

# **The Relationship between Magmatism and Borate Mineralisation in Western Turkey**

**By Duncan Anderson**

**June 1997**

**This thesis is submitted in fulfilment for the degree of Doctor of  
Philosophy in the Faculty of Science, University of Leicester**



UMI Number: U096034

All rights reserved

INFORMATION TO ALL USERS

The quality of this reproduction is dependent upon the quality of the copy submitted.

In the unlikely event that the author did not send a complete manuscript and there are missing pages, these will be noted. Also, if material had to be removed, a note will indicate the deletion.



UMI U096034

Published by ProQuest LLC 2013. Copyright in the Dissertation held by the Author.  
Microform Edition © ProQuest LLC.

All rights reserved. This work is protected against  
unauthorized copying under Title 17, United States Code.



ProQuest LLC  
789 East Eisenhower Parkway  
P.O. Box 1346  
Ann Arbor, MI 48106-1346

# **The Relationship between Magmatism and Borate Mineralisation in Western Turkey**

**By Duncan Anderson**

## **ABSTRACT**

A limited number of lacustrine basins in western Turkey contain world class borate reserves, with mineralisation present as strata bound deposits in Neogene volcano-sedimentary successions. This study examined in detail the relationship between magmatism and borate mineralisation in two of these basins (Emet and Kirka).

The magmatism comprised an Early Miocene K-rich acid phase, represented by granite, ignimbrite, rhyolite and dacite, and a more mafic K-rich, Middle - Late Miocene phase, represented by shoshonite and latite. Information from field observations, mineralogy, isotopic dates, immobile element concentrations and biotite compositions indicate that acid magmatism in Emet and Kirka Basins was closely related in both space and time to the deposition of the borate-host sediments, whilst mafic volcanism occurred later.

The mineralogical and geochemical composition of the borate-host sediments was strongly influenced by the post-depositional modification of rhyolitic, ignimbritic and granitic-derived material in a saline, alkaline environment. The result of the interaction between saline, alkaline waters and dominantly acid igneous products, was the generation of an authigenic mineral assemblage comprising mainly calcite, dolomite, borate, trioctahedral smectite and K-feldspar. Trioctahedral smectite, dolomite and K-feldspar, together with elevated concentrations of As, Sr and Li, correlate particularly well with borate mineralisation.

The geochemistry of the Early Miocene acid igneous rocks suggests that acid magmatism represented a likely source for B and Li, and probably also for As and Sr. Possible mechanisms for the transfer of B and other elements from an igneous source to the basin sediments include; transfer by igneous-driven geothermal fluids, rich in B as a result of hydrothermal leaching and contributions from magmatic waters and gases, and the break down of igneous material in saline, alkaline lakes. Trace element and Nd and Sr isotopic data indicate that the ultimate source of the B was assimilated upper continental crust, perhaps with some component of melted lithospheric mantle. Comparison with other borate provinces shows a common tectonic setting, characterised by former convergence with associated subduction and crustal thickening.

---

# CONTENTS

	Page numbers
<b>ABSTRACT</b>	
<b>CONTENTS</b>	<b>i-v</b>
<b>LIST OF FIGURES</b>	<b>v-ix</b>
<b>LIST OF TABLES</b>	<b>ix</b>
<b>LIST OF PLATES</b>	<b>x</b>
<b>ACKNOWLEDGEMENTS</b>	
<b>CHAPTER 1 (INTRODUCTION)</b>	<b>1.1-1.6</b>
1.1 BACK GROUND TO THESIS	1.1
1.2 LITERATURE REVIEW	1.1-1.5
1.2.1 Continental borate deposits	1.1-1.2
1.2.2 Geological evolution of western Turkey	1.2-1.5
1.2.2.1 Tethyan History	1.2-1.3
1.2.2.2 Post-Tethyan History	1.3-1.5
1.3 STUDY AREAS	1.5
1.4 METHODOLOGY	1.5
1.5 SPECIFIC OBJECTIVES	1.5-1.6
1.6 THESIS LAYOUT	1.6
<b>CHAPTER 2 (GEOLOGY OF THE EMET &amp; KIRKA AREAS)</b>	<b>2.1-2.23</b>
2.1 INTRODUCTION	2.1
2.2 GEOLOGY OF THE EMET BASIN AND THE SURROUNDING AREA (PREVIOUS STUDIES)	2.1-2.4
2.3 FIELD RELATIONS AND PETROLOGY OF IGNEOUS ROCKS FROM THE EMET AREA	2.4-2.12
2.3.1 Erigöz Granite	2.4-2.5
2.3.2 Volcanism in the Emet Basin	2.5-2.10
2.3.2.1 Emet Rhyolites	2.5-2.7
2.3.2.2 Emet Mafic Lavas	2.7
2.3.2.3 Volcaniclastic sediments in the Emet Basin	2.7-2.10
2.3.2.4 Emet Basin volcanic stratigraphy (from field and mineralogical evidence)	2.10
2.3.3 Volcanism south and west of Emet Basin	2.10-2.12
2.3.3.1 Rhyolites	2.10
2.3.3.2 Dacites	2.10



---

2.3.3.3 Mafic Lavas	2.10-2.11
2.3.3.4 Volcaniclastic sediments from south of Emet Basin	2.11
<b>2.4 GEOLOGY OF KIRKA BASIN AND THE SURROUNDING AREA (PREVIOUS STUDIES)</b>	<b>2.12-2.14</b>
<b>2.5 FIELD RELATIONS AND PETROLOGY OF IGNEOUS ROCKS FROM THE KIRKA AREA</b>	<b>2.14-2.22</b>
<b>2.5.1 Volcanism in the Kirka Basin</b>	<b>2.15-2.20</b>
2.5.1.1 Kirka Ignimbrites	2.15
2.5.1.2 Kirka Rhyolites and Dacites	2.16
2.5.1.3 Kirka Mafic Lavas	2.17
2.5.1.4 Volcaniclastic sediments from within Kirka Basin	2.17-2.20
2.5.1.5 Kirka Basin volcanic stratigraphy (from field and mineralogical evidence and K-Ar dates)	2.20
<b>2.5.2 Volcanism of the Afyon region</b>	<b>2.21-2.22</b>
2.5.2.1 Afyon Andesites and Dacites (sanidine-bearing)	2.21
2.5.2.2 Afyon Mafic Lavas	2.21
2.5.2.3 Volcaniclastic sediments from the Afyon region (Balmahmut)	2.22
<b>2.6 CONCLUDING POINTS</b>	<b>2.22-2.23</b>
 <b>CHAPTER 3 (TIMING OF MAGMATISM RELATIVE TO DEPOSITION OF BORATE-HOST SEDIMENTS)</b>	 <b>3.1-3.12</b>
<b>3.1 INTRODUCTION</b>	<b>3.1</b>
<b>3.2 CHEMICAL CLASSIFICATION OF THE MAGMATISM</b>	<b>3.1-3.4</b>
3.2.1 Alteration and element mobility	3.1-3.3
3.2.2 Nomenclature	3.3-3.4
<b>3.3 ISOTOPIC DATING</b>	<b>3.5-3.7</b>
3.3.1 Introduction	3.5
3.3.2 The Usak-Güre, Selendi and Emet area	3.6
3.3.3 The Kirka and Afyon areas	3.6-3.7
<b>3.4 CONSTRAINTS ON VOLCANIC STRATIGRAPHY FROM IMMOBILE ELEMENTS</b>	<b>3.7-3.9</b>
3.4.1 Introduction	3.7
3.4.2 Emet Basin	3.7-3.8
3.4.3 Usak-Güre and Selendi Basins	3.8
3.4.4 Kirka Basin	3.8-3.9
3.4.5 Afyon area (Balmahmut)	3.9
<b>3.5 CONSTRAINTS ON VOLCANIC STRATIGRAPHY FROM MINERAL CHEMISTRY</b>	<b>3.9-3.10</b>
3.5.1 Introduction	3.9

---

<b>3.5.2 Biotites</b>	<b>3.9-3.10</b>
<b>3.5.3 Feldspars</b>	<b>3.10</b>
<b>3.6 CONCLUDING POINTS</b>	<b>3.10-3.12</b>
 <b>CHAPTER 4 (ROLE OF MAGMATISM IN BORATE GENESIS)</b>	 <b>4.1-4.29</b>
<b>4.1 INTRODUCTION</b>	<b>4.1</b>
<b>4.2 INFLUENCE OF MAGMATISM ON THE COMPOSITION OF SEDIMENTS IN SALINE, ALKALINE LACUSTRINE BASINS; CONSTRAINTS FOR BORATE MINERALISATION</b>	<b>4.1-4.18</b>
<b>4.2.1 Previous investigations</b>	<b>4.1-4.3</b>
<i>4.2.1.1 Saline, alkaline basins in western USA</i>	<i>4.1-4.2</i>
<i>4.2.1.2 Borate-bearing basins in western Turkey and the Aegean</i>	<i>4.2-4.3</i>
<b>4.2.2 Influence of magmatism on the mineralogical and geochemical composition of sediments in the Borate and Red Formations of Emet Basin</b>	<b>4.3-4.14</b>
<i>4.2.2.1 Introduction</i>	<i>4.3</i>
<i>4.2.2.2 Methodology</i>	<i>4.3-4.4</i>
<i>4.2.2.3 Distribution of borate mineralisation in the sampled sections</i>	<i>4.4</i>
<i>4.2.2.4 Composition and post-depositional modification of igneous-derived sediment in Emet Basin</i>	<i>4.4-4.10</i>
(a) Introduction	4.4
(b) The Red Formation	4.4-4.5
(c) The Borate Formation	4.5-4.9
(d) Summary	4.9-4.10
<i>4.2.2.5 Implications for the distribution of borate mineralisation in Emet Basin</i>	<i>4.10-4.12</i>
<i>4.2.2.6 Importance of trioctahedral smectite, authigenic K-feldspar and illite to colemanite precipitation</i>	<i>4.12-4.13</i>
<i>4.2.2.7 The mineralogy and geochemistry of Emet Basin borate-hosting mudstones compared with other lacustrine sediments and upper continental crust</i>	<i>4.13-4.14</i>
<b>4.2.3 Comparison between the composition of sediments in the Emet Basin with those in the Selendi, Usak-Güre, Kirka and Afyon areas</b>	<b>4.14-4.17</b>
<i>4.2.3.1 Introduction</i>	<i>4.14</i>
<i>4.2.3.2 Selendi/Usak-Güre Basins</i>	<i>4.14-4.15</i>
<i>4.2.3.3 Kirka Basin</i>	<i>4.15-4.16</i>
<i>4.2.3.4 Afyon Area (Balmahmut)</i>	<i>4.17</i>
<b>4.2.4 Concluding points</b>	<b>4.17-4.18</b>
<b>4.3 EVALUATION OF MAGMATISM AS A SOURCE FOR ELEMENTS ASSOCIATED WITH BORATE MINERALISATION</b>	<b>4.18-4.27</b>
<b>4.3.1 Previous work</b>	<b>4.18-4.19</b>
<b>4.3.2 Investigation into the source potential of igneous rocks in the</b>	

---

<b>Usak-Güre, Selendi, Emet, Kirka and Afyon areas</b>	<b>4.19-4.27</b>
4.3.2.1 <i>Introduction</i>	4.19
4.3.2.2 <i>Geochemical Analysis</i>	4.19
4.3.2.3 <i>Concentrations of Sr, As, B &amp; Li in igneous rocks from the Usak-Güre, Selendi, Emet, Kirka and Afyon areas</i>	4.19-4.21
4.3.2.4 <i>Secondary mobilisation of B, As, Li and Sr</i>	4.21-4.23
4.3.2.5 <i>Discussion: implications for borate mineralisation</i>	4.23-4.27
(a) Source potential of Igneous rocks	4.23
(b) Transfer mechanisms	4.23-4.27
<b>4.3.3 Concluding points</b>	<b>4.27</b>
<b>4.4 MODEL FOR THE ROLE OF MAGMATISM IN THE GENESIS OF EMET AND KIRKA BORATE DEPOSITS</b>	<b>4.27-4.29</b>
<b>4.5 IMPLICATIONS FOR BORATE MINERAL EXPLORATION</b>	<b>4.29</b>
 <b>CHAPTER 5 (ORIGIN OF MIOCENE MAGMATISM IN THE TURKISH BORATE PROVINCE)</b>	 <b>5.1-5.19</b>
<b>5.1 INTRODUCTION</b>	<b>5.1</b>
<b>5.2 SUMMARY OF OLIGOCENE TO RECENT MAGMATISM IN WESTERN TURKEY (PREVIOUS STUDIES)</b>	<b>5.1-5.3</b>
<b>5.3 GENESIS OF MIOCENE MAGMATISM IN THE USAK-GÜRE, SELENDI, EMET, KIRKA AND AFYON AREAS</b>	<b>5.3-5.18</b>
5.3.1 Major and trace elements	5.3-5.5
5.3.2 Nd and Sr isotopes	5.5-5.6
5.3.3 Discussion	5.6-5.18
5.3.3.1 <i>Assimilation of upper crust</i>	5.6-5.8
5.3.3.2 <i>Lithospheric mantle sources</i>	5.8-5.12
5.3.3.3 <i>Implications for the source of B</i>	5.12-5.16
5.3.3.4 <i>The generation of Miocene magmatism in western Turkey within a tectonic framework</i>	5.16-5.18
<b>5.4 CONCLUDING POINTS</b>	<b>5.18-5.19</b>
 <b>CHAPTER 6 (CONCLUSIONS &amp; RECOMMENDATIONS FOR FUTURE WORK)</b>	 <b>6.1-6.8</b>
<b>6.1 INTRODUCTION</b>	<b>6.1</b>
<b>6.2 TIMING OF MAGMATISM RELATIVE TO DEPOSITION OF BORATE-HOST SEDIMENTS</b>	<b>6.1-6.3</b>
6.2.1 Field and petrologic evidence	6.1
6.2.2 Isotopic dating	6.1-6.2
6.2.3 Immobile elements and mineral compositions	6.2
6.2.4 Summary	6.2-6.3

---

---

<b>6.3 INFLUENCE OF MAGMATISM ON SEDIMENT COMPOSITION AND THE IMPLICATIONS FOR BORATE MINERALISATION</b>	<b>6.3-6.4</b>
<b>6.4 SOURCE POTENTIAL OF ACID MAGMATISM AND TRANSFER MECHANISMS FROM SOURCE TO BASIN SEDIMENTS</b>	<b>6.4-6.5</b>
6.4.1 Source potential of acid igneous rocks in the Emet and Kirka areas	6.4
6.4.2 Mechanisms for the transfer of B, As, Li, Sr and s from an igneous source to the basin sediments	6.4-6.5
<b>6.5 SUMMARY OF MODEL FOR THE ROLE OF MAGMATISM IN THE GENESIS OF EMET AND KIRKA BORATE DEPOSITS</b>	<b>6.5-6.6</b>
<b>6.6 ORIGIN OF MAGMATISM IN THE TURKISH BORATE PROVINCE; CONSTRAINTS FOR THE ULTIMATE SOURCE OF BORON</b>	<b>6.6-6.7</b>
<b>6.7 CONCLUDING POINTS</b>	<b>6.7</b>
<b>6.8 IMPLICATIONS FOR BORATE MINERAL EXPLORATION</b>	<b>6.7-6.8</b>
<b>6.9 SUGGESTIONS FOR FURTHER WORK</b>	<b>6.8</b>
<b>REFERENCES</b>	<b>R1-R11</b>
<b>APPENDICES</b>	

## LIST OF FIGURES

	Follows Page
<b>Chapter 1</b>	
Figure 1.1 Summary geological map of study areas	1.1
<b>Chapter 2</b>	
Figure 2.1 Map of the geology of the Emet area	2.1
Figure 2.2 Geological & location map of the Emet Borate District	2.1
Figure 2.3 Sections through the Red & Borate Formations of Emet Basin	2.7
Figure 2.4 Sections through the Inay Group of the Selendi Basin	2.11
Figure 2.5 Sections through the Inay Group of the Usak-Güre Basin	2.12
Figure 2.6 Map of the geology of the Kirka area	2.12
Figure 2.7 Geological & location map of Kirka Borate District	2.12
Figure 2.8 Sections through the Karaören Formation of the Kirka Basin	2.17
Figure 2.9 Sections through sedimentary sequences near to Balmahmut	2.22
<b>Chapter 3</b>	
Figure 3.1a Composition of glass in ignimbrite south of Kirka Basin	3.1
Figure 3.1b Alteration of feldspars to kaolinite in Emet rhyolites	3.1
Figure 3.2 Plots of selected elements vs Zr for volcanic and granitic samples from the Emet area	3.3

---

Figure 3.3	Plots of selected elements vs Zr for volcanic samples from the area S & W of Emet	3.3
Figure 3.4	Plots of selected elements vs Zr for volcanic samples from the Kirka area	3.3
Figure 3.5	Plots of selected elements vs Zr for volcanics from the Afyon area	3.3
Figure 3.6	Relationship between LOI & major element concentrations in igneous rocks from the Emet area	3.3
Figure 3.7	Alkali-silica plots for igneous rocks of the Emet region	3.4
Figure 3.8	Alkali-silica plots for igneous rocks of the Kirka & Afyon areas	3.4
Figure 3.9	AFM diagrams for the igneous rocks of Emet region	3.4
Figure 3.10	AFM diagrams for igneous rocks of the Kirka & Afyon areas	3.4
Figure 3.11	Immobile element concentrations in granite, volcanics & volcaniclastic sediments from the Emet area	3.7
Figure 3.12	Immobile element concentrations and ratios in granite, volcanics & volcaniclastic sediments from the Emet area	3.7
Figure 3.13	Immobile elements vs CaO in volcanics & volcaniclastic sediments from Emet Basin	3.7
Figure 3.14	Immobile element concentrations in volcanics & volcaniclastic sediments from the Selendi & Usak-Güre Basins	3.8
Figure 3.15	Immobile element concentrations & ratios in volcanics & volcaniclastic sediments from Selendi & Usak-Güre Basins	3.8
Figure 3.16	Immobile element concentrations in volcanics & volcaniclastic sediments from the Kirka area	3.8
Figure 3.17	Immobile element concentrations and ratios in volcanics and volcaniclastic sediments of the Kirka area	3.8
Figure 3.18	Immobile element concentrations in volcanics & volcaniclastic sediments of the Balmahmut area	3.9
Figure 3.19	Immobile element concentrations and ratios in volcanics and volcaniclastic sediments of the Balmahmut area	3.9
Figure 3.20	Composition of biotites from granitic, volcanic and volcaniclastic rocks of Emet Basin	3.10
Figure 3.21	Compositions of feldspars from granitic, volcanic and volcaniclastic rocks of Emet Basin	3.10
Figure 3.22	Generalised stratigraphy of Emet Basin	3.11
Figure 3.23	Generalised stratigraphy of Selendi & Usak-Güre Basins	3.11
Figure 3.24	Generalised stratigraphy of Kirka Basin	3.11
<b>Chapter 4</b>		
Figure 4.1	Multielement variation plots for volcaniclastic siltstones of the Red	

---

	Formation (Emet Basin)	4.4
Figure 4.2	Electron microprobe analyses of volcanoclastic siltstone from the Red Formation (Emet Basin)	4.4
Figure 4.3	Multielement variation plots for sediments of the Borate Formation (Section C - northern Emet Basin)	4.5
Figure 4.4a	Electron microprobe analyses of volcanoclastic siltstone in the Borate Formation (Section C - northern Emet Basin)	4.6
Figure 4.4b	Electron microprobe analyses of altered plagioclase from volcanoclastic siltstone in the Borate Formation (Section C - northern Emet Basin)	4.6
Figure 4.5	Multielement variation plots for sediments of the Borate Formation (Sections E & G - mid & southern Emet Basin)	4.9
Figure 4.6	Multielement variation plots for sediments from barren and colemanite-bearing mudstones (Borate Formation - Emet Basin)	4.10
Figure 4.7	XRD traces of borate-host & barren mudstone (Borate Formation - Emet Basin)	4.11
Figure 4.8	Concentrations of As, Sr & Li in sediments from the Borate Formation of Emet Basin (histograms)	4.11
Figure 4.9	Concentrations of As, Sr & Li in sediments from the Borate Formation of northern Emet Basin (alongside stratigraphic sections)	4.11
Figure 4.10	Concentrations of As, Sr & Li in sediments from the Borate Formation of southern Emet Basin (alongside stratigraphic sections)	4.11
Figure 4.11	Multielement variation plots comparing the Emet mudstones with other sediment databases	4.13
Figure 4.12	Multielement variation plots for mudstones of the Selendi & Usak-Güre Basins	4.14
Figure 4.13	Concentrations of As, Sr & Li in sediments from the Emet, Selendi, Usak, Kirka & Afyon areas of Emet Basin (histograms)	4.15
Figure 4.14	As vs Sr concentrations in sediments from the Emet, Selendi, Usak, Kirka and Afyon areas	4.15
Figure 4.15	Li vs Sr concentrations in sediments from the Emet, Selendi, Usak, Kirka and Afyon areas	4.15
Figure 4.16	Multielement variation plots for siltstones of the Karaören & Fetiye Formations (Kirka Basin)	4.15
Figure 4.17	Multielement variation plots for siltstones of the Sarikaya Formations (Kirka Basin)	4.16
Figure 4.18	Multielement variation plots for sediments from the Afyon area (Balmahmut)	4.17
Figure 4.19	Sr & As concentrations in igneous rocks from the Usak, Selendi,	

	Emet Kirka & Afyon areas	4.19
Figure 4.20	Remobilisation test multielement variation plots for igneous rocks of the Emet area	4.20
Figure 4.21	Remobilisation test multielement variation plots for igneous rocks of the Kirka area	4.20
Figure 4.22	B & Li concentrations in igneous rocks from the Usak, Selendi, Emet Kirka & Afyon areas	4.20
Figure 4.23	Block diagram illustrating a model for the role of magmatism in the genesis of Emet & Kirka borate deposits	4.27
<b>Chapter 5</b>		
Figure 5.1	Variations of major elements vs time for radiometrically dated igneous rocks from the Usak, Selendi, Emet & Kirka areas	5.3
Figure 5.2	Variations of major elements and selected trace element ratios vs time for radiometrically dated igneous rocks from the Usak, Selendi, Emet & Kirka areas	5.3
Figure 5.3	Variations of elemental ratios with SiO <sub>2</sub> wt %	5.4
Figure 5.4	Multielement variation plots for acid igneous rocks from the Usak, Selendi, Emet & Kirka areas	5.4
Figure 5.5	Multielement variation plots for trachyte/dacite, andesite, latite & shoshonite from the Usak, Selendi, Emet & Kirka areas	5.4
Figure 5.6	Multielement variation plots for volcanic rocks from the Afyon area	5.4
Figure 5.7	Multielement variation plots comparing variations within the Usak, Selendi, Emet, Kirka & Afyon suites with Tertiary & Quaternary volcanism from elsewhere in western Turkey	5.4
Figure 5.8	REE concentrations in igneous rocks from the Usak, Selendi, Emet & Kirka areas	5.4
Figure 5.9	Multielement plot comparing the Usak, Selendi, Emet, Kirka & Afyon data with upper continental crust	5.5
Figure 5.10	Nd & Sr isotopic compositions of the Usak, Selendi, Emet, Kirka and Afyon volcanics and granite compared with magmatism from the eastern Mediterranean region	5.5
Figure 5.11	SiO <sub>2</sub> and MgO variations with <sup>87</sup> Sr/ <sup>86</sup> Sr and ε <sub>Nd</sub>	5.6
Figure 5.12	B and B/Nb variations with <sup>87</sup> Sr/ <sup>86</sup> Sr and ε <sub>Nd</sub>	5.6
Figure 5.13	Nd & Sr isotopic compositions of the Usak, Selendi, Emet, Kirka and Afyon volcanics and granite compared with magmatism from the eastern Mediterranean region	5.6
Figure 5.14	Multielement variation plots comparing the Usak, Selendi, Emet, Kirka and Afyon acid magmatism with other databases	5.8

---

Figure 5.15	Multielement variation plots comparing the Usak, Selendi, Emet, Kirka and Afyon mafic magmatism with other databases	5.9
Figure 5.16	Ti/Y vs Nb/Y for the Usak, Selendi, Emet, Kirka and Afyon mafic lavas	5.9
Figure 5.17	Th/Y vs Nb/Y for the Usak, Selendi, Emet, Kirka and Afyon mafic lavas	5.9
Figure 5.18	B/Nb vs B for the Usak, Selendi, Emet, Kirka and Afyon volcanics & granite	5.14

## LIST OF TABLES

	Page
<b>Chapter 2</b>	
Table 2.1	Summary of authigenic minerals present in the Borate Formation (Emet Basin)
	2.3
Table 2.2	Summary petrology of intrusive & extrusive rocks in Emet Basin
	2.6
Table 2.3	Summary mineralogy of volcanoclastic sediments in the Red Formation (Emet Basin)
	2.8
Table 2.4	Summary mineralogy for volcanoclastic sediments of the Borate Formation (Emet Basin)
	2.9
Table 2.5	Summary petrology of volcanic rocks & volcanoclastic sediments from Selendi & Usak-Güre Basins
	2.11
Table 2.6	Summary of authigenic minerals present in the Sarikaya Formation (Kirka Basin)
	2.14
Table 2.7	Summary petrology of volcanic rocks from the Kirka area
	2.16
Table 2.8	Summary mineralogy of ignimbrite-derived volcanoclastic sediments in the Karaören Formation (Kirka Basin)
	2.18
Table 2.9	Summary mineralogy of sediments in the Sarikaya Formation (Kirka Basin)
	2.19
Table 2.10	Summary mineralogy of ignimbrite-derived lacustrine volcanoclastic sediments in the Fetiye Formation (Kirka Basin)
	2.20
Table 2.11	Summary petrology of volcanic lavas and volcanoclastic sediments from the Afyon area
	2.21
<b>Chapter 3</b>	
Table 3.1	Summary of alteration & recrystallisation in collected volcanic rock samples from the Emet & Kirka areas
	3.2
Table 3.2	Nomenclature of collected samples
	3.4
Table 3.3	K-Ar & $^{40}\text{Ar}/^{39}\text{Ar}$ ages for igneous rocks from the Emet, Selendi, Usak, Kirka & Afyon areas
	3.5



---

# LIST OF PLATES

Follows Page

## Chapter 2

Plate 2.1a	Emet Rhyolites near Kurtlubeyler (Emet Basin)	2.5
Plate 2.1b	Emet mafic lavas overlying mudstone (Emet Basin)	2.5
Plate 2.2a	Volcaniclastic siltstone bed in the Red Formation of Emet Basin	2.7
Plate 2.2b	Thin section of Red Formation volcaniclastic siltstone	2.7
Plates 2.3a & b	Possible remnant pumice in Red Formation volcaniclastic siltstone	2.7
Plate 2.4a	Section B (in Red Formation of Emet Basin)	2.8
Plate 2.4b	Thin section of Red Formation volcaniclastic siltstone	2.8
Plate 2.5a	Section C through Borate Formation (northern Emet Basin)	2.8
Plate 2.5b	Section Upper C showing colemanite nodules	2.8
Plate 2.6a	Kirka Ignimbrite at Köroglukalesi Tepe	2.15
Plate 2.6b	Fiamme in Kirka Ignimbrite	2.15
Plate 2.7a	Tent rocks in Kirka ignimbrite	2.15
Plate 2.7b	Kirka mafic lavas near Sancar overlying cherty limestone of the Sarikaya Formation (Kirka Basin)	2.15
Plate 2.8a	Glass shards in Kirka Ignimbrite (SEM image)	2.15
Plate 2.8b	Unfragmented glass in Kirka Ignimbrite (SEM image)	2.15
Plate 2.9a	Cherty limestone beds of the Sarikaya Formation overlying volcaniclastic sediments of the Karaören Formation (Kirka Basin)	2.17
Plate 2.9b	Tent rocks in volcaniclastic sediments of the Karaören Formation (Kirka Basin)	2.17
Plates 2.10a & 2.10b	Pumice infilled with calcite in volcaniclastic sediments of the Fetiye Formation (Kirka Basin)	2.19

## Chapter 4

Plates 4.1a & 4.1b	Authigenic K-feldspar in volcaniclastic siltstone of the Borate Formation (Emet Basin) (electron microprobe back scatter images)	4.6
Plate 4.2a	The main minerals present in volcaniclastic siltstone of the Borate Formation (Emet Basin) (electron microprobe back scatter image)	4.6
Plate 4.2b	The matrix of volcaniclastic siltstone of the Borate Formation (Emet Basin) (electron microprobe back scatter image)	4.6

## **Acknowledgements**

I would like to especially thank my three supervisors for all their assistance and enthusiasm during my PhD; Dr Barry Scott for setting up the project and for his help during the early stages, Dr Charlie Moon for his help and support throughout, and Professor Ansel Dunham for valuable assistance during the latter stages of this work. I have also received considerable assistance and advice from many of the staff at Leicester; Dr Andy Saunders (paper review), Professor John Tarney (writing grant proposal), Dr Mike Branney (reading chapter), Dr Ray Kent (reading chapter), Dr Tim Brewer (seeing samples from Nottingham), Dr Andy Kerr, Dr Jeremy Richards, Dr Alan Collins, Professor John Hudson, Dr Dickson Cunningham, Dr Mike Norry, Dr Mike Whately, Dr Jan Zalasiewicz and Andy Smith. The technical staff at Leicester have always been helpful and efficient and I would like to thank the following in particular; Bill Teasdale, Chris Beckett, Nick Marsh, Rob Kelley, Dougie Martin, Emma Mansley, Kevin Sharkey, Rob Wilson, Linda Marvin, Colin Cunningham, Rod Branson and Paul Ayto. On the administration side, Pat and Donna have cheered up many a dull day. From NIGL at Keyworth, I would particularly like to thank Barbara Barreiro and Geoff Nowell for analysing my samples and for showing an interest in my project.

From Turkey, Gürol Seyitoglu was a good friend as well as being a real help with the geology too and Cahit Helvacı provided me with useful information on the Turkish borates. Other people I would like to thank in Turkey are; Ismail (driver), the staff of Etibank at Emet, the staff of Hotel Ece in Afyon, the staff of the hotel at Eynal, the taxi drivers of Afyon and Ford Hassan. I also greatly appreciate financial aid whilst in Turkey from BHP Minerals and Turk Petroleum. I would like to thank Christophe Noblet and Nejat Somali of BHP minerals for their discussions on borates. Overall, I thoroughly enjoyed my time in Turkey, which is interesting, beautiful and very friendly place.

On the personal side, I want to thank all the many friends I have spent time with over this period, for all their abuse and generally good times. From outside Leicester, Paul, Rob, Fiona, Russell, Amanda, Gordon, Jilly, Becky, Ernie (+ the Worcester gang) and Jon particularly paid visits to the pubs of Leicester and some even to Turkey. At Leicester, I have many friends to thank for three and a half excellent years; Tanya for surviving three years in the same house as me, Ceri for being ridiculously laid back, Vivi for being Vivi, Adrian for not being competitive, Laurence for not being argumentative, Barney for not being abusive, Lynsey for not drinking much, Sarah for the use of her computer, for photographing my car as it dangled over a cliff and for not being dappy. Also, Vince, Joules, Liz, Jon, Jim, Jane, Andy Kerr, Chris Beckett, Chris Bert, Annette, Christina, Matt, Magnus, Joe, Robin, Emine, Al, Karine, Sam, Roz, Tiff, Graham, Steve Temperly, Steve Powell, Dickson, Trevor, Vasilis, Kate, Marion and Steph.

My parents and Malcolm, Niki and Neil have been brilliant over this extended period of my education, a more supportive family I could not wish for. In particular, I would like to thank my parents who have been of great support, financial and otherwise.

# 1 INTRODUCTION

## 1.1 BACKGROUND TO THESIS

Most of the world's commercial borate deposits are located in lacustrine basins, and are associated with continental sediments and volcanism of Neogene age (Kistler & Helvacı 1994). The assertion that volcanism has a genetic association with borate mineralisation stems from the presence of interbedded volcanic lavas and volcanoclastic sediments within many borate-hosting sequences (Kistler & Helvacı 1994). A number of workers have suggested a volcanic or thermal spring source for the boron in these deposits (Inan et al., 1973, Helvacı 1995, Smith & Medrano 1996). The purpose of this study was to examine in detail the possible relationship between magmatism and borate mineralisation in Miocene borate-hosting volcano-sedimentary basins in western Turkey.

## 1.2 LITERATURE REVIEW

### 1.2.1 Continental borate deposits

Cenozoic continental borate deposits provide more than 90% of the world's required boron compounds, while metamorphic complexes and borate minerals from pre-Cenozoic marine evaporites supply the remainder (Smith & Medrano 1996). Continental borate deposits from western Turkey, whose genesis is the subject of this thesis, accounted for 38% of world production in 1992, while similar deposits in USA and South America (Argentina, Chile, Bolivia & Peru) accounted for 39% and 15% respectively (Smith & Medrano 1996). These three regions therefore make up the world's largest and most economically important borate provinces.

Borate minerals from Cenozoic continental deposits are relatively rare members of a group of minerals generated under arid conditions in hydrologically closed lacustrine basins, where evaporation exceeds inflow. Common saline minerals in lacustrine evaporitic deposits include halite (NaCl), sylvite (KCl), gypsum ( $\text{CaSO}_4 \cdot 2\text{H}_2\text{O}$ ), epsomite ( $\text{MgSO}_4 \cdot 7\text{H}_2\text{O}$ ) and trona ( $\text{NaHCO}_3 \cdot \text{Na}_2\text{CO}_3 \cdot 2\text{H}_2\text{O}$ ) (Eugster 1980). The vast majority of continental brines are therefore represented by cations of Na, K, Mg and Ca, and anions of Cl,  $\text{SO}_4$  and  $\text{HCO}_3\text{-CO}_3$  (Eugster 1980). These ionic species are concentrated in brines during evaporation leading to the eventual generation of saline minerals.




According to Eugster (1980), the first mineral to precipitate from such brines is calcite, which leads to an increase in the Mg/Ca ratio of the residual solution, and the subsequent precipitation of high-Mg calcite and dolomite. Saline minerals such as gypsum and trona reach saturation later in the brine evolution (Eugster 1980). Sometimes, these evaporating brines become saturated in the borate species  $\text{B(OH)}_3$  and  $\text{B(OH)}_4^-$ , in addition to cations of Na, Ca and Mg, which leads to the precipitation of borate minerals (Smith & Medrano 1996). Furthermore, boron isotope studies on non-marine borate minerals have shown that borate minerals precipitate from alkaline solutions (generally  $> 8$  pH - Oi et al., 1989, Palmer & Helvacı 1995). Common borate minerals include borax ( $\text{Na}_2\text{B}_4\text{O}_7 \cdot 10\text{H}_2\text{O}$ ), colemanite ( $\text{Ca}_2\text{B}_6\text{O}_{11} \cdot 5\text{H}_2\text{O}$ ) and ulexite ( $\text{NaCaB}_5\text{O}_9 \cdot 8\text{H}_2\text{O}$ ) (Kistler & Helvacı 1994).

The Turkish Borate Province (Figure 1.1), the subject of this thesis, contains the largest known borate reserves in the world (Kistler & Helvacı 1994). The borate deposits are thought to have formed

**FIGURE 1.1-** Summary geological map and location of study areas (geology from Bingöl 1989)



**LEGEND**

-  Tertiary - Quaternary Volcanics
-  Metamorphic Complexes
-  Fault

**Figure 1.1**

during the Miocene in closed lacustrine basins under conditions of high salinity and alkalinity (Helvacı et al., 1993). The deposits in this region are found in basins in the Bigadiç, Sultançayırı, Kestelek, Emet, Kirka and Samos (Greece) areas (Figure 1.1); deposits at Bigadiç, Emet and Kirka are currently exploited commercially (Helvacı et al., 1993, Kistler & Helvacı 1994). Colemanite is present in all these deposits, and ulexite is present in all except the Sultançayırı deposit, while the only occurrence of borax is in the Kirka district (Helvacı 1984, 1994, 1995; Helvacı et al., 1993, Stamatakis & Economou 1991, Gündoğdu et al., 1996). Other evaporitic minerals found in these deposits include gypsum and celestite (Helvacı et al., 1993). The borate reserves are interbedded with lacustrine sediments, which include mudstone, sandstone and limestone, and all the basins were partially filled with a series of tuffaceous rocks and lavas (Helvacı et al., 1993, Kistler & Helvacı 1994).

### **1.2.2 Geological evolution of western Turkey**

In the following section, a brief outline is given of the geological evolution of western Turkey from the Late Palaeozoic to the present, and the place of Miocene borate-hosting basins within this established framework. The section is separated into Tethyan and post-Tethyan history. The former phase was dominated by interaction of the super continents Gondwana and Laurasia and the evolution of Tethyan oceanic basins between them (Sengör & Yilmaz 1981, Okay et al., 1996, Robertson et al., 1996), while the latter was dominated by upper crustal extension (Sengör et al., 1985, Hetzel et al., 1995).

#### **1.2.2.1 Tethyan History**

It has been established from palaeomagnetic data, that in Permo-Triassic times, two super continents, Gondwana and Laurasia, were separated by a westward narrowing gulf known as Tethys (Bullard et al., 1965). By the Early Tertiary, western Turkey had become a single entity, following the amalgamation of several continental fragments with independent Palaeozoic and Mesozoic geologic histories (Okay et al., 1996). The events leading up to assembling of the continental fragments that make up western Turkey are described below.

During the Late Permian to Mid Triassic, an ocean known as Palaeotethys, covered much of the eastern Mediterranean region (Sengör & Yilmaz 1981, Robertson & Dixon 1984, Sengör et al., 1984a, Stampfli et al., 1991, Dercourt et al., 1993, Okay et al., 1996). During the Permian, much of present Turkey constituted part of the northern margin of Gondwana, while the Pontides (Figure 1.1) are considered to mark the southern margin of the other super continent, Eurasia (Sengör & Yilmaz 1981, Robertson & Dixon 1984). A number of authors (Robertson and Dixon 1984, Robertson et al., 1996, Stampfli et al., 1991 and Dercourt et al., 1993) have suggested that the southern margin of Eurasia was active in the Late Palaeozoic, with northward subduction of Paleotethyan crust. Robertson et al. (1996) proposed that this northward subduction was active from the Late Palaeozoic to the Early Tertiary, jumping ocean ward as continental fragments collided with the trench. The northern Gondwana margin (ie. Africa) was seen as passive, at least from the Late Palaeozoic onwards (Robertson & Dixon 1984, Dercourt et al., 1986, Robertson et al., 1996). Furthermore, Robertson and

Dixon (1984) advocated the presence of a single Tethyan ocean that continuously existed in the Eastern Mediterranean from the Late Palaeozoic onwards.

This contrasts with the view of Sengör et al. (1984a) who envisaged the southern margin of Eurasia as being passive in the Late Palaeozoic to Early Mesozoic, whilst the northern margin of Gondwana was active. They proposed west to south-west subduction beneath the Gondwana margin during the Late Permian to Mid-Jurassic which led to rifting of an elongate Gondwana-derived continental fragment, Cimmeria, that drifted northwards opening a new (Neotethyan) back arc basin. During the Late Triassic to Early Jurassic, the northern branch of Neotethys (Vardar Ocean) began opening south of the Cimmerian continent (Sengör et al., 1984a). They regarded the new rifting event as renewed back arc activity over the still active Paleotethyan subduction zone (Sengör et al., 1984a). In their interpretation, Palaeotethys finally closed in the Mid Jurassic, with the welding of the Cimmerian continent to the southern margin of Laurasia, subsequently followed by Tibet type magmatism.

In common with Sengör et al. (1984a), Robertson and Dixon (1984) identified the Permo-Triassic as a time of important rifting of micro-continents, such as the Tauride platform (Figure 1.1) from Gondwana. In this view, during the Mesozoic, the south Tethyan region consisted of Gondwana-derived micro-continents and small ocean basins (Robertson et al., 1996). Both sets of authors envisaged progressive closure of Tethys in the eastern Mediterranean region during the Late Cretaceous to Early Tertiary. There is a consensus that the Eurasian margin was active from the Cretaceous to the Early Tertiary, and that northward subduction beneath the Eurasian margin during the latter stages of Tethyan closure gave rise to Andean type magmatism (Sengör et al., 1984a, Robertson and Dixon 1984, Robertson et al., 1996). During the Late Cretaceous to Early Eocene, the Gondwana-derived Anatolide-Tauride block collided with the Pontides (part of Eurasia) leading to the closure of the northern branch of Neotethys (Sengör & Yilmaz 1981). Ophiolite obduction took place in the Late Cretaceous as a trench collided with a continent, while final suturing with continent - continent collision occurred in the Late Eocene, leading to the formation of the Ankara-Izmir Zone (Figure 1.1) (Collins & Robertson 1997).

### *1.2.2.2 Post-Tethyan History*

Much of the current area of Anatolia was characterised by N-S intracontinental convergence during the Early Miocene, as a result of the Late Cretaceous-Eocene collision described above (Sengör et al., 1985). Crustal thickness at this time has been estimated at between 50 and 70 km (Sengör et al., 1985). This convergence also resulted in the thrusting of the Lycian nappes, which are composed of largely Mesozoic platform carbonates, pelagic sediments, and peridotite, and lie to the south of the Menderes Massif (Sengör & Yilmaz 1981, Sengör et al., 1985, Collins 1997, Collins & Robertson 1997). The Menderes Massif, which lies immediately to the south of the Izmir-Ankara Suture Zone (Figure 1.1), is generally believed to be a Gondwana-derived continental fragment (Robertson et al., 1996), that underwent intense deformation and metamorphism during the Middle Eocene (Hetzel & Reischmann 1996). The metamorphism was considered by Sengör et al. (1984b) to be the product of the latest Palaeocene collision across Neotethys, which resulted in the burial of the Menderes Massif

area beneath the Lycian nappe pile. Recent work on the structure and sedimentology of the Lycian nappe pile has shown a multiphase over thrust history with maximum metamorphism in the Menderes Massif coeval with Mid Eocene thrusting of the Lycian nappes as the northern strand of Neotethys finally closed (Collins 1997, Collins & Robertson 1997).

Arabia collided with Eurasia along the Bitlis suture in south-eastern Turkey in the Early-Late Miocene (Sengör & Yilmaz 1981, Aktas & Robertson 1984). This collision introduced such drastic changes in the tectonic evolution of all Turkey that it is a convenient time to separate the country's neotectonic development from its palaeotectonic development (Sengör et al., 1985). During the Middle-Late Miocene (Late Serravallian-Tortonian) there is some evidence for the westerly motion of the Anatolian block, which was largely facilitated by movement along the Northern and Eastern Anatolian strike slip faults (Sengör et al., 1985). This westerly motion of the Anatolian block, relative to Africa, has been taken up by subduction at the Hellenic trench in the Aegean Sea (Dewey & Sengör 1979). The inferred driving force for the westward 'escape' of the Anatolian block is the intracontinental convergence along the Bitlis Suture Zone (Dewey & Sengör 1979).

At around this time (Late Oligocene - Late Miocene), N-S extensional tectonics also began in western Turkey resulting in prominent east-west grabens, such as the Büyük Menderes and the Gediz grabens (Figure 1.1) (Sengör et al., 1985, Seyitoglu & Scott 1992a). Dewey and Sengör (1979) suggested that N-S extension began in western Turkey to relieve E-W shortening, which may be the result of the obstruction of the Anatolian plate's westerly motion due to the south-westerly bend in the course of the North Anatolian Fault Zone. Seyitoglu and Scott (1991) proposed that the extension is related to the spreading of thickened crust as a result of the Palaeogene compression. There is some controversy as to precisely when extension began in western Turkey; a number of workers have suggested that the Tortonian (Late Miocene) marked the onset of extension (Sengör et al., 1985, Görür et al., 1995), while others believe that extension started earlier in the Late Oligocene-Early Miocene (Seyitoglu et al., 1992, Seyitoglu & Scott 1992a, Hetzel et al. 1995). Extension has continued in western Turkey right up to the present day, and there has been approximately 30 % extension since the Tortonian (Sengör et al., 1985).

In addition to the E-W trending grabens, NE-SW and NW-SE trending basins are abundant in western Turkey (Seyitoglu & Scott 1991). The NW-SE and NE-SW trending basins generally have an older age than the E-W trending grabens (Seyitoglu & Scott 1991). The various explanations for sedimentary basin development and volcanism in the Early-Middle Miocene in western Turkey reflect the different views on the timing of extension. It has been suggested that NW-SE trending rifts with a Middle to Upper Miocene fill in south-western Turkey result from the previous N-S compressional regime, while E-W trending grabens filled with Plio-Quaternary rocks, result from the later N-S extensional regime (Görür et al., 1995). Sengör et al. (1985) have also suggested that Miocene basins in western Turkey may be resurrected Tibet type grabens, controlled by structures formed during the previous compressional regime. Seyitoglu and Scott (1991) however, imply that all Neogene basins in western Turkey were generated under the later N-S extensional regime. The Neogene basins in western Turkey are filled with Miocene and Pliocene fluvio-lacustrine sequences, consisting of

conglomerates, sandstones, siltstones, mudstones and a limestone capping (Steffens 1971). Some of the Miocene basins, such as the Emet and Kirka Basins, which are the subject of this study, are also host to extensive borate reserves (Helvacı et al., 1993).

Magmatism in western Turkey has evolved during the Tertiary from largely calc-alkaline and intermediate-acid in the Oligocene and Early Miocene to mainly alkaline and intermediate-basic in the Late Miocene and Quaternary (Yilmaz 1990, Güleç 1991, Seyitoglu & Scott 1991, 1992b). The Early calc-alkaline volcanism was accompanied by Oligocene-Early Miocene high level granitic intrusions (Bingöl et al., 1982, Yilmaz 1990). Yilmaz (1990) and Güleç (1991) proposed that the transition from calc-alkaline to alkaline volcanism reflected the change in the tectonic regime from compression to extension, while Seyitoglu and Scott (1992b) suggested that all Miocene volcanism was generated during extensional tectonics. They suggest that the change in the nature of the volcanism reflects an increasing asthenospheric contribution as a result of continuing extensional tectonics.

### 1.3 STUDY AREAS

The study areas are located in central western Turkey and include; the Emet and Kirka Basins and the areas immediately south of each basin (Figure 1.1). These two Miocene volcano-sedimentary basins host large reserves of borate mineralisation (Helvacı et al., 1993, Gündogdu et al., 1996). A considerable amount of detailed work has been conducted on the nature of the mineralisation in these basins (Inan et al., 1973, Helvacı 1977, Palmer & Helvacı 1995, Gündogdu et al., 1996), but the nature of Miocene magmatism within the basins and the surrounding areas has not been studied in detail. The basins therefore represent ideal locations to investigate the relationship between borate mineralisation and magmatism.

### 1.4 METHODOLOGY

Two field seasons, of five weeks and three months, were spent in western Turkey, sampling intrusives, extrusives and volcanoclastic sediments and examining their field relations. Two and a half years were subsequently spent at the University of Leicester undertaking mineralogical and geochemical investigations of the collected samples.

### 1.5 SPECIFIC OBJECTIVES

The overall aim of this thesis was to establish the complete magmatic history of two borate-hosting basins, such that the relationship between magmatism and borate mineralisation could be assessed. The specific objectives were therefore as follows:

- (i) To provide a thorough petrological and geochemical description of Miocene magmatism in the study areas.
- (ii) To determine the timing of magmatism relative to deposition of the borate-host lacustrine sediments.
- (iii) To assess the influence of magmatism on the composition of basin sediments, in particular the borate-host sediments.



(iv) To evaluate the potential of local magmatism as a source for elements associated with borate mineralisation.

(v) To establish the origin of the Miocene magmatism and therefore to constrain the ultimate source of boron.

### 1.6 THESIS LAYOUT

The layout of this thesis is designed to address each of the objectives above in a systematic manner:

**Chapter 2** - provides a field and petrological description of igneous rocks in the study area, and assesses the spatial and temporal position of magmatism relative to deposition of the borate-host sediments.

**Chapter 3** - the timing of magmatism relative to the deposition of the borate-host sediments is further constrained with the use of isotopic dating, immobile element concentrations and mineral chemical compositions.

**Chapter 4** - the influence of magmatism on the composition of the sediments, in particular the borate-host sediments, is considered, and an assessment is made of the potential of local magmatism as a source for elements associated with borate mineralisation.

**Chapter 5** - the detailed geochemistry of the igneous rocks of this region is presented with a view to establishing the origin of the magmatism and therefore the ultimate source of the boron.

**Chapter 6** - the main concluding points on the relationship between magmatism and borate mineralisation in western Turkey, as determined from this study, are presented, together with recommendations for future work.

A paper by Seyitoglu, Anderson, Nowell and Scott (1997), using data from this study, has been published on the evolution of magmatism in this area.

## **2. GEOLOGY OF THE EMET AND KIRKA AREAS**

### **2.1 INTRODUCTION**

The purpose of this chapter is to provide a review of the geology of the Emet and Kirka regions, and to present field and petrological information from the current study on the igneous rocks of this area. Field studies for this thesis were carried out mainly in the volcano-sedimentary basins at Emet and Kirka, although some additional work was undertaken in the surrounding areas; in Simav, Selendi and Usak-Güre Basins, and around the town of Afyon. Detailed sampling was undertaken of intrusives, extrusives and volcanoclastic sediments, and their field relations determined.

A major aim of this thesis is to infer the magmatic history of each basin in order to assess the influence of magmatism on borate mineralisation. This chapter therefore considers:

- (i) The igneous activity in this part of the Turkish Borate Province, by providing morphological and petrological descriptions of the extrusive and intrusive rocks.
- (ii) The spatial and temporal positions of extrusive and intrusive rocks relative to sedimentation, and in particular to borate-host sediments, in Emet and Kirka Basins.
- (iii) The provenance of the mineralised sediments, determined from their petrology, and in particular their volcanic content.

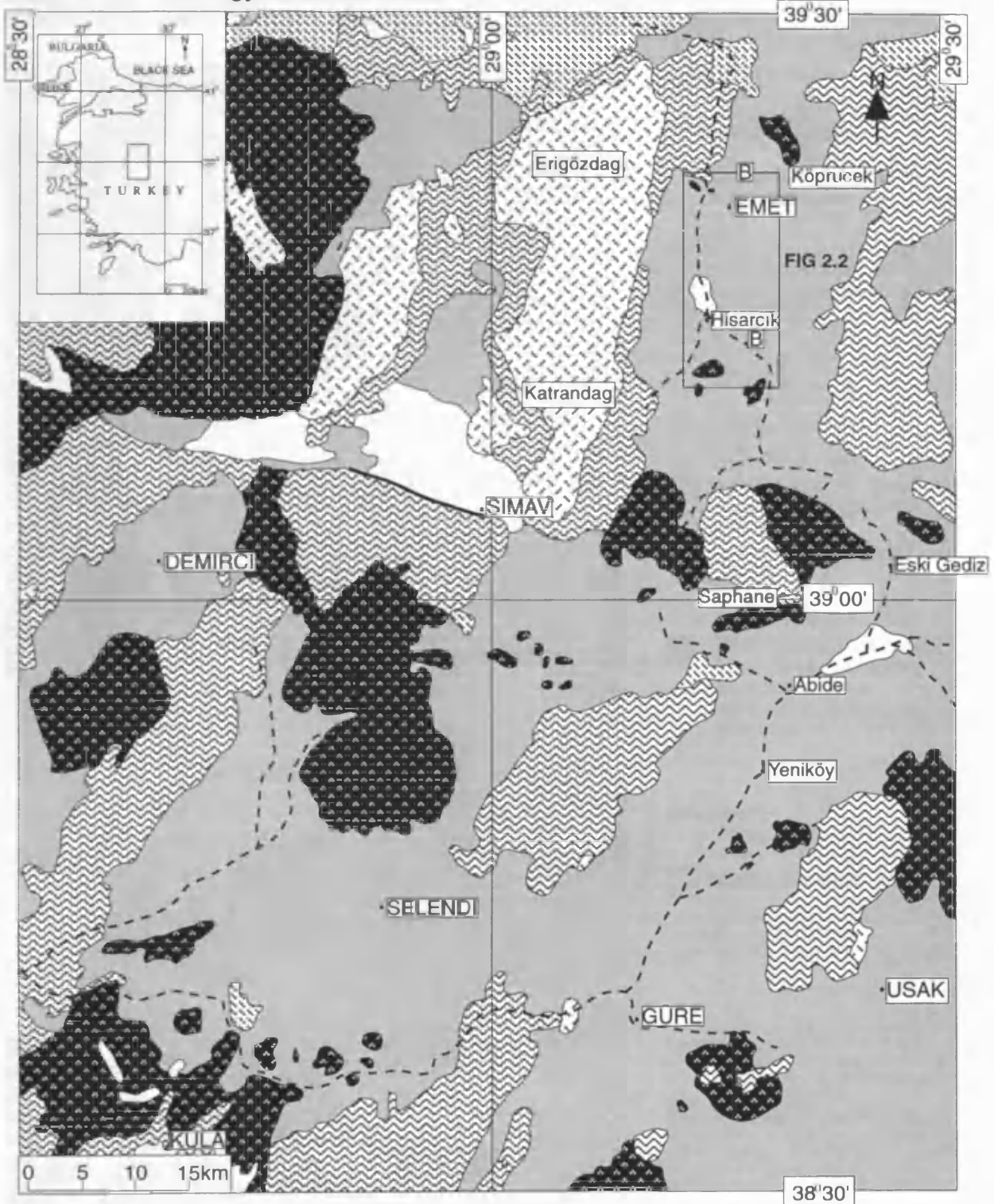
Subsequent chapters will build on this field and petrological information by discussing the geochemistry and detailed mineralogy of collected samples.

### **2.2 GEOLOGY OF THE EMET BASIN AND THE SURROUNDING AREA (PREVIOUS STUDIES)**

The Emet Basin is a structurally controlled basin with an infill of lacustrine and fluvial sediments. The basin is oriented in an approximate N-S direction and normal faults have been determined with NW-SE and NE-SW orientations, many of which are synsedimentary (Helvacı 1984, Yalçın et al., 1985). The faults have produced a distinct stepped topography (Helvacı 1977). The sediments in the Emet Basin are placed as Middle - Late Miocene on the basis of age determinations of diatomites (Yalçın et al., 1985), pollen (Gün et al., 1979) and ostracoda (Yalçın et al., 1985). Figure 2.1 shows that the Emet Basin is limited, by basement metasediments of presumed Palaeozoic age (Helvacı 1977), and igneous rocks of Tertiary age, which form elevated ground around the basin. The Erigöz Granite intruded basement metasediments on the western side of Emet Basin and it reaches over 2000 m to the north, while Saphane mountain at the south of the basin is again over 2000 m and is composed of both Tertiary volcanics and Palaeozoic basement rocks. The Palaeozoic basement rocks are comprised of marble, which forms elevated ground to the north and east, and of various schists, gneiss and quartzite to the west and north of the Emet Basin (Helvacı 1977, Kistler & Helvacı 1994).

The stratigraphy of the Emet Basin has been described with slight differences by a number of workers (Özpeker 1969, Helvacı 1977, Akdeniz 1977, Yalçın et al., 1985). A map of the Emet borate district, together with the basin stratigraphy, based on Helvacı (1977), is shown in Figure 2.2. South of the area shown on Figure 2.2, a basal conglomerate unconformably overlies the basement rocks

FIGURE 2.1 - Geology of the Emet Area



**LEGEND**

- Quaternary alluvium
- Neogene sediments
- Miocene volcanics
- Erigöz Granite

- Ultramafics
- Paleozoic & Permian basement

- Borate mineralisation
- Fault
- River

Based on MTA geological map 1:500,000 Izmir sheet (Kalafatcioglu 1964)

FIGURE 2.2 - Geological & location map of Emet Borate District (with minor modifications from Özpeker 1969, Helvacı 1977 & Helvacı 1984)

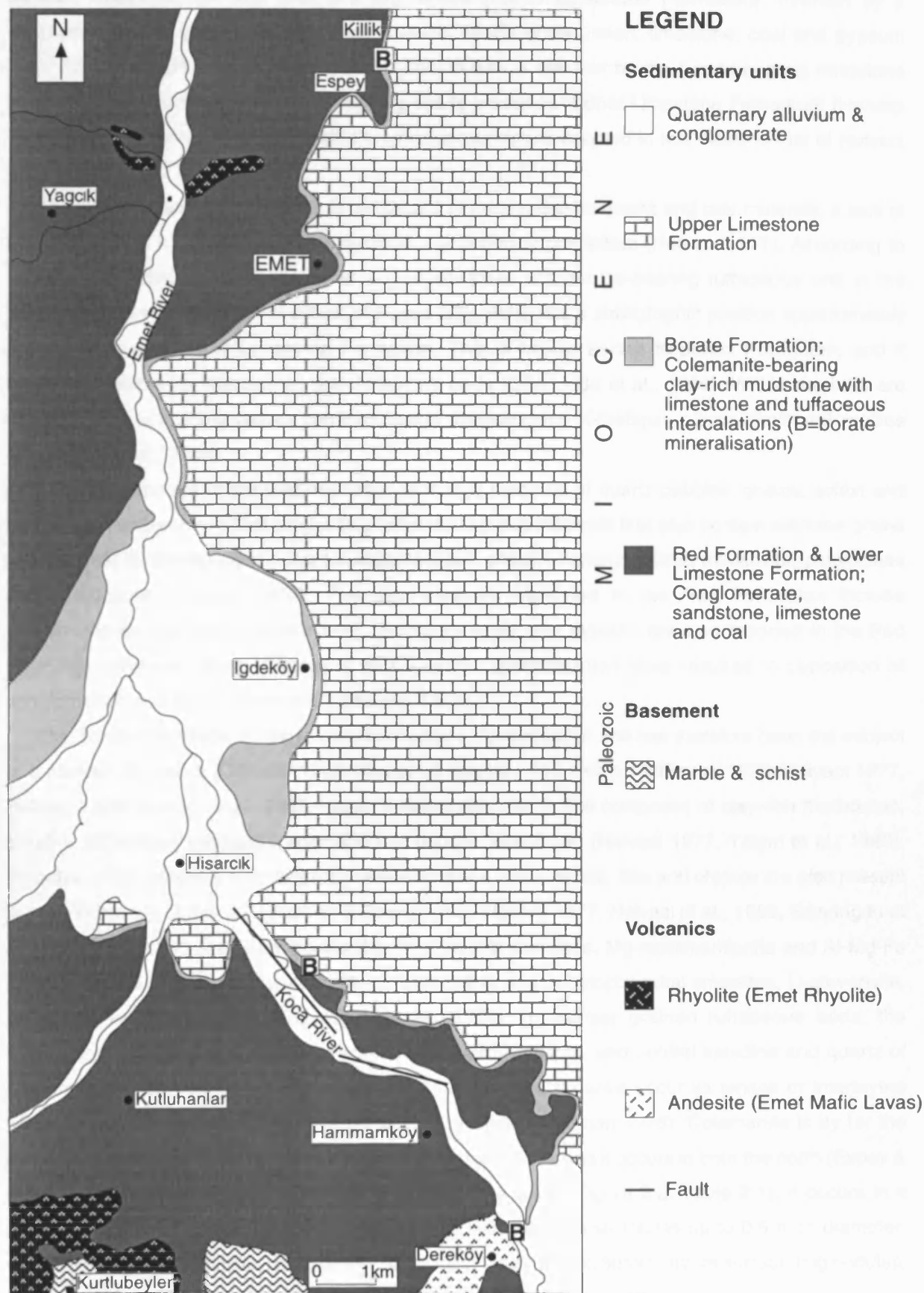


Figure 2.2

(Helvacı 1977, Helvacı & Firman 1976, Helvacı 1984). Above this, the sequence consists of a thin bedded limestone unit with marl and tuff lenses (Lower Limestone Formation), overlain by a conglomerate and sandstone unit which contains bands of clay, marl, limestone, coal and gypsum (Red Formation) (Helvacı & Firman 1976). This in turn is overlain by the borate-hosting mudstone horizon (Borate Formation) and by a capping cherty limestone (Upper Limestone Formation) (Helvacı 1977, Kistler & Helvacı 1994). The stratigraphic nomenclature adopted in this thesis is that of Helvacı (1977).

The Lower Limestone Formation is composed of calcite, detrital quartz and clay minerals; a lack of recorded fossils suggests that this limestone is a chemical precipitate (Helvacı 1977). According to Yalçın et al. (1985) and Gündoğdu et al. (1996), there is a zeolite-bearing tuffaceous unit in the southern part of the Emet Basin (south of Figure 2.2), which has a stratigraphic position approximately equivalent to the Lower Limestone Formation. This is known as the Köpenez Formation, and it comprises vitric tuffs intercalated with limestone beds (Gündoğdu et al., 1996). Within the tuffs are mineral zones containing various combinations of rhyolitic glass, K-feldspar, quartz, clays and zeolites (Gündoğdu et al., 1996).

The conglomerate of the Red Formation is mainly made up of quartz pebbles, gneiss, schist and granite rock fragments, which are loosely cemented by clay minerals that also contain siltstone grains (Helvacı 1977). Sandstones in this formation contain grains of quartz, biotite, muscovite, plagioclase and orthoclase (Helvacı 1977). The clay minerals identified in the Red Formation include montmorillonite and illite (Helvacı 1977). Bands of lignite and gypsum are also reported in the Red Formation (Helvacı 1984). Alternating high and low sedimentation rates resulted in deposition of conglomerate and lignite respectively (Helvacı 1977).

The Borate Formation is host to extensive borate mineralisation and has therefore been the subject of a number of studies (Özpeker 1969, Ataman & Baysal 1978, Helvacı & Firman 1976, Helvacı 1977, Helvacı 1984, Helvacı et al., 1993, Yalçın & Gündoğdu 1987). It is composed of clay-rich mudstones, borates, tuffaceous sediments, marl and thin bedded limestones (Helvacı 1977, Yalçın et al., 1985). Smectite is the dominant clay mineral, but illite-smectite mixed layers, illite and chlorite are also present in the mudstones of this unit (Ataman & Baysal 1978, Helvacı 1977, Helvacı et al., 1993, Gündoğdu et al., 1996). Smectites identified include the dioctahedral smectites, Mg-montmorillonite and Al-Mg-Fe montmorillonite (Ataman & Baysal 1978, Helvacı 1984), and the trioctahedral smectites, Li-stevensite, Al-stevensite and saponite (Gündoğdu et al., 1996). In coarser grained tuffaceous beds, the mineralogy consists of authigenic smectite, illite, and K-feldspar, and detrital sanidine and quartz of presumed volcanic derivation (Helvacı et al., 1993). Borate minerals occur as lenses or interlayers within these clay-rich and tuffaceous mudstones (Helvacı & Firman 1976). Colemanite is by far the most common borate mineral at Emet (Helvacı & Firman 1976), and it occurs in both the north (Espey & Killik deposits) and the south (Hisarcık deposits) of the basin (Figure 2.2, Table 2.1). It occurs in a number of different forms, including ovoid nodules with radiating structures up to 0.5 m in diameter, massive granular colemanite, disseminated crystals in a clay matrix, fibrous layers surrounding nodules, thin layers interbedded with clay and as vugh fillings (Helvacı & Firman 1976).

The Emet deposits also contain minor ulexite, hydroboracite and meyerhofferite (Kistler & Helvacı 1994) (Table 2.1). In addition Emet has the only recorded occurrences in Turkey of veatchite-A, teruggite and cahnite (Helvacı 1984) (Table 2.1). Therefore, in terms of borate mineralogy, Emet is dominated by calcium borates but Sr, Mg and Ca Na-bearing borates are also found. The extent of borate mineralisation in the northern deposits at Espey and Killik is estimated at 2.5 km by 1 km with a thickness of up to 100 m, while in the southern deposits at Hisarcık it covers an area of 2.5 km by 1 km with a thickness of up to 30 m (Scott pers. comm - 1993). Borate reserves for the Emet Basin are estimated at 110 Mt with a grade of 45 % B<sub>2</sub>O<sub>3</sub> (Helvacı & Firman 1976). Emet therefore represents one of the largest known colemanite deposits in the world.

Other minerals reported from the Borate Formation include calcite, celestite, gypsum, native sulphur, realgar, and orpiment (Helvacı & Firman 1976, Helvacı 1984, Helvacı et al., 1993, Kistler & Helvacı 1994, Yalçın & Gündoğdu 1987). Celestite is found in vugs of colemanite crystals and sulphur and realgar are found in borates and clays throughout the deposits. Much of the calcite is thought to be a feature of modern weathering, for instance of exposed colemanite outcrops (Helvacı & Firman 1976). Gypsum has been observed in fibrous form associated with the borates in the southern deposits (Helvacı & Firman 1976).

**Table 2.1 - Summary of authigenic minerals present in the Borate Formation (from Helvacı 1984)**

Minerals	Formula	Deposit
<b>Borates</b>		
Colemanite	Ca <sub>2</sub> B <sub>6</sub> O <sub>11</sub> ·5H <sub>2</sub> O	all deposits
Ulexite	NaCaB <sub>5</sub> O <sub>9</sub> ·8H <sub>2</sub> O	Killik, Espey
Meyerhofferite	Ca <sub>2</sub> B <sub>6</sub> O <sub>11</sub> ·7H <sub>2</sub> O	Killik, Espey
Veatchite-A	Sr <sub>2</sub> B <sub>11</sub> O <sub>16</sub> (OH) <sub>5</sub> ·H <sub>2</sub> O	Killik Espey
Tunellite	SrB <sub>6</sub> O <sub>9</sub> (OH) <sub>2</sub> ·3H <sub>2</sub> O	Killik Espey
Hydroboracite	CaMgB <sub>6</sub> O <sub>11</sub> ·6H <sub>2</sub> O	Killik, Espey, Hisarcık
Teruggite	Ca <sub>4</sub> MgAs <sub>2</sub> B <sub>12</sub> O <sub>22</sub> (OH) <sub>12</sub> ·14H <sub>2</sub> O	Hisarcık
Cahnite	Ca <sub>2</sub> B(OH) <sub>4</sub> AsO <sub>4</sub>	Killik, Espey, Hisarcık
<b>Other minerals</b>		
Celestite	SrSO <sub>4</sub>	Hisarcık, Espey
Realgar	AsS	Hisarcık, Espey
Gypsum	CaSO <sub>4</sub> ·2H <sub>2</sub> O	Hisarcık
Sulphur	S	Hisarcık, Espey
Calcite	CaCO <sub>3</sub>	all deposits
<b>Clay minerals</b>		
montmorillonite	(MgAl) <sub>2</sub> Si <sub>4</sub> O <sub>10</sub> (OH) <sub>2</sub> ·nH <sub>2</sub> O	all deposits
illite	(K,H <sub>3</sub> O)Al <sub>2</sub> (AlSi <sub>3</sub> O <sub>10</sub> )(OH) <sub>2</sub>	all deposits
chlorite	(SiAl) <sub>8</sub> (Mg,Fe) <sub>6</sub> O <sub>20</sub> (OH) <sub>4</sub>	all deposits

The oldest lava flows reported are rhyolites, dacites and trachytes, followed by trachyandesites and andesites and finally basaltic andesites (Helvacı 1977, Helvacı 1984). Yalçın et al. (1985) describe the oldest volcanics in the south of the Emet Basin as andesites and the youngest as olivine basalts. Stratigraphic columns by Yalçın et al. (1985), Helvacı et al. (1993) and Gündoğdu et al. (1996) imply that the older more evolved volcanism took place prior to deposition of the borate-host sediments, while the later mafic volcanism (basaltic andesite or olivine basalt) occurred after deposition of these sediments. Furthermore, the occurrence of tuffaceous rocks within the borate-host sediments suggests that volcanic activity may have taken place simultaneously with this phase of sedimentation

(Helvacı et al., 1993). Helvacı (1977) suggests that volcanic activity began during the deposition of the upper part of the Lower Limestone Formation on the basis that clay and volcanic ash was deposited at this time.

The Selendi and Usak-Güre Basins are located to the south of the Emet Basin (Figure 2.1) and they are both approximately N-S trending basins bounded by normal faults (Seyitoglu 1997). From palaeontological and palynological evidence, the sediments in these basins were dated from the Early Miocene to the Quaternary by Ercan et al. (1983, 1978). In common with the Emet Basin, the Selendi and Usak-Güre Basins contain fluvial and lacustrine sediments, which consist of a lower unit of largely conglomerate and sandstone (Hacıbekir Group), an intermediate unit of predominately mudstone with a capping limestone (Inay Group), and finally the youngest unit of sandstone and conglomerate (Seyitoglu 1997). The Inay Group is lithologically equivalent to the Borate and Upper Limestone Formations of the Emet Basin and the thick mudstone sequences of this unit are potential hosts for borate mineralisation. However, as yet, appreciable borate reserves have not been discovered in these basins. As at Emet Basin, volcanism occurred during sedimentation with the first phase of volcanic activity cross cutting the Hacıbekir Group and a second phase took place during deposition of the Inay Group (Seyitoglu 1997).

### 2.3 FIELD RELATIONS AND PETROLOGY OF IGNEOUS ROCKS FROM THE EMET AREA

In this section, field and petrological information from this study is discussed, in conjunction with the limited previous work on igneous rocks from the Emet area. This present study concentrates on intrusives, extrusives and volcanoclastic sediments from the Emet Basin, although the igneous activity of the Selendi and Usak-Güre Basins is also considered. An extensive sampling programme was carried out in these basins (sample localities in Appendices A & B), and all samples were collected by this author with the exception of a small number of volcanic rocks collected to the south of the Emet Basin by BHP Minerals consultants. All subsequent mineralogical and geochemical work on the samples was undertaken as part of this study.

#### 2.3.1 Erigöz Granite

The Erigöz Granite forms a significant topographical barrier to the west side of the Emet Basin reaching an elevation of over 2000 m, approximately 1000 m higher than the borate hosting sediments in the basin. It comprises at least one pluton which has intruded Palaeozoic sediments (Helvacı 1977). Aplite veins commonly cross cut the main Erigöz Granite, and they represent the late stage melts of the pluton. Granitic and aplite clasts can be found in conglomerate beds at a locality north of Emet in the Borate Formation (Section C), and at a locality to the south-west of Hisarcık (Section A) within the Red Formation. Helvacı (1977) also observed granite fragments in the Red Formation, and hence, granite emplacement clearly predated the deposition of the Red and Borate Formations. Bingöl et al. (1982) dated the Erigöz Granite using K-Ar dating on biotites and orthoclase, and obtained Early Miocene - Oligocene cooling ages of 20 - 20.4 Ma ( $\pm 0.7$ ) and 24.6 - 21.2 Ma ( $\pm 1.8$ ) respectively.

Evidence for hydrothermal activity associated with the pluton is present in the form of less than 20 m wide areas of hematite mineralisation within the granite. The granite body was sampled along its length in this study (Appendices A & B), and the main minerals present are plagioclase, K-feldspar, hornblende and biotite, while the accessory minerals comprise apatite, magnetite and chlorite (Table 2.2, Appendix D). Electron microprobe analyses (Appendix H) indicate that the plagioclases are albite ( $An_6$  - one analysis) and andesine ( $An_{31-45}$ ) whilst the K-feldspar is orthoclase ( $Or_{79-87}$ ). Plagioclases often show well developed multiple twinning and occasional zoning. Hornblende can be observed in basal section with two well developed cleavages. At least some biotite is secondary having replaced hornblende while chlorite has formed by secondary replacement of biotite. Apatite is included within biotite, and magnetite is closely associated spatially with biotite. The aplite is finer grained with a similar mineralogy to the granite except that hornblende is absent. Electron microprobe analyses reveal that the opaque phase in the granite is magnetite (approximately 33%  $Fe^{2+}$  and 67%  $Fe^{3+}$  - Appendix H). Hence, on petrological criteria, the Erigöz Granite can be described as an 'I-type' of Chappell and White (1974), from the presence of hornblende and magnetite, as well as apatite inclusions in biotite.

### 2.3.2 Volcanism in the Emet Basin

#### 2.3.2.1 Emet Rhyolites

There are a number of rhyolite exposures within the Emet Basin which occur near to the villages of Köprücek, Yagcık and Kurtlubeyler (Figures 2.1 & 2.2). The volcanics near Köprücek and Yagcık were briefly described in Helvacı's Ph.D. thesis (1977), and a limited description of the volcanics near Kurtlubeyler was given by Yalçın et al. (1985). Other rhyolite exposures discussed in this section are found along the southern margin of the basin around Saphane mountain, near the villages of Saphane, Taslık and Eski Gediz (Figure 2.1).

The rhyolite sheets of the Emet area form a number of low hills and often they outcrop in a linear fashion, such as near Yagcık and Kurtlubeyler where they form elongate jagged ridges suggesting fractural control. Although no caldera has been recognised in the Emet area, it is possible that the rhyolites are related to a caldera structure. Rapid erosion has produced a rugged topography as typified by the rhyolites near Kurtlubeyler shown in Plate 2.1a. Other common features include bedded breccia such as in the rhyolites from near Yagcık, and platy jointing found in the rhyolites from Köprücek and Eski Gediz.

The rhyolites of the Emet Basin were extensively sampled, with at least two samples collected from each rhyolite sheet. The rhyolites are porphyritic with phenocrysts of plagioclase, K-feldspar, quartz and biotite in a pale grey to purple quartz-feldspathic matrix (Table 2.2, Appendix D). The rhyolites at Köprücek and Eski Gediz contain fresh elongate plagioclase showing multiple twinning and zoning as well as K-feldspar with Carlsbad twinning. However, the feldspar from rhyolites near Kurtlubeyler and around Yagcık are often 'speckled' and altered to clay minerals (more detail in Chapter 3). Evidence of more intense alteration in the rhyolite is provided by a large area of alunite in the southern margin of Emet Basin near to the town of Saphane, and by a small zone of silicification in rhyolite close to the village of Yagcık in the north of the basin (Figures 2.1 & 2.2).





Plate 2.1a - Emet Rhyolite sheet near Kurtlubeyler, southern Emet Basin



Plate 2.1b - Emet mafic lavas overlying a mudstone sequence to the west of Dereköy

Electron microprobe analyses of unaltered feldspars from rhyolites of the Emet area show that the plagioclases comprise andesine and oligoclase (An<sub>27-50</sub>), while the K-feldspars comprise K-sanidine (Or<sub>73-75</sub>) (Appendix H). These feldspar compositions are similar to the nearby Erigöz acid intrusive. Apatite is present as an accessory phase in the Eski Gediz rhyolites, occurring as inclusions within the biotite. The matrix is generally fine grained and in the case of Köprücek and Eski Gediz, contains well developed spherulites. Such spherulites are common in acid volcanic glass. They normally comprise radiating aggregates of K-feldspar with or without quartz (Cas & Wright 1993) and result from high temperature devitrification of unstable glass (Lofgren 1970, McPhie et al., 1993).

**Table 2.2: Summary petrology of intrusive and extrusive rocks from Emet Basin**

Rock type and locality	Mineralogy (from thin sections, XRD, microprobe)
Erigöz Granite (W margin of Emet Basin)	Phenocrysts of plagioclase (rare albite, abundant oligoclase & andesine), K-feldspar (orthoclase), hornblende, biotite (with included apatite and chlorite alteration), quartz, minor magnetite.
Emet Rhyolite (within Emet Basin - Köprücek, Yagcık, Kurtlubeyler, southern margin of basin - Eski Gediz, Saphane, Taslık)	Phenocrysts of plagioclase (andesine & oligoclase), K-feldspar (K-sanidine), biotite (with included apatite), quartz. Feldspars often altered to clay minerals. Matrix is glassy and sometimes contains spherulites.
Emet mafic lavas (Dereköy)	Phenocrysts of augite and biotite in a matrix of fine needles of K-feldspar.

One of the objectives of this study was to determine the spatial and temporal position of this rhyolitic volcanism relative to deposition of the borate-host sediments. It is clear from the map in Figure 2.2 that the rhyolite exposures are closely spatially associated with borate mineralisation, but any genetic relationship between them is dependant on the timing of volcanic activity relative to sedimentation. Hence, an attempt was made to determine the temporal position of acid volcanism relative to mineralisation by evaluating the volcanic stratigraphy of the Emet Basin and the surrounding area, from field and petrological evidence. As pointed out above, the stratigraphic section of Kistler & Helvacı (1994) inferred that the acid volcanism at Emet predated deposition of the borate-host sediments, and the fieldwork in this study sought to evaluate this.

The rhyolites at Köprücek (Figure 2.1) are overlapped on their western side by cherty limestone beds of the Upper Limestone Formation, proving the acid volcanics to be at least partly older than these sediments. Rhyolites north-west of Eski Gediz (Figure 2.1) again appear to be overlapped by cherty limestone. To the west of Kurtlubeyler (Figure 2.2), just east of Karapinar River, a direct contact between the rhyolite sheet and beds of the Lower Limestone Formation is observed. The dip of the limestone increases towards the rhyolite sheet, but it is unclear whether the rhyolite intruded the limestone or if it was a lava deposited on the limestone. Both situations indicate that this rhyolite sheet is younger than at least part of the Lower Limestone Formation. The rhyolite sheet to the east of Yagcık and just east of Emet River (Figure 2.2), in places overlies limestone beds, and hence appears to post-date at least part of the Lower Limestone Formation (Helvacı 1977).

In summary, on the basis of field evidence alone, the acid volcanism of the Emet Basin appears to have occurred between the deposition of the Lower Limestone and the Upper Limestone Formations. The observed contacts between rhyolites and sediments in Emet Basin are such that a more accurate

assessment of the timing of this phase of volcanism relative to sedimentation is not possible. However, the volcanic stratigraphy of the Emet Basin will be further constrained later in this chapter when the mineralogy in the volcanoclastic sediments is described.

### 2.3.2.2 Emet Mafic Lavas

Basaltic andesite and andesite lavas outcrop around the village of Dereköy in the southern part of the Emet Basin (Figures 2.1 & 2.2), and they have briefly been described by Helvacı (1977) and Yalçın et al. (1985). In contrast to the rhyolites, these lavas form relatively flat lying flows and are often vesicular, sometimes with amygdaloids of calcite. Mineralogically, these lavas contain phenocrysts of augite and biotite in a matrix of fine feldspar needles (Table 2.2). Electron microprobe analyses of the feldspar laths in the andesite reveals that they are K-feldspars ( $Or_{41-70}$ ) (Appendix H). Helvacı (1977) described olivines in thin sections of these lavas but no olivine was found in this study using an electron microprobe.

Field observations indicate that the mafic volcanism occurred after the deposition of the borate-host mudstones, which is in accordance with Yalçın et al. (1985), Helvacı (1984) and Gündoğdu et al. (1996). West of Dereköy, this lava is clearly overlying a mudstone sequence (Plate 2.1b) and at a location between Hammamköy and Dereköy, just to the west of the Koca River, the Dereköy lavas outcrop above colemanite-hosting mudstone (Section G, Appendix A). Hence, it appears that these lavas were erupted after deposition of the Borate Formation mudstones, and therefore possibly after borate mineralisation.

### 2.3.2.3 Volcanoclastic sediments in the Emet Basin

The volcanic input into the sediments of the Emet Basin was examined in order to establish the volcanic stratigraphy, and hence the timing of volcanism relative to deposition of the borate-host sediments. Two sections were logged in the Red Formation (Sections A & B) and a further five in the Borate Formation (Sections C - G) (locations in Appendices A & B). A total of twenty three samples were collected from these units for detailed mineralogical and geochemical analysis; four from the Red Formation (VSE 1 - 4) and nineteen from the Borate Formation (VSE 5 - 23). In addition, samples were collected over 1.8 m intervals in the Borate Formation (67 samples) to monitor geochemical variations (Chapter 4).

Section A (Figure 2.3) through the Red Formation, is located south-west of Hisarcık and comprises conglomerate interbedded with red siltstone. The conglomerates contain abundant granite boulders up to 30 cm in diameter. Aplite clasts derived from the nearby Erigöz Granite also occur (Figure 2.3). Siltstones (Plate 2.2a) interbedded with the conglomerates contain abundant biotite in a crumbly red to grey matrix. The siltstone is poorly sorted, with angular crystals, particularly quartz (Plate 2.2b). Possible remnant pumices (Plate 2.3a & 2.3b) and mechanically damaged detrital biotite, which has been 'bent', also occur. Siltstone elsewhere in the Red Formation has a similar mineralogy and texture to that of Section A (Table 2.3), and is also poorly sorted with angular clasts, particularly quartz. Some of the siltstones contain rare fragments of spherulites, similar to those in the rhyolites. Section B, north

## Geology of the Emet and Kirka areas

**FIGURE 2.3 - Sections through Red and Borate Formations of the Emet Basin**

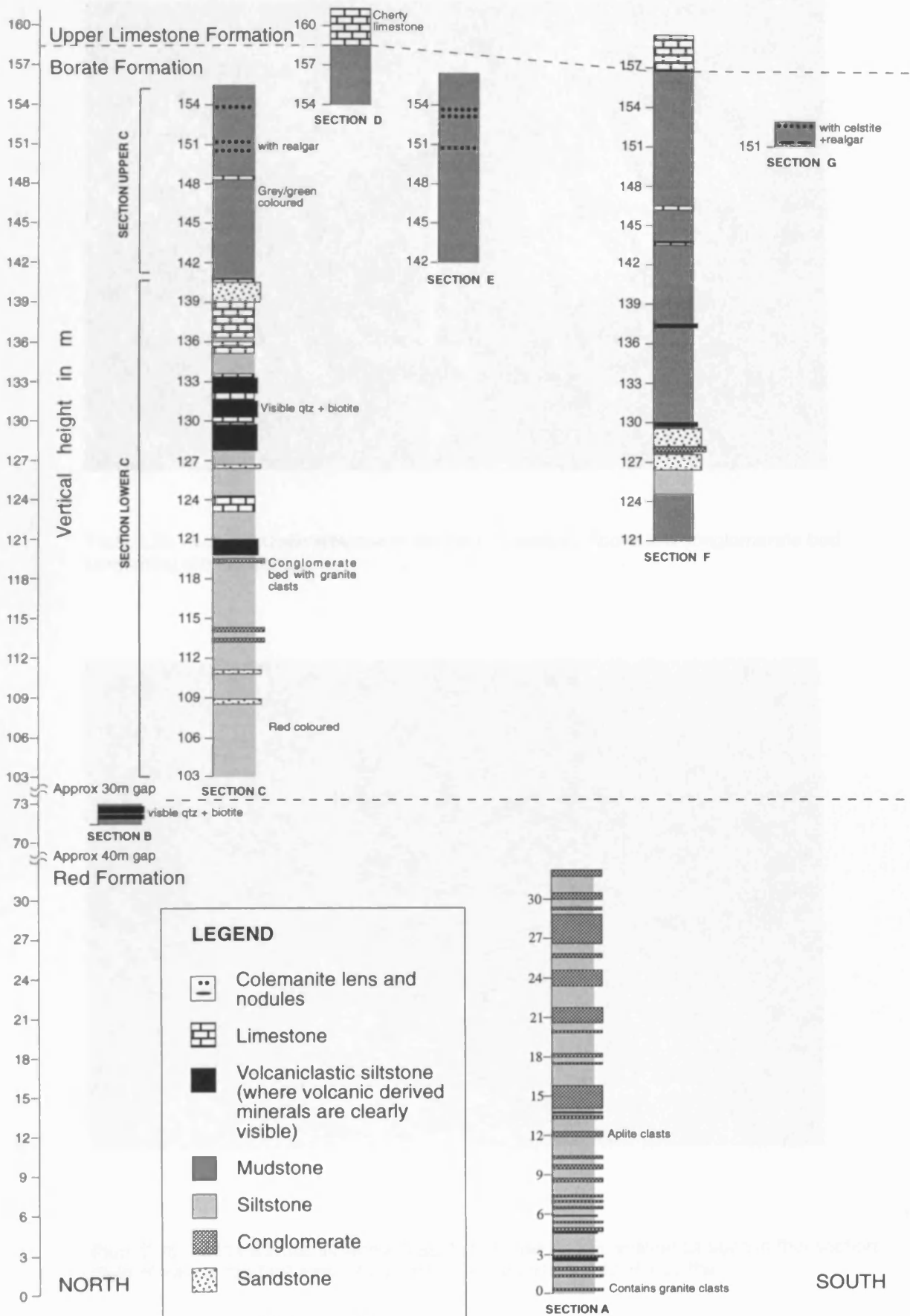


**Figure 2.3**





Plate 2.2a - volcaniclastic siltstone in the Red Formation. Above is a conglomerate bed containing granite clasts.

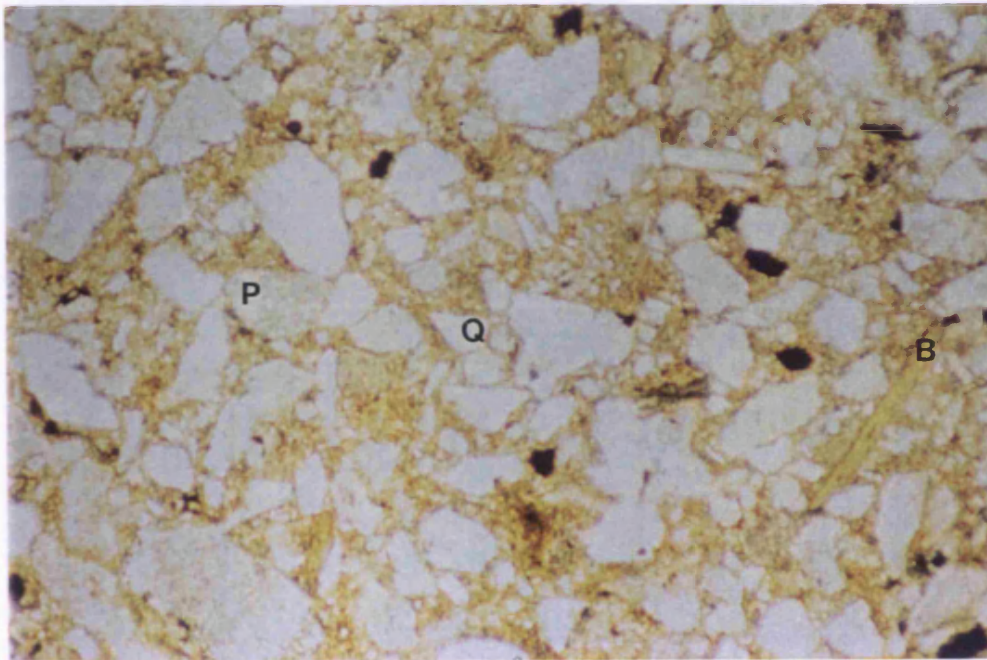


Plate 2.2b - volcaniclastic siltstone (VSE 1) from the Red Formation as seen in thin section (field of view 3 mm by 2 mm). P = pumice, Q = angular quartz, B = biotite



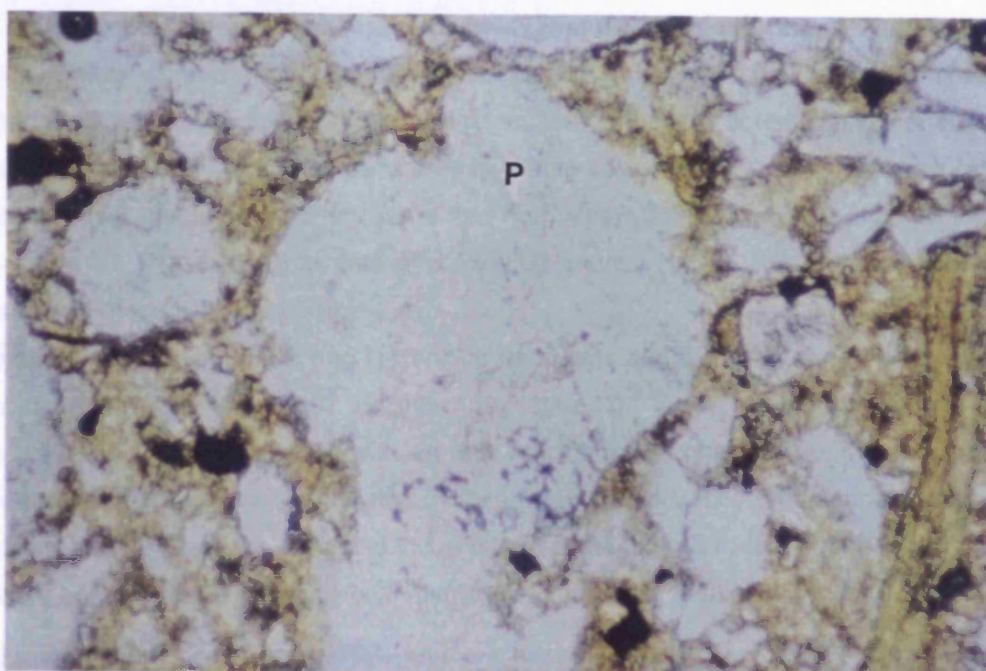


Plate 2.3a - possible remnant pumice (P) in volcaniclastic siltstone (VSE 1) from the Red Formation (Plain polarised light, field of view 1 mm by 0.67 mm)

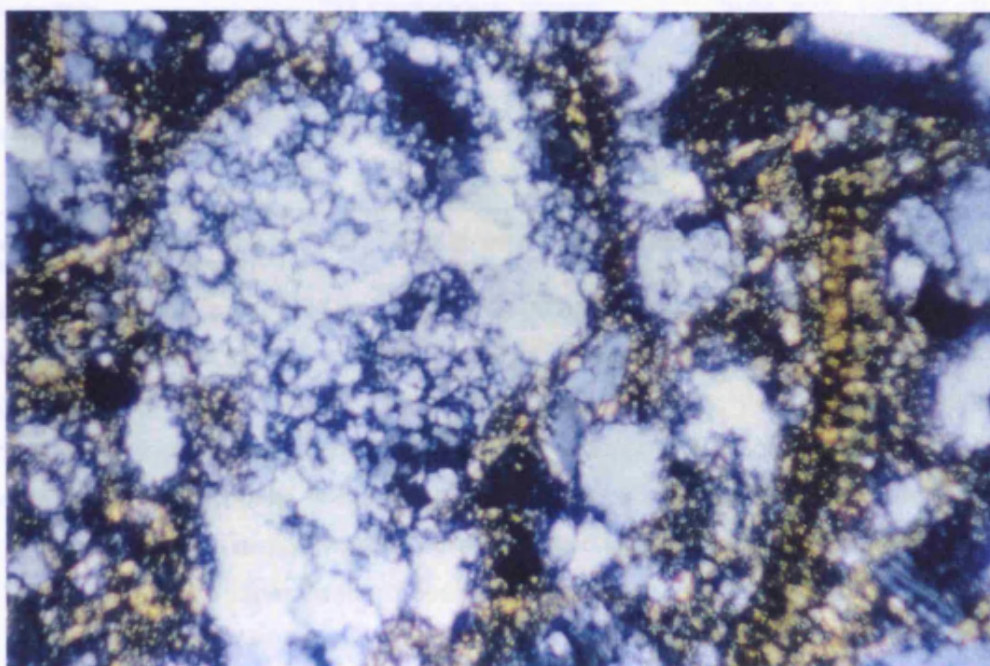


Plate 2.3b - the same view as above, but in cross polarised light

of the Espey/Killik mining operation in the northern part of the Emet Basin consists of volcanoclastic siltstone interbedded with finer grained mudstone (Figure 2.3 & Plate 2.4a). These siltstones lie several 10s of metres below the borate-hosting mudstones, either in the base of the Borate Formation or near the top of the Red Formation. They contain angular and poorly sorted crystals of quartz, biotite, K-feldspar and plagioclase, as well as pumice lapilli (Table 2.3, Plate 2.4b). XRD analyses (Appendices G) indicate a significant clay component in the Red Formation siltstones, comprising smectite, illite and kaolinite (Table 2.3, Appendix D) as also described by Helvacı (1977). Calcite and dolomite are also found in some of these siltstones (Table 2.3).

The presence of pumice lapilli and spherulitic fragments suggests that the rock is at least partly volcanoclastic (McPhie et al., 1993). Furthermore, abundant quartz, K-feldspar, biotite and some plagioclase (Table 2.3) is consistent with an acid volcanic  $\pm$  granitic source. The poor sorting and angular nature of the crystals also indicates a limited transport distance, and hence a local source for these sediments. The presence of apatite inclusions in some biotites further suggests an acid igneous source, since both Erigöz Granite and local rhyolite contain similar biotites.

**Table 2.3 - Summary mineralogy of volcanoclastic sediments in Red Formation**

<b>Red Formation</b>		
<b>Location</b>	<b>Sample</b>	<b>Mineralogy (from thin sections, XRD, microprobe)</b>
Section A - SW of Hisarcık	VSE 1 (volcanoclastic siltstone)	Biotite (with apatite inclusions), quartz, plagioclase, K-feldspar, illite, smectite, kaolinite, remnant pumice
NE of Hammamköy	VSE 2 (volcanoclastic siltstone)	Biotite, quartz, K-feldspar, calcite, illite/muscovite
NE of Yagcık	VSE 3 (volcanoclastic siltstone)	Biotite, quartz, K-feldspar, dolomite, illite/muscovite, pumice
Section B - N of Espey/ Killik	VSE 4 (volcanoclastic siltstone)	Glass, quartz, K-feldspar, plagioclase, pumice, illite/muscovite, smectite, kaolinite

**Previous work - Helvacı 1977** - sandstone in this formation contains quartz, plagioclase, K-feldspar, biotite and muscovite. Clay fractions identified are montmorillonite and illite

Borate mineralisation is found at three of the logged sections in the Borate Formation (Sections C, E & G) while the other two are barren (Sections D & F) (Figure 2.3 & Table 2.4). Therefore, as well as providing information on the igneous component in these sediments, studying their mineralogy might establish differences between barren and mineralised sediments. Section C, on the northern edge of the Espey/Killik borate deposits encompasses a sequence of red siltstones (Plate 2.5a) (Section Lower C) that grade up into distinctive grey - green mudstones which host the borate minerals (Section Upper C) (Figure 2.3). The mineralisation consists of colemanite nodules partly altered to calcite (Plate 2.5b) in mudstones which also contain abundant orange realgar. Conglomerates with granitic clasts and limestone beds are interbedded with the siltstones in the lower part of the sequence. In this thesis, the term volcanoclastic is used for siltstones that contain visible volcanic derived minerals such as biotite and quartz. Section D, near to Igdeköy consists of mudstones without borate mineralisation, capped by cherty limestone (Figure 2.3). Further south, Section E located to the north of Hisarcık, is again dominantly mudstone but here there are thin bands (0.25 m thick) of colemanite nodules partially





Plate 2.4a - interbedded volcaniclastic siltstone and mudstone of the Red Formation (Section B)

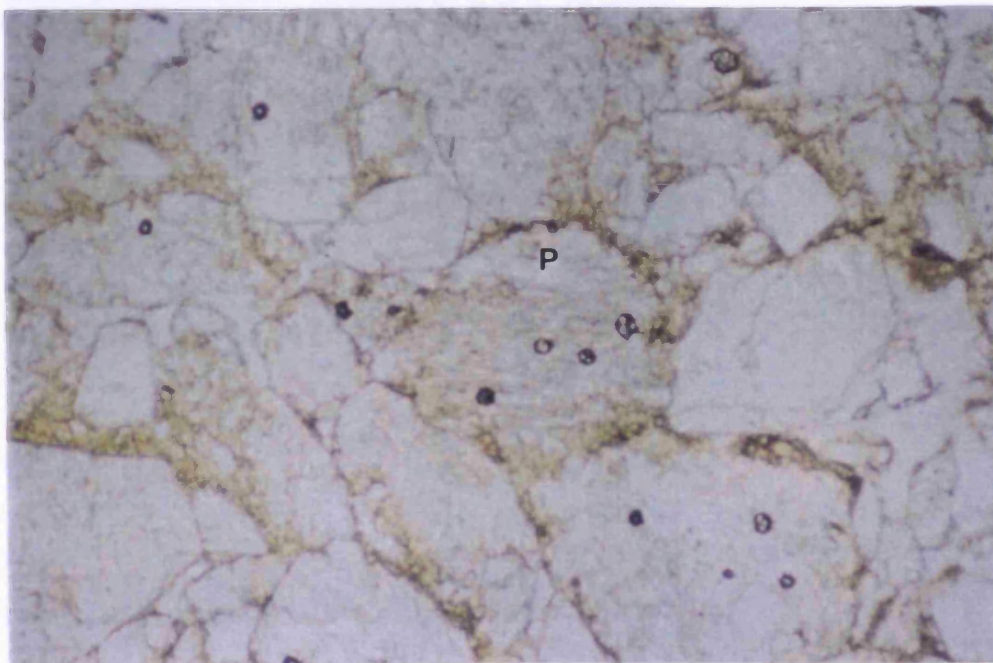


Plate 2.4b - pumice in volcaniclastic siltstone (VSE 4) from Section B. P = pumice





Plate 2.5a - red siltstones grade up into grey mudstone (Section C)



Plate 2.5b - colemanite nodules in grey mudstone (Section Upper C)

altered to calcite (Figure 2.3). Section F, south of the large Hisarcık open pit, comprises interbedded grey - green mudstone and siltstone with some limestone beds, but no observed borate mineralisation (Figure 2.3). Section G, north-east of Dereköy in the south of the Emet Basin, comprises grey - green mudstones with lenses and nodules of colemanite with associated celestite and realgar (Figure 2.3). Stratigraphically above the mudstone at this locality are the Emet mafic lavas.

The siltstones of the Borate Formation have a similar mineralogy to those of the Red Formation, with quartz, plagioclase, K-feldspar, biotite, illite, smectite and rare calcite (Table 2.4, Appendix D). Furthermore, the siltstones of this unit are poorly sorted and many of the crystals have an angular shape. As in the Red Formation, these textural features, and the presence of quartz and plagioclase, are consistent with a local acid igneous source. The presence of granitic clasts in some of the siltstones indicates that at least some of the material originated from the Erigöz Granite. It is likely that the finer grained material in the siltstones originated from rhyolitic ash falls, although pumice from such eruptions was not observed. These observations are consistent with work by Helvacı et al (1993) which describes the presence of quartz, K-feldspar, illite, smectite and high sanidine in tuffaceous sediments from the borate bearing sediments of the Emet Basin. They suggest that the K-feldspar, illite and smectite are authigenic while the sanidine and quartz are detrital.

**Table 2.4 - Summary mineralogy for volcanoclastic sediments of the Borate Formation**

Location	Sample	Mineralogy (from thin sections, XRD, electron microprobe)
<b>Section Lower C</b> - just N of Espey/Killik open pit,	VSE 5, 6, 8, 9 (volcanoclastic siltstone)	Quartz, K-feldspar, plagioclase, biotite, calcite, illite, smectite
	VSE 9, 10 (limestone)	Calcite
	VSE 7 (mudstone)	Quartz, calcite, illite, smectite
<b>Section Upper C</b> - just N of Espey/Killik open pit,	VSE 11, 12, 13, 14, 15, 16 (mudstone)	K-feldspar, calcite, dolomite, illite, smectite, colemanite, realgar
<b>Section D</b> - east of Igdeköy	VSE 17 (mudstone)	Calcite, illite, quartz
<b>Section E</b> - just N of Hisarcık	VSE 18, 19, 20 (mudstone)	Quartz, K-feldspar, calcite, gypsum, illite, smectite
<b>Section F</b> - NE of Hammamköy	VSE 21 (mudstone)	Quartz, calcite, illite
	VSE 22 (volcanoclastic siltstone)	Quartz, plagioclase, K-feldspar, calcite, illite, chromite
<b>Section G</b> - NE of Dereköy (colemanite, celestite and realgar observed)	VSE 23 (mudstone)	Quartz, calcite, K-feldspar, illite, smectite

**Previous work:** Helvacı 1977 - found smectite, illite, calcite and occasional biotite, quartz and muscovite in the borate hosting mudstones.

XRD analyses of the finer grained mudstones from the sections through the Borate Formation indicate the presence of illite, smectite, K-feldspar, dolomite, calcite and rare quartz (Table 2.4, Appendix G). Helvacı (1977) also described illite, smectite and quartz as well as biotite and calcite in the mudstones of this formation. This mineralogy is broadly similar to the coarser volcanoclastic siltstones and it is likely that the mudstones are also rich in volcanic-derived material. The mineralogy of these

mudstones is presented in more detail in Chapter 4 of this thesis.

### *2.3.2.4 Emet Basin volcanic stratigraphy (from field and mineralogical evidence)*

Field evidence from the Emet Basin suggests that acid volcanism, represented by the Emet Rhyolites, occurred between the deposition of the Lower and Upper Limestone Formations, while the Emet mafic lavas post-dated deposition of the borate-host sediments. The textural and mineralogical features of the volcanoclastic sediments from the Red and Borate Formations indicate a significant acid igneous input. The acid igneous content probably results from both a rhyolitic input in the form of volcanic ash erupted into the basin, and a granitic input from the weathering and subsequent transport of material from the Erigöz pluton. Clearly this implies that the rhyolitic phase of volcanism was active during deposition of both the Red and Borate Formations.

### **2.3.3 Volcanism South and West of Emet Basin**

Volcanic exposures in the Usak-Güre, Selendi and Simav Basins were sampled so as to provide a complete picture of the volcanic evolution of the Emet area. A secondary purpose was to compare the igneous rocks of the Usak-Güre and Selendi Basins with those of the Emet Basin, in order to evaluate their potential to also host borate mineralisation.

#### *2.3.3.1 Rhyolites*

North of the town of Selendi there is considerable exposure of Miocene volcanics (Figure 2.1) which are largely rhyolitic. The rhyolite sheet sampled in this study (Appendices A & B) has a similar mineralogy to the Emet Rhyolites, with phenocrysts of biotite, plagioclase, K-feldspar and quartz in a fine grained glassy matrix (Table 2.5). However, in contrast to the Emet rocks, these rhyolites have phenocrysts of hornblende. According to Seyitoglu (1997), the Selendi rhyolites cut the Hacibekir Group, making them at least younger than this unit. Above the Hacibekir Group, the Inay Group contains thick sequences of mudstones and is the equivalent of the Borate Formation in the Emet Basin, although borate minerals have not been recorded in this unit. Hence, as in the Emet Basin, rhyolitic volcanism was active in the Selendi Basin prior to and/or during deposition of a unit composed largely of mudstone.

#### *2.3.3.2 Dacites*

The dacites in this area are found to the south of the Emet Basin in the Usak-Güre Basin (Appendices A & B). The mineralogy of these samples comprises phenocrysts of plagioclase and biotite in a fine grained feldspathic matrix (Table 2.5). These volcanics cut the Inay Group (Seyitoglu 1997) and hence they are younger than at least some of these sediments.

#### *2.3.3.3 Mafic Lavas*

Basaltic andesites and andesites are abundant in this area and they form lava flows. Stratigraphically, these mafic lavas appear to occur near to the top of the sedimentary successions.

The Nasa andesite lava flows lie high up in the sedimentary sequence on the western side of the Erigöz Granite in the Simav Basin. South-east of the Emet Basin and north-east of Eski Gediz (Figure 2.1), the basaltic andesite lava flows underlie beds of cherty limestone, part of the Inay Group of the Usak-Güre Basin. Due to poor exposure of sediments, the stratigraphic positions of the andesites from near Saphane further east, (samples SE 26, 27 - Appendices A & B) were not discernible in the field. The remaining mafic samples were collected in the Usak-Güre Basin and are placed within the Inay Group (Seyitoglu 1997). A common feature of these lavas is columnar jointing which is clearly seen in andesites near Saphane in the north of the Selendi Basin (Figure 2.1). Such jointing is produced as a result of increases in viscosity and contraction on cooling of magma (McPhie et al., 1993). Phenocryst phases in these lavas include biotite and clinopyroxene and in the case of the andesites from Saphane, plagioclase and hornblende. The matrix invariably contains small feldspar laths (Table 2.5).

**Table 2.5: Summary petrology of volcanic rocks & volcanoclastic sediments from Selendi and Usak-Güre Basins**

Rock type and locality	Mineralogy (from thin sections, XRD, microprobe)
Rhyolite (N of Selendi)	Phenocrysts of plagioclase, K-feldspar, biotite, quartz and hornblende in a glassy matrix.
Dacites (N of Selendi & in Usak-Güre Basin)	Phenocrysts of plagioclase and biotite in a fine grained matrix.
Andesite (Saphane)	Phenocrysts of plagioclase, biotite, hornblende and clinopyroxene in a matrix of feldspar needles and glass.
Andesite & basaltic andesite (Usak-Güre Basin)	Phenocrysts of biotite and clinopyroxene with feldspar needles in the matrix.
Lacustrine sediments in Inay Group (VSS 1, Section H - west of Selendi)	Quartz, plagioclase, ankerite, smectite and illite.
Lacustrine sediments in Inay Group (VSS 2, Section I - N of Selendi)	K-feldspar, ankerite and illite.
Lacustrine sediments in Inay Group (VSUG 1, Section J - centre of Usak-Güre Basin)	illite and calcite.
Lacustrine sediments in Inay Group (VSUG 2, Section K - centre of Usak-Güre Basin)	K-feldspar, ankerite, illite, smectite.

## 2.3.3.4 Volcanoclastic sediments from south of Emet Basin

Four sections were sampled to the south of the Emet Basin, two in the Selendi Basin and two in the Usak-Güre Basin (Appendices A & B). All sections were logged in thick mudstone units which are overlain by cherty limestone, and which are part of the Inay Group (Seyitoglu 1997). Section H is located to the west of Selendi (Appendices A & B) and consists of interbedded mudstones and siltstones with occasional limestone beds (Figure 2.4). Quartz in a conglomerate bed could be of volcanic or metamorphic derivation. Minerals identified by XRD in mudstone from this section include quartz, plagioclase, ankerite, smectite and illite (Table 2.5, Appendix G). Section I is located to the north of Selendi and once again comprises mudstones, micaceous siltstones and occasional limestone beds (Figure 2.4). The mica in the siltstone may have been derived from volcanic or metamorphic rocks. Identified mineral phases include illite, ankerite and K-feldspar (Table 2.5, Appendix D).

The sections sampled in the mudstones of the Inay Group in the Usak-Güre Basin are located near the centre of the basin (Figure 2.1). Both Sections J and K comprise mudstone with thin beds of

FIGURE 2.4 - Sections through the Inay Group of the Selendi Basin

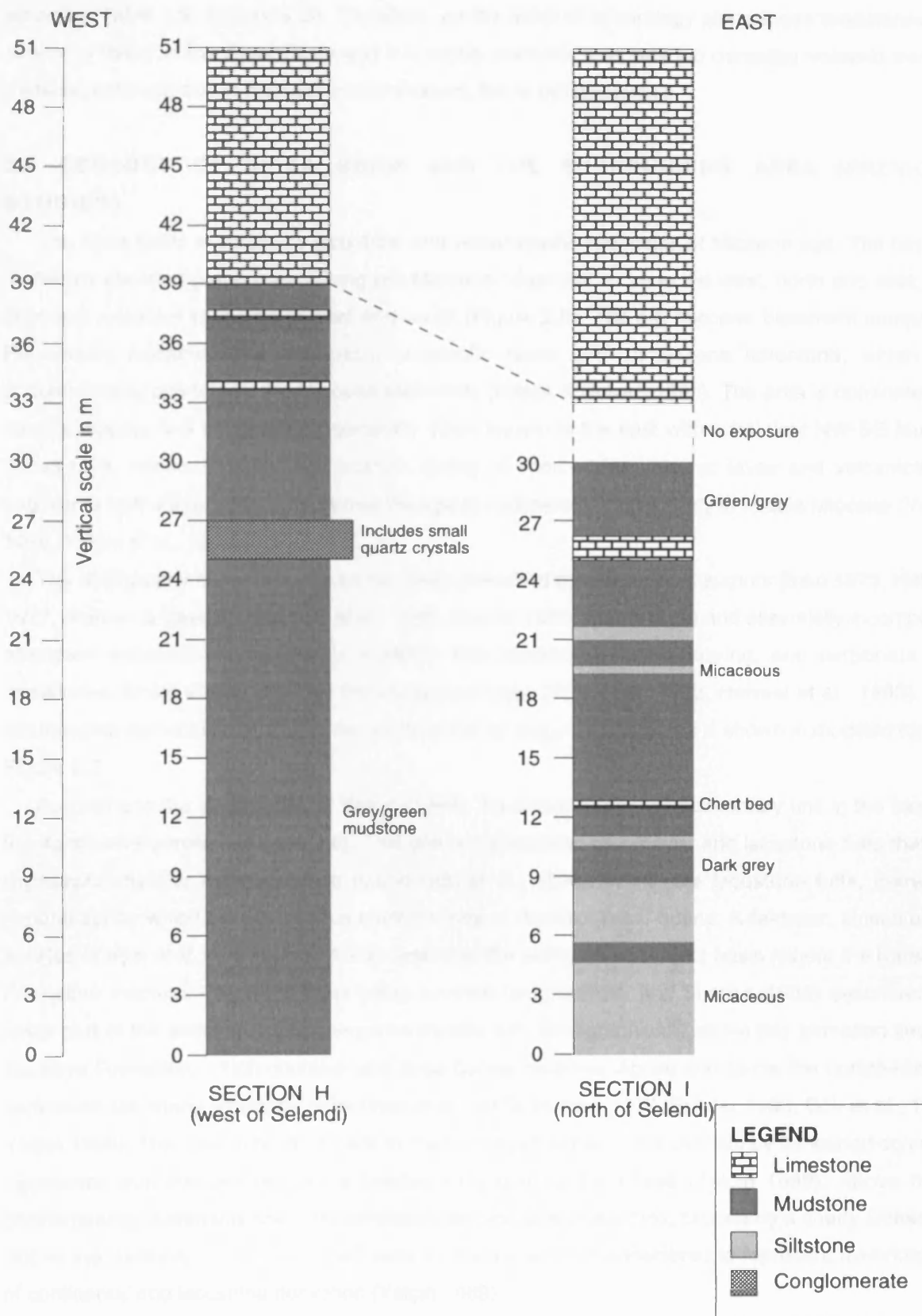


Figure 2.4

limestone (Figure 2.5), and there appears to be an absence of micaceous siltstones. Section J mudstone contains smectite, illite and calcite, while Section K contains K-feldspar, ankerite, illite and smectite (Table 2.5, Appendix D). Therefore, on the basis of mineralogy alone these mudstones are similar to those of the Emet Basin and it is highly plausible that they too comprise volcanic derived material, although due to their fine grained nature, this is not discernible.

### 2.4 GEOLOGY OF KIRKA BASIN AND THE SURROUNDING AREA (PREVIOUS STUDIES)

The Kirka Basin is infilled by lacustrine and volcanoclastic sediments of Miocene age. The basin is limited by elevated ground comprising pre-Miocene basement rocks to the west, north and east, and Miocene volcanics to the north-west and south (Figure 2.6). The pre-Miocene basement comprises Palaeozoic metamorphics, Mesozoic ultramafic rocks and an Eocene limestone, which are unconformably overlain by the Miocene sediments (Kistler & Helvacı 1994). The area is dominated by steeply dipping N-S normal faults generally down thrown to the east with subsidiary NW-SE faulting (Scott pers. comm - 1993). K-Ar isotopic dating of interbedded volcanic lavas and volcanoclastic sediments from Kirka basin indicate that the age of sedimentation was Early to Middle Miocene (Yalçın 1989, Yalçın et al., 1990).

The stratigraphy of the Kirka Basin has been described by a number of authors (Inan 1973, Helvacı 1977, Ataman & Baysal 1978, Gök et al., 1980, Sunder 1980, Yalçın 1989) and essentially it comprises abundant volcanoclastic sediments together with lacustrine, borate-bearing, and carbonate rich mudstones, which are encased by thick limestone units (Inan et al., 1973, Helvacı et al., 1993). The stratigraphic nomenclature used in this study is that of Yalçın (1989) which is shown in modified form in Figure 2.7.

According to the stratigraphy of Yalçın (1989), the oldest Neogene sedimentary unit in the basin is the Karaören Formation (Figure 2.6). This unit is represented by subaerial and lacustrine tuffs that are rhyodacitic-rhyolitic in composition (Gündoğdu et al., 1996). Within the lacustrine tuffs, there are mineral zones which include various combinations of rhyolitic glass, quartz, K-feldspar, smectite and zeolites (Yalçın et al., 1991). Inan (1972) described the eastern part of Kirka basin (where the Karaören Formation outcrops - Figure 2.7) as being covered by ignimbrite, and Sunder (1980) describes this lower part of the sedimentary sequence as rhyolite tuff. Stratigraphically above this formation lies the Sarıkaya Formation, which contains very large borate reserves. Above and below the borate-hosting sediments are cherty limestone units (Inan et al., 1973, Helvacı 1977, Sunder 1980, Gök et al., 1980, Yalçın 1989). The lower limestone beds in the Sarıkaya Formation are overlain by laminated dolomitic claystones with interbedded biotite bearing tuffs and borate lenses (Yalçın 1989). Above these borate-bearing sediments are more laminated claystones and dolomite, capped by a cherty limestone. Above the Sarıkaya Formation is the Fetiye Formation which is considered to represent reworked tuff of continental and lacustrine derivation (Yalçın 1989).

The borate mineralisation of the Sarıkaya Formation has been the subject of a number of studies (Inan 1972, Inan et al., 1973, Ataman & Baysal 1978, Gök et al., 1980, Sunder 1980, Yalçın 1989,



FIGURE 2.5 - Sections through the Inay Group of the Usak-Güre Basin

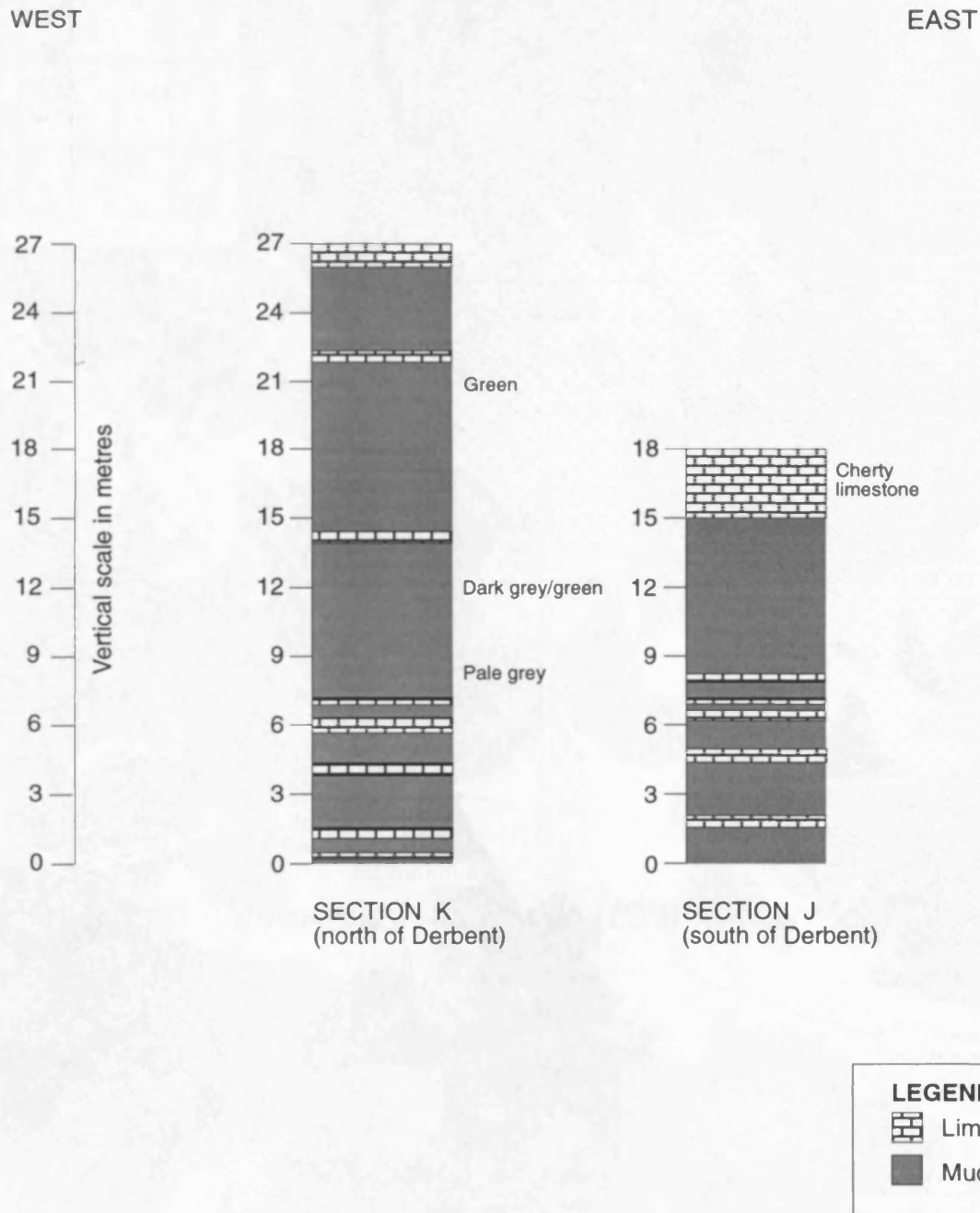
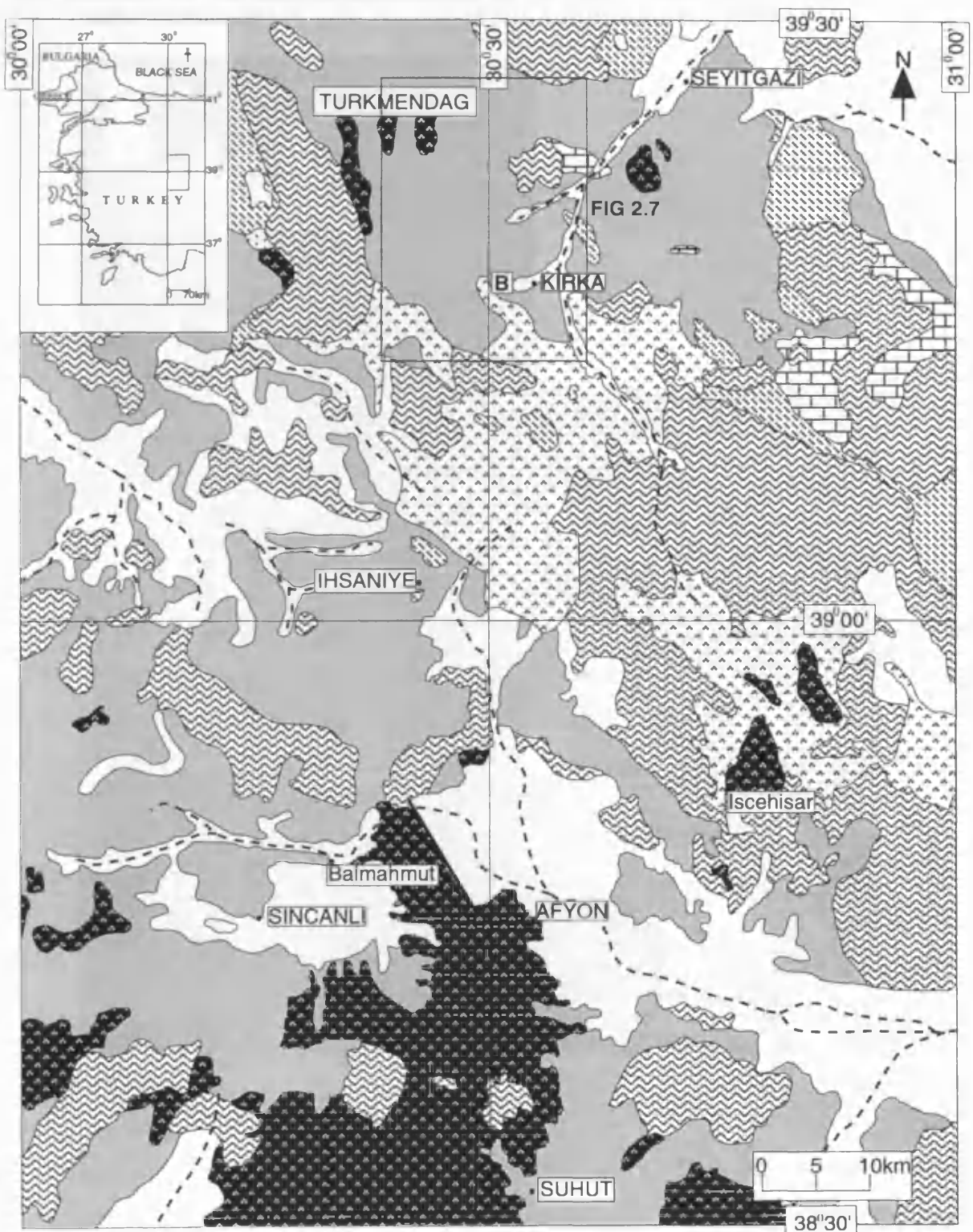


FIGURE 2.6 - The Geology of the Kirka area



LEGEND

- Quaternary alluvium
- Neogene sediments
- Miocene volcanic lavas
- Ignimbrite

- Pre-Miocene
- Eocene limestone
- Paleozoic & Permian basement
- Ultramafics

B = borate mineralisation

= Fault

= River

Based on MTA geological map 1:500,000 Ankara sheet (Erentöz 1963)

Figure 2.6



FIGURE 2.7 - Geological & location map of Kirka Borate District (with minor modifications from Yalçın1989 and Yalçın & Baysal 1991)

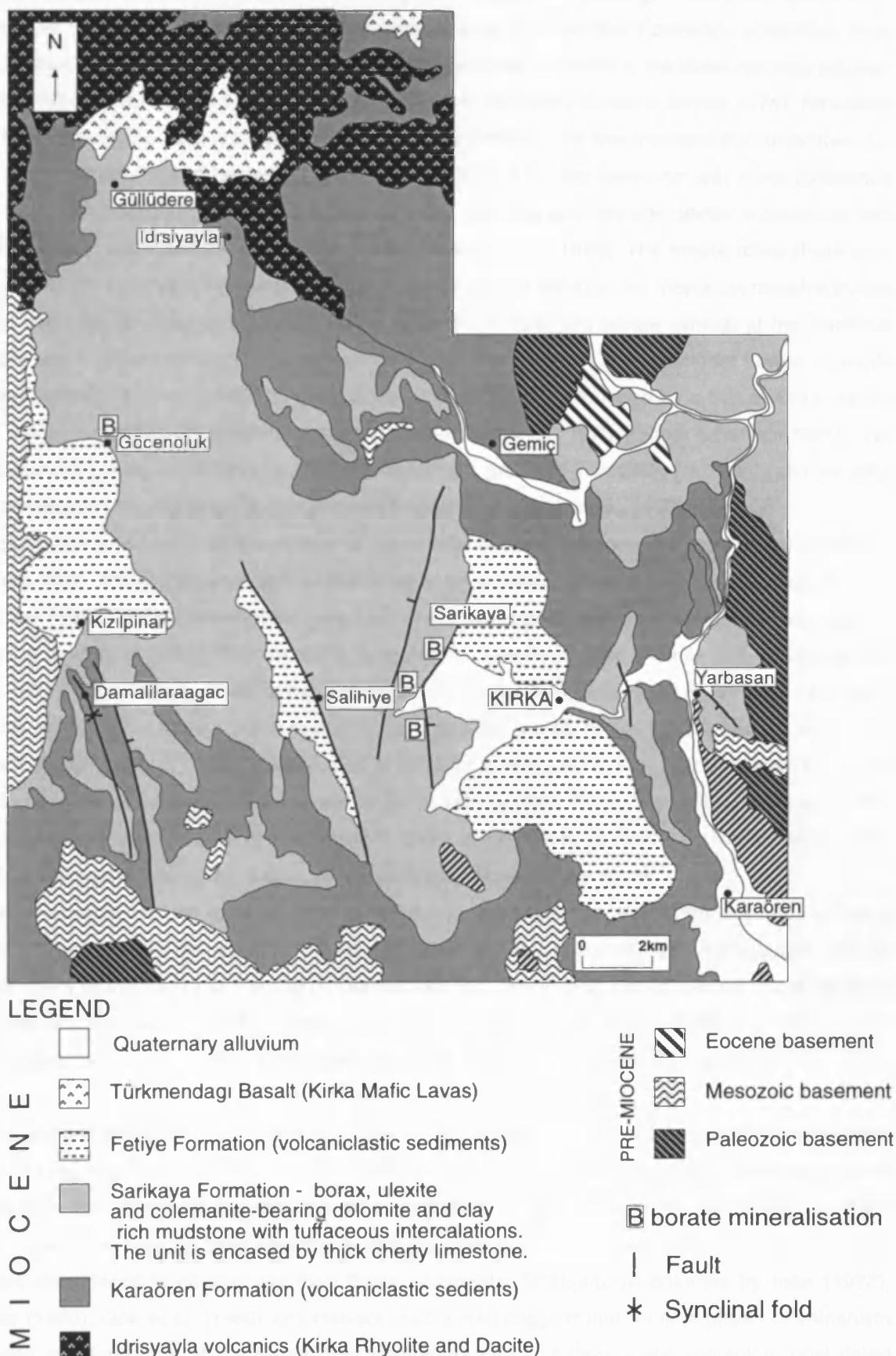


Figure 2.7

Yalçın et al., 1989a, Yalçın & Baysal 1991, Helvacı et al., 1993, Palmer & Helvacı 1995). The most extensive borate reserves in the basin are found just to the east of the village of Sarikaya, with smaller reserves at Göçenoluk (Figure 2.7). As described above, the Sarikaya Formation comprises thick cherty limestone above and below borate hosting mudstones. Smectite is the dominant clay mineral, but illite and chlorite are also present in the mudstones of this unit (Ataman & Baysal 1978). Smectites identified include the dioctahedral smectite, montmorillonite, and the trioctahedral smectites, Li-saponite, Li-stevensite and hectorite (Yalçın et al., 1989a). The clay layers contain some tuffaceous sediments, with authigenic K-feldspar, zeolite (erionite), smectite and illite and detrital volcanic-derived sanidine, albite, anorthoclase, quartz and calcite (Helvacı et al., 1993). The borate mineralisation at Kirka occurs as; thin layers interbedded with clay, disseminated within a clay matrix, as massive borate and as vugh fillings (Inan et al., 1973). Borax is the most abundant borate mineral at the Sarikaya deposits and it occurs chiefly in monomineralic zones (Inan 1972). Other abundant borate minerals include ulexite and colemanite. The borax body at Sarikaya is surrounded by a thin layer of ulexite which in turn is surrounded by a thin layer of colemanite (Inan et al., 1973, Palmer & Helvacı 1995). This borate mineral zoning at Sarikaya has been attributed to a gradually increasing  $\text{Na}^+/\text{Ca}^{2+}$  ratio resulting from precipitation of calcium carbonate followed by colemanite (Inan et al., 1973).

Colemanite is the major borate mineral at the smaller deposit of Göçenoluk, which is considered to be at the same stratigraphic level as the colemanite layer underlying the borax body at Sarikaya (Palmer & Helvacı 1995). Other borate minerals recorded at the main Sarikaya deposits include, tintalconite (an alteration product of borax), hydroboracite, kurnakovite, tunellite, inyoite, inderite and meyerhofferite (Inan 1972). Significantly, Kirka is the only basin in Turkey to contain sodium borates. The Kirka deposits are therefore dominated by sodium borates, but Ca, Ca Na, Sr and Mg borates are also found (Table 2.6). The extent of borate mineralisation at Sarikaya is estimated at 7 km N-S by at least 4 km E-W reaching a maximum of about 160 m thickness (Scott pers. comm - 1993). Total borate reserves for the Sarikaya deposit are estimated at 100 Mt with a grade of 20-25%  $\text{B}_2\text{O}_3$  (Kistler & Helvacı 1994). Kirka therefore represents one of the largest known reserves of borax in the world.

The sediments hosting mineralisation at Kirka are carbonate-rich, the carbonate mineral being dolomite (Yalçın 1989). Helvacı et al. (1993) and Kistler and Helvacı (1994) reported celestite, realgar and orpiment in the Sarikaya Formation, but the fact that Inan (1972) did not record these minerals suggests that they are rare at Kirka. Indeed, analyses for As, Sr and S reveal significantly lower values in the Sarikaya Formation of the Kirka Basin than in the Borate Formation of Emet Basin (Inan et al., 1973).

The volcanic lavas of the Kirka area are found mainly in the north-west of the basin. They have been separated into two main groups by Yalçın (1989); the Idrisyayla volcanics and the Türkmendagı basalt (Figure 2.7). The Idrisyayla volcanics are more evolved in composition and are considered by Yalçın (1989) to be older than the borate-hosting sediments while the Türkmendagı volcanics are more basic and are considered to be younger than these sediments. Stratigraphic columns by Inan (1972), Sunder (1980), Gök et al. (1980) and Helvacı (1977) also suggest that an acid phase of volcanism predated the deposition of the borate-host sediments and that more mafic volcanism post-dated

deposition of these sediments. K-Ar isotopic dating by Yalçın (1989) give ages for basal Idrisyayla rhyolite and andesite of 15.7-16.7 Ma ( $\pm 1$ ) and 15.4 Ma ( $\pm 1.1$ ) respectively, while Türkmendagı basalt was dated at 9.3 Ma ( $\pm 1$ ). The Karaören, Sarikaya and Fetiye Formations all contain tuffaceous sediments with volcanic derived minerals (Yalçın 1989, Helvacı et al., 1993) and there is therefore abundant evidence of volcanic activity throughout sedimentation in the Kirka Basin.

**Table 2.6 - Summary of authigenic minerals present in the Sarikaya Formation (from Inan 1973, Kistler & Helvacı 1994, Helvacı et al. 1993, Ataman & Baysal 1978, Sunder 1980)**

Minerals	Formula	Deposit
<b>Borates</b>		
Borax	$\text{Na}_2\text{B}_4\text{O}_7 \cdot 10\text{H}_2\text{O}$	Sarikaya
Tintalconite	$\text{Na}_2\text{B}_4\text{O}_7 \cdot 5\text{H}_2\text{O}$	Sarikaya
Colemanite	$\text{Ca}_2\text{B}_6\text{O}_{11} \cdot 5\text{H}_2\text{O}$	Sarikaya, Göçenoluk
Ulexite	$\text{NaCaB}_5\text{O}_9 \cdot 8\text{H}_2\text{O}$	Sarikaya, Göçenoluk
Meyerhofferite	$\text{Ca}_2\text{B}_6\text{O}_{11} \cdot 7\text{H}_2\text{O}$	Sarikaya
Tunellite	$\text{SrB}_6\text{O}_9(\text{OH})_2 \cdot 3\text{H}_2\text{O}$	Sarikaya
Hydroboracite	$\text{CaMgB}_6\text{O}_{11} \cdot 6\text{H}_2\text{O}$	Sarikaya
Inyoite	$\text{Ca}_2\text{B}_6\text{O}_{11} \cdot 13\text{H}_2\text{O}$	Sarikaya
Inderite	$\text{Mg}_2\text{B}_6\text{O}_{11} \cdot 15\text{H}_2\text{O}$	Sarikaya
<b>Other minerals</b>		
Dolomite	$\text{CaMgCO}_3$	Sarikaya
Celestite	$\text{SrSO}_4$	Sarikaya
Realgar	$\text{AsS}$	Sarikaya
Gypsum	$\text{CaSO}_4 \cdot 2\text{H}_2\text{O}$	Sarikaya
(Celestite, realgar & gypsum are reported only in Helvacı et al 1993 and Kistler & Helvacı 1994)		
<b>Clay minerals</b>		
montmorillonite	$(\text{MgAl})_2\text{SiO}_4)10(\text{OH})_2 \cdot n\text{H}_2\text{O}$	Sarikaya
illite	$(\text{K},\text{H}_3\text{O})\text{Al}_2(\text{AlSi}_3\text{O}_{10})(\text{OH})_2$	Sarikaya
chlorite	$(\text{SiAl})_8(\text{Mg},\text{Fe})_6\text{O}_{20}(\text{OH})_4$	Sarikaya

Volcanic activity to the south of Kirka Basin was widespread in the Neogene. For instance, ignimbrites cover an area of approximately 2000 km<sup>2</sup> (Figure 2.5), which overlie Palaeozoic schists and marbles and are laterally intercalated with Neogene sediments (Keller & Villari 1972). Further south, around the city of Afyon, intermediate-basic volcanic rocks occur and are also intercalated in places with Neogene sediments (Keller & Villari 1972). K-Ar dating on the Afyon lavas produced a Mid-Late Miocene age spectrum from 8.6 - 14.7 Ma (Besang et al., 1977).

## 2.5 FIELD RELATIONS AND PETROLOGY OF IGNEOUS ROCKS FROM THE KIRKA AREA

Field and petrological information from this study is discussed in this section, in conjunction with previous work on igneous rocks from the Kirka area. Volcanic rocks and volcanoclastic sediments from Kirka area formed the bulk of the present study but the igneous activity of the Afyon area, further south was also considered. An extensive sampling programme was carried out in these areas (sample localities in Appendices A & B).

### 2.5.1 Volcanism in the Kirka Basin

#### 2.5.1.1 Kirka Ignimbrites

The ignimbrites are exposed along the southern margin of the Kirka Basin where they cover an area of over 2000 km<sup>2</sup> (Figure 2.6). Due to the close proximity of the ignimbrites to the Kirka Basin, they are termed the Kirka Ignimbrites in this study. Keller and Villari (1972) described the rhyolitic ignimbrites as largely devitrified, both welded and unwelded, with common phenocrysts of quartz, sanidine and plagioclase, and occasional biotite. On the basis of stratigraphic relations, Keller & Villari (1972) suggested that the ignimbrites were erupted in the Pliocene. A caldera has been recognised within this ignimbrite field to the north of Afyon (Aydar et al., 1994).

In this study a number of ignimbrite localities were sampled to establish textural, mineralogical and geochemical variations and to compare primary ignimbrites with the volcanoclastic material interbedded with lacustrine sediments in the Kirka Basin. The sampling covered a wide area, from localities within the ignimbrite expanse to the south of the Kirka Basin (Köroglukalesi Tepe, Ayazini, Seyidler and Fetiye), and also at localities within and around the fringes of the basin (Büyükyayla, north-east of Karaören and west of Kümbet) (Appendices A & B).

A thick ignimbrite succession is observed at Köroglukalesi Tepe, approximately 15 km south of Kirka (Figure 2.6), comprising several 20 m high benches (Plate 2.6a), which may separate individual ignimbrites. Fiamme are found near the base of the ignimbrite succession (Plate 2.6b), and in places the pumice has been completely weathered away leaving fiamme-shaped holes. Also at the base of the ignimbrite, obsidian occurs where no devitrification has taken place. Above this, the ignimbrite is a homogeneous white - pale grey lapilli tuff. The rock has probably undergone almost total devitrification, apart from near the base (Keller and Villari 1972). Columnar cooling joints and well formed cones, sometimes called 'tent rocks', also occur (Plate 2.7a) (Francis 1993). The columnar joints indicate high emplacement temperatures. The 'tent rocks' are erosion features but may record former fumarole sites.

The ignimbrite has distinctive smokey quartz, K-feldspar, plagioclase and rare biotite, and porphyritic pumice lapilli up to 0.5 cm in diameter with spherical vesicles (Table 2.7). In more welded lithologies, such as at the base of the sequence at Köroglukalesi Tepe, the pumices are flattened producing fiamme. Dark grey volcanic lithic lapilli, up to 5 cm in diameter, with abundant quartz phenocrysts, also sometimes occur. Plagioclase feldspars show well developed multiple twinning while K-feldspars occasionally show Carlsbad twinning. Electron microprobe analyses of the plagioclases revealed oligoclase (An<sub>19-27</sub>) compositions (Appendix H), which is consistent with petrological studies by Keller and Villari (1972). The compositions of K-feldspars fall on the boundary between Na and K sanidine (Or<sub>69-71</sub>). Under high power using a scanning electron microscope (SEM), typical textural features of pyroclastic rocks can be observed. Plate 2.8a illustrates typical glass shards, which may have been produced by explosive fragmentation of the magma and perhaps also by attrition of glassy clasts during transport (McPhie et al., 1993). Plate 2.8b illustrates another area of the same sample which in contrast is dominantly unfragmented glass.



Plate 2.6a - Kirka Ignimbrite exposed at K roglukalesi Tepe

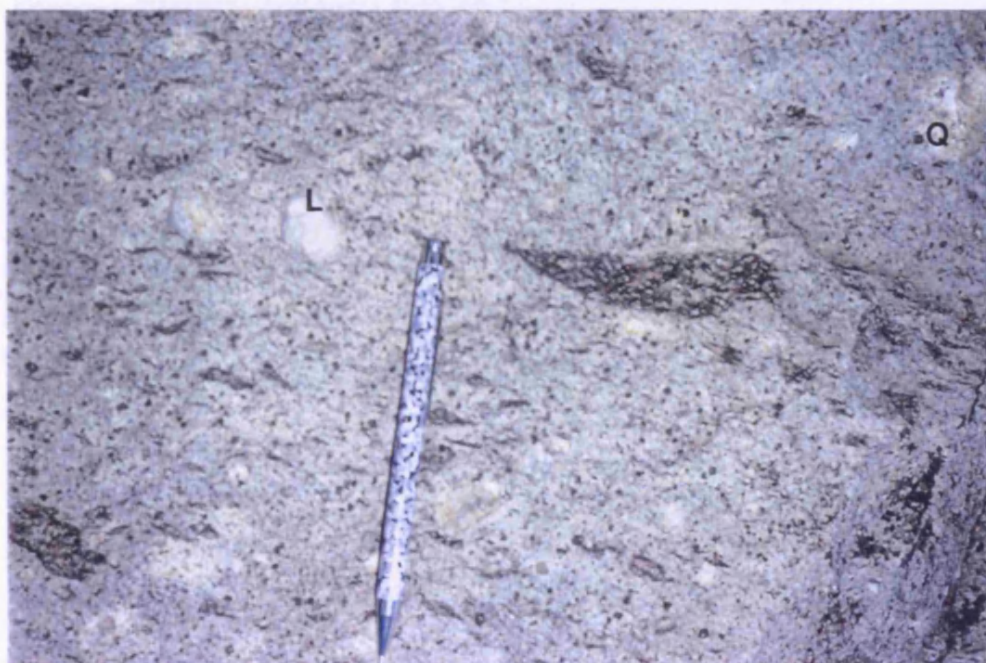


Plate 2.6b - fiamme in the Kirka Ignimbrite. Lithic clasts (L) and smoky quartz (Q) are also visible.





Plate 2.7a - tent rock in the Kirka Ignimbrite near Iscehisar



Plate 2.7b - Kirka mafic lavas near Sancar overlie cherty limestone beds of the Sarikaya Formation



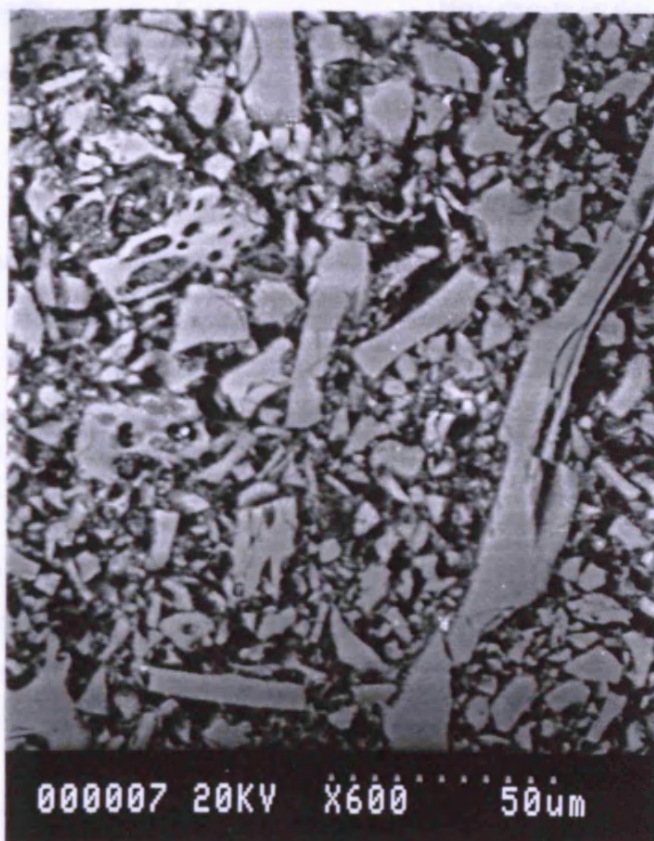


Plate 2.8a - SEM photomicrograph of glass shards in Kirka Ignimbrite (magnification X 600)

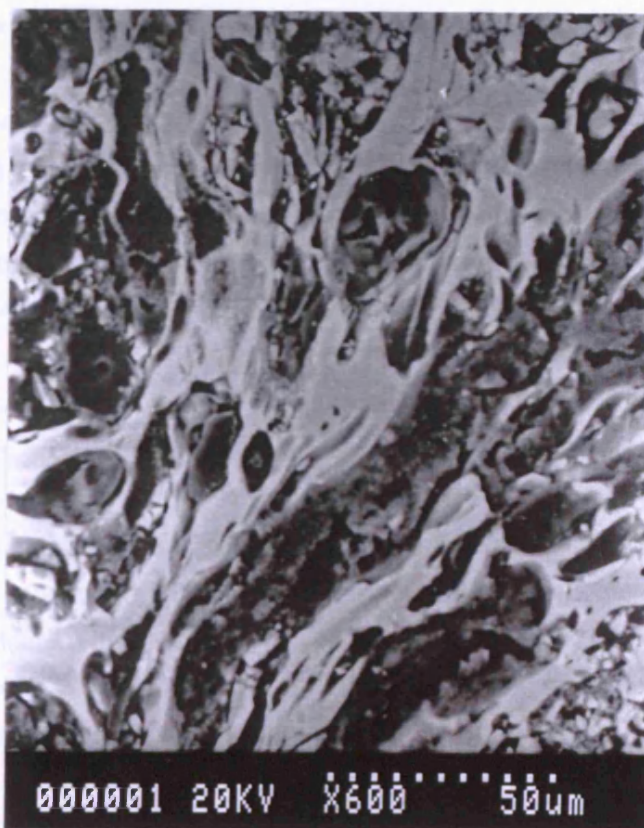


Plate 2.8b - SEM photomicrograph of unfragmented glass in Kirka Ignimbrite (magnification X 600)

## Geology of the Emet and Kirka areas

**Table 2.7 - Summary petrology of volcanic rocks from the Kirka area**

<i>Rock type and locality</i>	<i>Mineralogy (from thin section, XRD, microprobe)</i>
Kirka Ignimbrite (within and to the S of Kirka Basin)	Abundant phenocrysts of plagioclase (oligoclase), K-feldspar (Na/K sanidine), smokey quartz. Rare biotite. Pumice lapilli - sometimes compressed but more often contain rounded vesicles. Lithic lapilli present. Rock is largely devitrified with only occasional fresh glass and rare fiamme texture.
Kirka Rhyolite & Dacite (Idrisyayla - N Kirka Basin)	Phenocrysts observed include plagioclase (andesine), K-feldspar (sanidine), quartz, biotite and amphibole. Some rocks are fine grained with no phenocrysts. Spherulites are common in the matrix.
Kirka mafic lavas (Bozbel Tepe and Sancar - N and NE Kirka basin respectively)	Phenocrysts of plagioclase (bytownite-anorthite), olivine, clinopyroxene (augite) in a matrix of plagioclase needles.

### 2.5.1.2 Kirka Rhyolites and Dacites

Rhyolite and dacite sheets (Idrisyayla volcanics of Yalçın 1989) are exposed around Idrisyayla village, 7 km north-west of Kirka (Figure 2.7). They occupy the northern fringes of the basin, and form a series of small hills and ridges. These rhyolites and dacites were sampled in detail (Appendices A & B). As in the Emet Basin, rapid erosion of these sheets has left a rugged topography. Platey jointing is observed in some of the rhyolites.

Within the rhyolite and dacite sheets of this area, there is a spectrum from very fine grained to slightly porphyritic, with some quartz and feldspar phenocrysts, through to porphyritic rhyolites and dacites with abundant phenocrysts of biotite, plagioclase and K-feldspar (Table 2.7). The fine grained rhyolites contain only quartz and feldspar, while the porphyritic rhyolites and dacites have some or all of plagioclase, K-feldspar, biotite, quartz, and hornblende. Plagioclase often shows well developed multiple twinning and zoning, while the hornblende, although a rare phase in these rocks, can be seen in basal section showing two cleavages. Electron microprobe analyses of plagioclase feldspar phenocrysts in porphyritic rhyolite reveal the presence of andesine with a restricted compositional range ( $An_{32-37}$ ) (Appendix H), similar to the compositions of plagioclase in the Emet Rhyolites. The K-feldspars are K sanidines ( $Or_{73-74}$ ), very similar to compositions observed in the Emet Rhyolites. Spherulites are common in the glassy matrix of the rhyolites, and particularly north of Güllüdere village.

The volcanics occur immediately to the north of the Miocene Kirka lacustrine sediments and are therefore close enough spatially to have had an influence on the lake system. Contacts with sediments are not exposed in this area and hence to obtain information on the timing of this phase of volcanism relative to the mineralisation, evidence from basinal sediments is required. However, on the basis of K-Ar dating by Yalçın (1989), the Kirka Rhyolites and Dacites appear to have an Early Miocene age. Furthermore, Yalçın's (1989) K-Ar dating of volcanic-derived minerals in the Karaören and Sarıkaya Formation also gave Early Miocene ages.



### 2.5.1.3 Kirka Mafic Lavas

The Kirka mafic lavas (Türkmendagi volcanics of Yalçın 1989) are found at two localities, north of Idrisyayla, and also north of Sancar in the north-east of the basin midway between Kirka and Seyitgazi (Figures 2.6). The basaltic andesite lavas north of Idrisyayla form the highest hills, notably Türkmendagi and Bozbel Tepe. Similarly near Sancar the basaltic andesites form vesicular lava flows at the tops of a small hill. Mineralogically the lavas near Idrisyayla and Sancar are very similar, with phenocrysts of augite, olivine and sometimes elongate plagioclase in a matrix of small plagioclase needles (Table 2.7). Electron microprobe analyses of feldspars (Appendix H) reveal that the plagioclase is considerably more calcic than those of the more acid volcanics and, indeed, the Emet mafic lavas. The elongate plagioclases are bytownite and rarely anorthite ( $An_{69-97}$ ), typical plagioclase composition for basic rocks (Gribble & Hall 1993). The olivines are close to fayalite in composition ( $Fe_{16-39}Fa_{61-84}$ ), which is a somewhat more iron rich than that in most basic rocks (Gribble & Hall 1993).

The Kirka mafic lavas near Sancar provide useful stratigraphic information since the lava flows can be seen to directly overlie cherty limestone beds of the Sarikaya Formation (Plate 2.7b). Contacts between volcanics and sediments are more difficult to observe around Idrisyayla. However, to the north of the village of Güllüdere (Figure 2.7), although direct contacts are not visible, basaltic andesite appears to lie stratigraphically above both cherty limestone and rhyolite. A similar relationship is observed between the basaltic andesite and rhyolite directly to the north of Idrisyayla. These field observations are consistent with the stratigraphy determined by Yalçın (1989), which indicated that the Kirka mafic lavas are younger than both the Sarikaya Formation and the rhyolites. As already mentioned, this is confirmed by K-Ar dating, the basalt having a Late Miocene age while the acidic volcanism has an Early Miocene age (Yalçın 1989).

### 2.5.1.4 Volcaniclastic sediments from within Kirka Basin

As in the Emet Basin, the volcanic input into the sediments was examined in the Kirka Basin with a view to constraining the volcanic stratigraphy, and hence the timing of volcanism relative to the deposition of the borate-host sediments. Sampling was undertaken of volcaniclastic sediments over the whole extent of the Kirka Basin, within the Karaören, Sarikaya and Fetiye Formations (Appendices A & B).

Sedimentary logs were drawn through the Karaören Formation near; Gemiç in the north of the basin (Section L), near Yarbasan at Tekke Tepe in the eastern part of the basin (Section M), and near Karaören (Section N)(Appendices A & B). At these localities the stratigraphic position of the Karaören Formation sediments can be established. At Sections L, M and N, cherty limestone beds of the Sarikaya Formation overlie the volcaniclastic sedimentary rocks (Figure 2.8). This relationship can be seen at a locality just north of Karaören (Plate 2.9a) and to the west of Gemiç (Figure 2.7). There the overlying limestone was mapped by Gök et al. (1980) as a continuation of the unit lying directly above the borate-hosting sediments at the Sarikaya open pit. Limestone is also found above volcaniclastic sediment at the village of Damialıkaraagaç (Figure 2.7). Hence, cherty limestone beds of the Sarikaya Formation stratigraphically overlie the volcaniclastic sediments of the Karaören Formation at a number

**FIGURE 2.8 - Sections through the Karaören Formation of the Kirka Basin**

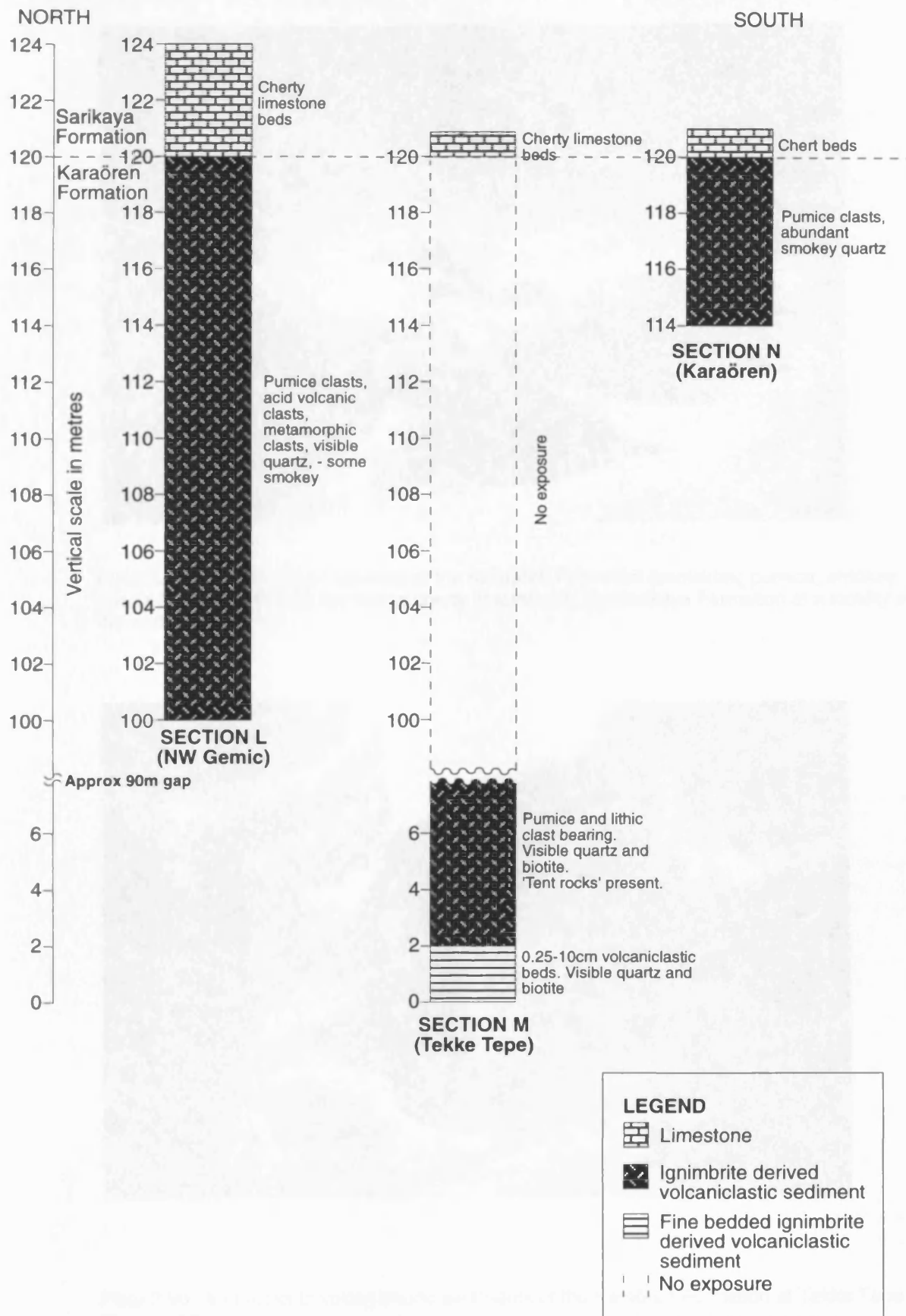


**Figure 2.8**



Plate 2.9a - volcaniclastic siltstone of the Karaören Formation (containing pumice, smokey quartz & lithic fragments) lies below cherty limestone of the Sarikaya Formation at a locality of the north of Karaören



Plate 2.9b - tent rocks in volcaniclastic sediments of the Karaören Formation at Tekke Tepe (Section M)

of localities, and therefore Yalçın's (1989) assertion that the Karaören Formation lies stratigraphically below the Sarıkaya Formation appears reasonable.

Section L (Figure 2.8) consists of beds of volcanoclastic sedimentary rocks which have a fine grained tuffaceous matrix with clasts of pumice, acid volcanics and metamorphic rocks. Section M (Figure 2.8) comprises fine bedded biotite rich sediments which give way to volcanoclastics which are massive and contain pumice and rhyolite lithic lapilli. These volcanoclastics in places have been eroded to form distinctive cones or 'tent rocks' (Plate 2.9b) similar to those observed in the ignimbrite south of the basin. Section N (Figure 2.8) comprises volcanoclastic sediments with pumice lapilli. Phenocrysts of quartz (often smokey), K-feldspar and plagioclase are abundant in all the samples (Table 2.8) and biotite is a rare phase. Hence, the mineralogy of these sediments is very similar to that of the ignimbrite. Furthermore, the presence of pumice clasts and lithic lapilli suggest an ignimbrite source.

However, the matrix material of these sediments is mainly calcite and vesicles in the pumice clasts are often filled with calcite (Table 2.8), probably the result of interaction between ignimbrite material and Ca-rich lake waters. Hence, these rocks are ignimbrite-derived volcanoclastics which were modified in a lacustrine environment. Volcanic clasts found in the volcanoclastic sediments of Section L in the north of the basin comprise phenocrysts of plagioclase, K-feldspar, biotite, hornblende and occasional quartz in a matrix containing spherulites (Table 2.8). The mineralogy is therefore very similar to the porphyritic Kirka Dacites and Rhyolites. The unaltered and unfractured nature of the minerals in the clasts further suggests that they have a local source. Hence, as well as there being an input into the Karaören sediments from the ignimbrite, there appears to have been an input from weathered local rhyolite/dacite sheets.

**Table 2.8 - Summary mineralogy of ignimbrite-derived lacustrine volcanoclastic sediments in the Karaören Formation**

<b>Karaören Formation</b>		
<b>Location</b>	<b>Sample</b>	<b>Mineralogy (from thin sections, XRD, microprobe)</b>
Section L - NW Gemiç village	VSK 265, 266 (volcanoclastic siltstone)	Quartz, K-feldspar, plagioclase. Pumice with calcite filled vesicles, calcite matrix.
	VSK 279 (acid volcanic clast)	Phenocrysts of plagioclase, K-feldspar, biotite and hornblende in a matrix with spherulites.
Section M - Tekke Tepe	VSK 255, 256, 257 (volcanoclastic siltstone)	Quartz, K-feldspar, plagioclase and biotite. Pumice with calcite filled vesicles, calcite matrix.
Section N - Karaören village	VSK 272 (volcanoclastic siltstone)	Quartz, K-feldspar, plagioclase and rare biotite. Abundant vesicular pumice.
W of Gemiç village	VSK 267, 268 (volcanoclastic siltstone)	Quartz, K-feldspar, plagioclase (oligoclase), clinoptilolite, some calcite in matrix, vesicular pumice.
N of Karaören village	VSK 273 (volcanoclastic siltstone)	Quartz, K-feldspar, plagioclase, vesicular pumice.
W of Damalıkkaraagaç village	VSK 275 (volcanoclastic siltstone)	Quartz, K-feldspar, plagioclase. Pumice with calcite filled vesicles, calcite matrix.

**Previous work - Yalçın 1989 Yalçın et al. 1991., Gündoğdu et al. 1996-** studies on the mineralogy of the Karaören Formation. Volcanoclastic sediments of this formation described as ash/dust tufts of rhyolitic composition, with zeolite (clinoptilolite, heulandite), smectite, calcite and K-feldspar. A K-Ar date on biotite from this formation gave an Early Miocene age.

The Sarıkaya Formation has been widely studied, as discussed previously in this chapter and this

section will only examine the possible igneous influence on these sediments. Yalçın (1989) described banded tuff interbedded with cherty limestone in the lower part of the Sarikaya Formation and laminated dolomitic claystone with interbedded biotite tuff and borate lenses in the centre of the unit. Tuffaceous samples from the Sarikaya borate hosting unit have been found to contain authigenic minerals (K-feldspar, zeolite, illite and smectite) and volcanic-derived detrital minerals (sanidine, albite, anorthoclase and quartz) by Helvacı et al. (1993). Hence, it is beyond doubt that there has been a significant volcanic input into the sediments hosting mineralisation at Sarikaya. Furthermore, an acidic volcanic source is indicated from the presence of detrital quartz.

As a result of a large amount of published literature (Helvacı et al., 1993, Yalçın 1989) and due to the poor exposure of the Sarikaya Formation in the Kirka Basin, only a limited amount of sampling of this unit was undertaken in this study. Mudstones were sampled from the host sediments at Sarikaya (west of open pit in a borax & ulexite-bearing zone) and Göçenoluk (in a colemanite-bearing zone) (Appendices A & B). The sediments at the former locality comprise thin beds of carbonate interbedded with mudstone which are too fine grained to identify individual minerals with the naked eye. XRD on these samples revealed that the mudstone contains dolomite and smectite, while the carbonate is pure dolomite (Table 2.9). Previous workers on the sediments at Sarikaya also described them as being high in carbonate (Kistler & Helvacı 1994, Yalçın 1989). The mudstone at Göçenoluk, which hosts colemanite mineralisation (Palmer & Helvacı 1995), contains smectite, illite and K-feldspar (Table 2.9) and is therefore very similar to the colemanite hosting mudstones at Emet. The mineralogy of the Sarikaya mudstones is presented in more detail in Chapter 4 of this thesis.

**Table 2.9 - Summary mineralogy of sediments in the Sarikaya Formation**

<b>Karaören Formation</b>		
<b>Location</b>	<b>Sample</b>	<b>Mineralogy (from XRD)</b>
Old mine workings - west of main Kirka open pit (ulexite + borax)	VSK 1- interbedded dark grey mudstone and light grey/white carbonate bands.	Smectite and dolomite
	VSK 2- dark grey mudstone.	Smectite and dolomite
	VSK 3 - light grey/white carbonate.	Dolomite
Göçenoluk (colemanite)	VSK 4 dark grey mudstone.	Smectite, illite, K-feldspar

**Previous work - Ataman & Baysal (1978)** found montmorillonite, illite and chlorite present in the mudstones, **Kistler & Helvacı (1994)** described the clays at Kirka as being carbonate rich, **Helvacı et al., (1993)** and **Yalçın (1989)** described volcanoclastic sediments - see above.

The Fetiye Formation is described by Yalçın (1989) as reworked tuff fragments which lie above the borate mineralisation of the Sarikaya Formation. Samples were taken in the current study from Salihiye and Kızılpınar (Figure 2.7, Appendices A & B). From the petrology and textures of these volcanoclastic sediments, it is clear that they have had a significant input from the nearby ignimbrite. The crystal phases are smokey quartz, K-feldspar, plagioclase and occasional biotite, while the matrix is calcite rich (Table 2.10), a probable feature of the interaction of these volcanoclastics with Ca-rich lake waters. The sediments are also pumice rich and vesicles within the pumice are filled with calcite (Plates 2.10a & 2.10b).

Volcanoclastic sediments to the north-west of Salihiye village in the western part of the Kirka Basin clearly lie above cherty limestone beds which are part of the upper limestone of the Sarikaya Formation



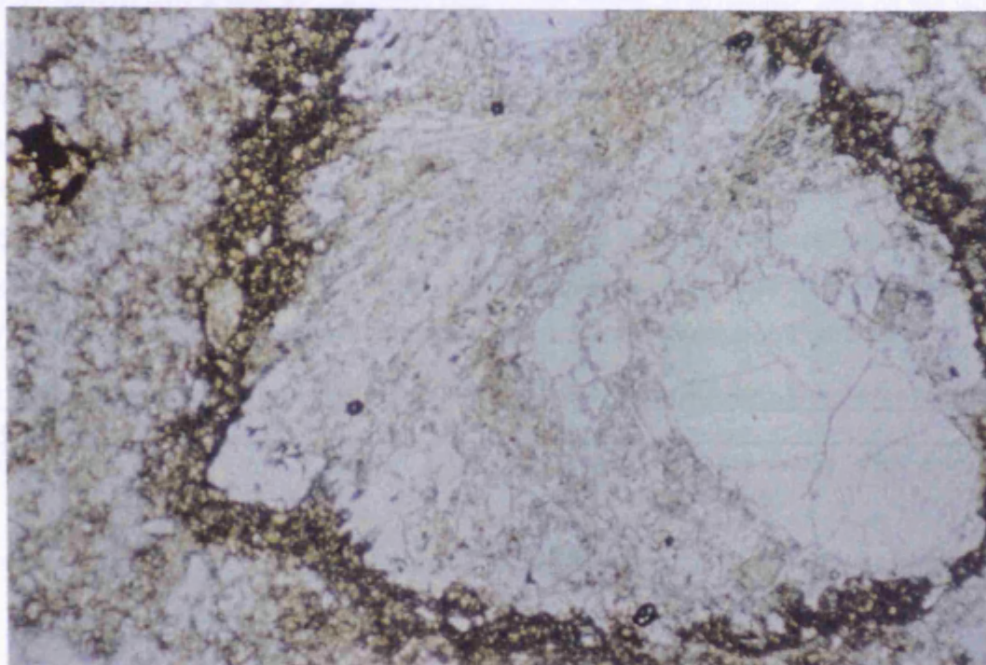


Plate 2.10a - vesicular pumice in volcanoclastic siltstone of the Fetiye Formation from near Salihiye (plain polarised light, field of view 3 mm by 2 mm)

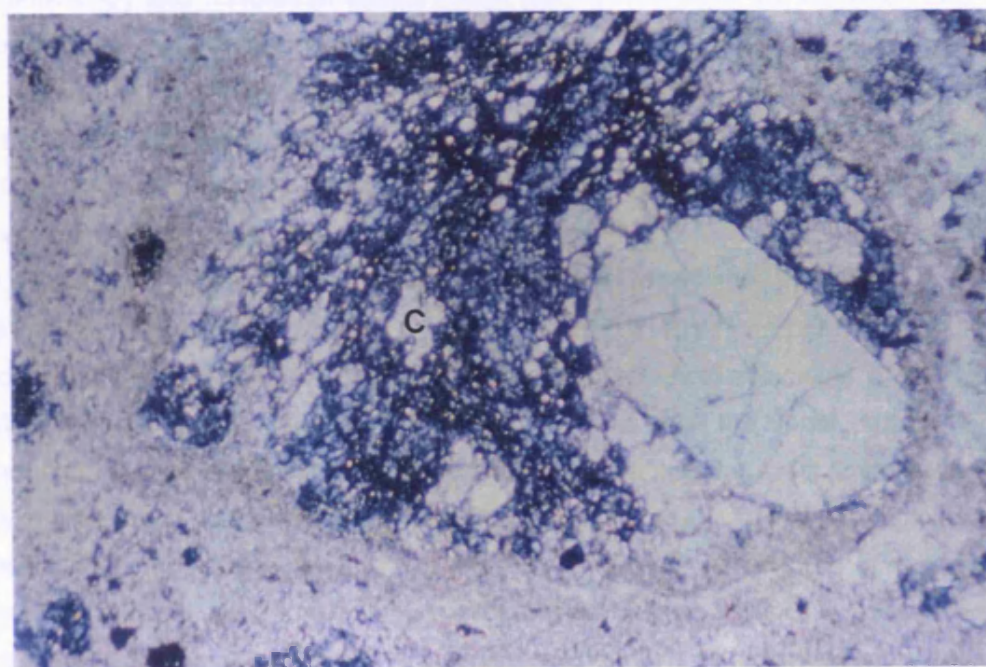


Plate 2.10b - as above, but viewed under cross polarised light. Calcite (C) can be seen in the vesicles of the pumice (field of view 3 mm by 2 mm)

(Figure 2.7). Similar exposures can be found near to the village of Kızılpınar, also on the western side of the basin (Figure 2.7), and although the field relations are less clear, they also appear to lie near the top of the sedimentary sequence. These observations that the Fetiye volcanoclastic sediments were deposited after the borate-host sediments are consistent with Yalçın (1989). His assertion that these represent reworked sediments therefore appears reasonable. There are no significant mineralogical differences between these sediments and those of the Karaören Formation, but the different stratigraphic positions suggest that the Fetiye Formation represents a reworking of ignimbrite material, either as a result of erosion from the primary ignimbrite or from the Karaören Formation.

**Table 2.10 - Summary mineralogy of ignimbrite-derived lacustrine volcanoclastic sediments in the Fetiye Formation**

<b>Fetiye Formation</b>		
<b>Location</b>	<b>Sample</b>	<b>Mineralogy (from thin section &amp; XRD)</b>
Salihiye village	VSK 261, 262 (volcanoclastic siltstone)	Quartz, K-feldspar, plagioclase, rare biotite. Pumices with calcite filled vesicles, calcite matrix.
Kızılpınar village	VSK 274 (volcanoclastic siltstone)	Quartz, K-feldspar, plagioclase. Pumices with calcite filled vesicles, calcite matrix.

## 2.5.1.5 Kirka Basin volcanic stratigraphy (from field and mineralogical evidence, and K-Ar dates)

The mineralogy and textures of volcanoclastic sediments in both the Karaören and the Fetiye Formation suggest a significant input from acid pyroclastics into these sediments. The presence of pumice, lithic lapilli and of smokey quartz are especially typical of the ignimbrite exposures found around the basin and these sediments appear to have had a largely ignimbritic provenance. Volcanoclastic sediments are also present in the Sarikaya Formation and the presence of detrital quartz in these sediments again suggests an acid volcanic source.

Field relations indicate that the Karaören volcanoclastics were deposited prior to deposition of at least the upper limestone of the Sarikaya Formation, while the Fetiye Formation appears to represent reworked ignimbrite, which was deposited later, after the borate-host sediments. It therefore appears that acid pyroclastic activity predated the deposition of at least the upper part of the Sarikaya Formation. It is not possible from field evidence alone to establish the exact timing of the ignimbrite eruptions relative to the borate mineralisation. The presence of rhyolite clasts in conglomerates below the Sarikaya cherty limestone indicates that the rhyolite sheets may also be of similar age to the ignimbrite. Field relations at Sancar clearly indicate that the basaltic andesite lavas were erupted after deposition of the borate host sediments. In contrast to Emet, K-Ar dates are available for some of the volcanic rocks at Kirka (Yalçın 1989). The dates confirm the proposed volcanic stratigraphy assigning the Kirka acid volcanism and volcanoclastic sediments of the Karaören and the Sarikaya Formations an Early Miocene age while the basaltic andesite volcanism was Late Miocene in age.

## **2.5.2 Volcanism of the Afyon region**

An extensive sampling programme was carried out in the Afyon area (Appendices A & B). The aim was to build on previous studies of Keller & Villari (1972) and Keller (1983), and to relate this volcanism to that of Kirka Basin further north. As mentioned, the volcanic rocks of this area are basic - intermediate in composition (Keller & Villari 1972) and have been dated at between 8.6 and 14.7 Ma (Besang et al., 1977). They are therefore intermediate in age between the Early Miocene acid volcanism and the Late Miocene, more mafic, volcanism of the Kirka Basin. The volcanics of the Afyon area can be separated into two groups on the basis of their field appearance. The first types are porphyritic andesites and dacites and the second are finer grained mafic lavas.

### **2.5.2.1 Afyon Andesites and Dacites (sanidine-bearing)**

These outcrop at the city of Afyon, to the south of Afyon at Kayadibi, Suhut and Büyükkalecik and to the west of Afyon near Balmahmut (Appendices A & B). The Afyon andesites and dacites form well preserved domes and large breccia bodies; one of the most spectacular domes forms the bedrock to the castle in the centre of Afyon. The breccias are considered to be partly of nuée origin and partly friction breccias connected to the extrusion of the domes (Keller & Villari 1972).

The most spectacular petrologic feature in these volcanics around Afyon is the presence of large (up to 5 cm) phenocrysts of sanidine, also noted by Keller & Villari (1972) and Çevikbas et al. (1988). Electron microprobe analyses of the large sanidine crystals reveals that the majority of each phenocryst is K-sanidine ( $Or_{70-74}$ ) with a small amount of intergrown andesine ( $An_{33-42}$ ) (Appendix H). Other phenocryst phases present in these rocks include hornblende (up to 2 cm), biotite, multiple twinned and sometimes zoned plagioclase (Table 2.11). The matrix is made up of small feldspar and augite crystals. Electron microprobe analyses of the plagioclase reveals andesine compositions ( $An_{30-43}$ ).

### **2.5.2.2 Afyon Mafic Lavas**

The mafic lavas have a dark grey colour and produce flows. They range from basaltic andesites to andesites and they outcrop near; Iscehisar to the north-east of Afyon, Köprülü, Elvanpasa and Çepni to the west of Afyon, near Nuhköy to the south-west of Afyon, and near Çalköy to the north-west of Afyon (Figures 2.6 & 2.7). These mafic lavas contain phenocrysts of biotite and clinopyroxene in a matrix of small feldspar needles (Table 2.11). The lavas are observed capping ignimbrite near to Iscehisar. According to Aydar et al. (1994), these capping lavas were erupted along ring fractures.

**Table 2.11 - Summary petrology of volcanic lavas and volcanoclastic sediments from the Afyon area**

<b>Rock type and locality</b>	<b>Mineralogy (from thin section, XRD, microprobe)</b>
Afyon sanidine-bearing andesites and dacites (Afyon, Kayadibi, Suhut, Büyükkalecik, Balmahmut)	Phenocrysts of sanidine, hornblende, plagioclase and biotite in a matrix of feldspar and augite.
Afyon mafic lavas (Iscehisar, Köprülü, Elvanpasa, Çepni, Nuhköy, Çalköy)	Phenocrysts of biotite and clinopyroxene in a matrix of small feldspar needles.
Balmahmut mudstone	illite/muscovite, K-feldspar, plagioclase, calcite.



### 2.5.2.3 Volcaniclastic sediments from the Afyon region (Balmahmut)

The sedimentary sequences studied in this project are found to the north of the village of Balmahmut, to the west of Afyon (Figure 2.6). These sediments were sampled in order to provide a mineralogical and geochemical comparison to the sediments associated with the volcanism in Kirka and Emet Basins. In this area Afyon andesite (sanidine-bearing) breccias are seen outcropping below volcaniclastic sediments. Section P is located east of Balmahmut and consists of mudstones and siltstones (Figure 2.9, Appendices A & B) which overlie Afyon andesitic breccias and lie below cherty limestone beds which cap the hill tops in this area. The volcanic breccia below these sediments is made up largely of a brown coloured biotite-bearing tuffaceous matrix with clasts of sanidine-bearing Afyon andesites. The matrix of this rock comprises phenocrysts of biotite, plagioclase and K-feldspar. Some of the siltstones contain abundant biotite, visible with the naked eye, probably of volcanic derivation. XRD analyses of mudstone (Appendix G) from these sediments reveals the presence of illite/muscovite, K-feldspar and calcite (Table 2.11). A similar sequence to the north of Balmahmut is recorded in Section O (Figure 2.9) and it is at the same stratigraphic level as Section P. It contains mudstone, volcaniclastic and limestone beds (Figure 2.9) which are situated above a 5 m band of volcaniclastics and below cherty limestone which cap the hillside. The mudstone comprises K-feldspar, plagioclase and illite/muscovite (Table 2.11). The volcaniclastics below the section are matrix supported with only occasional clasts of sanidine-bearing Afyon andesites. The matrix comprises phenocrysts of biotite, plagioclase and K-feldspar (Table 2.11). In summary, the presence of feldspar in the mudstone together with the close proximity of the Afyon sanidine-bearing andesites suggests an influence of volcanism on sedimentation in this area.

## 2.6 CONCLUDING POINTS

In general terms, the volcanic evolution in this area during the Miocene, was from acidic to less evolved, more mafic magmatism. Information from field and mineralogical work in this study and from the literature, indicates that a particular type of magmatism in both the Emet and Kirka Basins has a close spatial and temporal position to the borate hosting sediments. In both basins, it is an acidic phase of magmatism that appears to have been active before, and perhaps during the time of deposition of borate-host sediments. Mineralogical and textural studies of volcaniclastic sediments from the basins indicate that there was a high input into these sediments from local acid magmatism.

The Emet Basin is bordered on its western side by the large Erigöz pluton, which intruded Palaeozoic basement. The pluton is classified as an I type granite on the basis that it contains hornblende and magnetite. Field evidence indicates that the pluton predated most if not all sedimentation in Emet Basin. A series of rhyolite sheets were related closely in space and possibly in time with the pluton. These rhyolites are porphyritic with phenocrysts of plagioclase, K-feldspar, biotite and quartz in a glassy matrix often with spherulites. The field relations of these rhyolites, together with studies on volcaniclastic sediments reveals that acid volcanism at Emet took place prior to and perhaps during deposition of borate-host sediments. Volcaniclastic sediments in both the Red and Borate Formations appear, on the basis of textures and mineralogy, to be derived from both acid pyroclastic

FIGURE 2.9 - Sections through sedimentary sequence near to Balmahmut

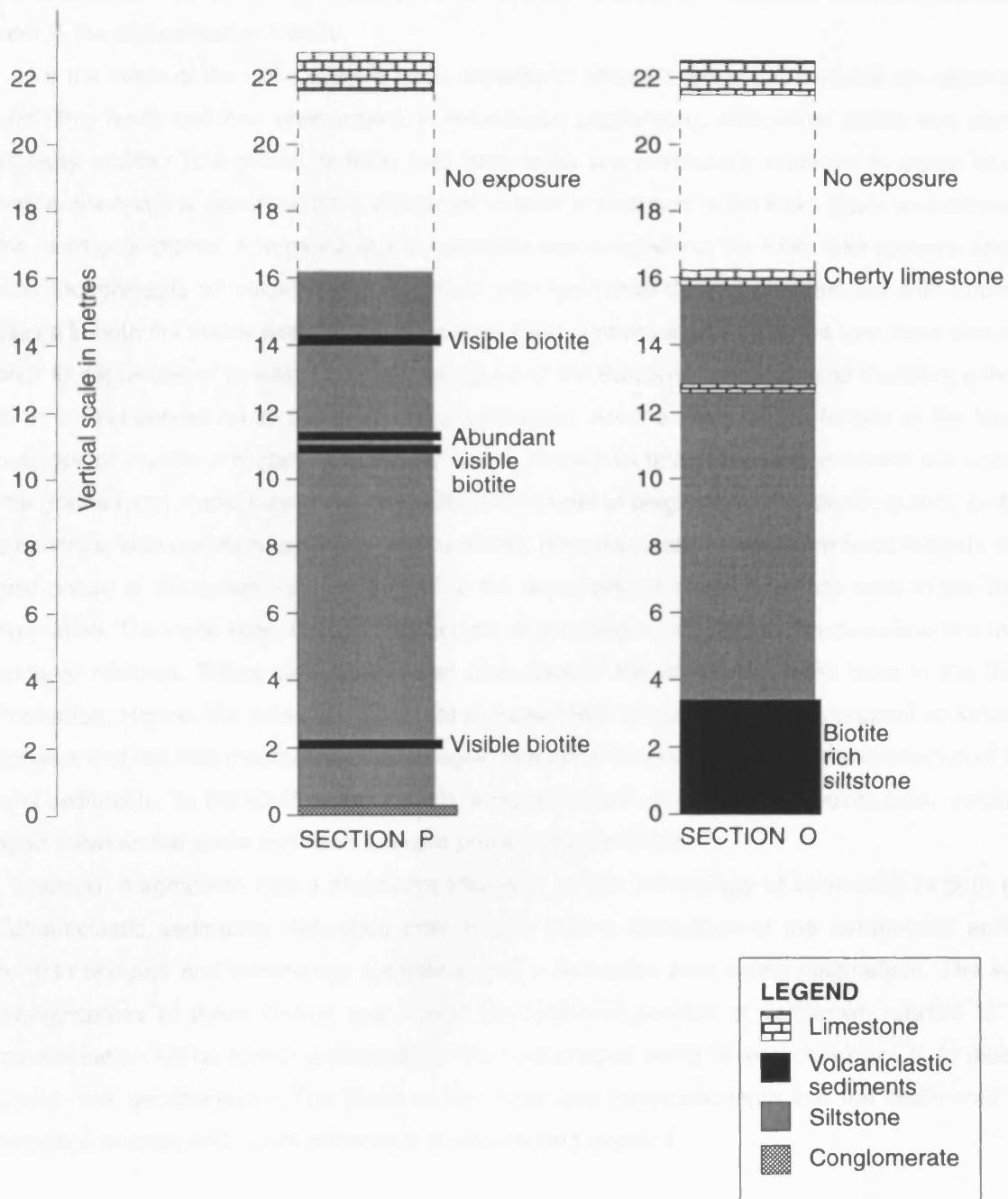


Figure 2.9

volcanism and erosion of the granite. The last phase of volcanism in the Emet Basin, which post dated deposition of the borate-host sediments, was the eruption of the Emet mafic lavas. The lavas contain phenocrysts of augite and biotite in a matrix of feldspar needles. Studies of the basins to the south of the Emet Basin reveal a similar situation with an evolution from acidic volcanism to more mafic volcanism later in the sedimentation history.

To the south of the Kirka Basin a large expanse of Miocene ignimbrite contains abundant pumice and lithic lapilli and has phenocrysts of K-feldspar, plagioclase, occasional biotite and distinctive smokey quartz. The quartz, pumice and lithic lapilli are particularly common in some lacustrine sediments and it is apparent that a significant volume of sediment in the Kirka Basin was derived from the nearby ignimbrite. A large volume of ignimbrite was erupted into the Kirka lake systems and this is now recognisable as volcanoclastic sediment with ignimbrite-derived minerals but with appreciable calcite in both the matrix and in pumice vesicles. Field relations indicate that the ignimbrite was erupted prior to deposition of at least the upper limestone of the Sarikaya Formation and therefore either prior to or during deposition of the borate-host sediments. Around the northern fringes of the basin are outcrops of rhyolite and dacite sheets, as well as mafic lava flows. The acid volcanics are sometimes fine grained and sometimes porphyritic with phenocrysts of plagioclase, K-feldspar, quartz, biotite and amphibole, with common spherulites in the matrix. Rhyolite clasts in basin sediments indicate that this acid phase of volcanism was active prior to the deposition of cherty limestone units in the Sarikaya Formation. The mafic lavas contain phenocrysts of plagioclase, olivine and clinopyroxene in a matrix of feldspar needles. These lavas post-dated deposition of the cherty limestone beds in the Sarikaya Formation. Hence, the evolution from acid to more mafic magmatism is also present at Kirka and it appears that the acid magmatism is once again in a close temporal position to the deposition of borate-host sediments. To the south of Kirka Basin, around the town of Afyon, intermediate-basic volcanism is aged between the acidic and mafic volcanic phases of Kirka Basin.

Hence, magmatism had a significant influence on the mineralogy of sediments in both basins. Volcanoclastic sediments deposited prior to and during deposition of the borate-host sediments contain textures and mineralogy consistent with a derivation from acidic magmatism. The volcanic stratigraphies of these basins and hence the temporal position of volcanism relative to borate mineralisation will be further constrained in the next chapter using mineral chemistry, K-Ar dating and whole rock geochemistry. The effect of this large acid magmatic input into the sediments on the formation of clays and borate minerals is considered in Chapter 4.

## 3 TIMING OF MAGMATISM RELATIVE TO DEPOSITION OF BORATE-HOST SEDIMENTS

### 3.1 INTRODUCTION

Field and mineralogical information discussed in the previous chapter indicates that acid magmatism in both Emet and Kirka Basins was related in space and possibly in time to the deposition of the borate-host sediments. In this chapter, geochemical data on granitic, volcanic and volcanoclastic rocks are presented, with a view to further constraining information from Chapter 2 on the timing of magmatism relative to the deposition of these sediments. Three approaches have been taken:

- (i) Isotopic dating of igneous rocks to provide absolute ages of magmatism in the area.
- (ii) The concentrations of 'immobile' elements in volcanoclastic sediments as compared with those in local granitic and volcanic rocks.
- (iii) The chemical compositions of minerals in volcanoclastic sediments as compared with those of local granitic and volcanic rocks.

The major and trace element data used in this chapter was produced by XRF analysis, while mineralogical studies were carried out using the electron microprobe and XRD, all at the University of Leicester Geology Department (Appendices G, H & I).

### 3.2 CHEMICAL CLASSIFICATION OF THE MAGMATISM

The nomenclature used to describe the magmatism is that recommended by the IUGS Subcommission on the Systematics of Igneous Rocks, which involves the chemical classification of rock samples using total alkalis-silica (TAS) diagrams (LeBas et al., 1992). Chemical classification using TAS diagrams is only valid when the analysed rocks are unaltered and therefore the freshest samples were collected. However there was evidence of some alteration, and in order that the geochemical plots could be interpreted correctly, an assessment of the affects of remobilisation was made.

#### 3.2.1 Alteration and Element Mobility

Table 3.1 provides a summary of the affects of alteration and recrystallisation in all the samples collected for igneous petrogenetic studies. With the exception of very minimal replacement of biotite by chlorite, samples collected from the Erigöz Granite are largely unaltered and hence are not included in the Table 3.1. As mentioned in the preceding chapter, ignimbrite and rhyolite from the Emet and Kirka areas show signs of recrystallisation; the ignimbrite has been largely devitrified with very little fresh glass remaining, and some of the rhyolites contain abundant spherulites in their matrices.

XRD studies on ignimbrite samples from south of Kirka Basin revealed the presence of small amounts of the clays smectite and illite (Table 3.1, Appendix G). The formation of these clays may have led to changes in the bulk chemistry of the ignimbrite. Electron microprobe studies were carried out on the ignimbrite in an attempt to determine the mode of formation of these clays, but analyses of pure smectite or illite were not obtained (Figure 3.1a). Pumice and glass shards from the ignimbrite have a composition close to that of illite while the matrix contains rare aggregates of a clay with the

**FIGURE 3.1a - Composition of glass in Ignimbrite south of Kirka Basin**

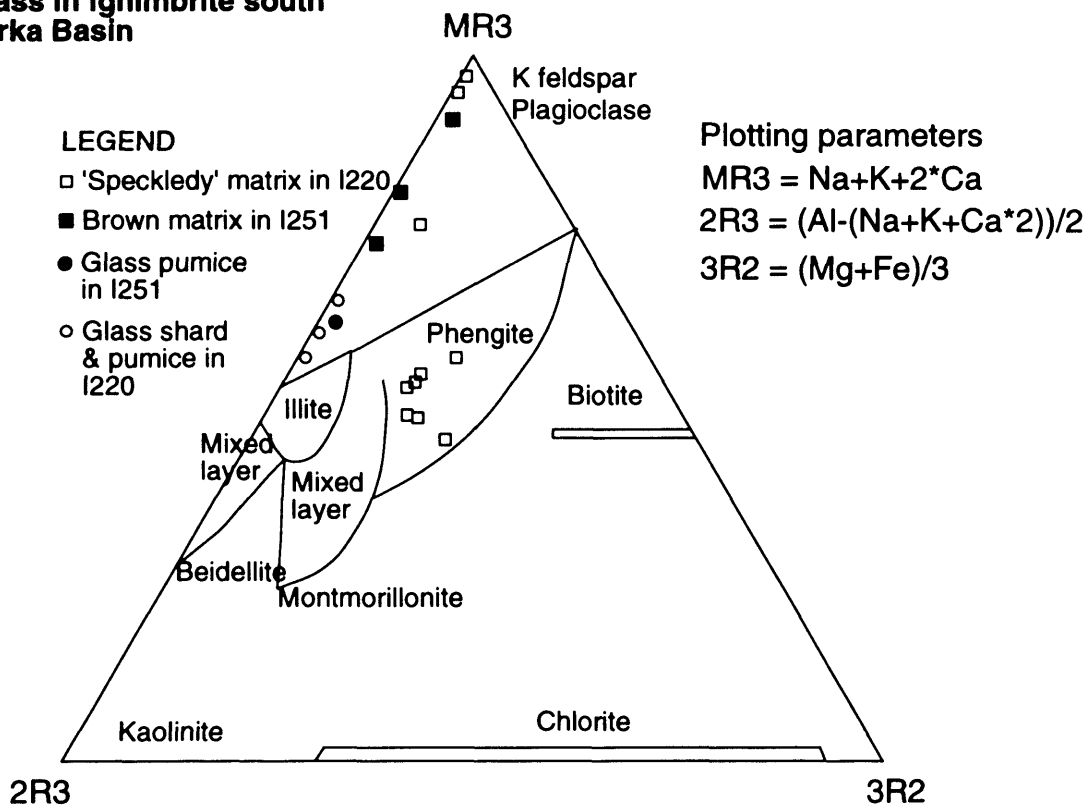
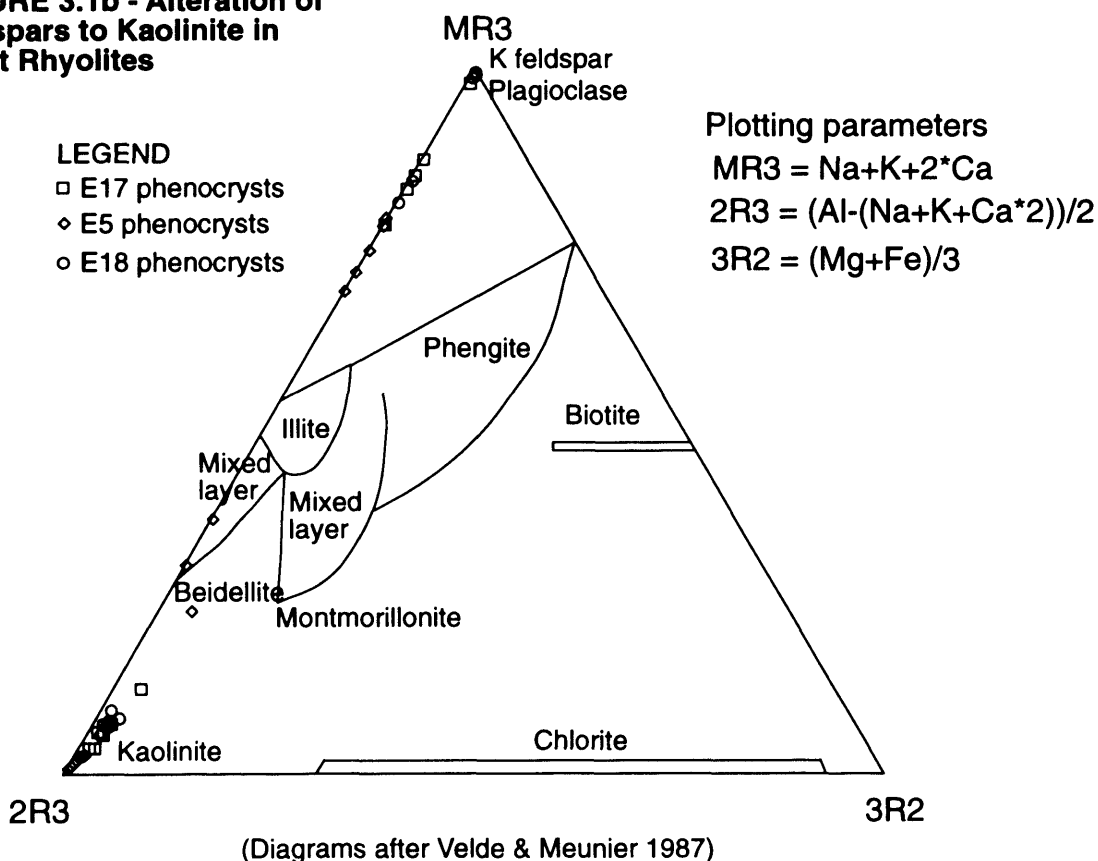


**FIGURE 3.1b - Alteration of feldspars to Kaolinite in Emet Rhyolites**



## Timing of magmatism relative to deposition of borate-host sediments

composition of phengite (Figure 3.1a), perhaps indicating partial alteration of volcanic glass towards smectite or illite compositions.

**Table 3.1 - Summary of alteration and recrystallisation in collected volcanic rock samples from the Emet and Kirka areas**

Rock Type	Locality & sample numbers	Alteration & recrystallisation affects	
Ignimbrite	I 208, 209, 219, 220, 221, 222, 250, 258, 259, 260, 271 (Within and to the south of Kirka Basin)	Matrix has been largely devitrified, little fresh glass remains.	
	I 219, 221, 250, 258 (Within and to the south of Kirka Basin)	XRD traces indicate the presence of smectite and illite.	
	I220 & 251 (South of Kirka Basin)	Microprobe analyses reveal clays with a composition of phengite in the matrix and glass shards and pumice with a composition close to illite.	
Rhyolites & Dacites	E 1,2 (Emet Basin) UG 28, 29 (Usak/Güre Basin) K 229, 230, 231, 232, 246, 247 (Kirka Basin)	Matrix is largely composed of spherulites. XRD revealed minor smectite in E 1 and 2	
	E 5, 6, 16, 17, 18, 19 (Emet Basin) K235 (Kirka Basin)	Contain 'speckledy' altered feldspars. Alteration product identified as kaolinite from XRD and microprobe analyses on E5, 16 & 18.	
	E 16 (Emet Basin) K 236, 235 (Kirka Basin) UG 63, 66, 67, 75 (Usak/Güre Basin)	Contain altered biotites with a dark brown 'blotchy' colouration.	
Andesites & Basaltic andesites	E 3, 4, 68 (Emet Basin) A 200, 205, 210, 213, 215, 218 A 248, 254 (Afyon area)	Biotites contain dark reaction rims. Microprobe analyses of these rims in E 4 & 68 indicates that they are Fe rich.	
	Silicified rock (alteration within rhyolite)	E 22 (northern Emet Basin)	Recrystallised quartz and Fe - oxides
	Alunite (altered rhyolite?)	SE 71 (Saphane - south of Emet Basin)	XRD trace reveals that the sample is largely composed of alunite & quartz.

Some of the rhyolites from Emet and Kirka contain altered feldspars. Electron microprobe analyses of this characteristically speckledy alteration product reveal that it is dominantly composed of kaolinite (Figure 3.1b), as do whole rock XRD analyses (Table 3.1). It is likely that the microprobe data (Figure 3.1b) represent an alteration trend from feldspar to kaolinite. The alteration of feldspar to kaolinite has been well documented (Velde 1992) and it results in the loss of Na and K. Further evidence of acid alteration in the rhyolite can be found to the south of the Emet Basin around the town of Saphane, with the presence of alunite and quartz, and in northern part of the basin, near Yagcık, with a small zone of silicification. XRD analysis of the rhyolite from Köprücek in the north of the Emet Basin shows that minor smectite is present, probably the result of alteration of volcanic glass.

In rhyolite through to basaltic andesite samples, biotite phenocrysts often appear altered. In the rhyolites the alteration appears dark brown and uneven, whilst in the more mafic lavas, distinct dark rims are observed around the biotite crystals. Electron microprobe analyses indicate that these rims are highly enriched in Fe, slightly enriched in Na, and highly depleted in Mg and K, relative to unaltered

biotite. The rims, whether produced by oxidation processes within magmas or near surface hydrothermal alteration, have possibly therefore resulted in subtle changes in the bulk chemistry of these rocks.

Hence, in the acid volcanics, devitrification, alteration of feldspars and glass to clays, and the alteration of biotites, may have led to subtle changes in the bulk chemistry of these rocks. In the more mafic samples, biotite alteration appears to be the only effect likely to change whole rock geochemistry. Figures 3.2-3.5 show a series of immobile and potentially mobile elements plotted against the highly incompatible and immobile element Zr, which is often used to monitor fractionation in igneous rock suites. Deviations from fractionation trends in these plots should indicate to what extent alteration and devitrification processes have mobilised certain elements (MacLean & Barrett 1993).

The High Field Strength Elements (HFSE) Ti and P are generally considered immobile during hydrothermal alteration and weathering processes (Floyd & Winchester 1975, Smith & Smith 1976, Finlow-Bates & Stumpfl 1981). Figures 3.2-3.5 show a strong correlation between  $\text{TiO}_2$  and  $\text{P}_2\text{O}_5$  in all the rock suites owing to fractionation and an absence of secondary mobilisation of these elements. The Light Rare Earth Elements (LREE), such as Nd are also often immobile during hydrothermal alteration (Tarney & Marsh 1991), although there are some records of their mobilisation (MacLean 1988). Rock suites in this study (Figures 3.2-3.5) suggest that Nd was immobile, following a similar fractionation trend to Ti and P against Zr. In the Simav/Selendi/Usak-Güre and Afyon suites (Figures 3.3 & 3.5), K and Rb follow the same fractionation trend, whilst in the Emet and Kirka suites (Figures 3.2 & 3.4), the rhyolites show a wide spread in values of these elements. This variation in Rb and K in the rhyolites could be the result of magmatic processes, such as crustal contamination, but the presence of altered feldspars and spherulites in these rocks strongly suggests that secondary remobilisation of these elements was caused by near surface weathering and recrystallisation. Interestingly, Na behaves in the opposite manner to K and Rb suggesting that the alteration may have caused alkali exchange in these rocks. Ba and Th show considerable variation against Zr in all the rock suites (Figures 3.2-3.5), but these variations do not correlate with K and Rb. Whether or not this variation is the result of magmatic processes or near surface alteration is not possible to ascertain.

Loss on ignition (LOI) values determined when samples are heated to drive off volatile components is often a good index of hydrothermal alteration (Tarney & Marsh 1991). Samples with higher LOI values are generally believed to be more altered. Most of the samples collected for this igneous petrogenetic study had an LOI value of < 3 % (99 % of samples) and many < 1 % (41 % of samples), suggesting minimal alteration. There is no correlation between Ti, K and Na concentrations and LOI for the Emet suite (Figure 3.6).

### 3.2.2 Nomenclature

Due to the apparent mobility of alkalis in a number of the Emet and Kirka Rhyolites, caution was taken when classifying these rocks on TAS diagrams. However, with the less evolved rocks, classification into alkaline and subalkaline groups was possible, because the alkalis have probably not been mobilised. Table 3.2 provides names for the igneous rock types present in this area while the



**FIGURE 3.2 - Volcanic and granitic samples from the Emet area**

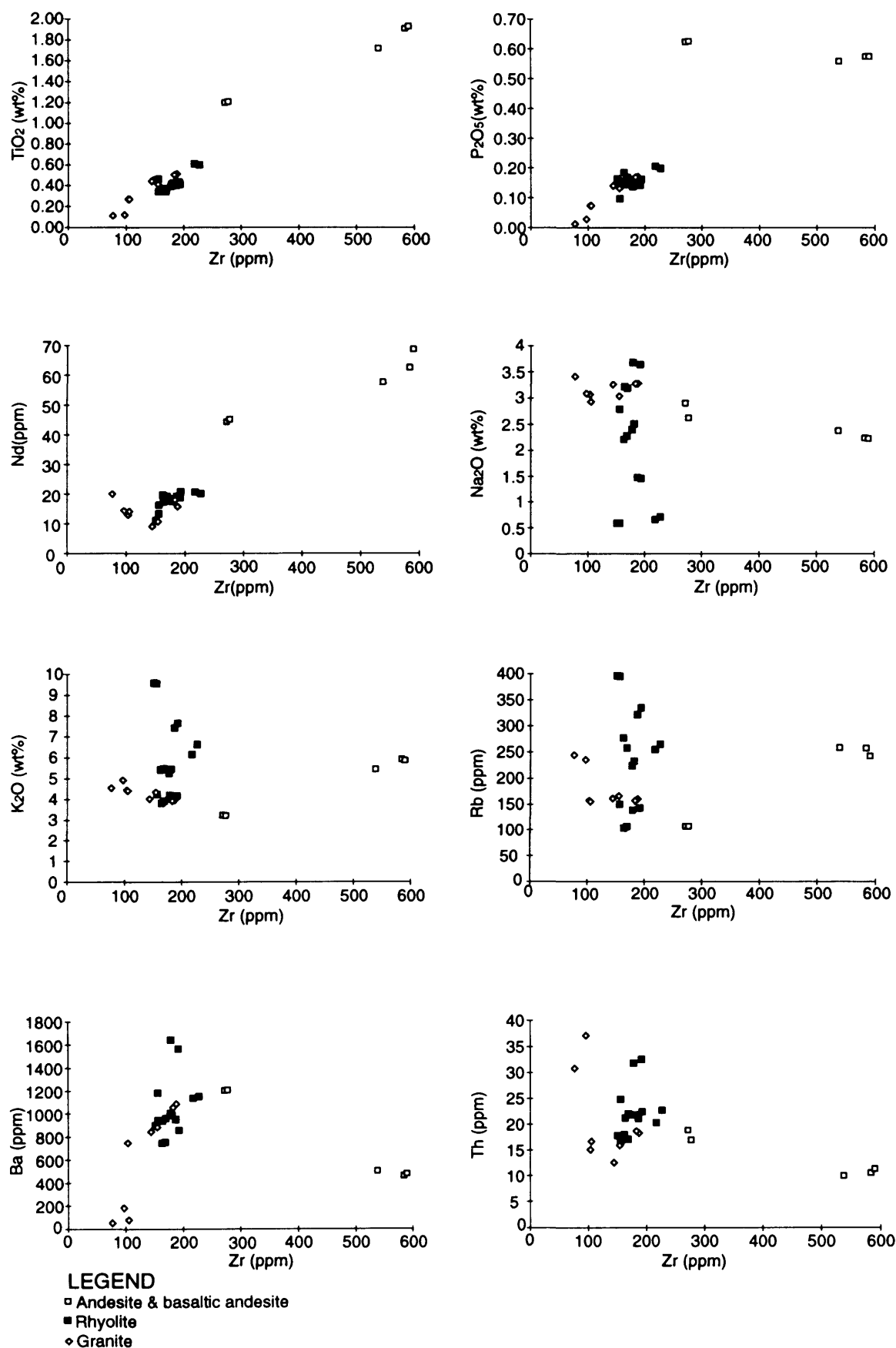


**Figure 3.2**

**FIGURE 3.3 - Volcanic samples from the areas to the south and west of Emet Basin (Simav, Selendi, Usak areas)**

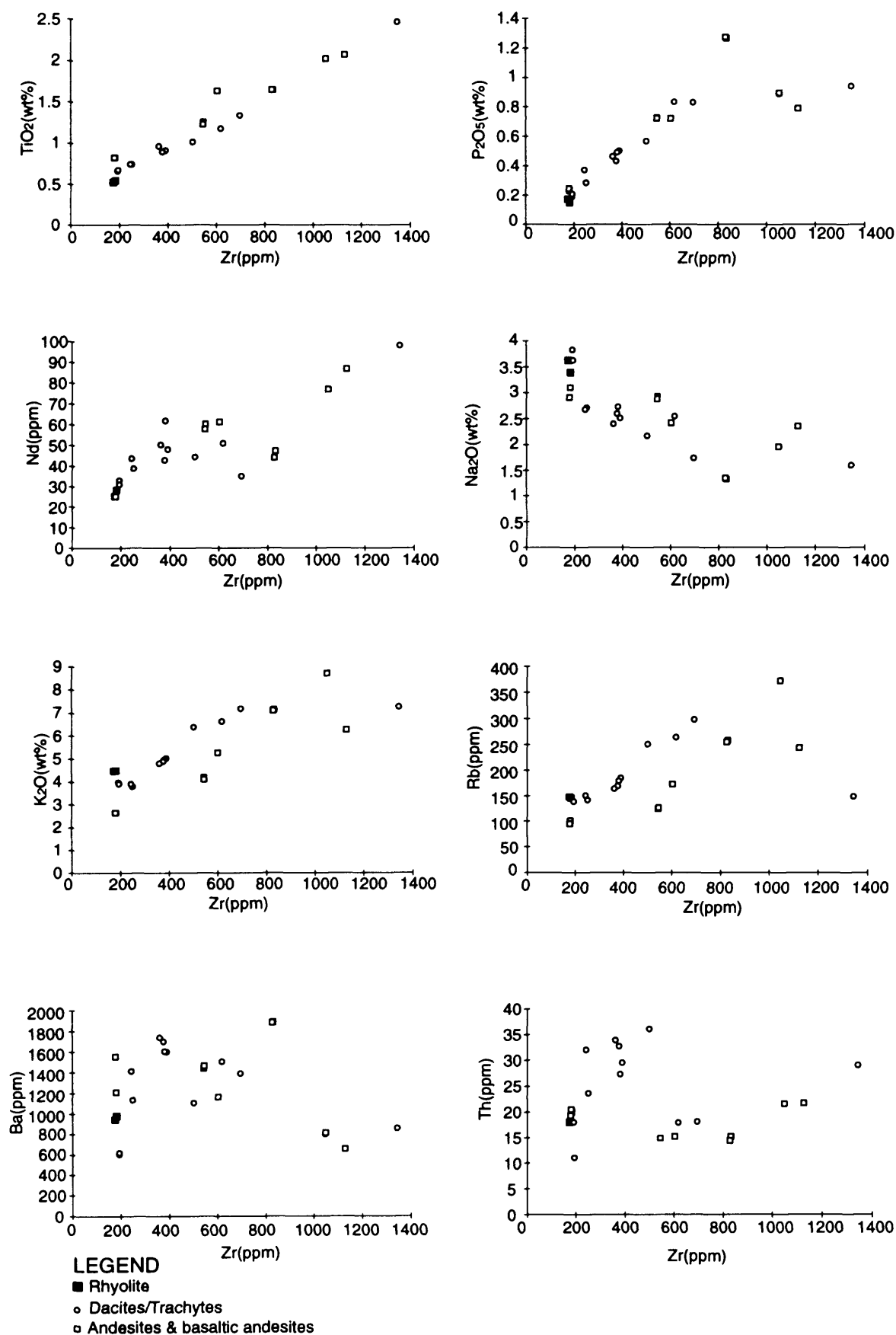


**Figure 3.3**

FIGURE 3.4 - Volcanic samples from the Kirka area

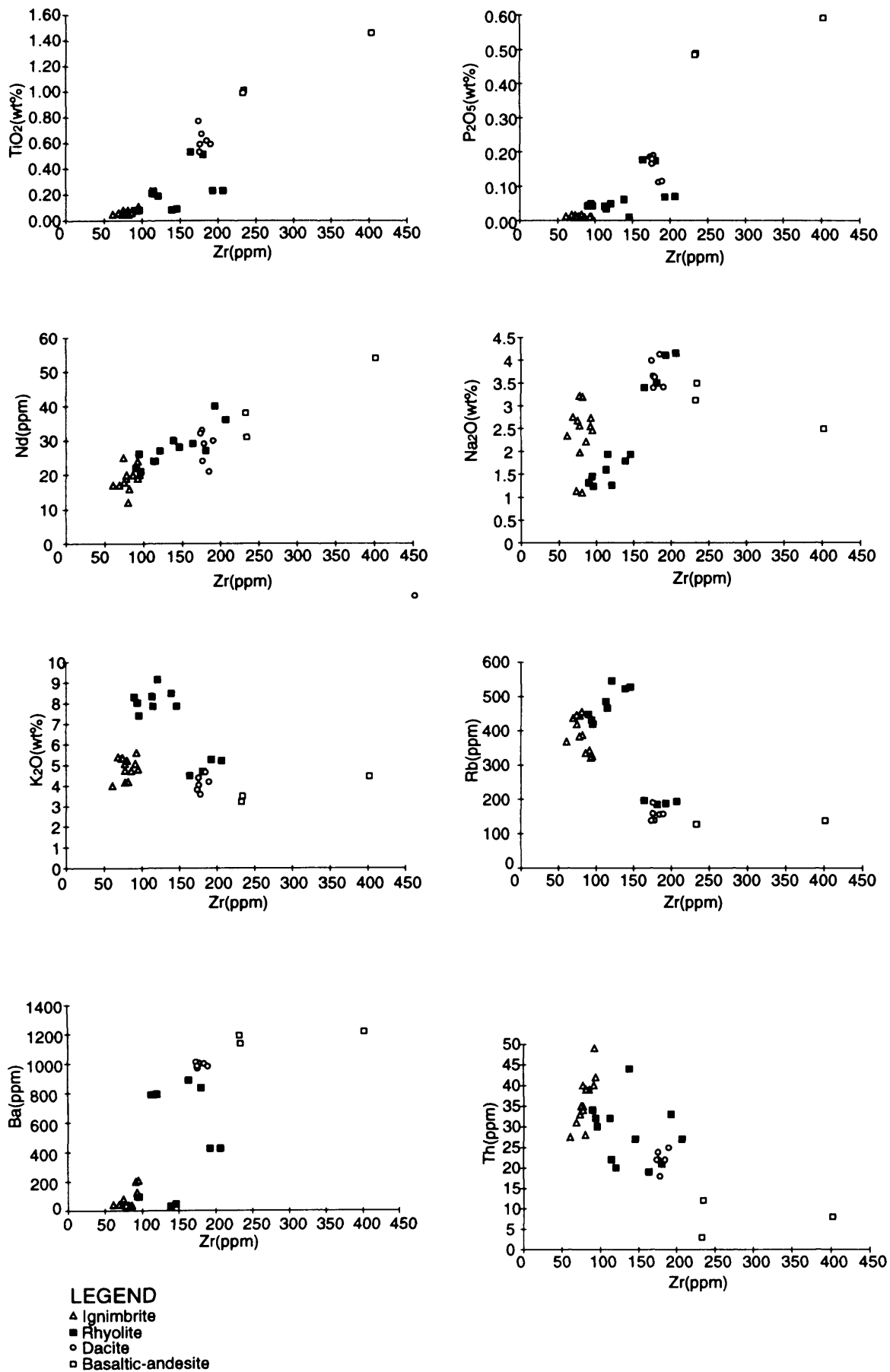
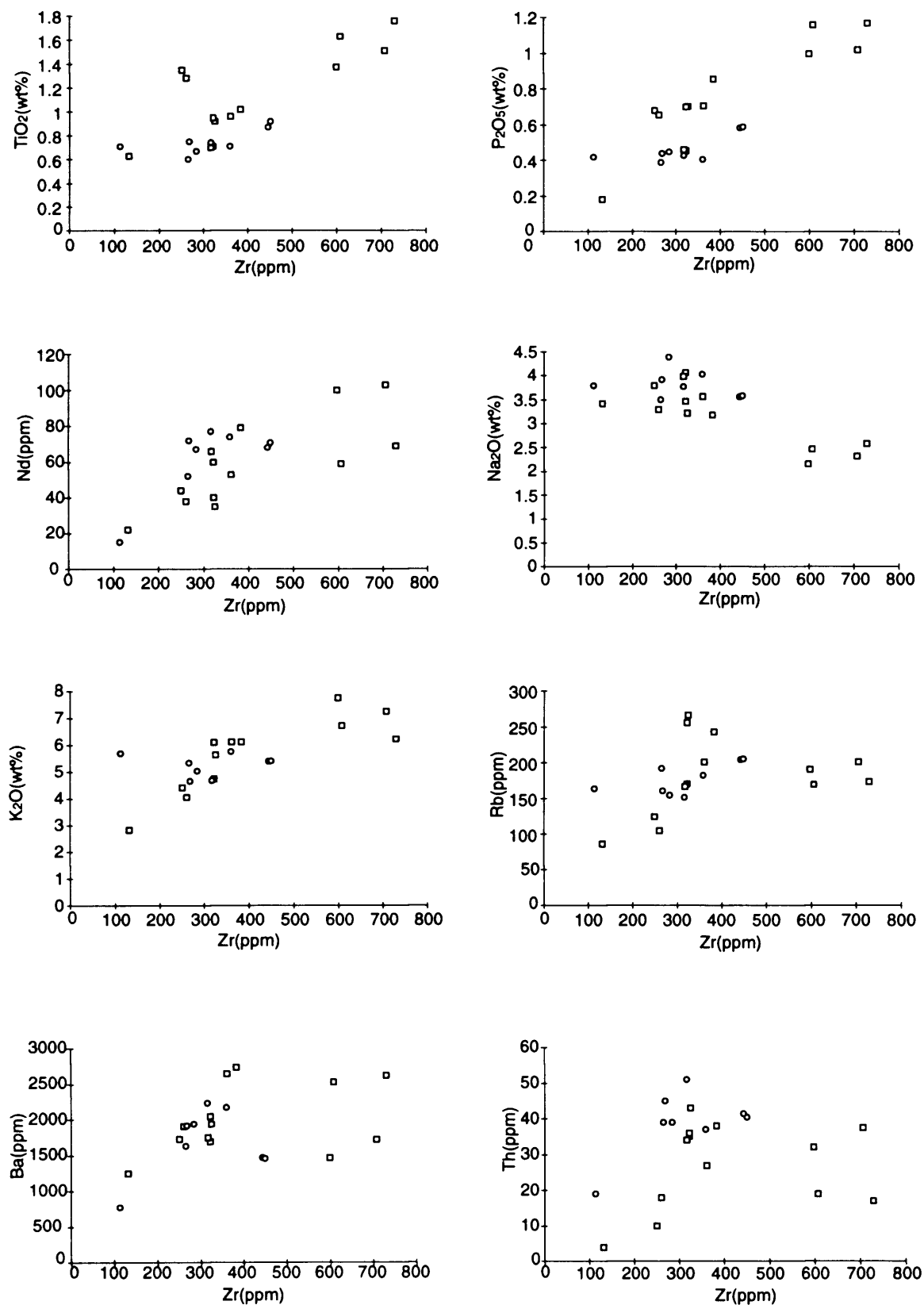


Figure 3.4

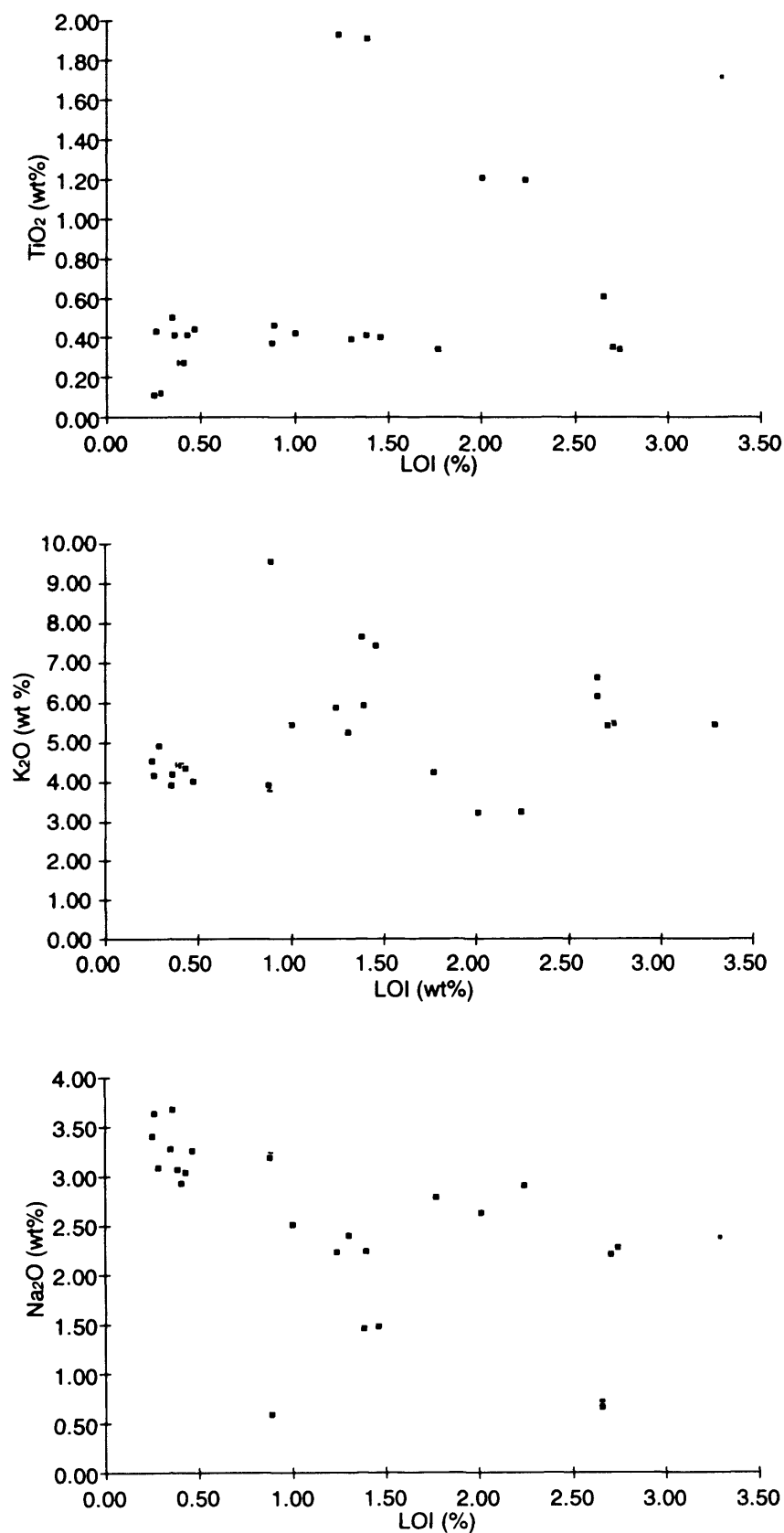
FIGURE 3.5 - Volcanic samples from the Afyon area



LEGEND

- Trachyte
- Basaltic-andesite & andesite

**FIGURE 3.6 - Relationship between loss on ignition (LOI) and selected major elements for the igneous rocks of the Emet area**



▪ Granite, rhyolite, latite & shoshonite from the Emet area

names of individual collected samples are found in Appendix D.

**Table 3.2 - Nomenclature of collected samples**

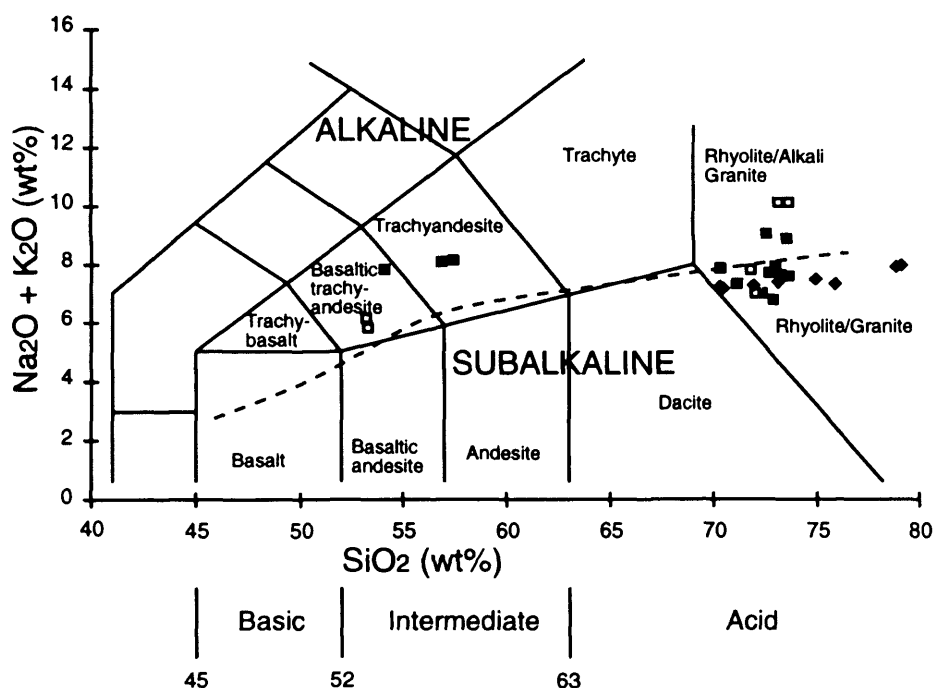
Locality	Field name	Final classification
<b>Emet area</b>		
Western margin of Emet Basin	Erığöz Granite	I Type Granite (on basis of mineralogy)
Within and on the southern margin of Emet Basin	Emet Rhyolites	Rhyolite (K rich)
Within (Dereköy) and on the southern margin (Eski Gediz) of Emet Basin	Emet Mafic Lavas	Latite & shoshonite
<b>South &amp; west of Emet area</b>		
Within Selendi Basin to the north of town of Selendi	Rhyolite	Rhyolite (K rich)
Within Selendi and Usak/Güre Basins	Dacites	Some dacites, mostly K-trachytes
Within Selendi & Usak/Güre Basins	Andesites	Some andesite, mostly latite
Within Simav Basin	Andesites	Latite
<b>Kirka area</b>		
Within & to the south of Kirka Basin	Kirka Ignimbrite	Ignimbrite (K-rich)
N Kirka Basin - Idrisyayla village	Kirka Rhyolites & Dacites	Rhyolite & trachyte (K-rich)
N & NE Kirka Basin - Idrisyayla & Sancar villages	Kirka Mafic Lavas	Shoshonite
<b>Afyon area</b>		
Afyon town & further south	Afyon Andesites and Dacites (sanidine-bearing)	Some latite, mostly K-trachyte
Throughout Afyon area	Afyon Mafic Lavas	Latite & shoshonite

The Erığöz Granite plots in the granite field (Figure 3.7) and as discussed in the previous chapter, has a mineralogy characteristic of an I type granite (Chappell & White 1974). The Emet Rhyolites and the rhyolite from north of Selendi, plot in the rhyolite field but due to the mobility of their alkalis it is not possible to discriminate between alkaline or subalkaline types. The Emet mafic lavas plot as basaltic trachyandesite and trachyandesite (Figure 3.7), and using the IUGS approved classification of Le Bas et al. (1992), they can be further divided into shoshonite and latite respectively where  $\text{Na}_2\text{O} - 2 < \text{K}_2\text{O}$ . Shoshonite is also found on the southern margin of the Emet Basin, north-east of Eski Gediz; dacite, K-trachyte, andesite and latite are found within the Selendi and Usak-Güre Basins, while latite is found in the Simav Basin (Table 3.2, Figure 3.7).

The ignimbrite and rhyolite of the Kirka area are also K-rich but again potential mobility of the alkalis renders characterisation of these rocks as alkaline and subalkaline impossible. The Kirka mafic lavas plot in the basaltic andesite field (Figure 3.8) and are therefore shoshonites. The sanidine bearing volcanics from the Afyon area comprise some latites but are mostly K-trachytes (Table 3.2, Figure 3.8). As shown in the previous section, there is no evidence of remobilisation of the alkalis in these volcanics and they can be assigned as K-trachyte (after Cox et al., 1979). The lavas from around Afyon with a more mafic appearance are latites and shoshonites (Table 3.2, Figure 3.8). On an AFM diagram (Figure 3.9 & 3.10) the Usak-Güre, Selendi, Emet, Kirka and Afyon (USEKA) suites all plot as calc-alkaline.

**FIGURE 3.7**

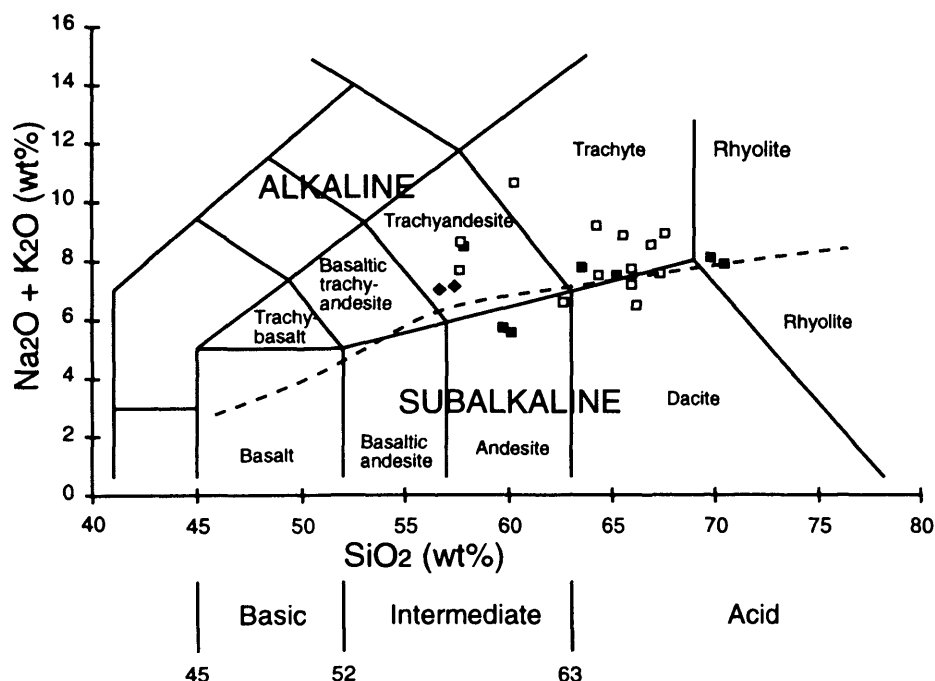
**Alkali-silica plot for magmatism of the Emet area**



**LEGEND**

- Volcanics from the southern margin of Emet Basin
- Volcanics from within Emet Basin
- ◆ Erigöz Granite

**Alkali-silica plot for magmatism to the south and west of Emet Basin (Simav, Selendi & Usak/Güre areas)**



**LEGEND**

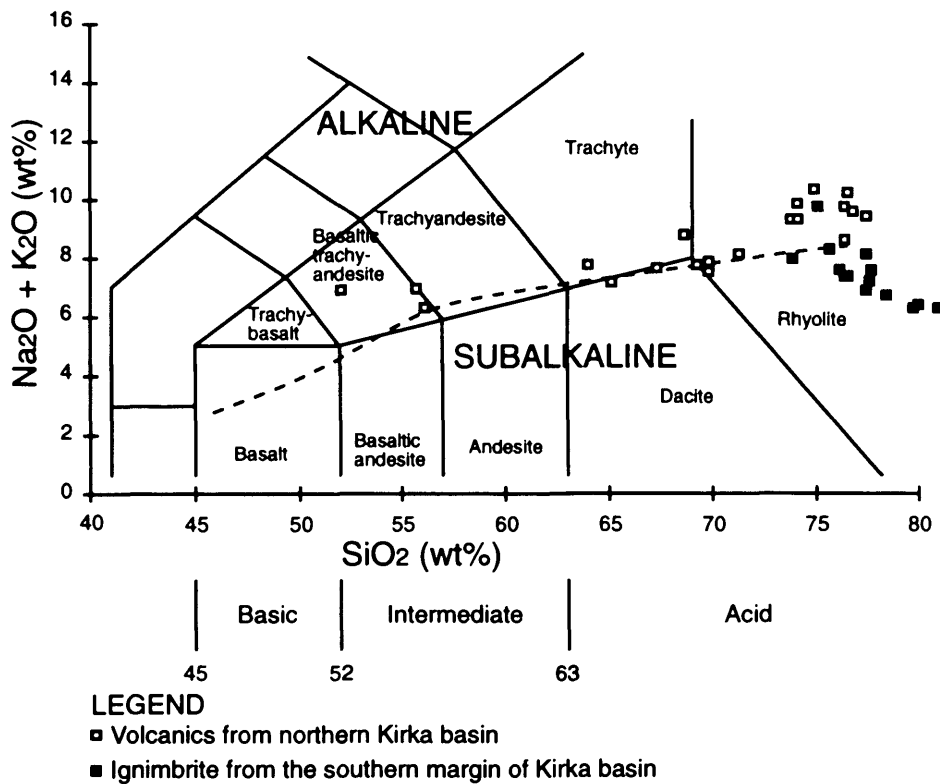
- Volcanics from Usak-Güre Basin
- Volcanics from Selendi Basin
- ◆ Volcanics from Simav Basin
- K-rich Trachyandesite = Latite
- K-rich Basaltic Trachyandesite = Shoshonite

Classification from Le Maitre et al., 1989  
Alkaline and subalkaline division from Kuno 1966

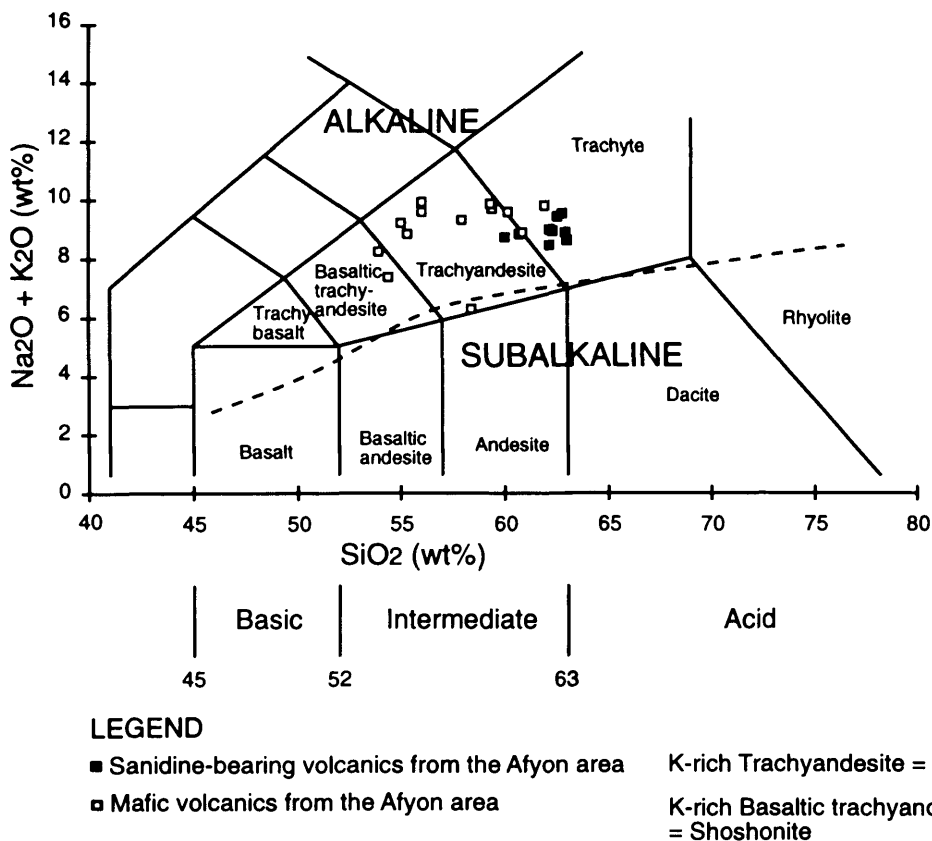


**FIGURE 3.8**

**Alkali-silica plot for magmatism of the Kirka area**

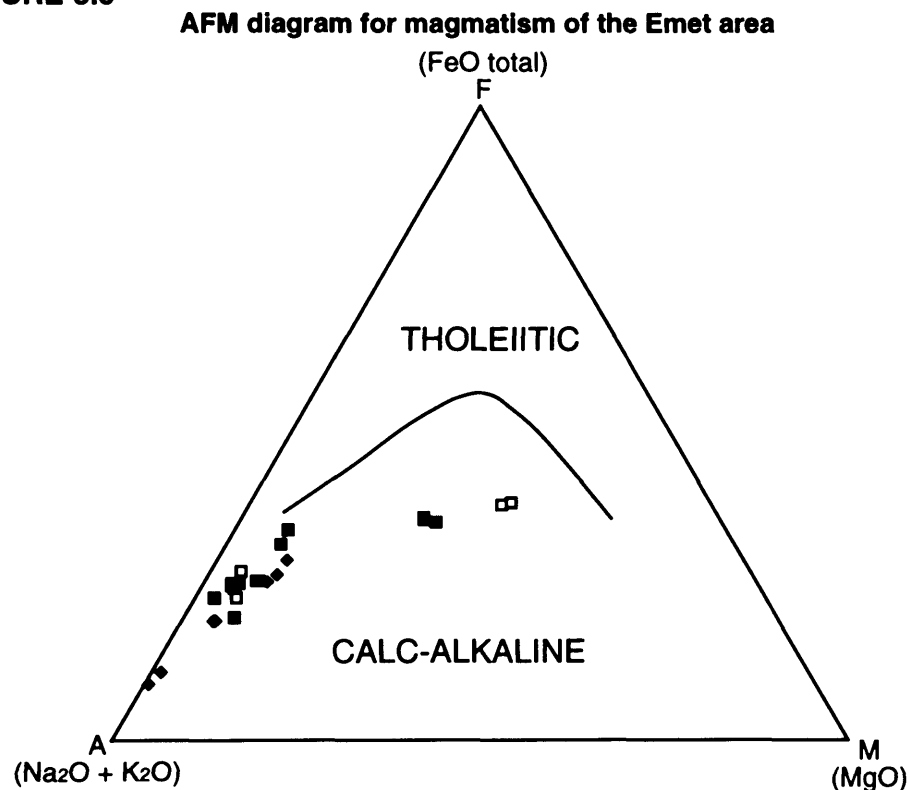


**Alkali-silica plot for magmatism of the Afyon area**



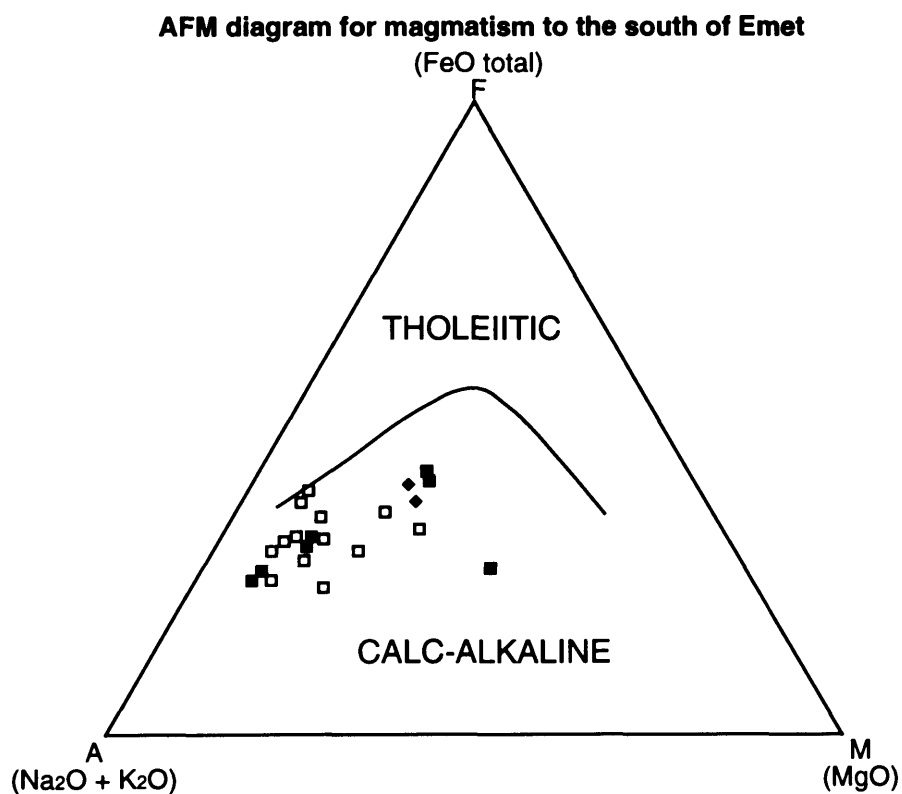
Classification from Le Maitre et al., 1989  
Alkaline and subalkaline division from Kuno 1966

**FIGURE 3.9**



**LEGEND**

- ◆ Granite
- Volcanics within Emet Basin
- Volcanics from southern margin of Emet Basin

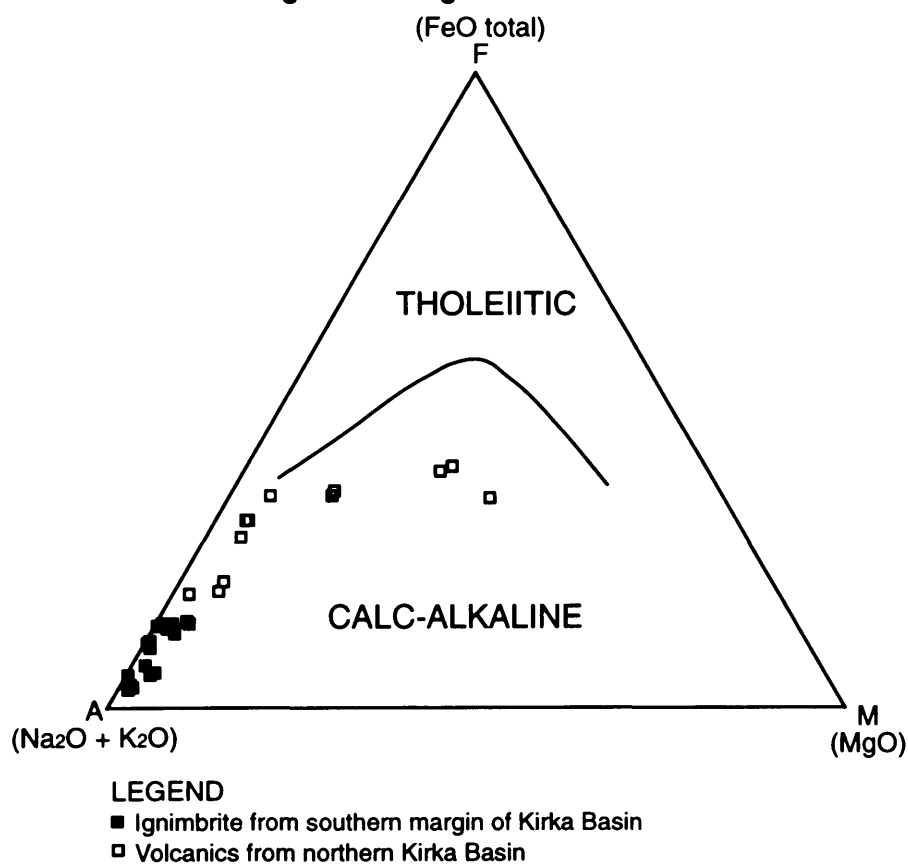


**LEGEND**

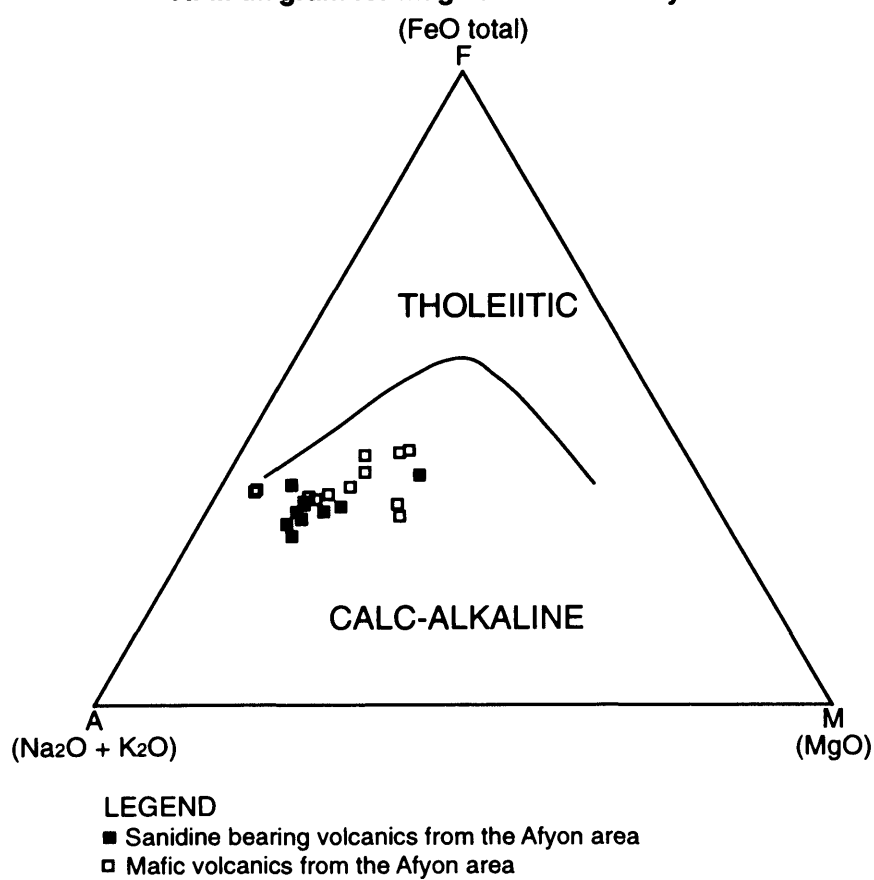
- ◆ Volcanics from Simav Basin
- Volcanics from Selendi Basin
- Volcanics from Usak-Güre Basin

(Dividing line after Irvine & Barager 1971)

**FIGURE 3.10** AFM diagram for magmatism of the Kirka area



**AFM diagram for magmatism of the Afyon area**



### 3.3 ISOTOPIC DATING

#### 3.3.1 Introduction

Isotopic dating provides the only absolute method of determining the timing of magmatism in this area. Prior to this project, igneous rocks from the Usak-Güre, Selendi and Emet (USE) area had not been isotopically dated, with the exception of the Erigöz Granite (Late Oligocene to Early Miocene - Bingöl et al., 1982) and the Kula lavas (Late Miocene to Quaternary - Ercan et al., 1985). In the Kirka and Afyon areas, K-Ar dates were available for a number of volcanic rocks and related sediments (Besang et al., 1977, Yalçın 1989), but prior to the current project, the Kirka Ignimbrite had not been isotopically dated. Therefore, in the course of this project, isotopic dating (K-Ar and  $^{40}\text{Ar}/^{39}\text{Ar}$ ) was carried out on a number of the USE igneous rocks and on the Kirka Ignimbrite. The K-Ar dates obtained in this study for granitic and volcanic rocks from the USE area have been published by Seyitoglu, Anderson, Nowell and Scott (1997).

Dating was carried out on separated biotites from the more acid volcanics and on whole rock fractions from the finer grained mafic rocks. Although evidence discussed earlier indicated remobilisation of the alkalis in the Emet Rhyolites, by the alteration of feldspars and devitrification of glass, the biotites selected were unaltered and therefore the age produced should accurately represent the time of their crystallisation. Ages for igneous rocks of the USEKA area are given in Table 3.3, and procedural details are given in Appendices E and F. K-Ar dating was carried out at the NERC Isotope Geoscience Laboratories and  $^{40}\text{Ar}/^{39}\text{Ar}$  dating at the Geology Department, University of Leeds.

**Table 3.3 - K-Ar and  $^{40}\text{Ar}/^{39}\text{Ar}$  ages for igneous rocks from the Emet, Selendi, Usak-Güre, Kirka and Afyon areas**

Sample	Locality	Dating system & material dated	Age (Ma)
<b>Dating from this study</b>			
E 1 (Rhyolite)	Northern Emet Basin	K-Ar (Biotite separate)	20.2 ( $\pm 0.4$ )
E 6 (Rhyolite)	Southern Emet Basin	K-Ar (Biotite separate)	20.3 ( $\pm 0.6$ )
E 3 (Latite)	Southern Emet Basin	K-Ar (Whole rock)	14.9 ( $\pm 0.3$ )
G 5 (Granite)	Western margin Emet Basin	K-Ar (Biotite separate)	17.7 ( $\pm 1.3$ )
G 8 (Granite)	Western margin Emet Basin	K-Ar (Biotite separate)	20.5 ( $\pm 0.6$ )
SE 25 (Rhyolite)	Southern margin Emet Basin	K-Ar (Biotite separate)	20.0 ( $\pm 0.6$ )
SE 1 (Rhyolite)	Selendi Basin	K-Ar (Biotite separate)	18.9 ( $\pm 0.6$ )
SE 3 (K-Trachyte)	Selendi Basin	K-Ar (Biotite separate)	14.9 ( $\pm 0.6$ )
SE 12 (Andesite)	Northern Selendi Basin	K-Ar (Whole rock)	16.8 ( $\pm 0.7$ )
UG 28 (Rhyolite)	Southern margin Emet Basin	K-Ar (Biotite separate)	17.6 ( $\pm 1$ )
UG 58 (K-Trachyte)	Usak-Güre Basin	K-Ar (Whole rock)	15.1 ( $\pm 0.4$ )
UG 63 (K-Trachyte)	Usak-Güre Basin	K-Ar (Whole rock)	14.6 ( $\pm 0.3$ )
UG 75 (K-Trachyte)	Usak-Güre Basin	K-Ar (Whole rock)	15.9 ( $\pm 0.4$ )
UG 142 (K-Trachyte)	Usak-Güre Basin	K-Ar (Whole rock)	15.2 ( $\pm 0.6$ )
UG 145 (Latite)	Usak-Güre Basin	K-Ar (Whole rock)	15.5 ( $\pm 0.4$ )
I 219 (Ignimbrite)	South of Kirka Basin	$^{40}\text{Ar}/^{39}\text{Ar}$ (Biotite separate)	18.6 ( $\pm 0.5$ )

**Previous dating:** (i) Bingöl et al. 1982 - Erigöz granite (20-20.4 $\pm$ 0.7 Ma - Biotite separate, 21.2-24.6 $\pm$ 1.8 Ma - orthoclase separate), (ii) Yalçın 1989 - Volcanics from Kirka basin; Türkmençay basalt (9.3 $\pm$ 1 Ma - whole rock), Idrisyayla andesite (15.4 $\pm$ 1.7 Ma - Biotite separate), Idrisyayla rhyolite (15.7 $\pm$ 1.1 & 16.7 $\pm$ 0.5 Ma - whole rock), Karaören Formation tuff (17.8 $\pm$ 0.6 Ma - Biotite separate), Sarıkaya Formation tuff (17.5  $\pm$ 0.6 Ma - Biotite separate), (iii) Besang et al. 1977 - lavas from around Afyon (8.6 - 14.7 Ma).

### 3.3.2 The Usak-Güre, Selendi and Emet area

Volcanics in the Usak-Güre, Selendi and Emet (USE) area evolved from Early Miocene rhyolites to Middle Miocene K-trachytes and latites (Table 3.3). Rhyolites dated from the Emet Basin range in age from 20.2 to 20.3 Ma, while rhyolites on the southern margin of the basin have an age of 17.6 to 20 Ma. The rhyolite dated in the Selendi Basin has an age of 18.9 Ma and hence the rhyolitic volcanism of the USE area was restricted to the Early Miocene. The Erigöz Granite also has an Early Miocene cooling age, 17.7 Ma in the southern part of the pluton, and 20.5 Ma midway along the length of intrusion. These two ages could indicate two separate phases of intrusion, although the age from the southern granite has a large error of 1.3 Ma. These granite ages are similar to those obtained by Bingöl et al. (1982) on biotite separates. All these dates indicate that the granite and the rhyolites of the Emet area were part of the same overall magmatic event. In contrast, the K-trachytes of Selendi and Usak-Güre Basins are slightly younger with Middle Miocene ages, ranging from 14.6 to 15.9 Ma (Table 3.3). Latites from Emet Basin and from Usak-Güre Basin also fall in the Middle Miocene range, from 14.9 to 15.5 Ma (Table 3.3).

Field and mineralogical information, discussed in the previous chapter, are compatible with the isotopic evidence. The combined evidence suggests that the Erigöz Granite pre-dated most sedimentation in Emet Basin, the rhyolitic volcanism occurred prior to and/or during deposition of the mineralised sediments and the latite/shoshonite volcanism occurred after deposition of the borate-host sediments. Biotites from volcanoclastic sediments in the Red and Borate Formations were not used for dating, due to alteration and the difficulty in separating them from white micas of non-igneous derivation.

### 3.3.3 The Kirka and Afyon areas

In the Kirka and Afyon areas, there was also an evolution from acid volcanism in the Early Miocene through to less evolved volcanism in the Middle Miocene (Table 3.3). The rhyolites dated from the Idrisyayla area (northern Kirka Basin) (Yalçın 1989) range in age from 15.7 to 16.7 Ma, and hence are slightly younger than the rhyolites from the USE area. However, these are subject to error, since Yalçın (1989) dated whole rock fractions, which may have undergone K remobilisation. Andesite from the northern part of Kirka Basin has a K-Ar biotite age of 15.4 Ma, while the Kirka shoshonite however was dated at 9.3 Ma, significantly younger than the acid volcanism (Yalçın 1989). Published ages for trachyte, latite and shoshonite from the Afyon area are mostly intermediate between the rhyolite and shoshonite of the Kirka area (Besang et al., 1977 - 8.6 to 14.7 Ma).

Field and mineralogical information discussed in the previous chapter indicated that the acid (rhyolite and ignimbrite) volcanism was active prior to and/or during deposition of the borate hosting Sarıkaya Formation in Kirka Basin, while the shoshonite volcanism probably post-dated deposition of these sediments. The information from isotopic dating is clearly consistent with these observations. The oldest dates obtained by Yalçın (1989) are from biotite separates in the volcanoclastic sediments of the Karaören and Sarıkaya Formations, which are aged 17.8 ( $\pm 0.6$  Ma) and 17.5 ( $\pm 0.6$  Ma) respectively. Providing these biotites have not been altered, the dates represent the time this mineral crystallised.

The ages are within errors of the  $^{40}\text{Ar}/^{39}\text{Ar}$  age obtained in this study for ignimbrite south of Kirka Basin ( $18.6 \pm 0.5$  Ma - Table 3.3). It is possible therefore that the biotite dated in the Karaören and Sarikaya Formations by Yalçın (1989) originated from the nearby ignimbrite, which is expected as it has already been demonstrated that much of the Karaören Formation comprises ignimbrite-derived material. It should be noted that the biotite in the Karaören and Sarikaya sediments might also have been derived from the Kirka Rhyolite and Dacite, but separated biotites from these acid volcanics have not been dated.

### 3.4 CONSTRAINTS ON VOLCANIC STRATIGRAPHY FROM IMMOBILE ELEMENTS

#### 3.4.1 Introduction

Since the volcanoclastic sediments may have been affected by saline alkaline lake fluids and diagenesis, and the granitic and volcanic rocks may have interacted with hydrothermal systems, it was decided to use immobile elements as indicators of sediment provenance. The aim was to use this information on provenance to further refine the volcanic stratigraphy of each basin, and therefore to better constrain the timing of magmatism relative to deposition of the borate-host sediments.

Studies have shown that Ti, Zr, P, Nb, Al and Y are generally immobile under conditions of low grade metamorphism and during hydrothermal alteration (Cann 1970, Pearce & Cann 1973, Smith & Smith 1976, Floyd & Winchester 1975, Finlow-Bates & Stumpfl 1981, MacLean & Kranidotis 1987, MacLean & Barrett 1993), while the REE are considered immobile during diagenesis (Fleet 1984). However, Milodowski & Zalasiewicz (1991) have recorded REE mobility during the diagenesis of mudrocks, and MacLean (1988) and Hellman et al. (1979) have described REE mobility during hydrothermal alteration and low grade metamorphism. In the light of these investigations, the current study uses P, Ti, Al, Nb, Zr, Y, Nd and Ce as potential immobile elements.

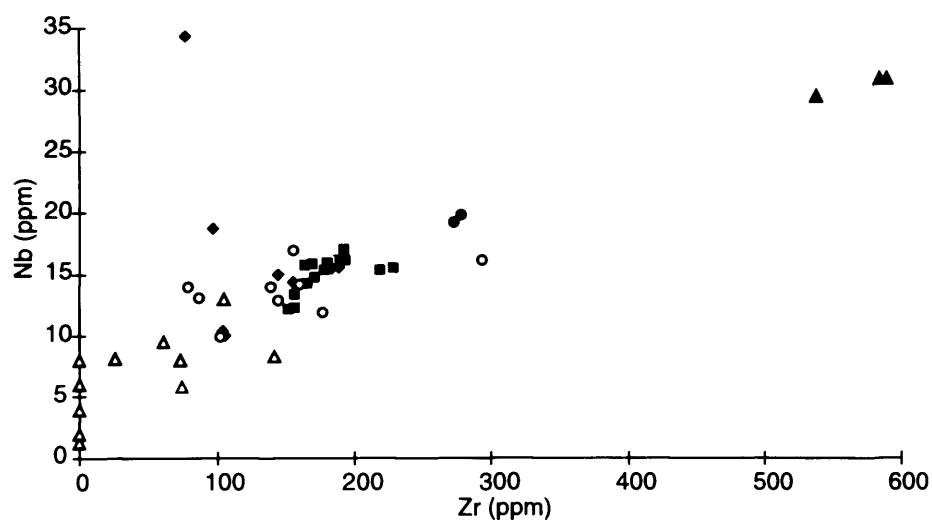
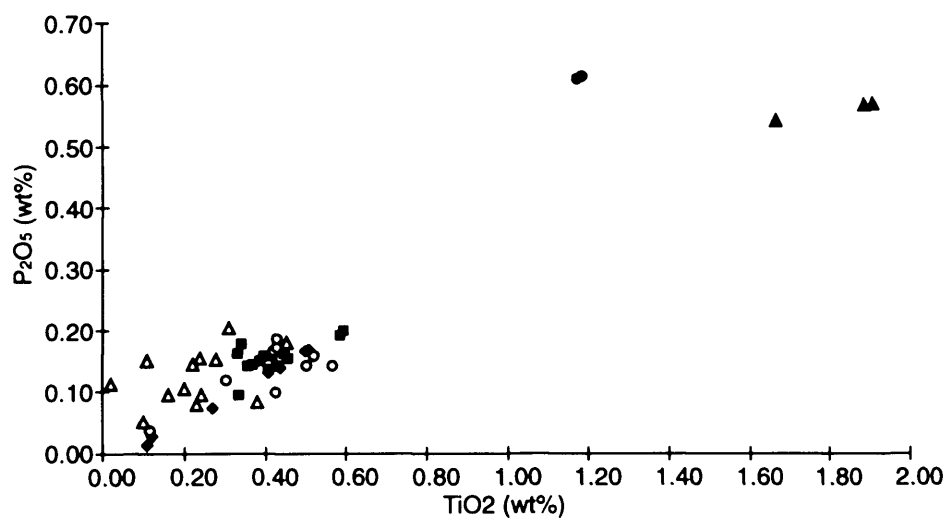
#### 3.4.2 Emet Basin

Figures 3.11 and 3.12 show the levels of immobile elements in a variety of rock types from the Emet Basin. Shoshonite and latite contain significantly higher concentrations of Zr, P, Nb, Ti and Nd than all the other volcanic related rock samples, whilst the granite, rhyolite and sediments all have broadly similar levels of most immobile elements (Figures 3.11 & 3.12). However, some of the sediments contain lower concentrations of Ti, Nb, Zr and Nd than the rhyolite and granite (Figures 3.11 & 3.12). Figure 3.13 reveals that concentrations of Ti, Al, Nb, Zr, Y and Nd decrease with increasing Ca, suggesting dilution by calcite precipitation. Figure 3.13 clearly shows that sediments with low Ca (< 5 wt %) have very similar concentrations of all the immobile elements to the rhyolite and the granite. In an attempt to remove the dilution affect,  $\text{TiO}_2/\text{Al}_2\text{O}_3$  is plotted against Nb/Y ratios (Figure 3.12), since the ratio of one immobile element to another should be unaffected by dilution (MacLean & Kranidotis 1987, MacLean & Barrett 1993). In this plot, there is definite overlap between the volcanoclastic sediments and the granite and rhyolite (Figure 3.12).

Therefore, providing Ca-rich sediments are excluded, or immobile element ratios are used, these data appear to support the contention made in the previous chapter, that the sediments of the Red



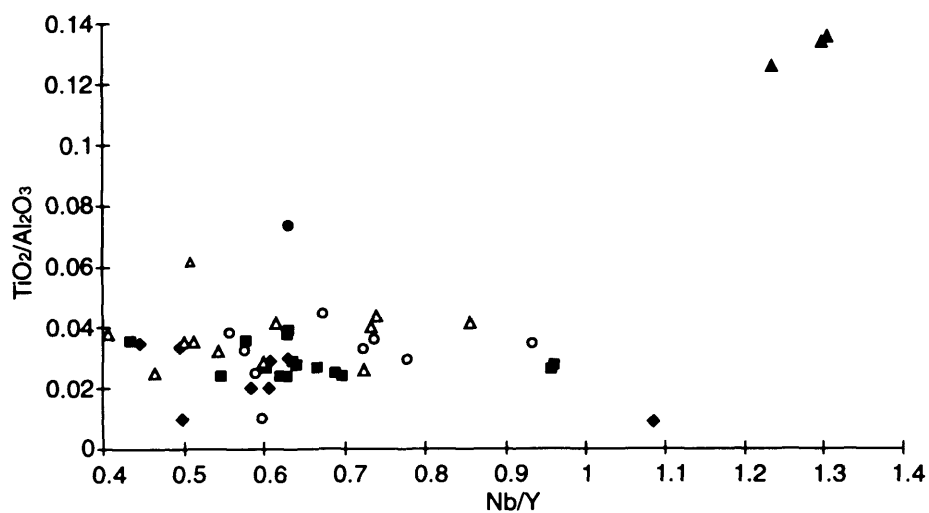
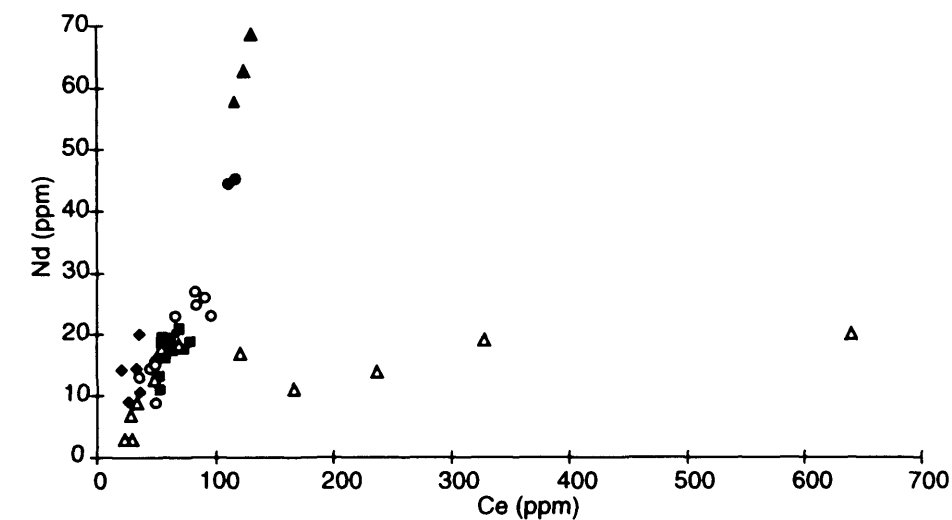
**FIGURE 3.11- Concentrations of selected immobile elements in granite, volcanics & volcanoclastic sediments from the Emet area**



#### LEGEND

- ▲ Shoshonite & latite (Emet Basin - Dereköy)
- Shoshonite (southern margin of Emet Basin)
- ◆ Granite (Erigöz)
- Rhyolite (within & southern margin of Emet Basin)
- Volcaniclastic sediments with <10wt% CaO (Red & Borate Formation)
- △ Volcaniclastic sediments with >10wt% CaO (Red and Borate Formation)

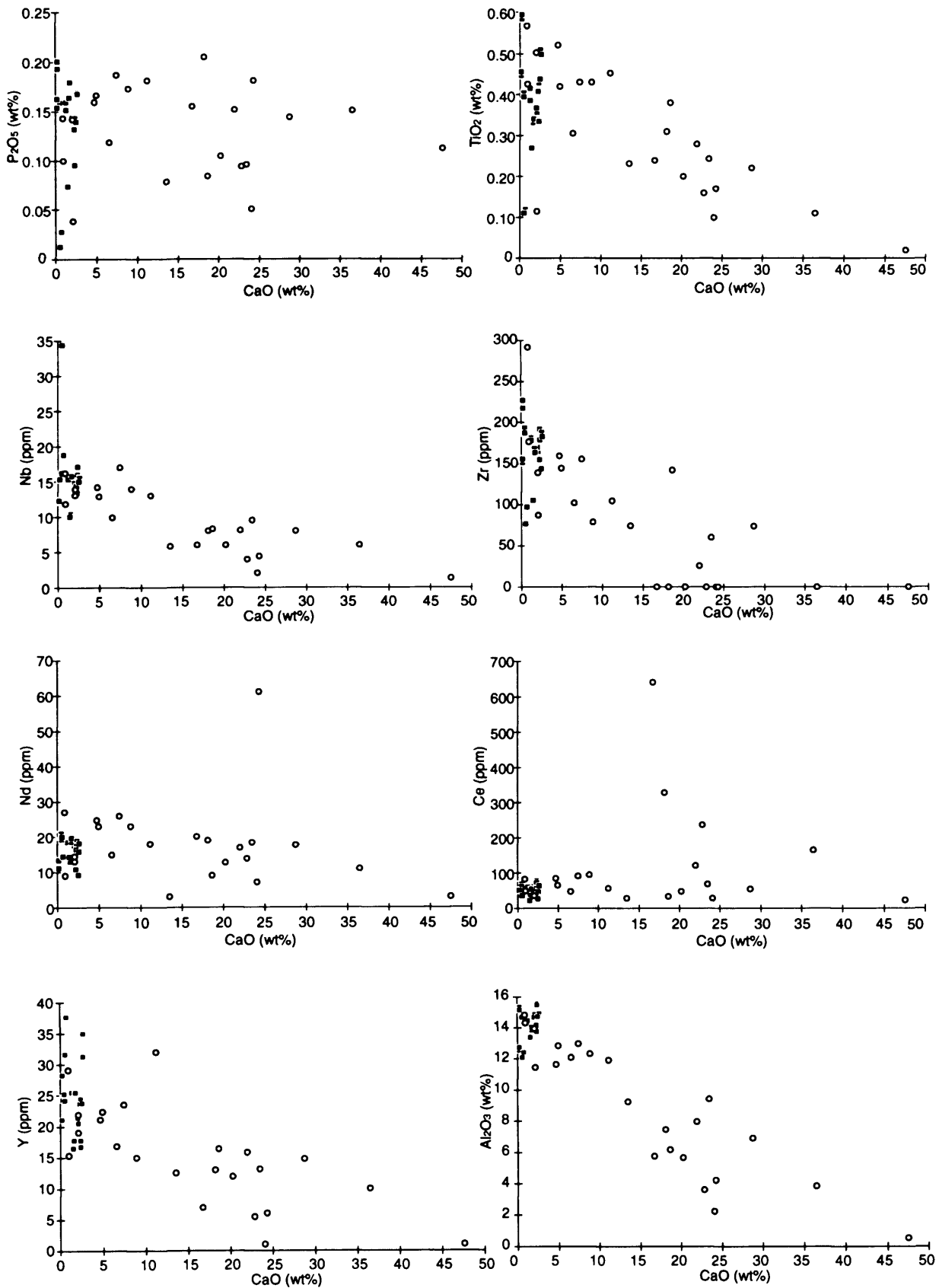
**FIGURE 3.12- Concentrations and ratios of selected immobile elements in granite, volcanics & volcanoclastic sediments from the Emet area**



#### LEGEND

- ▲ Shoshonite & latite (Emet Basin - Dereköy)
- Shoshonite (southern margin of Emet Basin)
- ◆ Granite (Erigöz)
- Rhyolite (within & southern margin of Emet Basin)
- Volcaniclastic sediments with <10wt% CaO (Red & Borate Formation)
- △ Volcaniclastic sediments with >10wt% CaO (Red and Borate Formation)

**FIGURE 3.13 - Selected immobile elements vs CaO for Emet Basin volcanics and volcaniclastic sediments**



**LEGEND**

- Rhyolites & granite (Emet area)
- Volcaniclastic sediments (Emet Basin)

and Borate Formations have had a significant input from local acid magmatism. Furthermore, the data indicate that the latite and shoshonite magmatic activity occurred after the deposition of the borate-host sediments consistent with the location of the Emet mafic lavas stratigraphically above the borates.

Some sediments from the Borate Formation show a pronounced enrichment in Ce (Figure 3.13). These enrichments could indicate that Ce has been partially mobilised in this environment, or that the sediments contain detrital REE-rich minerals such as monazite, but the lack of correlation of Ce with P does not support this hypothesis. As a result of these enrichments, Ce is clearly not suitable in determining the provenance of the Emet sediments.

### 3.4.3 Usak-Güre and Selendi Basins

The mudstones of the Inay Group in Selendi and Usak-Güre Basins contain similar concentrations of immobile elements to the rhyolite and trachyte/dacite whilst the least evolved rocks of the area, the latites, have considerably higher levels of all immobile elements than the sediments (Figure 3.14 & 3.15). This suggests that the sediments of the Inay Group in Selendi and Usak-Güre Basins have a close spatial and temporal relationship to acid volcanism as observed in the Emet Basin. The Ca dilution effect and Ce enrichment are also observed as in the Emet Basin.  $\text{TiO}_2/\text{Al}_2\text{O}_3$  and Nb/Y ratios, plotted to remove the affect of dilution, also indicate an acid volcanic provenance for the Inay Group mudstones (Figure 3.15).

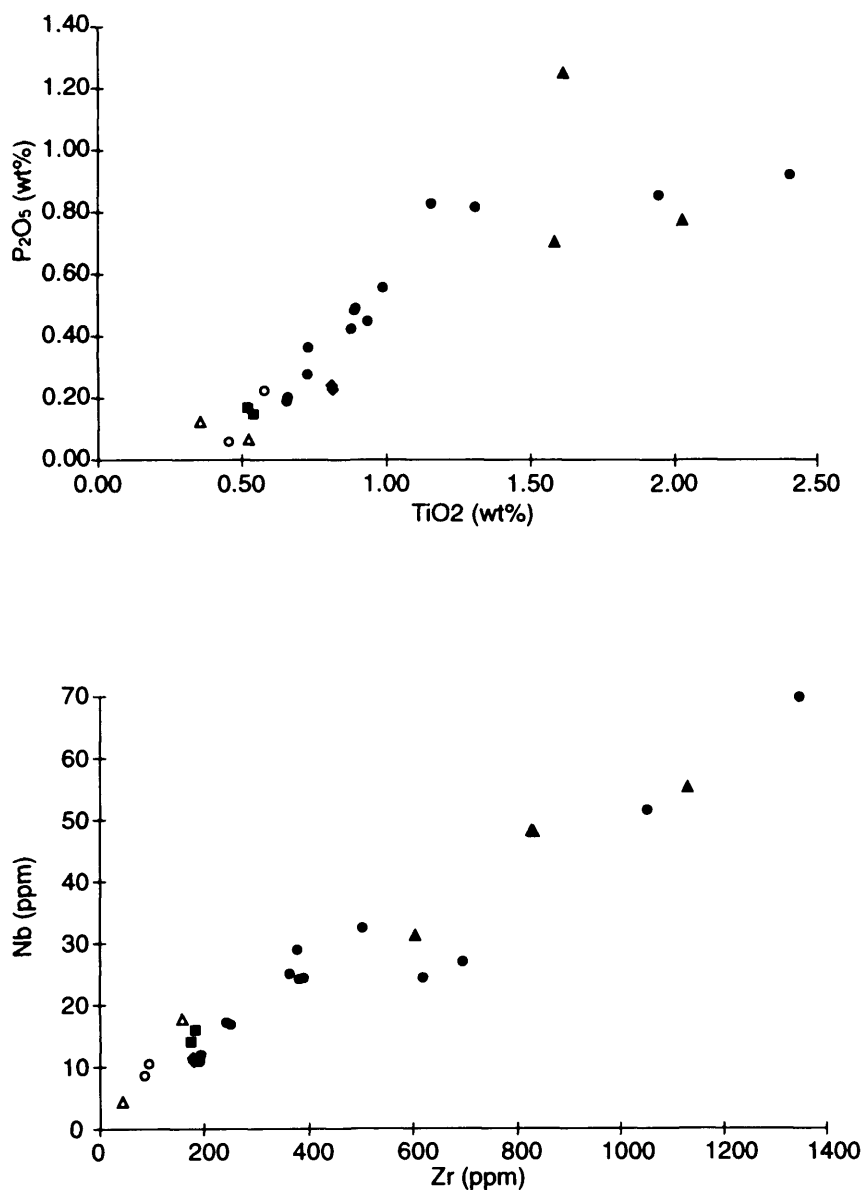
### 3.4.4 Kirka Basin

In the Kirka Basin, the shoshonites also differ in their immobile element concentrations from the more evolved volcanics (rhyolite and ignimbrite) and the sediments, with higher levels of P, Ti, Zr and Nd in the former (Figures 3.16 & 3.17). The Karaören and Fetiye Formation volcanoclastic sediments, which are found stratigraphically below limestone beds of the Sarikaya Formation, have similar levels of P, Ti, Zr, Nd and Ce to the Kirka Ignimbrite (Figures 3.16 & 3.17). This is consistent with textural and mineralogical observations that indicated an ignimbrite derivation for the majority of the Karaören and Fetiye Formation volcanoclastic sediments. The main mineralogical difference between the ignimbrite and the Karaören and Fetiye sediments is the presence of calcite in the latter, and, as at Emet, results in a Ca dilution effect, most pronounced with Nb (Figure 3.16).

The Göçenoluk mudstone, which is found in the colemanite-bearing part of the Sarikaya Formation, plots close to the Kirka Rhyolites in all except Ce, which is enriched (Figures 3.16 & 3.17) suggesting an acid volcanic input, as in the Emet Basin. Ca dilution of immobile elements in the dolomite-rich mudstones from the borax/ulexite-bearing part of the Sarikaya Formation makes assessing the provenance of these sediments impossible. Trace element ratios of these sediments could not be calculated due to measured trace elements concentrations below the XRF detection limit. However, a plot of  $\text{TiO}_2/\text{Al}_2\text{O}_3$  against Nb/Y confirms the acid volcanic provenance of the Göçenoluk mudstone and the volcanoclastics of the Karaören and Sarikaya Formations (Figure 3.17).

Hence these data indicate that as at Emet, acid volcanism has had a large influence on the chemical composition of much of the basin sediments, such as mudstone from the Sarikaya Formation near

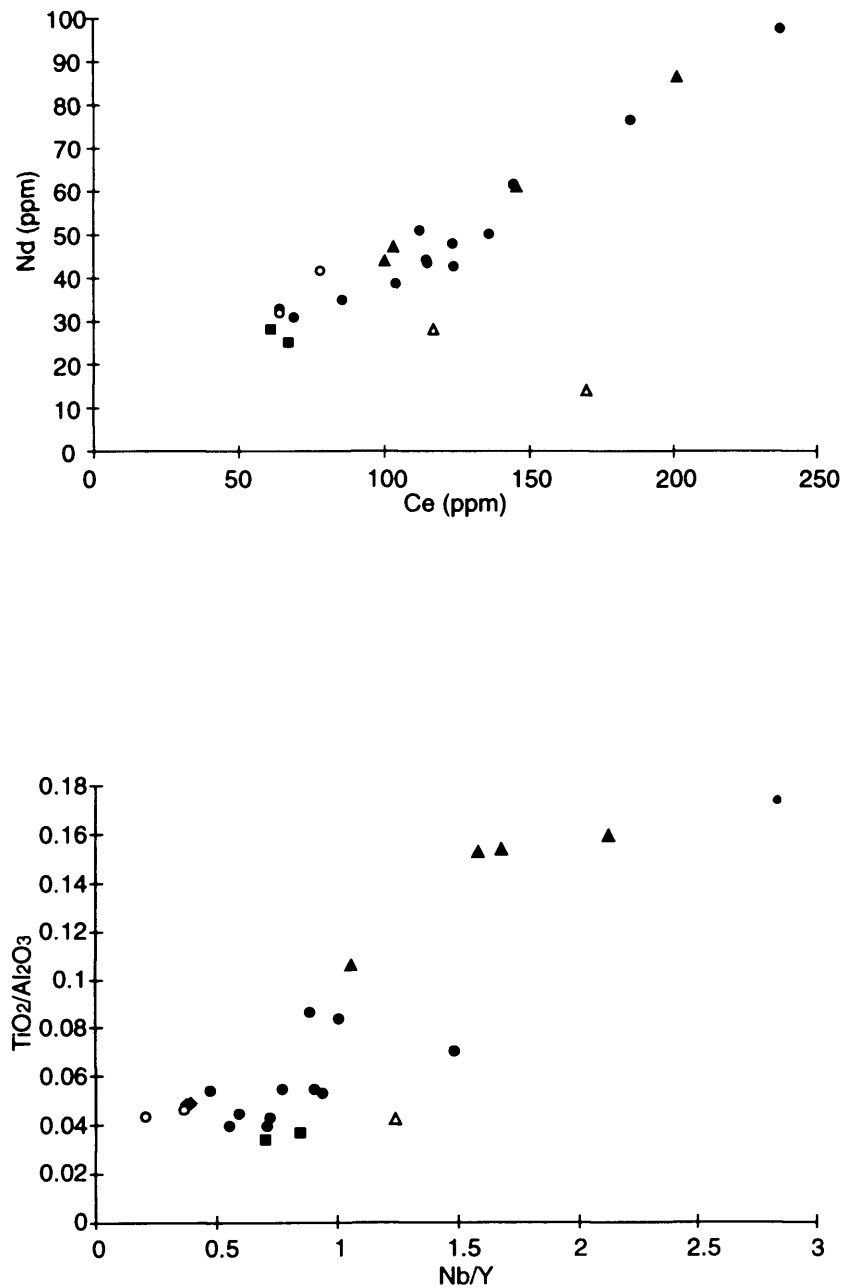
**FIGURE 3.14 - Concentrations of selected immobile elements in volcanics & volcaniclastic sediments from Selendi & Usak/Güre Basins**



#### LEGEND

- ▲ Latite (Selendi & Usak/Güre Basins)
- Andesite (northern Selendi Basin)
- Dacite & K-trachyte (Selendi & Usak/Güre Basins)
- Rhyolite (Selendi Basin)
- Volcaniclastic sediments - 9.60-11.67wt% CaO (Selendi Basin)
- △ Volcaniclastic sediments - 5.60-9.84wt% CaO (Usak/Güre Basin)

**FIGURE 3.15 - Concentrations of selected immobile element concentrations and ratios in volcanics & volcanoclastic sediments from Selendi & Usak/Güre Basins**

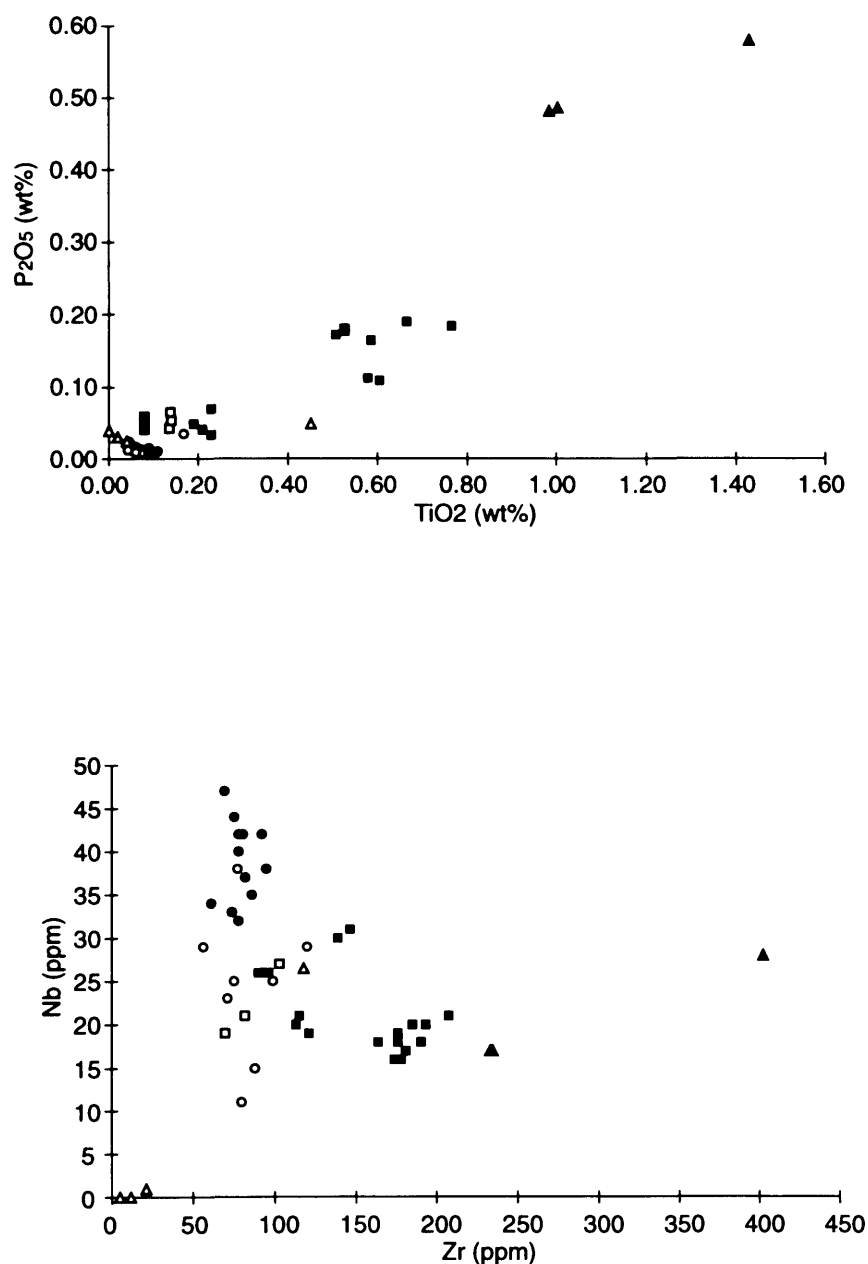


**LEGEND**

- ▲ Latite (Selendi & Usak/Güre Basins)
- ◆ Andesite (northern Selendi Basin)
- Dacite & K-trachyte (Selendi & Usak/Güre Basins)
- Rhyolite (Selendi Basin)
- Volcanoclastic sediments - 9.60-11.67wt% CaO (Selendi Basin)
- △ Volcanoclastic sediments - 5.60-9.84wt% CaO (Usak/Güre Basin)



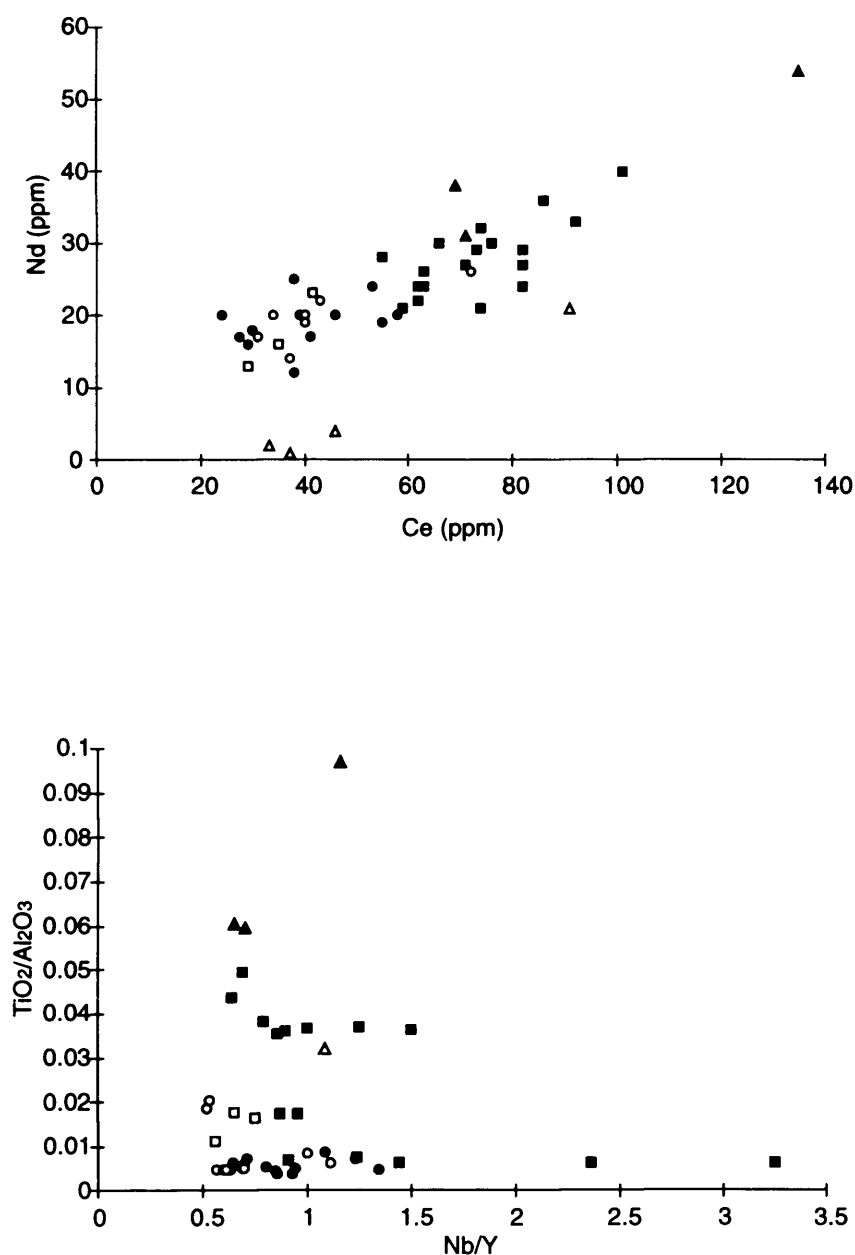
**FIGURE 3.16 - Concentrations of selected immobile elements for volcanics & volcanoclastic sediments of the Kirka area**



#### LEGEND

- ▲ Shoshonite (northern & eastern Kirka Basin)
- Ignimbrite (south & within Kirka Basin)
- Rhyolite, Dacite & Trachyte (northern Kirka Basin)
- Volcanoclastic sediment (Karaören)
- △ Mudstone & Dolomite (Sarikaya Formation - one sample from the colemanite-bearing mudstone at Göçenoluk and three samples from the ulexite & borax bearing mudstone and dolomite near Sarikaya)
- Volcanoclastic sediment (Fetiye Formation)

**FIGURE 3.17 - Concentrations and ratios of selected immobile elements for volcanics & volcanoclastic sediments of the Kirka area**



#### LEGEND

- ▲ Shoshonite (northern & eastern Kirka Basin)
- Ignimbrite (south & within Kirka Basin)
- Rhyolite, Dacite & Trachyte (northern Kirka Basin)
- Volcanoclastic sediment (Karaören)
- △ Mudstone & Dolomite (Sarıkaya Formation - one sample from the colemanite-bearing mudstone at Göçenoluk and three samples from the ulexite & borax-bearing mudstone and dolomite near Sarıkaya)
- Volcanoclastic sediment (Fetiye Formation)

(Note - Y concentrations in VSK 1, 2 and 3 are below the XRF detection limit and therefore these samples from the Sarıkaya Formation have been omitted from the element ratio plot)

Göçenoluk and volcanoclastics from the Karaören and Fetiye Formations. The affect of local volcanism on the chemical composition of the most carbonate-rich sediments in the Sarikaya Formation is very difficult to assess, which makes the precise timing of acid magmatism relative to deposition of the borate-host sediments at Kirka difficult to determine. However, the presence of ignimbrite-derived sediments below carbonate beds in the Sarikaya Formation suggests that the acid volcanism probably occurred prior to and perhaps during deposition of the mineralised sediments. The Fetiye sediments may therefore represent reworked ignimbrite.

### 3.4.5 Afyon area (Balmahmut)

Volcaniclastic sediments from the Balmahmut area contain similar levels of all the immobile elements to the Afyon sanidine bearing K-trachyte (Figures 3.18 & 3.19) which is expected as these rocks contain clasts of the Afyon volcanics. The mudstones found stratigraphically above these volcaniclastic sediments have similar concentrations of P, Nd, Ce and sometimes Zr to K-trachyte and shoshonite (Figures 3.18 & 3.19) which suggests that the chemistry of the sediments is also influenced by the local volcanism. The immobile element data are consistent with field observations which indicate that the Afyon K-trachyte volcanism occurred prior to or perhaps during the deposition of these sediments. However the mudstones have lower levels of Ti and Nb (Figure 3.18), which may also be a feature of dilution by the higher levels of Ca in the sediments. Immobile element ratios, which should be unaffected by dilution, show an overlap between the Balmahmut sediments and local volcanics (Figure 3.19).

## 3.5 CONSTRAINTS ON VOLCANIC STRATIGRAPHY FROM MINERAL CHEMISTRY

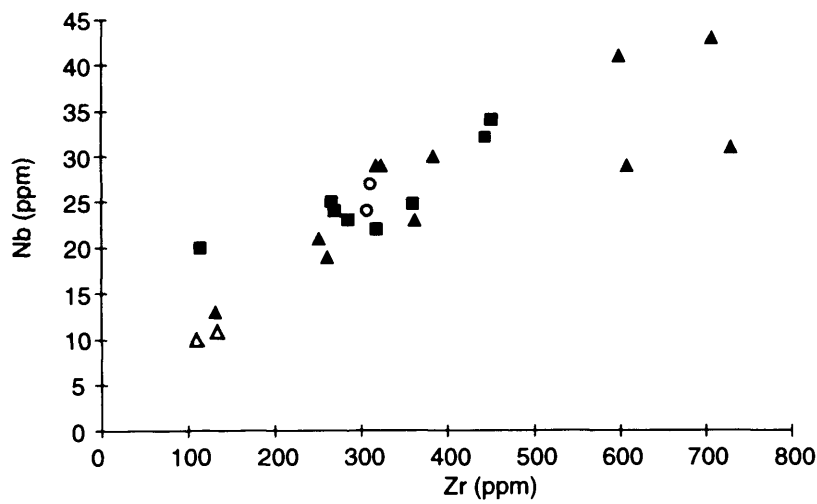
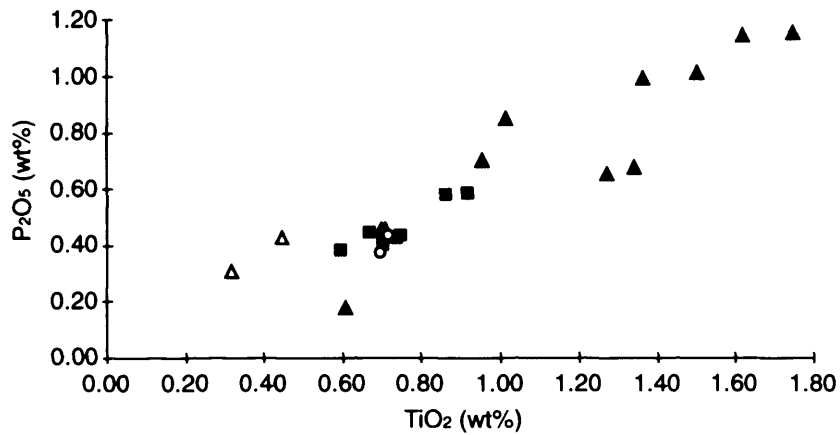
### 3.5.1 Introduction

The chemical composition of biotite and feldspar was determined in granitic, volcanic and volcaniclastic rocks from the Emet Basin using an electron microprobe, in order to determine the origin of these minerals in the volcaniclastic sediments, so that the timing of magmatism could be further constrained. This work was not carried out on the volcaniclastic sediments from Kirka Basin since textural, mineralogical and immobile element investigations already discussed, clearly indicated a largely ignimbritic source for the Karaören and Fetiye Formations.

### 3.5.2 Biotites

Biotite compositions depend largely upon the nature of the magma from which they crystallise (Abdel-Rahman 1993). Therefore, it is logical to expect higher concentrations of Mg in the biotites of the shoshonite and latite, than in the Mg-poor rhyolite and granite. However, alteration of biotites in the latite and shoshonite lead to an increase in Fe and a decrease in Mg, and therefore for the purpose of this study, it was essential to select unaltered biotites. This was achieved by selecting samples with biotites which have a fresh appearance in thin section, produce good electron microprobe analyses totals, and have compositions that plot directly in the biotite field on a chemiographic diagram by Velde and Meunier (1987) (c.f. Figure 3.1).

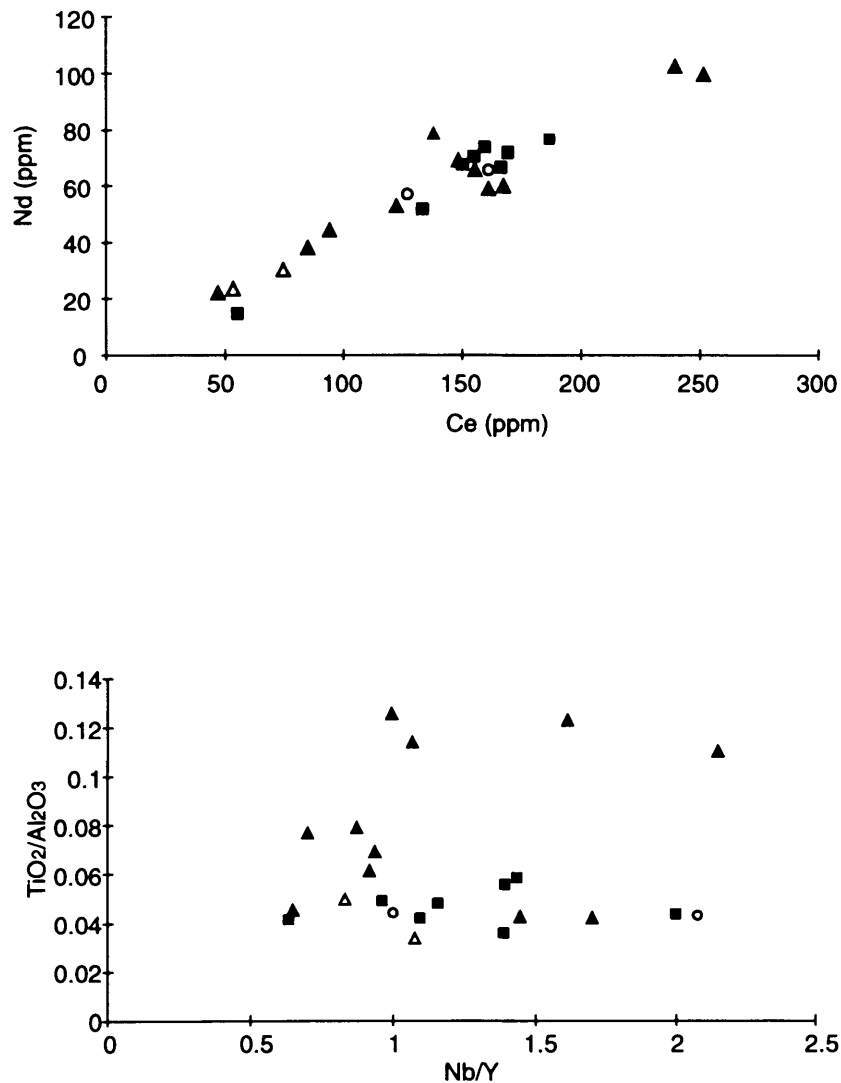
**FIGURE 3.18 - Concentrations of selected immobile elements in volcanics and volcanoclastic sediments of the Balmahmut area**



#### LEGEND

- ▲ Latite & shoshonite
- K-trachyte (often contains large sanidine phenocrysts)
- Volcaniclastic sediment (from just below Sections O & P near Balmahmut)
- △ Mudstone (Sections O & P)

**FIGURE 3.19 - Concentrations and ratios of selected immobile elements in volcanics and volcanoclastic sediments of the Balmahmut area**



#### LEGEND

- ▲ Latite & shoshonite
- K-trachyte (often contains large sanidine phenocrysts)
- Volcanoclastic sediment (from just below Sections O & P near Balmahmut)
- △ Mudstone (Sections O & P)

Shoshonite and latite do have higher Mg levels than the rest of the samples, a direct reflection of their higher whole rock Mg concentrations, whilst the biotites of the granite, the rhyolite and the volcanoclastic sediments plot in the same region of the diagram (Figure 3.20). This is consistent with the biotites in the volcanoclastic sediments of the Red and Borate Formations originating from local acid magmatism, either rhyolitic or granitic. However, it is not possible to distinguish between rhyolitic and granitic source for the biotites in the sediments.

### 3.5.3 Feldspars

Figure 3.21 shows electron microprobe analyses of unaltered feldspar (selected by the same method as the biotites) in the granite, volcanics and volcanoclastic sediments of the Emet Basin. As discussed in the previous chapter, the shoshonite and latite from the Emet Basin contain only small needles of K-feldspar whilst the granite, rhyolite and volcanoclastic sediments contain large feldspar phenocrysts of both plagioclase and K-feldspar. This indicates that the volcanoclastic sediments probably have a granitic or rhyolitic provenance. Furthermore, the slightly more calcic nature of the K-feldspars in the Dereköy latite and shoshonite compared with those in the sediments of the Red and Borate Formation (Figure 3.21) adds further weight to this argument. This is consistent with all the data presented so far, which indicated that the latite and shoshonite magmatism occurred after deposition of the borate-host sediments.

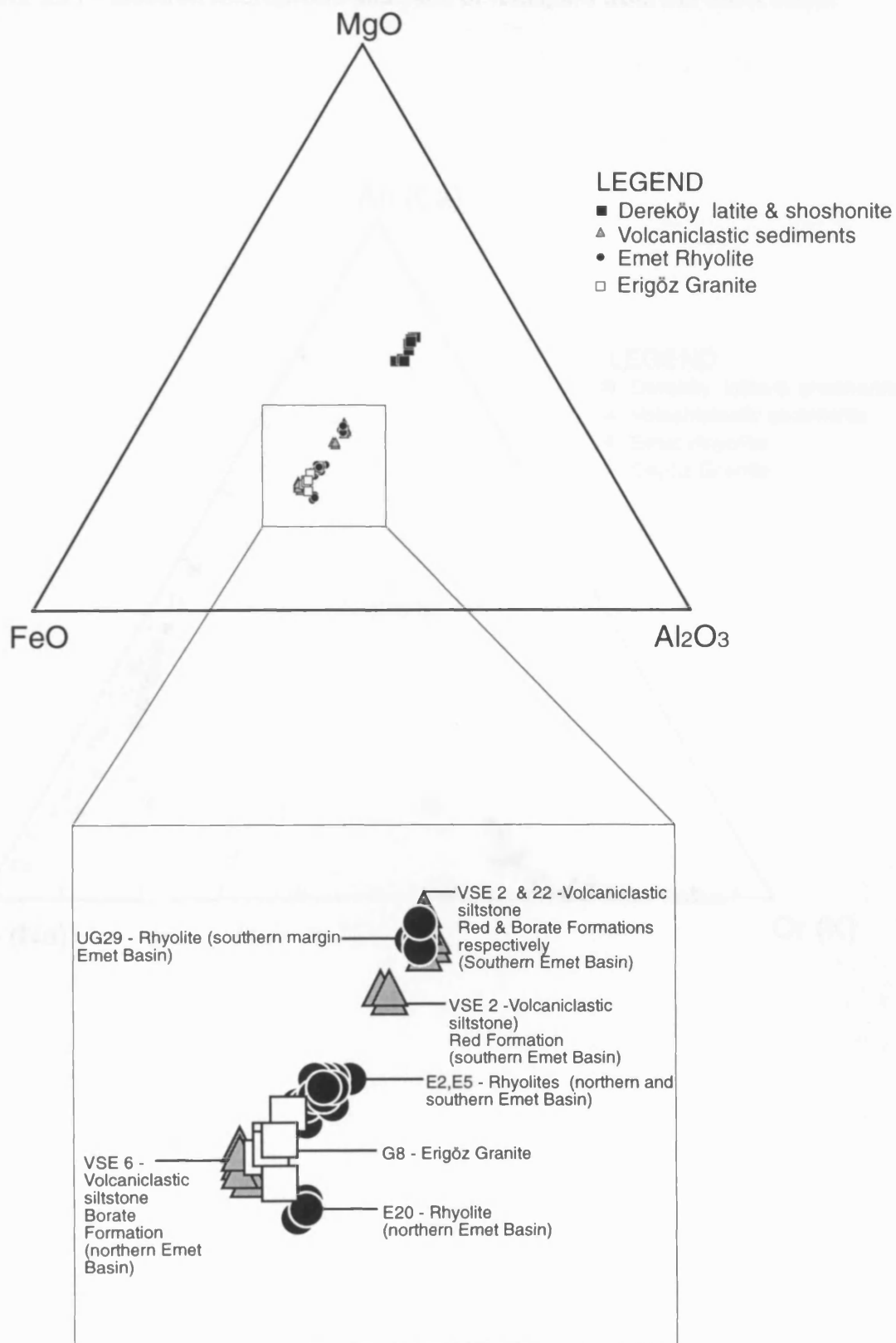
The compositions of K-feldspar phenocrysts in the volcanoclastic sediments overlap with those of the granite and rhyolite and hence at least some of the phenocrysts may have been derived from the local acid magmatism. However, the possibility that some of the K-feldspar phenocrysts analysed in the sediments may be authigenic, as proposed by Helvacı et al. (1993) and not clastic, cannot be discounted. The analysed plagioclase phenocrysts in the volcanoclastic sediments differ from those of the granite and rhyolite, being slightly more sodic (Figure 3.21). Although, further analysis of feldspars in the sediments, the rhyolites and the granite might produce some overlap in plagioclase compositions, it is also possible that the alkali elements Na and K have been mobilised in the lacustrine environment in which the sediments were deposited.

In summary, the feldspar analyses appear to preclude the involvement of the latite and shoshonite magmatism in sedimentation at the time of borate mineralisation but they also fail to provide clear evidence of derivation of the sediment feldspars from local acid magmatism.

## 3.6 CONCLUDING POINTS

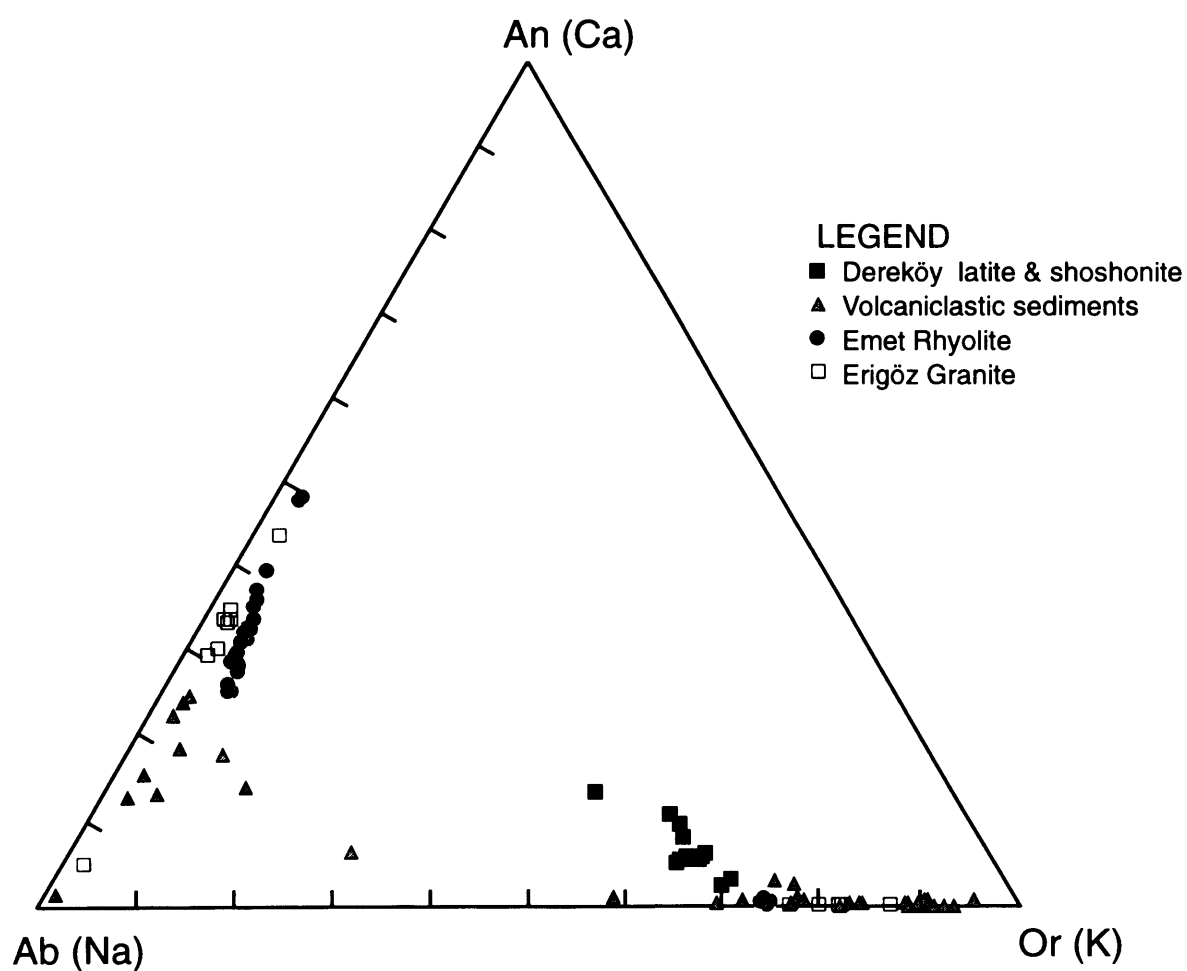
Isotopic dates reveal an Early Miocene phase of acid magmatism in this region, as represented by granite and rhyolite in the USE area, and ignimbrite and rhyolite in the Kirka area (this study, Bingöl et al., 1982, Yalçın 1989). Later magmatic activity in the Middle Miocene comprised trachyte, latite and shoshonite in the USE area, shoshonite in the Kirka area and trachyte, latite and shoshonite in the Afyon area (this study, Yalçın 1989, Besang et al., 1989). The overall evolution through the Miocene was from acidic to more mafic rocks, a trend consistent with Güleç's (1991) observation.

FIGURE 3.20 - Electron microprobe analyses of biotites from the Emet Basin





**FIGURE 3.21 - Electron microprobe analyses of feldspars from the Emet Basin**



A modified stratigraphic column of Emet Basin (after Helvacı 1984) is shown in Figure 3.22. K-Ar dating, immobile element concentrations and mineral compositions, confirm the observations made in Chapter 2, that acid magmatism was active in the Emet Basin prior to and possibly during the deposition of borate-host sediments, while the mafic magmatism occurred later. New K-Ar dates reveal that acid magmatism was active in the Emet Basin during the Early Miocene and that more mafic magmatism has a Middle Miocene age (Figure 3.22). Investigations of immobile element concentrations and compositions of biotites in the volcanoclastic sediments of the Red and Borate Formations indicated a derivation from local acid magmatism, but are unable to distinguish between rhyolitic or granitic provenance.

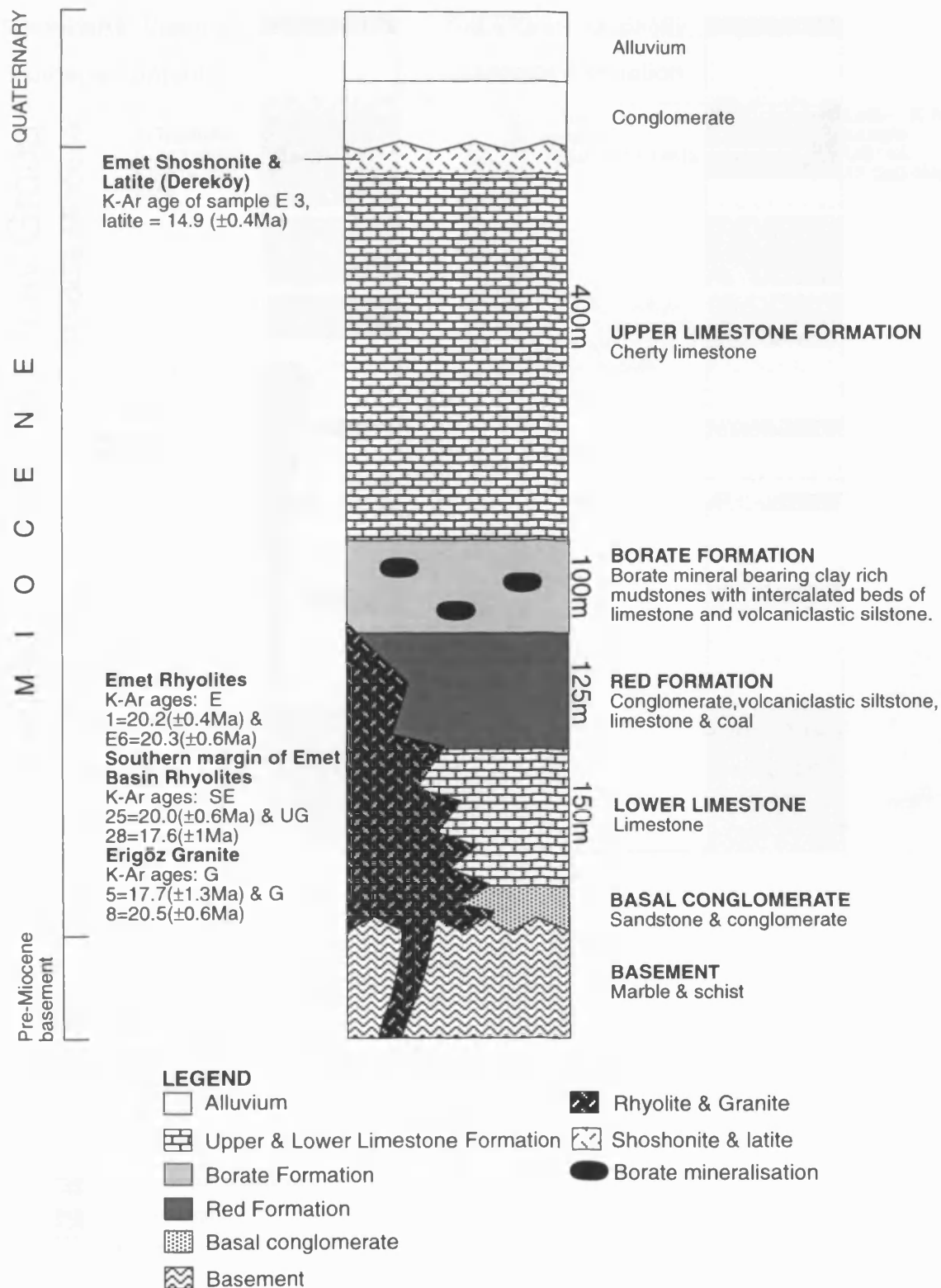
Granitic clasts found in sediments of both the Red and Borate Formations (c.f. Chapter 2) revealed that granite emplacement pre-dated most of the sedimentation in the Emet Basin. Volcanic material found in the sediments may have originated from the erosion of pre-existing rhyolite sheets and/or from the direct deposition of rhyolitic ash into the basins during active volcanism. The immature and largely unaltered nature of the volcanoclastic sediments would appear to suggest the latter possibility. Whatever the precise timing of acid magmatism relative to the mineralisation, it is clear that, as well as controlling the composition of the sediments, the granitic and rhyolitic magmatism may have provided a source for important elements associated with the borates.

Figure 3.23 shows the age bracketed stratigraphy of Selendi and Usak-Güre Basins (after Seyitoglu 1997). K-Ar dates reveal that like Emet this area had an Early Miocene acid volcanic phase with later less evolved volcanism in the Middle Miocene. Immobile element concentrations in mudstones of the Inay Group suggest an input from acid volcanism and they preclude the involvement of the latite volcanic phase. The rhyolite and trachyte appear therefore to have exerted some control on the composition of the Inay Group mudstones and these volcanics may represent a suitable source for elements associated with borate mineralisation. The similarity of these basins to the Emet Basin in terms of volcanic and sedimentary stratigraphy, suggest that the mudstone sequences of the Inay Group had the potential to host borate mineralisation.

Figure 3.24 is a modified stratigraphic column of the Kirka Basin (after Yalçın 1989). K-Ar dates published by Yalçın (1989) for the Kirka acid volcanics are consistent with field and mineralogical information, as discussed in Chapter 2. This indicated that acid volcanism (both rhyolitic and ignimbritic) was active prior to and possibly during the deposition of borate-host sediments, while mafic volcanism occurred later. The Early Miocene age obtained in this study for ignimbrite south of the Kirka Basin by  $^{40}\text{Ar}/^{39}\text{Ar}$  dating gives further credence to that view.

Field and mineralogical evidence (c.f. Chapter 2) indicated a largely ignimbritic provenance for the Karaören and Fetiye Formation sediments, with an additional rhyolitic clast component in the former. Geochemical evidence of an ignimbrite-derived component in the Karaören and Fetiye volcanoclastic sediments is provided by their immobile element concentrations. Further confirmation of an acid volcanic input into these sediments is given by the Early Miocene K-Ar age of biotite in the Karaören Formation (Yalçın 1989) which correlates within errors with the Early Miocene  $^{40}\text{Ar}/^{39}\text{Ar}$  age of the ignimbrite. As a result of dilution effects caused by high Ca levels in most Sarıkaya Formation

**FIGURE 3.22 - Generalised stratigraphy of the Emet Basin (volcanic stratigraphy modified from Helvacı 1984 and Kistler & Helvacı 1994)**



**Figure 3.22**

FIGURE 3.23 - Generalised stratigraphy of Selendi & Usak/Güre Basins (from Seyitoglu 1997, with K-Ar dates from this study)

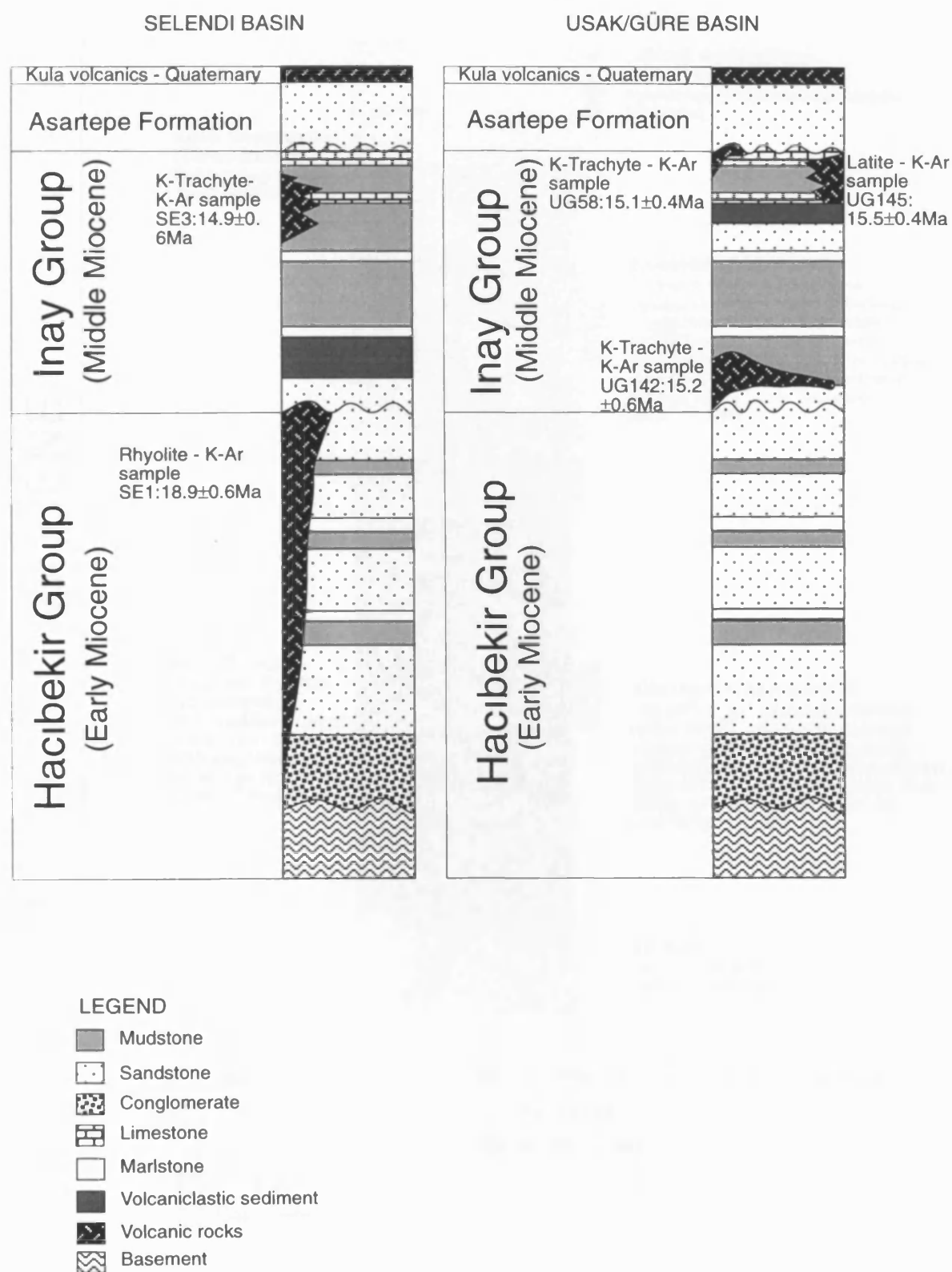
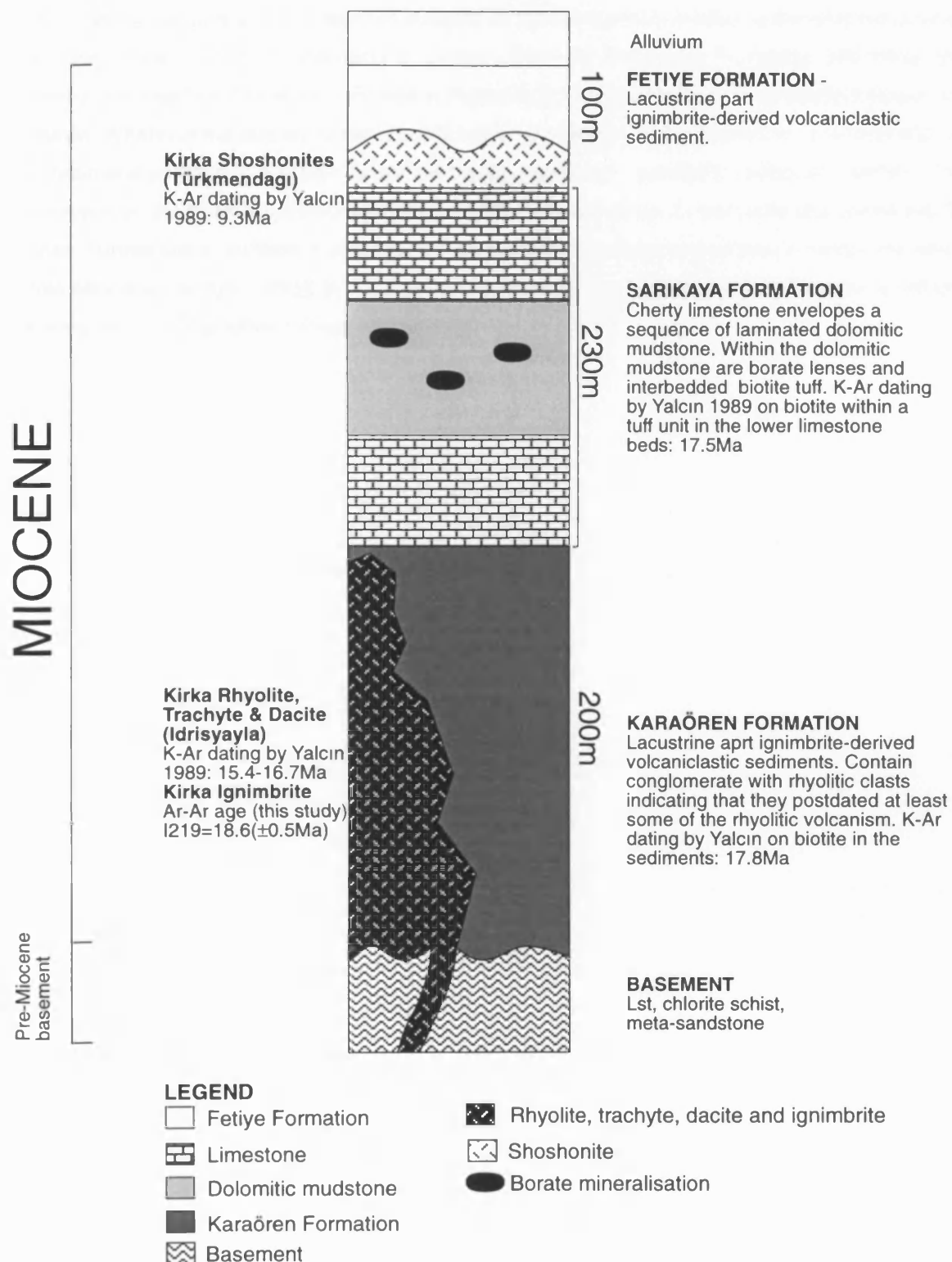


Figure 3.23

**FIGURE 3.24 - Generalised stratigraphy of the Kirka Basin (volcanic stratigraphy modified from Yalcin 1989)**



sediments, their provenance could not be determined using immobile element concentrations. However, the K-Ar age of biotite in the Sarikaya sediments (Yalçın 1989) is within errors of the age of biotite in both the Karaören Formation and the ignimbrite, strongly suggesting an ignimbritic input at around the time of deposition of the borate-host sediments.

Whether or not acid volcanic-derived material in the Sarikaya Formation is the product of direct deposition or the product of reworking is unclear. Similarly, the Fetiye Formation sediments may represent reworked ignimbrite, as indicated in Figure 3.24, or pyroclastic material erupted directly into the basin. Whatever the precise timing of acid volcanism relative to mineralisation, it is clear that the ignimbritic and probably to a lesser extent the rhyolitic volcanism, exerted considerable control on the composition of the Kirka sediments, and may have provided a source for elements associated with the borates. Further south, mudstone sequences near Balmahmut are closely related in space and time to Middle Miocene trachytic volcanism and immobile element concentrations also suggest a volcanic influence on the composition of these sediments.

## 4. ROLE OF MAGMATISM IN BORATE GENESIS

### 4.1 INTRODUCTION

Chapters two and three demonstrated that acid magmatism in the Emet and Kirka Basins was closely related in both space and time to the deposition of borate-host sediments. This chapter examines:

- (i) The influence of magmatism on the mineralogy and geochemistry of both borate mineralised and barren sediments.
- (ii) The potential of local magmatism as a source for elements associated with borate mineralisation.

This information has been combined to produce a model for the role of magmatism in borate genesis.

### 4.2 INFLUENCE OF MAGMATISM ON THE COMPOSITION OF SEDIMENTS IN SALINE, ALKALINE LACUSTRINE BASINS; CONSTRAINTS FOR BORATE MINERALISATION

Magmatic activity has significantly influenced the composition of sediments in many of the world's saline, alkaline continental basins (Hay 1977, Surdam 1977, Sheppard & Gude 1969, Stamatakis 1989, Banfield et al., 1991a) and a review of the literature is presented below. In order to assess the affects of local magmatism on sedimentation and particularly its role in the generation of borate mineralisation in western Turkey, a detailed mineralogical and geochemical investigation was carried out on lacustrine sediments in Emet Basin. The excellent exposure of borate mineralised and barren mudstones and the abundance of literature on the borate mineralisation made this basin an ideal locality for such a study. For comparative purposes less detailed studies were conducted in the Kirka, Selendi, Usak-Güre and Afyon regions.

#### 4.2.1 Previous investigations

##### 4.2.1.1 *Saline, alkaline basins in western USA*

The influence of magmatism on sediment composition in saline, alkaline continental basins has been particularly well documented in western USA (Sheppard & Gude 1969, 1973; Surdam 1977, Hay 1977, Barrows 1980, Jones 1986, Banfield et al., 1991a). Authigenic minerals such as clays, zeolites, K-feldspar and searlsite ( $\text{NaBSi}_2\text{O}_6\text{H}_2\text{O}$ ) are produced when saline, alkaline waters interact with volcanic material (Sheppard & Gude 1969, Surdam 1977, Hay 1977). Common volcanic reactants include glass, smectite, kaolinite, plagioclase and quartz (Hay 1977). The minerals in saline, alkaline continental basins, such as the Pleistocene Lake Tecopa Deposits in southern California, often show a lateral gradation; from the margin to the centre of a basin, of fresh glass, to zeolites and, finally, authigenic K-feldspar  $\pm$  searlesite (Surdam 1977).

In the Miocene Barstow Formation in California, a zone of analcime separates a K-feldspar zone from the other zeolites, dominantly clinoptilolite (Sheppard & Gude 1969). The zeolites clinoptilolite, chabazite, erionite, phillipsite and mordenite were produced by direct reaction of silicic glass with



alkaline, saline pore waters trapped within the tuffs during diagenesis (Sheppard & Gude 1973) whereas analcime and K-feldspar were formed by the alteration of the clinoptilolite group of zeolites under conditions of increased salinity, and locally they replaced plagioclase (Sheppard & Gude 1969). Strong evidence that authigenic K-feldspar and analcime are stable in highly saline conditions comes from the Kramer borate deposits in California, where these minerals were associated with borax-rich sediments, while clinoptilolite and phillipsite were associated with lower salinity sediments (Sheppard & Gude 1969).

A large proportion of clays found in saline, alkaline lakes are considered detrital, although authigenic smectites can be produced in such settings (Hellier 1995). In a detailed investigation of weathering and diagenesis around and within Abert Lake in Oregon, Banfield et al. (1991a) showed that the lake clays exhibit a greater average Mg content than clay in the pyroclastics around the basin. They attributed this to Mg uptake during diagenesis. Trioctahedral Mg-smectites, such as stevensite, hectorite and saponite, are indeed the most common authigenic smectites in alkaline lakes (Hellier 1995). More Mg-rich clays are generally found towards the centre of a basin, reflecting conditions of increased salinity (Jones 1986).

### *4.2.1.2 Borate bearing basins in western Turkey and the Aegean*

Volcanism had a significant impact on sediment composition in the borate bearing basins of western Turkey and Samos island (Greece), producing authigenic minerals similar to those found in saline, alkaline basins in western USA (Stamatakis 1989, Stamatakis et al., 1989, 1991; Yalçın et al., 1991, Helvacı et al., 1993, Helvacı 1995, Kistler & Helvacı 1994, Gündoğdu et al., 1996). For instance, authigenic K-feldspar, zeolites and smectites are found in all the major borate-bearing basins of this region and often show distinct diagenetic zonation (Yalçın and Gündoğdu 1987, Stamatakis 1989, Yalçın et al., 1991, Gündoğdu et al., 1996).

In the tuffs of the Karaören Formation in Kirka Basin (which pre-dates the deposition of the borate-host sediments; Yalçın 1989, this study), mineral zones of glass + smectite, clinoptilolite + opal-CT, and clinoptilolite/heulandite + K-feldspar  $\pm$  quartz have been described by Gündoğdu et al. (1996). They also show that in the tuffs of the Köpenez Formation (which pre-dates the Beyköy/Red Formation) in the south of Emet Basin, mineral zones consist of glass + smectite, clinoptilolite + opal C-T, clinoptilolite + K-feldspar  $\pm$  quartz  $\pm$  analcime, K-feldspar + analcime + quartz + smectite + illite/smectite mixed layers, and K-feldspar + smectite + quartz. In both basins, diagenetic transformation of K-rich rhyolitic glass lead to the generation of dioctahedral smectite and clinoptilolite (Gündoğdu et al., 1996). The lateral facies distribution is believed to have resulted from differences in the salinity and pH of pore waters, with formation of analcime and K-feldspar favoured by the highest salinity and pH (Gündoğdu et al., 1996).

In the borate-bearing sediments of Kirka Basin (Sarıkaya Formation), tuffaceous horizons contain authigenic K-feldspar, erionite, smectite and illite, whilst sanidine, albite, anorthoclase and calcite are apparently volcanic detritus (Helvacı et al., 1993). The smectites found in the Sarıkaya Formation are Li-stevensite, Li-saponite and hectorite (Yalçın et al., 1989a). Tuffaceous sediments from the Borate

Formation in the Emet Basin comprise authigenic K-feldspar, illite and smectite, whereas sanidine and quartz are considered volcaniclastic (Helvacı et al., 1993). Clays identified in the Borate Formation include Li-stevensite, Al-stevensite, saponite, dioctahedral smectite and illite-smectite mixed layers (Ataman & Baysal 1978, Yalçın & Gündoğdu 1985). Helvacı (1977; 1984) claimed that a complete transition from tuff to clay in the Borate Formation can be determined from field and geochemical evidence. The formation of clays from tuffs was accompanied by a decrease in Si and K and an increase in Mg, Na, Cr, Ni, B, As and Sr (Helvacı 1977). He suggested that some K was lost in solution while illite provided a sink for the remainder and Mg, Cr and Ni were incorporated into the montmorillonite structure. His study attributed enrichments in B, As and Sr to the presence in the mudstone of borate, celestite and realgar, as well as illite which absorbed B and smectite which absorbed As and Sr.

### **4.2.2 Influence of magmatism on the mineralogical and geochemical composition of sediments in the Borate and Red Formations of Emet Basin**

#### **4.2.2.1 Introduction**

Previous investigations (Helvacı 1977, 1984; Helvacı et al., 1993, Ataman & Baysal 1978, Yalçın & Gündoğdu 1985, Gündoğdu et al., 1996) provide a useful introduction to the impact of local volcanism on sediment composition in the Emet Basin. However, they have limitations; the study by Gündoğdu et al. (1996) concentrated on the mineralogy of the Köpenez Formation without detailed whole rock geochemistry, while Helvacı (1977) described the basic geochemistry of mudstone in the Borate Formation without detailed mineralogical information. Furthermore, previous studies have not attempted to compare borate mineralised and barren sediments.

The current study therefore builds on this previous work and provides the first fully integrated mineralogical and geochemical investigation of both mineralised and barren sediments in the Borate and Red Formations. The specific aim of the investigation was to assess the influence of local magmatism on the composition of the sediments and in particular on the distribution of borate mineralisation. The following section therefore examines:

- (i) The distribution of borate mineralisation in the sampled sections.
- (ii) The mineralogical and geochemical composition of igneous material deposited in both the Red and Borate Formations, and the nature and extent of post-depositional modification.
- (iii) The implications for the distribution of borate mineralisation in the basin.

#### **4.2.2.2 Methodology**

Sediment samples were collected from logged sections in both the Red and Borate Formations along the length of the Emet Basin (Chapter 2, Appendices A & B). Detailed mineralogical and geochemical studies, using XRD, XRF, ICP-AES and electron microprobe analyses, were conducted on twenty three selected samples (Appendices C, G, H & I); four from the Red Formation (VSE 1 - 4) and nineteen from the Borate Formation (VSE 5 - 23). Furthermore, As, Sr and Li concentrations were determined in 67 samples collected at 1.8 m intervals from sections C, D, E, F and G in the Borate

Formation. Li was analysed by ICP-AES, while As and Sr were analysed using XRF (Appendix I).

### 4.2.2.3 Distribution of borate mineralisation in the sampled sections

In order to assess the affect of the igneous input on the distribution of borate mineralisation, the location of borate minerals within the sampled sections needed to be accurately constrained. This was accomplished by a combination of field observations and XRD analyses. No attempt was made to analyse boron in the sediments, due to the expensive analytical procedure and the success of mineralogical studies in locating the borate mineralisation. The distribution of colemanite in the sampled sections, was shown in Chapter 2 (Figure 2.3); colemanite was identified in Sections C, E and G, but not in Sections D and E.

### 4.2.2.4 Composition and post-depositional modification of igneous-derived sediment in Emet Basin

#### (a) Introduction

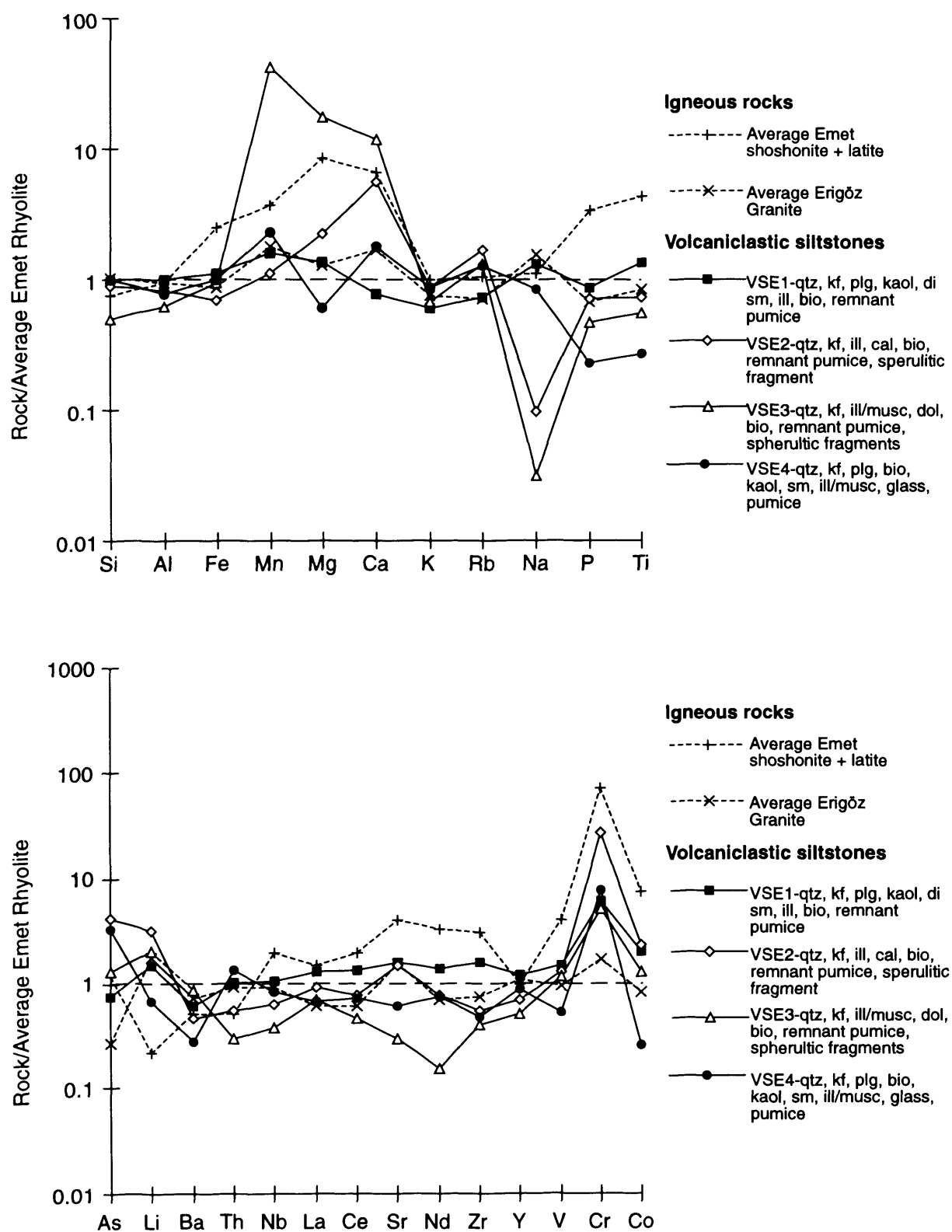
In Chapters 2 and 3, the occurrence of quartz, plagioclase, low-Mg biotites and the concentrations of immobile elements in volcanoclastic siltstones in the Red and Borate Formations were used as evidence for a derivation from local acid magmatism. On mineralogical and geochemical criteria alone, weathered granite cannot be distinguished from rhyolitic ash, but the presence of pumice and spherulitic fragments in some volcanoclastic siltstones indicates definite pyroclastic input. It is therefore probable that the volcanoclastic siltstones of Emet Basin were largely derived from rhyolitic ash, although they may also contain a component from weathered granite (Chapter 2). Immobile element levels in the mudstones of the Borate Formation are again consistent with a derivation from local acid magmatism, although concentrations in many cases have been diluted by the precipitation of calcite (Chapter 3). The following discussion concentrates on the mineralogical and geochemical post-depositional modifications of these acid igneous-derived sediments.

#### (b) The Red Formation

The elemental abundances of four volcanoclastic siltstone samples from the Red Formation have been normalised to average Emet Rhyolite so that post-depositional changes to the original acid igneous input can be easily observed. Samples VSE 1 and 4 contain concentrations of most elements similar to average Emet Rhyolite and Erigöz Granite, including the more mobile elements such as K, Rb, Na and Sr (Figure 4.1). It is therefore likely these volcanoclastic siltstones have not been significantly modified since deposition. The mineralogy of these samples is also largely comparable with that of the Emet Rhyolite; quartz, K-feldspar, plagioclase, biotite and kaolinite all remain. Furthermore, XRD analysis of sample VSE 4 (Appendix G) indicates an abundance of fresh glass.

XRD analyses reveal that illite is also present in samples VSE 1 and 4 (Appendix G) and electron microprobe studies on sample VSE 1 (Appendix H) show that the illite occurs in the form of white mica crystals (Figure 4.2). These illite crystals were probably detritally derived from local basement rocks, whilst micas with biotite to chlorite compositions originated from rhyolitic volcanism  $\pm$  weathered granite (Figure 4.2). On the basis of an XRD peak at approximately 15.5 Å, smectite in samples VSE 1 and 4 is

FIGURE 4.1- Geochemistry of volcanoclastic siltstones from the Red Formation



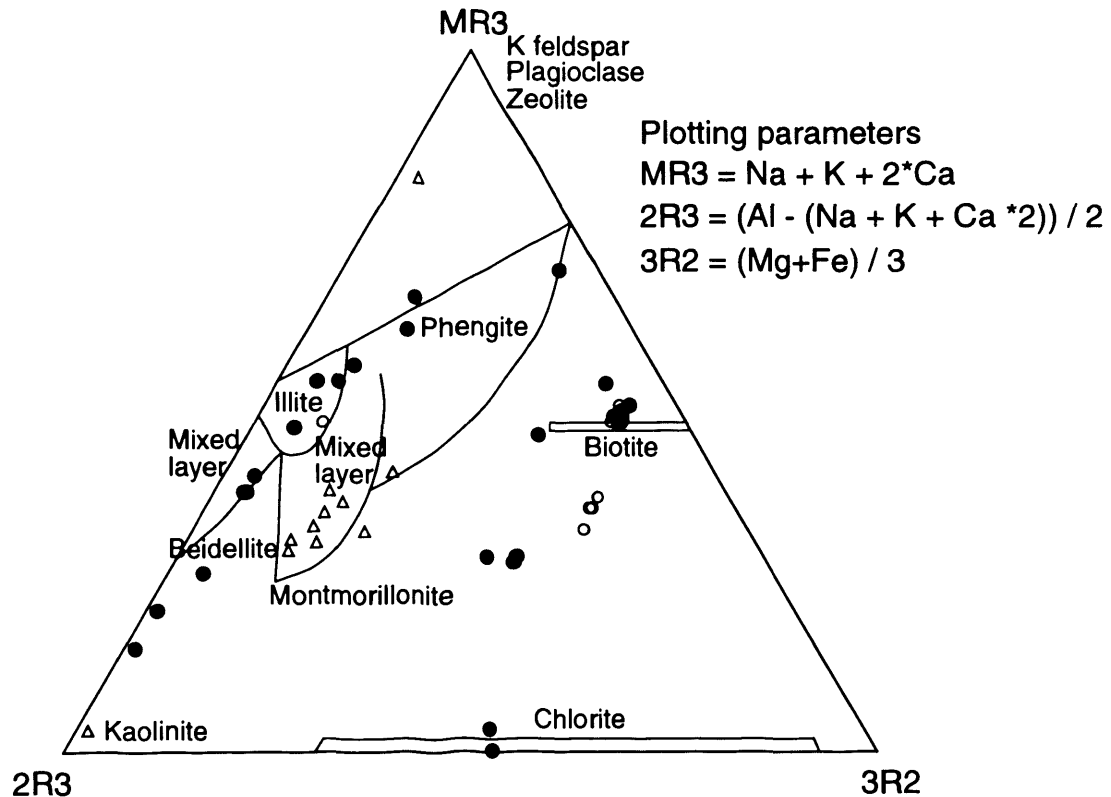
LEGEND: qtz=quartz, kf=K-feldspar, plg=plagioclase, bio=biotite, cal=calcite, dol=dolomite, di sm=diocahedral smectite, ill=illite, musc=muscovite, kaol=kaolinite

Average Emet Rhyolite = average of E1, 2, 5, 6, 16, 17, 18, 19, 21

Average Emet Shoshonite & Latite = average of E3, 4, 68

Average Erigöz Granite = average of G1, 2, 4, 5, 7, 8, 23

**FIGURE 4.2 - Electron microprobe analyses of volcanoclastic siltstone in the Red Formation**



**LEGEND**

- Micas in sample VSE2
- Micas in sample VSE1
- △ Matrix in sample VSE1

(Clay discrimination diagram after Velde & Meunier 1987)

classified as the MgCa variety (Brown & Brindley 1980). This peak shows characteristic smectite behaviour; a shift from ~15 Å to ~17 Å on treatment with ethylene glycol followed by partial collapse at 330°C and total collapse at 550°C (Appendix G, Brown & Brindley 1980). Further identification of the smectite using XRD proved problematical due to an overlap between the d(060) peaks of illite and montmorillonite (Moore & Reynolds 1989). However, electron microprobe analyses showed that montmorillonite and illite-montmorillonite mixed layers occur in the matrix of sample VSE 1 (Figure 4.2). The montmorillonite probably formed by the alteration of rhyolitic glass in the matrix of acidic volcanic ash deposited into the basin. Alteration of volcanic glass to dioctahedral smectite can occur during diagenetic reactions in a saline environment, or weathering reactions (Jones 1986, Banfield et al., 1991b, Gündogdu et al., 1996).

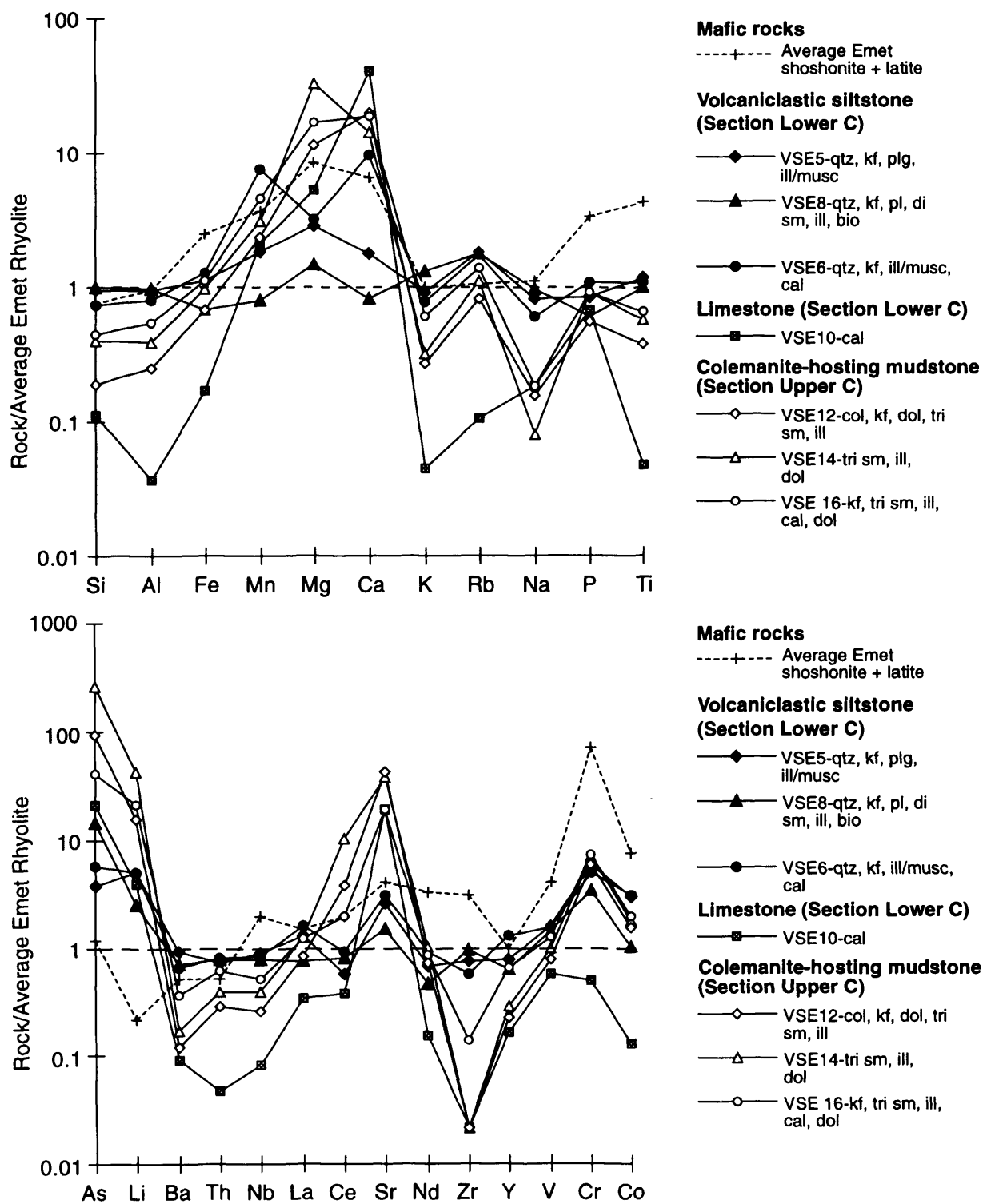
In contrast, samples VSE 2 and 3 comprise rhyolitic ± granitic-derived sediment which has been modified since deposition. They contain calcite (VSE 2) and dolomite (VSE 3) but no glass, smectite, plagioclase or kaolinite. This geochemistry reflects the mineralogy with higher concentrations of Mg and Ca but lower Na than average rhyolite (Figure 4.1). Dolomite and calcite which occur in the matrices of these sediments and in the case of sample VSE 3, in the pumice vesicles too, are common authigenic phases in alkaline, saline lakes (Surdam 1977, Deike & Jones 1980, Banfield et al., 1991a). Precipitation of calcite leads to a increase of the Mg/Ca ratio in the residual solution and the subsequent precipitation of high-Mg calcite and finally dolomite (Eugster & Jones 1979, Eugster 1980).

It therefore appears that the interaction of rhyolitic ± granitic material with Ca, Mg and carbonate-rich saline, alkaline waters lead to the precipitation of carbonate and the breakdown of glass, plagioclase and kaolinite. This breakdown releases silica and the cations of Na, Ca, Sr, K and Al. Figure 4.1 shows that the loss of Na was particularly pronounced and this reflects the lack of any Na-bearing phases in samples VSE 2 and 3. The breakdown of plagioclase probably also resulted in the loss of some Ca and Sr to solution. Loss of Al and Si has taken place in sample VSE 3 but K levels have not changed significantly relative to average Emet Rhyolite (Figure 4.1) since K still resides in K-feldspar. The Emet Rhyolites contain small concentrations of CaO (0.28-2.08 wt%) and MgO (0.26-0.72 wt%) and hence would have supplied only minor amounts of these elements to the lake waters. Gündogdu et al. (1996) have suggested that a more significant source of Ca and Mg may have been the local carbonate and ophiolitic basement rocks. Slightly elevated As and Li levels in sample VSE 2 relative to average Emet Rhyolite (Figure 4.1) was also probably the result of interaction with lake waters. All samples have elevated levels of Cr relative to average Emet Rhyolite (Figure 4.1), which might indicate an input from a mafic rock source, such as ophiolitic basement, but there is no direct evidence for this.

### (c) The Borate Formation

The geochemistry of siltstone, limestone and mudstone from Section C in the Borate Formation of northern Emet Basin is shown in Figure 4.3. The siltstone and limestone (VSE 5, 6, 8, 10) were sampled from the lower part of the section (Section Lower C) while the mudstone (VSE 12, 14, 16) was obtained from the borate mineralised upper portion of the section (Section Upper C) (Figure 2.3). Like

**FIGURE 4.3 Geochemistry of sediments from the Borate Formation (Section C - northern Emet Basin)**



LEGEND: qtz=quartz, kf=K-feldspar, plg=plagioclase, bio=biotite, cal=calcite, dol=dolomite, di sm=di octahedral smectite, tri sm=trioctahedral smectite, ill=illite, musc=muscovite, kaol=kaolinite, col=colemanite

Average Emet Shoshonite & Latite = average of E3, 4, 68



some of the siltstones of the Red Formation, samples VSE 5 and 8 from Section Lower C are very similar in terms of geochemistry to average Emet Rhyolite (Figure 4.3), and even the mobile elements K, Rb, Sr and Na have remained largely unchanged since deposition. This mineralogy is also very similar to that of the Emet Rhyolites, with quartz, plagioclase, K-feldspar and biotite. As in the Red Formation, the presence of white micas in sample VSE 8 with an illitic composition (Figure 4.4a) and the Cr enrichment in samples VSE 5 and 8, suggest an additional input from eroded basement rocks. Some interaction with lake or pore waters has probably occurred due to slightly elevated levels of As and Li in both samples and of Mg, Ca and Sr in VSE 5 (Figure 4.3).

Detailed electron microprobe work on sample VSE 8, from Section Lower C, revealed that these acid volcanoclastic sediments have been modified to a minor extent since deposition. The composition of a single plagioclase phenocryst which has been partially altered is shown in Figure 4.4b. Plagioclase has been altered to illite and to illite-smectite mixed layer clay minerals (Figure 4.4b), either during diagenesis or by weathering. It is likely that this alteration occurred after the deposition of these sediments since feldspars in volcanics around the basin have been affected by a more acidic alteration producing kaolinite (Chapter 3).

In addition, small (1-40  $\mu\text{m}$ ) rhombic K-feldspar phenocrysts were observed in the matrix of sample VSE 8 (Plates 4.1a & b). These phenocrysts have different compositions to magmatic K-feldspars analysed in the rhyolites and granite (Chapter 2), since they are virtually Na-free ( $\text{Or}_{96-98\%}$  Appendix H). They are therefore interpreted as authigenic K-feldspars which have grown during diagenesis. Similar Na-free authigenic K-feldspar formed by the replacement of glass during diagenesis in the saline and alkaline Abert Lake in Oregon (Banfield et al., 1991a). Authigenic K-feldspar has also been observed by Helvacı et al. (1993) and Gündoğdu et al. (1996) in the Borate Formation of the Emet Basin and similar K-feldspar are common in saline, alkaline lake environments all over the world (Sheppard & Gude 1969; 1973, Hay 1977, Surdam 1977, Stamatakis 1989, Banfield et al., 1991a). As described above, the presence of authigenic K-feldspar is indicative of interstitial water with the highest salinity and pH (Sheppard & Gude 1973).

Plate 4.2a shows the main phenocryst phases of plagioclase, K-feldspar, quartz, and biotite in sample VSE 8, while Plate 4.2b shows a high magnification electron back scatter image of the matrix. The lighter phase in Plate 4.2b has a composition close to K-feldspar, whilst the darker phase contains less K but higher levels of Mg and Fe, and trends towards phengite and montmorillonite in composition (Figure 4.4a). The dioctahedral smectite (montmorillonite) and authigenic K-feldspar have probably directly or indirectly replaced rhyolitic glass, as described in the Köpenez tuffs lower in the stratigraphy of Emet Basin by Gündoğdu et al. (1996). The abundance of authigenic K-feldspars in the Köpenez Formation has been attributed to a high K content in the glasses (Gündoğdu et al., 1996), which is clearly a reflection of the overall high K level in the local rhyolitic volcanism (average Emet Rhyolite = 5.60 %  $\text{K}_2\text{O}$ ). Identification of the smectite type by XRD is difficult due to an overlap between the d(060) peaks of illite and montmorillonite, but the lack of a d(060) peak at 1.52-1.53 Å suggests that trioctahedral smectites are not present (Moore & Reynolds 1989).

Sample VSE 6, a siltstone also from Section Lower C is very similar in terms of geochemistry to

**Figure 4.4a - Electron microprobe analyses in volcaniclastic siltstone in the Borate Formation**

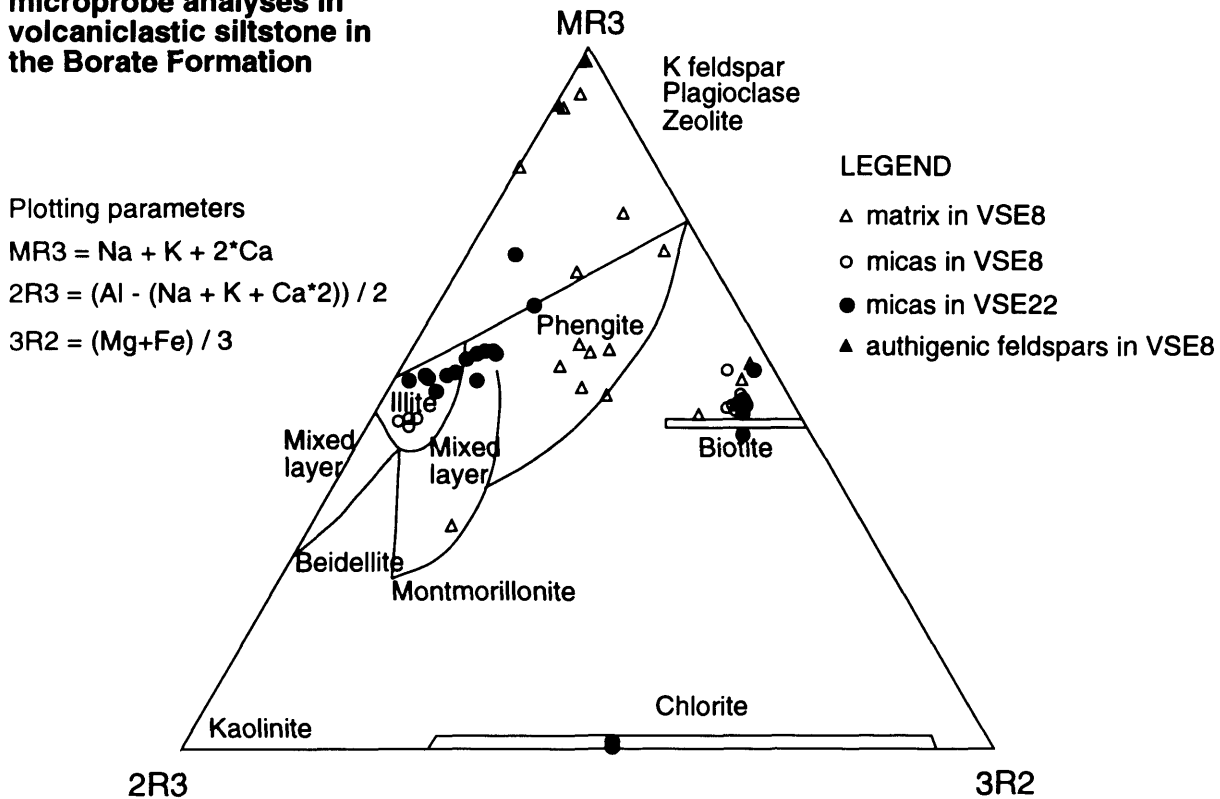
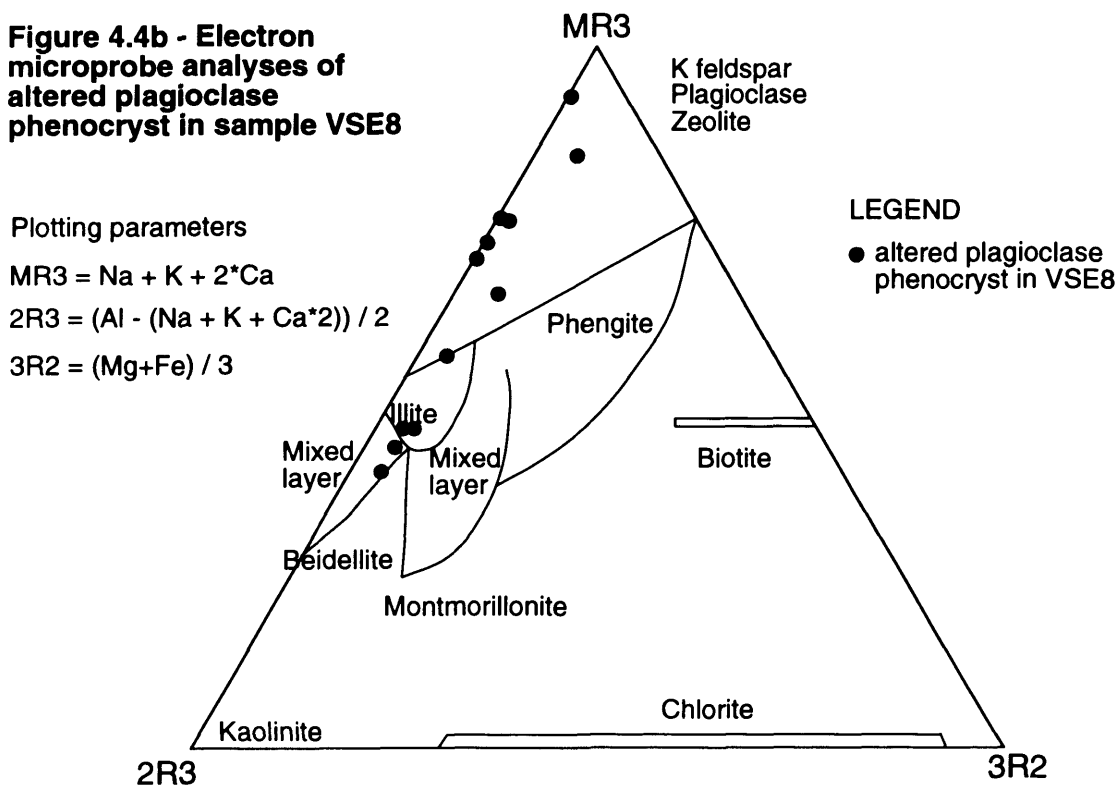


**Figure 4.4b - Electron microprobe analyses of altered plagioclase phenocryst in sample VSE8**



(Clay discrimination diagram after Velde & Meunier 1987)

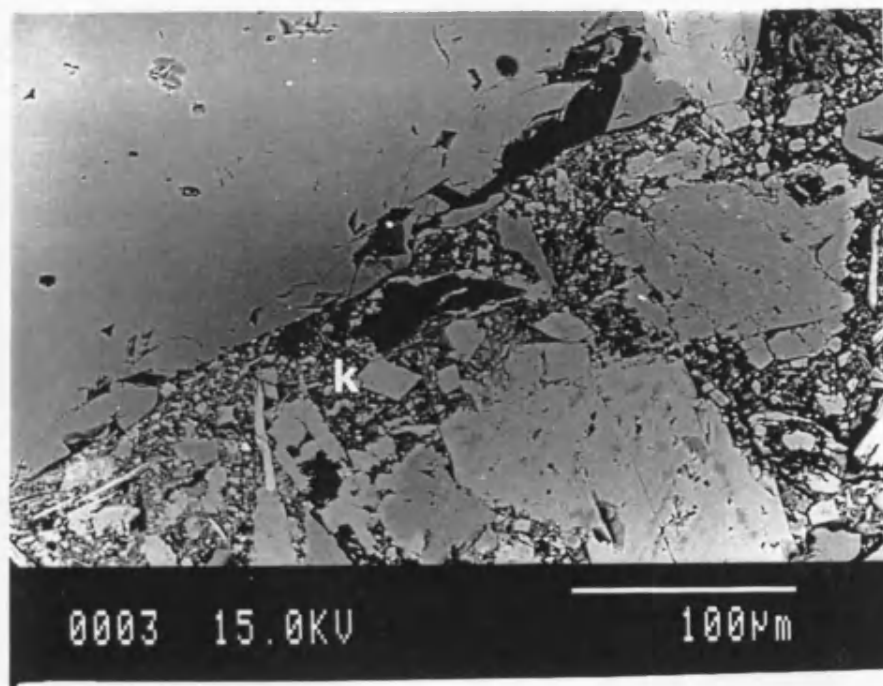


Plate 4.1a - an electron microprobe back scatter image of sample VSE 8 showing an authigenic K-feldspar crystal (K)

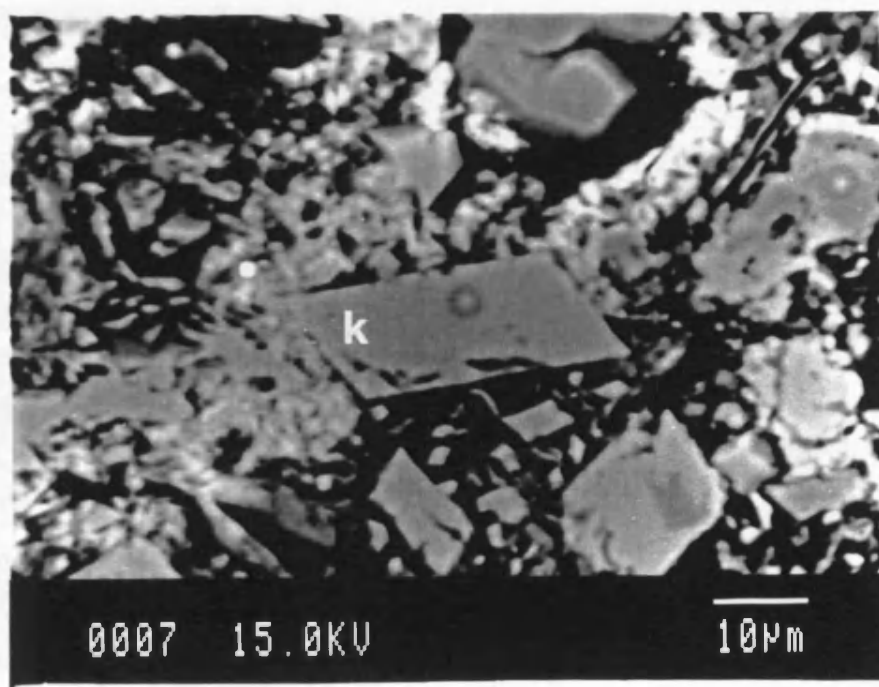


Plate 4.1b - the same authigenic K-feldspar crystal (K) viewed under higher power

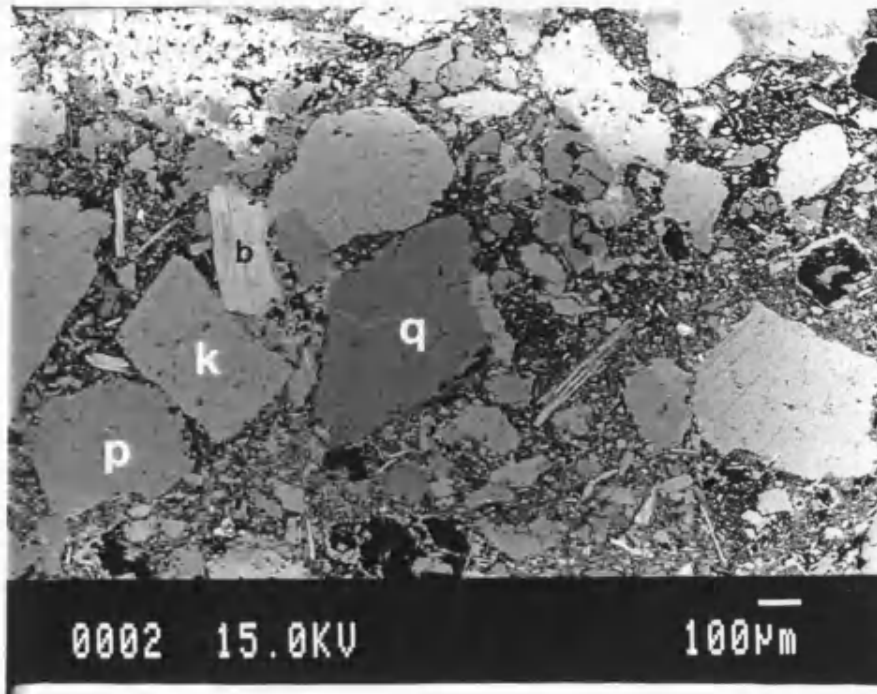


Plate 4.2a - an electron microprobe back scatter image of sample VSE 8 showing the main mineral phases present of quartz (q), biotite (b), K-feldspar (k) and plagioclase (p)

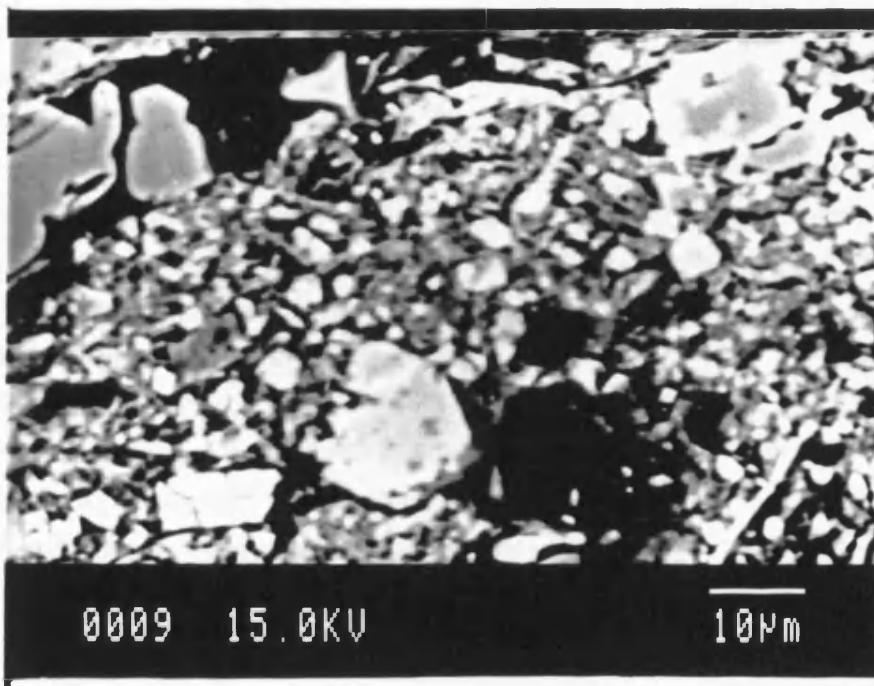


Plate 4.2b - a high magnification image of the matrix. The lighter phase has a composition close to K-feldspar, while the darker phase has a composition trending towards phengite and montmorillonite

samples VSE 5 and 8 except that it contains slightly lower Na than average Emet Rhyolite, reflecting the breakdown of plagioclase, and it contains higher Ca, reflecting the presence of calcite (Figure 4.3). Sample VSE 5 also has elevated levels of Mn and Sr relative to average Emet Rhyolite (Figure 4.3) which is probably a consequence of the substitution of  $\text{Mn}^{2+}$  and  $\text{Sr}^{2+}$  for  $\text{Ca}^{2+}$  in calcite (Deer et al., 1992). Sample VSE 10 is a limestone composed of calcite chemically precipitated from lake waters and the immobile element concentrations in this rock clearly bear no resemblance to volcanism in the basin (Figure 4.3). The calcite contains elevated Sr, As and Li (Figure 4.3) which probably reflect the concentration of these elements in the lake waters and the substitution of  $\text{Sr}^{2+}$  for  $\text{Ca}^{2+}$ .

The mineralogy and geochemistry of the colemanite-hosting mudstones (VSE 12, 14, 16) in Section Upper C (Figure 2.3) is significantly different to that of the siltstones found lower in the section. It seems likely that these mudstones are the product of the post-depositional modification of acid igneous material (similar to that of the siltstone sample VSE 8). The borate-hosting mudstones contain depleted levels of Si, Al, K, Na, Ti, Ba, Th, Nb, Zr and Y and enriched levels of Mn, Mg, Ca, As, Li, Ce, Sr and Cr relative to average Emet Rhyolite (Figure 4.3). The most pronounced enrichments are in Mg, Ca, As, Li and Sr, (Figure 4.3) which is probably a reflection of the high concentration of these elements in the lake brines. Rhyolite  $\pm$  granite-derived quartz, and plagioclase, which are present in the acid volcanoclastic siltstones in Section Lower C, are absent in the borate-hosting mudstones and Si, Al and Na are depleted relative to average Emet Rhyolite in these samples (Figure 4.3), reflecting the breakdown of these minerals.

The particularly pronounced depletion in Na is expected since there are no Na-bearing phases in the mudstones. The Na zeolite, analcime, which often forms in highly saline waters such as the colemanite deposits at Bigadiç in western Turkey (Helvacı 1995) and in the borax deposits of Kramer in California (Sheppard & Gude 1969) is absent here. However, analcime has been recorded lower in the stratigraphy in the pyroclastic rocks of the Köpenez Formation, where it apparently formed during diagenesis under saline conditions (Gündoğdu et al., 1996). Illite in the mudstones is probably the only detrital mineral remaining and it provides a sink for Al, Si and K (Deer et al., 1992). Some Mg and Fe might also occur in the octahedral sites of the illite (Velde 1995). As indicated above some authigenic illite may also be present which formed by the alteration of feldspar. Authigenic illite-smectite mixed layers have been reported elsewhere in the Borate Formation (Gündoğdu et al., 1996).

The K-feldspar in samples VSE 12 and 16 (Figure 4.3) is considered to be largely authigenic on the basis of the rhombic authigenic crystals observed in Section Lower C. Some detrital K-feldspar might remain but the authigenic variety is typical of extremely saline, alkaline conditions (Sheppard & Gude 1973) such as clearly existed in this environment of colemanite precipitation. The depletion in K relative to average Emet Rhyolite (Figure 4.3) in the mudstones indicates that some K was lost in solution with the breakdown of glass and detrital K-feldspar. However, the presence of illite and authigenic K-feldspar and the lack of any Na bearing phase has maintained and often increased the high K/Na ratio inherited from the local rhyolitic volcanism. Rb is not depleted relative to average Emet Rhyolite (Figure 4.3) and it presumably resides in these K-bearing minerals. Carbonate, both dolomite and calcite, is a major phase in the mudstones, which is reflected in their high Mn, Ca and Mg

concentrations (Figure 4.3). Yalçın et al. (1985) provide the only other record of dolomite in the Borate Formation. As discussed above, local acid magmatism probably contributed minimal Mg or Ca to the lake waters. The increasing content of Ca and Mg may at least in part explain the depleted levels of Si, Al, Ti, Ba, Th, Nb, Zr and Y relative to average Emet Rhyolite (Figure 4.3).

Another sink for Ca, Mn and particularly Mg in these mudstones is smectite and whole rock and clay separate XRD analyses (Appendix G) illustrate that CaMg smectite is present with a peak at approximately 15 Å (Brindley & Brown 1980). Further attempts to classify the smectite were made using 060 reflections which can discriminate between dioctahedral and trioctahedral smectites (Moore & Reynolds 1989, Hay et al., 1991). Values from whole rock XRD analyses of d(060) for the smectites in these mudstones range between 1.52 and 1.53 Å (Appendix G), which is indicative of trioctahedral smectites (Moore & Reynolds 1989, Hay et al., 1991). However, caution should be taken using this method of identification, since calcite has a peak in the same region. In order to overcome this problem, the ratio of the 3.03 to the 1.52 Å peak was measured in a calcite-rich sample (VSE 10); the proportion of the 1.52 Å peak taken up by calcite in mudstone samples could therefore be determined. In all cases, calcite alone cannot account for the intensity of the 060 reflections and it is therefore concluded that trioctahedral smectites are present.

The identification of trioctahedral smectite is consistent with the observations of Gündogdu et al. (1996), who state that saponite and stevensite are present in the Borate Formation, and with Ataman and Baysal (1978) who showed that the clays in the Borate Formation are Mg-rich (up to 7.89 % MgO) while Ca (up to 0.53 % CaO) and Na concentrations (upto 0.48 % Na<sub>2</sub>O) are lower. Trioctahedral Mg smectites, such as saponite and hectorite, are the most commonly reported authigenic smectites in alkaline lakes (Hellier 1995) and Mg-rich smectites are characteristic of basin centres where salinity is highest (Jones 1986).

The evidence presented in this study and by Gündogdu et al. (1996) indicates that dioctahedral smectites were produced by the alteration of rhyolitic glass and feldspar during weathering and diagenesis in the Köpenez, Red and lower Borate Formations, while further diagenesis under conditions of increased salinity lead to the generation of trioctahedral smectites in the borate-hosting mudstones. This is a very similar situation to that observed by Banfield et al (1991a, b) in their study of Lake Abert in Oregon, where di-trioctahedral smectite in the lake clays were produced by the addition of authigenic trioctahedral smectite to dioctahedral aluminous volcanic weathering products. The authigenic growth mechanism might involve the overgrowth of new layers onto existing clay flakes or the uptake of Mg into interlayer sites, with subsequent addition of Si to form new smectite layers (Jones 1986). Similarly, authigenic Mg-smectite in Searles Lake in California is thought to form by the addition of Mg silicate to dioctahedral smectite either by precipitation onto a montmorillonite template or by interstratification (Hay et al., 1991). Hence, it appears that dioctahedral smectite, produced from the weathering of volcanics, is an important precursor to lacustrine Mg-rich trioctahedral smectites. Furthermore, it has been suggested that the exchange of Mg for Ca into interlayer sites might provide a source for Ca in the precipitation of calcite (Jones 1986).

Apart from Mg and Ca, the trioctahedral smectites contain Si and Al and possibly Li (Deer et al.,

1992). In a trioctahedral smectite, Si occupies tetrahedral sites, Al can occupy tetrahedral and octahedral sites, Mg occupies octahedral sites, Li can occupy octahedral sites and Na and Ca occupy the interlayer sites (Deer et al., 1992, Velde 1995). Samples VSE 12, 14 and 16 contain significantly higher Li than the siltstones in Lower Section C (Figure 4.3) which is consistent with the identification of trioctahedral smectites in the colemanite-hosting mudstones. Gündoğdu et al. (1996) state that Li-stevensite is the Li-bearing trioctahedral smectite in the Borate Formation. It is possible that K, Rb, Sr and Ba might also reside in the interlayer sites in the smectite, having exchanged for Ca and Na (Deer et al., 1992). Other authigenic minerals found in the mudstones of Section C include colemanite and realgar, which are indicative of high B, Ca, S and As in the precipitating brines. The enrichments relative to average Emet Rhyolite of Cr and Co probably reflect a small input from mafic basement rocks, while elevated Ce (Figure 4.3) might indicate the presence of detrital monazite, although there appears to be no corresponding increase in P.

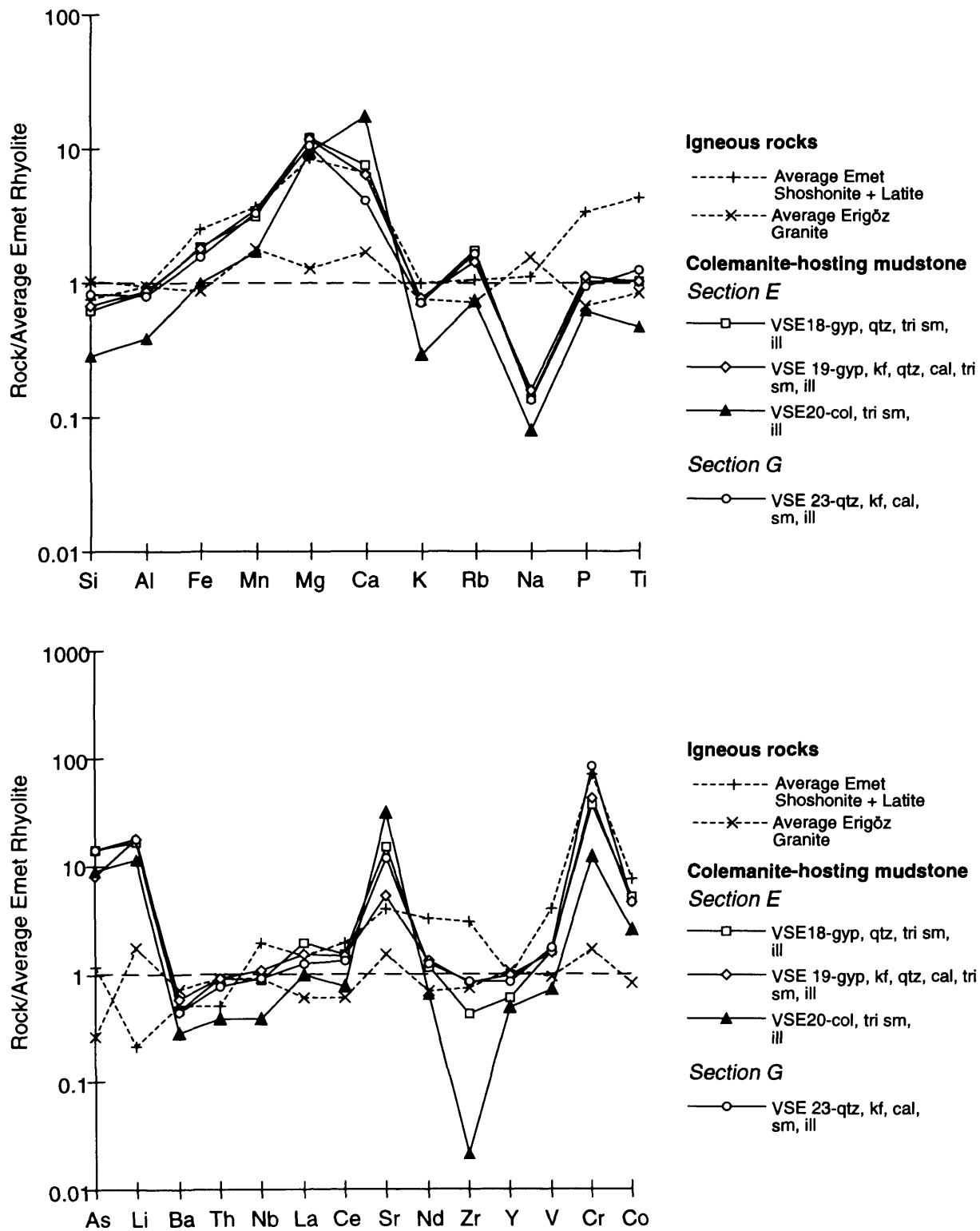
The borate-hosting mudstones of Sections E and G from the southern part of Emet Basin generally have a similar composition to the mudstones of Upper Section C, containing trioctahedral smectite, K-feldspar, calcite and illite; depletions relative to average Emet rhyolite in Si, Al, K, Na, Ba and Zr, and enrichments in Mn, Mg, Ca, As, Li, Sr, Cr and Co (Figure 4.5). As in the Upper Section C mudstones, the most pronounced enrichments are in Ca, Mg, Mn, As, Li, and Cr while the most pronounced depletion is in Na (Figure 4.5). Trioctahedral smectite was identified by  $d(060)$  at  $1.52 \text{ \AA}$  (Appendix G); all the samples also have 060 reflections at  $1.50 \text{ \AA}$  which is diagnostic of dioctahedral smectite but a definite identification cannot be made due to overlap with the illite peak (Moore & Reynold 1989). Differences with the Upper Section C mudstones include the presence of gypsum and quartz in Section E and celestite in Section G. Furthermore, these mudstones have a slight enrichment in Fe relative to average Emet Rhyolite (Figure 4.5), which might indicate substitution of this element into the octahedral sites of illite, or perhaps into the carbonate phase.

### (d) Summary

A mineralogical and geochemical transition can be observed from largely unmodified acid volcanoclastic siltstones, containing an abundance of rhyolitic/granitic detrital minerals, to mudstones which have been extensively modified during diagenesis. This transition can be clearly observed within Section C over approximately 20 m of stratigraphy. The mineralogy and geochemistry of unmodified siltstones reflects the rhyolitic, and possibly granitic, input into the sediments; the presence of pumice, glass, spherulitic fragments, quartz, plagioclase, K-feldspar, biotite, dioctahedral smectite, kaolinite and a geochemical signature similar to that of the local rhyolitic volcanism. The first changes to occur in these acid igneous-derived sediments on interaction with saline, alkaline waters and during early diagenesis, were the breakdown of glass, plagioclase and kaolinite and the precipitation of calcite and dolomite in interstitial spaces. The former led to the release of K, Na, Al and silica while the latter resulted in an increase in Ca, Mg, Sr and Mn in the sediment. At least some of the rhyolitic glass was replaced by dioctahedral smectite and authigenic K-feldspar. The presence of authigenic K-feldspar and detrital illite explains the partial retention of K in these sediments.



**FIGURE 4.5- Geochemistry of sediments from the Borate Formation (Sections E & G - mid and southern Emet Basin)**



LEGEND: qtz=quartz, kf=K-feldspar, plg=plagioclase, bio=biotite, cal=calcite, dol=dolomite, tri sm=trioctahedral smectite, ill=illite, musc=muscovite, kaol=kaolinite, gyp=gypsum

Average Emet Shoshonite & Latite = average of E3, 4, 68

Average Erigöz Granite = average of G1, 2, 4, 5, 7, 8, 23

Further post-depositional modification of acid igneous-derived sediments, through diagenesis and interaction with highly saline brines, appears to have led to the generation of the borate-hosting mudstones, in which the only remaining detrital volcanic mineral is rare quartz. These mudstones show pronounced enrichments in Mn, Mg, Ca, As, Li and Sr and depletion in Na relative to local rhyolitic volcanism. The high levels of Mn, Mg, Ca, As, Li and Sr in the mudstones reflect brines enriched in these elements which led to the precipitation of calcite, dolomite, colemanite, gypsum and celestite. The rhyolitic/granitic input probably only supplied a minor amount of Ca (from dioctahedral smectite modification and plagioclase breakdown) and Mg to these brines, and local carbonate basement is considered a more significant source for these elements. The significance of local magmatism on the concentrations of B, As, Li and Sr in the brines is investigated in detail later in this chapter. The high K/Na ratio of the rhyolitic input led to the growth of authigenic K-feldspar and despite an overall reduction in K during diagenesis, the ratio was maintained due to the extreme depletion in Na and the absence of any authigenic Na phase. The modification under highly saline conditions of dioctahedral smectite, which was formed by the alteration of volcanic minerals and glass, probably led to the generation of Mg-bearing trioctahedral smectite.

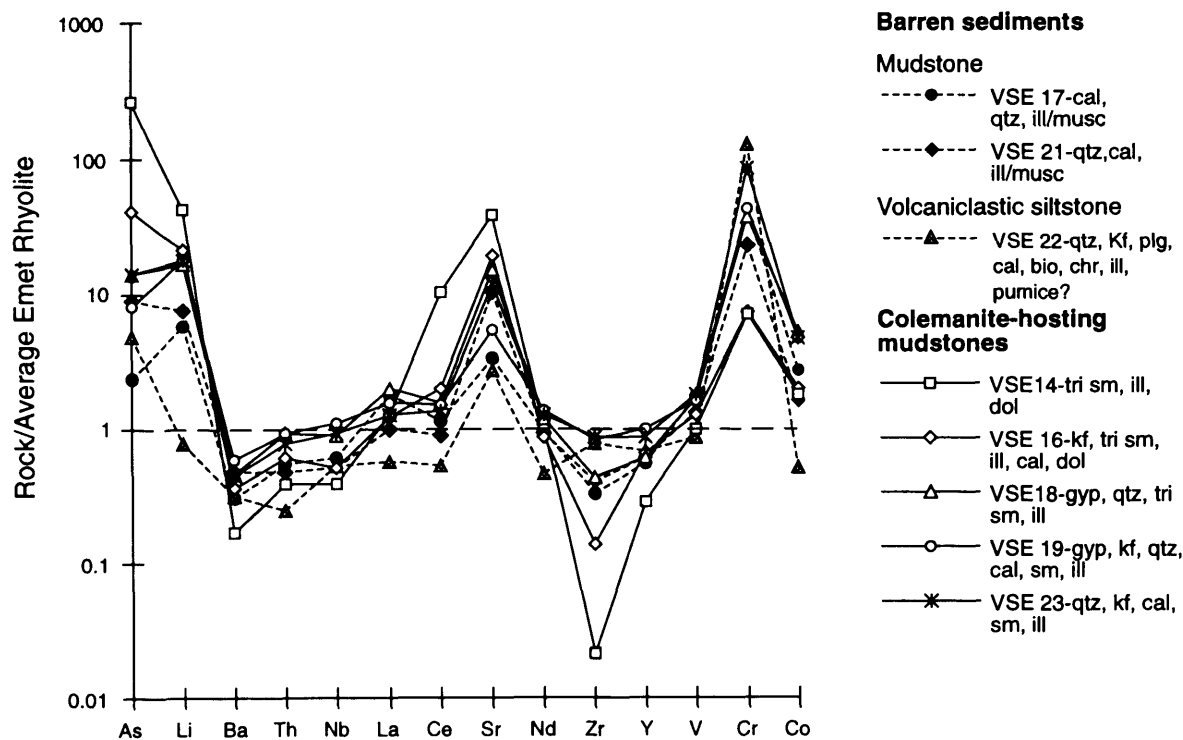
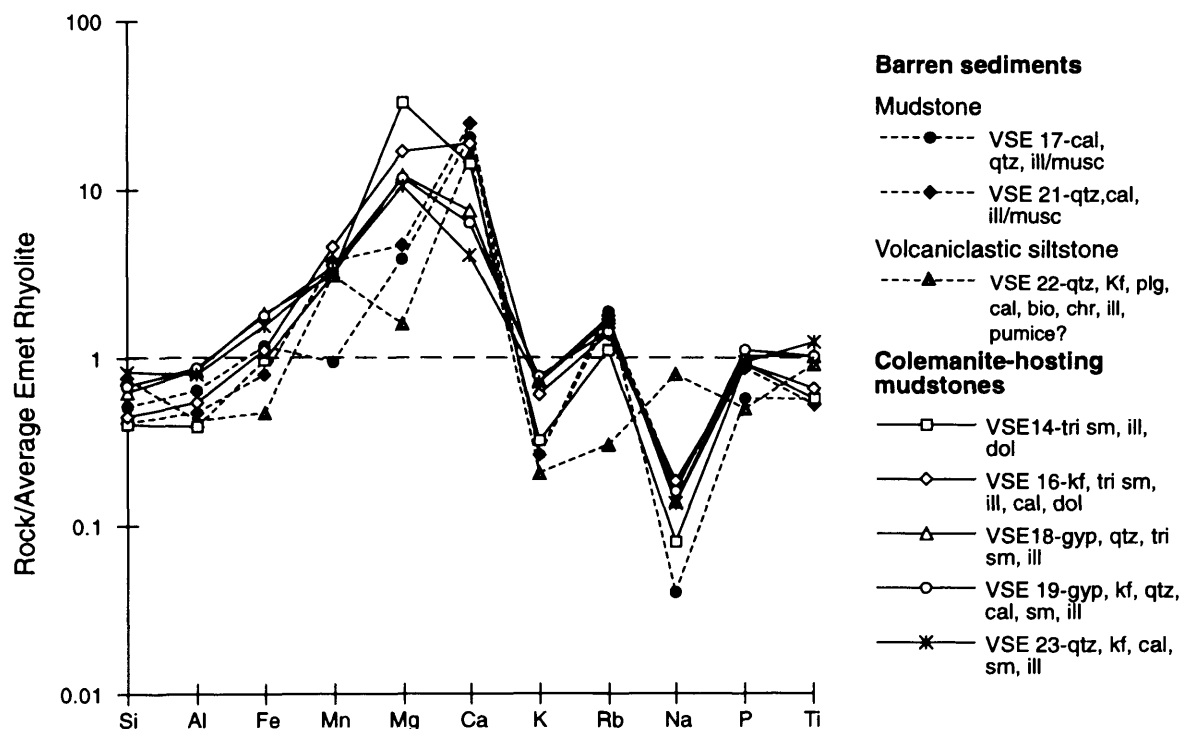
The occurrence of borates, authigenic K-feldspar, trioctahedral smectite, together with high concentrations of Mg, Ca, As, Li and Sr indicate that these mudstones developed in a highly saline, alkaline environment, probably near to the centre of an evaporitic (playa) lake where extreme concentration took place. Lower in the stratigraphy (Köpenez Formation) clinoptilolite was produced under less saline conditions, and analcime was generated where the K/Na ratios in glass were lower (Gündoğdu et al., 1996). The presence of illite and enriched Cr in the Borate Formation suggests an additional input to acid magmatism, such as eroded local basement. Ultramafic rocks may account for the elevated Cr, but no direct evidence for such rocks was found.

#### *4.2.2.5 Implications for the distribution of borate mineralisation within Emet Basin*

In order to assess the impact of local magmatism on the distribution of borate mineralisation within the Borate Formation, comparisons have been made between the mineralogy and geochemistry of mineralised (C, E, and G) and barren sections (D and F) (Figure 4.6).

Sample VSE 22 is a volcanoclastic siltstone from barren Section F which has similar mineralogy to Ca-rich siltstones from elsewhere in the basin (eg. VSE 3 from the Red Formation and VSE 6 from Section Lower C in the Borate Formation), with a calcite cement, white mica, biotite, quartz, plagioclase and K-feldspar. The geochemistry of this siltstone (Figure 4.6) suggests that high Ca has led to a relative dilution of Si and Al, but most of the immobile element concentrations are similar to those of average Emet Rhyolite, indicating an acid igneous derivation for these sediments in common with other parts of the basin. However, smectite, common in the mineralised sediments, is lacking in sample VSE 22 from barren Section F. As observed elsewhere in the basin, the Ca enrichment in sample VSE 22 is accompanied by enhanced Mn, Mg and Sr relative to average Emet Rhyolite (Figure 4.6). A pronounced Cr enrichment in this siltstone (Figure 4.6) can be explained by the presence of detrital chromite crystals in the sample, which were analysed by the electron microprobe. They presumably

**FIGURE 4.6 - Comparison between geochemistry of sediments from barren (Sections D & F) and colemanite-bearing (Sections C, E & G) mudstones in the Borate Formation**



LEGEND: qtz=quartz, kf=K-feldspar, plg=plagioclase, bio=biotite, cal=calcite, dol=dolomite, di sm=di octahedral smectite, tri sm=tri octahedral smectite, ill=illite, musc=muscovite, kaol=kaolinite, col=colemanite, chr=Cr bearing mineral

originated from the erosion of local basement rocks. The white micas are illitic in composition (Figure 4.4a) and were probably also derived from local basement.

In contrast to the borate mineralised mudstones of Sections Upper C, E and G, colemanite, realgar, celestite, gypsum, dolomite, smectite and K-feldspar were absent in XRD traces of the mudstones of barren Sections D and F (Figure 4.6). The barren mudstones are comprised of illite, calcite and quartz. The XRD trace of barren mudstone from Section D indicates a very gradual increase in intensity at around 15 Å (~6 degrees Two Theta), but no distinct smectite peak is observed, which contrasts with the extremely sharp peaks observed in this region in the colemanite-hosting mudstones (Figure 4.7). Peaks at 1.525 and 1.527 Å in the barren mudstone samples VSE 21 and 17 respectively are in the region of trioctahedral smectites but these peaks are taken up by calcite, which is abundant in these sediments. A lack of smectite and dolomite in the barren sediments explains the lower levels of Mg relative to the mineralised mudstones while the lack of K-feldspar explains the low K levels in these sediments (Figure 4.6).

Sediments from Section Lower C are also barren, although they are close to the borate-host mudstones of Section Upper C (Figure 2.3). These sediments from Section Lower C also lack dolomite, but they contain authigenic K-feldspar and smectite, which as discussed earlier, appears to be dioctahedral. Hence, barren sediments in all cases lack dolomite and trioctahedral smectite (Sections Lower C, D & F), and sometimes lack authigenic K-feldspar and dioctahedral smectite (Sections D & F).

As discussed above, authigenic K-feldspar and Mg-rich clays are typically developed under conditions of high salinity near to the centre of basins (Sheppard & Gude 1969; 1973, Jones 1986). Therefore, the barren sediments of Sections D and F, may have been developed under relatively low conditions of salinity, since they lack authigenic K-feldspar and trioctahedral smectite. The presence of authigenic K-feldspar in Section Lower C probably indicates slightly more saline conditions, while the occurrence of authigenic K-feldspar, trioctahedral smectite and borates in the mineralised sections indicate the highest salinity conditions. Therefore, it seems likely that the distribution of borate mineralisation within a closed basin reflects the area occupied by the palaeolake which was in turn controlled by the palaeotopography of the basin. The evidence suggests that the igneous input was fairly uniform throughout the basin although the total lack of smectite in Sections D and F might reflect some variation in the supply of detrital dioctahedral smectite or of volcanic material which could be altered to this clay.

The barren sediments of Sections D and F also contain less As, Li and sometimes Sr than the mineralised sediments (Figure 4.6, 4.8, 4.9 & 4.10) consistent with the lack of observed realgar, celestite and trioctahedral smectite. The data presented indicate that high concentrations of As, Li and perhaps Sr appear to correlate with colemanite mineralisation, consistent with the observations of Helvacı (1977) and Gündogdu et al. (1996). They described high As and Sr concentrations and Li-bearing trioctahedral smectites respectively in the borate-hosting sediments. The assertion of Kistler and Helvacı (1994) that Sr, As and Li are useful elements for borate exploration was tested in detail in the Emet Basin.

FIGURE 4.7 - XRD traces of borate-host and barren mudstone from Emet Basin

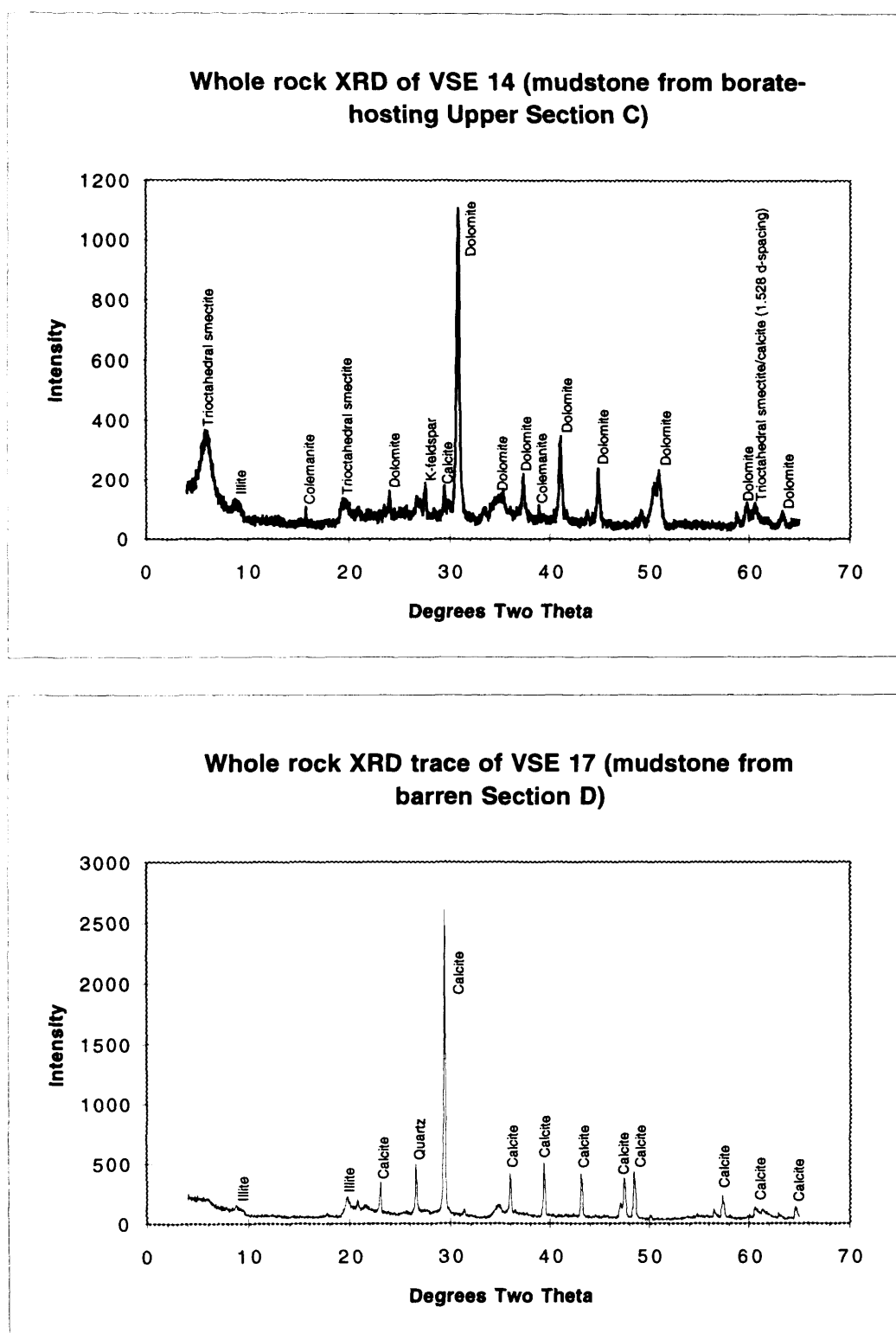


**FIGURE 4.8 - Concentrations of As, Sr and Li in sediments from the Borate Formation**

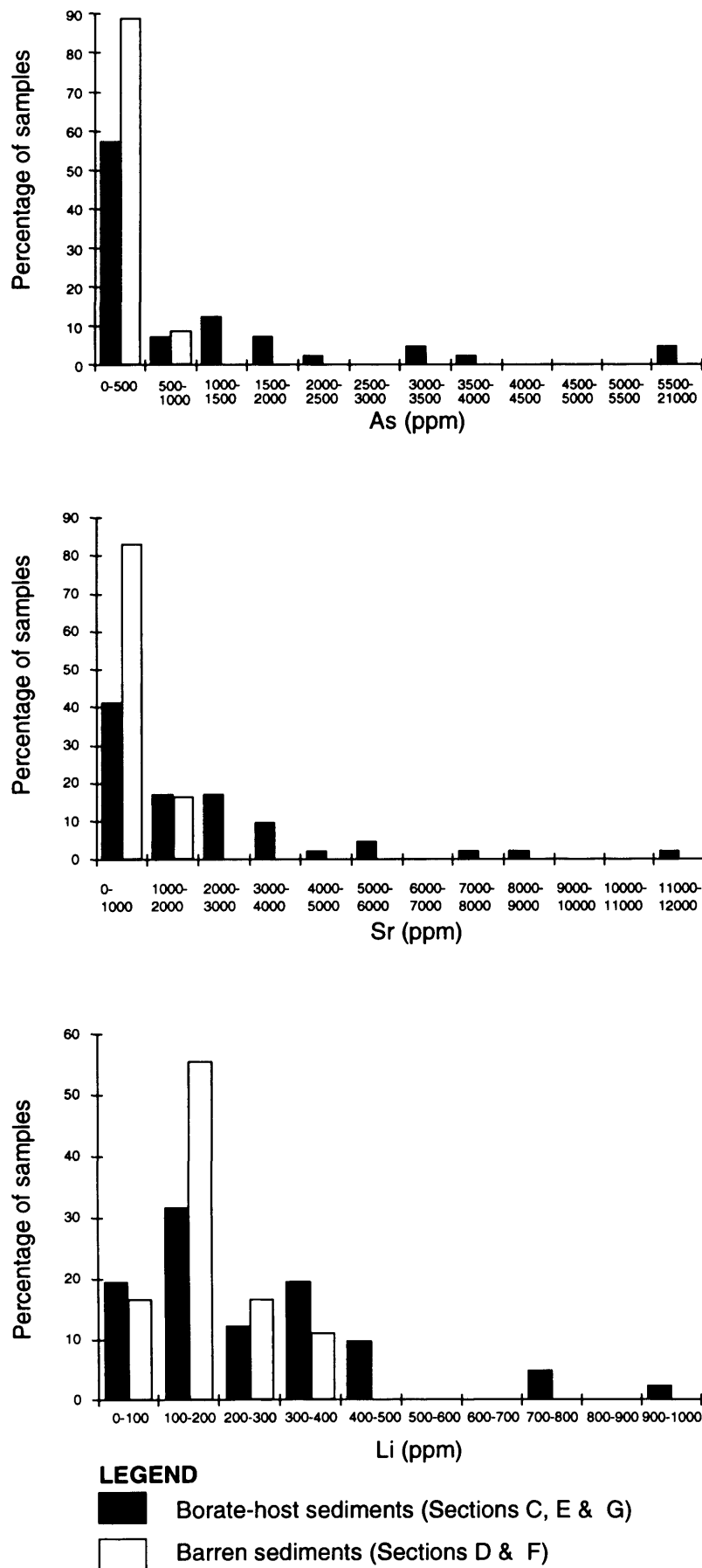


**FIGURE 4.9 - Concentrations of As, Li and Sr in the Borate Formation - Northern Emet Basin**

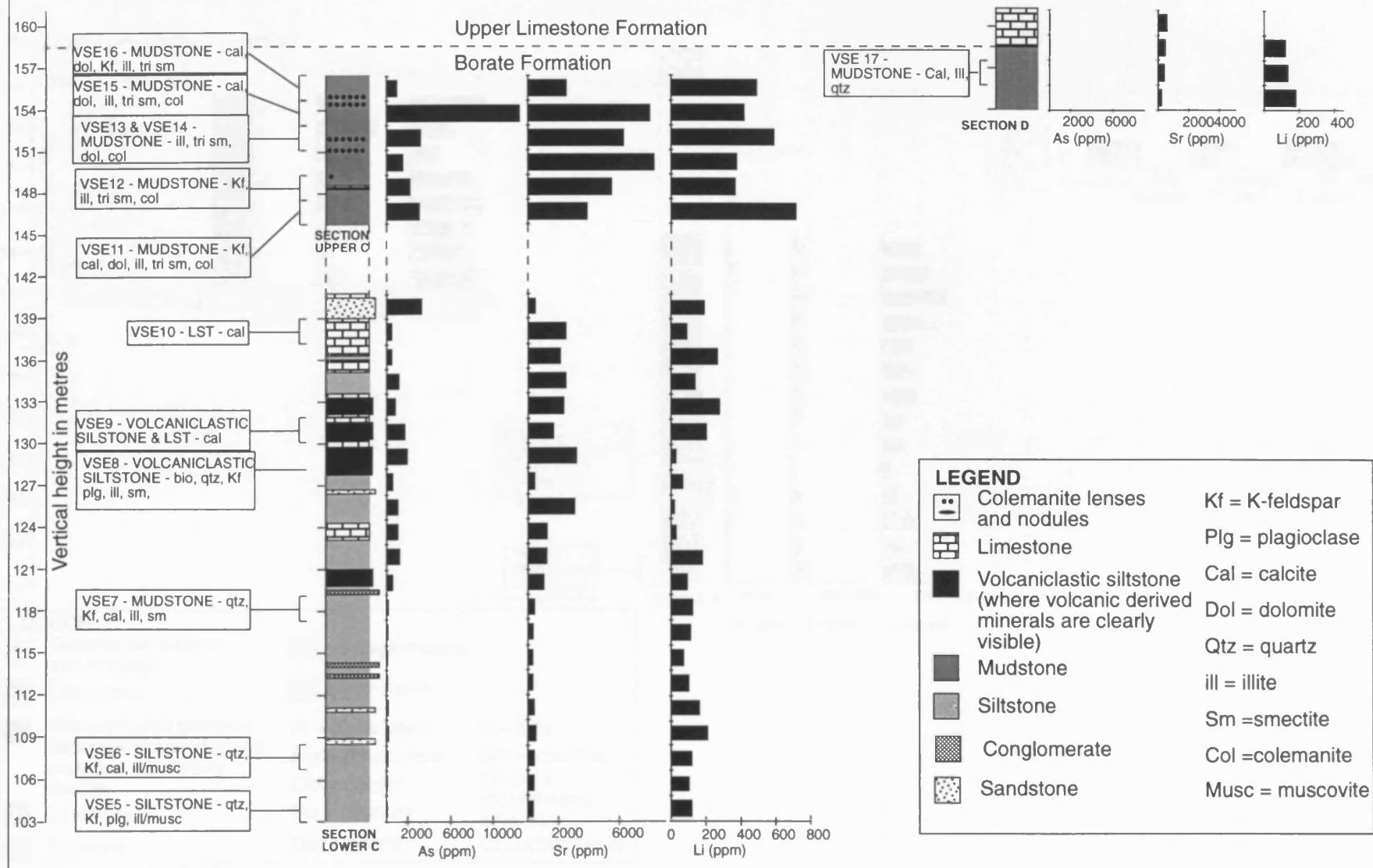
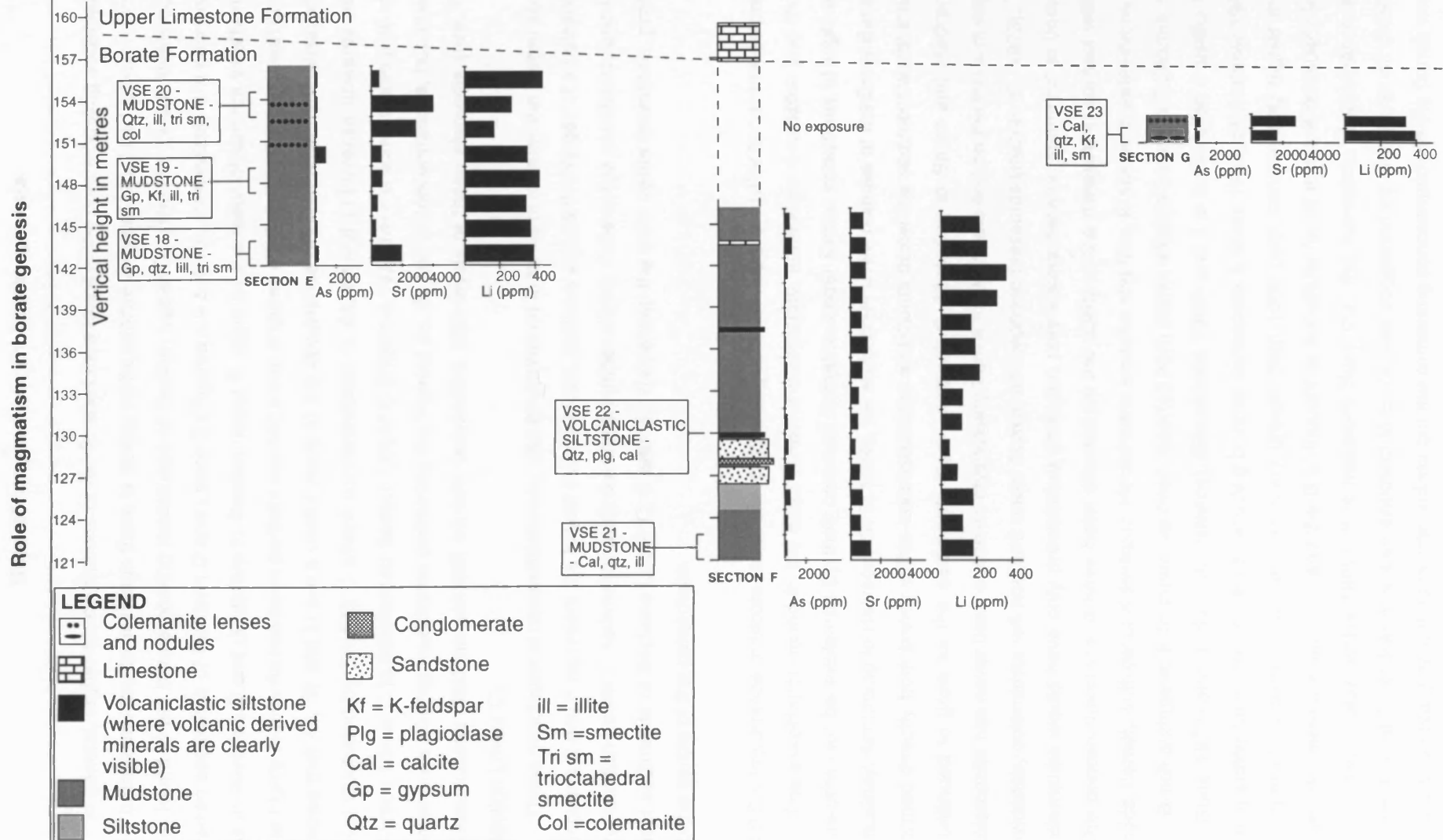


**FIGURE 4.10 - Concentrations of As, Li and Sr in the Borate Formation - Southern Emet Basin**





In general, higher concentrations of As, Sr and Li are found in the borate-hosting sediments than in the barren sediments, although there is clearly some overlap (Figure 4.8). The highest concentrations are found in the borate-hosting mudstones of Section Upper C, while the lowest levels occur in the barren sediments of Sections D and Lower C (Figures 4.9 & 4.10). Reasonably low concentrations of As in Sections E and G relative to Section Upper C might be the result of surface weathering, where the highly mobile As has been partially washed away (Figures 4.9 & 4.10). Overall however, this study shows that As, Sr and Li are a useful guide to the occurrence of colemanite mineralisation, perhaps best illustrated by Section C where concentrations of As, Sr and Li increase upwards from barren Section Lower C to mineralised Section Upper C (Figure 4.19). There is some lithological control with colemanite-hosting mudstones containing the highest As, Sr and Li concentrations, but limestone and volcanoclastic siltstone can still contain reasonably high levels of these elements (see Figure 4.9, Section Lower C).

These geochemical observations can also be explained in terms of salinity; the barren sediments of Sections D and F represent the lowest salinity facies, perhaps around the fringes of a palaeolake, while the Section Lower C sediments were developed under slightly more saline conditions, and the borate-host sediments of Sections Upper C, E and G experienced the most saline conditions, probably near to the centre of the palaeolake.

### *4.2.2.6 Importance of trioctahedral smectite, authigenic K-feldspar and illite to colemanite precipitation*

The association found in the Emet Basin of colemanite, authigenic K-feldspar and trioctahedral smectite can be explained by their common formation under similar conditions of high salinity and alkalinity. According to Helvacı (1977; 1984), the early colemanite nodules of the Emet Basin probably formed directly from brines within unconsolidated sediments below the sediment/water interface and continued to grow as the sediments were compacted. According to Smith and Medrano (1996), colemanite has never been observed crystallising from a modern lake and on the basis of experimental evidence, colemanite will not form under normal atmospheric pressures (Inan et al., 1973). Therefore, colemanite would have only precipitated when the pore waters became saturated in borate anions. The concentration would have been affected by the ability of the minerals in contact with the pore fluids, namely authigenic K-feldspar, trioctahedral smectite and illite, to absorb borate anions.

B-rich authigenic K-feldspar has been reported from saline, alkaline basins in California (Sheppard & Gude 1973) and in Samos, (Greece) (Stamatakis 1989) and it is considered a useful tool in the prospecting for saline minerals including borates (Sheppard & Gude 1973, Stamatakis 1989). The B content of these feldspars is commonly greater than 1000 ppm, considerably higher than that of volcanic derived K-feldspar and the B is thought to substitute for Al in the K-feldspar (Sheppard & Gude 1973, Stamatakis 1989). It is therefore likely that the authigenic K-feldspar in the Borate Formation of Emet Basin is also enriched in B, as was suggested by Helvacı et al. (1993). The K-feldspar probably absorbed borate anions but the remaining concentration in the brines was still high enough for colemanite and other borate minerals to precipitate. In contrast, at the Beypazari Trona Deposit in central Turkey, boron-bearing K-feldspar formed, but not borate minerals, presumably

because the remaining borate anion concentration was too low (Helvacı et al., 1993).

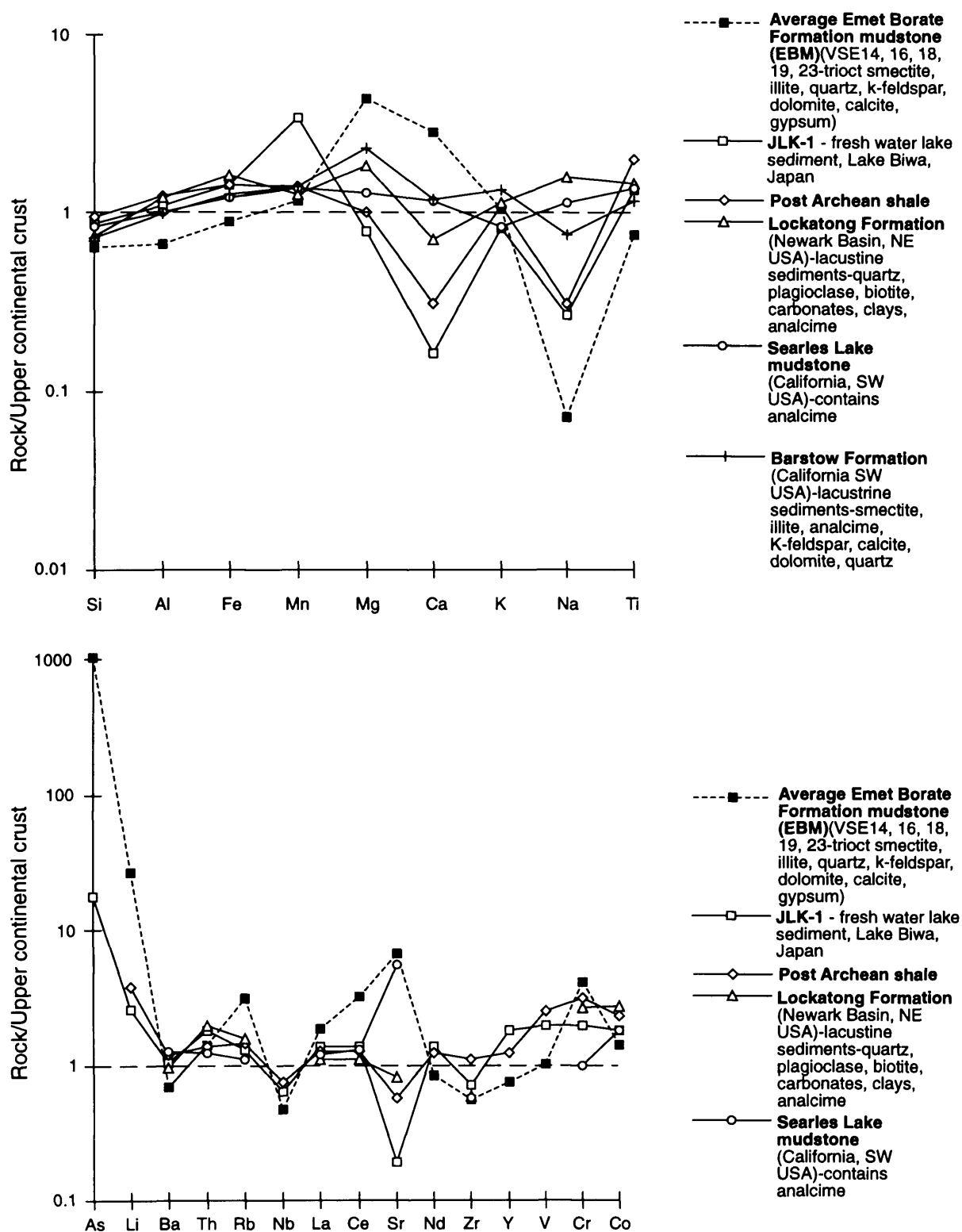
A number of workers have demonstrated that illite is considerably more effective at absorbing borate species than smectite (Stubican & Roy 1962, Fleet 1965, Keren & Mezuman 1981, Keren & O'Connor 1982, Mosser 1983, Keren & Talpaz 1984), although trioctahedral smectites (saponite) can still contain appreciable B (Stubican & Roy 1962). Experiments show that alkaline conditions are highly favourable for the absorption of borate species by clays (Keren & Mezuman 1981). This can be explained by the fact that boron speciation is pH dependent, with  $\text{B(OH)}_3$  stable below pH 7 and  $\text{B(OH)}_4^-$  stable at higher pHs, and that clays have a stronger affinity for  $\text{B(OH)}_4^-$  than for  $\text{B(OH)}_3$  (Keren & Mezuman 1981, Keren & Talpaz 1984). From B isotope evidence, colemanite is thought to precipitate from brines with a pH of about 8 (Palmer & Helvacı 1994, Oi et al., 1989). Hence, in the alkaline pore waters of the Emet Basin, it is likely that illite and trioctahedral smectite provided a sink for  $\text{B(OH)}_4^-$  anions. The experiments of Keren & Mezuman (1981) indicate that clay absorption of  $\text{B(OH)}_4^-$  decreases rapidly at highly alkaline conditions (above pH 10) due to an increase in competition between  $\text{OH}^-$  and  $\text{B(OH)}_4^-$ . It is tempting to suggest therefore that colemanite precipitation began as a result of reduced borate absorption by clays at high pHs. However, this does not appear to be the case since the colemanite precipitated from pHs of less than 10 (Oi et al., 1989, Palmer & Helvacı., 1994), before a significant reduction in borate absorption by clays would have occurred (Keren & Mezuman 1981).

The available evidence suggests therefore that authigenic K-feldspar, illite and trioctahedral smectite are all good absorbents of borate anions, especially in alkaline conditions. It is likely that the brines at Emet contained such high concentrations of borate anions, that even if the minerals discussed above absorbed borate species, concentrations in the residual fluids were still high enough to precipitate colemanite. It is possible that all the absorption/exchange sites in authigenic K-feldspar, trioctahedral smectite and illite became used up by borate anions, producing a compacting mudstone incapable of further absorption. This mudstone saturated in borate anions may then have served to localise or trap B-rich brines leading to the precipitation of colemanite. Once crystallised, colemanite is highly susceptible to surface weathering such as to calcite (Helvacı 1977) and hence the mudstone encasing the nodules would have ensured their preservation.

#### *4.2.2.7 The mineralogy and geochemistry of Emet Basin borate-hosting mudstones compared with other lacustrine sediments and upper continental crust*

Figure 4.11 compares the geochemistry of the average Emet borate-hosting mudstone (EBM) with other mudstone and shale databases and the average upper continental crust. Lacustrine sediments from the Triassic-Jurassic Lockatong Formation in north-east USA, the Miocene Barstow Formation and Quaternary Searles Lake in south-west USA provide good analogues for the mudstones of the Emet Basin, since they too experienced diagenesis under saline, closed basin conditions and are derived at least in part from acid igneous rocks (Sheppard & Gude 1969, Hay et al., 1991, van de Kamp & Leake 1996). Borates are not reported from the Lockatong Formation (van de Kamp & Leake 1996) or the Barstow Formation (Sheppard & Gude 1969, van de Kamp & Leake 1996). Colemanite is,

FIGURE 4.11 - Comparison of Emet mudstones with other sediment databases



Data sources: Emet Basin (this study), JLK-1 (Imai et al., 1996), Post Archean shale, upper continental crust (Taylor & McLennan 1985), Lockatong Formation & Searles Lake (Van de Camp & Leake 1996), Barstow Formation (Sheppard & Gude 1969)

however, reported in contemporaneous lacustrine sediments only 10 miles from the latter (Sheppard & Gude 1969) and searlesite ( $\text{NaBSi}_2\text{O}_6\text{H}_2\text{O}$ ) and borax have been reported from Searles Lake (Smith 1979, Hay et al., 1991, Kistler & Helvacı 1994). Data for fresh water sediment from Lake Biwa in Japan (JLK-1 - Imai et al., 1996) and Post Archean Shale (Taylor & McLennan 1985) are also included in this comparison as representative sediments which have not experienced saline, alkaline and evaporitic conditions.

Relative to average upper continental crust (Taylor & McLennan 1985), EBM is considerably depleted in Na but shows pronounced enrichments in Mg, Ca, As, Li, Rb, Ce, Sr, and Cr (Figure 4.11). EBM, Lockatong, Barstow and Searles Lake mudstones contain higher concentrations of Mg and Ca relative to JLK-1 and Post Archean Shale (Figure 4.10), which appears to be a feature of the high salinity environment of the former. However, EBM differs from the Lockatong Formation, the Barstow Formation and Searles Lake in having even higher concentrations of Mg and Ca, but lower concentrations of Si, Al and Fe (Figure 4.11); the probable result of dilution by the high carbonate content. Na concentrations are also considerably lower in EBM relative to all the other databases, and the highest levels are found in the Lockatong, Barstow and Searles Lake mudstones which contain analcime (Figure 4.11). The analcime in the mudstone of Searles Lake and the Lockatong Formation is thought to have formed during diagenesis as a result of high Na levels in the brines (van de Kamp & Leake 1996).

EBM is enriched in As, Li, and Sr compared to JLK-1 and Post Archean Shale (Figure 4.11). However, Searles Lake, probably a modern analogue of the Emet brines, is enriched in Li and B (Kistler & Helvacı 1994, Ludington et al., 1992) and the mudstone from there contains similar high Sr to EBM (Figure 4.11). The higher Rb, La and Ce of average EBM relative to the other sediments probably reflects the provenance of the Emet sediments; higher Rb and La the rhyolitic input (see Figure 4.3) and high Ce levels the presence of a detrital mineral such as monazite.

### **4.2.3 Comparison between the composition of sediments in the Emet Basin with those in the Selendi, Usak-Güre, Kirka and Afyon areas**

#### **4.2.3.1 Introduction**

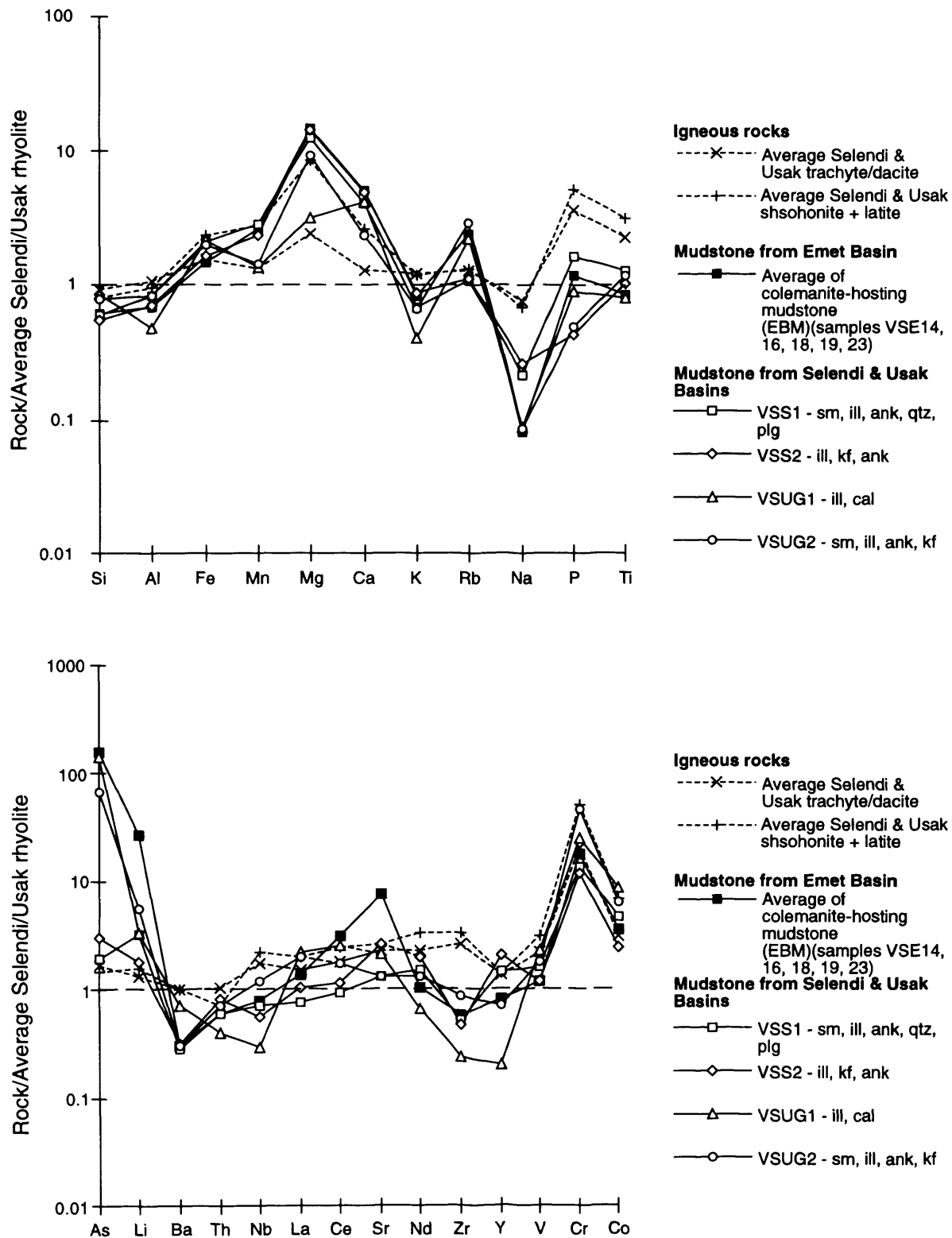
The aim of this (less detailed) work in the Selendi, Usak-Güre, Kirka and Afyon areas is:

- (i) To determine the influence of local magmatism on sediment composition.
- (ii) To provide a local comparison for the sediments of the Emet Basin.
- (iii) To assess the potential of sediments to host borate mineralisation.

#### **4.2.3.2 Selendi/Usak-Güre Basins**

Figure 4.12 shows the normalised mineralogy and geochemistry of four mudstone samples from the Selendi and Usak-Güre Basins with EBM plotted for comparison. As described in Chapter 3, the concentrations of some immobile elements such as P, Ti, Nb and Zr are similar in both the mudstones and average Selendi/Usak Rhyolite (Figure 4.12) suggesting that the sediments of all these basins were at least in part derived from local acid magmatism. The overall geochemical pattern in these

FIGURE 4.12 - Geochemistry of mudstones from the Selendi and Usak Basins



**LEGEND:** qtz=quartz, kf=K-feldspar, plg=plagioclase, cal=calcite, ank=ankerite, tri sm=trioctahedral smectite, sm=smectite, ill=illite

Average Selendi + Usak-Güre rhyolite - SE1, 2, 72, UG28, 29

Average Selendi + Usak-Güre Trachyte/Dacite - SE3, 4, UG58, 63, 64, 65, 66, 67, 75, 76, 126

Average Selendi + Usak-Güre Shoshonite + Latite - SE12, 13, 26, 27, UG7, 8, 73, 142, 145

mudstones is broadly similar to that of EBM (Figure 4.12), which as discussed above, has undergone significant post-depositional modification during diagenesis and interaction with saline, alkaline pore waters.

In detail, samples VSS 1, VSS 2 and VSUG 2 are similar to EBM in terms of major elements, while VSUG 1 differs with lower Mg and K (Figure 4.12). The former contain ankerite, illite, and sometimes smectite  $\pm$  K-feldspar and they therefore have a similar mineral assemblage to EBM. On the basis of the study at Emet, it appears that smectite (VSS 1), K-feldspar (VSS 2, VSUG 2) and Mg carbonate (VSS 1, VSS 2, VSUG 2) have a common association with borate mineralisation. The presence of ankerite as opposed to dolomite and calcite in these samples reflects their higher Fe content relative to the EBM (Figure 4.12). Sample VSUG 1 more closely resembles the barren mudstones of the Emet Basin, with the presence of only illite and calcite. This mineral assemblage explains the lower K and Mg in sample VSUG 1 relative to EBM and the other mudstone samples from this area.

Trace element patterns for samples VSS 1, VSS 2, VSUG 2 are similar to EBM, while VSUG 1 differs with lower Th, Nb, Nd, Zr, Y and V (Figure 4.12). All samples contain the distinctive enrichment in Cr, which was observed in the Emet Basin (Figure 4.12). The Selendi and Usak-Güre samples show at least some enrichment in As, Sr and Li relative to average local rhyolite (Figure 4.12), and they are enriched relative to other lacustrine sediment databases (eg. JLK 1-27 ppm As, 67.5 ppm Sr, 51.5 ppm Li - Imai et al., 1996). However, concentrations of these elements in the Selendi and Usak-Güre samples are in general lower than those found in the Emet mudstones, although there is some overlap (Figures 4.13, 4.14 & 4.15).

Hence, on the basis of the study in Emet, the presence of smectite, K-feldspar and Mg carbonate in at least some of the Selendi and Usak-Güre sediments suggests that these basins represent potential targets for borate mineral exploration. The similar chemistry of three of the samples to average EBM, with pronounced enrichments in Mn, Mg, Ca, As, Li, and Sr, further indicate a potential for borate mineralisation.

### 4.2.3.3 Kirka Basin

The mineralogy and geochemistry (normalised to average Kirka Ignimbrite) of four siltstone samples from the Karaören and Fetiye Formations in the Kirka Basin is presented in Figure 4.16 and average Emet Basin Red Formation siltstone is plotted for comparison. On both mineralogical and geochemical criteria, the volcanoclastic siltstones of the Karaören Formation are clearly ignimbrite derived (Chapters 2 & 3). Sample VSK 267 has a similar mineralogy to the ignimbrite south of the basin, except that it contains clinoptilolite and minor calcite. Clinoptilolite was also found in the Karaören Formation by Gündogdu et al. (1996). The clinoptilolite was apparently formed by the diagenetic transformation of rhyolitic glass in a saline environment (Gündogdu et al., 1996). Hence, the presence of clinoptilolite indicates that some post-depositional modification of this ignimbrite material has taken place, but the fact that glass and pumice still remain (Figure 4.16) shows that the changes were only minor.

**FIGURE 4.13 - Concentrations of sediments from the Emet, Selendi, Usak, Kirka and Afyon areas**

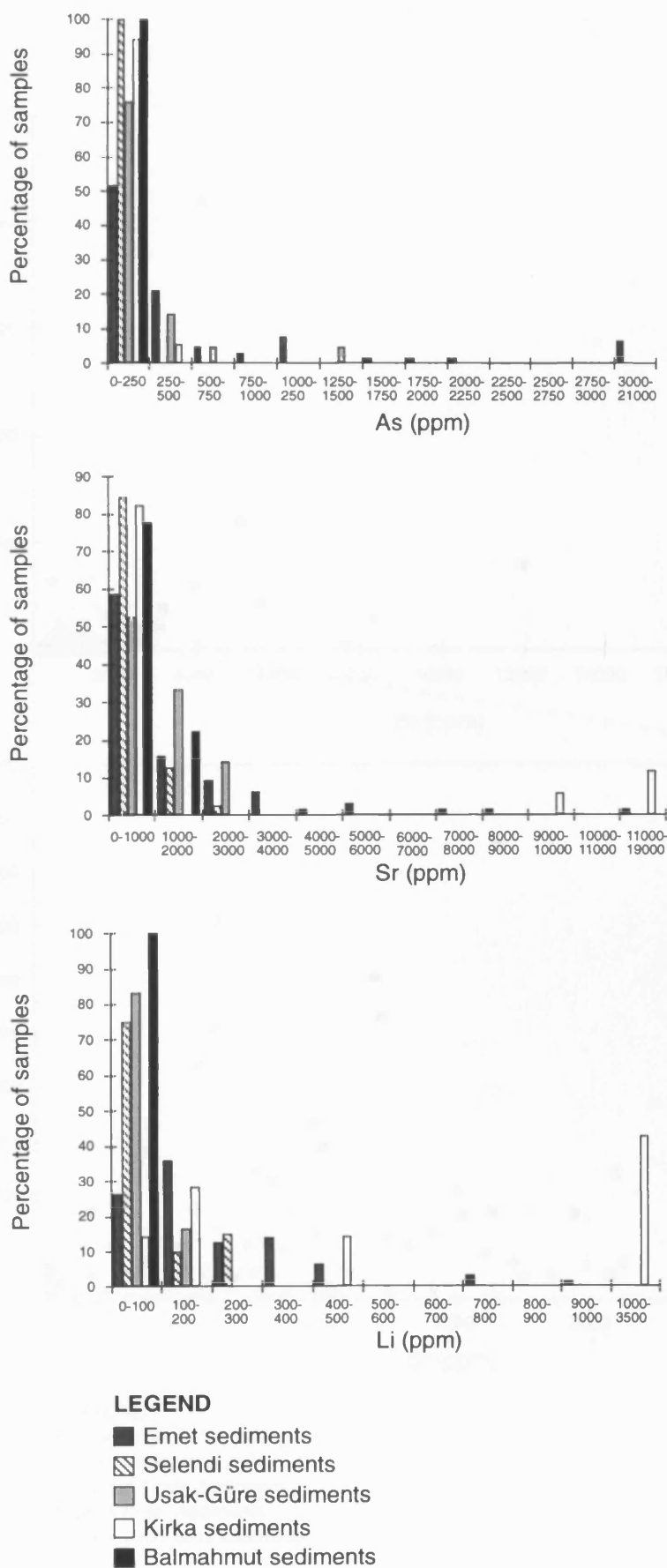


**FIGURE 4.14- As vs Sr concentrations in sediments from the Emet, Selendi, Usak, Kirka and Afyon areas**

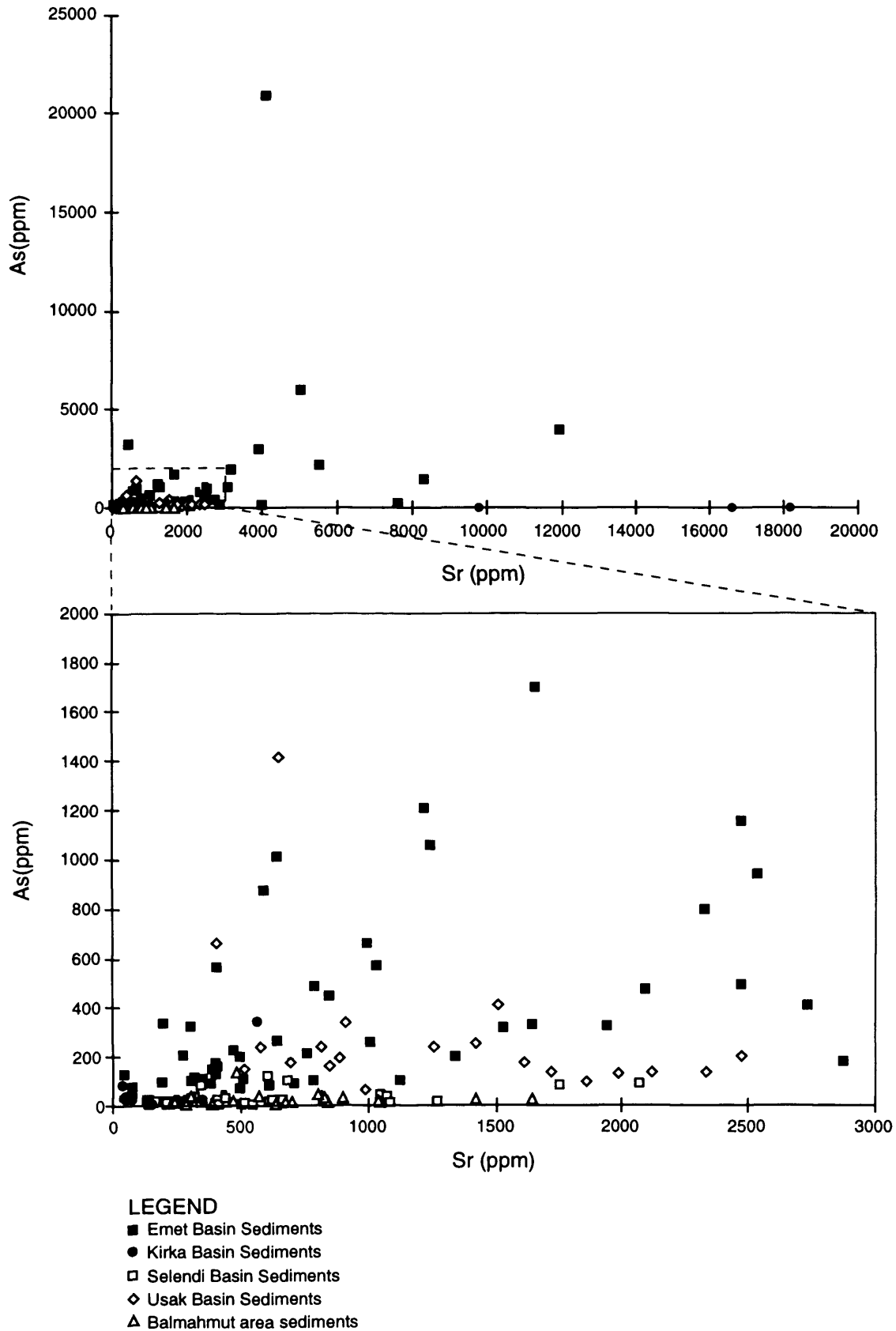




**FIGURE 4.15- Li vs Sr concentrations in sediments from the Emet, Selendi, Usak, Kirka and Afyon areas**

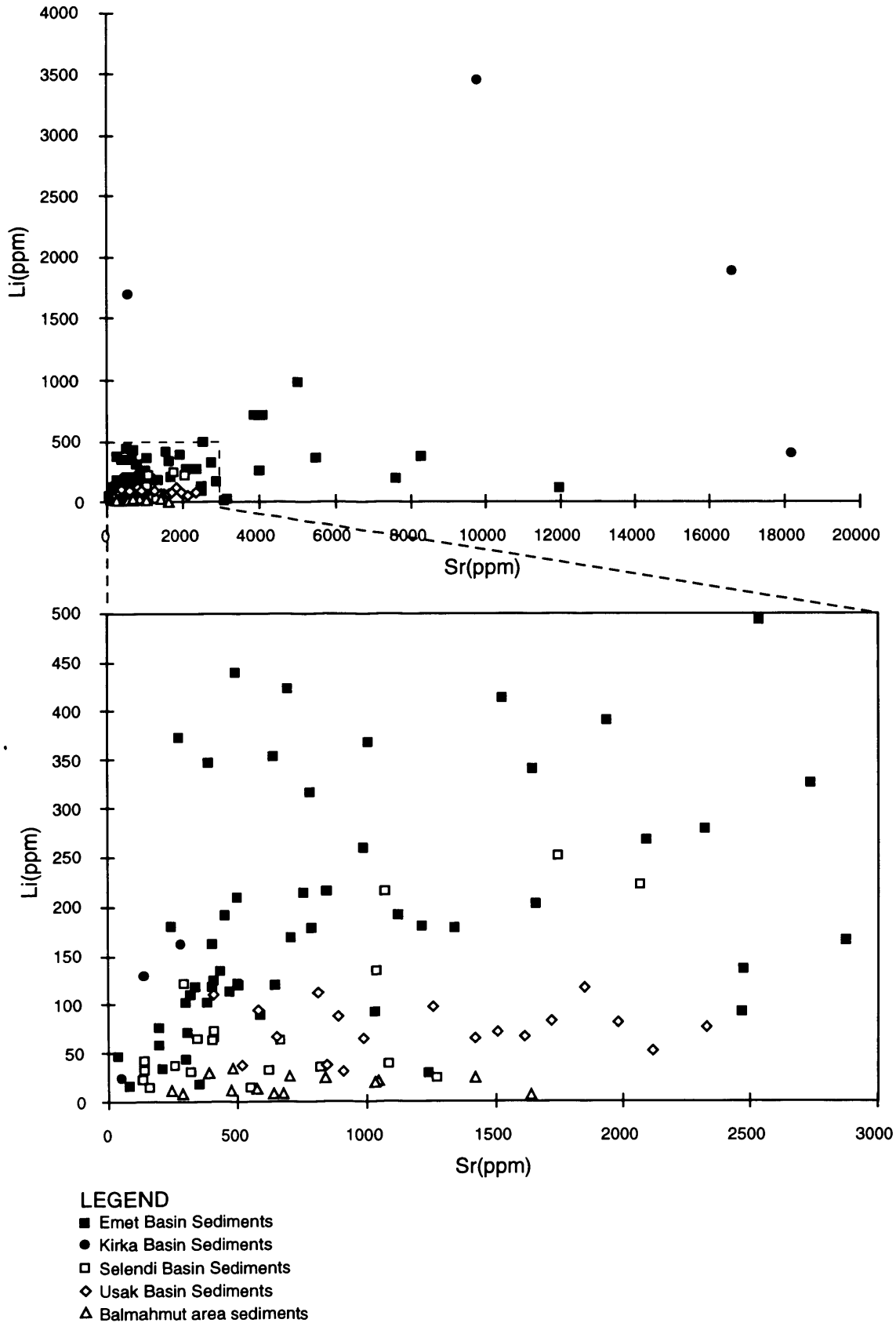
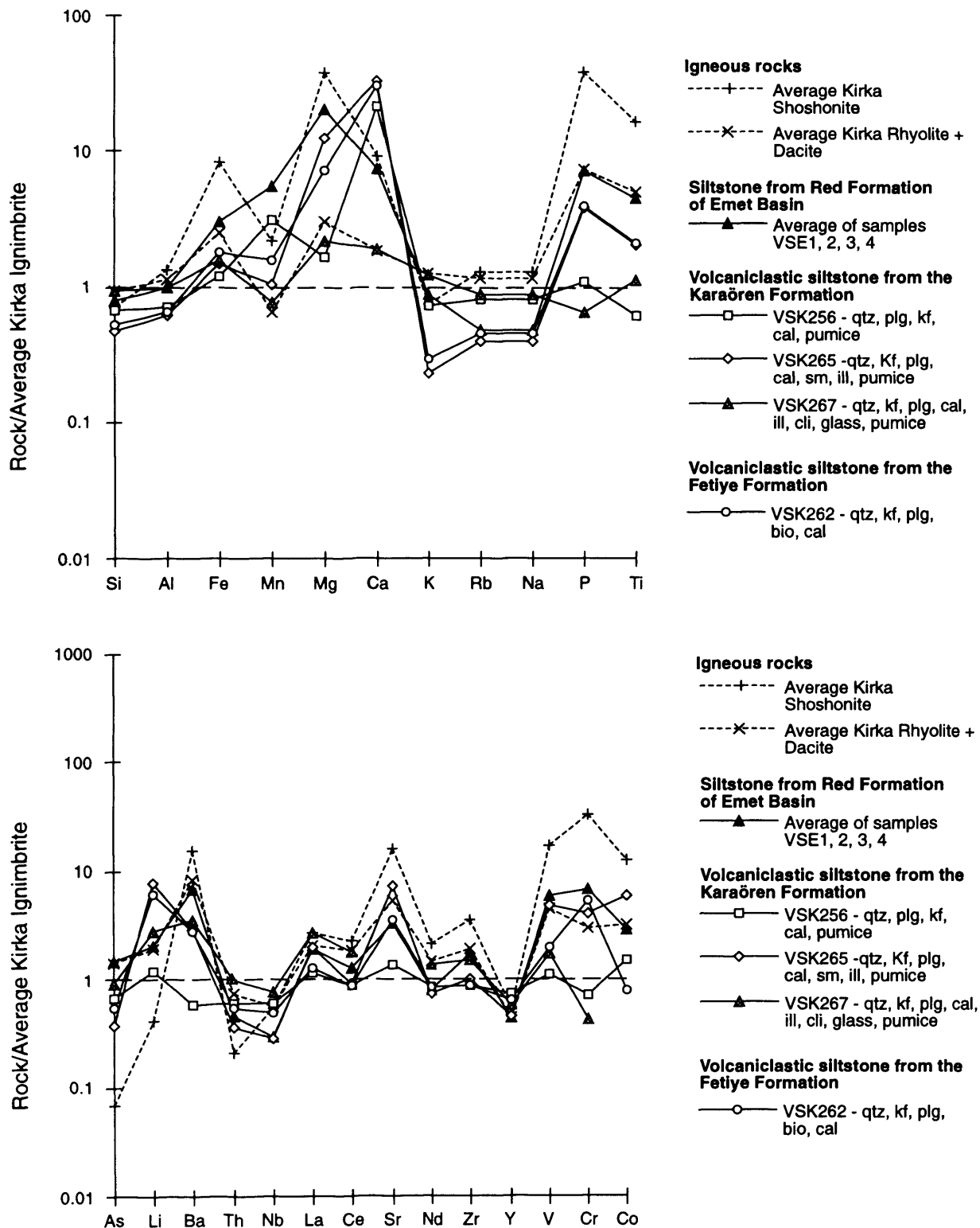


**FIGURE 4.16 - Geochemistry of siltstones from the Karaören and Fetiye Formations (Kirka Basin)**



**LEGEND:** qtz=quartz, plg=plagioclase, kf=K-feldspar, bio=biotite, sm=smectite, ill=illite, cal=calcite, cli=clinoptilolite

Average Kirka Ignimbrite - I208, 209, 219, 220, 221, 222, 250, 251, 252, 258, 259, 260, 271

Average Kirka Shoshonite - K223, 225, 226

Average Kirka Rhyolite/Dacite - K227, 228, 229, 230, 231, 232, 233, 234, 235, 236, 237, 238, 239, 244, 245, 247, 277

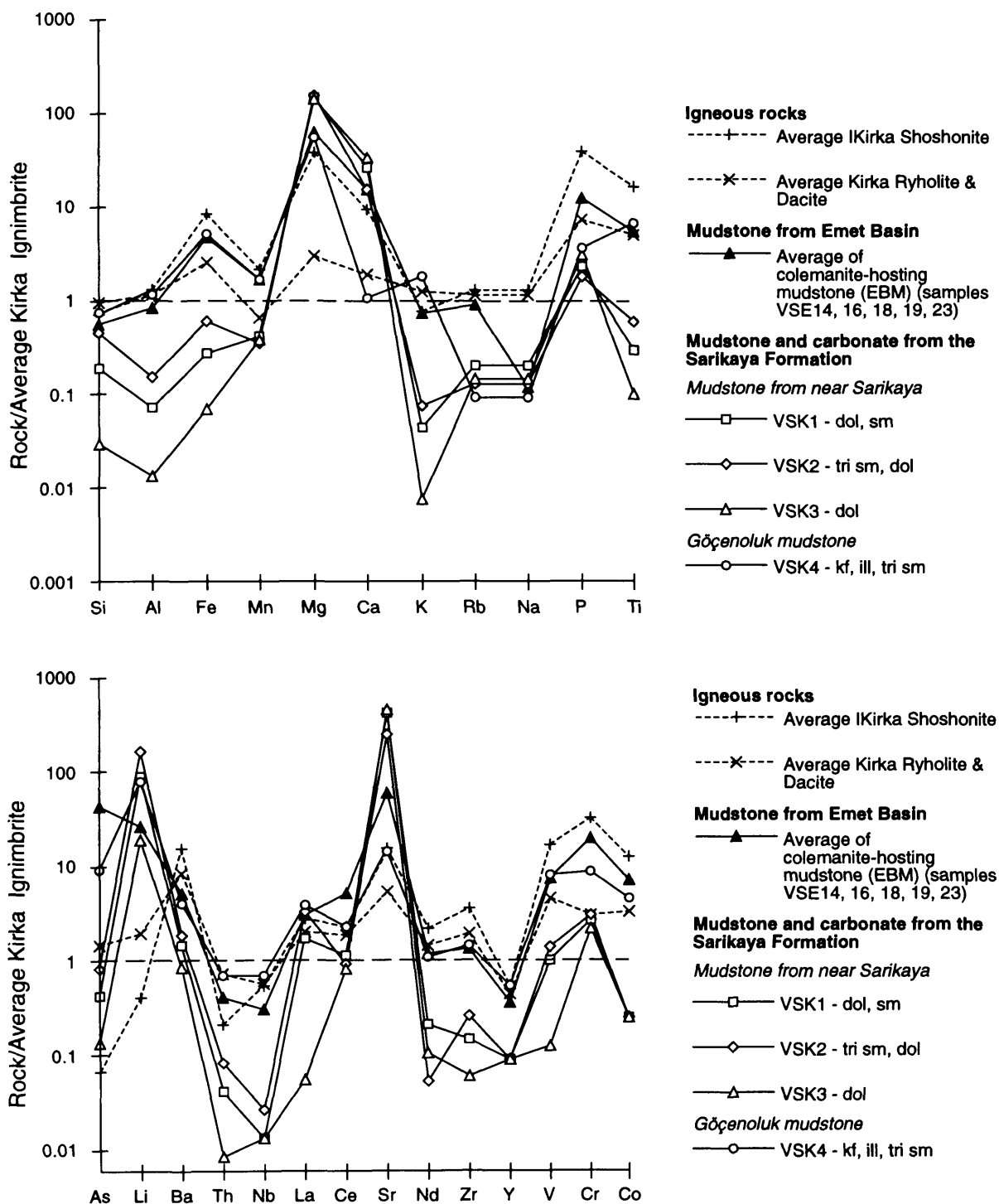
Samples VSK 256, 265 and 262 all contain abundant calcite and therefore, like the Red Formation siltstones from Emet Basin, they have elevated levels of Ca and Mg relative to average Kirka Ignimbrite (Figure 4.16). As in the Emet Basin, it appears that many of the siltstones of the Karaören and Fetiye Formation have interacted with Ca and Mg-rich waters. The calcite was precipitated in interstitial spaces such as in the matrix and the pumice vesicles (see Chapter 2). The samples have slightly elevated levels of Sr relative to average Kirka Ignimbrite, perhaps reflecting substitution for  $\text{Ca}^{2+}$  in calcite. Some of the samples contain minor Li enrichment while none show elevated As (Figure 4.16), suggesting that pore waters were poor in As but perhaps slightly enriched in Li.

The mineralogy and geochemistry of four sediment samples from the Sarikaya Formation in the Kirka Basin is presented in Figure 4.17 together with other local volcanics and EBM plotted for comparison. Samples VSK 1, 2 and 3 are borax and ulexite-hosting sediments from near the main Sarikaya open pit, while VSK 4 is colemanite-hosting mudstone from Göçenoluk (see Chapter 2). As in the Emet Basin, the mudstones from the Kirka Basin are considered to represent acid igneous-derived material that has undergone significant post-depositional modification, although this is difficult to establish due to the dilution of immobile trace element concentrations by high levels of Ca (see Chapter 3).

The colemanite-hosting mudstone from Göçenoluk (VSK 4) is similar in terms of mineralogy and geochemistry to EBM (Figure 4.17). As in EBM, K-feldspar and trioctahedral smectite are present, suggesting a highly saline environment, but unlike at Emet, carbonate is absent. The high Mg content in sample VSK 4, similar to that in average EBM (Figure 4.17), suggests that the trioctahedral smectite is Mg-rich, since other Mg-bearing minerals were not identified. The ulexite and borax hosting sediments (VSK 1, 2, 3) differ from EBM in having no K-feldspar, which is reflected in their low K concentration (Figure 4.17). Trioctahedral smectite and dolomite are present in these mudstones and hence they have very high levels of both Mg and Ca which exceed levels in EBM (Figure 4.17). Analyses of clay separates from the Kirka Basin confirm the Mg-rich nature of the trioctahedral smectite with 7.56-23.3 wt% MgO, 0.09-1.4 wt% CaO and 0.07-0.64 wt%  $\text{Na}_2\text{O}$  (Ataman & Baysal 1978).

As described in Chapter 3, high carbonate levels in samples VSK 1, 2 and 3 led to a dilution of a number of the other elements, such as Si, Al, Fe, Ti, Th, Nb, La, Nd, Zr and Y (Figure 4.17). Levels of Cr are also lower in these samples relative to both Emet and Göçenoluk mudstone, which might reflect different inputs from the basement. Samples VSK 1, 2, and 3 contain lower As but higher Li and Sr than the colemanite-hosting mudstones of Göçenoluk and Emet (Figure 4.17). The lower As is consistent with the observation by Inan et al. (1973) that the Emet deposits were more enriched in this element than those at Kirka. The higher Sr in samples VSK 1, 2, and 3 is probably due to their higher carbonate content. Some of the Kirka samples (VSK 1, 2, 3) have the highest Sr and Li levels of all sediments analysed in this study, while As concentrations are generally lower than those at Emet (Figures 4.13, 4.14 & 4.15). This study therefore suggests that colemanite-hosting mudstone in western Turkey has higher As, but lower Li and Sr than ulexite/borax-bearing sediment, although it should be noted that the database for the latter rock type is small.

**FIGURE 4.17 - Geochemistry of sediments from the Sarikaya Formation (Kirka Basin)**



**LEGEND:** kf=K-feldspar, dol=dolomite, ill=illite, tri sm=trioctahedral smectite, sm=smectite

Average Kirka Ignimbrite - I208, 209, 219, 220, 221, 222, 250, 251, 252, 258, 259, 260, 271

Average Kirka Shoshonite - IK223, 225, 226

Average Kirka Ryholite/Dacite - IK227, 228, 229, 230, 231, 232, 233, 234, 235, 236, 237, 238, 239, 244, 245, 247, 277

### 4.2.3.4 Afyon Area (*Balmahmut*)

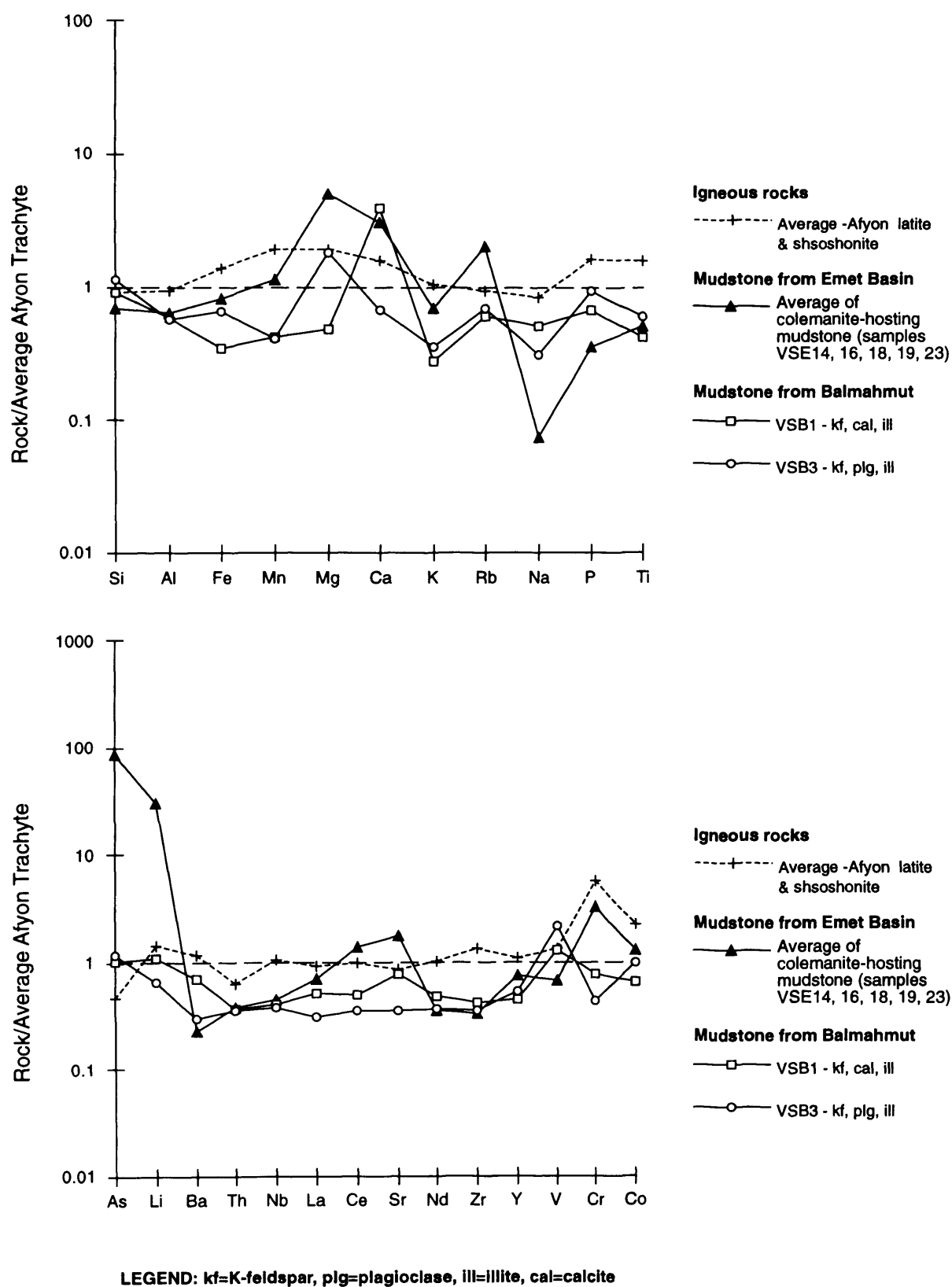
The mineralogy and geochemistry of two mudstones from the Afyon area (normalised to Afyon Trachyte) is presented in Figure 4.18 with local volcanics and EBM plotted for comparison. Similar levels of P in the mudstone and the average Afyon Trachyte suggests that local volcanism affected the composition of these sediments (Figure 4.18), although dilution by elevated Ca may have produced lower concentrations of some of the other immobile elements (see Chapter 3). Relative to EBM, the Balmahmut sediments do not contain a significant Mg, As, Li, Sr or Cr enrichment or the pronounced Na depletion (Figure 4.18). The lower Mg reflects the lack of either dolomite or trioctahedral smectite in these sediments, while the higher Na can at least in part be explained by the presence of plagioclase in one of the samples (Figure 4.18). The lower Mg, As, Li and Sr appears to indicate that pore waters associated with these sediments were not enriched in these elements, while lower Cr suggests a lack of basement input. The Balmahmut sediments contain the lowest As and Li of all the basins analysed (Figures 4.13, 4.14 & 4.15). The lack of trioctahedral smectite and Mg carbonate, together with the relatively Mg, As, Li and Sr-poor, but Na-rich nature of these sediments indicates that they are not likely to host borate mineralisation.

### 4.2.4 Concluding points

This study has shown that local acid magmatism exerted a strong control on the composition of siltstones and mudstones in the Emet Basin. The mudstones appear to be the result of the diagenetic alteration of dominantly rhyolite  $\pm$  granite-derived material in a saline, alkaline environment. Diagenesis and interaction with saline, alkaline waters led to the breakdown of all rhyolite  $\pm$  granite detrital minerals and the development of an authigenic mineral assemblage comprising carbonate, borate, trioctahedral smectite and authigenic K-feldspar. The breakdown and alteration of acid igneous detrital minerals provided an abundant supply of Si, Al and K, together with lesser amounts of Ca and Sr to the basin, thereby having some influence on the authigenic mineral assemblage produced. The presence of detrital illite and chromite however, suggests an additional input from the basement, which may also have provided a more significant supply of Ca and Mg. Ultramafic basement in particular would be able to account for the observed detrital chromite and elevated Ca and Mg.

Trioctahedral smectite, authigenic K-feldspar, dolomite and borate mineralisation have a common association in the Emet Basin. Barren sediments in the basin lack dolomite and trioctahedral smectite and sometimes lack authigenic K-feldspar and diocetahedral smectite. This suggests that the borate minerals formed in the centres of paleolakes where extremely saline waters collected with high Mg concentrations. In these highly saline environments, modification of volcanic derived diocetahedral smectite through Mg uptake resulted in the generation of trioctahedral smectite, while the formation of K-feldspar reflected the K-rich nature of the igneous input. It therefore seems likely that the distribution of borate mineralisation depended on the locations of paleolakes, and therefore on the palaeotopography of the basins. The evidence indicates that the igneous input was fairly uniform throughout the basin although some variation is suggested by the lack of any smectite in some of the barren sediments.

FIGURE 4.18 - Geochemistry of sediments from the Afyon area



Average Afyon Trachyte - A202, 203, 204, 205, 210, 242, 243, 216

Average Afyon Shoshonite + Latite - A200, 201, 206, 207, 217, 218, 241, 253, 254, 248, 249

Mudstones within the Selendi, Usak-Güre and Kirka Basins are very similar in terms of mineralogy and geochemistry to those of the Emet Basin, and they also appear to be the result of the diagenetic alteration of predominantly acid volcanic-derived material in a saline, alkaline environment. All the sediments in these basins are variably enriched in As, Li and Sr with the borate mineralised sediments of the Emet and Kirka Basins containing the highest concentrations. The sediments from the Afyon area (near Balmahmut) differ in that they contain lower Mg, As, Li, Sr and Cr than the other basins, and they have no trioctahedral smectite or Mg-carbonate. These differences in Mg and Cr might reflect the lack of a mafic basement input in this area. The following section examines the affect of local magmatism on the As, Sr and Li concentrations in the lacustrine sediments of the different basins.

### 4.3 EVALUATION OF MAGMATISM AS A SOURCE FOR ELEMENTS ASSOCIATED WITH BORATE MINERALISATION

#### 4.3.1 Previous work

In 1851, Veach (in Hanks 1883) concluded that the source of boron in a Quaternary evaporate Lake in California (Borax Lake) was local thermal springs related to geologically young volcanic rocks. Since then, a large number of workers have suggested a volcanic or thermal spring source for the boron in non-marine borate deposits (Inan et al., 1973, Rettig et al., 1980, Sunder 1980, Kistler & Smith 1983, Papke 1985, Siefke 1985, Helvacı 1985, Alonso et al., 1988, Stamatakis & Economou 1991, Ludington et al., 1992, Kistler & Helvacı 1994, Smith & Medrano 1996, Palmer & Helvacı 1995).

Studies of recent borate deposits have stimulated many of the theories concerning the origin of borate mineralisation. These deposits are often clearly associated with thermal springs (Kistler & Smith 1983, Barker & Barker 1985, Helvacı & Alonso 1994, Kistler & Helvacı 1994, Crowley 1996), and in South America, cones and aprons of ulexite  $\pm$  borax have built up around vents from which thermal waters and gases are in many cases still emanating (Muessig 1966). Furthermore, many of the B, Li and Sr rich lakes and salars (playas or salt flats) in South America are fed by igneous-related geothermal springs (Risacher & Fritz 1991, Alonso et al., 1991, Orris et al., 1992). Elevated levels of B and Li have been found in thermal springs (up to 30.7 ppm B & 9.42 ppm Li) and rivers (up to 244 ppm B & 105 ppm Li) associated with B and Li-rich lakes and salars in Bolivia (Orris et al., 1992).

Evidence for an association between geothermal activity and older borate deposits is more difficult to find. However, the presence of arsenic and antimony-bearing minerals in the Tertiary Kramer borax deposit in California has been taken as evidence for hydrothermal springs in the area (Smith 1985, Smith & Medrano 1996). Additional evidence for the involvement of hot springs in the genesis of Tertiary borate deposits comes from B isotope studies, where the range of B isotope compositions for borate minerals from the Kirka Basin are consistent with a derivation of B from geothermal waters (Palmer & Helvacı 1995).

Muessig (1966) speculated that the B in South American springs had a source related to volcanism and studies by Rettig et al. (1980) and Risacher and Fritz (1991) indicated that the Li and B in thermal springs and rivers result from the leaching and drainage of volcanic rocks. However, B enrichment in geothermal waters is sometimes found where there is no clear evidence for magmatic involvement. For

instance, in the Lardarello region in Italy, natural steam associated with geothermal waters carries boric acid believed to be derived from the sedimentary host rocks (Barker & Barker 1985, Kistler & Helvacı 1994).

Thermal springs associated with local volcanic activity and streams which carry eroded volcanic material have also been cited as a source for the borate mineralisation in Tertiary Turkish deposits, although direct evidence is lacking (Helvacı 1984; 1994, Helvacı & Firman 1976, Helvacı & Kistler 1994, Inan et al., 1973). The deposition of volcanic ash into saline, alkaline lakes and the subsequent release of B during the diagenetic transformation of volcanic glass has been suggested as an additional B source in the Tertiary borate deposits of western Turkey (Gündoğdu et al., 1996, Helvacı 1984).

### **4.3.2 Investigation into the source potential of igneous rocks in the Usak-Güre, Selendi, Emet, Kirka and Afyon areas**

#### **4.3.2.1 Introduction**

The potential of igneous activity as a source of the elemental suite, B, As, Sr and Li, enriched in the Emet and Kirka Basins, was assessed by;

- (i) Determining whether the primary (unaltered) igneous rocks were enriched.
- (ii) Using the evidence of remobilisation of these elements by hydrothermal fluids.

#### **4.3.2.2 Geochemical Analysis**

Sr and As were analysed by XRF and Li by ICP-AES at the University of Leicester; B was determined by prompt gamma activation analysis (PGAA) at a commercial laboratory in Ontario, Canada (Appendix I).

#### **4.3.2.3 Concentrations of Sr, As, B & Li in igneous rocks of the Usak-Güre, Selendi, Emet, Kirka and Afyon areas**

In common with other igneous rock suites (eg. calc-alkaline series from the Sunda Arc - Foden 1983), Sr concentrations in the Usak-Güre, Selendi, Emet, Kirka and Afyon (USEKA) rocks, decrease with increasing SiO<sub>2</sub>, such that the granite, ignimbrite and rhyolite have the lowest Sr levels (Figure 4.19). The concentrations of Sr in these acid igneous rocks are generally lower than average upper continental crust (350 ppm Sr - Taylor & McLennan 1985), while the levels in the latites and shoshonites are considerably higher (Figure 4.19). Igneous rocks with similar high levels of Sr to the mafic rocks of this area include island arc calc-alkaline basalts (eg. 550 ppm Sr - Sun 1980), continental margin alkali basalts (eg. 871 ppm Sr in the CVZ in the Andes - Thorpe et al., 1984) and average ocean island basalt (660 ppm Sr - Sun & McDonough 1989).

A large proportion of the rocks analysed in this study contain greater than 20 ppm As (Figure 4.19), which is the highest recorded concentration for fresh igneous rocks (Govindaraju 1994), with particular enrichment in rhyolite from the Kirka Basin and rhyolite and alunite from the southern margin of the Emet Basin (Figure 4.19). Within the Emet area, the rhyolite, latite and shoshonite have higher



**FIGURE 4.19 - Sr and As concentrations in igneous rocks from the USE, Afyon and Kirka areas**

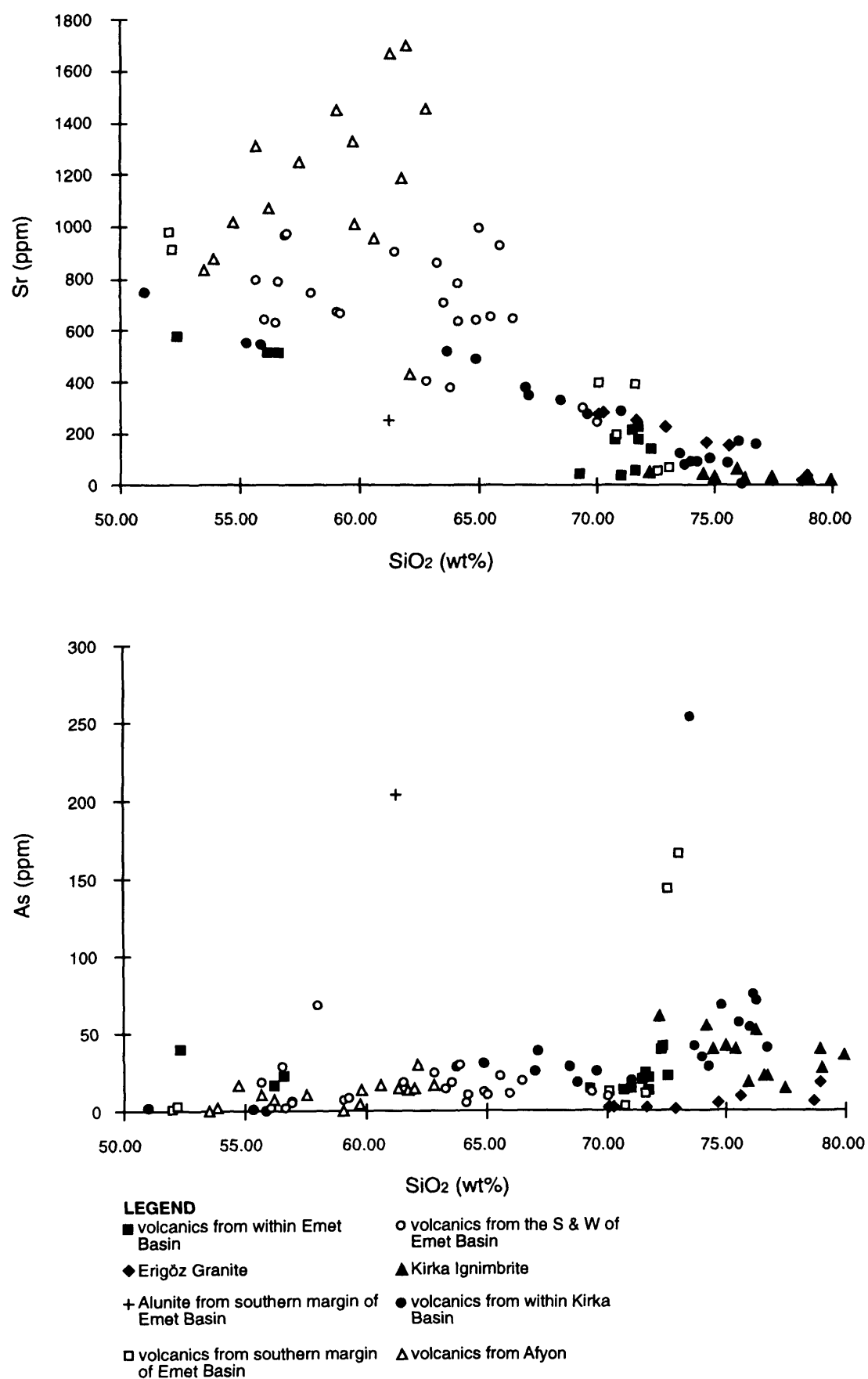


**Figure 4.19**

concentrations of As than the Erigöz Granite (Figure 4.20 a & b), whilst within the Kirka area, the rhyolite, dacite and ignimbrite contain higher levels than the shoshonite (Figure 4.21 a & b). Previous analyses of four volcanic rock samples from the Emet Basin showed similar elevated concentrations of As (43-93 ppm - Helvacı 1984). All the acid volcanics of this area are enriched in As relative to average upper continental crust (Taylor & McLennan 1985) (Figure 4.20 & 4.21).

B concentrations in igneous rocks from the USEKA area fall within the limits of previous reports of igneous rocks (Figure 4.22, Wright et al., 1975, Langmuir et al., 1977, Bryan et al., 1979, Langmuir et al., 1986, Miller et al., 1992, Ryan & Langmuir 1993, Edwards et al., 1994, Imai et al., 1996, Leeman & Sissons 1996 and references within). A positive correlation between B and SiO<sub>2</sub> for the volcanic rocks from this study area (Figure 4.22) is consistent with the contention that B tends to be enriched in the silicic differentiates of magmatism (London et al., 1996). The most B-rich igneous rock in this area is the Kirka Ignimbrite (47-145 ppm); the glass-bearing ignimbrite samples (I252 & 219) contain higher B levels than the devitrified samples (I208, 250, 222). Similar observations have been made in the rhyolitic tuff of Valles caldera, New Mexico (White et al., 1992). This is consistent with the 'fugitive' behaviour of B in magmatic environments which is likely to result in the concentration of B into the glass (Arnórsson & Andrésdóttir 1995).

The Erigöz Granite is depleted in B (6-21 ppm) relative to the acid volcanic rocks (Figure 4.22). This granite contains similar B levels to average upper continental crust (Taylor & McLennan 1985), whilst all the acid volcanics are enriched (Figures 4.20 & 4.21). Higher B concentrations are found in the aplite than in the main granite body (Figure 4.20b), indicating that this element was concentrated in the late stage residual fluids. The Erigöz Granite falls at the low end of the spectrum for analysed granites, which range from below upper crustal values to highly enriched tourmaline-bearing bodies (Leeman & Sisson 1996); for example, the Gangotri pluton in the Himalayas which contains up to 513 ppm B (Scaillet et al., 1990) and tourmaline-bearing granite from south-west England (London & Manning 1995). The B concentrations in the Emet and Kirka rhyolites, dacites and ignimbrites (24-145 ppm B) fall in the range for rhyolites and acid pyroclastics generated at former convergent margins or in areas characterised by significant crustal thickening, which generally contain between 20 and 200 ppm B (Higgins 1988, Webster et al., 1989, Dunbar & Hervig 1992, Duffield & Ruiz 1992, Imai et al., 1996), although the Macusani glass in south-east Peru is exceptionally enriched with 1930 ppm B (Leeman & Sisson 1996). Rhyolites generated from B-depleted crustal sources or B-poor precursor magmas, such as those of the Colorado Plateau have a relatively low B content of less than 25 ppm (Leeman & Sisson 1996), which is clearly lower than most of the Emet and Kirka acid volcanics.

The Li concentrations of the USEKA suite also fall within the field for previously reported igneous rock (Figure 4.22, Wright 1971, Kay 1976, Bryan & Moore 1977, Bryan et al., 1979, Langmuir et al., 1986, Ryan & Langmuir 1987, Imai et al., 1996). Ryan & Langmuir (1987) described a positive correlation between Li and SiO<sub>2</sub> within individual rock suites, and this is approximately found in the Emet and Kirka suites with the highest concentrations in the more silicic rocks (Figure 4.22). The highest Li concentrations in igneous rocks of this area are found in the Erigöz Granite from the Emet area and some samples of ignimbrite and rhyolite from the Kirka area (Figure 4.22). In contrast to B, Li is

**FIGURE 4.20 - Concentration and remobilisation of elements in igneous rocks of the Emet area**

**Figure 4.20a**

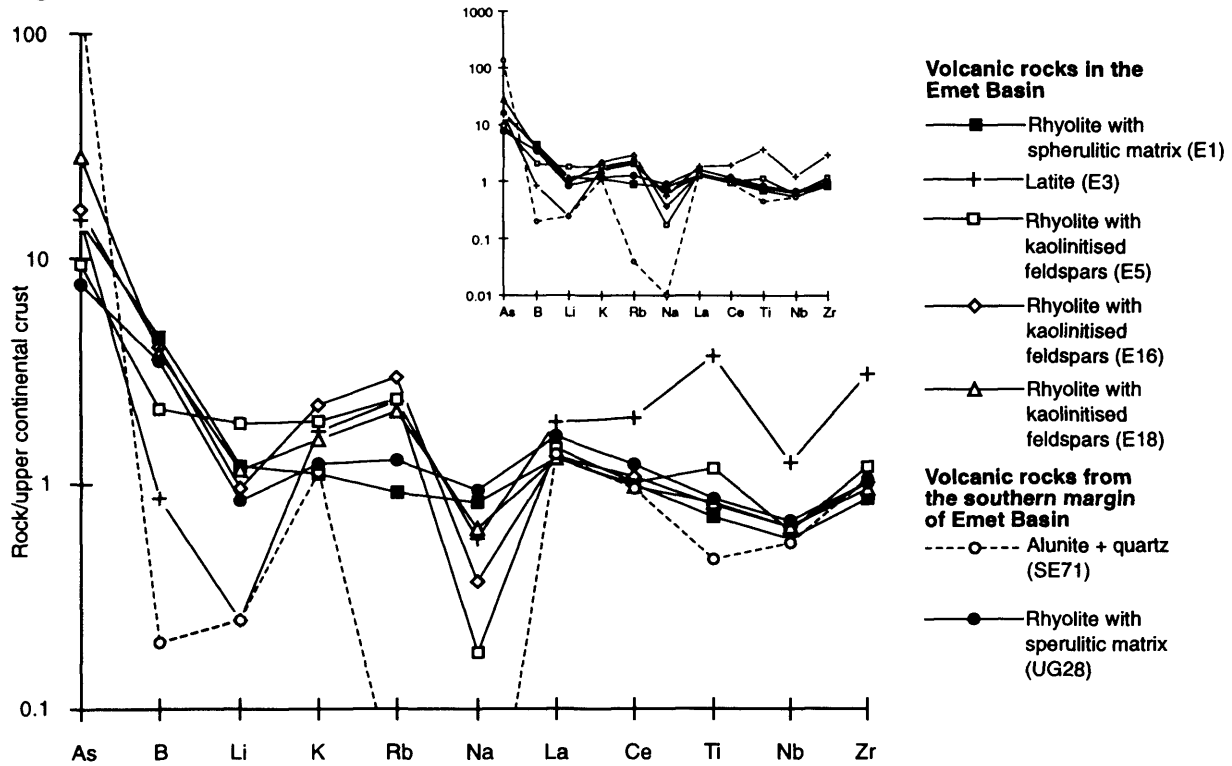


**Figure 4.20b**

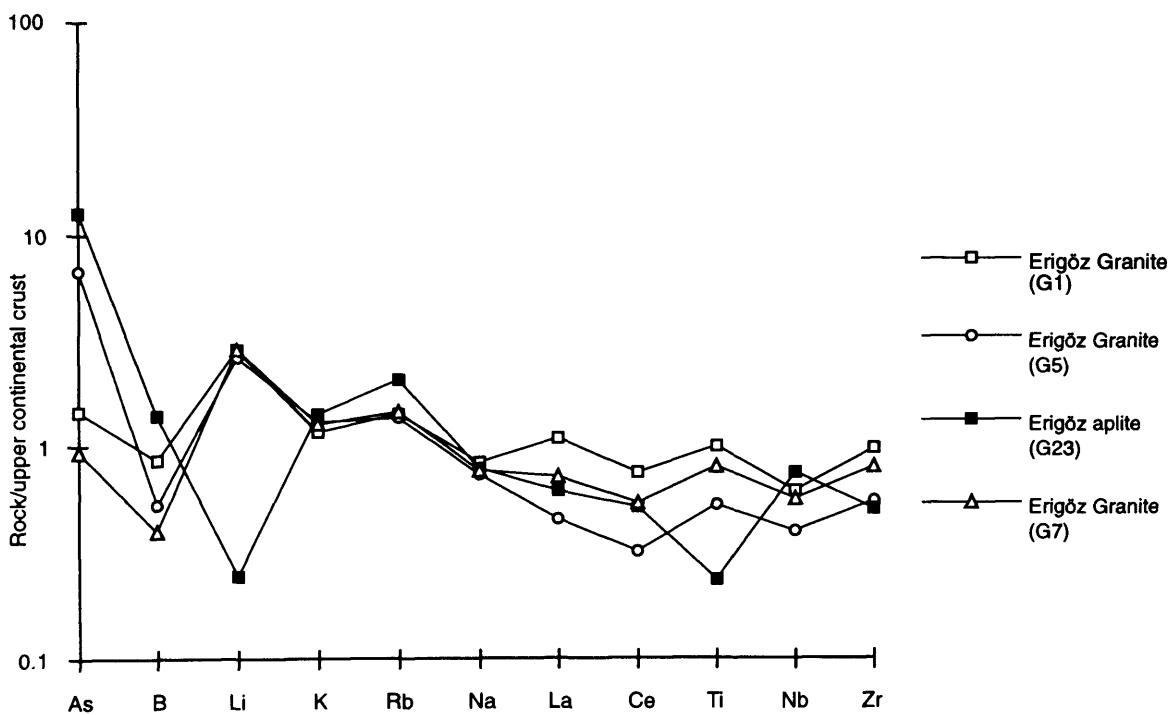


**FIGURE 4.21 - Concentration and remobilisation of elements in igneous rocks of the Kirka area**

**Figure 4.21a**

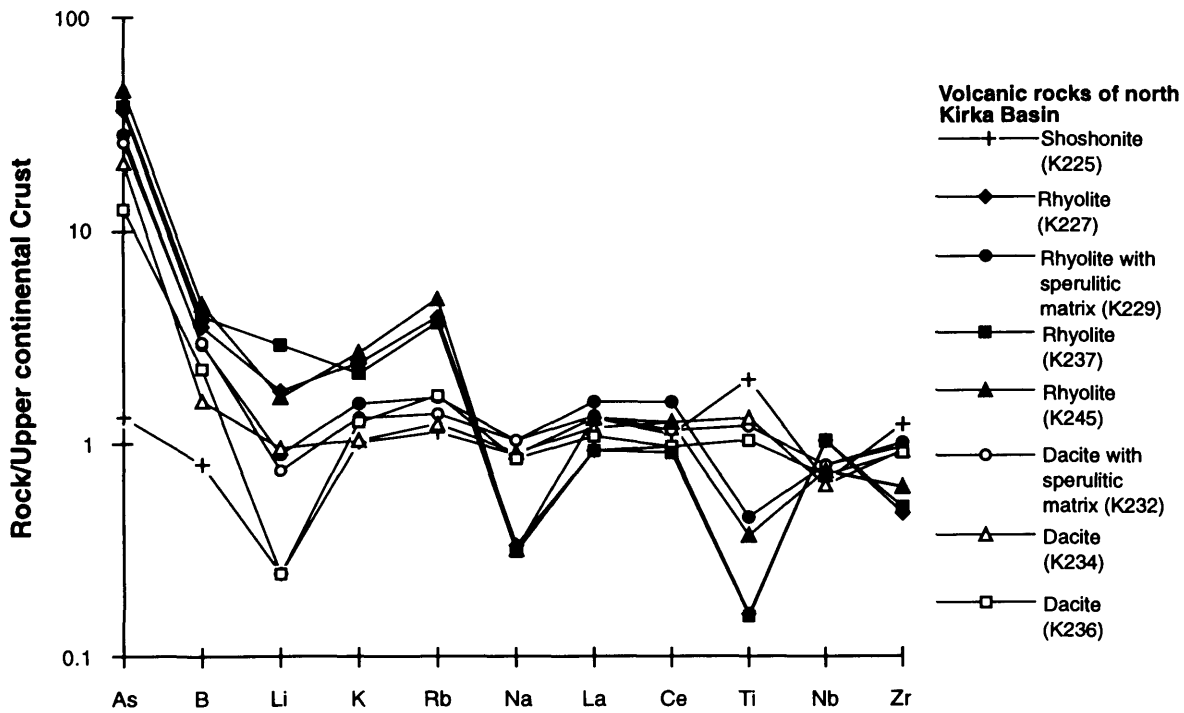


**Figure 4.21b**

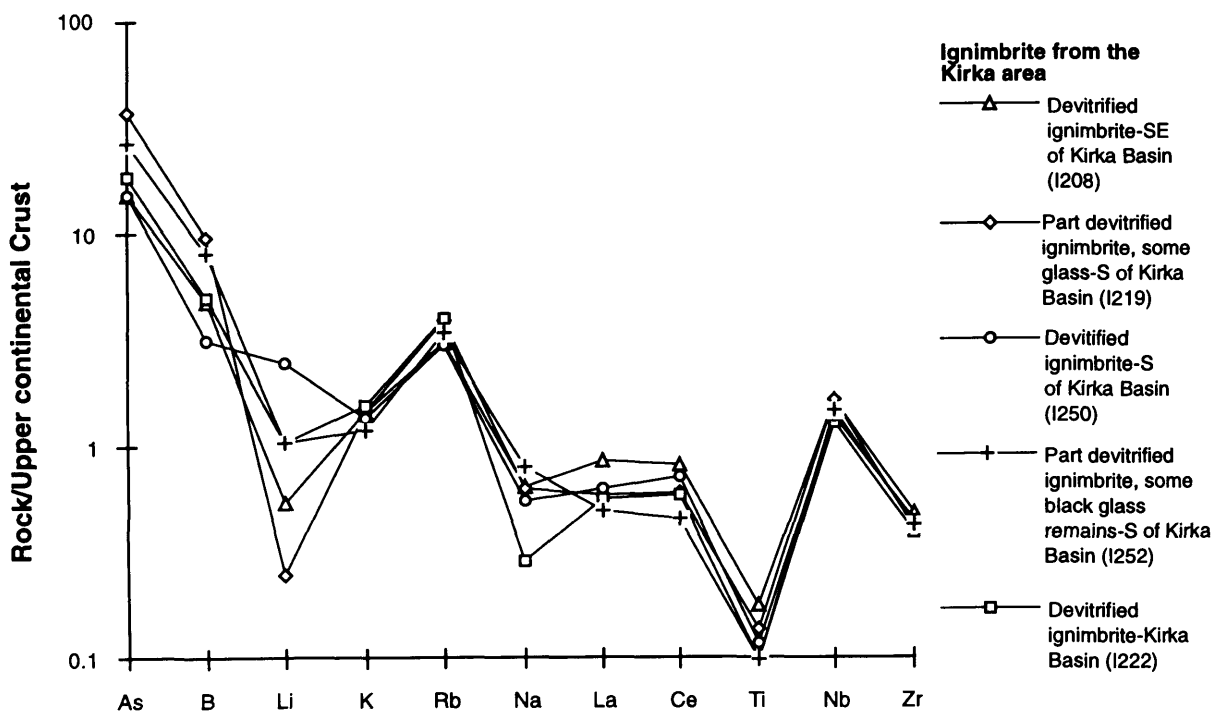


**FIGURE 4.22 - B and Li concentrations in igneous rocks from the USE, Afyon and Kirka areas**

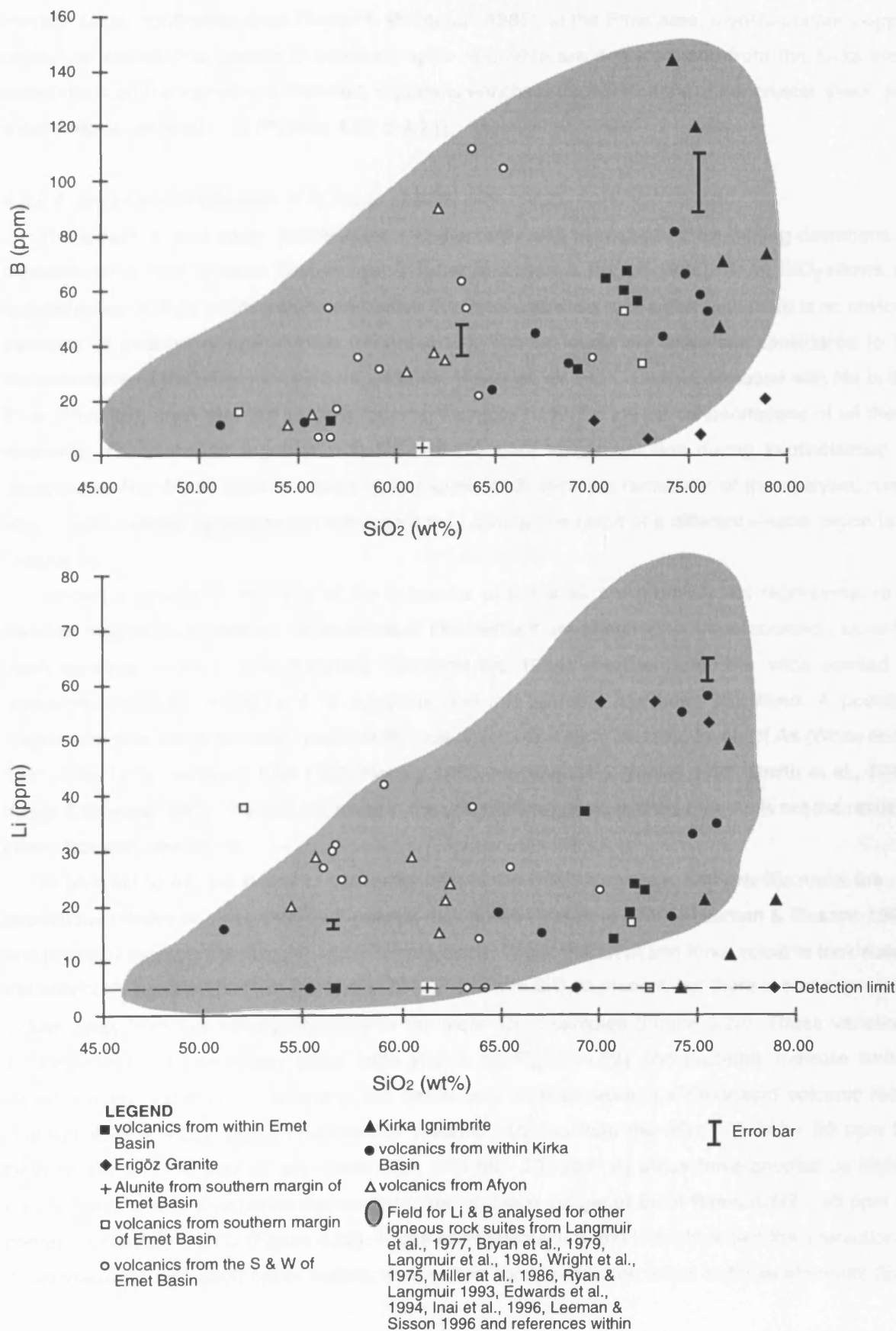


**Figure 4.22**

not apparently concentrated into the residual Erigöz granitic fluids, and aplite is depleted in Li relative to average upper continental crust, while the main granite body is enriched (Figure 4.20b). Relative to average upper continental crust (Taylor & McLennan 1985); in the Emet area, rhyolite contains upper crustal concentrations, granite is enriched, aplite and latite are depleted, and from the Kirka area, ignimbrite is both enriched and depleted, rhyolite is enriched, dacite contains upper crustal levels, and shoshonite is depleted in Li (Figures 4.20 & 4.21).

### 4.3.2.4 Secondary mobilisation of B, As, Li and Sr

The extent of secondary remobilisation of elements was assessed by examining deviations of concentrations from igneous fraction trends (after MacLean & Barrett 1993). Sr vs SiO<sub>2</sub> shows an approximately straight fractionation trend within the Emet and Kirka rock suites, and there is no obvious evidence of secondary mobilisation (Figure 4.19). The Sr levels are therefore considered to be representative of the parental melt compositions. However, Sr and Ca levels decrease with Na in the Emet Rhyolites, such that the kaolinite-bearing samples have the lowest concentrations of all these elements. Therefore, Sr together with Na and Ca were lost to solution during kaolinitisation of plagioclase. The Afyon volcanics have higher levels of Sr than the remainder of the analysed rocks which might indicate remobilisation although it may also be the result of a different source region (see Chapter 5).

Concentrations of As in many of the volcanics of this area are probably not representative of parental magma compositions, since levels of this element are often higher than recorded values for fresh igneous rocks in the literature (Govindaraju 1994). Furthermore, the wide spread in concentration of As in Figure 4.19 suggests that this element has been mobilised. A possible mechanism was interaction with geothermal fluids which often carry elevated levels of As (White et al., 1971, Ellis 1979, Henley & Ellis 1983, Henley 1985, Hedenquist & Henley 1985, Smith et al., 1987, Krupp & Seward 1990). The lack of calcite in the volcanics suggests that the high As is not the result of interaction with lake brines.

In contrast to As, the B and Li concentrations of the USEKA volcanic and granitic rocks are not anomalous relative to other analysed igneous rock suites (Imai et al., 1996, Leeman & Sissons 1996) and probably represent parental magma compositions. Within the Emet and Kirka volcanic rock suites, the previously reported positive correlation of B and Li with SiO<sub>2</sub> is present, but there is some spread in values away from this trend particularly in the more silicic samples (Figure 4.22). These variations exceed analytical uncertainty (error bars shown on Figure 4.22) and probably indicate limited remobilisation. Variations in B and Li are particularly pronounced in the Kirka acid volcanic rocks (Figures 4.21 & 4.22). Some intermediate volcanic samples from the Afyon (A 242 - 90 ppm B), Selendi (SE 3 - 112 ppm B) and Usak-Güre (UG 58 - 105 ppm B) areas have anomalous high B concentrations; one shoshonite sample from the southern margin of Emet Basin (UG7 - 38 ppm Li) contains unusually high Li (Figure 4.22). These enrichments in B and Li might reflect the interaction of these volcanics with geothermal waters, which often contain elevated levels of these elements (Ellis

1979, Henley & Ellis 1983). This interaction is unlikely to have been recent, as currently active hot springs in the Emet area do not contain appreciable B or As (Helvacı 1984).

A further test of mobility is the homogeneity of multivariation plots. The mobility of the elements plotted on Figures 4.20 and 4.21 approximately increases from right to left, and a greater degree of variation in concentrations on the left relative to the right of the diagram indicates remobilisation. With the exception of Na, both mobile and immobile element concentrations show little variation within the Emet Rhyolite suite (Figure 4.20a), suggesting that B and Li have not been remobilised in these rocks. There is no evidence in this plot to suggest that devitrification or kaolinitisation in some of the rhyolites mobilised Li and B (Figure 4.20a). The decrease in Na is the result of the alteration of plagioclase to kaolinite as discussed above (Figure 4.20a). The higher Ti and Li, but lower B, of sample E 5 relative to the other rhyolites (Figure 4.20a), is probably the result of concentration of B into the most evolved siliceous melt (lowest Ti) as is observed in the aplite of the Erigöz pluton (Figure 4.20b).

In contrast, sample SE 71 (alunite & quartz) from the southern margin of the Emet Basin was the product of the acid alteration of rhyolite, which has resulted in the leaching of Na, Rb, Li and B from the rock but has led to an increase in As (Figure 4.20a). The leaching of B and Li from acidic volcanic rocks by thermal solutions has been noted elsewhere, both in the field (Shaw & Sturchio 1992) and in the laboratory (Ellis & Mahon 1964, 1967, White et al., 1992). Other evidence for hydrothermal activity in the Emet area is provided by a small zone of silicification within a rhyolite exposure in the north of Emet Basin (Chapter 2). This silicified rock composed of quartz and Fe-oxides, contains 71 ppm As, which provides additional evidence that the hydrothermal solutions carried high As concentrations. Silicification and alunite, features of high sulphidation epithermal ore deposits where host rock has been leached by acidic fluids are known elsewhere in western Turkey; for example in the Biga Peninsula (Pirajno 1994).

Similar plots of the Kirka area show higher B and Li levels in the rhyolite compared to the dacite of north Kirka Basin (Figure 4.21a). This is best explained by the concentration of these elements into more silicic magmas. However, the ignimbrite samples show little variation in Ti and other immobile elements, but significant variation in Li and B (Figure 4.21b), suggesting that remobilisation of these elements has occurred; possibly by devitrification since glass-bearing samples both contain the highest B of the ignimbrite samples. Studies of other silicic terranes have shown that B and Li can be lost or gained during devitrification (Higgins 1988, Stix et al., 1995).

Caution must be exercised with the interpretation of the B and Li data, since even when there is no evidence of post emplacement/eruption remobilisation, the B and Li concentrations in analysed volcanics are likely to be lower than those of the parental magmas (Leeman & Sisson 1996, Webster & Duffield 1991). Studies of the composition of glass inclusions in the quartz of rhyolites indicate that B and Li have been lost from the bulk samples during or following eruption (Webster & Duffield 1991). Both B and Li can be lost in exsolving aqueous fluids prior to eruption (Webster & Duffield 1991) and B can be lost during degassing of magmas (Shaw & Sturchio 1992, Arnórsson & Andriessdóttir 1995) such that fumarole gases and encrustations are often B-rich (Kanazki et al., 1979, Nomura et al., 1982, Fogg & Duce 1985, Quisefit et al., 1989, Garavelli & Vurro 1994).

The evidence therefore suggests that Sr has not been remobilised in these rocks, except during kaolinitisation, while As has been extremely mobile resulting in considerable enrichment of this element in many of the samples. Only minimal remobilisation of B and Li has taken place in most of the rhyolites, dacites and Erigöz Granite, but effective leaching has removed these elements from some rhyolites to the south of Emet Basin. Furthermore, devitrification has led to minor remobilisation of B and Li in the Kirka ignimbrite. Finally, the measured concentrations of B and Li may be lower than in the parental magmas due to loss through exolving fluids and degassing.

### *4.3.2.5 Discussion: implications for borate mineralisation*

#### **(a) Source Potential of Igneous Rocks**

The data above provide evidence that although the acid igneous rocks of this area contain significantly less Sr than the younger more mafic rocks, they still represent a potential source for this element. However, marble basement in the area may have provided a more significant source for Sr, as suggested by Helvacı (1984). The evidence presented above demonstrated widespread mobilisation of As in this area, and it is therefore not possible to determine the parental magma concentrations of this element. Hence, a direct assessment of the source potential of the Emet and Kirka igneous rocks for As, is impossible. However, data for fresh igneous rock suites elsewhere suggest that As is enriched in the more silicic magmas (Imai et al., 1996). Furthermore, sulphosalts of As, including realgar, are commonly found in volcanic fumarolic encrustations (Quisefit et al., 1989, Garavelli & Vurro 1994). It therefore appears that volcanism, particularly when silicic, is a potential source of As, and hence the acid volcanism of the Emet and Kirka areas probably represents a source for at least some As.

Comparatively high B and Li in the ignimbrite, rhyolite and dacite of this area suggest that acid volcanism was a viable source for these elements. Furthermore the acid pyroclastic volcanism of this area contained large amounts of glass and this study has shown that fresh glass is a repository for B. In addition, the B and Li levels of the parental acid magmas may have been even higher than the current levels, due to degassing and the loss of exolving fluids prior to eruption or emplacement. High Li but low B levels in the Erigöz Granite suggests that it may have also provided a significant source for the former element. The absence of acid volcanics and therefore of high B and Li concentrations in the Afyon area might explain the lack of borates and the low Li and As levels in the Balmahmut sediments.

#### **(b) Transfer mechanisms**

As discussed above, geothermal fluids, rivers and pyroclastic activity have been proposed for the transfer of B from an igneous source to basin sediments (Helvacı 1984, Barker & Barker 1985, Gündoğdu et al., 1996). The release of B to geothermal fluids from igneous bodies is thought to occur by hydrothermal leaching (Barker & Barker 1985, Helvacı 1995). The transfer of B into lake waters from igneous material transported to basins by rivers and pyroclastic activity, occurs during post depositional modification of such material in saline, alkaline conditions (Gündoğdu et al., 1996). This section discusses these transfer mechanisms in detail, utilising the data presented above.



Direct evidence for geothermal activity during the Miocene in the Emet and Kirka areas is difficult to find. However, the occurrence of silicification and alunite alteration zones within rhyolite exposure in the Emet area, provides evidence for hydrothermal activity. The precise age of this acid alteration is unknown, but it seems likely that the geothermal fluids were driven by heat from active Early Miocene magmatism. The study of modern silicic terranes has shown that geothermal systems are common in such settings where dominantly meteoric waters are driven by heat from magma bodies in the crust and acid sulphate hot springs, such as those which produced the alunite in the southern margin of the Emet Basin, are common (Henley & Ellis 1983). Additional evidence for Miocene geothermal activity in the Emet and Kirka areas is provided by the As data described above, which strongly suggests that As-rich hydrothermal solutions interacted with the Miocene volcanics. It is therefore extremely likely that the Early Miocene silicic volcanism of the Emet and Kirka areas was accompanied by geothermal activity.

Based on a study of Mt St Helens, it appears that two hydrothermal systems typically form after a pyroclastic eruption; one located close to the magma conduit ('magma-driven system') and one at some distance from the conduit where meteoric waters are driven by heat given off from the cooling pyroclastic deposits ('pyroclastic-driven system') (Shevenell & Goff 1995). Their study suggests that fumaroles and hot springs associated with the pyroclastic deposits are likely to be short lived compared with those driven by the magma of the conduit. Tent rocks observed in the Kirka Ignimbrite may represent fossil fumaroles associated with pyroclastic flows (Chapter 2), but it is likely that much of the evidence for this low temperature hydrothermal circulation has been eroded away. However, both magma-driven and pyroclastic-driven geothermal systems probably existed during active rhyolitic volcanism in the Early Miocene in the Emet and Kirka Basins.

Evidence discussed above indicated that As-rich acidic solutions in the southern margin of the Emet Basin effectively leached B and Li from the associated rhyolitic rock, while kaolinitisation of feldspar by acid alteration or weathering of the Emet Rhyolites led to the release of Sr into solution. Experimental studies have illustrated that appreciable quantities of B and Li can be leached from volcanic rocks by hydrothermal solutions in relatively short reaction times (Ellis & Mahon 1964, 1967; White et al., 1992). Ellis and Mahon (1964) also demonstrated that large proportions of B could be leached before the volcanic rocks showed appreciable signs of alteration. Furthermore it has been shown that aqueous alteration of rhyolitic glass from Yellowstone, USA, released both B and Li to solution (Shaw & Sturchio 1992). Hence, evidence from the Emet Basin, in addition to information from the literature, suggest that hydrothermal leaching may have been an important mechanism for the transferring of B, Li, Sr and perhaps As from igneous bodies to the Emet and Kirka Basins.

In general, the concentrations of Li and B in geothermal waters reflect the levels of these elements in the associated country rocks (Ellis 1979, Arnórsson & Andrésdóttir 1995, Shevenell & Goff 1995). For example, low B contents in geothermal waters in Iceland are generally thought to reflect the low content of B in the host basaltic rock and elevated levels of B in the geothermal waters of one area are attributed to the presence of silicic volcanics with a higher B content (Arnórsson & Andrésdóttir 1995). In a similar way, the concentrations of Li in geothermal waters are considered to reflect the abundance

in the surrounding rocks and hence waters in basaltic areas generally have low concentrations compared with those in rhyolitic and andesitic areas (Ellis 1979). Since, the rhyolites, dacites and ignimbrites in the Emet and Kirka areas contain relatively high B and Li concentrations, thermal solutions in contact with these rocks would potentially be enriched in these elements. The abundance of glass in the pyroclastic rocks of this area is likely to have provided a particularly abundant supply of As and B, since these are incompatible elements likely to be concentrated into glass (Arnórsson & Andrédóttir 1995, Noll et al., 1996). Furthermore, experiments by Mahon and Ellis (1964) showed that pumice, which is abundant in the pyroclastic rocks of this area, is particularly reactive with hydrothermal solutions due to its large surface area. In addition, the porous nature of ignimbrite, particularly when unwelded, would have provided a relatively permeable rock through which thermal fluids could easily pass. The leaching of the Erigöz pluton by hydrothermal fluids may have provided a small supply of B and a more significant amount of Li on the basis of concentrations measured in this study. The leaching of shoshonite, latite and trachyte in the Afyon area would have produced geothermal fluids with lower B and Li concentrations than those in contact with more acid volcanics, which probably explains the absence of borates and the lower Li in the sediments of this area.

Mass balance calculations for the required amount of volcanic source rock to yield borate deposits of the size of Emet and Kirka are shown below. The calculations assume 50% leaching of B from the source rocks, and a value of 50 ppm in the source rocks prior to leaching.

### **Boron - mass balance (Emet Basin):**

Reserves 110 Mt at 45%  $B_2O_3$  = 49.5 Mt  $B_2O_3$  =  $4.95 \times 10^{10}$  Kg  $B_2O_3$   
=  $1.5558 \times 10^{10}$  KgB

Source rock, assuming 50 ppm B:  $3.1 \times 10^{14}$  kg required

Taking density of acid volcanics as  $2520 \text{ kg m}^{-3}$  =  $1.23 \times 10^{11} \text{ m}^3$

= 123 km<sup>3</sup> of volcanic source  
rock required at 50 ppm B  
if 100% rock leaching. At 50%  
leaching, 246 km<sup>3</sup> of volcanic  
source rock required

### **Boron - mass balance (Kirka Basin):**

Reserves 100 Mt at 25%  $B_2O_3$  = 25 Mt  $B_2O_3$  =  $2.5 \times 10^{10}$  Kg  $B_2O_3$   
=  $7.8 \times 10^9$  KgB

Source rock, assuming 50 ppm B:  $1.56 \times 10^{14}$  kg required

Taking density of acid volcanics as  $2520 \text{ kg m}^{-3}$  =  $6.19 \times 10^{10} \text{ m}^3$

= 62 km<sup>3</sup> of volcanic source  
rock required at 50 ppm B if  
100% rock leaching. At 50%  
leaching, 124 km<sup>3</sup> of volcanic source  
rock required

Given the large expanse of igneous rock in these areas (Figures 2.1 & 2.6), it is therefore plausible that leaching volcanic and granitic rocks may have provided enough B to yield these large borate

deposits. For instance, the Kirka Ignimbrite covers an area of ~ 2000 km<sup>2</sup>, although the volume of these volcanics is unknown.

There is no direct evidence for transferring B from igneous bodies to geothermal fluids, other than by hydrothermal leaching, but it is likely that magmatic waters and gases were important. Geothermal fluids are dominated by meteoric water, but magmatic fluids are commonly present too, and the transfer of Li and B, and perhaps As, in exsolving fluids from magmas (Webster & Duffield 1991, Hedenquist & Lowenstern 1994), may have provided an additional mechanism for enriching geothermal waters in these elements in the Emet and Kirka areas. For instance, in the Taylor Creek rhyolite in New Mexico, Li is considered to have separated from the melt as chloride complexes at a depth of less than 1.6 km (Webster & Duffield 1991). Furthermore, the degassing of magmatic B(OH)<sub>3</sub> and SO<sub>2</sub>, has been observed in some fumaroles (Kanazaki et al., 1979) and degassing of magma intrusives is thought to have increased the B content of thermal waters in Iceland (Arnórsson & Andrédóttir 1995). It is therefore likely that degassing of magmas in the Emet and Kirka areas also provided a mechanism for the transfer of B and S to geothermal fluids. For instance, degassing of SO<sub>2</sub> from rhyolitic magmas may have provided a source for the S in the alunite produced by acid alteration in the Emet area.

It is likely that the drainage of B and Li-rich silicic igneous terranes would have provided an additional source for these elements to the Emet and Kirka Basins, as observed with the inflow into the Salar of Uyuni, Bolivia (Rettig et al., 1980, Risacher & Fritz 1991). However, on the basis of the experiments by Ellis and Mahon (1964), little B and Li would have been dissolved from the country rock, unless the pyroclastic flows or rhyolite lavas were still hot (150°C). The streams though, were probably able to carry small amounts of eroded igneous material, as suggested by Helvacı (1984) to the palaeolake systems. An abundance of granite clasts are found in the Emet Basin, which must have been transported in this way.

It was illustrated in the preceding parts of this chapter, that rhyolitic ± granitic material, transported to the basins either as ash fall during eruptions, or by streams, was broken down in the saline, alkaline lake waters. During the break down of this igneous material, chemical constituents would have been released to solution. Given the high B, Li and possibly As in the Emet and Kirka igneous rocks, appreciable quantities of these elements would have been released. Volcanic glass, a repository for B and possibly for As, may have released considerable amounts of these elements. The break down of igneous plagioclase and K-feldspar described above, would also have released Sr to the lake waters. This enrichment of B and Li in pore waters as a result of the breakdown of volcanic material was suggested by Gündoğdu et al. (1996).

The principal mechanisms therefore, for the transfer of B from an igneous source to the Emet and Kirka Basins included:

(i) Transfer by igneous-driven geothermal fluids; the fluids obtained B, Li, As, Sr and S by hydrothermal leaching, and from contributions of magmatic waters and gases. The alunite altered rhyolite in the Emet area provides direct evidence for the leaching of B and Li from acid volcanics, while the degassing of B(OH)<sub>3</sub> and SO<sub>2</sub> and the transfer of Li, B and perhaps As in magmatic fluids are inferred from investigations involving recent volcanism.

(ii) Breakdown of acid igneous material within saline, alkaline basins; this material included fluvially transported eroded igneous rock and pyroclastics erupted directly into the basin.

### 4.3.3 Concluding points

The data presented indicates that the potential source rocks, the acid volcanics, are depleted in Sr, but largely enriched in B and Li relative to average upper continental crust. The B concentrations fall within the field for acid volcanics generated at former convergent margins or in areas characterised by crustal thickening. The Erigöz Granite has similar concentrations of Sr and Li to the acid volcanics, but it is depleted in B, suggesting that this element was concentrated into the volcanic phase of Early Miocene magmatism. Concentrations of As are anomalous in most of the USEKA volcanics relative to levels recorded in fresh igneous rocks from elsewhere.

The data described above indicates that only limited remobilisation of Sr, B and Li has taken place in most of the USEKA rock suite, and hence the measured concentrations are generally representative of the parental melts. Some mobility of Sr however, has resulted from the kaolinitisation of plagioclase, while devitrification in the ignimbrite led to limited remobilisation of B and Li. In contrast, As appears to have been very mobile in this environment with probable widespread interaction between As-rich hydrothermal fluids and volcanics.

The acid volcanics therefore represent a viable source for B, Li and to a lesser extent Sr, while the Erigöz Granite was a potential source of Li, and less so of B. The potential of the acid volcanics as a source for As is impossible to assess due to remobilisation, but it is likely that local acid magmatism supplied at least some As to local hydrothermal fluids.

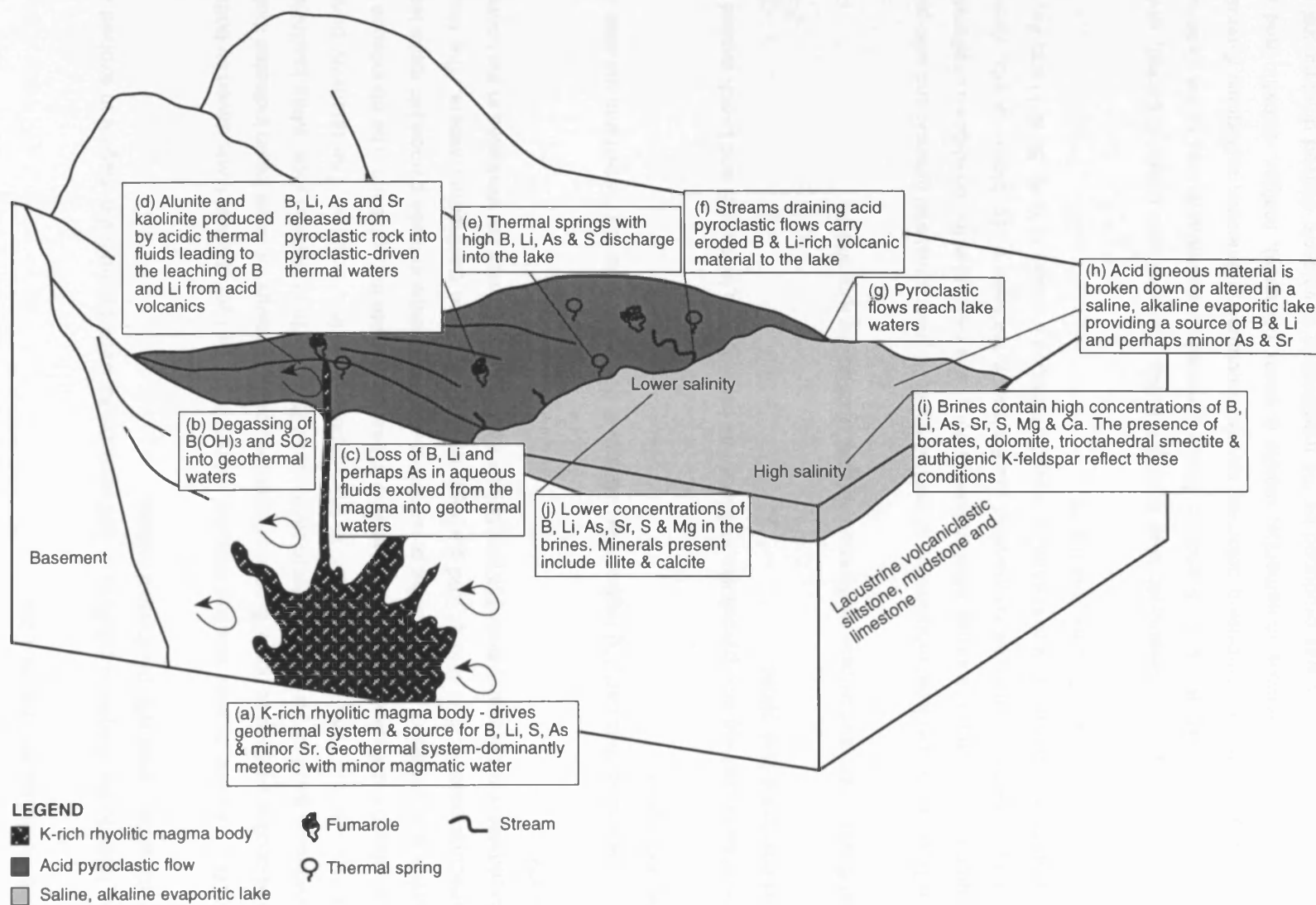
The main mechanisms for the transfer of B, Li, Sr, As and S from an acid igneous source to the basins probably included transfer by igneous-related geothermal fluids and the break down of igneous material within the saline, alkaline basins. Evidence for geothermal activity is provided by acidic hydrothermal alteration (alunite and silicification) in the Emet area and by elevated As in volcanics from much of the USEKA area. Alunite altered rhyolitic rock from south of Emet Basin, provided evidence of hydrothermal leaching of B and Li from acid volcanics. Mass balance calculations show that hydrothermal leaching is a realistic mechanism for releasing sufficient B to yield borate deposits. Although direct evidence is clearly not available, magmatic fluids and gases may also have released B, As, Li and S to geothermal fluids. Finally, the large volumes of acid igneous material in the Emet and Kirka Basins was modified after deposition within a saline, alkaline environment, with the result that minerals were broken down and B, Li, Sr and probably As were released to lake and pore waters.

## 4.4 MODEL FOR THE ROLE OF MAGMATISM IN THE GENESIS OF EMET AND KIRKA BORATE DEPOSITS

On the basis of the information gained in the course of this study, a model for the role of magmatism in the genesis of Emet and Kirka borate deposits has been proposed. This model is summarised below and illustrated in a schematic block diagram (Figure 4.23).

**FIGURE 4.23 - Model for the role of magmatism in the genesis of Emet and Kirka borate deposits**

(Basic geology of block diagram extensively modified from Eugster & Hardie 1975)



## Role of magmatism in borate genesis

---

(a) A K-rich rhyolitic magma body at high crustal level generated a circulating hydrothermal system dominated by heated meteoric water but containing some magmatic water. The magma provided a source for B, Li, S, As and minor Sr.

(b) Near to the magma conduit, there was direct degassing of  $\text{B(OH)}_3$  and  $\text{SO}_2$  from the magma into geothermal waters (Figure 4.23).

(c) Near to the magma conduit, B, Li and perhaps As were lost from the magma in exolved aqueous fluids which mixed with geothermal waters.

(d) B, Li, As and Sr were leached from the country rocks by hydrothermal fluids driven by both magma and cooling pyroclastic flows. Evidence from the southern margin of Emet Basin indicates that alunite-producing geothermal waters effectively leached B and Li from rhyolitic rock, while kaolinitisation of feldspar in the Emet Rhyolites led to the release of Sr into solution. The relatively porous acid pyroclastic rocks allowed geothermal waters to easily percolate through them. The abundance of glass, which is a repository for B, and the presence of reactive pumice in these pyroclastic rocks lead to the effective release of B and Li and perhaps As and Sr to the geothermal waters. The leaching of basement rocks probably provided an additional source but this was not evaluated in the course of this study.

(e) Thermal springs carrying high concentrations of B, Li, S and As discharged into the lake and local ground waters.

(f) Streams draining acid pyroclastic rocks carried considerable loads of B and Li-rich eroded volcanic material to the lake brines.

(g) B and Li-rich acid pyroclastic flows sometimes reached the lake waters.

(h) The post-depositional modification of dominantly acid igneous material (granitic and acid pyroclastic material) took place in a saline, alkaline lake system. This resulted in the breakdown or alteration of all detrital volcanic minerals which included plagioclase, K-feldspar, glass, biotite, quartz, kaolinite and dioctahedral smectite. This acid igneous material provided a supply of K, Al, Si, B, Li and As, together with minor Na, Ca and Sr to the lake brines.

(i) In the centre of the evaporitic lake (playa) the most concentrated brines collected, which were enriched in Ca, Mg, B, As, Li, S and Sr. These elevated concentrations lead to the generation of a mineral assemblage comprising dolomite, calcite, trioctahedral smectite, authigenic K-feldspar (not always present), borates (colemanite, ulexite & borax primarily), realgar, celestite and gypsum. Trioctahedral smectite was produced by the modification of volcanic derived dioctahedral smectite

through Mg uptake. The high K content of the magmatic input resulted in the replacement of volcanic glass by authigenic K-feldspar.

(j) Lower salinity waters near to the edge of the playa lake contained lower concentrations of Mg, K, B, As, Li, S and Sr and therefore trioctahedral smectite, authigenic K-feldspar, dolomite, borates, realgar, celestite and gypsum are not stable here. The mineral assemblage is comprised of illite and calcite.

### 4.5 IMPLICATIONS FOR BORATE MINERAL EXPLORATION

Information gained in the course of this study has implications for borate mineral exploration and particularly for large Tertiary lacustrine deposits. It is well established that borate minerals in the Turkish Borate Province formed in saline, alkaline closed basins under arid conditions (Helvacı et al., 1993). The specific contribution of this study is in the role of magmatism in borate genesis. Based on Emet and Kirka deposits, the following geological situations are considered favourable for borate mineralisation in western Turkey;

(i) For the location of potential borate-bearing basins;

- The occurrence of dacite, trachyte, rhyolite and acid pyroclastics in close temporal and spatial position with lacustrine sediments in closed basins. The presence of K-rich acid volcanics ( > 3.5 wt % K<sub>2</sub>O) with ~20-150 ppm B and ~10-60 ppm Li.
- The presence of elevated concentrations of As in acid volcanics (frequently > 20 ppm As) which provides evidence of geothermal spring activity.
- The presence of acid volcanic-derived lacustrine sediments (ie. sediment with an ignimbrite mineral assemblage but with calcite precipitated within pumice vesicles).

(ii) For the location of borate-hosting sediments within a basin;

- The presence of lacustrine mudstone sequences containing some or all of authigenic K-feldspar, trioctahedral smectite and dolomite.
- The presence of elevated As (> 150 ppm), Sr (> 300 ppm) and Li (> 150 ppm) in lacustrine mudstone and interbedded carbonate.
- The presence of high Mg concentrations (> 6.5 wt % MgO) in lacustrine mudstone.

## 5 ORIGIN OF MIOCENE MAGMATISM IN THE TURKISH BORATE PROVINCE

### 5.1 INTRODUCTION

The preceding chapters illustrated that Early Miocene acid volcanism and related geothermal activity were probably the major suppliers of B to Emet and Kirka Basins. The aim of this chapter is to investigate the origin of Miocene magmatism in the Usak-Güre, Selendi, Emet, Kirka and Afyon (USEKA) area in order to place constraints on the ultimate source of B. To fulfil this objective, a detailed investigation has been undertaken on the major, trace and rare earth element concentrations and the Sr and Nd isotope characteristics of the igneous rocks of this area. This information is incorporated into our existing understanding of the tectonic and volcanic evolution of western Turkey, and comparisons are made with volcanism in similar tectonic settings around the world including the other major borate provinces. Some of the information from this study has been published in a paper by Seyitoglu, Anderson, Nowell and Scott (1997).

### 5.2 SUMMARY OF OLIGOCENE TO RECENT MAGMATISM IN WESTERN TURKEY (PREVIOUS STUDIES)

Tertiary and younger magmatism in western Turkey has evolved from dominantly calc-alkaline in the Oligocene and Early Miocene to mostly alkaline in the Late Miocene and Quaternary (Yilmaz 1990, Güleç 1991, Seyitoglu & Scott 1991, Seyitoglu & Scott 1992b). The calc-alkaline volcanics were intermediate-acid in composition, while the Late Miocene, Pliocene and Quaternary volcanism had a basic-intermediate nature (Yilmaz 1990, Güleç 1991, Seyitoglu & Scott 1992b, Seyitoglu et al., 1992). The early calc-alkaline volcanism was accompanied by Oligocene-Early Miocene high level granitic intrusions, although older Tertiary granitoids (Palaeocene-Eocene) are also found in north-west Turkey (Bingöl et al., 1982, Yilmaz 1990). The alkaline rocks changed from a potassic nature in the Miocene - Pliocene to sodic in the Quaternary (Güleç 1991).

The calc-alkaline volcanics typically show enrichments in the large ion lithophile elements (LILE - Ba, Th, Rb, K) but distinctive depletions in the high field strength elements (HFSE - Nb, Ti, P) relative to ocean island basalt (OIB) (Yilmaz 1990, Seyitoglu & Scott 1992b) and they have high  $^{87}\text{Sr}/^{86}\text{Sr}$  (0.70501 - 0.70953) and low  $^{143}\text{Nd}/^{144}\text{Nd}$  isotopic ratios (0.51269 - 0.51229) (Güleç 1991). Yilmaz (1990) suggested that the calc-alkaline volcanics contain a significant crustal component and Keller and Villari (1972) advocated an anatectic origin for the rhyolitic ignimbrite in the Afyon area. Güleç (1991) suggested the calc-alkaline volcanics were derived from continental lithospheric or shallow asthenospheric mantle, contaminated by upper continental crust. She attributed the contamination to earlier subduction-related enrichment of the lithosphere and the operation of an assimilation-fractional crystallisation (AFC) process (Güleç 1991). However, Seyitoglu and Scott (1992b) advocate a purely lithospheric mantle source modified by previous subduction.

Most of the Miocene and Pliocene alkaline volcanics have trace element and isotope ratios similar to the calc-alkaline rocks (Güleç 1991). Quaternary alkaline volcanics (Kula lavas) also have enriched



concentrations of the LILE but they have low Ba/Nb ( $\sim 8$ ) and high  $\text{TiO}_2$  ( $\sim 2\%$ ) relative to the Tertiary calc-alkaline and alkaline rocks ( $\text{Ba/Nb} > 15$ ;  $\text{TiO}_2 \leq 1.77\%$ ) (Güleç 1991). The Kula lavas therefore resemble rift or intraplate volcanics (Güleç 1991, Seyitoglu & Scott 1992b). Furthermore, the Quaternary rocks have lower  $^{87}\text{Sr}/^{86}\text{Sr}$  (0.70313 - 0.70363) and higher  $^{143}\text{Nd}/^{144}\text{Nd}$  ratios (0.512998 - 0.512749) and they plot within the mantle array (Güleç 1991). The generation of these volcanics was apparently controlled by melts derived from relatively deep, isotopically depleted mantle regions, such as the asthenosphere (Güleç 1991, Seyitoglu & Scott 1992b). The Quaternary alkaline lavas suffered only minimal crustal contamination in contrast to the earlier calc-alkaline volcanics (Güleç 1991). However, in order to account for the enrichment of the LILE in the Kula lavas, Paton (1992), Richardson-Bunbury (1992) and McKenzie and O'Nions (1995) argued for a source region in the lithospheric mantle, rather than the asthenosphere.

Arc volcanism is still active in the southern Aegean (in the south Aegean arc) where the African plate is being subducted beneath the Aegean plate (Fytikas et al., 1984). However, the South Aegean Arc does not generally appear to have exerted an influence on recent volcanism in western Turkey; for instance, the most recent activity at Kula (Late Miocene - Quaternary) was clearly intraplate and not arc related. However, it has been suggested that the Late Miocene to Pliocene Söke and Bodrum volcanics located in the extreme western part of Turkey may be related to the nearby Aegean arc (Pe & Gledhill 1975, Seyitoglu & Scott 1992b).

The tectonic framework of Oligocene - Miocene volcanism in western Turkey has been the subject of much debate, which has generally centred around the timing of north - south extension. One view is that north - south shortening and compression continued until the Late Miocene (Tortonian), and was subsequently followed by north - south extension (Sengör and Yilmaz, 1981, Sengör et al., 1985). Within this tectonic framework, it has been suggested that the compressional and extensional regimes were associated with periods of calc-alkaline and alkaline volcanism respectively (Yilmaz 1989 1990; Güleç, 1991). However, others suggest that north - south extensional tectonics may have begun as early as the Late Oligocene - Early Miocene and that the demise of the earlier compressional regime had occurred by the Late Oligocene in western Turkey (Seyitoglu and Scott, 1991 1992b; Seyitoglu et al., 1992, Hetzel et al., 1995). This implies that the Early Miocene calc-alkaline volcanism was associated with extension as opposed to compression (Seyitoglu & Scott 1992b). The volcanic evolution of western Turkey is therefore considered to reflect an increasing asthenospheric contribution, facilitated by a thinned extended lithosphere arising from extensional tectonics (Seyitoglu & Scott 1992b).

The mechanisms for the generation of the Early Miocene calc-alkaline volcanism largely depend on the timing of extensional tectonics in western Turkey. Under a compressional regime, delamination of subcontinental lithosphere beneath a thickened crust may have taken place, followed by partial melting of the crust to produce anatectic melts (Pirajno 1995). Yilmaz (1990) stated that continental under thrusting played an important role in the generation of calc-alkaline magmas during the late stages of a compressional regime. However, the tectonic framework of Seyitoglu & Scott (1992b) suggests that extension initiated decompressional melting and the subsequent generation of Early

Miocene calc-alkaline magmas. Seyitoglu and Scott (1992b) suggested that extension led to asthenosphere dominated alkaline volcanism in the Pliocene to Quaternary, but Richardson and Bunbury (1992) and McKenzie and O'Nions (1995) argued that melting of anhydrous asthenosphere would have been unlikely, since the degree of lithospheric extension was too small and because there is no evidence of elevated mantle temperatures beneath western Turkey. They therefore suggest that the Late Miocene - Quaternary Kula lavas originate from enriched subcontinental lithosphere, which is able to melt after only modest amounts of extension (Paton 1992, Richardson & Bunbury 1992, McKenzie & O'Nions 1995).

### 5.3 GENESIS OF MIOCENE MAGMATISM IN THE USAK-GÜRE, SELENDI, EMET, KIRKA AND AFYON AREAS

Isotopic dates presented in Chapter 3 showed that there was an Early Miocene phase of calc-alkaline acid magmatism, represented by granite and rhyolite in the Usak-Güre, Selendi and Emet (USE) area (K-Ar: 20.3-17.6 Ma - this study) as well as by ignimbrite ( $^{40}\text{Ar}/^{39}\text{Ar}$ : 18.6 Ma - this study) and rhyolite (K-Ar: 16.7-15.7 Ma - Yalçın 1989) in the Kirka area. This was followed by a Mid - Late Miocene less evolved phase of magmatism which included K-trachyte from Selendi and Usak-Güre Basins (15.9-14.6 Ma - this study), latite from Emet and Usak-Güre Basins (15.5-14.9 Ma - this study), shoshonite from Kirka Basin (9.3 Ma - Yalçın 1989) and basalt, latite and trachyte from the Afyon area (14.7 - 8.6 Ma - Besang 1977). The alkaline Kula basalts are located just to the south of the USE area (Figure 2.1) and they represent the youngest phase of volcanism in western Turkey (7.6 Ma - recent - Ercan et al., 1985). Hence, these isotopic dates reveal a change from largely calc-alkaline acid magmatism in the Early Miocene to predominately alkaline, less silicic volcanism in the Mid to Late Miocene, which is consistent with observations made elsewhere in western Turkey (Yilmaz 1990, Güleç 1991, Seyitoglu & Scott 1992b). Field evidence discussed in Chapter 2 corroborates the information from isotopic dating.

#### 5.3.1 Major and trace elements

All major and trace elements were analysed by XRF, with the exception of Li and B, which were determined by ICP-AES and Prompt GAA respectively (Appendix I). Figures 5.1 and 5.2 show the concentrations of a number of elements and selected element ratios plotted against time for radiometrically dated igneous rocks from this study. For comparative purposes, data for the Kula lavas (Late Miocene to Quaternary) (Ercan et al., 1985) are also plotted. Reflecting the change from acid to more mafic magmatism, there is a decrease in  $\text{SiO}_2$  and an increase in  $\text{MgO}$  from the Early to Middle Miocene (Figure 5.1 a, b). Ni, V, Cr and Co are also markedly higher in some of the Middle Miocene lavas relative to the Early Miocene volcanics, consistent with a more mafic nature. Furthermore, there is an increase in  $\text{Fe}_2\text{O}_3$  and CaO from the Early to Middle Miocene (Figure 5.1 c, d).

The Late Miocene to Quaternary Kula lavas contain much higher  $\text{Na}_2\text{O}$  and generally lower  $\text{K}_2\text{O}$  than the Early to Middle Miocene volcanics (Figure 5.1e, f), resulting in higher  $\text{K}_2\text{O}/\text{Na}_2\text{O}$  ratios in most of the latter (Figure 5.2 a). Therefore, in this area, there is an evolution in time from potassic volcanism

**Figure 5.1 - Variations of major elements vs time for radiometrically dated igneous rocks from the USE and Kirka areas**

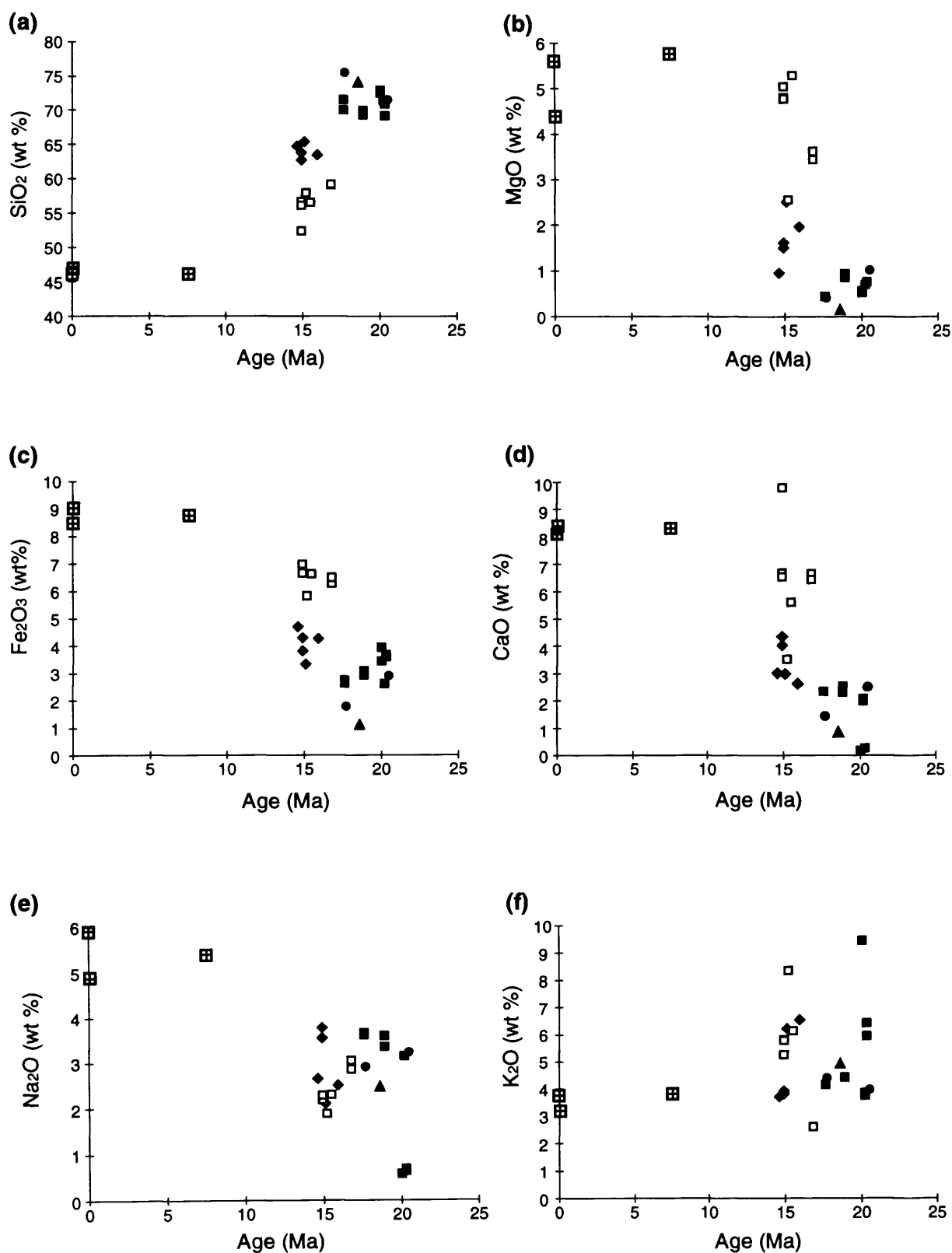
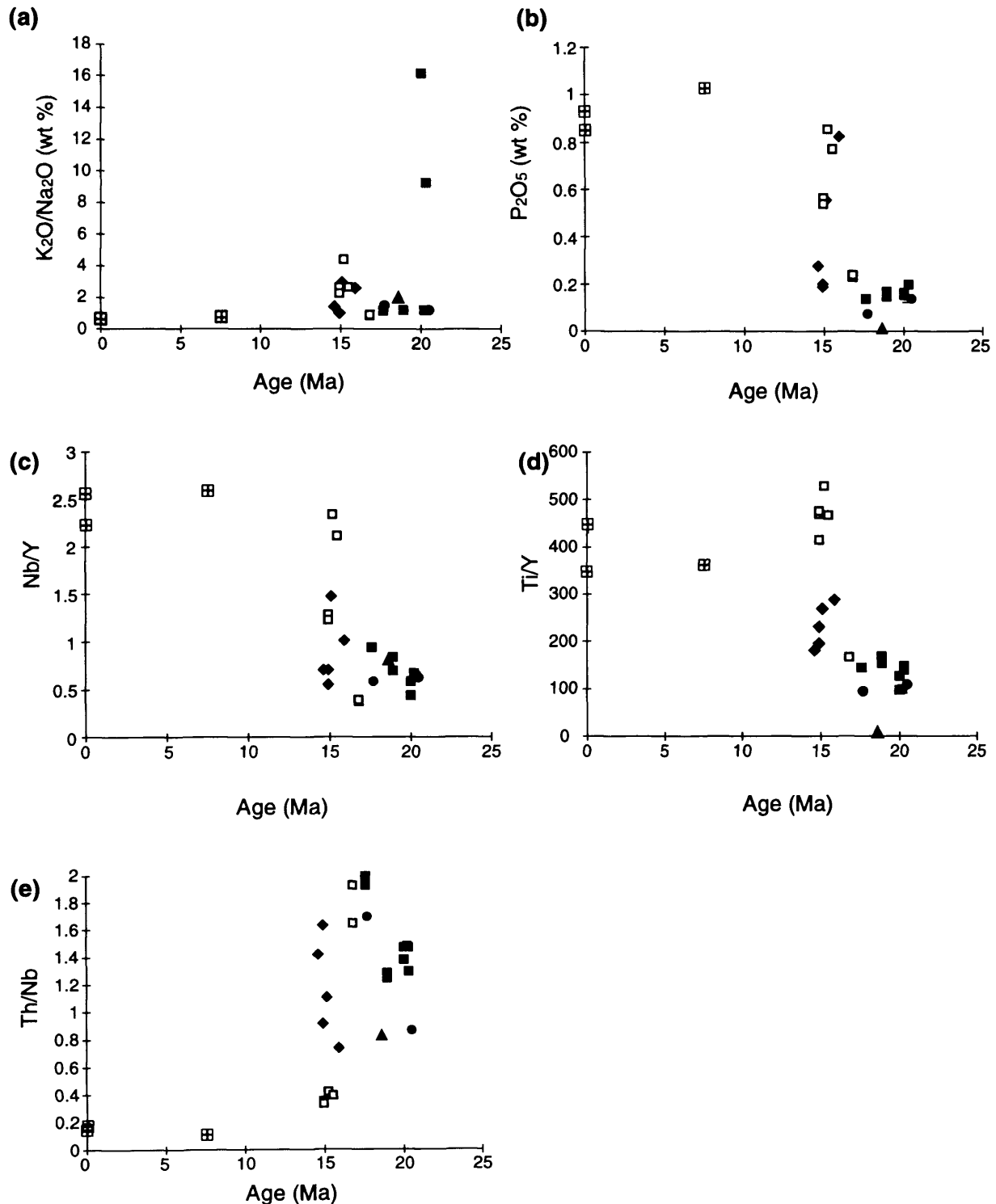


**Figure 5.2 - Variations of major elements and selected trace element ratios with time for radiometrically dated igneous rocks from the USE and Kirka areas**



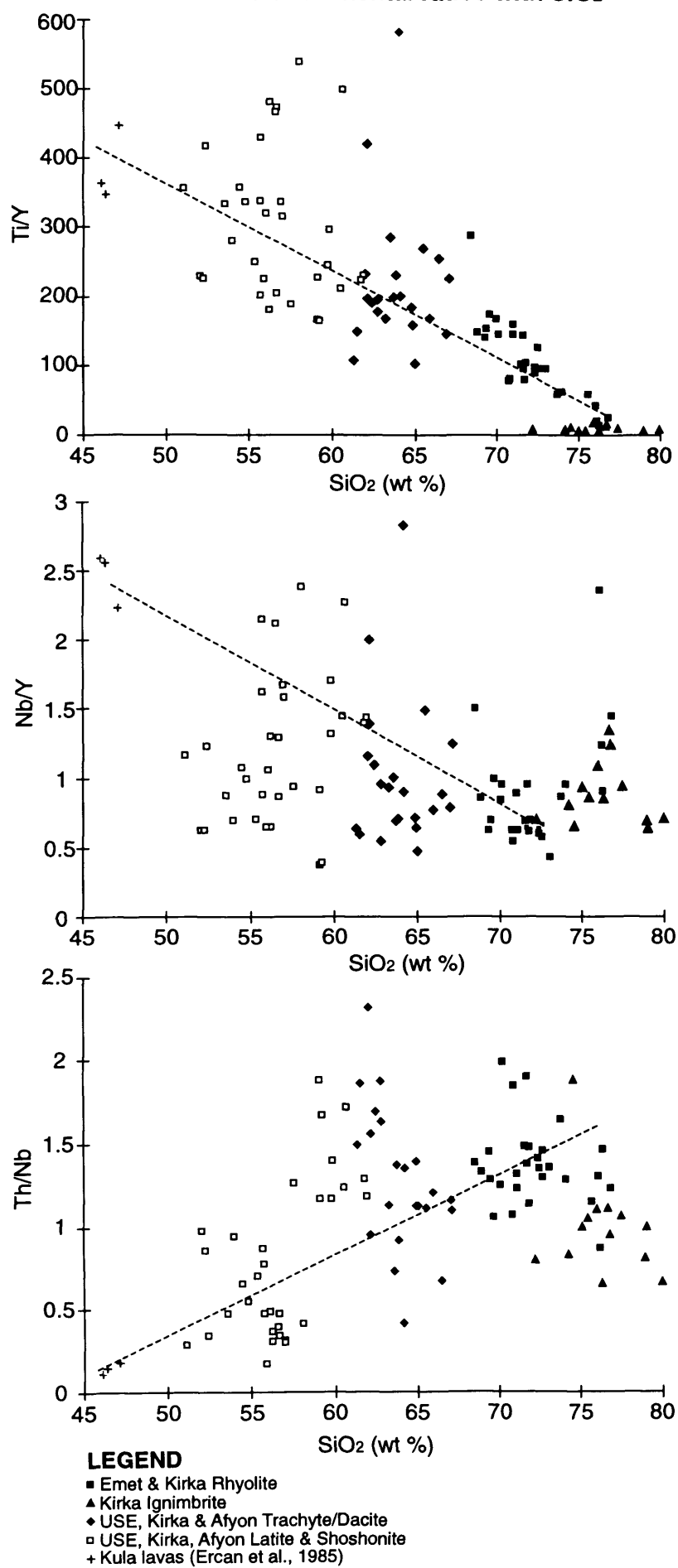
in the Early to Middle Miocene to sodic volcanism in the Late Miocene to Quaternary, a trend previously noted in western Turkey by Güleç (1991). All the USEKA volcanics are strongly potassic (2.6 - 9.48 wt %  $K_2O$ ), and the shoshonite and latite can be further classified into potassic ( $MgO > 3$  wt %,  $K_2O/Na_2O < 2 > 1$ ) and ultrapotassic ( $MgO > 3$  wt %,  $K_2O/Na_2O > 2$ ) according to the classification of Foley et al. (1987). The USE and Afyon areas contain both ultrapotassic and potassic Middle Miocene lavas, whilst the Kirka mafic lavas are potassic.

Higher levels of the HFSE are found in some of the Middle Miocene lavas relative to the earlier more silicic volcanics (Figure 5.2 b - e). These elevated concentrations occur in the shoshonite and latite leading to generally higher  $P_2O_5$ , Nb/Y and Ti/Y, but lower Th/Nb in these rocks compared to the rhyolite, ignimbrite, granite and trachyte (Figure 5.2 b, c, d, e). Overall, there is considerable variation in  $P_2O_5$ , Nb/Y, Ti/Y, and Th/Nb within the Middle Miocene lavas (Figure 5.2 b - e). Figure 5.3 shows these ratios plotted against  $SiO_2$  for all the samples analysed in this study. There are trends of decreasing Ti/Y and Nb/Y, but increasing Th/Nb, with increasing  $SiO_2$ , although there is a considerable spread in the data, particularly with the latite and shoshonite samples (Figure 5.3). Since the Kula basalts are less evolved ( $SiO_2 < 48.4$  wt % - Güleç 1991) than even the most mafic USEKA lavas, geochemical comparisons between the two suites should be made with caution. Attempts have been made to extrapolate the elemental ratios against  $SiO_2$  in the USEKA mafic lavas to establish possible ratios at  $SiO_2$  concentrations equivalent to those of the Kula basalts (Figure 5.3). The trends appear to suggest that, at lower  $SiO_2$  concentrations (equivalent to the Kula basalts) Ti/Y, Nb/Y and Th/Y ratios in the USEKA mafic suite would be similar to those in the Kula basalts. As described above, the most significant geochemical difference between the Late Miocene-Quaternary Kula lavas and the Middle Miocene mafic USEKA lavas is that the former is sodic and the latter potassic in nature.

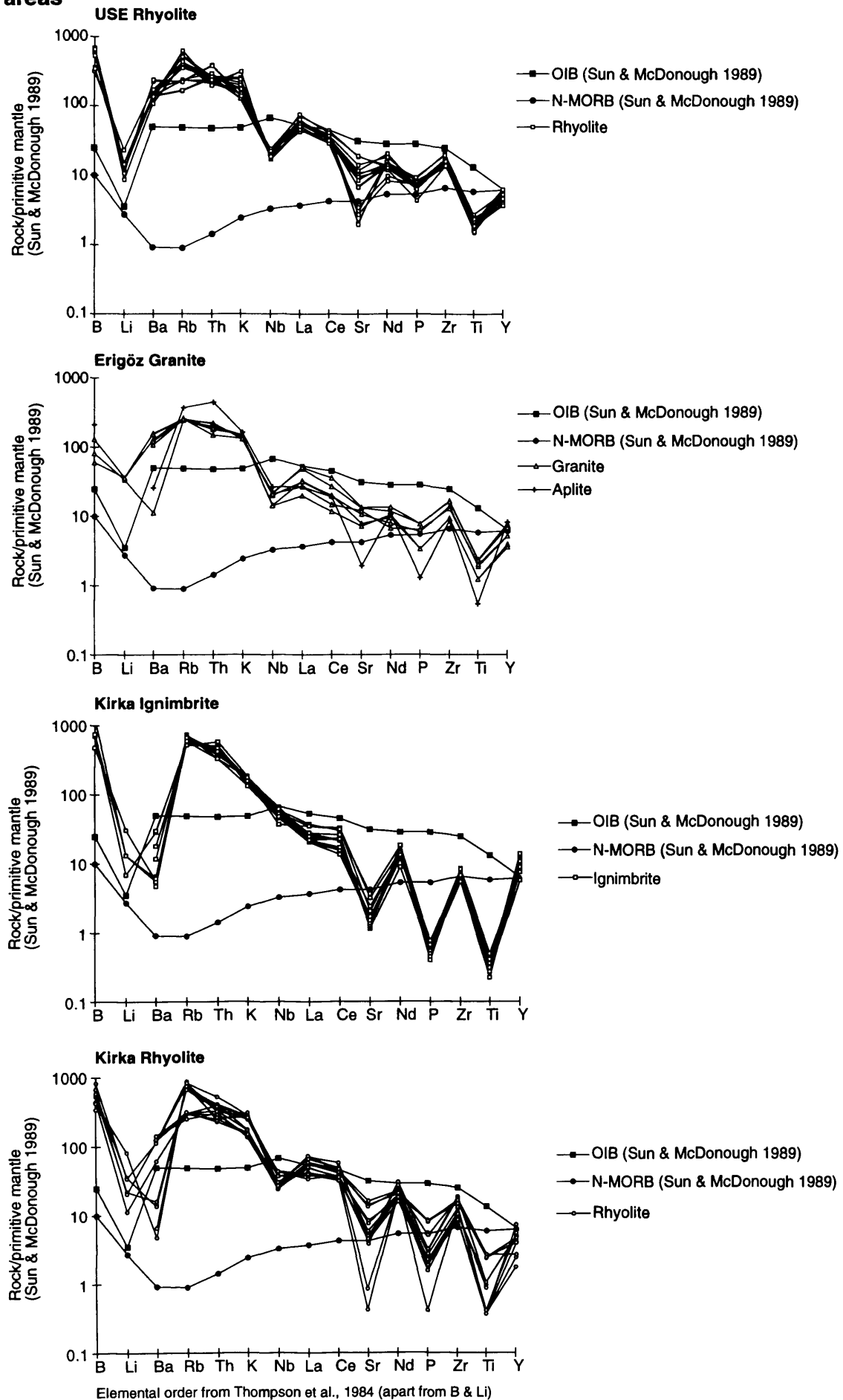
The compositions of igneous rocks collected in this study are shown in Figures 5.4 to 5.8 on primitive mantle normalised multi-element diagrams. Some caution should be taken when interpreting the significance of the concentrations of the mobile elements B, Li, Ba, Rb and K, as a result of a limited amount of remobilisation of these elements, particularly in the more acidic rocks (Chapters 3 & 4). Due to the widespread remobilisation of As in most of the samples (Chapter 5), this element is not plotted in these diagrams.

All the suites from acid to intermediate rocks are enriched in the LILE and B and depleted in Nb relative to average ocean island basalt (OIB) (Figures 5.4, 5.5, 5.6, 5.7). Although Li is enriched, relative to Li contents in OIB, in all the collected samples, it is less enriched than the LILE and B, therefore producing a negative anomaly (Figure 5.4, 5.5, 5.6, 5.7). As described in the previous chapter, the average shoshonite and latite contain lower levels of B than the more silicic volcanics in the area (Figure 5.7). The acid igneous rocks from Emet and Kirka show distinctive negative anomalies in Sr, P, Ti, Eu and sometimes Ba (Figures 5.4, 5.7, 5.8) and these troughs appear to result from crystal fractionation of various mineral phases. The Sr, Ba and Eu anomalies indicate the removal of feldspar from the melt by crystal fractionation or the retention of feldspar in the source. Ti concentration is probably controlled by Fe-Ti oxides, such as magnetite which is present in the Erigöz Granite, and the P levels are likely to be related to the crystal fractionation of apatite, an accessory phase found in the

**FIGURE 5.3 - Variations of elemental ratios with SiO<sub>2</sub>**

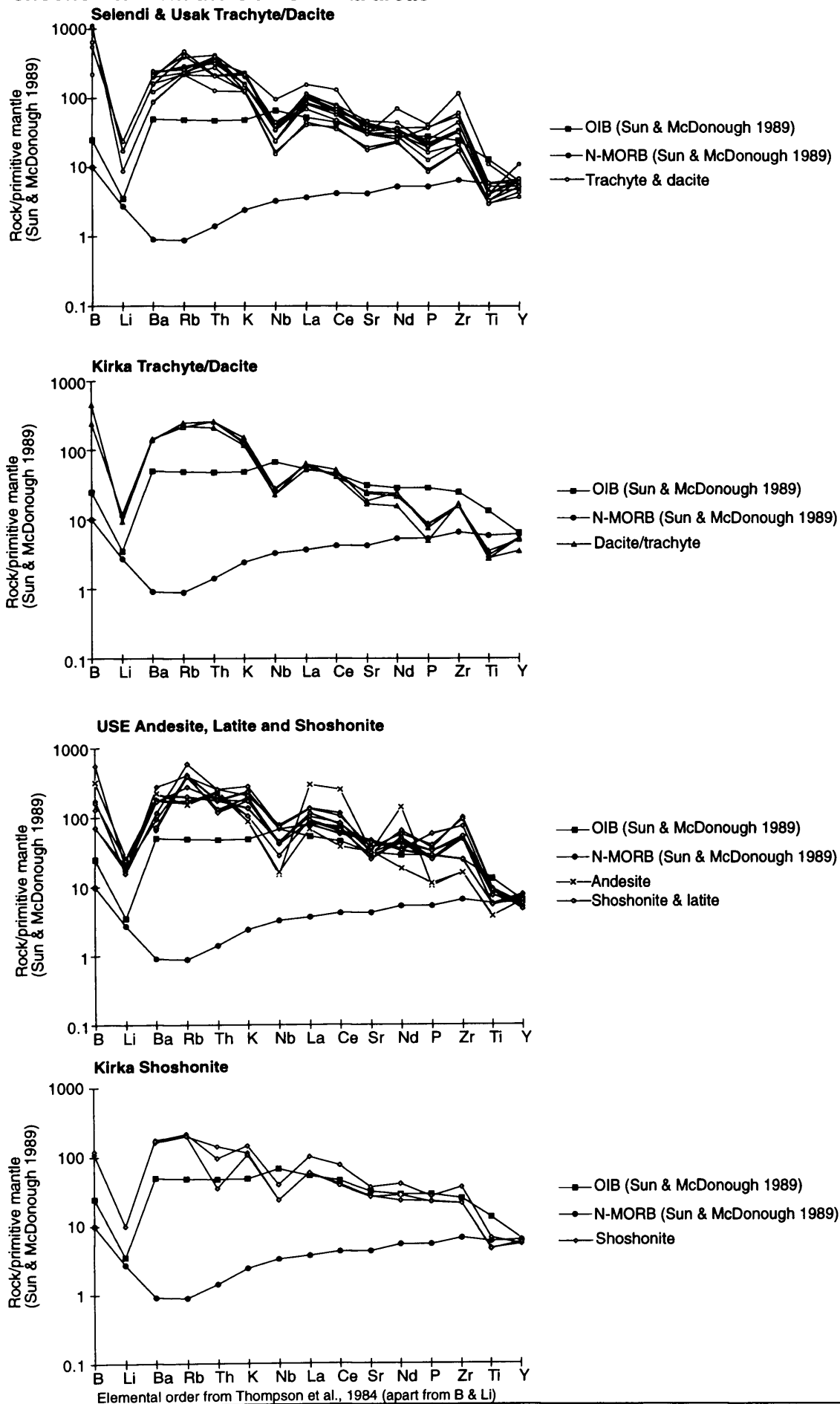


**FIGURE 5.4 - Multielement variation plots for acid igneous rocks from the USE and Kirka areas**



**Figure 5.4**

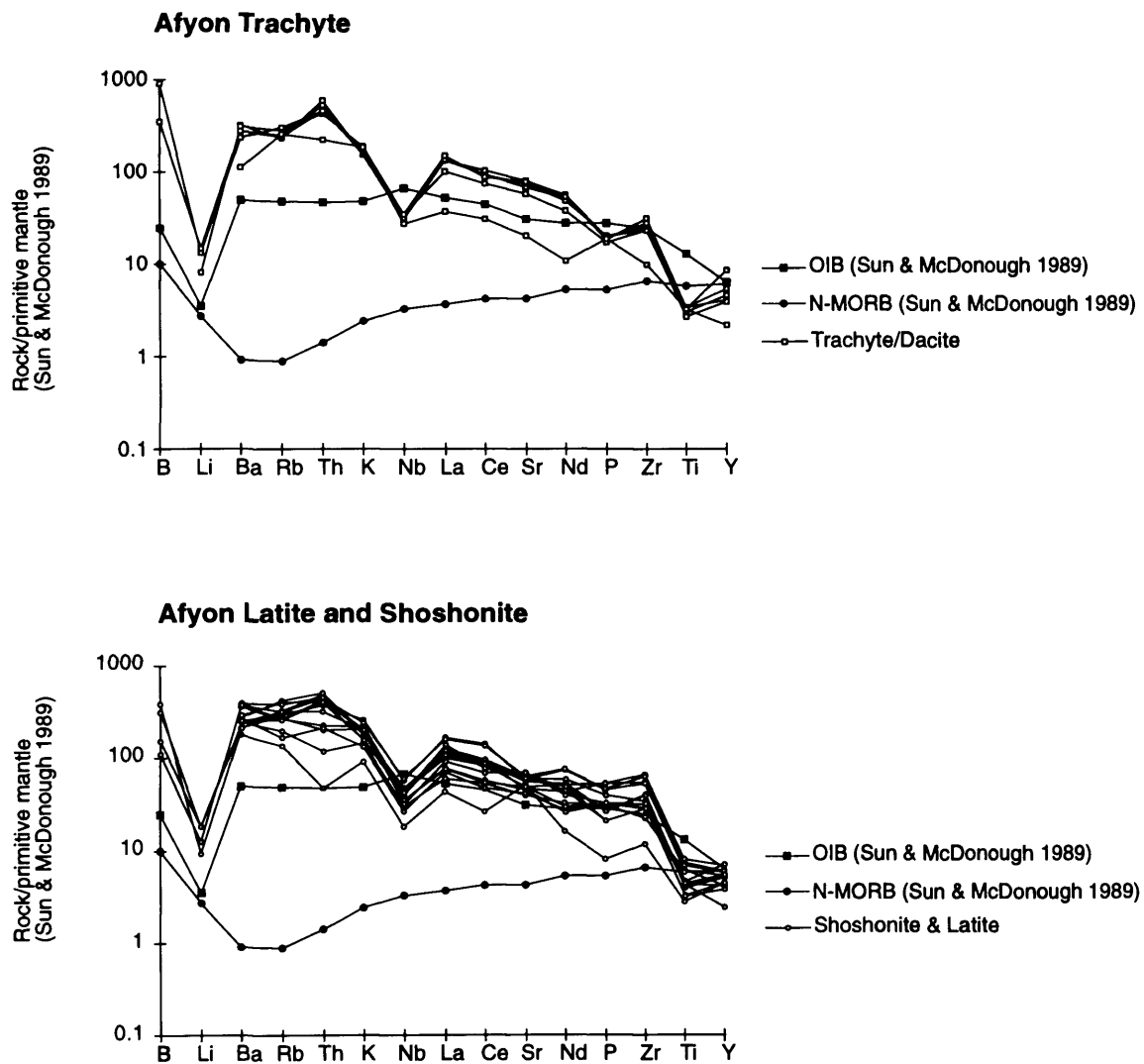
**FIGURE 5.5 - Multielement variation plots for trachyte/dacite, andesite, latite & shoshonite from the USE & Kirka areas**



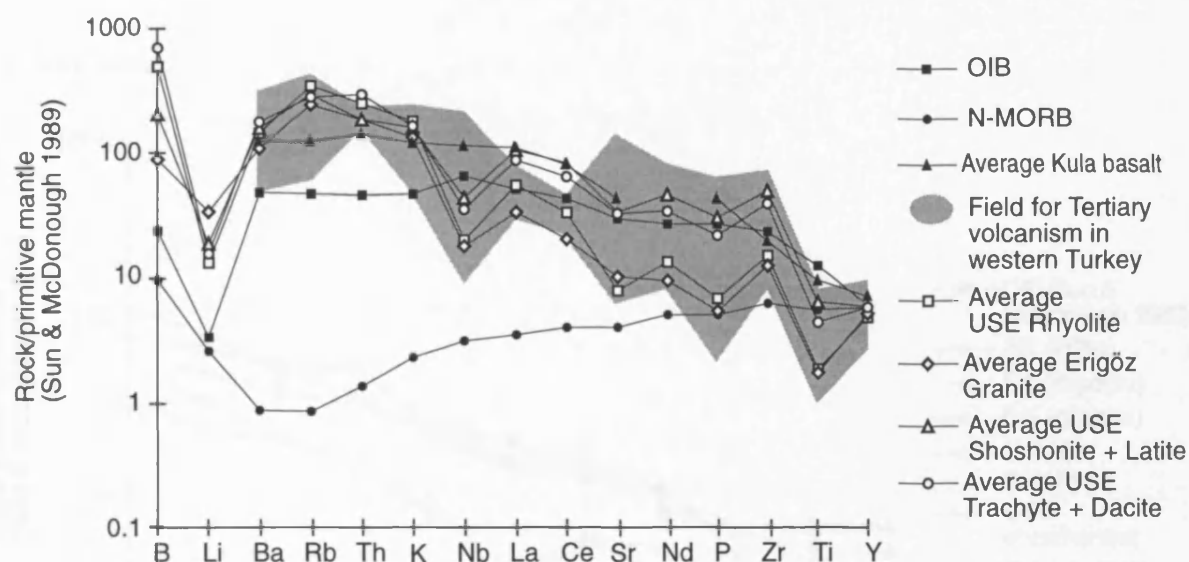
**Figure 5.5**



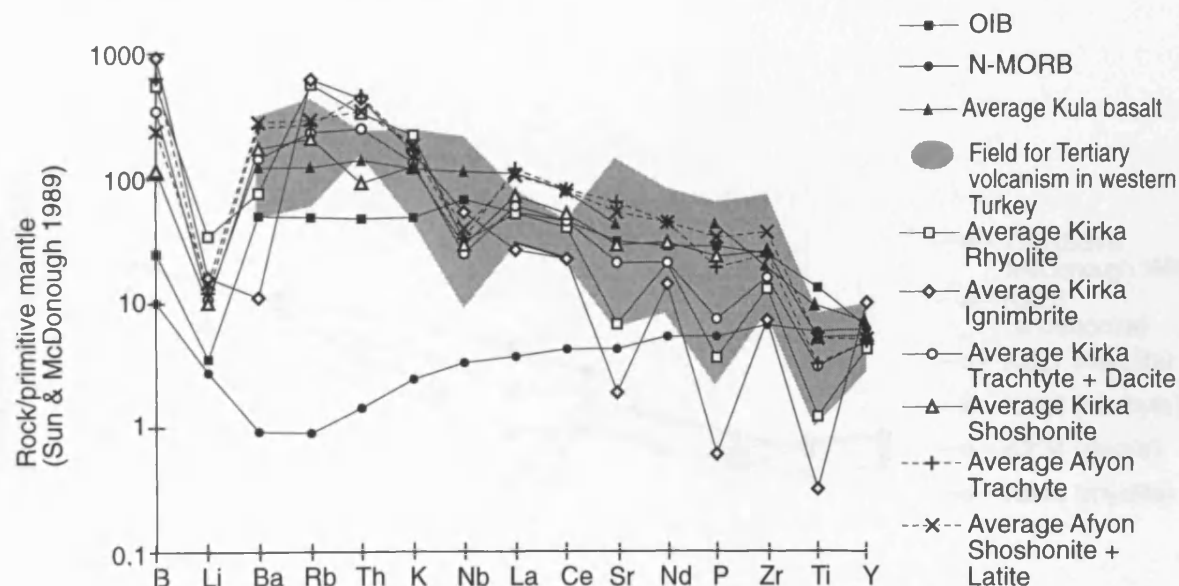
FIGURE 5.6 - Multielement variation plots for volcanic rocks from the Afyon area



**FIGURE 5.7a - Multielement plot comparing variations within the USE suite with Tertiary and Quaternary volcanism elsewhere in western Turkey**



**FIGURE 5.7b - Multielement plot comparing variations within the Afyon and Kirka suites with Tertiary and Quaternary volcanism elsewhere in western Turkey**



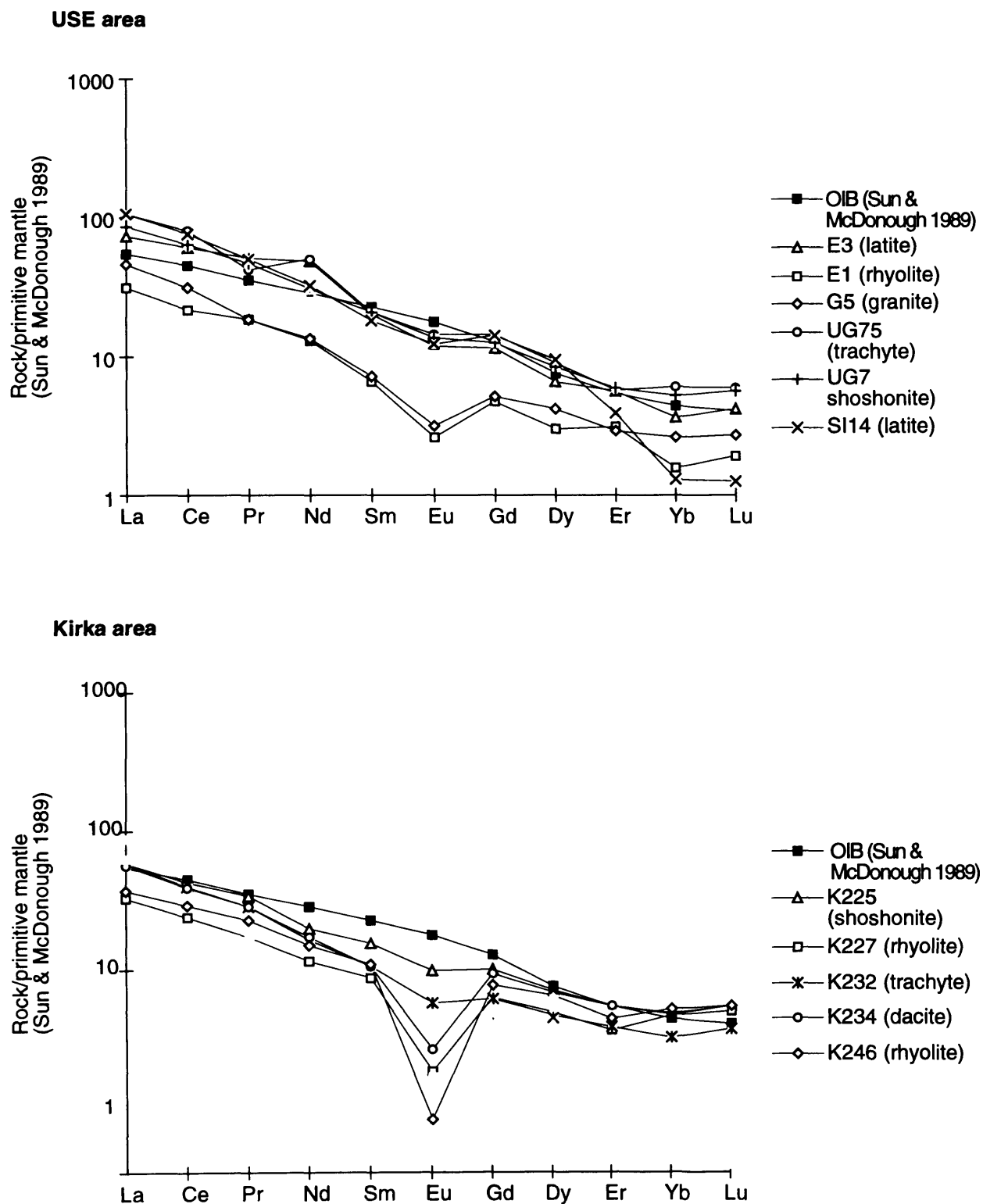
**Data sources**

OIB and N-MORB from Sun & McDonough 1989

Kula basalts from Ercan et al., 1985

Western Turkey Tertiary volcanism - Güleç 1991, Seyitoglu et al., 1992

**FIGURE 5.8 - Rare earth element concentrations in igneous rocks from the USE and Kirka areas**



acid volcanics and the Erigöz Granite. Smaller negative anomalies in Sr, Ti, Eu and P are present in the dacite and trachyte from this area, but these troughs are virtually absent in the least evolved USEKA rocks, the latite and shoshonite (Figures 5.5, 5.6, 5.7, 5.8). Hence, concentrations of Sr, Ti, Eu and P gradually increase as fractionation decreases. The other main difference between the evolved and the mafic lavas is that the latter contain higher levels of all the REE and Zr (Figures 5.7 & 5.8). The acid igneous rocks often show depletions in La, Ce, Nd and Zr, while the mafic lavas are largely enriched in these elements relative to OIB (Figures 5.4, 5.5, 5.6, 5.7, 5.8).

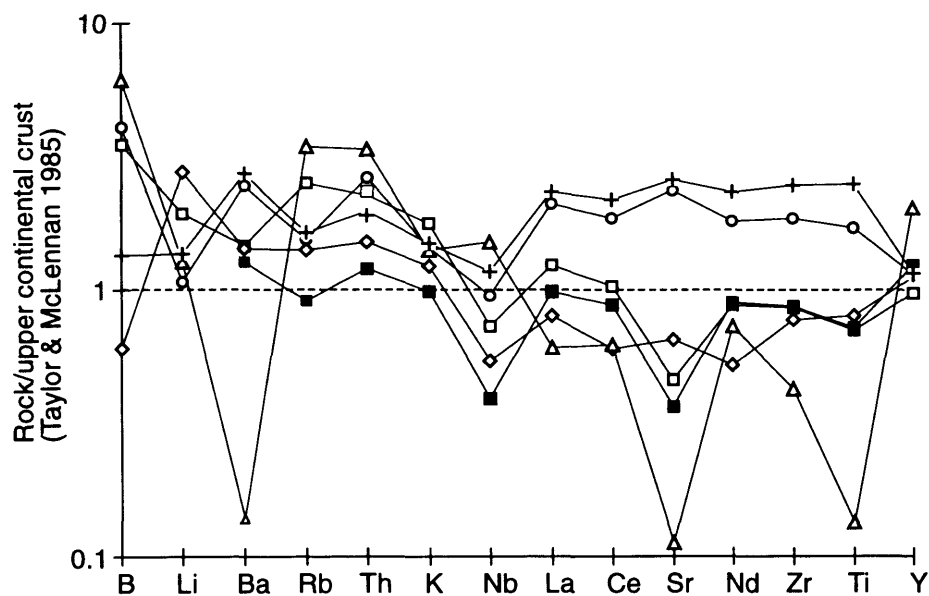
All the igneous rocks from this study plot within the field for previously analysed Tertiary volcanics from west Turkey, with the exception of the Kirka Ignimbrite which contains anomalously low concentrations of Ba, Sr, P and Ti as described above (Figures 5.7 a & b). However the USEKA igneous rocks contain higher concentrations of the LILE and lower Nb than the Late Miocene to Quaternary Kula basalts (Figure 5.7). The Kula basalts appear more similar to OIB except that they show greater enrichments in those elements to the left of Sr on the multielement variation diagram (Figure 5.7).

Figure 5.9 shows the data from this study normalised to average upper continental crust (Taylor & McLennan 1985). Average metasediment (upper crust) from the Aegean islands of Paros and Serifos is plotted for comparison (Stouraiti 1995, McGrath - pers. comm, 1995). As pointed out by Güleç (1991), there is a lack of data for the west Turkish upper continental crust; eg. for the Menderes Massif. The elemental composition of the Erigöz Granite and the USE and Kirka Rhyolite is reasonably similar to both the average upper continental crust of Taylor and McLennan (1985) and that of Paros and Serifos (Stouraiti 1995, McGrath - pers. comm, 1995) (Figure 5.9). However, the USE and Kirka Rhyolite differs from mean upper continental crust in containing elevated concentrations of Rb, Th, K and B (Figure 5.9). The Kirka Ignimbrite also differs from upper continental crust in containing high levels of Rb, Th, K and B, but in addition it is depleted in Ba, Sr and Ti, the result of extensive fractionation. As shown above, the USEKA trachyte, dacite, latite and shoshonite contain similar concentrations of the LILE to the acid volcanics, but they have much greater amounts of La, Ce, Sr, Nd, Zr and Ti. Hence, these less evolved volcanics are considerably enriched in the light REE, Sr, Zr and Ti relative to upper continental crust and the enrichment is greater in the latite and shoshonite than in the trachyte and dacite (Figure 5.9). Overall therefore, the acid igneous rocks are more similar to upper continental crust than the mafic lavas, although all (except the granite) show a marked enrichment relative to the crust in Rb, Th, K and B.

### 5.3.2 Nd and Sr isotopes

Nd and Sr isotopic ratios were analysed in selected samples at the National Isotope Geoscience Laboratories (NIGL) (details in Appendix J). All the samples analysed from the USEKA area plot in the enriched quadrant of the  $\epsilon_{Nd}$  vs  $^{87}Sr/^{86}Sr$  diagram (Figure 5.10 - all data age corrected, except for recent Kula lavas). The USE and Kirka data have been grouped together due to their similar isotopic compositions shown by samples from these areas (Figure 5.10). The USE and Kirka samples have a

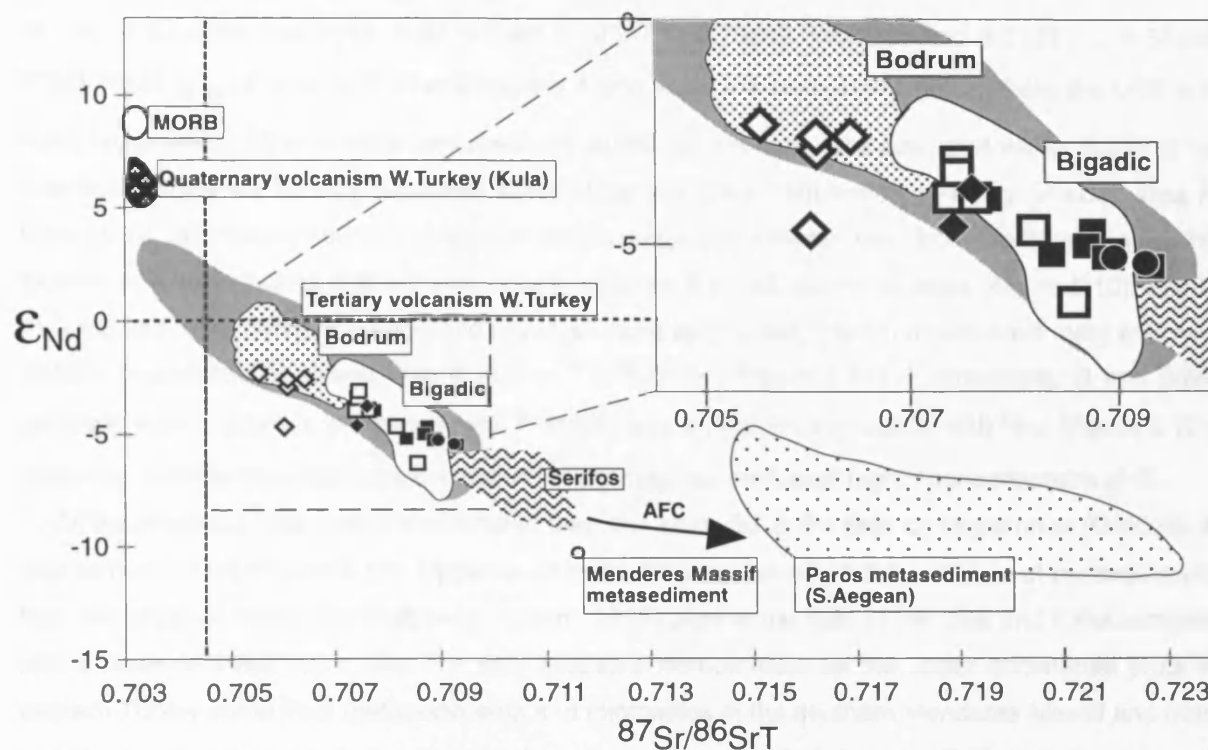
FIGURE 5.9 - Magmatism of the USEKA area compared to upper continental crust



#### LEGEND

- Average Paros & Serifos greywackie  
(Stouraiti 1995, McGrath 1995)
- Average USE & Kirka Rhyolite
- Average USEKA Trachyte + Dacite
- ◇— Average Erigöz Granite
- △— Average Kirka ignimbrite
- +— Average USEKA Shoshonite & Latite

**FIGURE 5.10 - Nd and Sr isotopic compositions of the USEKA volcanics and granite compared with magmatism from the eastern Mediterranean region**



#### LEGEND

- USE & Kirka rhyolite (Early Miocene) (68.42-76.76 wt % SiO<sub>2</sub>, 0.16-0.94 wt % MgO)
- ◆ USE dacite/trachyte (Mid-Miocene) (63.54-64.85 wt % SiO<sub>2</sub>, 0.96-1.97 wt % MgO)
- USE & Kirka latite & shoshonite (Mid - Late Miocene) ( 55.89-59.23 wt % SiO<sub>2</sub>, 3.46-5.31 wt % MgO)
- Erigöz Granite (early Miocene/Oligocene) (71.68-75.61 wt % SiO<sub>2</sub>, 0.42-1.03 wt % MgO)
- ◇ Afyon latite & trachyte (Mid-Miocene) (56.21-62.40 wt % SiO<sub>2</sub>, 1.68-4.16 wt % MgO)
- Menderes Massif metasediment (sample 888/2 - from near Kula)
- MORB (Mid Atlantic Ridge - Sun & McDonough 1989)
- Kula volcanism (Gulec 1991) (45.48-48.43 wt % SiO<sub>2</sub>, 4.87-7.31 wt % MgO)
- Tertiary volcanism, western Turkey - Gulec 1991, Robert et al., 1992 (49.54-71.88 wt % SiO<sub>2</sub>, 0.38-10.73 wt % MgO)
- Bigadic (Borate-bearing basin - western Turkey - Gulec 1991) (59.12-67.01 wt % SiO<sub>2</sub>, 0.74-3.43 wt % MgO)
- Bodrum (Robert et al., 1992) (48.64-52.09 wt % SiO<sub>2</sub>, 4.79-11.19 wt % MgO)
- Serifos granite (Stouraiti 1995)
- Paros metasediment (McGrath 1995)

All data are age corrected apart from the recent volcanism of Kula

range in  $^{87}\text{Sr}/^{86}\text{Sr}$  from 0.70738 to 0.70931 and a range in  $^{143}\text{Nd}/^{144}\text{Nd}$  from 0.51246 to 0.51230 ( $\epsilon_{\text{Nd}}$  -3.1 to -6.3), while the Afyon suite contain 0.70557 to 0.70643  $^{87}\text{Sr}/^{86}\text{Sr}$  and 0.51251 to 0.51238  $^{143}\text{Nd}/^{144}\text{Nd}$  ( $\epsilon_{\text{Nd}}$  -2.3 to -4.7). Therefore, the Afyon lavas are isotopically distinct from the USE and Kirka lavas which have a more 'enriched' signature. All the data, however, plot within the field for previously analysed Tertiary (Miocene & Pliocene) volcanics from western Turkey (shaded area in Figure 5.10, after Güleç 1991). The isotopic characteristics of volcanic rocks from the Bigadiç area, the location of a major borate deposit, also closely matches the USE and Kirka lavas (Figure 5.10). Within the USE and Kirka suites, the silicic and low MgO samples (rhyolite, granite) mostly have more enriched isotopic signatures (ie. lower  $\epsilon_{\text{Nd}}$  & higher  $^{87}\text{Sr}/^{86}\text{Sr}(\text{T})$  - Figure 5.11). Furthermore, B and B/Nb generally have a positive correlation with  $^{87}\text{Sr}/^{86}\text{Sr}$  and a negative correlation with  $\epsilon_{\text{Nd}}$  (Figure 5.12), indicating that the more isotopically enriched silicic magmas contained higher concentrations of B.

All the analysed USE and Kirka samples from this study fall in the field for upper crust (DePaolo & Wasserburg 1979) (Figure 5.13). Upper crust in the Aegean, based on the analyses of metasediment from the island of Paros (McGrath pers. comm - 1995) plots to the right of the USE and Kirka samples with a more enriched signature. The only available isotopic data on the upper continental crust in western Turkey come from metasediments and migmatites in the southern Menderes Massif and from tonolite and granitic meta-igneous rocks from the northern part of the massif (Satir & Friedrichsen 1986). The  $^{87}\text{Sr}/^{86}\text{Sr}$  ratios of these rock types range from 0.70851 to 0.70137 in the former and from 0.70660 to 0.70729 in the latter (Satir & Friedrichsen 1986). This field overlaps with the USEKA field and also extends to higher ratios. In addition, a single sample of amphibolite facies pelite from further north in the Menderes Massif near Kula (Verge pers. comm - 1995) was analysed during this study and has an isotopic composition of  $\epsilon_{\text{Nd}}$  -10.3 and  $^{87}\text{Sr}/^{86}\text{Sr}$  0.71159 (age corrected to 18 Ma, which is the time of active acid magmatism in the area). This pelite therefore plots between the USEKA magmatism and the Paros metasediment (Figure 5.10). However, to gain a more complete knowledge of the isotopic composition of the upper continental crust in western Turkey, considerably more data are required from a whole range of basement units. The available data from western Turkey and the Aegean suggests that upper crustal isotopic compositions in this region range from ratios near to USEKA lavas to considerably higher ratios.

### 5.3.3 Discussion

#### 5.3.3.1 Assimilation of upper crust

The data from the USEKA area reveal a change from largely calc-alkaline acidic volcanism in the Early Miocene to predominantly alkaline, less silicic volcanism in the Middle Miocene. The continental crust over western Turkey in the Miocene is believed to have been between 50 and 70 km thick (Sengör et al., 1985) and hence there is a strong likelihood that crystal fractionation and crustal contamination processes played an important role in the modification of the early Miocene USE and Kirka magmas. The Middle Miocene more mafic USEKA volcanism contained higher concentrations of

FIGURE 5.11

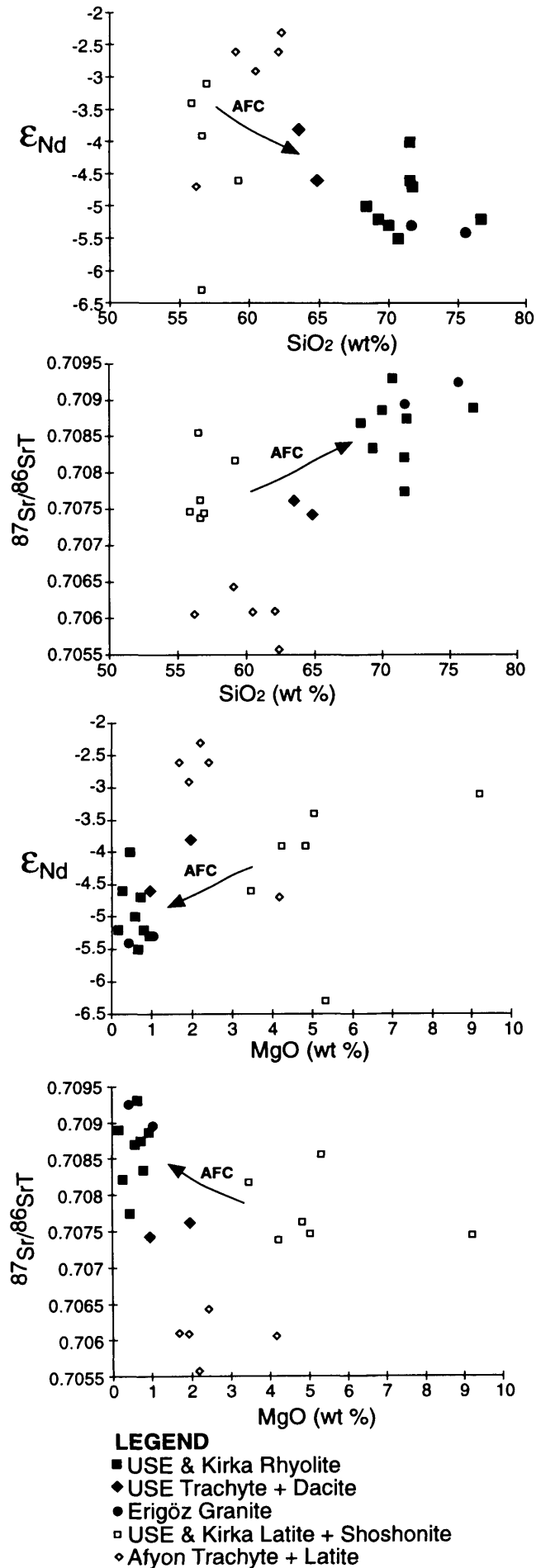
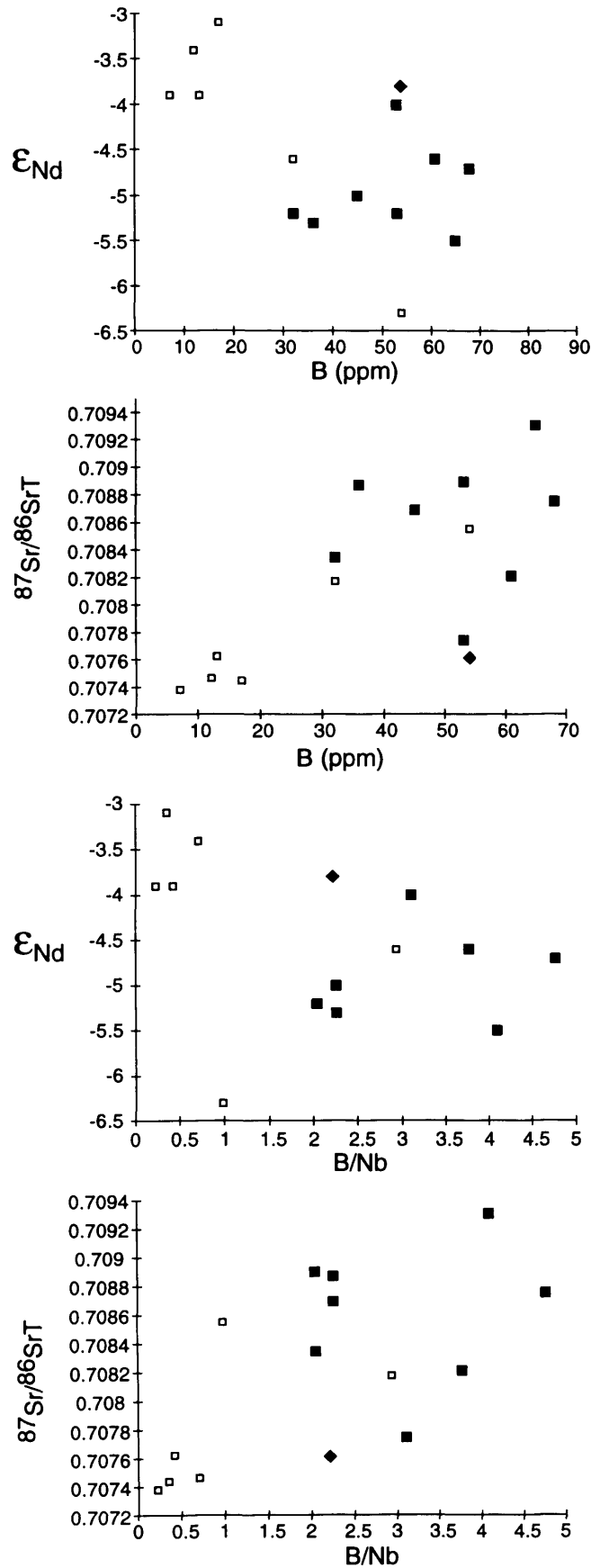


Figure 5.11



FIGURE 5.12

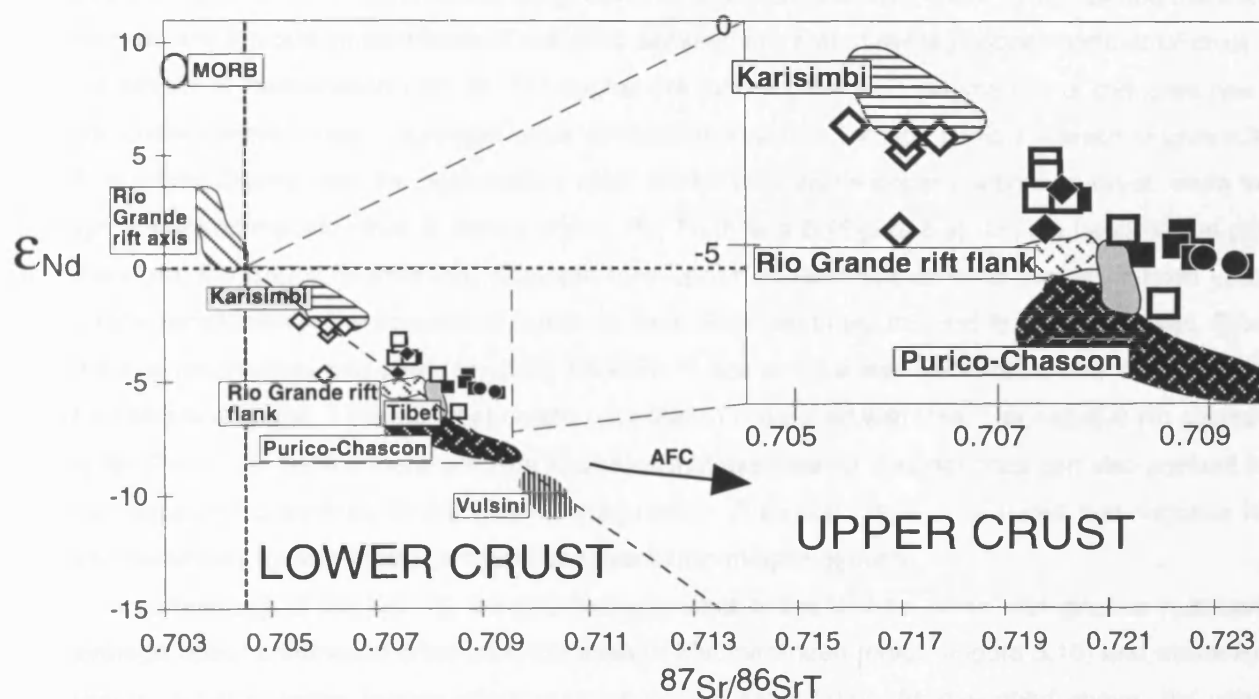


**LEGEND**

- USE & Kirka Rhyolite
- ◆ USE Trachyte
- USE & Kirka Latite + Shoshonite

B values for samples K228, K231, K226 & SE13 taken from analyses of duplicates from the same localities

**FIGURE 5.13 - Nd and Sr isotopic compositions of USEKA volcanics and granite compared with selected volcanic provinces from around the world**



# **LEGEND**

- USE & Kirka rhyolite (Early Miocene) (68.42-76.76 wt % SiO<sub>2</sub>, 0.16-0.94 wt % MgO)
- ◆ USE dacite/trachyte (Mid-Miocene) (63.54-64.85 wt % SiO<sub>2</sub>, 0.96-1.97 wt % MgO)
- USE & Kirka latite & shoshonite (Mid - Late Miocene) ( 55.89-59.23 wt % SiO<sub>2</sub>, 3.46-5.31 wt % MgO)
- Erigöz Granite (early Miocene/Oligocene) (71.68-75.61 wt % SiO<sub>2</sub>, 0.42-1.03 wt % MgO)
- ◇ Afyon latite & trachyte (Mid-Miocene) (56.21-62.40 wt % SiO<sub>2</sub>, 1.68-4.16 wt % MgO)
- MORB (Mid Atlantic Ridge - Sun & McDonough 1989)
- ▨ Karisimbi (Rogers et al., 1985) (43.66-47.27 wt % SiO<sub>2</sub>, 8.48-9.41 wt % MgO)
- ▩ Vulsini (Rogers et al., 1985) (44.70-56.09 wt % SiO<sub>2</sub>, 4.15-12.84 wt % MgO)
- ▧ Rio Grande rift flank (Gibson et al., 1993) (53.84-54.33 wt % SiO<sub>2</sub>, 4.16-7.65 wt % MgO)
- ▦ Rio Grande rift axis (Gibson et al., 1993) (43.75-53.39 wt % SiO<sub>2</sub>, 6.96-12.02 wt % MgO)
- ▤ NW Tibet (Arnaud et al., 1992) (49.80-57.09 wt % SiO<sub>2</sub>, 3.67-5.6 wt % MgO)
- ▣ Purico-Chascon (Hawkesworth et al., 1982) (56.4-70.4 wt % SiO<sub>2</sub>)

Continental crust (DePaolo & Wasserburg 1979)

All data is age corrected apart from the recent volcanism of East Java, Vulsini and Karisimbi

MgO, Fe<sub>2</sub>O<sub>3</sub>, CaO, Ni, V, Cr and Co than the earlier acid magmas, probably reflecting a decrease in fractional crystallisation and, perhaps, crustal assimilation through time. An attempt to assess the degree of crustal assimilation in the magmatism of this area has been made by comparing the trace element and isotopic compositions of collected samples with that of average upper continental crust. If the effects of fractionation (Ba, Sr, Ti troughs) are ignored, the acid magmatism of this area has a composition more similar to average upper continental crust than the later mafic volcanism (Figure 5.9). The Erigöz Granite has the composition most similar to average upper continental crust, while the ignimbrite and rhyolite differ in having higher Rb, Th, K and B (Figure 5.9). On the basis of this plot, therefore, the Erigöz Granite may originate from upper crustal anatexis while the assimilated upper crustal component in the volcanics appears to have decreased from the acid to the mafic lavas. Since the acid magmatism was generally Early Miocene in age and the less silicic volcanism was Middle to Late Miocene in age, it appears that crustal assimilation decreased with time. The negative Nb anomaly in the Paros and Serifos metasediment illustrates that assimilation of upper crust can also account for the negative Nb anomaly in the USEKA magmatism. Rollinson (1993) also noted that negative Nb anomalies may be an indicator of crustal involvement in magma genesis.

A comparison of the Nd - Sr isotopic characteristics of the USEKA lavas with igneous rocks and average upper continental crust from the eastern Mediterranean region (Figure 5.10) and elsewhere (Figure 5.13) provides further information on crustal assimilation. As described above, the upper continental crust from this region contains rock types with higher <sup>87</sup>Sr/<sup>86</sup>Sr and lower  $\epsilon_{Nd}$  than the USEKA magmatism (eg. Paros metasediment - McGrath 1995 - pers comm, & Menderes Massif basement - this study & Satir & Friedrichsen 1986). The fact that the silicic, low MgO samples from the USE and Kirka areas generally have higher <sup>87</sup>Sr/<sup>86</sup>Sr and lower  $\epsilon_{Nd}$  than the less evolved mafic samples (Figures 5.10, 5.11, 5.12), and therefore plot closer to upper continental crust (Figure 5.10), strongly suggests that the former contain a greater component of assimilated upper crust. The positive correlation between <sup>87</sup>Sr/<sup>86</sup>Sr<sub>T</sub> and SiO<sub>2</sub>, and a negative one between  $\epsilon_{Nd}$  and SiO<sub>2</sub> (Figure 5.11) further indicate that contamination took place by AFC processes. The conclusions made from this study are broadly consistent with Güleç (1991), who, on the basis of Nd and Sr isotopes, stated that most of the Tertiary volcanics in western Turkey have been subjected to contamination at crustal levels through AFC processes, with a gradual decrease in the amount of contamination with time. Her study also illustrated that the highest <sup>87</sup>Sr/<sup>86</sup>Sr and lowest  $\epsilon_{Nd}$  signatures are found in the most silicic volcanics. However, additional data on the upper crust of western Turkey is required to further constrain the amounts of crustal assimilation and the precise compositions of the contaminants involved.

The Late Miocene Serifos granite in the Aegean has slightly higher <sup>87</sup>Sr/<sup>86</sup>Sr and lower  $\epsilon_{Nd}$  than the USE and Kirka samples (Figure 5.10). The Serifos pluton is thought to result from the melting and subsequent mixing of relatively isotopically depleted amphibolite with more enriched greywacke (which has a similar Nd - Sr isotopic composition to Paros metasediment), both of which are present in

the local basement (Stouraiti 1995). The Erigöz Granite has a similar isotopic and trace element (except for the slightly higher LILE) composition to the Serifos pluton (Figures 5.10 & 5.14a) and therefore it is plausible that the Erigöz Granite was also generated from the melting and mixing of enriched (high  $^{87}\text{Sr}/^{86}\text{Sr}$  & low  $\epsilon_{\text{Nd}}$ ) local metasediment in the basement with a more depleted (lower  $^{87}\text{Sr}/^{86}\text{Sr}$  & higher  $\epsilon_{\text{Nd}}$ ) source. As already mentioned though, the elemental composition of the Erigöz Granite closely approximates that of upper continental crust (Figure 5.9) and hence a partly crustal source seems likely in this case. The similarity in chemical and isotopic composition of the USE and Kirka Rhyolite with the Erigöz Granite (Figures 5.4, 5.5, 5.9 & 5.10) indicates a similar source.

Suitable comparisons for the USE and Kirka acid volcanics include the Central Volcanic Zone (CVZ) of the Andes and north-west Tibet, which, like western Turkey, have both experienced significant crustal thickening and compression. The Purico-Chascon acid igneous complex in the southern CVZ (northern Chile) has Nd - Sr isotopic compositions similar to those of the USE and Kirka rhyolites, although  $\epsilon_{\text{Nd}}$  is slightly lower (more enriched) in the former (Figure 5.13). The Purico-Chascon rocks are considered to have formed from the partial melting of pre-existing crust of intermediate to mafic composition (Hawkesworth et al., 1982). Similarly, the late Miocene ignimbrite 'flare up' which resulted in the Altiplano-Puna volcanic complex further north in the CVZ (Bolivia & Peru) was also apparently the consequence of widespread crustal melting (de Silva 1989). The Nd and Sr isotopic composition of the Altiplano-Puna volcanic complex overlaps with that of the Purico-Chascon volcanics (de Silva 1989). The thickness of crust in this region is thought to have been approximately 70 km (de Silva 1989), which is a similar figure to that suggested for western Turkey in the Miocene (Sengör et al., 1985). Hence, the acid volcanism of the central Andean region appears to provide a good analogue for the silicic magmatism of the USE and Kirka areas with both containing a significant crustal contribution.

Rhyolite from north-west Tibet (Arnaud et al., 1992) has a very similar chemical composition to average USE and Kirka Rhyolite, with considerable enrichment relative to OIB in Rb, Th and K (Figure 5.14). It also has a similar  $\epsilon_{\text{Nd}}$  composition (-5.5) to the western Turkish rhyolite, although the  $^{87}\text{Sr}/^{86}\text{Sr}$  ratio is somewhat higher (0.7137) (Arnaud et al., 1992). The north-west Tibetan rhyolite is considered to be an AFC product of associated basaltic rocks, which have similar trace element patterns (Arnaud et al., 1992). The origin of these associated basaltic rocks, together with the more mafic rocks of the USEKA area, is discussed in the following section.

### 5.3.3.2 Lithospheric mantle sources

In order to place constraints on the mantle source of the Miocene western Turkish volcanism, this section compares the elemental and isotopic composition of mafic lavas (> 3 wt % MgO) from the USEKA area with volcanics from similar tectonic settings around the world. In common with average USEKA shoshonite and latite, potassic lavas from Vulsini (Roman province, Italy - Rogers et al., 1985), Karisimbi (Virunga province, Rwanda - Rogers et al., 1992), the Rio Grande rift flank (south-west USA - Gibson et al., 1993) and north-west Tibet (Arnaud et al., 1992), exhibit enrichment in the LILE and light

**FIGURE 5.14 - Comparison of the elemental compositions in the USEKA acid magmatism with other databases**

**Figure 5.14a - Erigöz Granite**

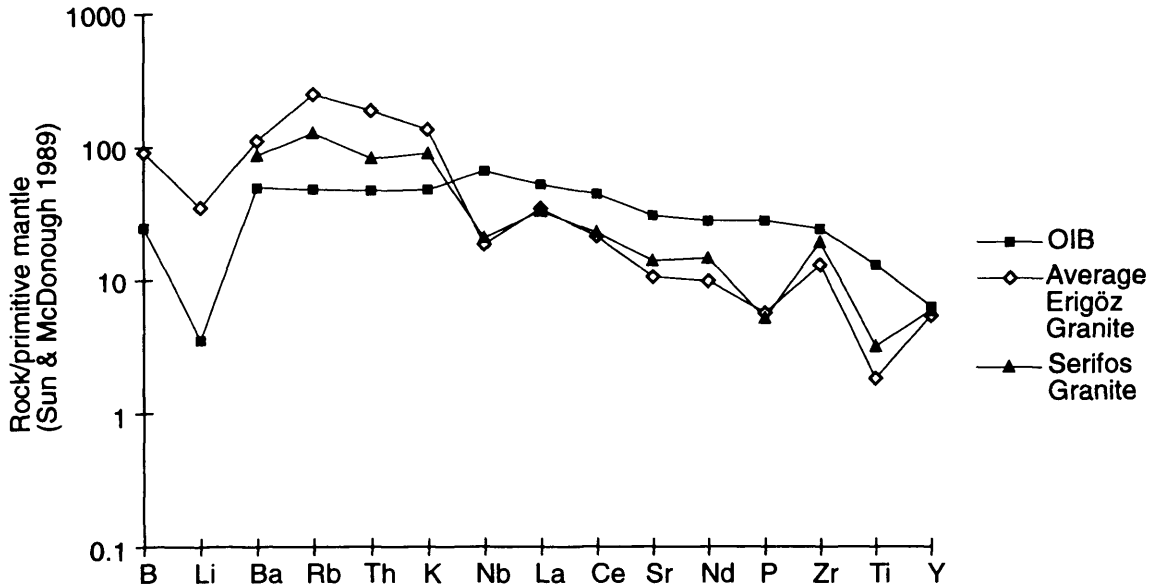
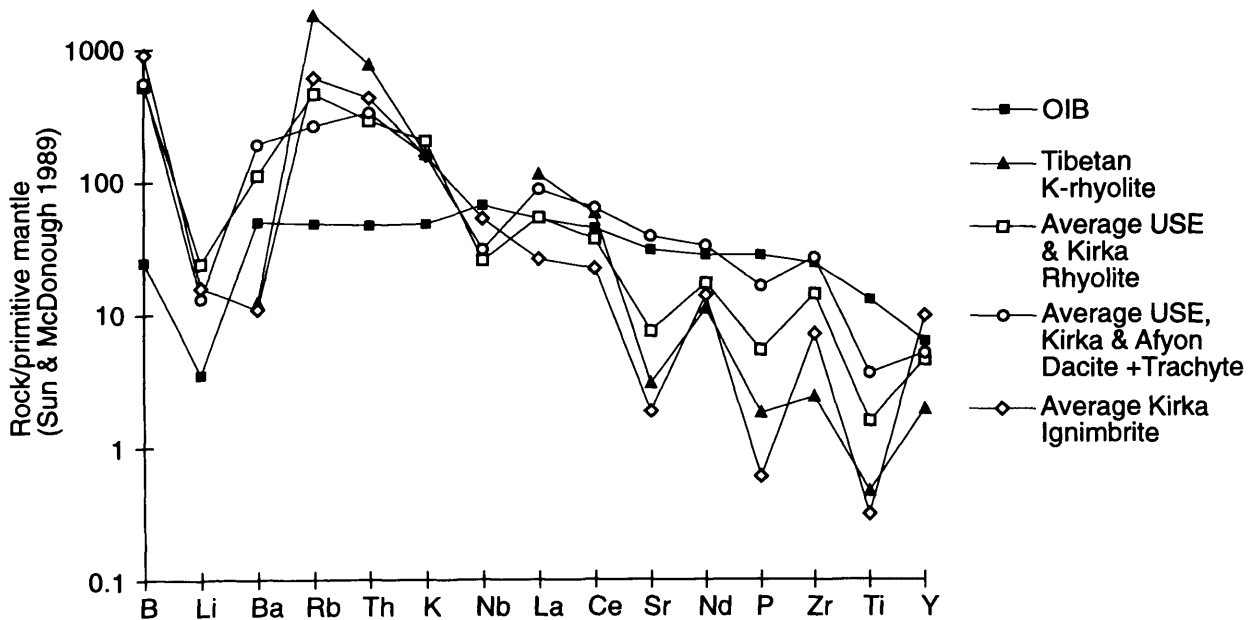


**Figure 5.14b - Acid volcanism of the USEKA area**



**Data sources**

OIB from Sun & McDonough 1989  
Tibetan K-rhyolite from Arnaud et al., 1992  
Serifos granite - from Stouraiti 1995

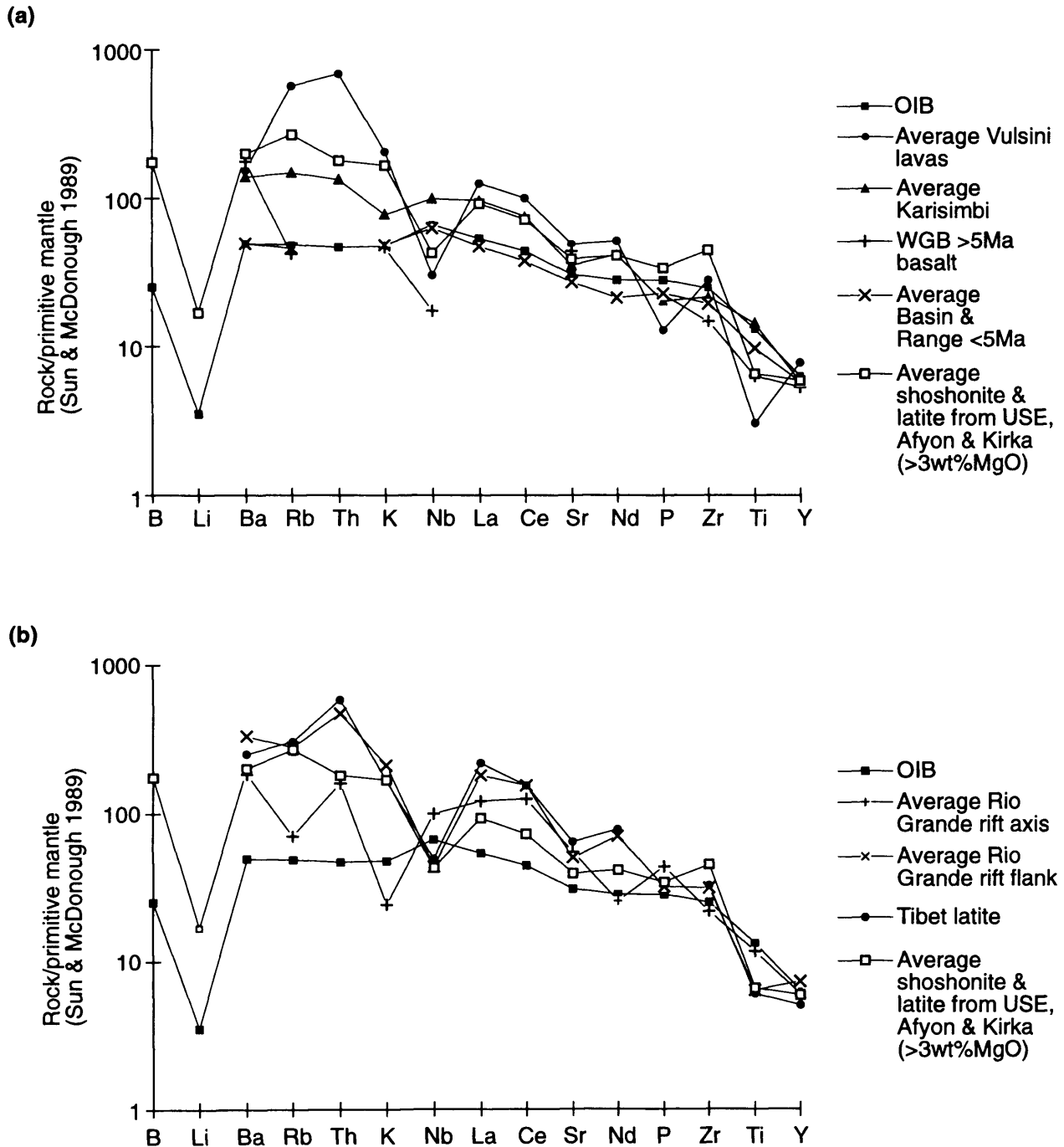
REE relative to OIB (Figure 5.15 a, b). These high concentrations of the LILE and light REE have been attributed to an enriched source region in the subcontinental mantle (Rogers et al., 1985, Rogers et al., 1992, Rogers 1992, Arnaud et al., 1992, Gibson et al., 1993, Turner et al., 1996). Although not enriched in K, lavas from the Western Great Basin (WGB) (> 5 Ma) in south-west USA are enriched in the light REE relative to OIB (Figure 5.15a), and are also considered to originate from an enriched subcontinental mantle source (Kempton et al., 1991). However, lavas from the Basin and Range (< 5 Ma) and the Rio Grande rift axis in south-west USA are similar to OIB in composition (Figure 5.15 a, b) and are therefore thought to have an asthenospheric mantle source (Kempton et al., 1991, Gibson et al., 1993).

Figure 5.16 shows the variation of Ti/Y with Nb/Y and Figure 5.17 Th/Y with Nb/Y for the mafic samples from the USEKA area, together with lavas from the selected volcanic provinces discussed above. It is apparent from Figures 5.16 and 5.17 that there are two end member potassic provinces, represented by the Vulsini and Karisimbi lavas, which can be related to two contrasting mantle enrichment processes (Rogers 1992). The Vulsini province are characterised by lower Nb/Y and Ti/Y but higher Th/Nb than the Karisimbi lavas (Figures 5.16 & 5.17). Low Nb/Y and Ti/Y ratios such as those measured in the Vulsini lavas (Figure 5.16) have typically been attributed to subduction-related processes (Rogers 1992), while high Th/Nb ratios (Figure 5.17) indicate crustal involvement in magma genesis (Kempton et al., 1991). Rogers et al. (1985) consider that, in the case of the Vulsini lavas, this crustal involvement occurs in the form of subducted crustal sediments from which fluids or melts are released. Lavas from the WGB, the Rio Grande rift flank and north-west Tibet plot in a similar position to the Vulsini lavas in Figure 5.16 and they are considered to have inherited their chemical characteristics from a lithospheric mantle source possibly enriched by previous subduction events (Fitton et al., 1991, Kempton et al., 1991, Arnaud et al., 1992, Gibson et al., 1993). The reason for the low Nb and Ti content of subduction-related melts is that the HFSE are insoluble in hydrous fluids and relatively insoluble in hydrous melts and they therefore remain in the subducted slab and the adjacent parts of the mantle (Saunders et al., 1991).

The Karisimbi lavas (Rogers et al., 1992) have high Ti/Y and Nb/Y (Figure 5.16) which suggests that their source was enriched in the HFSE in contrast to the subduction modified source of the Vulsini lavas. In Figure 5.17, the Karisimbi lavas plot in the OIB field with a restricted range of Th/Nb ratios. Since crustal rocks typically have higher Th/Nb ratios (Kempton et al., 1991), there appears to be no crustal involvement in the genesis of the Karisimbi lavas. Rogers (1992) suggests that these lavas are the result of melting of subcontinental lithosphere, previously enriched by migrating small degree melts of depleted upper mantle. Such small degree melts often have high levels of Ti (Navon et al., 1988, McKenzie 1989) which could account for the high Ti/Y ratios of the Karisimbi lavas (Figure 5.16). These melts are extremely rich in K with direct evidence provided by fluid inclusions in diamonds (Navon et al., 1988).

It is generally accepted that the potassic lavas of western Turkey are derived from an enriched lithospheric mantle source, although the nature of the mantle enrichment process remains a matter of debate. Keller (1983) suggested that the source for the K-rich lavas at Afyon was enriched via

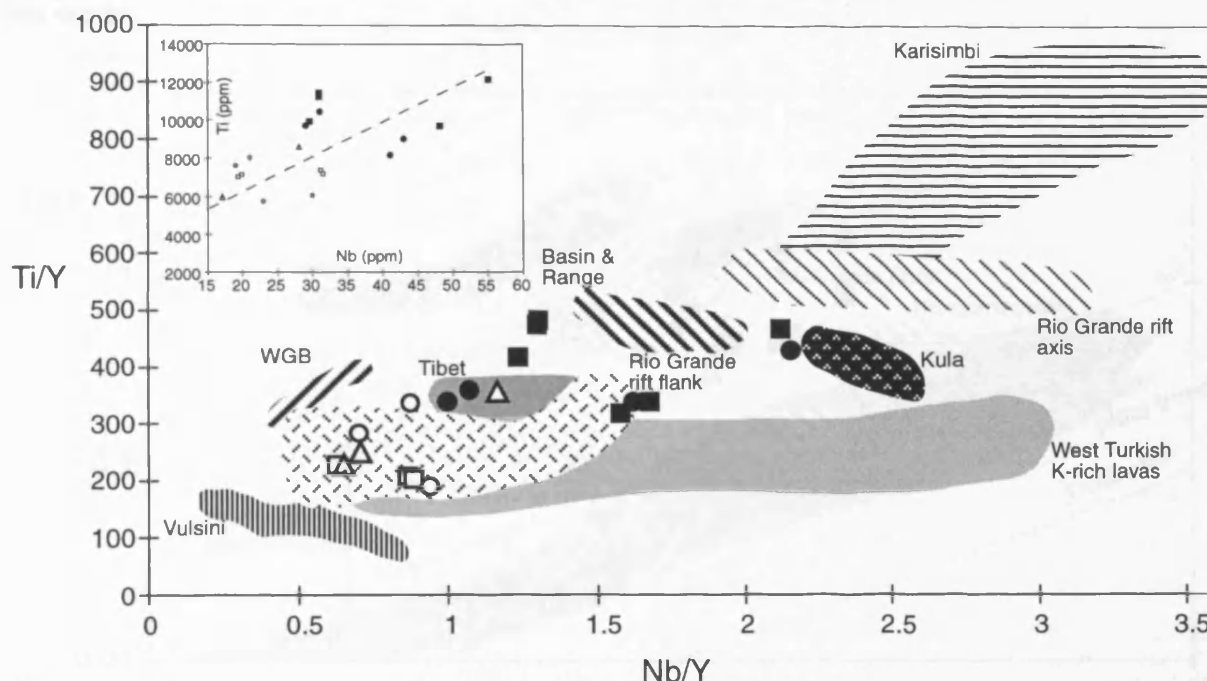
**FIGURE 5.15 - Comparison of the elemental compositions in the USEKA mafic volcanics with other data**



**Data sources**

Vulsini K-rich lavas (45-58wt% SiO<sub>2</sub>) (Rogers et al., 1985)  
 Karisimbi basanite (44-47wt% SiO<sub>2</sub>) (Rogers et al., 1992)  
 Western Great Basin (WGB) >5Ma basalt (47-52wt% SiO<sub>2</sub>) (Ormerod 1988)  
 Basin & Range <5Ma basalt (45-48wt% SiO<sub>2</sub>) (Kempton et al., 1991)  
 Rio Grande rift flank (Gibson et al., 1993)  
 Rio Grande rift axis (Gibson et al., 1993)  
 Tibet latite (Arnaud et al., 1992)

FIGURE 5.16 - Ti/Y vs Nb/Y diagram for USEKA mafic lavas, other K-rich lavas from western Turkey and selected volcanic provinces from around the world

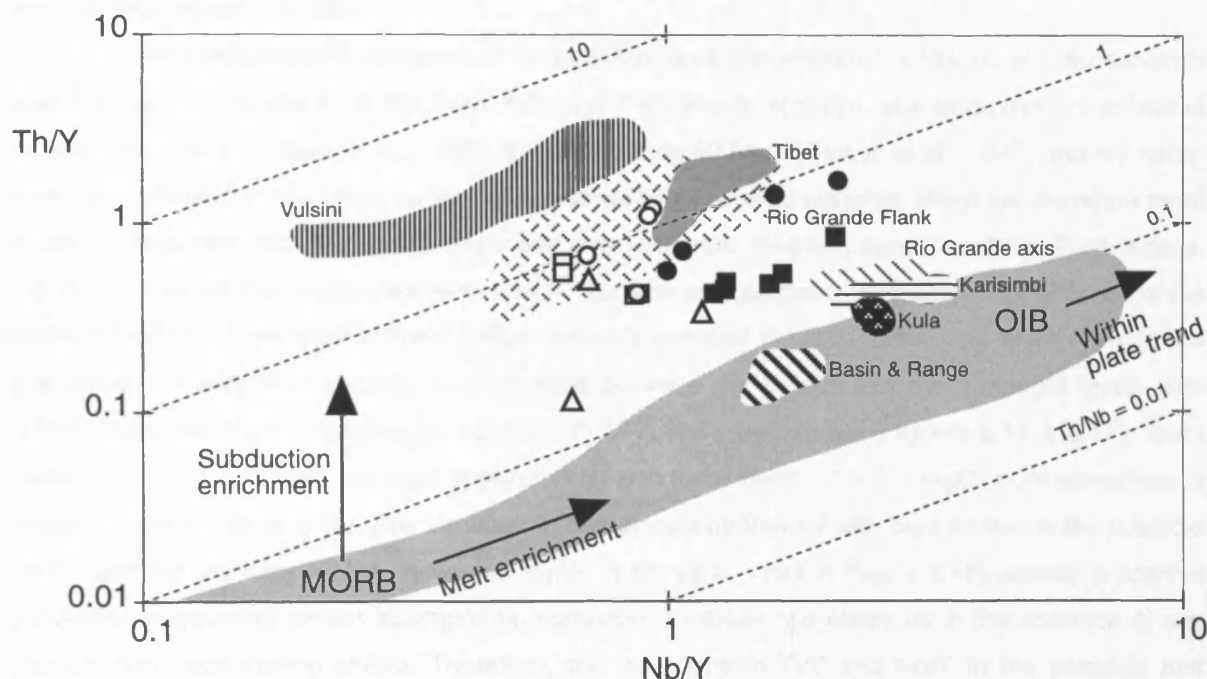


LEGEND

- : Ultrapotassic ( $K_2O/Na_2O > 2$ ) USE lavas - 5-9 wt % MgO, 52-57 wt %  $SiO_2$
- : Potassic ( $> 3\%$  MgO,  $K_2O/Na_2O > 1 < 2$ ) USE lavas - 4-7 wt % MgO, 52-57 wt %  $SiO_2$
- : Ultrapotassic Afyon lavas - 3-6 wt % MgO, 54-56 wt %  $SiO_2$
- : Potassic Afyon lavas - 3-4 wt % MgO, 53-57 wt %  $SiO_2$
- △: Potassic Kirka lavas - 5-7 wt % MgO, 51-56 wt %  $SiO_2$
- : Tertiary west Turkish ultrapotassic & potassic lavas (Güleç 1991) - 4-8 wt % MgO, 49-60 wt %  $SiO_2$
- : Kula sodic lavas ( $K_2O/Na_2O < 1$ ) (Ercan et al. 1985) - 4-6 wt % MgO, 46-47 wt %  $SiO_2$
- : Vulsini ultrapotassic & potassic lavas (Rogers et al., 1985) - 4-13 wt % MgO, 45-56 wt %  $SiO_2$
- : Karisimbi potassic lavas (Rogers et al., 1992) - 9-10 wt % MgO, 44-47 wt %  $SiO_2$
- : Western Great Basin (WGB) sodic lavas (Fitton et al., 1991) - 5-7 wt % MgO, 52 wt %  $SiO_2$
- : Basin & Range - Post 5 Ma sodic lavas (Kempton et al., 1991) - 8-10 wt % MgO, 45-48 wt %  $SiO_2$
- : Rio Grande rift flank ultrapotassic lavas (Gibson et al., 1993) - 4-9 wt % MgO, 50-56 wt %  $SiO_2$
- : Rio Grande rift axis sodic lavas (Gibson et al., 1993) - 13-14 wt % MgO, 40-43 wt %  $SiO_2$
- : Tibet potassic lavas (Arnaud et al., 1992) - 4-6 wt % MgO, 50-57 wt %  $SiO_2$



**FIGURE 5.17 - Th/Y vs Nb/Y diagram for USEKA mafic lavas, other K-rich lavas from western Turkey and selected volcanic provinces from around the world**



**LEGEND**

- : Ultrapotassic ( $K_2O/Na_2O > 2$ ) USE lavas - 5-9 wt % MgO, 52-57 wt %  $SiO_2$
- : Potassic ( $> 3\%$  MgO,  $K_2O/Na_2O > 1 < 2$ ) USE lavas - 4-7 wt % MgO, 52-57 wt %  $SiO_2$
- : Ultrapotassic Afyon lavas- 3-6 wt % MgO, 54-56 wt %  $SiO_2$
- : Potassic Afyon lavas- 3-4 wt % MgO, 53-57 wt %  $SiO_2$
- △: Potassic Kirka lavas - 5-7 wt % MgO, 51-56 wt %  $SiO_2$
- ▨: Vulsini ultrapotassic & potassic lavas (Rogers et al., 1985) - 4-13 wt % MgO, 45-56 wt %  $SiO_2$
- ▤: Karisimbi potassic lavas (Rogers et al., 1992) - 9-10 wt % MgO, 44-47 wt %  $SiO_2$
- ▥: Basin & Range - Post 5 Ma sodic lavas (Kempton et al., 1991) - 8-10 wt % MgO, 45-48 wt %  $SiO_2$
- ▧: Rio Grande rift flank ultrapotassic lavas (Gibson et al., 1993) - 4-9 wt % MgO, 50-56 wt %  $SiO_2$
- ▩: Rio Grande rift axis sodic lavas (Gibson et al., 1993) - 13-14 wt % MgO, 40-43 wt %  $SiO_2$
- : Tibet potassic lavas (Arnaud et al., 1992) - 4-6 wt % MgO, 50-57 wt %  $SiO_2$
- ▬: Kula sodic lavas ( $K_2O/Na_2O < 1$ ) (Ercan et al. 1985) - 4-6 wt % MgO, 46-47 wt %  $SiO_2$

(Diagrams based on that by Kempton et al., 1991)

subduction related processes, whereas, for the K-rich lavas of Bodrum, Robert et al. (1992) invoked enrichment of the source by small degree melts derived from the convecting upper mantle. On the basis of Nd and Sr isotopic ratios, Robert et al. (1992) suggest that the enrichment event or events were ancient (about 1.25 Ga).

The USEKA potassic and ultrapotassic lavas plot on a vector between the Vulsini and the Karisimbi end members in Figures 5.16 and 5.17. Although the majority of these data fields are comprised of basalts, the Vulsini (Rogers et al., 1992), the Rio Grande rift flank (Gibson et al., 1993) and the north-west Tibet (Arnaud et al., 1992) suites contain some more evolved magmas which are therefore more closely comparable with the ultrapotassic and potassic mafic magmas from this study. Furthermore, Figure 5.3 showed that comparison with less evolved lavas is probably valid since extrapolation of the ratios in the USEKA samples to lower SiO<sub>2</sub> levels only changed the ratio values by a small amount and this would not alter their general position lying between the Vulsini and the Karisimbi lavas. The USEKA samples show considerable variation in Ti/Y, Nb/Y and Th/Nb (Figures 5.16 & 5.17). Such variations in Ti/Y and Nb/Y are also apparent in K-rich lavas (with > 3 wt % MgO) from elsewhere in western Turkey (Figure 5.16). The variation in Ti/Y should be treated with caution due to the possible fractionation of titanomagnetite. However, a plot of Nb vs Ti (inset in Figure 5.16) reveals a positive correlation suggesting similar incompatible behaviour by these two elements in the absence of any titanium-rich fractionating phase. Therefore, the variations in Ti/Y and Nb/Y in the potassic and ultrapotassic USEKA magmas appear to reflect variations in their source composition.

These data indicate that the potassic and ultrapotassic USEKA lavas may have been derived from a heterogeneous subcontinental lithospheric mantle source enriched by subduction processes, which result in high K but low HFSE levels ('Vulsini-like source') and by small degree melts of depleted upper mantle, which resulted in high K and high HFSE levels ('Karisimbi-like source'). Figure 5.17 clearly illustrates these two enrichment processes, which each produce a different vector. Subduction enrichment increases Th/Y relative to Nb/Y (Kempton et al., 1991), whilst enrichment by small degree melts leads to a similar increase of both Th/Y and Nb/Y (Figure 5.17). Enrichment from previous subduction events is plausible since there is a long history of subduction episodes in the Eastern Mediterranean region, and from at least the Late Cretaceous to the Middle Eocene, western Turkey and the Aegean were affected by subduction related volcanism (Paton 1992). For instance, extensive Upper Cretaceous calc-alkaline volcanism in the Pontides is thought to have been related to northward subduction of Neo-Tethyan crust (Sengör & Yilmaz 1981). Earlier subduction in the region was related to the closure of Palaeotethys (Mid Triassic-Early Jurassic) (Sengör & Yilmaz 1981). Both Seyitoglu and Scott (1992) and Güleç (1991) suggest the low HFSE levels in Miocene volcanics in western Turkey originate from lithospheric mantle modified by previous subduction events.

The enrichment probably occurs within a 'freezing layer' within the mechanical boundary layer (MBL) (McKenzie 1989). The MBL comprises both lithosphere and crust and is separated from the convecting upper mantle (asthenosphere) by the thermal boundary layer (TBL) (McKenzie 1989). The significance of the separation from the asthenosphere is that enrichments within the MBL are preserved and large isotopic anomalies can build up through time as radiogenic isotopes decay

(McKenzie 1989). Both enrichment processes produce low Sm/Nd and high Rb/Sr ratios and therefore when the MBL is affected by such enrichments, it eventually develops an isotopic composition with low  $^{143}\text{Nd}/^{144}\text{Nd}$  and high  $^{87}\text{Sr}/^{86}\text{Sr}$  through the decay of  $^{87}\text{Rb}$  to  $^{87}\text{Sr}$  and  $^{147}\text{Sm}$  to  $^{143}\text{Nd}$  (McKenzie 1989, Rogers 1992). The isotopic compositions of the Vulsini (Rogers et al., 1985), Karisimbi (Rogers et al., 1992), Rio Grande rift flank (Gibson et al., 1993) and north-west Tibet (Arnaud et al., 1992) K-rich lavas all plot within the enriched quadrant of the  $\epsilon_{\text{Nd}}$  vs  $^{87}\text{Sr}/^{86}\text{Sr}$  diagram (Figure 5.17). The enriched isotopic characteristics of the K-rich Vulsini lavas are thought to result from the subduction of sediment (Rogers et al., 1985), while the Karisimbi signature is explained by the enrichment of a lithospheric source by small degree melts at approximately 1 Ga (Rogers et al., 1992, Rogers 1992). The Nd and Sr isotopic characteristics of the Rio Grande rift flank and the north-west Tibet lavas (Figure 5.17) are also thought to result from previous enrichment events and subsequent isotopic decay within the subcontinental lithospheric mantle (Arnaud et al., 1992, Gibson et al., 1993). Within western Turkey, the Bodrum lavas also have an enriched isotopic signature (Figure 5.16), which according to Robert et al. (1992) can be explained by the isolation of small degree melts from depleted mantle in the lithosphere for about 1.25 Ga.

The position of the USEKA mafic lavas (latite and shoshonite) within the enriched quadrant of Figures 5.10 and 5.13 and their high LILE and light REE concentrations (and MgO content of 3-9 wt %) is therefore consistent with a lithospheric mantle source. Such a source would have been isolated from the convecting upper mantle thereby allowing the radiogenic isotopes to decay through time to their current enriched ratios. It has already been suggested that the acid volcanics and granite formed at least in part from melted upper continental crust, due to their more enriched isotopic signatures. However, as mentioned above, their position in the  $\epsilon_{\text{Nd}}$  vs  $^{87}\text{Sr}/^{86}\text{Sr}$  diagram to the left of known upper continental crustal compositions in the region suggests an additional input from a more depleted source. Figure 5.9 showed that the acid volcanics are enriched in Rb, Th and K relative to average upper continental crust. It is possible that these elevated LILE concentrations originate from the subcontinental lithosphere and that the USE and Kirka acid magmas may have been generated by a mixture of lithospheric and upper continental crustal melts. By the Middle Miocene, the amount of assimilated upper continental crust has decreased and the lithospheric component increased. As described above, this is reflected by the more mafic nature of the Middle Miocene volcanism compared to the silicic Early Miocene magmas.

Within the USEKA mafic lava group, the Afyon suite is the least isotopically enriched despite the fact that it does not contain the most primitive lavas in the study. Lavas from the USE and Kirka areas have lower  $\text{SiO}_2$ , higher MgO, but higher  $^{87}\text{Sr}/^{86}\text{Sr}$  than the Afyon volcanics. It therefore appears that the lithospheric source for the Afyon lavas has a different isotopic composition to that of the USE and Kirka mafic rocks. It seems that an isotopically heterogeneous subcontinental lithospheric mantle beneath western Turkey melted to generate K-rich lavas.

The most recent phase of volcanism in western Turkey is represented by the Kula lavas which, as shown in Figures 5.16 and 5.17 contain similar trace element ratios to the Karisimbi, post 5 Ma Basin

and Range (from south-west USA - Kempton et al., 1991) and the Rio Grande rift axis lavas. However, the Karisimbi volcanics are potassic ( $K_2O/Na_2O > 1$ ) and have high initial Sr and low initial Nd ratios (Figure 5.17), whereas the Basin and Range and Rio Grande rift axis volcanics are sodic ( $K_2O/Na_2O < 1$ ) and have Sr and Nd initial ratios which fall within the mantle array (Rio Grande rift in Figure 5.17, Basin & Range - Kempton et al., 1991). Fitton et al. (1991) and Gibson et al. (1993) suggest an asthenospheric source for the post 5 Ma Basin and Range and Rio Grande rift axis lavas respectively, since they are chemically and isotopically indistinguishable from OIB. By contrast, the Nd and Sr initial ratios of the Karisimbi lavas are considered to be the result of isotopic decay within lithosphere isolated from the convecting upper mantle over 1 Ga (Rogers 1992).

The Kula lavas are similar to the post 5 Ma Basin and Range and the Rio Grande rift axis lavas, being sodic and having Sr and Nd initial ratios which lie within the mantle array (Güleç 1991, Figure 5.17). It has therefore been suggested that the Kula lavas have an asthenospheric component (Güleç 1991, Seyitoglu & Scott 1992b). However, Paton (1992), Richardson-Bunbury (1992) and McKenzie and O'Nions (1995) suggested that the Kula lavas were generated from continental lithosphere that had been previously enriched, since they contain higher abundances of the LILE than OIB (Figure 5.7) and such levels cannot be produced by a single stage melting event of depleted or primitive mantle. The Nd and Sr isotope characteristics of the Kula lavas cannot distinguish whether the source was asthenospheric or lithospheric, but if the source was enriched lithosphere, the enrichment process must have been recent. Furthermore, if the source was enriched lithosphere, it must have contained extremely high Na levels relative to the lithospheric mantle source of the earlier Middle Miocene K-rich magmas. The geochemical characteristics of the Kula lavas can be explained if the initial melts were derived from an asthenospheric mantle source and that these melts were subsequently contaminated by enriched lithospheric mantle during their ascent. Such lithospheric contamination of asthenosphere derived melts could easily account for the elevated levels, relative to OIB, of incompatible elements seen in the Kula lavas. A similar model of contamination of asthenospheric melts by small degree ultrapotassic melts derived from the lithospheric mantle, has been used by Thompson et al. (1989) to account for the geochemical composition of minettes from north-west Colorado in the USA.

### 5.3.3.3 Implications for the source of B

On the basis of the discussion above, the potential sources for B in the Miocene USEKA magmas include upper continental crust and enriched subcontinental lithospheric mantle. It was established in the previous chapters that the Early Miocene acid volcanism represents the most likely source for B in the borate deposits and therefore this project is particularly concerned with the genesis of this phase of magmatism. As discussed above, the more evolved and isotopically enriched nature of the Early Miocene acid magmatism compared to later Middle Miocene mafic volcanism have been taken as evidence for a greater component of upper continental crust in the former. Figure 5.12 shows that B and B/Nb have a positive correlation with  $^{87}Sr/^{86}Sr$ , but a negative one with  $\epsilon_{Nd}$ . Hence, if the more

enriched volcanics do indeed contain a greater proportion of assimilated upper crust, the highest B lavas are those with the greatest upper crustal component. This suggests that upper continental crust may be the most important source for B in the acid magmatism. However, the granite has low B levels and yet appears to have been generated largely by the anatexis of upper crust. It seems that B was concentrated into the volcanic phases of the acid magmatism and not in the plutons.

Figure 5.9 shows that all the lavas of the USEKA area are enriched in B relative to average upper continental crust (Taylor & McLennan 1985). However, the upper crust of western Turkey may well contain a higher B concentration than the average values for upper crust (eg. 15 ppm B - Taylor & McLennan 1985, 16.8 ppm B - Leeman & Sisson 1996). There is evidence of B-rich crust in the southern sector of the Menderes Massif in western Turkey; tourmaline augen gneisses (derived from an S type granitic protolith), tourmaline-rich dykes and tourmaline porphyroblasts in semi-pelites (Bozkurt et al., 1995). They suggest that the granite protolith of the gneiss resulted from the melting of amphibolite-facies metagreywackes, which may have had a marine sediment component. Modern marine sediments have a B content of between 40 and 180 ppm (Leeman & Sisson 1996) and they therefore represent a potential source of B. Furthermore, tourmaline-bearing amphibolite facies pelite is found further north in the Menderes Massif near to the town of Kula (Verge pers. comm - 1995). A sample of this pelite (888/2), which is considered to have a mudstone or claystone protolith (Verge pers. comm - 1997), was found to contain 527 ppm B. As described earlier, the isotopic signature of this pelite indicates that it may have been a source for the Early Miocene silicic magmas. Hence, the melting of such B-rich upper crust in western Turkey is likely to have provided a source for B in the Early Miocene acid volcanism which had a close spatial and temporal position with the borate-host sediments. It should also be noted that, due to the incompatible nature of B in basaltic magmas, it is likely to be concentrated in the most differentiated magmas (Ryan et al., 1993, Arnórsson & Andrésdóttir 1995). This is generally the case for the USEKA magmatism, where the more acid volcanics normally contain greater concentrations of B than the less evolved lavas (Chapter 4). It is also likely that the melting of upper continental crust in the genesis of acid volcanics in this area may have provided a source for Li and As, which have average upper crustal values of 20 and 1.5 ppm respectively (Taylor & McLennan 1985).

As discussed above, the more mafic lavas from this area largely originate from the melting of subcontinental lithospheric mantle, and the acid volcanics may also contain a component of such lithosphere. Therefore, the subcontinental lithosphere is a potential source for B in the mafic magmas and, and perhaps partly for B in the silicic magmas. Since the lithosphere in this region appears to have been enriched by both previous subduction events and the upwards migration of small degree melts of depleted upper mantle, both of these mechanisms need to be examined. Figures 5.4 to 5.6 showed that the volcanics from this region contain similar enrichments relative to primitive mantle of B to LILE. It would therefore appear that B has behaved in a similar fashion to the LILE, which might be explained by enrichment events from prior subduction. It is well established that the LILE and the light REE are efficiently transferred from a subducted slab to the overlying mantle wedge, as a result of their mobility in hydrous fluids (Saunders et al., 1991) and is also now known that B is progressively

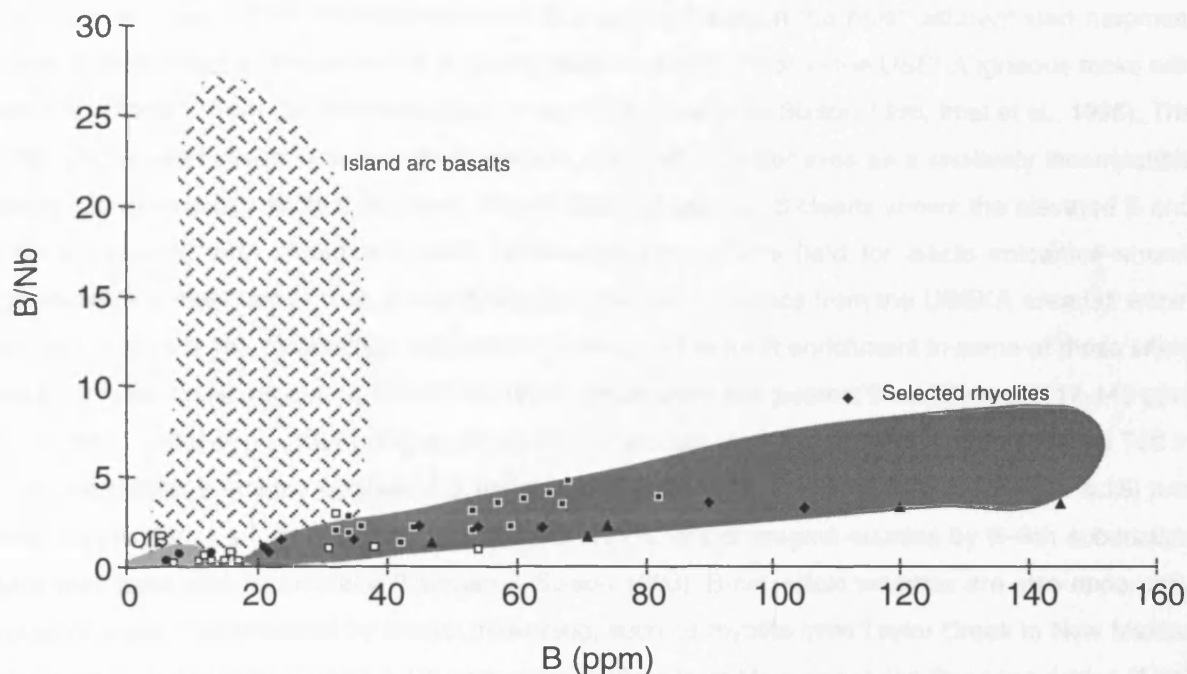
mobilised and removed from a subducted slab via solution in aqueous fluids released during prograde dehydration reactions (Morris et al., 1990, Moran et al., 1992, Leeman & Sisson 1996, Ryan et al., 1996, Noll et al., 1996, Ryan & Langmuir 1993). However, Ryan and Langmuir (1993) suggest that B may differ from the alkalis and other enriched lithophile trace elements at arcs in that it is mobilised more readily in the earlier stages of the subduction process. In addition to B, aqueous fluids released from subducted slabs are also thought to contain As (Leeman & Sisson 1996, Noll et al., 1996). As a result, arc lavas are enriched in B (Figure 5.18) and As, more so than expected assuming normal magmatic processes (Noll et al., 1996). Hence, it seems likely that previous subduction events led to enrichment of B and As in the MBL of the lithospheric mantle beneath western Turkey, in the same way that K was enriched.

Much of the B and As was probably added to oceanic crust prior to subduction (Noll et al., 1996). The early enrichment of As is most likely related to hydrothermal convection cells established in new oceanic crust at mid-ocean ridges which produce sulphide mineralisation throughout the ocean crust and deposit metalliferous sediments onto the oceanic crust (black smokers) (Puecker-Ehrenbrink et al., 1994). It is also well established that altered oceanic crust is enriched in B (Leeman & Sisson 1996, You et al., 1993, Seyfried et al., 1984, Bebout et al., 1993). Such B enrichment is associated with smectite which is produced during the alteration of basalt by sea water at relatively low temperatures (eg. 150°C - Seyfried et al., 1984). Another B-rich reservoir in the oceanic crust is pelagic sediment which contains terrigenous detritus (illite dominated, 30 - 150 ppm B), biogenic carbonate (< 20 ppm B), siliceous oozes (> 40 ppm B) and marine smectites (> 100 ppm B) (Leeman & Sisson 1996). Sea water represents an additional source with on average 4.5 ppm B (Bebout et al., 1993).

In contrast to B and As, Li has concentrations in arc basalts similar to those in MORB (Ryan & Langmuir 1987). Furthermore, Li is not enriched to the extent of incompatible elements such as K in arc magmas, and therefore arc volcanics have elevated K/Li ratios (Ryan & Langmuir 1987). This is despite the fact that Li behaves very similarly to K during sea floor alteration and sedimentation, where it is concentrated in ocean sediments and altered oceanic crust (Holland 1980, Donnelly et al., 1980). The USEKA mafic lavas are clearly more evolved than basalts and hence the enrichments in Li relative to average OIB and N-MORB (Figure 5.9) may result from differentiation, although an input from crustal assimilation is also possible. However, the USEKA mafic lavas show an enrichment of the LILE and B relative to Li (Figures 5.5 & 5.6) perhaps reflecting a lithospheric source region influenced by prior subduction events. Hence, although the melting of such a source may have supplied some Li to magmas, subduction enrichment events would have been relatively more important in providing B and As.

Since B and As are incompatible and Li is moderately incompatible in basaltic magmas (Ryan & Langmuir 1987, Noll et al., 1996), small degree melts of depleted upper mantle are likely to be enriched in these elements. Therefore, the enrichment of the lithospheric mantle by melts from the asthenosphere, is also likely to enrich the MBL in B and As and to a lesser extent Li. Hence, both the enrichment processes discussed above are capable of generating elevated levels of B in the lithospheric mantle. When adiabatic decompression melting occurred in the lithospheric mantle

FIGURE 5.18 - B/Nb vs B



LEGEND

- USE & Kirka rhyolite
- ♦ USE, Afyon & Kirka trachyte/dacite
- USE, Afyon, Kirka latite & shoshonite
- ▲ Kirka Ignimbrite
- Erigöz Granite & Aplite
- Ocean island basalt (OIB) - Hawaii (1 - 9 ppm B, 0.05 - 0.7 B/Nb), Society islands (1 - 2 ppm B, 0.02 - 0.07 B/Nb) Gough islands (3 - 12 ppm B, 0.05 - 0.1 B/Nb) (Ryan et al., 1996)
- ▨ Island arc basalts & andesites - Mt St Helens (4 - 6 ppm B, 0.1 - 0.4 B/Nb), Marianas (13 ppm B, 26 B/Nb), Sandwich islands (19.5 ppm B, 10 B/Nb), Salvador (20 ppm B, 8 B/Nb), Costa Rica (11 - 13 ppm B, 5 - 7 B/Nb), Japan (9 - 30 ppm B, 0.3 - 19 B/Nb) (Leeman & Sisson 1996, Inai et al., 1996)
- Selected acid volcanics - Inyo dome obsidian and Bishop tuff tephra & ignimbrite (California), Taylor Creek rhyolite lava (New Mexico), JR-1 & JR-2 rhyolite (Japan) (Leeman & Sisson 1996, Inai et al., 1996)

beneath western Turkey at the onset of extension, the melts produced would therefore have been enriched in B in addition to other incompatible elements such as K.

In summary, the B in the USEKA acid volcanism probably largely originated from upper continental crust possibly with a minor contribution from the subcontinental lithospheric mantle. The acid nature of the volcanism has further implications since B is concentrated in the most differentiated magmas. Figure 5.18 provides a comparison of B abundances and B/Nb ratios in the USEKA igneous rocks with selected volcanics from the literature (Ryan et al., 1996, Leeman & Sisson 1996, Imai et al., 1996). The B/Nb ratio is used as an indicator of enrichment since Nb also behaves as a relatively incompatible element in most silicic melts (Leeman & Sisson 1996). Figure 5.18 clearly shows the elevated B and B/Nb associated with island arcs and subduction zones. The field for silicic volcanics shows considerable enrichment in both B and B/Nb, and the acid volcanics from the USEKA area fall within this field (Figure 5.18). Subduction appears to be responsible for B enrichment in some of these silicic rocks, such as the island arc rhyolites from Japan which show the greatest B enrichment (117-145 ppm B, 7.7 B/Nb) (Imai et al., 1996) (Figure 4.18). Acid volcanics from the Inyo Domes and Bishop Tuff in California exhibit a smaller degree of B enrichment (28-53 ppm B, 0.9 - 2.4 B/Nb) (Figure 4.18) and since they occur at a former convergent margin, enrichment of magma sources by B-rich subduction fluids may have also taken place (Leeman & Sisson 1996). B-rich silicic magmas are also apparently typical of areas characterised by crustal thickening, such as rhyolite from Taylor Creek in New Mexico (19.5 ppm B, 0.43 B/Nb) (Figure 4.18) and volcanic glass from Macusani in the Peruvian Andes (1930 ppm B, 46.7 B/Nb) (Leeman & Sisson 1996).

This information therefore broadly suggests that areas of thickened crust and regions which have experienced or are experiencing episodes of subduction are likely to produce B-rich magmas. As described above, western Turkey in the Miocene had both a thickened crust and had experienced prior subduction events. Where continental crust is involved in the genesis of silicic magmas, the B content of the protolith clearly controls the B concentration of the magmatism generated. For instance, some rhyolites from the Colorado Plateau in south-west USA have relatively low B/Nb ratios ( $< 0.2$ ) which is thought to reflect a derivation from previously depleted crustal sources (eg. granulites) (Leeman & Sisson 1996). Furthermore, low B Miocene rhyolites of the Snake River Plain (Idaho) are found to the east, while coeval high B rhyolites (eastern Oregon) are found to the west of the Western Idaho Suture Zone; the former had a B-depleted granulite protolith and the latter had a B-rich amphibolite oceanic crust protolith (Leeman & Sisson 1996). Studies have shown that B concentrations decrease with increasing metamorphic grade, since B is systematically remobilised at higher temperatures (Bebout et al., 1993, Leeman & Sisson 1996). Therefore, the B concentrations of representative metapelite suites world-wide show a decrease from greenschist through amphibolite to granulite facies rocks (Leeman & Sisson 1996). On the basis of the small amount of mineralogical and geochemical information available on the West Turkish crust, the amphibolite facies Menderes Massif rocks (Bozkurt et al., 1995, Verge pers comm - 1994) have retained a considerable amount of B and therefore represent a protolith which would be likely to generate B-rich magmas.

As described in the previous chapters, the other major borate provinces in the world can be found



in the central Andes of South America and in south-west USA. Borate deposition has occurred on the Altiplano-Puna plateau in the central Andes for the past 7 to 8 Ma (Alonso et al., 1991) and acid volcanism has been active in the region for much of this time (de Silva 1989). The acid volcanism has generated an abundance of ignimbrites since the Late Miocene, which as described above, are considered to result from crustal melting (de Silva 1989, Hawkesworth et al., 1982). Borate deposition has occurred in SW USA from the Miocene to the present (Kistler & Helvacı 1994) and volcanism has been active in the region through much of this time (Kempton et al., 1991, Fitton et al., 1991). As in western Turkey and the Central Andes, this volcanism followed a time of crustal thickening (Coney & Harms 1984). The elemental and isotopic geochemistry of magmatism ( $< 17$  Ma) in this region indicates that subduction enriched lithospheric mantle was involved in the generation of all extension related basic magmas until recently (Fitton et al., 1991, Kempton et al., 1991). Hence, magmatism in the three main borate provinces of western Turkey, the Central Andes and south-west USA was generated after periods of convergence (with subduction) and crustal thickening. On this basis, suitable regions in which to carry out exploration for large lacustrine borate deposits are former or current continental margins which have experienced episodes of subduction and crustal thickening.

### *5.3.3.4. The generation of Miocene magmatism in western Turkey within a tectonic framework*

Views as to what initiated the Early Miocene volcanism in western Turkey depend largely on whether there was a compressional or extensional regime at the time. Seyitoglu and Scott (1992b) believe that the Early Miocene acid - intermediate volcanism was related to the onset of N-S extension in western Turkey. They made comparisons with the Basin and Range in south-west USA where crustal extension began synchronously with calc-alkaline intermediate-silicic volcanism (Wernicke et al., 1987, Gans et al., 1989). Yilmaz (1990) however believes that the Early Miocene acid - intermediate volcanism was generated in a compressional regime which lasted until the Middle Miocene when extension began. Under this compressional regime, anatectic melts were produced in the continental crust leading to calc-alkaline volcanic activity (Yilmaz 1990).

Regardless of the precise timing of each regime, it is clear that the Early Miocene acid magmatism was generated at a time when western Turkey had an overthickened crust (50 - 70 km - Sengör et al., 1985). Two different mechanisms for the generation of magmatism in regions of overthickened crust have been put forward for volcanism in northern Chile and north-west Tibet (Hawkesworth et al., 1982, Arnaud et al., 1992). It has been suggested that the Purico-Chascon acid igneous complex in the CVZ (northern Chile) was produced in response to crustal thickening (Hawkesworth et al., 1982). These workers consider that a rise in isotherms may have taken place as a result of radioactive decay within the thickened crust. Hence, the thickening of the crust would make it more difficult for mantle-derived magmas to reach the surface, and partial melting probably occurred at higher levels within the crust as the temperature increased. Delamination of the base of the lithosphere has been suggested for the generation of K-rich volcanism in north-west Tibet, another region of crustal thickening (Arnaud et al., 1992). They consider that, following thickening, it is possible that the lithosphere became unstable and part of it may have collapsed into the asthenosphere below. Thermal erosion of the base of the

remnant lithosphere (MBL) would generate basaltic magmas as a result of upward movement of the asthenosphere compensating for the displaced volume in the lithosphere (Arnaud et al., 1992). Both lithospheric delamination and radioactive decay may have led to lithospheric and/or crustal melting in western Turkey in the Early Miocene. If extension had already begun by the Early Miocene in western Turkey, melting of an enriched MBL (in the subcontinental lithosphere) might have occurred by adiabatic decompression (McKenzie 1989) which in turn may have led to crustal melting. As discussed above, the source of the Early Miocene silicic magmas of the USEKA area was probably melted upper continental crust, perhaps with some contribution from the lithosphere.

In the Middle Miocene, mafic lavas became common in the USEKA area, and they contained higher concentrations of MgO, CaO, Fe<sub>2</sub>O<sub>3</sub>, Ni, V, Cr and Co, lower levels of SiO<sub>2</sub> and less enriched Nd and Sr isotopic signatures than the Early Miocene silicic volcanism, interpreted above to indicate a decreasing amount of crustal contamination during the Miocene with an increasing proportion of lithospheric melts. There appears to be a consensus of opinion that extension began before or at least during the Middle Miocene in western Turkey (Seyitoglu et al., 1992, Yilmaz 1990) and therefore, most of the mafic volcanics of the USEKA area were probably generated in an extensional environment. An enriched subcontinental lithospheric mantle source, such as that indicated by the high levels of certain incompatible elements (eg. K, light REE) in the mafic lavas, would have been able to melt by decompression melting at low degrees of extension (Hawkesworth & Gallagher 1993) at the hydrous solidus at approximately 1000°C (McKenzie & O'Nions 1995).

The increasing dominance of mafic magmas in the Mid Miocene, which have suffered less crustal contamination than previous Early Miocene evolved volcanics, can be explained in a number of ways. Firstly, the magmas may have ascended via routes taken by earlier magmas, hence providing easier pathways and resulting in less crustal assimilation. Direct evidence for this is hard to find, but near to the town of Iscehisar in the Afyon region, ultrapotassic latite is found directly overlying ignimbrite flows (Chapter 2) and it is possible that the former followed the route of the latter through the crust. Secondly, if extension had begun by the Middle Miocene, crustal fracturing may have been common thereby facilitating the passage of the mafic magmas. A similar trend of magmas becoming less and less contaminated by crust through time as extension proceeds, has also been observed in the Basin and Range of the western USA (Glazner & Ussler 1989).

Continued extension in western Turkey until the Quaternary resulted in the cessation of potassic volcanism, and more sodic volcanism at Kula appears to represent a mixture of melts from the asthenosphere and subcontinental lithosphere previously enriched by small degree melts of upper mantle. However, McKenzie and O'Nions (1995) argue that with no evidence for elevated temperatures beneath western Turkey (ie. a mantle plume) and, given the degree of lithospheric extension, melting of anhydrous asthenosphere is unlikely. Hence, they inferred melt generation solely from a previously enriched continental lithosphere (McKenzie & O'Nions 1995). They believed that melting of anhydrous asthenosphere would not be expected in view of the recent extension rates in western Turkey and the current crustal thickness (approximately 40 km - McKenzie & O'Nions 1995). Furthermore, REE inversion modelling has shown that the Kula lavas give melt generation

depths of between 55 and 70 km, a region that is 100°C or more below the solidus for anhydrous asthenospheric mantle (McKenzie & O'Nions 1995). They suggest that anhydrous mantle at normal upper mantle temperatures only begins to melt when it is brought up to a depth of about 45 km, a statement based on major element modelling by McKenzie and Bickle (1988).

### 5.4 CONCLUDING POINTS

The USEKA magmatism was largely calc-alkaline and acidic in the Early Miocene and became progressively more mafic in the Middle Miocene. The mafic Middle Miocene magmas contained higher concentrations of MgO, Fe<sub>2</sub>O<sub>3</sub>, CaO, V, Co, Cr and Ni but lower levels of SiO<sub>2</sub> than the Early Miocene more acid magmatism. All the USEKA samples have enriched Nd and Sr isotopic signatures, but the most enriched compositions are generally found in the Early Miocene silicic volcanics and the Erigöz Granite. The combined elemental and isotopic information therefore indicate a decreasing importance of AFC processes through time. The modification of magmas during their ascent by such processes was likely given the occurrence of an overthickened crust (50-70 km) in western Turkey in the Early Miocene. Comparisons of the elemental and isotopic composition of the USEKA suite with available data on upper crust from this region provide further evidence of a larger amount of crustal assimilation by the Early Miocene acid magmas relative to the Middle Miocene mafic lavas. Possible mechanisms for generating crustal melting include; radioactive decay in an overthickened crust, delamination of the lithosphere and adiabatic decompression melting in the lithosphere as a result of extension. The decreasing importance of AFC processes through the Miocene suggests that magmas found passage through the crust easier with time, possibly due to the extensional regime.

All the USEKA magmas were K-rich and the occurrence of more mafic (up to 9.24 MgO wt %) potassic and ultrapotassic lavas in the Middle Miocene, enables an assessment of the mantle source to be made. Enrichments of a range of incompatible elements relative to OIB suggest an enriched lithospheric mantle source. The data from the USEKA lavas indicates that two enrichment processes have modified the lithospheric mantle beneath western Turkey; (1) a subduction-related enrichment process and (2) an enrichment process involving the migration of small degree melts of upper mantle. Lithospheric mantle enriched by subduction-related processes, melted to produce magmas with high Th/Nb but low Nb/Y and Ti/Y ratios, as typified by the Vulsini lavas. The melting of lithospheric mantle enriched by small degree melts of asthenosphere resulted in magmas with low Th/Nb but high Nb/Y and Ti/Y, as typified by the Karisimbi lavas. The USEKA mafic lavas lie on a vector between these two end member compositions, indicating a heterogeneously enriched subcontinental lithosphere beneath western Turkey in the Miocene. The enriched isotopic composition of the mafic lavas is the result of isotopic decay within an isolated MBL, but isotopic variations within the suite provide additional evidence of a heterogeneous subcontinental lithospheric mantle. Such enriched lithospheric mantle could have melted by decompression after only a small degree of extension in the Miocene. The Nd and Sr isotopic composition of the Early Miocene silicic magmatism is slightly less enriched than most of the upper crust in this region, suggesting that a more depleted component may also be involved in their genesis. Since the rhyolite and ignimbrite contain elevated levels of Rb, Th, K

and B relative to upper continental crust, they may also contain a component from melted enriched lithospheric mantle which could account for these elevated LILE concentrations.

In summary therefore, the Early Miocene silicic magmatism was largely generated by the melting of upper continental crust, possibly with a small contribution from lithospheric melts, while the more mafic and less isotopically enriched Middle Miocene lavas reflect a considerable subcontinental lithospheric input with a decrease in the amount of assimilated upper crust. By the Late Miocene to Quaternary (Kula basalts), asthenospheric melting is suggested by the change from potassic to sodic volcanism and by the change from enriched Nd and Sr isotopic compositions to more depleted signatures. However, elevated levels of various incompatible elements relative to OIB indicate that an enriched lithosphere was also involved in the genesis of the Kula lavas.

This information suggests that the likely source rocks for the borate deposits, namely the Early Miocene acid volcanics, attained their B from assimilated upper crust and possibly from melted enriched lithospheric mantle. The former is considered the major source, since B and B/Nb have a positive correlation with  $^{87}\text{Sr}/^{86}\text{Sr}$ , but a negative one with  $\epsilon_{\text{Nd}}$  and the most isotopically enriched volcanics are interpreted as having the greatest proportion of assimilated upper continental crust. The silicic nature of the Early Miocene volcanism is also important in providing a B-rich source rock, since this element is concentrated during differentiation. Although information is currently limited, there is some evidence that the upper crust of western Turkey would have provided a suitable B-rich protolith. It is also likely that subcontinental lithosphere enriched by subduction and small degree melts of asthenosphere would have contained elevated levels of B and therefore represented another potential source. It is interesting to note that the other major borate provinces, in south-west USA and the Central Andes, also occur in tectonic environments which have experienced convergence and associated crustal thickening together with previous subduction events.

## 6 CONCLUSIONS AND RECOMMENDATIONS FOR FUTURE WORK

### 6.1 INTRODUCTION

The overall aim of this thesis was to establish a complete history of magmatism in the Emet and Kirka areas, so that the relationship between magmatic activity and borate mineralisation could be investigated. This study therefore provides a detailed mineralogical and geochemical description of granite, volcanics and volcanoclastic sediments from these areas, together with an assessment of the spatial and temporal position of magmatism relative to borate-host sediments. This information has been used to establish: the influence of local magmatism on the mineralogy and geochemistry of the borate-host sediments, the potential of local magmatism as a source for elements associated with borate mineralisation and the ultimate origin of B in Miocene magmas.

### 6.2 TIMING OF MAGMATISM RELATIVE TO DEPOSITION OF BORATE-HOST SEDIMENTS

#### 6.2.1 Field and petrologic evidence

The stratigraphic relations of volcanic exposures with sediments in Emet and Kirka Basins enabled some constraints to be placed on the timing of volcanism relative to sedimentation, and particularly to the timing of deposition of the borate-host sediments. Examples of clear field observations include the positions of the Emet mafic lavas above borate-host mudstones in the Emet Basin, and the Kirka Ignimbrite below the limestone of the Sarıkaya Formation in Kirka Basin. Overall, field observations in Emet Basin suggest that acid volcanism (rhyolitic) was active between the deposition of the Lower and Upper Limestone units, while the mafic volcanism (latitic and shoshonitic) post-dated deposition of the Borate Formation. A similar situation, with an evolution from acid to more mafic volcanism is observed in the Usak-Güre and Selendi Basins. Investigations in the Kirka Basin indicate that acid volcanism (ignimbritic, rhyolitic, dacitic) was active prior to deposition of at least the upper part of the Sarıkaya Formation, while the mafic volcanism (shoshonitic) post-dated deposition of this unit.

Textural and mineralogical observations of the sediments from each basin indicate a significant local acid igneous input. The presence of quartz, plagioclase and biotite with apatite inclusions in sediments from the Red and Borate Formations in Emet Basin are consistent with a local rhyolitic  $\pm$  granitic provenance, and the occurrence of pumice and spherulitic fragments in some volcanoclastic sediments confirms at least some pyroclastic input. Volcanoclastic sediments from the Karaören and Fetiye Formations of Kirka Basin are largely ignimbrite-derived, as indicated by the presence of pumice, lithic clasts and smokey quartz.

Hence, field and petrologic evidence indicates that acid volcanism was active prior to and possibly during the deposition of borate-host sediments in both Emet and Kirka Basins.

#### 6.2.2 Isotopic dating

Isotopic dates from this study and others (Besang 1977, Yalçın 1989) have provided the only

absolute method of determining the timing of magmatism in this area. They revealed that in the Usak-Güre, Selendi, Emet, Kirka and Afyon (USEKA) area there was an Early Miocene phase of calc-alkaline acid magmatism (represented by granite, rhyolite and ignimbrite), followed by a Middle - Late Miocene phase of less evolved, predominantly alkaline, magmatism (K-trachyte, latite and shoshonite). This study contributed fifteen K-Ar age determinations on USE volcanic and granitic rocks, and one  $^{39}\text{Ar}/^{40}\text{Ar}$  age determination on the Kirka Ignimbrite.

At the Emet Basin, an Early Miocene I-type granite (Erigöz Granite) has intruded the Palaeozoic basement and field observations indicate that it predated much of the sedimentation in the basin. Closely related in both space and time with the granite, are a series of Early Miocene rhyolite sheets (Emet Rhyolites), while the last phase of magmatism in Emet Basin took place in the Middle Miocene and consisted of latite and shoshonite flows (Emet mafic lavas). Miocene volcanism to the south and west of the Emet Basin (Usak-Güre, Selendi and Simav Basins) comprised Early Miocene rhyolite followed by Middle Miocene K-trachyte, andesite and latite.

In the Kirka area there was an Early - Middle Miocene phase of acid volcanism, consisting of ignimbrite (Kirka Ignimbrite), and rhyolite, trachyte and dacite (Kirka acid volcanics), while Late Miocene volcanism comprised shoshonite flows (Kirka mafic lavas). To the south of the Kirka Basin, around Afyon, Middle - Late Miocene volcanism included trachyte, latite and shoshonite.

Overall, the isotopic ages corroborate observations made in the field; Early Miocene acid volcanics are dominantly found in the lower parts of the sedimentary successions and Middle Miocene volcanics mainly found higher up in the sedimentary sequences.

### 6.2.3 Immobile elements and mineral compositions

The volcanic stratigraphy of the basins was further constrained by comparing the immobile element concentrations and the chemical composition of minerals in volcanoclastic lacustrine sediments with local volcanic and granitic rocks. Sediments in the Red and Borate Formations of Emet Basin contain low-Mg biotites and low concentrations of the immobile elements, P, Ti, Nb, Zr and Nd and low values of  $\text{TiO}_2/\text{Al}_2\text{O}_3$  and Nb/Y, indicating a provenance from local rhyolite  $\pm$  granite. Immobile element concentrations in mudstones from the Inay Group of Selendi and Usak-Güre Basins also suggest an input from local acid volcanism, and preclude the involvement of the latite volcanic phase. Data from the Karaören and Fetiye Formations of Kirka Basin also confirm their derivation from acid volcanic material but the provenance of most of the borate-hosting Sarikaya sediments could not be determined by these means due to dilution affects by high Ca levels. However, mudstone from the Sarikaya Formation at Göçenoluk has not been affected by calcite dilution, and it has an acid igneous derivation. The immobile element concentrations in mudstone from sequences near to the village of Balmahmut, west of Afyon, indicate the influence of local trachytic volcanism on sedimentation.

### 6.2.4 Summary

Overall, this information from field observations, mineralogy, isotopic dates, immobile element concentrations and biotite compositions therefore indicates that:

(i) Acid magmatism in Emet and Kirka Basins, represented by granite, ignimbrite, rhyolite and dacite, was closely related in both space and time to the deposition of the borate-host sediments.

(ii) Mafic volcanism in the Emet and Kirka Basins, represented by shoshonite and latite, post-dated deposition of the borate-host sediments.

### 6.3 INFLUENCE OF MAGMATISM ON SEDIMENT COMPOSITION AND THE IMPLICATIONS FOR BORATE MINERALISATION

A detailed mineralogical and geochemical study of lacustrine mudstones from the Borate Formation in Emet Basin suggests that they were largely the product of the diagenetic alteration of dominantly rhyolite  $\pm$  granite-derived material in a saline, alkaline environment. Diagenesis and interaction with saline, alkaline waters resulted in the complete breakdown of rhyolitic and granitic detrital minerals and the development of an authigenic mineral assemblage of calcite, dolomite, borate, trioctahedral smectite, authigenic K-feldspar, celestite, gypsum and realgar. These post-depositional modifications resulted in the enrichment of Mn, Mg, Ca, As, Li and Sr and depletion of Na in the sediments relative to local rhyolitic volcanism. The breakdown of granitic and rhyolitic detrital minerals, provided an abundant supply of Si, Al and K, together with lesser amounts of Ca and Sr to the basin, thereby having some influence on the authigenic mineral assemblage produced. For instance, the generation of authigenic K-feldspar, at least in part from the alteration of volcanic glass, reflects the K-rich nature of the volcanic input. The trioctahedral smectite was probably generated by the modification of dioctahedral smectite which originated from the alteration of volcanic material, such as glass, during weathering or diagenesis. Furthermore, the borate-hosting sediments are enriched in Rb relative to upper continental crust and other sediment databases, which can be explained by the Rb-rich nature of the volcanic input. In contrast, the depletion in Na in the borate-hosting sediments indicates the lack of a Na-bearing phase, which may be the result of the relatively low Na content in the volcanic input. The presence of detrital illite and chromite suggests an additional input, from the basement, which may also have provided a significant supply of Ca and Mg.

Trioctahedral smectite, authigenic K-feldspar, dolomite and borates have a common association in the Emet Basin. Barren sediments in the basin lack dolomite and trioctahedral smectite and sometimes lack authigenic K-feldspar and dioctahedral smectite. In terms of geochemistry, the borate-host sediments are generally enriched in Mg, As, Li and Sr relative to the barren sediments. These observations can be explained if the borate-host sediments experienced high salinity conditions where concentrations of Mg, As, Li, Sr and B were high and authigenic K-feldspar and trioctahedral smectite were stable, while the barren sediments were developed in less saline conditions. This information suggests that the distribution of borate mineralisation largely depended on the palaeotopography of the basin which was controlled the positions of the palaeolakes. It appears that the igneous input into Emet Basin was fairly uniform, although some variation is suggested by the lack of any smectite in some of the barren sediments.

Mudstones from Selendi, Usak-Güre and Kirka Basins are very similar in terms of mineralogy and

geochemistry to those of Emet Basin, and they also seem to be the result of the diagenetic alteration of predominantly acid-derived volcanic material in a saline, alkaline environment. The borate-hosting sediments from Kirka Basin also contain some, or all of, trioctahedral smectite, authigenic K-feldspar and dolomite. Hence, as at the Emet Basin these minerals appear to have a common association with borate mineralisation. In common with the Emet Basin, the mudstone from the Kirka Basin also contains elevated Li, Sr and As. The presence of smectite, K-feldspar and Mg-carbonate, together with some elevated As, Li and Sr concentrations in at least some of the sediments from Selendi and Usak-Güre Basins suggests these basins represent favourable targets for borate minerals. By contrast, sediments from the Afyon area (near Balmahmut) contain lower Mg, As, Li, Sr and Cr than the other basins, and smectite and Mg-carbonate are absent. They are therefore unlikely to host borate mineralisation.

### **6.4 SOURCE POTENTIAL OF ACID MAGMATISM AND TRANSFER MECHANISMS FROM SOURCE TO BASIN SEDIMENTS**

#### **6.4.1 Source potential of acid igneous rocks in the Emet and Kirka areas**

The potential of Early Miocene acid magmatism (granite, ignimbrite, rhyolite, dacite) as a source for the elements associated with borate mineralisation (B, Li, As and Sr) was evaluated in this study by examining concentrations and remobilisation of these elements. The acid igneous volcanics of the USEKA area are depleted in Sr, but largely enriched in B and Li relative to average upper continental crust. The Erigöz Granite contains similar concentrations of Sr and Li to the acid volcanics, but is depleted in B. Concentrations of As are anomalous in most of the USEKA volcanics relative to levels recorded from fresh igneous rocks elsewhere.

The data indicates only minimal remobilisation of Sr, B and Li in most of the rocks and therefore the measured concentrations of these elements are probably representative of their parental melts. By contrast, the As data suggests that it was highly mobile in this environment, and measured concentrations do not appear to be representative of those in the parental melts.

Overall, this information indicates that the acid volcanics represent a viable source for B, Li and to a lesser extent Sr. The Erigöz Granite was a potential source of Li, but less so of B. The potential of the acid igneous rocks as a source for As is impossible to assess, but it seems likely that local acid magmatism supplied at least some as to geothermal fluids.

#### **6.4.2 Mechanisms for the transfer of B, As, Li, Sr and S from an igneous source to the basin sediments**

The main mechanisms for the transfer of B, As, Li, Sr and S from an igneous source to the basin sediments probably included transfer by igneous-driven geothermal fluids and the breakdown of igneous material in the basins by saline, alkaline lake and pore waters.

In the Emet area, the presence of alunite and silicification alteration, provides some evidence for geothermal activity. Furthermore, elevated As concentrations in many of the igneous rocks of the USEKA area, were probably the result of interaction with As-rich geothermal fluids. These fluids



## **Conclusions and recommendations for future work**

---

probably obtained B, Li, As, Sr and S from the igneous source by hydrothermal leaching, and by contributions of magmatic waters and gases. Direct evidence for the former is provided by the alunite altered rhyolitic rock in the Emet area, from which B and Li have been hydrothermally leached, while the latter processes are inferred from the study of modern magma systems.

Igneous material was transported into Emet and Kirka Basins both by fluvial action and by pyroclastic activity. This acid igneous material would have been unstable in the saline, alkaline lake waters, resulting in the break down of most igneous-derived minerals, with the subsequent release of B, Li, Sr and perhaps As. This study has shown that volcanic glass is a repository for B and hence the abundance of glass-bearing acid pyroclastics could have supplied appreciable amounts of B to the lake systems. The data from this study also shows that feldspar break down in the basin resulted in the release of Sr to solution.

### **6.5 SUMMARY OF MODEL FOR THE ROLE OF MAGMATISM IN THE GENESIS OF EMET AND KIRKA BORATE DEPOSITS**

On the basis of information gained in the course of this study, a model for the role of magmatism in the genesis of the Emet and Kirka borate deposits has been proposed:

- K-rich rhyolitic magma at high crustal level generated a circulating hydrothermal system dominated by heated meteoric water, but with some magmatic water.
- The geothermal waters obtained  $B(OH)_3$  and  $SO_2$  from magma degassing, B, Li and perhaps As from magmatic fluids, and B, Li, As and Sr from the hydrothermal leaching of country rocks. The data from this study indicates that ignimbrite, rhyolite and dacite may have provided an abundant supply of B and Li by this latter mechanism.
- Thermal springs, which carried high concentrations of B, Li, S and As, discharged into the lake and local ground water systems.
- Acid igneous material with high concentrations of B, Li and perhaps As, was transported to the basin by fluvial action and pyroclastic activity.
- This acid igneous material was broken down in the saline, alkaline lake and pore waters, resulting in loss of K, Si, B, Li, Sr and, perhaps As, to solution.
- Borate minerals precipitated near to the centre of the lake where the highest salinity waters are located with particularly high concentrations of B, Li, As, S, Sr, Ca and Mg. Other authigenic minerals stable in this environment included trioctahedral smectite, K-feldspar, dolomite, calcite, realgar, celestite and gypsum. Trioctahedral smectite was probably generated by the modification of volcanic-derived dioctahedral smectite and authigenic K-feldspar formed by the alteration of K-

rich volcanic glass.

- Around the edge of the lake, the waters were less saline, and the mineral assemblage developed comprised illite and calcite.

### 6.6 ORIGIN OF MAGMATISM IN THE TURKISH BORATE PROVINCE; CONSTRAINTS FOR THE ULTIMATE SOURCE OF BORON

This early phase of calc-alkaline acid magmatism, which had a close spatial and temporal position with the borates, became progressively more mafic in the Middle Miocene. The mafic Middle Miocene magmas contained higher concentrations of MgO, Fe<sub>2</sub>O<sub>3</sub>, CaO, V, Co, Cr and Ni, lower levels of SiO<sub>2</sub> and higher  $\epsilon_{Nd}$  and lower <sup>87</sup>Sr/<sup>86</sup>Sr than the silicic Early Miocene potential source magmas. This combined elemental and isotopic information indicates a decreasing importance of AFC processes through time. The modification of magmas during their ascent through the crust was likely since western Turkey contained an overthickened crust during the Early Miocene. Comparisons of the elemental and isotopic compositions of the USEKA magmatism with the limited amount of available data from upper crust in western Turkey and the Aegean provides further evidence that the Early Miocene silicic lavas contained a greater component of assimilated upper continental crust than the Middle Miocene mafic lavas. Possible mechanisms for generating crustal melting include: radioactive decay within an overthickened crust, delamination of the lithosphere and adiabatic decompression melting of the lithosphere as a result of extension.

The occurrence of more mafic (up to 9.2 wt % MgO) lavas in the Middle Miocene, enables an assessment of the mantle sources to be made. Enrichments of a range of incompatible elements relative to OIB suggest an enriched lithospheric mantle source. Comparison of the data from the USEKA mafic suite with potassic lavas from elsewhere indicates that two enrichment processes have modified the lithospheric mantle beneath western Turkey: a subduction-related enrichment process which led to lithosphere with high Th/Nb but low Nb/Y and Ti/Y ratios, and an enrichment process involving the migration of small degree melts of upper mantle which led to lithosphere with low Th/Nb, but high Nb/Y and Ti/Y.

Although less enriched than the Early Miocene silicic lavas, the mafic Middle Miocene lavas still plot in the enriched quadrant of an  $\epsilon_{Nd}$  vs <sup>87</sup>Sr/<sup>86</sup>Sr diagram and have low  $\epsilon_{Nd}$  and high <sup>87</sup>Sr/<sup>86</sup>Sr. This can be explained by isotopic decay within an isolated MBL in the subcontinental lithospheric mantle. Such enriched lithospheric mantle would be able to melt by adiabatic decompression after only small amounts of extension. Elevated Rb, Th, K and B, but slightly higher  $\epsilon_{Nd}$  and lower <sup>87</sup>Sr/<sup>86</sup>Sr in the Early Miocene silicic magmatism relative to upper continental crust suggests that a component of lithospheric mantle, in addition to a crust component, may also have been involved in their genesis.

Within the Emet and Kirka volcanic suites, there is a positive correlation between B and SiO<sub>2</sub> and between B and <sup>87</sup>Sr/<sup>86</sup>Sr. Hence, the most B-rich igneous rocks are the Early Miocene acid volcanics, which have been the most affected by AFC processes. It appears therefore that AFC processes

generated B-rich magmas, suggesting that the west Turkish crust is a major B source. If, as proposed above, the Early Miocene silicic source volcanics also contained a component from the lithospheric mantle, it too may have provided a source for B. This seems likely, since enrichment of the lithospheric mantle by previous subduction processes and by the migration of small degree melts of asthenosphere is likely to concentrate B in a similar fashion to other incompatible elements.

### **6.7 CONCLUDING POINTS**

- Early Miocene acid magmatism had a close spatial and temporal position with the deposition of the borate-host sediments in Emet and Kirka Basins.
- The mineralogical and geochemical composition of the borate-host sediments was strongly influenced by the post-depositional modification of rhyolitic, ignimbritic and granitic-derived material in a saline, alkaline environment.
- The geochemistry of the Early Miocene acid igneous rocks suggests that acid magmatism represented a likely source for important elements (B, Li, As, Sr & S) associated with borate-mineralisation.
- Possible mechanisms for the transfer of B and other elements from an igneous source to basin sediments include transfer by igneous - driven geothermal fluids and the break down of igneous material in saline, alkaline lake waters.
- Trace element and isotopic data for the acid igneous rocks indicate that the ultimate source of the B was assimilated upper continental crust, perhaps with some component of melted lithospheric mantle.

### **6.8 IMPLICATIONS FOR BORATE MINERAL EXPLORATION**

On the basis of this study, the following geological situations are considered favourable for the location of borate mineralisation:

- Regions with volcanism developed after episodes of convergence and crustal thickening.
- The occurrence of K-rich ignimbrite, rhyolite and dacite (with elevated As concentrations) in close spatial and temporal position with lacustrine sediments in closed basins.
- The presence of acid volcanic-derived lacustrine basin sediments.

## **Conclusions and recommendations for future work**

---

- The presence of As, Sr and Li-rich lacustrine mudstone sequences containing some or all of authigenic K-feldspar, trioctahedral smectite and dolomite.
- The presence of high Mg concentrations in lacustrine mudstone.

### **6.9 SUGGESTIONS FOR FURTHER WORK**

(1) Similar detailed studies of volcanism and related sediments in other borate-host basins in SW USA and the Central Andes would provide a useful comparison with this thesis. In particular, such studies could determine whether K-rich acid volcanism had a genetic relationship with borate mineralisation, as in western Turkey.

(2) An investigation of the B concentrations in individual minerals, in granite, volcanics and volcanoclastic sediments would provide a clearer understanding of the behaviour of this element in both magmatic and lacustrine basin environments, i.e. determination of the main B repositories in igneous rocks (glass?), and in lacustrine sediments (illite?). Suitable analytical techniques include (a) the ion probe which can analyse in situ B concentrations (Chaussidon & Libourel 1993), and (b) prompt gamma activation analysis (PGAA) of mineral separates (Hoffman 1992).

(3) A detailed study of the volcanoclastic sediments and their alteration to clay minerals using analytical electron microscope (AEM) and transmission electron microscope (TEM) studies. This would enable the chemical composition of individual clay particles to be determined as in a study of Abert Lake by Banfield et al. (1991a).

(4) Additional geochemical data is required for the upper continental crust of western Turkey in order to further assess crustal assimilation processes in the genesis of Early Miocene silicic magmatism, and to further constrain the ultimate source of B. Useful data would include major, trace element and B concentrations, as well as Nd and Sr isotope ratios.

(5) Further analyses of B are required in volcanic and granitic rocks elsewhere to gain a more complete understanding of the behaviour of this element. In particular, data are required for igneous rocks, associated with thickened crust and convergent settings and those associated with enriched subcontinental lithospheric melts.

# REFERENCES

- Abdel-Rahman, A. M., 1994, Nature of biotites from alkaline, calc-alkaline, and peraluminous magmas: *Journal of Petrology*, v. 35, p. 525-541.
- Aktas, G., and Robertson, A. H. F., 1984, The Maden Complex, SE Turkey: evolution of a Neotethyan active margin, in Dixon, J. E., and Robertson, A. H. F., eds., *The geological evolution of the eastern Mediterranean*, 17, *Geol Soc sp pub*, p. 375-402.
- Alonso, R. N., Helvacı, C., Sureda, R. J., and Viramonte, J. G., 1988, A new Tertiary borax deposit in the Andes: *Mineralium Deposita*, v. 23, p. 299-305.
- Alonso, R. N., Jordan, T. E., Tabbutt, K. T., and Vandervoort, D. S., 1991, Giant evaporite belts of the Neogene central Andes: *Geology*, v. 19, p. 401-404.
- Arnaud, N. O., Vidal, P., Tapponnier, P., and Matte, P., 1992, The high K<sub>2</sub>O volcanism of northwestern Tibet: Geochemistry and tectonic implications: *Earth and Planetary Science Letters*, v. 111, p. 351-367.
- Arnórsson, S., and Andrésdóttir, A., 1995, Processes controlling the distribution of boron and chlorine in natural waters in Iceland: *Geochimica et Cosmochimica Acta*, v. 59, p. 4125-4146.
- Ataman, G., and Baysal, O., 1978, Clay mineralogy of Turkish borate deposits: *Chemical Geology*, v. 22, p. 233-247.
- Aydar, E., Bayhan, H., and Erkan, Y., 1994, Köroğlu caldera, mid-west Anatolia, Turkey (abstract): *International Volcanological Congress (IAVCEI)*, Ankara, Turkey, 1994.
- Banfield, J. F., Jones, B. F., and Veblen, D. R., 1991a, An AEM-TEM study of weathering and diagenesis, Abert Lake, Oregon: II. Diagenetic modification of the sedimentary assemblage: *Geochimica et Cosmochimica Acta*, v. 55, p. 2795-2810.
- Banfield, J. F., Jones, B. F., and Veblen, D. R., 1991b, An AEM-TEM study of weathering and diagenesis, Abert Lake, Oregon: I. Weathering reactions in the volcanics: *Geochimica et Cosmochimica Acta*, v. 55, p. 2781-2793.
- Barker, C. E., and Barker, J. M., 1985, A re-evaluation of the origin and diagenesis of borate deposits, Death Valley Region, California, in Barker, J. M., and Lefond, S. J., eds., *Borates: Economic geology and production*, New York, Society of Mining Engineers of the American Institute of Mining, Metallurgical and Petroleum Engineers, Inc., p. 101-135.
- Barrows, K. J., 1980, Zeolitization of Miocene volcanoclastic rocks, southern Desatoya Mountains, Nevada: *Geological Society of America Bulletin*, v. 91, p. 199-210.
- Bebout, G. E., Ryan, J. G., and Leeman, W. P., 1993, B-Be Systematics in subduction-related metamorphic rocks: Characterisation of the subducted component: *Geochimica et Cosmochimica Acta*, v. 57, p. 2227-2237.
- Besang, C., Eckhardt, F. J., Harre, W., Kreuzer, H., and Müller, P., 1977, Radiometrische altersbestimmungen an neogenen Eruptivgesteinen der Türkei: *Geologisches Jahrbuch*, v. B25, p. 3-36.
- Bingöl, E., Delaloye, M., and Ataman, G., 1982, Granitic intrusions in western Anatolia: a contribution to the geodynamic study of this area: *Eclogae Geol. Helv*, v. 75, p. 437-446.
- Bingöl, E., 1989, Geological map of Turkey: MTA, Ankara.
- Bozkurt, E., and Park, R. G., 1994, Southern Menderes Massif: an incipient metamorphic core complex in western Anatolia: *Journal of the Geological Society, London*, v. 151, p. 213-216.
- Brown, G., and Brindley, G. W., 1980, X-ray diffraction procedures for clay mineral identification, in Brindley, G. W., and Brown, G., eds., *Crystal structures of clay minerals and their x-ray identification*: London, Mineralogical Society.
- Bryan, W. B., and Moore, J. G., 1977, Compositional variations of young basalts in the Mid Atlantic Ridge rift valley, near lat. 36°49'N: *Geol. Soc. Am. Bull*, v. 88, p. 556-570.
- Bryan, W. B., Thompson, G., and Micheal, P. J., 1979, Compositional variation in a steady state zoned magma chamber: Mid Atlantic Ridge at 36°50'N: *Tectonophysics*, v. 55, p. 63-85.
- Bullard, E. C., Everett, J. E., and Smith, A. G., 1965, Fit of continents around the Atlantic, in Blackett, P. M. S., Bullard, E. C., and Runcorn, S. K., eds., *A symposium on continental drift*, Ser A. 258, *Phil. Trans. Roy. Soc. London*, p. 41-75.

## References

---

- Cann, J. R., 1970, Rb, Sr, Y, Zr and Nb in some ocean floor basaltic rocks: *Earth and Planetary Science Letters*, v. 10, p. 7-11.
- Cas, R. A. F., and Wright, J. V., 1993, *Volcanic successions modern and ancient*, Unwin Hyman Ltd.
- Çevikbas, A., Ercan, T., and Metin, S., 1988, Geology and regional distribution of Neogene volcanics between Afyon - Suhut: *Metu Journal of Pure and Applied Sciences*, v. 21, p. 479-499.
- Chappell, B. W., and White, A., J. R., 1974, Two contrasting granite types: *Pacific Geology*, v. 8, p. 173-174.
- Chaussidon, M., and Libourel, G., 1993, Boron partitioning in the upper mantle: An experimental and ion probe study: *Geochimica et Cosmochimica Acta*, v. 57, p. 5053-5062.
- Collins, A. S., 1997, Tectonic evolution of Tethys in the Lycian Taurides, southwest Anatolia: Unpub. PhD thesis, University of Edinburgh.
- Collins, A. S., and Robertson, A. H. F., 1997, Lycian melange, southwestern Turkey: An emplaced Late Cretaceous accretionary complex: *Geology*, v. 25, p. 225-258.
- Coney, P. J., and Harms, T. A., 1984, Cordilleran metamorphic core complexes: Cainozoic extensional relics of Mesozoic compression: *Geology*, v. 12, p. 550-554.
- Cox, K. G., Bell, J. D., and Pankhurst, R. J., 1979, *The interpretation of igneous rocks*: London, Allen & Unwin.
- Crowley, J. K., 1996, Mg- and K-bearing borates and associated evaporites at Eagle Borax Spring, Death Valley, California: A spectroscopic exploration: *Economic Geology*, v. 91, p. 622-635.
- de Silva, S. L., 1989, Altiplano-Puna volcanic complex of the central Andes: *Geology*, v. 17, p. 1102-1106.
- Deer, W. A., Howie, R. A., and Zussman, J., 1992, *An introduction to the rock forming minerals*, Longman Scientific Technical.
- DePaolo, D. J., and Wasserburg, G. J., 1979, Petrogenetic mixing models and Nd-Sr isotopic patterns: *Geochimica et Cosmochimica Acta*, v. 43, p. 615-627.
- Dercourt, J., Ricou, L. E., Kazmin, V. G., Le Pichon, X., Knipper, A. L., Grandjacquet, C., Sbertshnikov, I. M., Geyssant, J., Lepvrier, C., Perchersky, D. H., Boulain, J., Sibuet, J. C., Savostin, L. A., Sorokhtin, O., Westpahl, M., Bazhrnov, M. L., Lauer, J. P., and Biju-Duval, B., 1986, Geological evolution of the Tethys belt from the Atlantic to the Pamirs since the Lias: *Tectonophysics*, v. 123, p. 241-315.
- Dercourt, J., Ricou, L. E., and Vrielynck, B., 1993, *Atlas Tethys Palaeoenvironmental Maps.*, Beicip-Franlab.
- Dewey, J. F., and Sengör, A. M. C., 1979, Aegean and surrounding regions: Complex multiplate and continuum tectonics in a convergent zone: *Geological Society of America Bulletin*, Part 1, v. 90, p. 84-92.
- Donnelly, T. W., Thompson, G., and Salisbury, M. H., 1980, The chemistry of altered basalts at site 417, Deep Sea Drilling Project leg 51, in Powell, R., and Laughter, F., eds., *Initial reports. DSDP 51-53*, p. 1319-1330.
- Droop, G. T. R., 1987, A general equation for estimating Fe<sup>3+</sup> concentrations in ferromagnesian silicates and oxides from microprobe analyses, using stoichiometric criteria: *Mineralogical Magazine*, v. 51, p. 431-435.
- Duffield, W. A., and Ruiz, J., 1992, Compositional gradients in large reservoirs of silicic magma as evidenced by ignimbrites versus Taylor Creek Rhyolite lava domes: *Contrib Mineral Petrol*, v. 110, p. 192-210.
- Dunbar, N. W., and Hervig, R. L., 1992, Petrogenesis and volatile stratigraphy of the Bishop Tuff: evidence from melt inclusion analysis: *J Geophys Res*, v. 97, p. 15129-15150.
- Edwards, C. M. H., Menzies, M. A., Thirwall, M. F., Morris, J. D., Leeman, W. P., and Harmon, R. S., 1994, The transition of potassic alkaline volcanism in Island Arcs: The Ringgit-Beser Complex, East Java: *Journal of Petrology*, p. 1557-1595.
- Ellis, A. J., 1979, Explored Geothermal Systems, in Barnes, H. L., ed., *Geochemistry of hydrothermal ore deposits*, John Wiley & Sons, New York, p. 632-683.
- Ellis, A. J., and Mahon, W. A. J., 1964, Natural hydrothermal systems and experimental hot-water/rock interactions: *Geochimica et Cosmochimica Acta*, v. 28, p. 1323-1357.
- Ellis, A. J., and Mahon, W. A. J., 1967, Natural hydrothermal systems and experimental hot water/rock interactions (Part II): *Geochimica et Cosmochimica Acta*, v. 31, p. 519-538.

## References

- Ercan, E., Dinçel, A., Metin, S., Türkecan, A., and Günay, E., 1978, Geology of the Neogene Basins in the Usak region (in Turkish): Bulletin of the Geological Society of Turkey, v. 21, p. 97-106.
- Ercan, E., Türkecan, A., Dinçel, A., and Günay, E., 1983, Geology of the Kula - Selendi area (in Turkish): Geological Engineering, v. 17, p. 3-28.
- Ercan, T., Satır, M., Kreuzer, H., Türkecan, A., Günay, E., Çevikbas, A., Ates, M., and Can, B., 1985, Batı Anadolu Senozoyik volkanitlerine ait yeni kimyasal, izotopik ve radyometrik verilerin yorumu (Interpretation of new chemical, isotopic and radiometric data on Cenozoic volcanics of western Anatolia): Bulletin of the Geological Society of Turkey, v. 28, p. 121-136.
- Erentöz, C., 1963, Geological map of Turkey 1:500,000 - Ankara sheet, Institute of mineral research and exploration, Ankara, Turkey.
- Eugster, H. P., 1980, Geochemistry of evaporitic lacustrine deposits: Ann. Rev. Earth Planet. Sci., v. 8, p. 35-63.
- Eugster, H. P., and Jones, B. F., 1979, Behaviour of major solutes during closed-basin brine evolution: Am. J. Sci., v. 279, p. 609-31.
- Eugster, H. P., and Hardie, L. A., 1975, Sedimentation in an ancient playa-lake complex: the Wilkins Peak member of the Green River Formation of Wyoming: Geological Society of America Bulletin, v. 86, p. 319-334.
- Finlow-Bates, T., and Stumpfl, E. F., 1981, The behaviour of so-called immobile elements in hydrothermally altered rocks associated with volcanogenic submarine-exhalative ore deposits: Mineral Deposita, v. 16, p. 319-328.
- Fitton, J. G., James, D., and Leeman, W. P., 1991, Basic magmatism associated with Late Cenozoic extension in the Western United States: Compositional variations in space and time: Journal of Geophysical Research, v. 96, p. 13693-13711.
- Fleet, A. J., 1984, Aqueous and sedimentary geochemistry of the rare earth elements, in Henderson, P., ed., Rare Earth Element Geochemistry, 2. Developments in Geochemistry, Elsevier.
- Fleet, M. E. L., 1965, Preliminary investigations into the sorption of boron by clay minerals: Clay Minerals, v. 6, p. 3-16.
- Floyd, P. A., and Winchester, J. A., 1975, Magma type and tectonic setting discrimination using immobile elements: Earth and Planetary Science Letters, v. 27, p. 211-218.
- Fogg, T. R., and Duce, R. A., 1985, Boron in the troposphere: distribution and fluxes: Journal of Geophysical Research, v. 90, p. 3781-3796.
- Foley, S. F., Venturelli, G., Green, D. H., and Toscani, L., 1987, The ultrapotassic rocks: Characteristics, classification and constraints for petrogenetic models: Earth Science Reviews, v. 24, p. 81-134.
- Francis, P., 1993, Volcanoes, a planetary perspective, Clarendon Press.
- Fytikas, M., Innocenti, F., Manetti, P., Mazzuoli, R., Peccerillo, A., and Villari, L., 1984, Tertiary to Quaternary evolution of volcanism in the Aegean region, in Dixon, J. E., and Robertson, A. H. F., eds., The geological evolution of the Eastern Mediterranean: Geological Society London Special Publication, v. 17, p. 687-699. For The Geological Society by Blackwell Scientific Publications.
- Gans, P. B., Mahood, G. A., and Schermer, E., 1989, Synextensional magmatism in the Basin and Range Province: A case study from the eastern Great Basin.: Geol. Soc. Am. Spec. Pap 223.
- Garavelli, A., and Vurro, F., 1994, Barberiite,  $\text{NH}_4\text{BF}_4$ , a new mineral from Vulcano, Aeolian Islands, Italy: American Mineralogist, v. 79, p. 381-384.
- Gibson, S. A., Thompson, R. N., Leat, P. T., Morrison, M. A., Hendry, G. L., Dickin, A. P., and Mitchell, J. A., 1993, Ultrapotassic magmas along the flanks of the Oligo-Miocene Rio Grande rift, USA: monitors of the zone of lithospheric mantle extension and thinning beneath a continental rift: Journal of Petrology, v. 34, p. 187-228.
- Glazner, A. F., and Ussler III, W., 1989, Crustal contamination, crustal density and the evolution of Cenozoic magmatism in the Basin and Range of the Western United States: Journal of Geophysical Research, v. 94, p. 7952-7960.
- Gök, S., Çakır, A., and Dündar, A., 1980, Stratigraphy, petrography and tectonics of the borate - bearing Neogene in the vicinity of Kirka: Bulletin of the Geological Congress of Turkey, v. 2, p. 53-62.
- Görür, N., Sengör, A. M. C., Sakiç, M., Tüysüz, O., Akkök, R., Yigitbas, E., Oktay, F. Y., Barka, A., Sarica, N., Ecevitoglu, B., Demirbag, E., Ersoy, S., Algan, O., Güneysu, C., and Aykol, A., 1995, Rift formation in the

## References

---

- Gökova region, southwest Anatolia: implications for the opening of the Aegean Sea: *Geol. Mag.*, v. 132, p. 637-650.
- Govindaraju, K., 1994, Compilation of working values for geostandards: *Geostandards Newsletter*, v. XVIII.
- Gribble, C. D., and Hall, A. J., 1993, *Optical mineralogy. Principles & practice*, UCL Press Ltd.
- Güleç, N., 1991, Crust - mantle interaction in western Turkey: Implications from Sr and Nd isotope geochemistry of Tertiary and Quaternary volcanics: *Geological Magazine*, v. 128, p. 417-435.
- Gün, H., Akdeniz, N., and Günay, E., 1979, Geology and problems of dating of Neogene basins in Gediz and southern Emet (in Turkish): *Geological Engineering*, v. 8, p. 1-13.
- Gündoğdu, M. N., Yalçın, H., Temel, A., and Clauer, N., 1996, Geological, mineralogical and geochemical characteristics of zeolite deposits associated with borates in the Bigadiç, Emet and Kirka Neogene lacustrine basins, western Turkey: *Mineral. Deposita*, v. 31, p. 492-513.
- Hanks, H. G., 1883, Report on the borax deposits of California and Nevada: *Calif State Mining Bur.*, v. 3, p. 1-111.
- Hawkesworth, C. J., and Gallagher, K., 1993, Mantle hotspots, plumes and regional tectonics as causes of intraplate magmatism: *Terra Nova*, v. 5, p. 552-559.
- Hawkesworth, C. J., Hammill, M., Glenhill, A. R., van Calsteren, P., and Rogers, G., 1982, Isotope and trace element evidence for late-stage intro-crustal melting in the High Andes: *Earth and Planetary Science Letters*, v. 58, p. 240-257.
- Hay, R. L., 1977, Geology of zeolites in sedimentary rocks, in Mumpton, F. A., ed., *Mineralogy and geology of natural zeolites*, 4. Reviews in Mineralogy, Mineralogical Society of America Short Course Notes.
- Hay, R. L., Guldman, S. G., Mathews, J. C., Lander, R. H., Duffi, M. E., and Kyser, T. K., 1991, Clay mineral diagenesis in core KM-3 of Searles Lake, California: *Clays and Clay Minerals*, v. 39, p. 84-96.
- Hedenquist, J. W., and Henley, R. W., 1985, Hydrothermal eruptions in the Waiotapu geothermal system, New Zealand: Their origin, associated breccias, and relation to precious metal mineralisation: *Econ Geol.*, v. 80, p. 1640-1668.
- Hedenquist, J. W., and Lowenstern, J. B., 1994, The role of magmas in the formation of hydrothermal ore deposits: *Nature*, v. 370, p. 519-526.
- Hellier, S., 1995, Erosion, sedimentation and sedimentary origin of clays, in Velde, B., ed., *Origin and Mineralogy of Clays (clays and the environment)*, Springer, p. 162-219.
- Hellman, P., L., Smith, R. E., and Henderson, P., 1979, The mobility of rare earth elements; evidence and implications from selected terrains affected by burial metamorphism: *Contrib. Mineral. Petrol.*, v. 71, p. 23-44.
- Helvacı, C., 1977, Geology, mineralogy and geochemistry of the borate deposits and associated rocks at the Emet valley, Turkey: Unpub. Ph.D dissertation thesis, University of Nottingham, England.
- Helvacı, C., 1984, Occurrence of rare borate minerals: veatchite-A, tunellite and caninite in the Emet borate deposits, Turkey: *Mineral. Deposita*, v. 19, p. 217-226.
- Helvacı, C., 1994, Mineral assemblages and formation of the Kestelek and Sultancayırı borate deposits: *Proc. 29th Intl. Geol. Congr.*, Part A., p. 245-264.
- Helvacı, C., 1995, Stratigraphy, Mineralogy, and Genesis of the Bigadic Borate Deposits, Western Turkey: *Economic Geology*, v. 90, p. 1237-1260.
- Helvacı, C., and Alonso, R. N., 1994, An occurrence of primary inyoite at Lagunita Playa, Northern Argentina: *Proc. 29th Int'l. Geol.*, 1994, p. 299-308.
- Helvacı, C., and Firman, R. J., 1976, Geological setting and mineralogy of Emet borate deposits, Turkey: *Trans. Institution of Mining and Metallurgy Transactions*, section B, v. 85, p. 142-152.
- Helvacı, C., Stamatakis, M. G., Zagourogrou, C., and Kanaris, C., 1993, Borate minerals and related authigenic silicates in northeastern Mediterranean late Miocene continental basins: *Exploration and Mining Geology*, v. 2, p. 171-178.
- Henley, R. W., 1985, The geothermal framework of epithermal deposits, in Berger, B. R., and Bethke, P. M., eds., *Geology and geochemistry of epithermal systems*, 2. Reviews in Economic Geology, Society of Economic Geologists, p. 1-24.



## References

---

- Henley, R. W., and Ellis, A. J., 1983, Geothermal systems ancient and modern: A geochemical review: *Earth Science Reviews*, v. 19, p. 1-50.
- Hetzl, R., and Reischmann, T., 1996, Intrusion age of Pan-African augen gneisses in the southern Menderes Massif and the age of cooling after Alpine ductile extensional deformation: *Geological Magazine*, v. 133, p. 565-572.
- Hetzl, R., Ring, U., Akal, C., and Troesch, M., 1995, Miocene NNE directed extensional unroofing in the Menderes Massif, Southwestern Turkey: *Journal of Geological Society, London*, v. 152, p. 639-654.
- Higgins, M. D., 1988, Trace element geochemistry of the Inyo volcanic chain, California: evidence for multiple magma sources, magma mixing and post-eruption loss of boron: *Journal of Volcanology and Geothermal Research*, v. 35, p. 97-110.
- Hoffman, E. L., 1992, Instrumental neutron activation in geoanalysis: *Journal of Geochemical Exploration*, v. 44, p. 297-319.
- Holland, H. D., 1980, *The chemical evolution of the Atmosphere and Oceans*: Princeton, Princeton Univ. Press.
- Imai, N., Sakuramachi, H., Terashima, S., Itoh, S., and Ando, A., 1996, Database on Internet for Geological Survey of Japan, geochemical reference samples: *Geostands Newsletter*, v. 20, p. 161-164.
- Inan, K., 1972, New borate district, Eskisehir-Kirka province, Turkey: *Trans. Instn. Min. Metall. (Sect B: Applied earth sci)*, v. 81, p. B163-165.
- Inan, K., Dunham, A. C., and Esson, J., 1973, Mineralogy, chemistry and origin of Kirka borate deposit, Eskisehir Province, Turkey: *Institution of Mining and Metallurgy Transactions, section B*, v. 82, p. 114-123.
- Irvine, T. N., and Baragar, W. R. A., 1971, A guide to the chemical classification of the common volcanic rocks: *Can. J. Earth. Sci.*, v. 8, p. 523-548.
- Jones, B. F., 1986, Clay mineral diagenesis in lacustrine sediments, in Mumpton, F. A., ed., *Studies in Diagenesis*, 1578, U.S. Geological Survey Bulletin, p. 291-300.
- Kalafatcioglu, A., 1964, Geological Map of Turkey 1:500.000 - Izmir sheet., Institute of mineral research and exploration, Ankara, Turkey.
- Kanzaki, T., Yoshida, M., Nomura, M., Kakihana, H., and Ozawa, T., 1979, Boron isotopic composition of fumarolic condensates and sassolites from Satsuma Iwo-jima, Japan: *Geochimica et Cosmochimica Acta*, v. 43, p. 1859-1863.
- Kay, R. W., 1976, Geochemical constraints on the origin of Aleutian magmas, in Talwani, M., and Pitman, W. C., eds., *Island Arcs, Deep Sea Trenches and Back Arc Basins*, 1, Maurice Ewing Series, p. 229-242.
- Keller, J., 1983, Potassic volcanism of the Mediterranean area: *Journal of Volcanology and Geothermal Research*, v. 18, p. 321-325.
- Keller, J., and Villari, L., 1972, Rhyolitic ignimbrites in the region of Afyon (Central Anatolia): *Bull. Volcanol*, v. 36, p. 342-358.
- Kempton, P. D., Fitton, J. G., Hawkesworth, C. J., and Ormerod, D. S., 1991, Isotopic and trace element constraints on the composition and evolution of the lithosphere beneath the southwestern United States: *Journal of Geophysical Research*, v. 96, p. 13713-13735.
- Keren, R., and Mezuman, U., 1981, Boron absorption by clay minerals using a phenomenological equation: *Clays and Clay Minerals*, v. 29, p. 198-204.
- Keren, R., and O'Connor, G. A., 1982, Effect of exchangeable ions and ionic strength on boron absorption by montmorillonite and illite: *Clays and Clay Minerals*, v. 30, p. 341-346.
- Keren, R., and Talpaz, H., 1984, Boron absorption by montmorillonite as affected by particle size: *Soil Sci. Soc. Am. J.*, v. 48, p. 555-559.
- Kistler, R. B., and Hevaci, C., 1994, Boron and borates, in Carr, D. D., ed., *Industrial minerals and rocks*, Society of Mining, Metallurgy and Exploration, Inc, p. 171-186.
- Kistler, R. B., and Smith, W. C., 1983, Boron and borates, in Lefond, S. J., ed., *Industrial minerals and rocks*, Society of Mining Engineers, New York, p. 533-560.
- Krupp, R. E., and Seward, T. M., 1990, Transport and deposition of metals in the Rokokawa geothermal system, New Zealand: *Mineral. Deposita*, v. 25, p. 73-81.

## References

---

- Kuno, H., 1966, Lateral variation of basalt magma types across continental margins and island arcs: *Bull. Volcanol.*, v. 29, p. 195-222.
- Langmuir, C. H., Bender, J. F., and Batiza, R., 1986, Petrologic and tectonic segmentation of the East Pacific Rise, 5°30'-14°30'N: *Nature*, v. 322, p. 422-429.
- Langmuir, C. H., Bender, J. F., Bence, A. E., Hanson, G. N., and Taylor, S. R., 1977, Petrogenesis of basalts from the FAMOUS area: Mid-Atlantic Ridge: *Earth Planet. Sci. Lett.*, v. 36, p. 133-156.
- Le Bas, M. J., Le Maitre, R. W., and Wooley, A. R., 1992, The construction of the total Alkali-Silica chemical classification of volcanic rocks: *Mineralogy and Petrology*, v. 46, p. 1-22.
- Le Maitre, R. W., Bateman, P., Dudek, A., Keller, J., Le Bas, M. J., Sabine, P. A., Schmid, R., Sorensen, H., Streckeisen, A., Woolley, A. R., and Zanettin, B., 1989, A classification of igneous rocks and glossary of terms: Oxford, Blackwell.
- Leeman, W. P., and Sisson, V. B., 1996, Geochemistry of boron and its implications for crustal and mantle processes, *in* Grew, E. S., and Anovitz, L. M., eds., *Boron, mineralogy, petrology and geochemistry*, 33. *Reviews in Mineralogy*, Mineralogical Society of America, p. 645-707.
- Lofgren, G., 1970, Experimental devitrification rates of rhyolitic glass: *Geol. Soc. Am. Bull.*, v. 81, p. 553-560.
- London, D., and Manning, D. A. C., 1995, Chemical variation and significance of tourmaline from southwest England: *Econ Geol.*, v. 90, p. 495-519.
- London, D., Morgan VI, G. B., and Wolf, M. B., 1996, Boron in granitic rocks and their contact aureoles, *in* Grew, E. S., and Anovitz, L. M., eds., *Boron, mineralogy, petrology and geochemistry*, 33. *Reviews in Mineralogy*, Mineralogical Society of America, p. 299-330.
- Ludington, S., Orris, G. J., Cox, D. P., Long, K. R., and Asher-Bolinder, S., 1992, Mineral deposit models, *Geology and mineral resources of the Altiplano and Cordillera Occidental, Bolivia*, U.S. Geological Survey Bulletin 1975, U.S. Geological Survey and Servicio Geologico de Bolivia, p. 63-89.
- MacLean, W. H., 1988, Rare earth element mobility at constant inter-REE ratios in the alteration zone at the Phelps Dodge massive sulphide deposit, Matagami, Quebec: *Mineral. Deposita*, v. 23, p. 231-238.
- MacLean, W. H., and Barrett, T. J., 1993, Lithogeochemical techniques using immobile elements: *Journal of Geochemical Exploration*, v. 48, p. 109-133.
- MacLean, W. H., and Kranidotis, P., 1987, Immobile elements as monitors of mass transfer in hydrothermal alteration: Phelps Dodge massive sulphide deposit, Matagami, Quebec: *Economic Geology*, v. 82, p. 951-962.
- McGrath, A., 1995, Unpublished data, Personal communication.
- McKenzie, D., 1989, Some remarks on the movement of small melt fractions in the mantle: *Earth and Planetary Science Letters*, v. 95, p. 53-72.
- McKenzie, D., and Bickle, M. J., 1988, The volume and composition of melt generated by extension of the lithosphere: *Journal of Petrology*, v. 29, p. 625-679.
- McKenzie, D., and O'Nions, R. K., 1995, The source regions of Ocean Island Basalts: *Journal of Petrology*, v. 36, p. 133-159.
- McPhie, J., Doyle, M., and Allen, M., 1993, *Volcanic textures: a guide to the interpretation of textures in volcanic rocks*, Hobart Centre for Ore Deposit and Exploration Studies, University of Tasmania.
- Miller, D., M., Langmuir, C. M., Goldstein, S. L., and Franks, A., 1992, The importance of parental magma composition to calc-alkaline and tholeiitic evolution: Evidence from Unmak island in the Aleutians: *J. Geophys. Res.*, v. 97, p. 321-343.
- Milodowski, A. E., and Zalasiewicz, J. A., 1991, Redistribution of rare earth elements during diagenesis of turbidite/hemipelagite mudrock sequences of Llandovery age from central Wales, *in* Morton, A. C., Todd, S. P., and Haughton, P. D. W., eds., *Developments in sedimentary provenance studies*, No. 57, Geological Society Special Publication, p. 101-124.
- Moore, D. M., and Reynolds, R. C., 1989, *X-ray diffraction and identification and analysis of clay minerals*: Oxford, Oxford University Press.
- Moran, A. E., Sisson, V. B., and Leeman, W. P., 1992, Boron depletion during progressive metamorphism: implications for subduction processes: *Earth Planet. Sci. Lett.*, v. 111, p. 331-349.

## References

---

- Morris, J. D., Leeman, W. P., and Tera, F., 1990, The subducted component in island arc lavas: constraints from Be isotopes and B-Be Systematics: *Nature*, v. 344, p. 31-36.
- Mosser, C., 1983, The use of B, Li and Sn in determining the origin of some sedimentary clays: *Chemical Geology*, v. 38, p. 129-139.
- Muessig, S., 1966, Recent South American borate deposits: 2nd Symposium on Salt, Cleveland, Ohio, 1966, p. 151-159.
- Navon, O., Hutcheon, I. D., Rossman, G. R., and Wasserburg, G. J., 1988, Mantle derived fluids in diamond micro-inclusions: *Nature*, v. 335, p. 784-789.
- Noll Jr, P. D., Newsom, H. E., Leeman, W. P., and Ryan, J. G., 1996, The role of hydrothermal fluids in the production of subduction zone magmas: Evidence from siderophile and chalcophile trace elements and boron: *Geochimica et Cosmochimica Acta*, v. 60, p. 587-611.
- Nomura, M., Kanzaki, T., Ozawa, T., Okamoto, M., and Kakihana, H., 1982, Boron isotopic composition of fumarolic condensates from some volcanoes in Japanese island arcs: *Geochimica et Cosmochimica Acta*, v. 46, p. 2403-2406.
- Oi, T., Nomura, M., Ohsaka, T., Okamoto, M., and Kakihana, H., 1989, Boron isotopic compositions of some boron minerals: *Geochimica et Cosmochimica Acta*, v. 53, p. 3189-3195.
- Okay, A. I., Satir, M., Maluski, H., Siyako, M., Monie, P., Metzger, R., and Akyüz, S., 1996, Paleo- and Neo-Tethyan events in northwestern Turkey: Geologic and geochronologic constraints, in Yin, A., and Harrison, T. M., eds., *Tectonic evolution of Asia*, Cambridge University Press, p. 420-441.
- Ormerod, D. S., Hawkesworth, C. J., Rogers, N. W., Leeman, W. P., and Menzies, M. A., 1988, Tectonic and magmatic transitions in the Eastern Great Basin, USA: *Nature*, v. 333, p. 349-353.
- Orris, G. J., Asher-Bolinder, S., Soria-Escalante, E., and Enriquez-Romero, R., 1992, Mineral deposits associated with lakes and salars, Geology and mineral resources of the Altiplano and Cordillera Occidental, Bolivia, U.S. Geological Survey Bulletin 1975, U.S. Geological Survey and Servicio Geológico de Bolivia.
- Özpeker, I., 1969, Western Anatolian borate deposits and their genetic studies (in Turkish): Unpub. PhD thesis, Technical University of Istanbul, Turkey.
- Palmer, and Helvacı, C., 1995, The boron isotope geochemistry of the Kirka borate deposit, western Turkey: *Geochimica et Cosmochimica Acta*, v. 59, p. 3599-3605.
- Palmer, M. R., Spivak, A. J., and Edmond, J. M., 1987, Temperature and pH controls over isotopic fractionation during absorption of boron on marine clay: *Geochimica et Cosmochimica Acta*, v. 51, p. 2319-2323.
- Papke, K. G., 1985, Borates in Nevada, in Barker, J. M., and Lefond, S. J., eds., *Borates: Economic geology and production*, New York, Society of Mining Engineers of the American Institute of Mining, Metallurgical and Petroleum Engineers, Inc., p. 89-100.
- Paton, S., 1992, The relationship between extension and volcanism in western Turkey, the Aegean Sea and central Greece: Unpub. PhD thesis, Cambridge.
- Pe, G. G., and Gledhill, A., 1975, Strontium isotopic ratios in volcanic rocks from the south-eastern part of the Hellenic arc: *Lithos*, v. 8, p. 209-214.
- Pearce, J. A., and Cann, J. R., 1973, Tectonic setting of basic volcanic rocks determined using trace element analyses: *Earth and Planetary Science Letters*, v. 19, p. 290-300.
- Pirajno, F., 1992, *Hydrothermal Mineral Deposits - Principles and Fundamental Concepts for the Exploration Geologist*, Springer-Verlag.
- Pirajno, F., 1995, Volcanic-hosted epithermal systems in northwest Turkey: *S. Afr. J. Geol.*, v. 98, p. 13-24.
- Puecker-Ehrenbrink, B., Hoffman, A. W., and Hart, S. R., 1994, Hydrothermal lead transfer from mantle to continental crust: the role of metalliferous sediments: *Earth Planet. Sci. Lett.*, v. 125, p. 129-142.
- Quisefit, J. P., Toutain, J. P., Bergametti, G., Javoy, M., Cheynet, B., and Person, A., 1989, Evolution versus cooling of gaseous volcanic emissions from Momotombo volcano, Nicaragua: Thermochemical model and observations: *Geochimica et Cosmochimica Acta*, v. 53, p. 2591-2608.
- Rettig, S. L., Jones, B. F., and Risacher, F., 1980, Geochemical evolution of brines in the salar of uyuni, Bolivia: *Chemical Geology*, v. 30, p. 57-79.

## References

---

- Rex, D. C., and Guise, P. G., 1986, Age of the Tinto felsite, Lanarkshire: a possible  $^{40}\text{Ar}$  -  $^{39}\text{Ar}$  monitor.: *Bulletin of Liason and Information.*, v. I.G.C.P. Project 196.
- Rex, D. C., Guise, P. G., and Wartho, J.-A., 1993, Disturbed  $^{40}\text{Ar}$  -  $^{39}\text{Ar}$  spectra from hornblendes: thermal loss or contamination?: *Chemical Geology*, v. 103, p. 271-281.
- Richardson-Bunbury, J. M., 1992, The basalts of Kula: Unpub. PhD thesis, Cambridge.
- Risacher, F., and Fritz, B., 1991, Geochemistry of Bolivian salars, Lipez, southern Altiplano: Origin of solutes and brine evolution: *Geochimica et Cosmochimica Acta*, v. 55, p. 687-705.
- Robert, U., Foden, J., and Varne, R., 1992, The Dodecanese Province, SE Aegean: A model for tectonic control on potassic magmatism: *Lithos*, v. 28, p. 241-260.
- Robertson, A. H. F., and Dixon, J. E., 1984, Introduction: aspects of the geological evolution of the Eastern Mediterranean, in Dixon, J. E., and Robertson, A. H. F., eds., *The geological evolution of the Eastern Mediterranean*, For The Geological Society by Blackwell Scientific Publications.
- Robertson, A. H. F., Dixon, J. E., Brown, S., Collins, A., Morris, A., Pickett, E., Sharp, I., and Ustaömer, T., 1996, Alternative tectonic models for the Late Palaeozoic-Early Tertiary development of Tethys in the Eastern Mediterranean region, in Morris, A., and Tarling, D. H., eds., *Palaeomagnetism and Tectonics of the Mediterranean Region*, 105, Geological Society Special Publication, p. 239-263.
- Rogers, N. W., 1992, Potassic magmatism as a key to trace element enrichment processes in the upper mantle: *Journal of Volcanology and Geothermal Research*, v. 50, p. 85-99.
- Rogers, N. W., De Mulder, M., and Hawkesworth, C. J., 1992, An enriched mantle source for potassic basanites: evidence from Karisimbi volcano, Virunga province, Rwanda: *Contributions to Mineralogy and Petrology*, v. 111, p. 543-556.
- Rogers, N. W., Hawkesworth, C. J., Parker, R. J., and Marsh, J. S., 1985, The geochemistry of potassium lavas from Vulsini, Central Italy and implications for mantle enrichment processes beneath the Roman region: *Contributions to Mineralogy and Petrology*, v. 90, p. 244-257.
- Rollinson, H. R., 1993, *Using geochemical data: evaluation, presentation, interpretation*, Longman Singapore Publishers (Pte) Ltd.
- Ryan, J. G., and Langmuir, C. H., 1987, The Systematics of lithium abundances in young volcanic rocks: *Geochimica et Cosmochimica Acta*, v. 51, p. 1727-1741.
- Ryan, J. G., and Langmuir, C. H., 1993, The Systematics of boron abundances in young volcanic rocks: *Geochim. Cosmochim. Acta*, v. 57, p. 1489-1498.
- Ryan, J. G., Leeman, W. P., Morris, J. D., and Langmuir, C. H., 1996, The boron Systematics of intraplate lavas: Implications for crust and mantle evolution: *Geochimica et Cosmochimica Acta*, v. 60, p. 415-422.
- Satir, M., and Friedrichsen, H., 1986, The origin and evolution of the Menderes Massif, W-Turkey: A rubidium/strontium and oxygen isotope study: *Geologische Rundschau*, v. 75/3, p. 703-714.
- Saunders, A. D., Norry, M. J., and Tarney, J., 1991, Fluid influence on the trace element composition of subduction zone magmas: *Phil. Trans. R. Soc. Lond. A*, v. 335, p. 377-392.
- Scaillet, B. F.-L., C., and Le Fort, P., 1990, Badrinath-Gangotri plutons (Gharwal, India): petrological and geochemical evidence for fractionation processes in a high Himalayan leucogranite: *J Volc Geotherm Res*, v. 44, p. 163-188.
- Scott, B. C., 1993, The Sarikaya borax deposit, Turkey and a comparison with the Kramer borax deposit, USA, Personal Communication.
- Sengör, A. M. C., Görür, N., and Saroglu, F., 1985, Strike-slip deformation basin formation and sedimentation: Strike-slip faulting and related basin formation in zones of tectonic escape: Turkey as a case study: *Society of Economic Palaeontologists and Mineralogist, Special Publication*, v. 37, p. 227-64.
- Sengör, A. M. C., Satir, M., and Akkök, R., 1984b, Timing of tectonic events in the Menderes Massif, western Turkey: implications for tectonic evolution and evidence for Pan-African basement in Turkey: *Tectonics*, v. 3, p. 693-707.
- Sengör, A. M. C., and Yılmaz, Y., 1981, Tethyan evolution of Turkey: A plate tectonic approach: *Tectonophysics*, v. 75, p. 181-241.

## References

---

- Sengör, A. M. C., Yilmaz, Y., and Sungurlu, O., 1984a, Tectonics of the Mediterranean Cimmerides: nature and evolution of the western termination of Palaeo-Tethys, *in* Dixon, J. E., and Robertson, A. H. F., eds., The geological evolution of the Eastern Mediterranean, For The Geological Society by Blackwell Scientific Publications.
- Seyfried Jr, W. E., Janecky, D. R., and Mottl, M. J., 1984, Alteration of the oceanic crust: Implications for geochemical cycles of lithium and boron: *Geochimica et Cosmochimica Acta*, v. 48, p. 557-569.
- Seyitoglu, G., 1997, Late Cenozoic tectano-sedimentary development of the Selendi and Usak-Güre basins: a contribution to the discussion on the development of east-west and north trending basins in western Turkey: *Geol. Mag.*, v. 134 (2), p. 163-175.
- Seyitoglu, G., Anderson, D., Nowell, G., and Scott, B., 1997, The evolution from Miocene potassic to Quaternary sodic magmatism in western Turkey: implications for enrichment processes in the lithospheric mantle: *Journal of Volcanology and Geothermal Research*, v. 76, p. 127-147.
- Seyitoglu, G., and Scott, B. C., 1991, Late Cenozoic crustal extension and basin formation in west Turkey: *Geological Magazine*, v. 128, p. 155-166.
- Seyitoglu, G., and Scott, B. C., 1992a, The age of the Büyük Menderes graben (west Turkey) and its tectonic implications: *Geological Magazine*, v. 129, p. 239-242.
- Seyitoglu, G., and Scott, B. C., 1992b, Late Cenozoic volcanic evolution of the NE Aegean region: *Journal of Volcanology and Geothermal Research*, v. 54, p. 157-176.
- Seyitoglu, G., Scott, B. C., and Rundle, C. C., 1992, Timing of Cenozoic extensional tectonics in west Turkey: *Journal of the Geological Society, London*, v. 149, p. 533-538.
- Shaw, D. M., and Sturchio, N. C., 1992, Boron-lithium relationships in rhyolites and associated thermal waters of young silicic calderas, with comments on incompatible element behaviour: *Geochimica et Cosmochimica Acta*, v. 56, p. 3723-3731.
- Sheppard, R. A., and Gude, A. J., 1969, Diagenesis of tuffs in the Barstow Formation, Mud Hills, San Bernardino County, California: *Geological Survey Professional Paper*, v. 634, p. 1-34.
- Sheppard, R. A., and Gude, A. J., 1973, Boron-bearing potassium feldspar of authigenic origin in closed-basin deposits: *Jour. Research U.S. Geol. Survey*, v. 1, p. 377-382.
- Shevenell, L., and Goff, F., 1995, Evolution of hydrothermal waters at Mount St. Helens, Washington, USA: *Journal of Volcanology and Geothermal Research*, v. 69, p. 73-94.
- Siefke, J. W., 1985, Geology of the Kramer borate deposit, Boron, California, *in* Barker, J. M., and Lefond, S. J., eds., *Borates: Economic geology and production*, New York, Society of Mining Engineers of the American Institute of Mining, Metallurgical and Petroleum Engineers, inc., p. 157-166.
- Smith, C. L., Ficklin, W. H., and Thompson, J. M., 1987, Concentrations of arsenic, antimony and boron in steam and steam condensates at the Geysers, California: *Journal of Volcanology and Geothermal Research*, v. 32, p. 329-341.
- Smith, G. I., 1979, Subsurface stratigraphy and geochemistry of Late Quaternary evaporites, Searles Lake, California: *Geological Survey Professional Paper*, v. 1043, p. 1-122.
- Smith, G. I., 1985, Borate deposits in the United States: Dissimilar in Form, Similar in Geologic Setting, *in* Barker, J. M., and Lefond, S. J., eds., *Borates: Economic geology and production*, New York, Society of Mining Engineers of the American Institute of Mining, Metallurgical and Petroleum Engineers, Inc., p. 37-52.
- Smith, G. I., and Medrano, M. D., 1996, Chapter 6 Continental borate deposits of Cenozoic age, *in* Grew, E. S., and Anovitz, L. M., eds., *Boron, mineralogy, petrology and geochemistry*, 33. *Reviews in Mineralogy*, Mineralogical Society of America, p. 263-298.
- Smith, R. E., and Smith, S. E., 1976, Comments on the use of Ti, Zr, Y, Sr, K, P and Nb in classification of basaltic magmas: *Earth and Planetary Science Letters*, v. 32, p. 114-120.
- Stamatakis, M. G., 1989, Authigenic silicates and silica polymorphs in the Miocene saline-alkaline deposits of the Karlovassi Basin, Samos, Greece: *Economic Geology*, v. 84, p. 788-798.
- Stamatakis, M. G., and Economou, G. S., 1991, A colemanite and ulexite occurrence in a Late Miocene saline-alkaline lake of west Samos Island, Greece: *Economic Geology*, v. 86, p. 166-172.

## References

---

- Stamatakis, M. G., Hein, J. R., and Magganas, A. C., 1989, Geochemistry and diagenesis of Miocene lacustrine siliceous sedimentary and pyroclastic rocks, Mytilinii basin, Samos Island, Greece: *Sedimentary Geology*, v. 64, p. 65-78.
- Stampfli, G., Marcoux, J., and Baud, A., 1991, Tethyan margins in space and time: *Palaeogeography, Palaeoclimatology, Palaeoecology*, v. 87, p. 373-410.
- Steffens, P., 1971, Remarks on the Upper Cenozoic of West Anatolia: *Newsletter Stratigraphy*, v. 1-3, p. 47-50.
- Steiger, R., and Jager, E., 1977, Convention on use of decay constants in geo- and cosmochemistry: *Earth Planet. Sci. Lett.*, v. 36, p. 359-362.
- Stix, J., Layne, G. D., and Spell, T. L., 1995, The behaviour of light lithophile and halogen elements in felsic magma: geochemistry of the post-caldera Valles Rhyolites, Jemez Mountains Volcanic Field, New Mexico: *Journal of Volcanology and Geothermal Research*, v. 67, p. 61-77.
- Stouraiti, C., 1995, Geochemistry and petrogenesis of the Serifos Granite, in relation to other Aegean Granitoids: Unpub. PhD thesis, University of Leicester.
- Stubican, V., and Roy, R., 1962, Boron substitution in synthetic micas and clays: *The American Mineralogist*, v. 47, p. 1166-1173.
- Sun, S. S., 1980, Lead isotope study of young volcanic rocks from mid-ocean ridges, ocean islands and island arcs: *Phil Trans R. Soc. Lond.*, v. A297, p. 409-445.
- Sun, S. S., and McDonough, W. F., 1989, Chemical and isotopic Systematics of oceanic basalts: implications for mantle composition and processes, in Saunders, A. D. a. N., M. J. (Editors), ed., *Magmatism in the ocean basins*, 42, Geological Society of London, Special Publication, p. 313-345.
- Sunder, M. S., 1980, Geochemistry of the Sarikaya borate deposits (Kirka-Eskisehir) (in Turkish): *Bulletin of the Geological Congress of Turkey*, v. 2, p. 19-34.
- Surdam, R. C., 1977, Zeolites in closed hydrologic systems, in Mumpton, F. A., ed., *Mineralogy and geology of natural zeolites*, 4. Reviews in Mineralogy, Mineralogical Society of America Short Course Notes.
- Tarney, J. T., and Marsh, N. G., 1991, Major and trace element geochemistry of holes CY-1 and CY-4: implications for petrogenetic models, in Gibson, I. L., Malpas, J., Robinson, P. T., and Xenophontos, C., eds., *Cyprus crustal study project: initial report, holes CY-1 and 1a*, Paper 90-20, Geological Survey of Canada, p. 133-176.
- Taylor, S. R., and McLennan, S. H., 1985, *The continental crust: its composition and evolution*, Blackwell, Oxford.
- Thompson, R. N., Leat, P. T., Dickin, A. P., Morrison, M. A., Hendry, G. L., and Gibson, S. A., 1989, Strongly potassic mafic magmas from lithospheric mantle sources during continental extension and heating: evidence from Miocene minettes of northwest Colorado, USA: *Earth and Planetary Science Letters*, v. 98, p. 139-153.
- Thorpe, R. S., Francis, P. W., and O'Callaghan, L., 1984, Relative roles of source composition, fractional crystallisation and crustal assimilation in the petrogenesis of Andean volcanic rocks: *Phil Trans R. Soc. Lond.*, v. A310, p. 675-692.
- Turner, S., Arnaud, N., Liu, J., Rogers, N., Hawkesworth, C., Harris, N., Kelley, S., Van Calsteren, P., and Deng, W., 1996, Post-collision, shoshonitic volcanism on the Tibetan Plateau: implications for convective thinning of the lithosphere and the source of ocean island basalts: *Journal of Petrology*, v. 37, p. 45-71.
- van de Kamp, P. C., and Leake, B. E., 1996, Petrology, geochemistry, and Na metasomatism of Triassic-Jurassic non-marine clastic sediments in the Newark, Harford, and Deerfield rift basins, northeastern USA: *Chemical Geology*, v. 133, p. 89-124.
- Velde, B., 1995, Composition and mineralogy of clay minerals, in Velde, B., ed., *Origin and mineralogy of clays, clays and the environment*, Springer, p. 8-42.
- Velde, B., and Meunier, A., 1987, Petrologic phase equilibria in natural clay systems, in Newman, A. C. D., ed., *Chemistry of clays and clay minerals*, Mineralogical Society Monograph 6, Longman Scientific and Technical, p. 423-458.
- Verge, N., 1995, Personal communication.
- Webster, J. D., and Duffield, W. A., 1991, Volatiles and lithophile elements in Taylor Creek Rhyolite: constraints from glass inclusion analysis: *American Mineralogist*, v. 76, p. 1628-1645.

## References

---

- Webster, J. D., Holloway, J. R., and Hervig, R. L., 1989, Partitioning of lithophile trace elements between H<sub>2</sub>O and H<sub>2</sub>O + CO<sub>2</sub> fluids and topaz rhyolite melt: *Econ Geol*, v. 84, p. 116-134.
- Wernicke, B. P., Christiansen, R. L., England, P. C., and Sonder, L. J., 1987, Tectonomagmatic evolution of Cenozoic extension in the North American Cordillera, in Coward, M. P., Dewey, J. F., and Hancock, P. L., eds., *Continental Extensional Tectonics*, 28, *Geol. Soc. London Spec. Publ.*, p. 203-221.
- White, A. F., Chuma, N. J., and Goff, F., 1992, Mass transfer constraints on the chemical evolution of an active hydrothermal system, Valles caldera, New Mexico: *Journal of Volcanology and Geothermal Research*, v. 49, p. 233-253.
- White, D. E., Muffler, L. J. P., and Truesdell, A. H., 1971, Vapor-dominated hydrothermal systems compared with hot water systems: *Econ Geol*, v. 66, p. 75-97.
- Wright, T. L., 1971, Chemistry of Kilauea and Mauna Loa lavas in space and time: U.S. Geol. Survey. Prof. Paper, v. 735.
- Wright, T. L., Swanson, D. A., and Duffield, W. A., 1975, Chemical compositions of Kilauea east rift lavas: *Journal of Petrology*, v. 16, p. 110-133.
- Yalçın, H., 1989, Stratigraphic and tectonic features of Kirka (Eskisehir) volcanosedimentary lacustrine basin of Neogene age (in Turkish): *Faculty of Engineering Bulletin, Cum, University, Serie A. Earth Sciences*, v. 6, 7, p. 165-181.
- Yalçın, H., and Baysal, O., 1991, The geological location, distribution, and origin of the kirka borate deposits (in Turkish): *MTA Journal*, v. 113, p. 93-104.
- Yalçın, H., and Gündoğdu, M. N., 1985, Emet Neogene lacustrine basin clay minerals (in Turkish): *National Clay Symposium, Ankara, Turkey, 1985*, p. 155-169.
- Yalçın, H., and Gündoğdu, M. N., 1987, Mineralogic-petrographic investigation of Emet lacustrine volcanosedimentary basin of Neogene age: formation and distribution of neoformation minerals (in Turkish): *Bulletin of Earth Sciences Application and research Centre of Hacattepe University*, v. 14, p. 45-61.
- Yalçın, H., Gündoğdu, M. N., and Liewig, N., 1989a, Clay mineralogy and geochemistry of Kirka Neogene lacustrine basin. Relationships between smectites and carbonate minerals (in Turkish): *Clay symposium, Sivas, Turkey, 1989a*.
- Yalçın, H., Gündoğdu, M. N., and Liewig, N., 1989b, Distribution, diagenetic evolution and occurrence of neoformation minerals in Kirka (Eskisehir) volcanosedimentary lacustrine basin of Neogene age, north-western Anatolia, Turkey: *EUG V, Strasbourg, 1989b*, p. 294.
- Yalçın, H., Gündoğdu, M. N., and Liewig, N., 1989c, Relationships between smectite and carbonate in the Kirka volcanosedimentary lacustrine basin, Eskisehir, Turkey: *9th International Clay Conference, Strasbourg, 1989c*, p. 437.
- Yalçın, H., Gündoğdu, M. N., and Liewig, N., 1991, Investigation of diagenetic silicate and carbonate minerals in the Kirka basin (in Turkish): *Faculty of Engineering, Cum University. Serie A. Earth Sciences Serie A*, v. 8, p. 31-45.
- Yalçın, H., Liewig, N., Bayhan, H., and Gündoğdu, M. N., 1990, Geochronology and geochemistry of volcanic and pyroclastic rocks of the Kirka area, northwestern Turkey: *International Volcanological Congress, Mainz, 1990*.
- Yalçın, H., Semelin, B., and Gündoğdu, M. N., 1985, Geological investigation of Emet lacustrine basin of Neogene age (south of Hisarcık) (in Turkish): *Bulletin of Earth Sciences Application and Research Centre of Hacattepe University*, v. 12, p. 39-52.
- Yilmaz, Y., 1989, An approach to the origin of young volcanic rocks of western Turkey, in Sengör, A. M. C., ed., *Tectonic evolution of the Tethyan Region*, Kluwer Academic Publishers, p. 159-189.
- Yilmaz, Y., 1990, Comparison of young volcanic associations of western and eastern Anatolia formed under a compressional regime: a review: *Journal of volcanology and Geothermal Research*, v. 44, p. 69-77.
- You, C. F., Spivak, A. J., Smith, J. H., and Gieskes, J. M., 1993, Mobilisation of boron in convergent margins: Implications for the boron geochemical cycle: *Geology*, v. 21, p. 207-210.

# APPENDICES

	Page numbers
<b>Appendix A - sample locations on maps</b>	<b>A1 - A4</b>
Figure A1 (sample locations in USE area)	A1
Figure A2 (sample locations in Emet Basin)	A2
Figure A3 (sample locations in Kirka and Afyon areas)	A3
Figure A4 (sample locations in Kirka Basin)	A4
<b>Appendix B - sample localities (grid references)</b>	<b>B1 - B3</b>
<b>Appendix C - summary of analytical techniques used</b>	<b>C1 - C4</b>
<b>Appendix D - petrology of samples</b>	<b>D1 - D4</b>
<b>Appendix E - K-Ar dating</b>	<b>E 1</b>
Sample preparation	E1
Analytical procedure	E1
Results	E1
<b>Appendix F - <math>^{40}\text{Ar}/^{39}\text{Ar}</math> dating</b>	<b>F1 - F2</b>
Analytical procedure	F1
Results	F1
Figure F1 (Ar spectra)	F2
<b>Appendix G (XRD)</b>	<b>G1 - G5</b>
Sample preparation	G1
Analytical conditions	G1
Results	G1 - G3
Clay identification	G3
Figure G1 (examples of XRD spectra)	G4
Figure G2 (example of XRD spectrum)	G5
<b>Appendix H (electron microprobe analysis)</b>	<b>H1 - H17</b>
Procedural details	H1
Electron microprobe data	H1 - H17
<b>Appendix I (XRF, PGAA, ICP-AES)</b>	<b>I1 - I38</b>
Sample preparation and analytical procedure	I1-I3
Accuracy and precision (of XRF, PGAA & ICP-AES)	I3-4
Table I1 (XRF data from granitic and volcanic rocks of the USEKA area)	I5 - I19
Table I2 (XRF data from volcanoclastic sediments of the USEKA area)	I20 - I25
Table I3 (As, Sr & Li concentrations of USEKA sediments)	I26 - I29
Table I4 (XRF major element international standard data)	I30 - I31

---



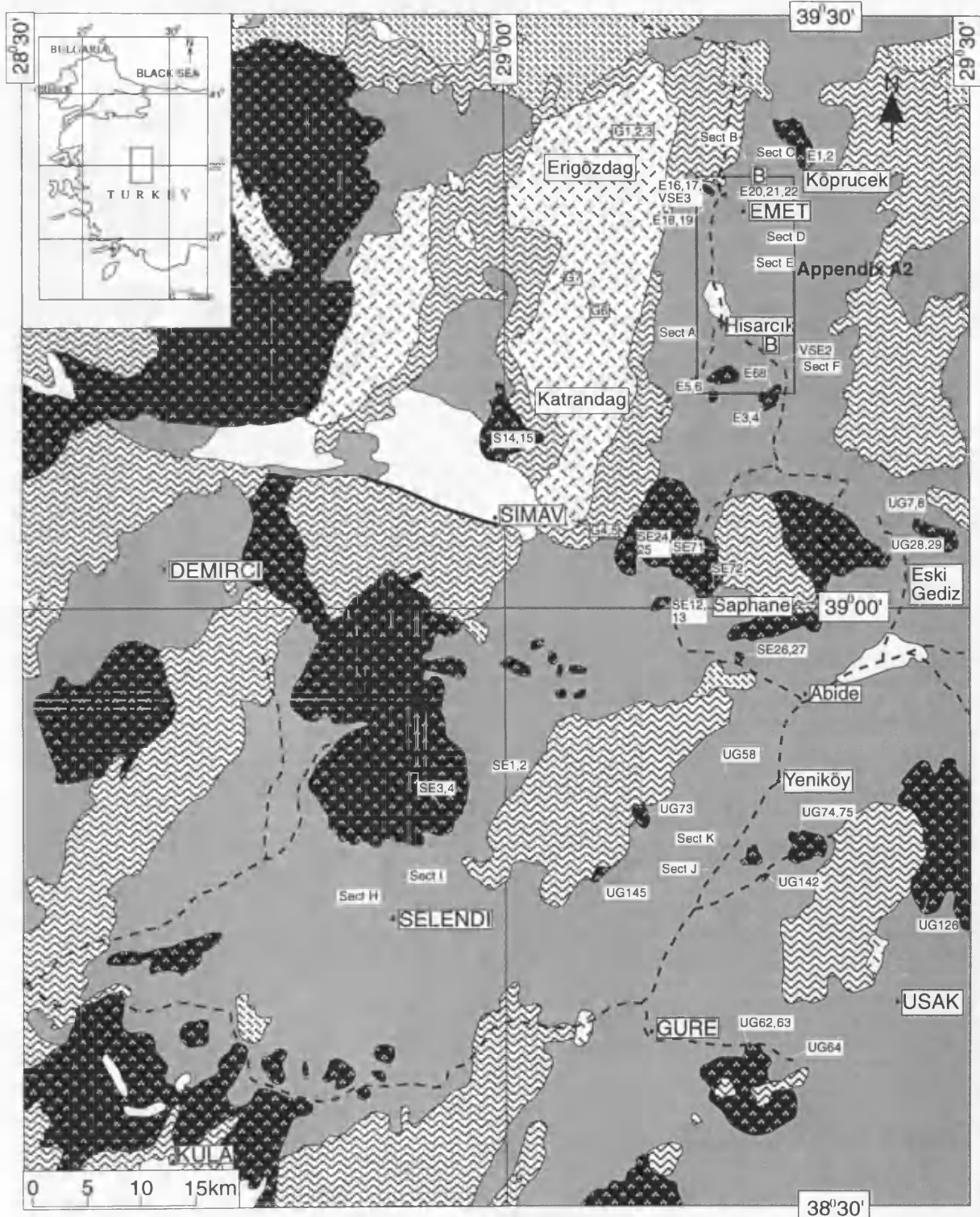
## Appendices

---

Table I5 (XRF trace element international standard data)	I32 - I33
Figure I1 (powder pellet TiO <sub>2</sub> vs fusion bead TiO <sub>2</sub> )	I34
Figure I2 (XRF accuracy plots)	I35
Figure I3 (XRF precision plots)	I36
Figure I4 (comparison of XRF & ICP-AES data)	I37
Table I6 (accuracy & precision of PGAA & ICP-AES)	I38
<b>Appendix J - Nd &amp; Sr isotope data</b>	<b>J1 - J2</b>
Analytical procedure	J1
Results	J1 - J2

---

Figure A1 - sample localities of the Usak, Selendi and Emet area



### LEGEND

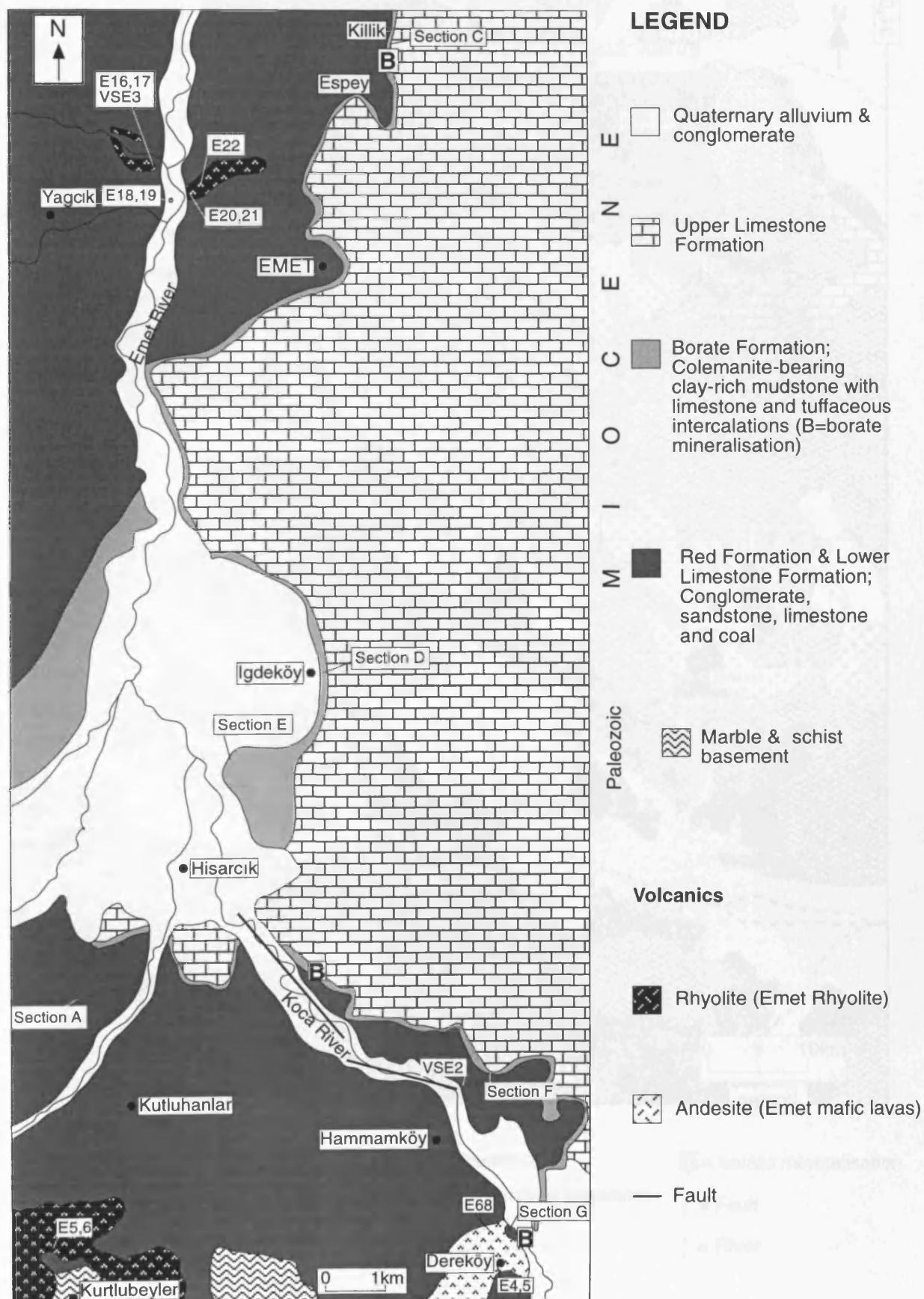
- Quaternary alluvium
- Neogene sediments
- Miocene volcanics
- Erigöz Granite

- Ultramafics
- Paleozoic & Permian basement

- Borate mineralisation
- Fault
- River

Based on MTA geological map 1:500,000 Izmir sheet (Kalafatcioglu 1964)





Figure A2 - sample locations for the Emet area

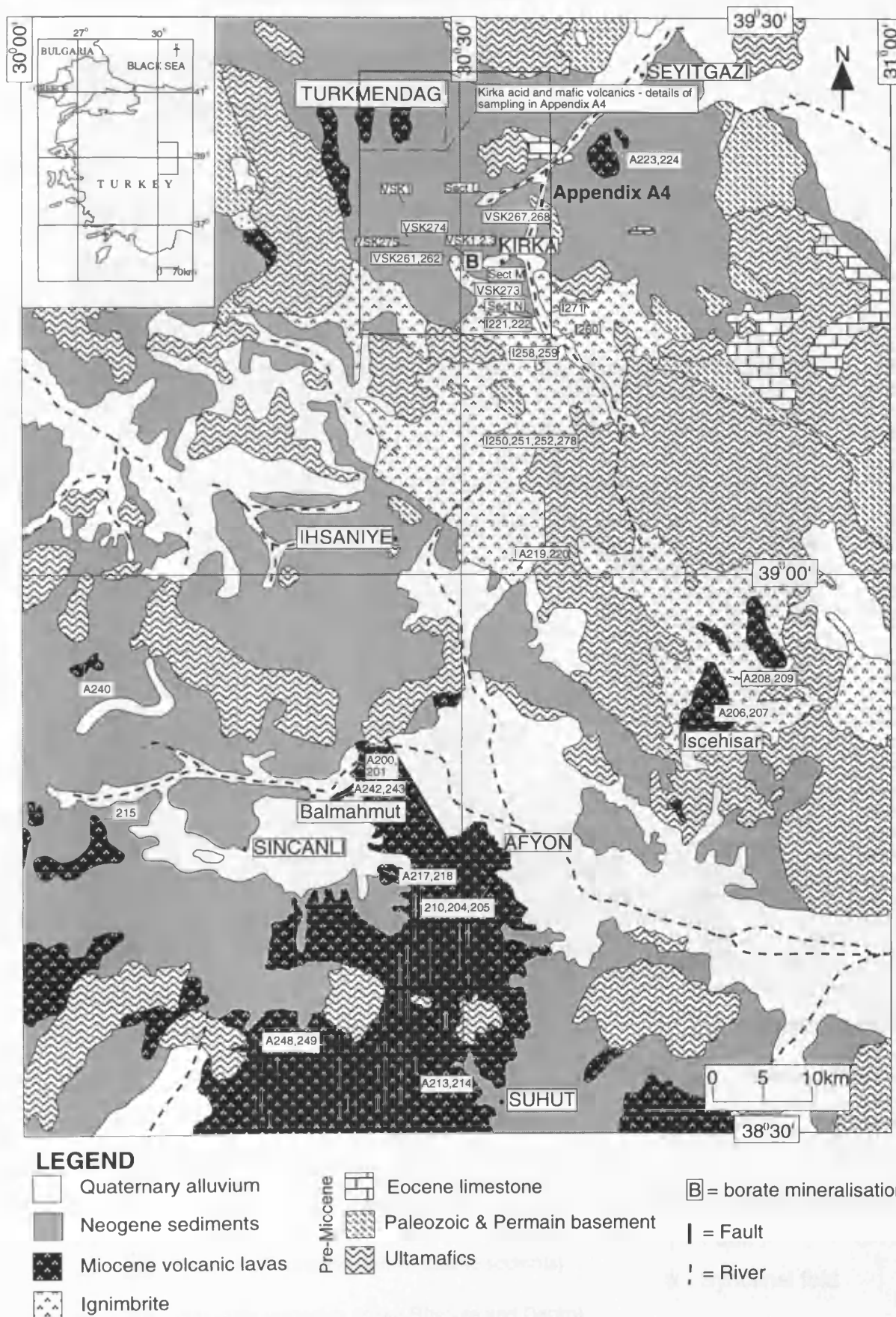


**Figure A3 - sample localities of the Kirka and Afyon areas**



Based on MTA geological map 1:500,000 Ankara sheet (Erentöz 1963)

- PRE-MIOCENE
-  Eocene basement
  -  Mesozoic basement
  -  Paleozoic basement
-  borate mineralisation
- | Fault
- \* Synclinal fold

## SAMPLE LOCALITIES

(co-ordinates from the grid system on Turkish topographical maps)

### ERİĞÖZ GRANITE

G 1, G 2, - from the northern area of the pluton at Kusoyunagi Tepe, approx 6 km west of Eriğöz (855,655 Kütahya J22).  
G 7, G 8 - from the central portion of the pluton, 3 km east of Darci (751,490 Kütahya J22).  
G 4, G 5, G 23 - from the southern portion of the pluton, located to the east of the town Simav, 3.4 km from the turn off outside Simav along the Simav-Abide road (765, 295 Kütahya J22).

### VOLCANICS WITHIN EMET BASIN

#### Emet Rhyolites

E 1, E 2 - from the northern area of the basin at Köprücek (001,608 Kütahya J22).  
E 5, E 6 - from the southern area of the basin 0.5 km north-west of Kurtubeyler (905,406 Kütahya J22).  
E 16, E 17 - from the north-western area of the basin 1.5 km north-east of Yagcık (917,593 Kütahya J22).  
E 18, E 19 - from the north-western area of the basin 2 km east of Yagcık. Located on the western side of Emet river (921,585 Kütahya J22).  
E 20, E 21, E 22 - from the north-western area of the basin 2.5 km east of Yagcık and just east of Emet river (923,587 Kütahya J22).

#### Emet Latite & Shoshonite

E 3, E 4 - from the southern area of the basin west of Dereköy (978,393 Kütahya J22).

*Additional sample collected by BHP Minerals geologists*

E68 - from the southern area of the basin, north of Dereköy (976,4142 Kütahya J22).

### SEDIMENTS IN THE EMET BASIN

**Section A** - from the southern area of the basin, 600m to west of Beyköy and just to the south-eastern side of the Simav-Hisarçık road (903,448 Kütahya J22).  
VSE 1 - 5.4 m (Figure 2.3 in main text).

**Section B** - from the northern area of the basin, approx 4 km north of Emet (942,624 Kütahya J22).  
VSE 4 - 1 m (Figure 2.3 in main text).

*Additional samples from the Red Formation*

VSE 2 - from the southern area of the basin, approx 1 km north-east of Hammamköy (970,437 Kütahya J22).

VSE 3 - from north-western area of basin, 1.5 km north-east of Yagcık (918,594 Kütahya J22).

**Section Lower C** - from the northern area of basin, 4 km west of Köprücek Tepe and 1.5 km north-west of Çalcaagil (956,621 Kütahya J22).  
VSE 5 - 103-104.8 m, VSE 6 - 106.6-108.4 m, VSE 7 - 117.4-119.2 m, VSE 8 - 128 m, VSE 9 - 130-131.8 m, VSE 10 - 137.2-139 m (Figures 2.3 & 4.8 in main text). Additional samples taken from every 1.8 m of section.

**Section Upper C** - from the northern area of basin, 4 km west of Köprücek Tepe and 1.5 km north-west of Çalcaagil (956,621 Kütahya J22).  
VSE 11 - 146-147.8, VSE 12 - 147.8-149.4 m, VSE 13 - 151.2-153, VSE 14 - 151.2-153 m, VSE 15 - 153-154.8 m, VSE 16 - 154.8-156.6 m (Figures 2.3 & 4.8 in main text). Additional samples taken from every 1.8 m of section.

**Section D** - from mid area of basin, 1 km east of Igdeköy (954,504 Kütahya J22).  
VSE 17 - 155.8-157.6 m (Figures 2.3 & 4.8 in main text). Additional samples taken from every 1.8 m of section.

**Section E** - from mid area of basin, just after road forks at Köprübası Tepe, approx 2 km north of Hisarçık (925,497 Kütahya J22).  
VSE 18 - 142-143.8 m, VSE 19 - 147.4-149.2 m, VSE 20 - 152.8-154.6 m (Figures 2.3 & 4.8 in main text). Additional samples taken from every 1.8 m of section.

**Section F** - from southern area of basin, 1 km north-east of Hammamköy village, to the east of Emet river (976,435 Kütahya J22).  
VSE 21 - 121-122.8 m, VSE 22 - 130 m (Figures 2.3 & 4.8 in main text). Additional samples taken from every 1.8 m of section.

**Section G** - from southern area of the basin, 1 km north-east of Dereköy, just to west of Emet river (983,402 Kütahya J22).  
VSE 23 - 151-152 m (Figures 2.3 & 4.8 in main text). Additional samples taken from every 1 m of section.

### VOLCANICS TO THE SOUTH AND WEST OF EMET BASIN (SELENDİ, USAK-GÜRE & SIMAV BASINS)

#### Rhyolites

UG 28, UG 29 - from the northern most part of the Güre/Usak basin 0.8 km north-west of Eski Gediz on road to Akcaalan. (081,252 Kütahya J22)  
SE 1 & SE 2 - from Selendi Basin, 1 km north-east of Yaikarieskin village, approx 6 km east of Yumru Dagı (714,025 Usak K21).



## APPENDIX B (grid references of sample localities)

*SE 24, SE 25* - from the approximate boundary between Emet and Selendi Basins, 0.5 km SE of Taslik village, on Kocakaya Tepe. (833,266 Kütahya J22)

### K-Trachytes

*SE 3, SE 4* - 1 km to east of Yumru Dagı (666,029 Usak K21).

### Andesite, latite & shoshonite

*UG 7, UG 8* - from the north-west of Eski Gediz, which lies just to the south-east of Emet basin and in the northern most part of Güre/Usak basin. Sample taken from beside main road to Kütahya 2.2 km from junction at Eski Gediz (098, 266 Kütahya J22).

*SE 12, SE 13* - from the northern most part of the Selendi basin 1.5 km south-west of Saphane (912,204 Kütahya J22)

*SE 26, SE 27* - from the northern most area of Selendi Basin, 6.6 km by road from Abide along the

main Simav-Abide road (938, 148 Usak K22).

*SI 14, SI 15* - from Simav Basin, at Nasa village (703,364 Kütahya J21).

*Additional samples collected by BHP Minerals geologists;*

### Rhyolites

*SE 72* - from the approximate boundary between Emet and Selendi Basins, at Saphane (926,2143 Kütahya J22).

*SE 71* - from the approximate boundary between Emet and Selendi Basins north-west of Saphane (906,2343 Kütahya J22).

### Dacites & K-Trachytes

*UG 58* - from the Usak/Güre Basin (966,0143 Usak K22).

*UG 62, UG 63* - from the southern area of the Usak/Güre Basin, east of Güre (966,7942 Usak K22).

*UG 64* - from the southern area of the Usak/Güre Basin (007,7942 Usak K22).

*UG 66, UG 67* - from the southern area of the Usak/Güre Basin (856,6142 Usak K22).

*UG 74, UG 75* - from the southern area of the Usak/Güre Basin (996,9842 Usak K22).

*UG 126* - from the Usak/Güre Basin (127,9542 Usak K22).

### Andesite & latite

*UG 65* - from the southern area of the Usak/Güre Basin (876,6542 Usak K22).

*UG 73* - from the southern area of the Usak/Güre Basin (876,9842 Usak K22).

*UG 142* - from the Usak/Güre Basin (966,9442 Usak K22).

*UG 145* - from the Usak/Güre Basin (826,9442 Usak K22).

## SEDIMENTS IN SELENDI BASIN

**Section H** - 1 km east of Yukarıgüllüce village. 548,900 (Usak K21)

*VSS 1* - 3.6-5.4 m (Figure 2.4). Additional samples taken from every 1.8 m of section.

**Section I** - 3 km north of Selendi, just to west of small river (612,930 Usak K21).

*VSS 2* - 16.2-18 m (Figure 2.4). Additional samples taken from every 1.8 m of section.

## SEDIMENTS IN USAK-GÜRE BASIN

**Section J** - 2 km south-west of Derbent (907,935 Usak K22)

*VSUG 1* - 5.4-5.6 m, (Figure 2.5). Additional samples taken from every 1.8 m of section.

**Section K** - 0.5 km north of Derbent (917,955 Usak K22).

*VSUG 2* - 10.8-12.6 m, (Figure 2.5). Additional samples taken from every 1.8 m of section.

## VOLCANICS OF THE KIRKA AREA

### Kirka Ignimbrite

*I 208, I 209* - from south-east of Kirka Basin 1.5 km north north-west of Seyidler village (119,079 Eskisehir J25).

*I 219, I 220* - from south of Kirka Basin 800 m north-west of Ayazini village (892,218 Eskisehir J25).

*I 221, I 222* - from south of Kirka Basin 1 km south-west of Fetiye village (869,444 Eskisehir J25).

*I 250* - from south of Kirka Basin 200 m west of main Afyon-Kirka road, Köroglukalesi Tepe (898,298 Eskisehir J25).

*I 251, I 252* - from south of Kirka Basin just to west of main road, Köroglukalesi Tepe (901,297 Eskisehir J25).

*I 258, I 259* - from southern area of Kirka Basin approx 2 km north of Büyükyayla (895,419 Eskisehir J25).

*I 260* - from southern area of Kirka Basin west of the village of Kümbet (922,426 Eskisehir J25).

*I 271* - from south-eastern area of Kirka Basin north-east of Karaören village, to east of river (924,463 Eskisehir J25).

### Kirka Rhyolites, Trachytes & Dacites

*K 227, K 228* - from northern area of Kirka Basin 1 km north-east of Bozbel Tepe (798,672 Eskisehir J24).

*K 229, K 230* - from northern area of Kirka Basin 1.5 km north-west of Bozbel Tepe (773,677 Eskisehir J24).

*K 231, K 232* - from northern area of Kirka Basin 2 km north of Bozbel Tepe (781,681 Eskisehir J24).

*K 233* - from northern area of Kirka Basin 2 km north of Bozbel Tepe (783,682 Eskisehir J24).

*K 234, K 235* - from northern area of Kirka Basin in river gully 2 km north-east of Bozbel Tepe (796,680 Eskisehir J24).

*K 236* - from northern area of Kirka Basin 1.5 km north north-east of Bozbel Tepe (788,679 Eskisehir J24).

*K 237* - from northern area of Kirka Basin 1 km north-east of Bozbel Tepe (795,671 Eskisehir J24).

*K 238, K 239* - from northern area of Kirka Basin 1 km west of Lütfiye village (703,652 Eskisehir J24).

*K 244, K 245* - from northern area of Kirka Basin 1 km to east of Idrisyayla village (782,648 Eskisehir J24).

## APPENDIX B (grid references of sample localities)

---

K 246, K 247 - from northern area of Kirka Basin 2.5 km north of Güllüdere (733,683 Eskisehir J24).  
K 277 - from northern area of Kirka Basin 1 km north-west of Idrisyayla village (764,650 Eskisehir J24).

### Kirka Shoshonite

K223, K224 - from north-eastern area of Kirka Basin 2 km north of Sancar village (977,656 Eskisehir J25).  
K225, K226 - from northern area of Kirka Basin Bozbel Tepe, north-east of the village of Idrisyayla (785,662 Eskisehir J24).

### SEDIMENTS IN KIRKA BASIN

**Section L** - from northern area of Kirka Basin 1 km north-west of Gemiç (836,598 Eskisehir J24).  
VSK 265, VSK 266 - 110 m, VSK 279 - 120 m (Figure 2.8 in main text).

**Section M** - from the eastern area of Kirka Basin to the east of Tekke Tepe, 2 km west of Yarbaskan & 2 km east of Kirka (894,511 Eskisehir J25).  
VSK 257 - 1.5 m, VSK 255 & VSK 256 - 6 m (Figure 2.8 in main text)

**Section N** - from the eastern area of Kirka Basin 300 m north-west of Karaören (910,459 Eskisehir J25).  
VSK 272 - 3 m (Figure 2.8 m in main text).

#### *Additional samples collected from the Karaören Formation*

VSK 267, VSK 268 - from the northern area of Kirka Basin 1.5 km west of Gemiç (833,582 Eskisehir J24).  
VSK 273 - from the eastern area of Kirka Basin 2 km north of Karaören (902,472 Eskisehir J25).  
VSK 275 - from the western area of Kirka Basin to west of Damialıkaraağaç village. 732,519 (Eskisehir J24)

### Samples from the Sarikaya Formation

VSK 1 - from old mine workings just west of the main Sarikaya open pit (810,513 Eskisehir J24).  
VSK 2 - from old mine workings just west of the main Sarikaya open pit (810,513 Eskisehir J24).  
VSK 3 - from old mine workings just west of the main Sarikaya open pit (810,513 Eskisehir J24).  
VSK 4 - from colemanite deposit at Göçenoluk (733,590 Eskisehir J24).

### Samples from the Fetiye Formation

VSK 261, VSK 262 - from the western area of Kirka Basin 0.5 km north-west of Salihiye, 100 m to west of road (952,513 Eskisehir J24).  
VSK 274 - from the western area of Kirka Basin at Kızılıpınar (728,539 Eskisehir J24).

### VOLCANICS FROM THE AFYON AREA

#### Afyon K-trachyte & latite (with large sanidine phenocrysts)

A 202, A 203 - Afyon (847,942 Eskisehir K25).  
A 204, A 205 - approx 8 km south of Afyon on hill to south of Büyükkalecik (821,849 Eskisehir K25).  
A 210 - approx 8 km south of Afyon on hill to east of Büyükkalecik village (828,854 Eskisehir K25).  
A 217, A 218 - approx 10 km west south of Afyon 500 m east of Kayadibi (743, 898 Eskisehir K24).  
A 242, A 243 - approx 13 km west of Afyon 2 km east of Balmahmut beside main road (700,978 Eskisehir K24).

#### Afyon mafic lavas

A 200, A 201 - approx 10 km west west north of Afyon north-east of Köprülü village (731,012 Eskisehir K24).  
A 206, A 207 - 5 km along road to north-east of Iscehisar (093,056 Eskisehir K25).  
A 213, A 214 - 1 km west of Suhut (843,683 Eskisehir K25).  
A 216 - 800 m east of Elvanpasa (433,978 Eskisehir K24).  
A 241 - 1 km to east of Çalköy (471,129 Eskisehir K24).  
A 248, A 249 - approx 4 km to west of Nuhköy (638,770 Eskisehir K24).  
A 253, A 254 - 200 m west of Çepni, close to small stream (413,773 Eskisehir K24).

### SEDIMENTS FROM THE AFYON AREA (Balmahmut)

**Section O** - 2 km north of Balmahmut, just north of railway (688,995 Afyon K24).  
VSB 3 - 9-10.8 m (Figure 2.9 m in main text).

**Section P** - 3 km north-east of Balmahmut (716,992 Afyon K24).  
VSB 1 - 10.8-12.6 m (Figure 2.9 m in main text).

#### Longitude and latitude covered by each topographical map

Kütahya J22 39°00'-39°30'N by 29°00'-29°30'E  
Usak K22 38°30'-39°00'N by 29°00'-29°30'E  
Kütahya J21 39°00'-39°30'N by 28°30'-29°00'E  
Afyon K25 38°30'-39°00'N by 30°30'-31°00'E  
Afyon K24 38°30'-39°00'N by 30°00'-30°30'E  
Eskisehir J24 39°00'-39°30'N by 30°00'-30°30'E  
Eskisehir J25 39°00'-39°30'N by 30°30'-31°00'E



**APPENDIX C - summary of techniques used**

Sample	petrographic TS	XRD whole rock	XRD clay separation	Electron microprobe	XRF majors & traces	ICP-AES (Li)	ICP-AES (REES)	PGAA (B)	K/Ar dating	<sup>39</sup> Ar/ <sup>40</sup> Ar dating	Nd & Sr isotopes
G1	●				●	●		●			
G2	●			●	●						
G4	●			●	●						
G5	●				●	●	●	●	●		●
G7	●				●	●		●			
G8	●			●	●				●		●
G23	●				●	●		●			
E1	●				●	●	●	●	●		●
E2	●	●		●	●						
E3	●	●			●	●	●	●	●		●
E4	●			●	●						
E5	●	●		●	●	●		●			●
E6	●				●				●		
E16	●	●			●	●		●			●
E17	●			●	●						
E18	●	●		●	●			●			
E19	●				●						
E20	●				●	●		●			●
E21	●	●			●						
E22	●	●			●						
E68	●			●	●						
VSE1	●	●	●	●	●	●					
VSE2	●	●		●	●	●					
VSE3	●	●			●	●					
VSE4	●	●			●	●					
VSE5		●			●	●					
VSE6		●			●	●					
VSE7		●			●	●					
VSE8	●	●	●	●	●	●					
VSE9		●			●	●					
VSE10		●			●	●					
VSE11		●			●	●					
VSE12		●			●	●					
VSE13		●			●	●					
VSE14		●			●	●					
VSE15		●			●	●					
VSE16		●	●		●	●					
VSE17		●			●	●					
VSE18		●			●	●					

XRD-X-ray diffraction; XRF- X-ray fluorescence; TS- thin section; EM- electron microprobe; ICP-AES-inductively coupled plasma -atomic emission spectroscopy; PGAA-prompt gamma activation analysis

**Appendix C (summary of analytical techniques used)**

**APPENDIX C - summary of techniques used**

Sample	petrographic TS	XRD whole rock	XRD clay separation	Electron microprobe	XRF majors & traces	ICP-AES (Li)	ICP-AES (REES)	PGAA (B)	K/Ar dating	<sup>39</sup> Ar/ <sup>40</sup> Ar dating	Nd & Sr isotopes
VSE19		●			●	●					
VSE20		●			●	●					
VSE21		●			●	●					
VSE22		●		●	●	●					
VSE23		●	●		●	●					
UG7	●				●	●	●	●			
UG8	●				●	●					
UG28	●				●	●		●	●		●
UG29	●				●						
UG58	●				●	●		●	●		
UG63	●				●				●		●
UG64	●				●						
UG65	●				●						
UG66	●				●						
UG67	●				●						
UG73	●				●	●		●			
UG74	●				●						
UG75	●				●	●	●	●	●		●
UG126	●				●	●	●	●			
UG142	●				●	●	●		●		
UG145	●				●	●		●	●		●
SE1	●				●	●		●	●		●
SE2	●				●						
SE3	●				●	●		●	●		
SE4	●				●						
SE12	●				●	●		●	●		
SE13	●				●						●
SE24	●				●	●		●			
SE25	●				●				●		
SE26	●				●	●		●			●
SE27	●				●						
SE71	●	●			●	●	●	●			
SE72	●	●			●						
SI14	●				●	●	●	●			●
SI15	●				●						
VSS1		●			●	●					
VSS2		●			●	●					
VSUG1		●			●	●					
VSUG2		●			●	●					

XRD-X-ray diffraction; XRF- X-ray fluorescence; TS- thin section; EM- electron microprobe; ICP-AES-inductively coupled plasma -atomic emission spectroscopy; PGAA-prompt gamma activation analysis

**Appendix C (summary of analytical techniques used)**

**APPENDIX C - summary of techniques used**

Sample	petrographic TS	XRD whole rock	XRD clay separation	Electron microprobe	XRF majors & traces	ICP-AES (Li)	ICP-AES (REES)	PGAA (B)	K/Ar dating	<sup>39</sup> Ar/ <sup>40</sup> Ar dating	Nd & Sr isotopes
I208	●				●	●		●			
I209	●				●						
I219	●	●	●		●	●		●		●	
I220	●			●	●						
I221	●	●			●						
I222	●				●	●		●			
I250	●	●			●	●		●			
I251	●	●		●	●						
I252	●	●			●	●		●			
I258	●	●			●						
I259	●				●						
I260	●				●						
I271	●				●						
K223	●				●	●	●	●			
K225	●				●	●	●	●			
K226	●			●	●						●
K227	●				●	●	●	●			
K228	●				●						●
K229	●				●	●	●	●			
K230	●				●						
K231	●				●						●
K232	●			●	●	●	●	●			
K233	●				●						
K234	●				●	●	●	●			
K235	●				●						
K236	●				●	●		●			
K237	●				●	●		●			
K238	●				●						
K239	●				●						
K244	●				●						
K245	●				●	●	●	●			
K246	●				●	●	●	●			
K247	●				●						
K277	●				●	●	●	●			
VSK1		●			●	●					
VSK2		●	●		●	●					
VSK3		●			●	●					
VSK4		●	●		●	●					

XRD-X-ray diffraction; XRF- X-ray fluorescence; TS- thin section; EM- electron microprobe; ICP-AES-inductively coupled plasma -atomic emission spectroscopy; PGAA-prompt gamma activation analysis

**Appendix C (summary of analytical techniques used)**

**APPENDIX C - summary of techniques used**

Sample	petrographic TS	XRD whole rock	XRD clay separation	Electron microprobe	XRF majors & traces	ICP-AES (Li)	ICP-AES (REES)	PGAA (B)	K/Ar dating	<sup>39</sup> Ar/ <sup>40</sup> Ar dating	Nd & Sr isotopes
VSK255	●				●						
VSK256	●	●		●	●	●					
VSK261	●				●						
VSK262	●	●			●	●					
VSK265	●	●		●	●	●					
VSK266	●				●						
VSK267	●	●			●	●					
VSK268	●			●							
VSK272	●				●						
VSK273	●				●						
VSK274	●				●						
VSK275	●				●						
VSK279	●										
A200	●				●	●		●			
A201	●				●						
A202	●				●	●		●			
A203	●				●						
A204	●				●						
A205	●				●						
A206	●				●	●		●			
A207	●				●						
A210	●				●	●		●			●
A213	●				●						
A214	●				●						
A216	●				●	●					
A217	●				●	●		●			●
A218	●				●						
A241	●				●						
A242	●				●	●		●			
A243	●				●						
A248	●				●						
A249	●				●						
A253	●				●						
A254	●				●						
VSΒ1		●			●	●					
VSΒ3		●			●	●					
VSΒ269	●				●						
VSΒ270	●				●						

XRD-X-ray diffraction; XRF- X-ray fluorescence; TS- thin section; EM- electron microprobe; ICP-AES-inductively coupled plasma -atomic emission spectroscopy; PGAA-prompt gamma activation analysis

## BRIEF PETROLOGICAL DESCRIPTION OF SAMPLES

### ERIGÖZ GRANITE

*G 1, G 2* - granite pluton; medium grained grey rock with plagioclase (oligoclase & andesine), K-feldspar, hornblende, and biotite. Biotite has replaced hornblende and chlorite has replaced biotite. Accessory magnetite present.  
*G 7, G 8* - granite pluton; medium grained grey rock with plagioclase (albite & andesine), K-feldspar (orthoclase), hornblende, biotite, quartz with accessory apatite in the biotites and magnetite.  
*G 4, G 5* - granite pluton; medium grained pink rock with plagioclase, K-feldspar, biotite, and quartz, with accessory apatite in the biotites, chlorite which has replaced biotite and magnetite found associated with the biotites.  
*G 23* - aplite vein in granite pluton; finer grained pink-purple rock with quartz, multiple twinned plagioclase, K-feldspar, biotite and magnetite.

### VOLCANICS WITHIN EMET BASIN

#### Emet Rhyolites

*E 1, E 2* - rhyolite sheet; pale pink rock with phenocrysts of K-feldspar (orthoclase), plagioclase (oligoclase & andesine), biotite and quartz in a matrix dominated by spherulites. Minor smectite present.  
*E 5, E 6* - rhyolite sheet; purple porphyritic rock with phenocrysts of biotite (with apatite inclusions), quartz and feldspar in a quartzofeldspathic matrix. Feldspars are part altered to kaolinite.  
*E 16, E 17* - rhyolite sheet; purple porphyritic rock with phenocrysts of biotite, quartz and feldspars, in an altered glassy matrix. Feldspars are part altered to kaolinite.  
*E 18, E 19* - rhyolite sheet; purple porphyritic rock with phenocrysts of biotite, quartz and feldspars in a fine grained matrix. Feldspars are part altered to kaolinite.  
*E 20, E 21* - rhyolite sheet; grey rock with phenocrysts of biotite, plagioclase, and K-feldspar, in a fine grained quartzofeldspathic matrix.  
*E 22* - hydrothermal alteration product; rusty brown silicified rock which consists of recrystallised quartz and Fe-oxides.

#### Emet Latite & Shoshonite

*E 3, E 4* - latite lava; grey rock with phenocrysts of biotite and augite in a matrix containing fine needles of K-feldspar.

*Additional sample collected by BHP Minerals geologists*

*E 68* - shoshonite lava; grey rock with phenocrysts of biotite and augite in a matrix of fine feldspar needles.

### SEDIMENTS IN THE EMET BASIN

#### Section A

Section through the Red Formation, which consists of conglomerates interbedded with red sandstones and siltstones (Figure 2.3 in main text).

*VSE 1* - volcaniclastic siltstone; brown-green sediment with biotite (with apatite inclusions), quartz, plagioclase and K-feldspar crystals, rare illite, dioctahedral smectite, kaolinite, remnant pumice.

#### Section B

Section through the Red Formation, which consists of volcaniclastic siltstone interbedded with fine grained mudstone (Figure 2.3 in main text).

*VSE 4* - volcaniclastic siltstone; grey 'crumbly' sediment with biotite, quartz, plagioclase and K-feldspar crystals, glass, pumice, illite/muscovite, smectite, kaolinite.

*Additional samples from the Red Formation*

*VSE 2* - volcaniclastic siltstone; 'crumbly' grey-green sediment with biotite, quartz, K-feldspar and illite crystals, calcite aggregates, possible remnant pumice (recrystallised quartz) and spherulitic fragments.

*VSE 3* - volcaniclastic siltstone; green-grey sediment with biotite, quartz, and K-feldspar crystals, illite/muscovite, spherulitic fragments and dolomite in both the matrix and within remnant pumice vesicles.

#### Section Lower C

Section through the Borate Formation, which consists largely of red-grey siltstones (Figure 2.3 in main text)

*VSE 5* - siltstone; Quartz, K-feldspar, plagioclase, illite/muscovite

*VSE 6* - siltstone; Quartz, K-feldspar, calcite, illite/muscovite.

*VSE 7* - mudstone; Quartz, plagioclase, calcite, illite, smectite.

*VSE 8* - volcaniclastic siltstone; biotite, quartz, plagioclase, K-feldspar (some authigenic), illite, dioctahedral? smectite.

*VSE 9* - volcaniclastic siltstone and limestone; calcite.

*VSE 10* - limestone; calcite.

#### Section Upper C

Section through the Borate Formation, which consists of colemanite-hosting green-grey mudstone (Figure 2.3 in main text).

*VSE 11* - mudstone; K-feldspar (authigenic?), calcite, dolomite, illite, trioctahedral smectite, colemanite.

*VSE 12* - mudstone; K-feldspar (authigenic?), illite, dolomite, trioctahedral smectite, colemanite.

*VSE 13* - mudstone and colemanite; mainly colemanite.

*VSE 14* - mudstone; - dolomite, illite, trioctahedral smectite, K-feldspar, colemanite.

*VSE 15* - mudstone; calcite, dolomite, illite, trioctahedral smectite, colemanite.

*VSE 16*; mudstone; K-feldspar (authigenic?), calcite, dolomite, illite, trioctahedral smectite.

## APPENDIX D (petrology of samples)

---

### Section D

Section through grey mudstone of Borate Formation and capping limestone of Upper Limestone Formation (Figure 2.3 in main text)  
*VSE 17 - mudstone; calcite, quartz, illite/muscovite.*

### Section E

Section through colemanite-hosting grey mudstone of the Borate Formation (Figure 2.3 in main section).

*VSE 18 - mudstone; gypsum, quartz, illite, trioctahedral smectite.*

*VSE 19 - mudstone; gypsum, K-feldspar (authigenic?), quartz, calcite, illite, trioctahedral smectite.*

*VSE 20 - mudstone; illite, trioctahedral smectite, colemanite.*

### Section F

Section through grey mudstone and siltstone of the Borate Formation (Figure 2.3 in main section).

*VSE 21 - mudstone; quartz, calcite, illite/muscovite.*

*VSE 22 - volcanoclastic siltstone; K-feldspar (authigenic?), quartz, plagioclase, biotite and illite crystals, chromite, calcite.*

### Section G

Section through grey colemanite-hosting mudstone (Figure 2.3 in main section).

*VSE 23 - mudstone; K-feldspar (authigenic?), quartz, calcite, illite, smectite.*

## VOLCANICS TO THE SOUTH AND WEST OF EMET BASIN (SELENDI, USAK-GÜRE & SIMAV BASINS)

### Rhyolites

*UG 28, UG 29 - rhyolite sheet; pale pink rock with phenocrysts of biotite (with included apatite), plagioclase and K-feldspar, with a dominantly spherulitic matrix.*

*SE 1 & SE 2 - rhyolite sheet; grey porphyritic rock with phenocrysts of biotite, plagioclases, K-feldspars, quartz and hornblende in a fine grained glassy matrix.*

*SE 24, SE 25 - rhyolitic lithic tuff; pale brown rock with angular fragments of K-feldspar, biotite and quartz in a quartz feldspathic matrix.*

### K-Trachytes

*SE3 & SE 4 - K-trachyte sheet; grey porphyritic micaceous rock with phenocrysts of biotite and plagioclase in a fine grained matrix.*

### Andesite, latite & shoshonite

*UG7, UG 8 - shoshonite lava; dark grey rock with phenocrysts of biotite and augite, with a matrix of feldspar needles. Biotite often replaced by chlorite.*

*SE 12, SE 13 - andesite lavas; dark grey rock with phenocrysts of biotite, hornblende, plagioclase and augite in a matrix of feldspar needles and glass.*

*SE 26, SE 27 - latite lava flow; dark grey micaceous rocks with phenocrysts of biotite and augite with some calcite amygdalae.*

*SI 14, SI 15 - latite lava flow; dark grey rock with clinopyroxene phenocrysts, plagioclase needles in the matrix, large calcite amygdalae.*

*Additional samples collected by BHP Minerals geologists*

### Rhyolites

*SE 72 - rhyolite sheet; pale brown rock with phenocrysts of biotite, K-feldspar, plagioclase and quartz in a speckledly altered quartz feldspathic matrix.*

*SE71 - altered acid volcanics; grey-white rock with speckledly appearance in thin section, original crystal forms still visible but their identities are not discernible. XRD identified alunite and quartz.*

### Dacites & K-Trachytes

*UG58 - trachyte sheet; grey porphyritic rock with phenocrysts of biotite, plagioclase, occasional augite in a fine grained glassy matrix.*

*UG 62, UG 63 - dacite sheet; purple rock with phenocrysts of altered biotite, plagioclase, fine grained matrix.*

*UG 64 - trachyte sheet; grey rock with phenocrysts of altered biotite in a feldspathic matrix.*

*UG 66, UG 67 - dacite sheet; purple rock with phenocrysts of biotite and plagioclase in a feldspathic matrix.*

*UG 74, UG 75 - trachyte sheet; dark grey porphyritic rock with phenocrysts of biotite in a fine grained feldspathic matrix.*

*UG 126 - dacite sheet; purple porphyritic rock with feldspar phenocrysts in a fine grained matrix.*

### Andesite & latite

*UG 65 - andesite sheet; grey rock with phenocrysts of biotite, plagioclase and augite, in a feldspathic matrix.*

*UG 73 - latite sheet; grey rock with phenocrysts of augite, calcite amygdalae and a matrix of small feldspar needles.*

*UG 142 - latite lava flow; grey rock with phenocrysts of biotite in a feldspathic matrix.*

*UG 145 - latite lava flow; grey rock with phenocrysts of augite in a fine grained feldspathic matrix.*

## SEDIMENTS IN SELENDI BASIN

### Section H

Section through the Inay Group, which consists of mudstones and siltstones with some limestone beds (Figure 2.4 in main text).

*VSS 1 - mudstone; quartz, plagioclase, ankerite, illite, smectite.*

## APPENDIX D (petrology of samples)

---

### Section I

Section through the Inay Group, which consists of mudstones, siltstones and occasional limestones beds (Figure 2.4 in main text).  
*VSS 2 - mudstone; K-feldspar, ankerite, illite.*

### SEDIMENTS IN USAK-GÜRE BASIN

#### Section J

Section through the Inay Group, which consists of mudstone with limestone beds. (Figure 2.5 in main text)  
*VSUG 1 - mudstone; calcite, illite.*

#### Section K

Section through the Inay Group, which consists of mudstone with thin beds of limestone. (Figure 2.5 in main text)  
*VSUG 2 - mudstone; K-feldspar, ankerite, illite, smectite.*

### VOLCANICS OF THE KIRKA AREA

#### Kirka Ignimbrites

*I 208, I 209 - ignimbrite; white-grey tuffaceous rock with contains smokey quartz, plagioclase and K-feldspar crystals, pumices and lithic fragments.*

*I 219, I 220 - ignimbrite; white-grey tuffaceous rock with phenocrysts of plagioclase, K- feldspar, smokey quartz, glass and rare biotite in a fine grained matrix. Clasts of fibrous pumice which contain empty vesicles. Clay fractions include illite and smectite.*

*I 221, I 222 - ignimbrite; white-grey tuffaceous rock with phenocrysts of plagioclase (oligoclase), K- feldspar (Na & K sanidine), smokey quartz and biotite in a fine grained matrix. Clasts of pumice where vesicles are sometimes infilled with calcite.*

*I 250 - ignimbrite; pale grey tuffaceous rock with smokey quartz, plagioclase, K-feldspar and lithic lapilli.*

*I 251, I 252 - ignimbrite; pale grey and black rock with phenocrysts of K- feldspar, smokey quartz, plagioclase (oligoclase) and occasional biotite in a fine grained matrix. Flattened pumices observed with fresh black volcanic glass but no vesicles. Crystals of quartz and plagioclase observed in the pumices.*

*I 258, I 259 - ignimbrite; grey-white tuffaceous rock with phenocrysts of plagioclase, smokey quartz, K- feldspar and occasional biotite in a fine grained matrix. Pumices present.*

*I 260 - ignimbrite; grey tuffaceous rock with phenocrysts of plagioclase, smokey quartz, K- feldspar and occasional biotite in a fine grained matrix. Pumices present.*

*I 271 - ignimbrite; pale grey tuffaceous rock with phenocrysts of quartz, K- feldspar, plagioclase and occasional biotite in a fine grained matrix. Abundant pumices with empty vesicles and also lithic clasts present.*

#### Kirka Rhyolites, Trachytes & Dacites

*K 227, K 228 - rhyolite sheet; white-pink porphyritic rock with phenocrysts of quartz, K- feldspar and biotite in a speckled fine grained matrix.*

*K 229, K 230 - rhyolite sheet; red-brown porphyritic rock with phenocrysts of multiple twinned and zoned plagioclase, K- feldspar, biotite, quartz and occasional basal amphibole in a spherulite dominated matrix.*

*K 231, K 232 - rhyolite sheet; pale pink rock with phenocrysts of biotite, K-feldspar (K sanidine) and multiple twinned and zoned plagioclase (andesine) in a spherulite dominated matrix.*

*K 233 - dacite sheet; pale grey porphyritic rock with phenocrysts of plagioclase and biotite in a fine grained matrix.*

*K 234, K 235 - dacite sheet; grey porphyritic rock with phenocrysts of biotite, basal amphibole and multiple twinned and zoned plagioclase in a glassy matrix.*

*K 236 - rhyolite sheet; purple porphyritic with phenocrysts of plagioclase in a fine grained matrix.*

*K 237 - rhyolite sheet; orange porphyritic rock with same mineralogy as K 227 & K 228 but contains iron oxide staining.*

*K 238, K 239 - rhyolite sheet; purple porphyritic rock with phenocrysts of biotite and plagioclase in a fine grained matrix.*

*K 244, K 245 - rhyolite sheet; fine grained banded pink to white rock with visible quartz and feldspar but no phenocrysts observed.*

*K 246, K 247 - rhyolite sheet; purple banded rock with occasional phenocrysts of quartz and K- feldspar, in a matrix dominantly of spherulites.*

*K 277 - rhyolite sheet; fine grained pale grey rock (no phenocrysts)*

#### Kirka Shoshonite

*K 223,- shoshonite lava flow; dark grey rock with phenocrysts of clinopyroxene and olivine in a matrix of plagioclase needles.*

*K 225, K 226 - shoshonite lava flow; dark grey rock with phenocrysts of clinopyroxene (augite), olivine (close to fayalite) and elongate plagioclase (bytownite, anorthite) in a matrix of small plagioclase needles.*

### SEDIMENTS IN KIRKA BASIN

#### Section L

Section through the Karaören Formation, which consists of ignimbrite-derived volcanoclastics with occasional conglomerate beds and a capping limestone (Figure 2.8 in main text).

*VSK 265, 266 - ignimbrite-derived volcanoclastics; grey-green tuffaceous rocks with quartz, K-feldspar and plagioclase crystals, and pumice lapilli in a calcite matrix. Pumice vesicles infilled by calcite.*

*VSK 279 - volcanic clast; phenocrysts of plagioclase, K-feldspar, biotite and basal hornblende in a matrix dominated by spherulites.*

#### Section M

Section through the Karaören Formation, which consists of fine grained tuffaceous beds which grade upwards into coarser tuff (Figure 2.8 in main text).

*VSK 255, 256, 257 - ignimbrite-derived volcanoclastics; pale green tuffaceous rock with quartz, K-feldspar, plagioclase, and rare biotite phenocrysts and pumice lapilli in a calcite matrix. Pumice vesicles infilled by calcite.*

## APPENDIX D (petrology of samples)

---

### Section N

Section through the Karaören Formation, which consists of ignimbrite-derived volcanoclastics below cherty limestone beds (Figure 2.8 in main text).

VSK 272 - *ignimbrite-derived volcanoclastics*; contains quartz, K-feldspar, plagioclase and rare biotite phenocrysts, and pumice lapilli in a fine grained matrix.

*Additional samples collected from the Karaören Formation;*

VSK 267, VSK 268 - *ignimbrite-derived volcanoclastics*; pale green tuffaceous rock with quartz, K-feldspar (Na & K sanidine), and plagioclase (oligoclase) phenocrysts, and pumice lapilli in matrix with some calcite. Also contains glass and clinoptilolite.

VSK 273 - *ignimbrite-derived volcanoclastics*; contains quartz, K-feldspar and plagioclase phenocrysts, and pumice lapilli in a fine grained matrix.

VSK 275 - *ignimbrite-derived volcanoclastics*; grey - white tuffaceous rock with quartz, K-feldspar and plagioclase phenocrysts, and pumice lapilli in a matrix of calcite. Pumice vesicles infilled by calcite.

### Samples from the Sarikaya Formation

VSK 1 - *interbedded carbonate and mudstone*; The light brown carbonate is dolomite and the grey mudstone beds largely comprise smectite.

VSK 2 - *mudstone bed*; trioctahedral smectite & dolomite.

VSK 3 - *carbonate*; dolomite.

VSK 4 - *mudstone*; trioctahedral smectite, illite and K-feldspar (authigenic?).

### Samples from the Fetiye Formation

VSK 261, VSK 262 - *ignimbrite-derived volcanoclastics*; pale brown cemented rock with quartz, K-feldspar, plagioclase and rare biotite phenocrysts, and pumice lapilli in a calcite matrix. Pumice vesicles infilled with calcite.

VSK 274 - *ignimbrite-derived volcanoclastics*; pale brown tuffaceous rock with quartz, K-feldspar and plagioclase phenocrysts, and pumice lapilli in a calcite matrix. Pumice vesicles infilled with calcite.

## VOLCANICS FROM THE AFYON AREA

### Afyon K-Trachyte & Latite

A 202, A 203 - *latite*; purple porphyritic rock with phenocrysts of sanidine, biotite, hornblende and zoned and multiple twinned plagioclase in a matrix which contains clinopyroxenes and feldspars.

A 204, A 205 - *K-trachyte*; grey porphyritic rock with phenocrysts of sanidine, hornblende, clinopyroxene, zoned and multiple twinned plagioclase (andesine) and biotite in a matrix of feldspar needles.

A 210 - *K-trachyte*; light grey porphyritic rock with phenocrysts of sanidine, hornblende, clinopyroxene, multiple twinned plagioclase (andesine) and K-feldspar in a matrix largely of feldspar needles. The large sanidine crystals can be several cm in length.

A 217, A 218 - *latite*; purple porphyritic rock with phenocrysts of sanidine (K sanidine with andesine intergrowths), biotite, hornblende and plagioclase in a matrix of feldspar needles.

A 242, A 243 - *latite*; pale grey porphyritic rock with phenocryst of sanidine, biotite, hornblende, clinopyroxene and plagioclase in a fine grained matrix.

### Afyon Mafic Lavas

A 200, A 201 - *latite sheet*; dark grey-purple rock with phenocrysts of altered biotite and clinopyroxene in a matrix of small feldspar needles.

A 206, A207- *latite lava flow*; dark grey vesicular rock with phenocrysts of clinopyroxene in a matrix of small feldspar needles.

A 213, A 214 - *latite lavas*; pale grey rock with phenocrysts of highly altered biotite, plagioclase and clinopyroxene in a matrix of small feldspar needles.

A 216 - *K-trachyte sheet*; pale grey rock with phenocrysts of altered biotite and clinopyroxene in a matrix of feldspar needles.

A 241- *shoshonite lavas*; dark grey rock with phenocrysts of clinopyroxene and biotite in a matrix of feldspar needles.

A 248, A 249 - *latite sheet*; grey rock with phenocrysts of altered biotite, clinopyroxene and plagioclase in a matrix of feldspars.

A 253, A 254 - *shoshonite lavas*; purple rock with phenocrysts of altered biotite, clinopyroxene and plagioclase in a matrix of small feldspar needles.

## SEDIMENTS FROM THE AFYON AREA (Balmahmut)

### Section O

Section consisting of siltstones and mudstones, which lie above Afyon sanidine-bearing latite and below cherty limestone.

VSB 3 - *mudstone*; K-feldspar, plagioclase, illite/muscovite.

VSB 270 - *tuffaceous material below section*; crumbly grey tuffaceous rock with phenocrysts of biotite, plagioclase, K-feldspar, rare quartz and some pumice in a fine grained matrix.

### Section P

Section consisting of mudstone with conglomerate and limestone beds which lies above a 15m thick bedded tuff unit and below thick cherty capping limestone.

VSB 1- *mudstone*; K-feldspar, calcite, illite/muscovite.

VSB 269 - *tuffaceous matrix of the agglomerates from below the section*; brown tuffaceous rock with phenocrysts of biotite, plagioclase, K-feldspar and it contains pumices with a fine grained matrix.



## Appendix E (K-Ar Dating)

The K-Ar dating of fifteen igneous samples from the USE area was carried out at the NERC Isotope Geoscience Laboratories (NIGL) in 1994. The whole rock and mineral separate fractions were prepared by this author, while the analytical work was conducted by Dr Geoff Nowell.

### Sample Preparation

Dating was carried out on separated biotite where possible. In the finer grained mafic samples this was not possible and therefore dating was conducted on whole rock fractions. Coarse grained rock crush was first produced at Leicester University with a 'fly press'. This coarse grained crush was then sieved into 125-250 and 250-500  $\mu\text{m}$  fractions at NIGL. The sieved fractions were washed in de-ionised water to remove any fine powder and dried at  $<150^\circ\text{C}$ . Biotite was separated from the two fractions using a Frantz magnetic separator and by manual separation on a clean piece of paper.

### Analytical Procedure

Potassium was analysed in at least duplicate by conventional mixed-acid digestion and flame photometry using a lithium internal standard. Errors are expressed as the difference between the mean and individual values expressed as a percentage. Argon was extracted from the sample by fusion under vacuum using external RF induction heating and analysed by the isotope dilution method on a MM1200 mass spectrometer. Errors for the argon determinations are compounded from the errors on the isotope ratio measurements and spike calibration and include any error magnification due to correction for contaminating atmospheric argon. Both the potassium and argon systems are calibrated regularly against international rock standards. Ages were calculated using the decay and other constants recommended by Steiger and Jager (1977) and errors are quoted at 95% confidence level.

### Results

**Analytical details and results of K-Ar dating on the USE volcanic and granitic samples**

Sample	Type	K (%)	n	Error (%)	Argon Run no.	Ar (g)	Atmos $^{40}\text{Ar}$ (nl)	Atmos $^{40}\text{Ar}$ (%)	Rad. $^{40}\text{Ar}$ (nl/g)	Error (%)	Age (Ma)	Error (Ma)
E1	Biotite	6.84	2	0.11	3977	0.2106	0.31	21.50	5.3992	1.1	<b>20.2</b>	0.4
E6	Biotite	6.52	2	0.28	4044	0.2891	1.8	54.53	5.184	1.6	<b>20.3</b>	0.6
E3	WR	5.03	2	0.03	3998	1.8134	0.75	12.38	2.933	1	<b>14.9</b>	0.3
G5	Biotite	5.45	3	3.43	4000	0.2581	1.31	57.30	3.7746	1.7	<b>17.7</b>	1.3
G8	Biotite	5.48	3	1.01	4001	0.2248	0.47	32.07	4.3859	1.1	<b>20.5</b>	0.6
SE 25	Biotite	6.78	3	1.04	3978	0.2307	0.46	27.3	5.3036	1.1	<b>20</b>	0.6
SE 1	Biotite	6.78	2	1.19	4046	0.2199	0.46	29.43	5.009	1.1	<b>18.9</b>	0.6
SE3	Biotite	5.11	3	1.49	4045	0.4324	0.51	28.32	2.9784	1.1	<b>14.9</b>	0.6
SE 12	WR	2.05	2	0.90	3981	1.9064	3.51	57.73	1.3472	1.7	<b>16.8</b>	0.7
UG 28	Biotite	6.53	3	2.47	3982	0.2513	1.12	49.67	4.491	1.4	<b>17.6</b>	1
UG58	WR	5.28	3	0.91	4027	1.9969	1.39	18.23	3.1174	1	<b>15.1</b>	0.4
UG 63	WR	2.76	2	0.52	4030	2.4851	0.94	19.41	1.5757	1	<b>14.6</b>	0.3
UG 75	WR	5.19	2	0.15	4029	1.7345	3.82	40.73	3.209	1.2	<b>15.9</b>	0.4
UG 142	WR	6.94	3	0.99	4024	2.9027	13.79	53.61	4.1103	1.6	<b>15.2</b>	0.6
UG 145	WR	5.24	2	0.74	4026	1.7015	1.36	20.19	3.1607	1	<b>15.5</b>	0.4

n = number of analyses used to determine the mean K content. WR = whole rock fraction used.

## Appendix F ( $^{40}\text{Ar}/^{39}\text{Ar}$ dating)

$^{40}\text{Ar}/^{39}\text{Ar}$  dating of the Kirka Ignimbrite (sample I219) was carried out at the University of Leeds by Mr Dave Rex in 1994. The date was obtained from a biotite fraction. The analytical procedure followed by the University of Leeds  $^{40}\text{Ar}/^{39}\text{Ar}$  laboratory is outlined below.

### Analytical Procedure

$^{40}\text{Ar}/^{39}\text{Ar}$  analysis followed the method described by Rex et al., (1993) with the following variations: Samples were irradiated at the Ford Reactor, Ann Arbor, Michigan, interference correction factors were  $(40/39)\text{K} = 0.03$ ,  $(36/39)\text{Ca} = 1000$  and  $(37/39)\text{Ca} = 0.24$ . Standards used to monitor the neutron fluence were 5 aliquots each of Tinto biotite (Rex & Guise 1986) and hornblendes MMHb1 and Hb3gr (qv Rex et al. 1993). Argon isotope analyses were performed using a modified MS 10 mass spectrometer with 4.2k Gauss magnet and voltage peak jumping under computer control. Ion beams were detected by a VG pre-amplifier with  $4 \times 10^{10}$  ohm resistor, digitised with a Keithley<sup>TM</sup> 2000 voltmeter and stored on computer disc for subsequent processing. Measured atmospheric  $^{40}\text{Ar}/^{36}\text{Ar}$  was  $287.8 \pm 0.2$  and sensitivity  $1.35 \times 10^{-7} \text{ cm}^3\text{V}^{-1}$ .

### Results

Figure F1 shows a flat spectrum giving an age of  $18.6 \pm 0.5$  Ma for the separated biotite from sample I 219. Additional data from the analysis is presented below.

Sample I 219, run 2128, weight = 0.0149g, J value =  $0.00390 \pm 0.5 \%$

Temp ( $^{\circ}\text{C}$ )	$^{39}\text{ArK}$ $\times 10^{-9} \text{ cm}^3$	$^{37}\text{ArCa}$ $\times 10^{-9} \text{ cm}^3$	$^{38}\text{ArCl}$ $\times 10^{-9} \text{ cm}^3$	Ca/K	$^{40/39}\text{ArK}$	%Atm $^{40}\text{Ar}$	Age (Ma)	Error (Ma)	% $^{39}$
635	1.0	0.05	0.3	0.091	2.754	86.3	19.3	6.4	3.5
770	6.5	0.05	1.6	0.016	2.841	9.9	19.9	0.9	22.9
840	2.9	0.02	0.7	0.013	2.485	20.2	17.4	2.2	10.4
915	7.5	0.03	1.8	0.009	2.639	8.4	18.5	0.6	26.7
975	9.3	0.02	2.2	0.005	2.637	7.2	18.5	0.7	33.0
1025	1.0	0.07	0.2	0.145	2.100	31.8	14.7	4.8	3.5

Integrated values, analytical and J errors

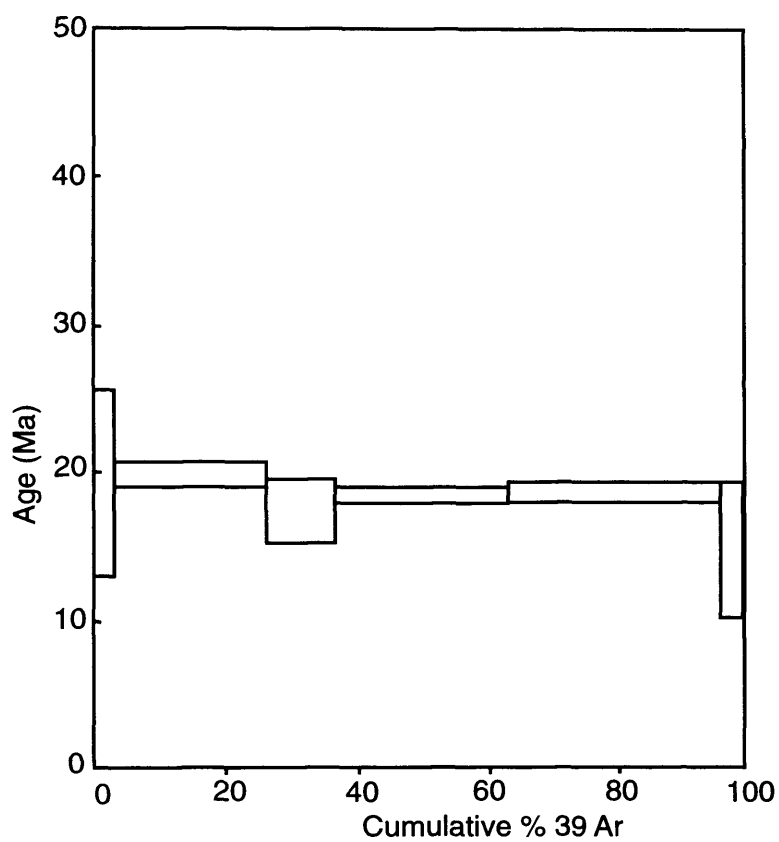
**Age (Ma)** 18.6      0.5      0.5

$^{40/39}\text{ArK}$  2.654      2.7%

Wt % K = 6.9,  $^{40}\text{Ar} = 50.3 \times 10^{-7} \text{ cm}^3 \text{ g}^{-1}$

Errors are  $2 \sigma$ ,  $^{40}\text{Ar} \equiv \text{vol. Radiogenic } ^{40}\text{Ar}$ , gas volumes corrected to STP.

**FIGURE F1 - Argon spectra for biotite separate from the Kirka Ignimbrite (sample I219)**



## Appendix G (X-Ray Diffraction)

X-ray diffraction (XRD) was carried out at the University of Leicester. XRD analyses were conducted on whole rock fractions from a range of volcanic and volcanoclastic rocks from the USEKA area, and on clay fractions ( $< 2 \mu\text{m}$ ) from selected Emet and Kirka Basin sediments.

### Sample preparation

Whole rock fractions consisted of fine grained powders, which were produced by crushing whole rock samples using a fly press followed by an agate mill. These powders were packed carefully into Al holders and then loaded directly into the XRD machine.

Fine grained powders were also used for the preparation of clay fractions ( $< 2 \mu\text{m}$ ). The powder was first mixed with a deflocculation agent (hexametaphosphate) and then allowed to settle over night. The clay fractions were subsequently separated from the coarser fractions using a centrifuge. The clay fractions were then pipetted onto a glass plate and allowed to dry in air. The glass plates were placed in the Al holders, and XRD analyses were carried out on these air dried samples.

After XRD analysis, the glass plates were placed in a dessicator containing ethylene glycol at  $60^{\circ}\text{C}$  over night. These glycolated samples were re-run using the same XRD operating conditions as for the air dried run. The next stage was to heat the samples in a furnace at  $330^{\circ}\text{C}$  for one hour, before analysing again. Finally, the samples were heated to  $550^{\circ}\text{C}$  for one hour and re-run. Hence, four XRD scans were generated from the clay fractions; air dried, glycolated,  $330^{\circ}\text{C}$ ,  $550^{\circ}\text{C}$ .

### Analytical conditions

The XRD analyses were carried out using a Philips PW 1729 X-ray generator equipped with a PW 1710 computerised control unit. The machine was operated at 40 kV and 30 mA, using Cu-K alpha radiation and a scanning speed of  $1^{\circ} 2\theta/\text{min}$ .

### Results

A summary of minerals identified in the USEKA samples is presented below:

#### *Emet volcanics*

- E2 - plagioclase, K-feldspar, mica, smectite (whole rock)
- E4 - augite, K-feldspar, mica, smectite (whole rock)
- E16 - quartz, K-feldspar, mica, kaolinite (whole rock)
- E18 - quartz, K-feldspar, plagioclase, mica, kaolinite (whole rock)
- E21 - quartz, plagioclase, mica (whole rock)
- E22 - quartz (whole rock)
- SE 72 - quartz, plagioclase, K-feldspar, mica (whole rock)
- SE71 - alunite, quartz (whole rock)

## Appendix G (XRD)

---

### *Emet Basin sediments*

VSE 1 - smectite, illite, kaolinite, quartz, K-feldspar, plagioclase (whole rock); smectite, illite, kaolinite (clay separation)

VSE 2 - illite, quartz, K-feldspar, calcite (whole rock)

VSE 3 - illite, quartz, K-feldspar, dolomite (whole rock)

VSE 4 - smectite, illite, kaolinite, glass, quartz, K-feldspar, plagioclase (whole rock)

VSE 5 - illite, quartz, K-feldspar, plagioclase (whole rock)

VSE 6 - illite, quartz, K-feldspar, calcite (whole rock)

VSE 7 - smectite, illite, quartz, plagioclase, calcite (whole rock)

VSE 8 - smectite, illite, K-feldspar (whole rock); smectite, illite (clay separation)

VSE 9 - calcite (whole rock)

VSE 10 - calcite (whole rock)

VSE 11 - trioctahedral smectite, illite, K-feldspar, colemanite, calcite, dolomite (whole rock)

VSE 12 - trioctahedral smectite, illite, K-feldspar, colemanite, dolomite (whole rock)

VSE 13 - colemanite (whole rock)

VSE 14 - trioctahedral smectite, illite, K-feldspar, colemanite, dolomite (whole rock)

VSE 15 - trioctahedral smectite, illite, colemanite, dolomite, calcite (whole rock)

VSE 16 - trioctahedral smectite, illite, K-feldspar, dolomite, calcite (whole rock); smectite, illite (clay separation)

VSE 17 - illite, calcite, quartz (whole rock)

VSE 18 - trioctahedral smectite, illite, quartz, gypsum (whole rock)

VSE 19 - trioctahedral smectite, illite, K-feldspar, quartz, gypsum, calcite (whole rock)

VSE 20 - trioctahedral smectite, illite, colemanite (whole rock)

VSE 21 - illite, calcite, quartz (whole rock)

VSE 22 - illite, quartz, plagioclase, K-feldspar, calcite (whole rock)

VSE 23 - smectite, illite, quartz, K-feldspar, calcite (whole rock); smectite, illite (clay separation)

### *Selendi Basin sediments*

VSS 1 - smectite, illite, quartz, plagioclase, ankerite (whole rock)

VSS 2 - illite, K-feldspar, ankerite (whole rock)

### *Usak-Güre Basin sediments*

VSUG 1 - illite, calcite (whole rock)

VSUG 2 - smectite, illite, K-feldspar, ankerite (whole rock)

### *Kirka Ignimbrite*

I219 - smectite, illite, glass, quartz, K-feldspar, plagioclase (whole rock); smectite, illite (clay separation)

I 221 - smectite, illite, quartz, K-feldspar (whole rock)

## Appendix G (XRD)

---

I250 - smectite, illite, quartz, K-feldspar, plagioclase (whole rock)

I252 - smectite, illite, glass, quartz, plagioclase (whole rock)

I258 - smectite, illite, quartz, K-feldspar, plagioclase (whole rock)

### *Kirka Basin sediments*

VSK 1 - smectite, dolomite (whole rock)

VSK 2 - trioctahedral smectite, dolomite (whole rock); smectite (clay separation)

VSK 3 - dolomite (whole rock)

VSK 4 - trioctahedral smectite, illite, K-feldspar (whole rock); smectite, illite (clay separation)

VSK 256 - plagioclase, calcite (whole rock)

VSK 262 - calcite (whole rock)

VSK 265 - smectite, illite, calcite (whole rock)

VSK 267 - illite, glass, quartz, K-feldspar, clinoptilolite (whole rock)

### *Sediments from Afyon area (Balmahmut)*

VSF 1 - illite, K-feldspar, calcite

VSF 3 - illite, K-feldspar, plagioclase

## Examples of XRD traces

Examples of XRD traces are shown over leaf. VSE 14 is a mudstone sample from Section Upper C (Figure G 1), while VSE 20 is a colemanite-rich mudstone sample from Section E (Figure G 2) in Emet Basin.

## Clay identification

Smectite was identified on the basis of a peak at  $\sim 15 \text{ \AA}$  ( $\sim 6$  two theta) in both whole rock and clay separation fractions (eg. VSE 16, Figure G 1). After glycollation, the peak shifted from  $\sim 15$  to  $\sim 17 \text{ \AA}$ , and after heat treatment the peak eventually collapsed. Further identification into trioctahedral smectite was on the basis of the 060 reflections. A peak of  $1.52\text{-}1.53 \text{ \AA}$  in the whole rock traces was considered diagnostic of trioctahedral smectite. However, calcite also has a peak in this region and hence the ratio between the  $3.03$  and  $1.52 \text{ \AA}$  peaks was measured in calcite-rich samples (VSE 10 & VSE 17). The proportion of 060 reflection ( $\sim 1.52 \text{ \AA}$ ) taken up by calcite in any given sample could then be determined. In most of the Emet and Kirka mudstone samples, the presence of calcite alone, could not account for the intensity of the  $\sim 1.52 \text{ \AA}$  peaks and it was therefore concluded that trioctahedral smectite was also present. Identification of dioctahedral smectite by XRD methods proved more difficult, due to overlap between the  $1.50 \text{ \AA}$  peak of this smectite and illite.

## Appendix G (XRD)

FIGURE G 1 - whole rock and clay separation XRD traces of sample VSE 16

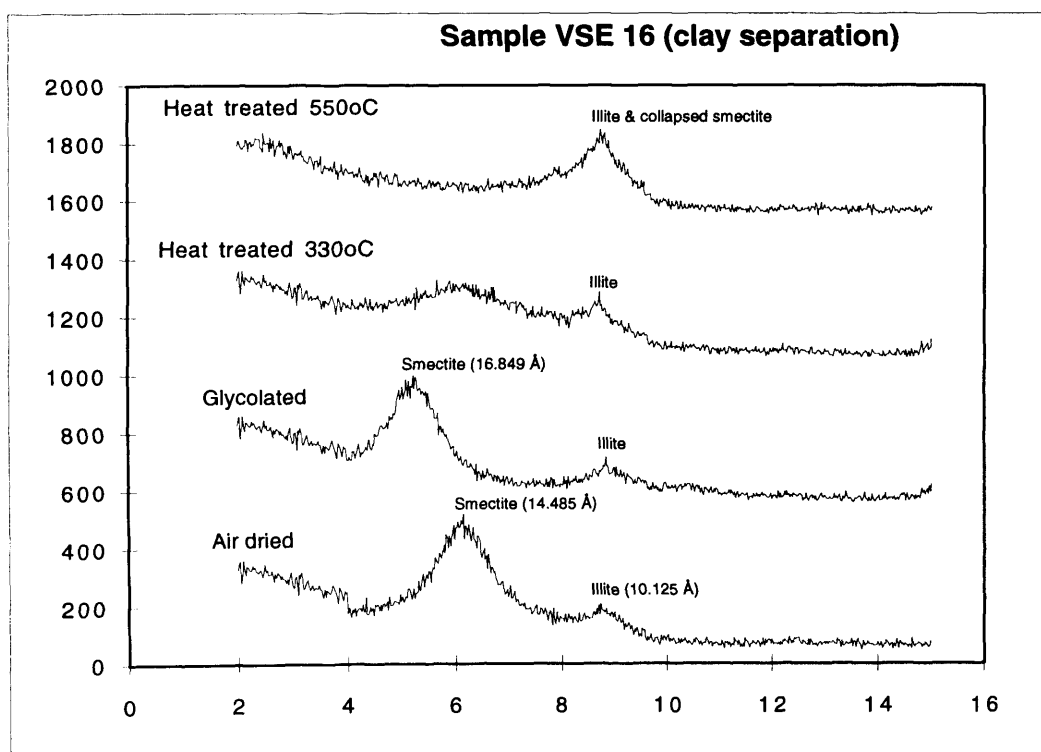
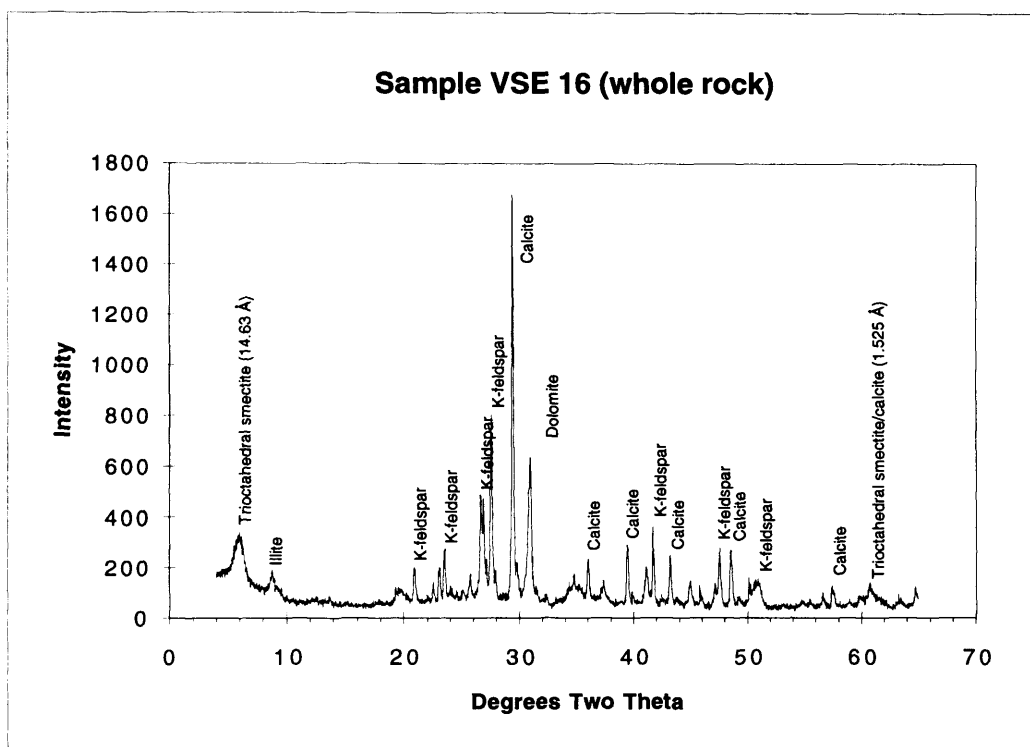
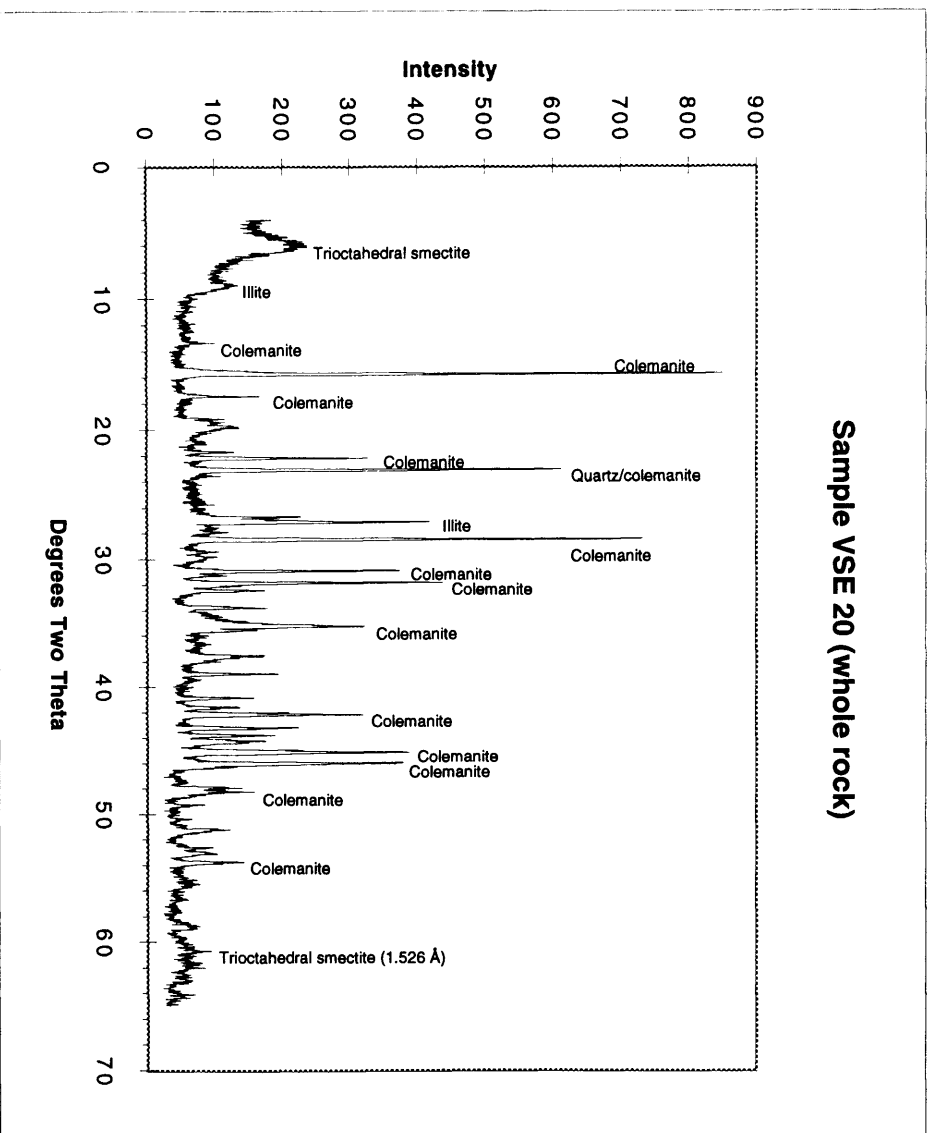


FIGURE G 2 - whole rock XRD trace of sample VSE 20





## Appendix H (electron microprobe analyses)

### Procedural details

Electron microprobe analyses were carried out at the University of Leicester on a JEOL JXA-8600 Superprobe running a wavelength dispersive system. The analyses were conducted on polished thin sections of granitic, volcanic and volcanoclastic samples from the USEKA area. The samples were analysed using a general silicate programme which was calibrated to the following standards; natural wollastonite for Si and Ca, natural rhodonite for Mn, natural jadeite for Na and Al, natural rutile for Ti, natural microcline for K and synthetic standards for Fe, Mg, Cr, and Ni. The operating voltage was 15 kv, the probe current was  $3 \times 10^{-8}$  A, and the beam diameters used were  $< 1 \mu\text{m}$  (for clay minerals) and  $15 \mu\text{m}$  (for feldspar, biotite, olivine). The analysed element was measured with a peak count of 20 seconds and a background count of 20 seconds. Estimated precision at  $2\sigma$  for the common petrogenetic minerals is  $\pm 0.25\%$  at 50 wt % oxide (calculated from standard deviations of raw intensity data).

### Electron microprobe data

Electron microprobe data used in this study is presented in the following pages. Analysed minerals include:

Plagioclase, K-feldspar and biotite from granitic, volcanic and volcanoclastic rocks of the USEKA area (number of ions on the basis of 32 O for feldspar and 22 O for biotite).

Magnetite from the Erigöz Granite (number of ions on the basis of 32 O).

Olivine from the Kirka Shoshonite (number of ions on the basis of 4 O).

Illite from Emet Basin volcanoclastics (Text Figures 4.2 & 4.4) (number of ions on the basis of 22 O).

Smectite from volcanoclastic sediments of the Red Formation in Emet Basin (Text Figure 4.2) (number of ions on the basis of 22 O).

Glass and matrix (clay) of the Kirka Ignimbrite (Text Figure 3.1a) (number of ions on the basis of 22 O).

Altered feldspar from the Emet Rhyolite (Text Figure 3.1b) (number of ions on the basis of 22 O).

Matrix (clay) of Borate Formation volcanoclastics (Text Figure 4.4a) (number of ions on the basis of 22 O).

Authigenic K-feldspar from Borate Formations volcanoclastics (Text Figure 4.4a) (number of ions on the basis of 32 O).

Altered plagioclase from Borate Formation volcanoclastics (Text Figure 4.4b) (number of ions on the basis of 22 O).

## Appendix H (electron microprobe)

### Plagioclase analyses

Sample	G8	G8	G8	G8	G8	G8	G8	G8	E2	E2	E2	E2	E2	E29
Run	dja1	dja1	dja1	dja1	dja1	dja1	dja1	dja1	dja15	dja3	dja3	dja3	dja3	dja5
Analysis	8	9	10	11	12	13	18	19	18	31	32	33	34	7
Mineral	Plag	Plag	Plag	Plag	Plag	Plag	Plag	Plag	Plag	Plag	Plag	Plag	Plag	Plag
SiO <sub>2</sub>	59.18	56.9	58.7	60.22	59.28	66.45	58.17	59.92	59.1	61.56	61.41	60.24	58.16	59.69
TiO <sub>2</sub>	0.01	0	0.01	0.01	0.01	0	0.01	0.01	0.01	0.01	0.01	0.02	0.01	0.01
Al <sub>2</sub> O <sub>3</sub>	25.41	26.93	24.71	24.31	24.77	19.73	24.62	24.41	24.88	23.17	23.67	24.45	25.78	24.01
Cr <sub>2</sub> O <sub>3</sub>	0.04	0.02	0	0	0	0	0.01	0	0.02	0.01	0.04	0.04	0.01	0.02
FeO	0.25	0.18	0.21	0.15	0.11	0.08	0.16	0.2	0.17	0.1	0.05	0.19	0.12	0.23
MnO	0.01	0.03	0.03	0.01	0.01	0.03	0.03	0.02	0.03	0.01	0.03	0.02	0.03	0
MgO	0	0	0	0	0	0.03	0	0	0.01	0	0	0	0	0
CaO	7.44	9.18	7.15	6.41	7.02	1.17	7.18	6.48	7.64	5.33	5.54	6.6	8.28	6.54
Na <sub>2</sub> O	7.28	6.17	7.35	8.02	7.33	11.06	7.36	7.77	7.13	7.78	7.83	7.35	6.53	7.16
K <sub>2</sub> O	0.29	0.39	0.28	0.36	0.33	0.27	0.4	0.47	0.69	1.07	0.99	0.79	0.54	0.85
NiO	0.02	0.03	0.03	0.03	0.04	0.03	0	0.01	0.02	0	0	0.02	0.02	0
Total	99.93	99.83	98.47	99.52	98.9	98.85	97.94	99.29	99.7	99.04	99.57	99.72	99.48	98.51
Si	10.592	10.246	10.656	10.797	10.698	11.808	10.627	10.774	10.627	11.059	10.982	10.787	10.477	10.819
Al	5.360	5.715	5.286	5.139	5.267	4.131	5.302	5.174	5.274	4.906	4.989	5.162	5.475	5.130
Fe <sub>2</sub>	0.038	0.026	0.032	0.022	0.016	0.013	0.026	0.029	0.026	0.016	0.006	0.029	0.019	0.035
Na	2.525	2.154	2.586	2.787	2.563	3.811	2.608	2.707	2.486	2.710	2.714	2.554	2.282	2.515
Ca	1.427	1.773	1.392	1.232	1.357	0.224	1.405	1.248	1.472	1.027	1.062	1.267	1.600	1.270
K	0.067	0.090	0.064	0.083	0.077	0.061	0.093	0.109	0.157	0.246	0.227	0.179	0.125	0.195
Total	20.010	20.003	20.016	20.061	19.978	20.048	20.061	20.042	20.042	19.965	19.981	19.978	19.978	19.965
An%	36	45	35	31	35	6	35	32	37	27	28	33	41	34
Or%	3	4	2	3	3	2	3	4	6	8	8	7	5	7

### Plagioclase analyses

Sample	E2	E2	E2	E2	E2	E2	E2	E2	E2	E29	E29	E29	E29	E20
Run	dja15	dja15	dja15	dja15	dja15	dja3	dja3	dja3	dja3	dja5	dja5	dja5	dja5	dja2
Analysis	19	20	21	22	23	27	28	29	30	13	14	17	18	49
Mineral	Plag	Plag	Plag	Plag	Plag	Plag	Plag	Plag	Plag	Plag	Plag	Plag	Plag	Plag
SiO <sub>2</sub>	59.93	55.79	55.66	55.89	58.43	61.05	61.98	60.89	60.81	60.89	61	59.75	60.04	59.37
TiO <sub>2</sub>	0.01	0.01	0.01	0.03	0.01	0.01	0.02	0.03	0.04	0.01	0.01	0.01	0.01	0.01
Al <sub>2</sub> O <sub>3</sub>	25.08	27.83	27.97	28.03	25.95	23.79	23.26	23.88	23.99	23.45	23.4	24.28	24.11	24.59
Cr <sub>2</sub> O <sub>3</sub>	0.01	0.01	0.04	0.02	0.04	0.02	0.03	0.04	0.02	0	0.04	0.02	0.04	0.02
FeO	0.18	0.19	0.21	0.22	0.14	0.1	0.13	0.19	0.15	0.25	0.22	0.23	0.24	0.13
MnO	0.01	0	0.01	0	0.03	0.03	0.03	0.02	0.03	0.03	0.01	0.03	0.03	0
MgO	0	0.01	0	0	0.01	0	0	0	0.01	0.01	0	0	0.01	0
CaO	6.86	10.09	10.2	10.25	7.88	6.02	5.37	6.2	6.1	5.8	5.77	6.74	6.56	6.92
Na <sub>2</sub> O	7.25	5.7	5.66	5.65	6.77	7.52	7.89	7.6	7.62	7.38	7.47	7.03	7.09	7.26
K <sub>2</sub> O	0.78	0.39	0.39	0.37	0.58	0.96	1.11	0.87	0.86	0.99	1.01	0.8	0.77	0.76
NiO	0.04	0.01	0.02	0.01	0	0.02	0.02	0.01	0.02	0.01	0.03	0.02	0	0.02
Total	100.2	100.1	100.19	100.5	99.87	99.52	99.84	99.73	99.65	98.82	98.96	98.91	98.9	99.08
Si	10.691	10.048	10.019	10.026	10.480	10.934	11.056	10.896	10.886	10.976	10.982	10.787	10.829	10.714
Al	5.274	5.910	5.936	5.926	5.485	5.021	4.890	5.037	5.062	4.982	4.966	5.168	5.126	5.232
Fe <sub>2</sub>	0.026	0.029	0.032	0.032	0.022	0.016	0.019	0.029	0.022	0.038	0.032	0.035	0.035	0.019
Na	2.509	1.990	1.974	1.965	2.355	2.611	2.730	2.637	2.643	2.579	2.608	2.461	2.480	2.541
Ca	1.312	1.949	1.968	1.971	1.514	1.155	1.027	1.187	1.171	1.120	1.114	1.302	1.267	1.338
K	0.176	0.090	0.090	0.083	0.131	0.221	0.253	0.198	0.195	0.227	0.234	0.186	0.176	0.176
Total	19.987	20.016	20.019	20.003	19.987	19.958	19.974	19.984	19.981	19.923	19.936	19.939	19.914	20.019
An%	34	49	50	50	39	31	27	31	31	30	30	35	34	34
Or%	7	4	4	4	5	8	8	7	7	8	8	7	7	6

Legend - Plag = plagioclase feldspar

## Appendix H (electron microprobe)

### Plagioclase analyses

Sample	E29	E29	E29	E29	VSE 8	VSE 8	VSE 8	VSE 8	VSE 8	VSE 8	VSE 8	VSE 8	VSE 8	I251
Run	dja5	dja5	dja5	dja5	dja4	dja4	dja4	dja8	dja8	dja8	dja8	dja8	dja8	dja3
Analysis	9	10	11	12	43	44	45	9	11	16	31	34	35	16
Mineral	Plag	Plag	Plag	Plag	Plag	Plag	Plag	Plag	Plag	Plag	Plag	Plag	Plag	Plag
SiO <sub>2</sub>	59.61	58.85	60.29	61.05	64.38	61.7	61.41	72.51	72.46	72.41	63.9	65.56	62.21	63.61
TiO <sub>2</sub>	0.01	0.06	0	0.01	0.01	0.01	0.01	0.03	0.05	0.07	0.06	0.01	0.01	0.02
Al <sub>2</sub> O <sub>3</sub>	24.73	24.98	23.96	23.56	20.54	23.33	23.34	20.41	22.06	21.75	23.34	20.44	22.86	22.16
Cr <sub>2</sub> O <sub>3</sub>	0	0.04	0	0.04	0	0.04	0.04	0.04	0.04	0.01	0.01	0.04	0.02	0.02
FeO	0.26	0.31	0.23	0.19	0.12	0.15	0.14	0.02	0.04	0.04	0.23	0.16	0.08	0.09
MnO	0.01	0.01	0.03	0.03	0	0.01	0	0	0.03	0.02	0.02	0.01	0.03	0.03
MgO	0	0.02	0	0.01	0.02	0	0.01	0	0	0	0.07	0	0.01	0
CaO	7.08	7.68	6.37	5.79	3.71	5.13	5.31	0.35	1.83	1.68	4.57	2.7	4.8	3.87
Na <sub>2</sub> O	7	6.87	7.43	7.38	8.21	8.53	8.42	5.43	5.06	5.44	6.52	9.53	8.71	8.76
K <sub>2</sub> O	0.77	0.67	0.85	0.96	0.8	0.48	0.48	0.15	0.22	0.3	0.44	0.44	0.42	1.01
NiO	0.02	0.02	0.01	0.01	0.03	0.01	0.02	0.02	0.01	0.02	0	0.01	0.02	0.02
Total	99.49	99.51	99.17	99.03	97.82	99.39	99.18	99.03	101.8	101.8	99.3	98.9	99.17	99.59
Si	10.714	10.602	10.854	10.976	11.594	11.034	11.011	12.410	12.131	12.150	11.299	11.664	11.130	11.318
Al	5.238	5.306	5.085	4.992	4.362	4.918	4.934	4.118	4.355	4.301	4.864	4.285	4.822	4.646
Fe <sub>2</sub>	0.038	0.048	0.035	0.029	0.019	0.022	0.022	0.003	0.006	0.006	0.035	0.022	0.013	0.013
Na	2.438	2.400	2.595	2.573	2.867	2.957	2.928	1.802	1.642	1.770	2.237	3.286	3.021	3.021
Ca	1.363	1.482	1.229	1.117	0.717	0.982	1.021	0.064	0.330	0.301	0.867	0.515	0.922	0.739
K	0.176	0.154	0.195	0.221	0.182	0.109	0.109	0.032	0.048	0.064	0.099	0.099	0.096	0.230
Total	19.968	19.990	19.994	19.907	19.741	20.022	20.026	18.429	18.512	18.592	19.402	19.872	20.003	19.968
An%	36	38	32	30	20	25	26	3	17	15	28	14	23	20
Or%	7	6	7	8	6	4	4	2	3	3	4	3	3	7

### Plagioclase analyses

Sample	E20	VSE 8	VSE 8	VSE 8	VSE 1	VSE 1	VSE 1	VSE 22	VSE 22	VSE 22	I251	I251	I251	I268
Run	dja2	dja4	dja4	dja4	dja8	dja8	dja8	dja5	dja5	dja5	dja3	dja3	dja3	dja6
Analysis	50	40	41	42	65	73	74	40	31	32	13	14	15	8
Mineral	Plag	Plag	Plag	Plag	Plag	Plag	Plag	Plag	Plag	Plag	Plag	Plag	Plag	Plag
SiO <sub>2</sub>	59.46	65.55	63.49	63.08	74.08	72.85	71.99	66.55	62.57	59.61	64.06	63.59	63.34	64.67
TiO <sub>2</sub>	0.01	0.01	0.02	0.07	0	0.08	0.08	0	0.01	0.1	0.01	0.01	0	0.01
Al <sub>2</sub> O <sub>3</sub>	24.52	19.47	20.9	21.86	20.26	20.92	20.62	18.94	21.33	21.41	22.12	22.06	22.04	21.7
Cr <sub>2</sub> O <sub>3</sub>	0.02	0.02	0.01	0.01	0.01	0.03	0.03	0.01	0	0.02	0.02	0.02	0.03	0
FeO	0.09	0.08	0.16	0.12	0.02	0.05	0.06	0.01	0.1	2.81	0.1	0.07	0.07	0.09
MnO	0.01	0.03	0.02	0.05	0.03	0.03	0.01	0.03	0.03	0.05	0.01	0.02	0.01	0.03
MgO	0	0.01	0.07	0.01	0	0	0	0.01	0.01	1.35	0	0	0	0
CaO	6.8	1.32	2.75	3.81	0.15	0.87	0.84	0.33	3.23	2.74	3.71	3.85	3.86	3.14
Na <sub>2</sub> O	7.19	7.5	9.19	8.47	4.4	3.73	5.71	10.88	9.12	7.77	8.86	8.69	8.79	8.61
K <sub>2</sub> O	0.72	4.94	0.91	1.72	0.13	0.11	1.63	0.12	0.45	2.24	1.16	1.13	0.99	1.33
NiO	0.02	0.01	0.01	0.01	0.02	0.02	0.01	0	0.03	0.02	0.04	0.02	0	0.02
Total	98.84	98.94	97.53	99.21	99.16	98.75	101	96.88	96.88	98.12	100.1	99.46	99.13	99.6
Si	10.742	11.818	11.501	11.309	12.573	12.429	12.243	11.990	11.402	10.989	11.344	11.331	11.322	11.472
Al	5.222	4.138	4.461	4.621	4.051	4.208	4.134	4.022	4.582	4.653	4.618	4.634	4.643	4.538
Fe <sub>2</sub>	0.013	0.013	0.026	0.019	0.003	0.006	0.010	0.000	0.016	0.432	0.016	0.010	0.010	0.013
Na	2.518	2.621	3.229	2.944	1.446	1.235	1.882	3.802	3.222	2.778	3.043	3.002	3.046	2.960
Ca	1.315	0.256	0.534	0.733	0.029	0.160	0.154	0.064	0.630	0.541	0.704	0.736	0.739	0.598
K	0.166	1.136	0.211	0.394	0.029	0.022	0.355	0.029	0.106	0.528	0.262	0.256	0.227	0.301
Total	19.978	19.981	19.962	20.019	18.131	18.061	18.778	19.907	19.958	19.920	19.987	19.968	19.987	19.882
An%	34	9	14	20	2	11	8	2	16	16	19	20	20	17
Or%	6	30	6	12	2	2	16	1	3	16	8	8	7	9

Legend - Plag = plagioclase feldspar

## Appendix H (electron microprobe)

### Plagioclase analyses

Sample	I220	I220	I220	I220	I220	I220	I220	K232	K232	K226	K226	K226	K226	K226
Run	dja3	dja3	dja3	dja3	dja3	dja3	dja3	dja14	dja14	dja14	dja14	dja14	dja14	dja14
Analysis	47	48	49	51	52	55	56	67	73	33	34	35	36	40
Mineral	Plag	Plag	Plag	Plag	Plag	Plag	Plag	Plag	Plag	Plag	Plag	Plag	Plag	Plag
SiO <sub>2</sub>	61.93	62.03	61.85	63.13	63.37	63.46	63.27	59.29	59.58	50.24	50.37	50.74	50.87	49.85
TiO <sub>2</sub>	0.01	0	0.01	0	0	0.01	0.01	0.01	0.01	0.03	0.01	0.01	0.05	0.04
Al <sub>2</sub> O <sub>3</sub>	23.05	22.97	23.41	22.54	22.3	22.3	22.14	25.18	25	30.61	30.74	30.78	30.7	30.78
Cr <sub>2</sub> O <sub>3</sub>	0.02	0.04	0.03	0.01	0.01	0.04	0.03	0.01	0.04	0.04	0.02	0.02	0.04	0.01
FeO	0.08	0.16	0.1	0.09	0.1	0.1	0.08	0.25	0.25	0.64	0.63	0.61	0.52	0.57
MnO	0.03	0	0	0	0.03	0.01	0.03	0.03	0.04	0.01	0.01	0.03	0.02	0.03
MgO	0	0	0	0	0	0	0.01	0	0	0.15	0.16	0.17	0.08	0.14
CaO	5.11	5.02	5.37	4.32	4.06	4.12	3.97	7.15	6.9	14.04	14.16	13.86	13.75	14.32
Na <sub>2</sub> O	8.25	8.25	8.19	8.74	8.68	8.68	8.7	6.95	7.09	3.22	3.28	3.27	3.48	3.22
K <sub>2</sub> O	0.78	0.8	0.71	0.92	1.01	0.92	0.95	0.85	0.88	0.4	0.39	0.39	0.37	0.34
NiO	0.04	0.03	0.02	0	0.05	0.01	0.01	0.02	0.02	0.02	0.01	0.02	0.02	0
Total	99.3	99.3	99.69	99.75	99.61	99.65	99.2	99.74	99.81	99.4	99.78	99.9	99.9	99.3
Si	11.088	11.104	11.034	11.229	11.283	11.286	11.302	10.640	10.682	9.245	9.235	9.277	9.299	9.190
Al	4.864	4.848	4.922	4.726	4.678	4.675	4.662	5.325	5.283	6.640	6.643	6.634	6.614	6.688
Fe <sub>2</sub>	0.013	0.022	0.016	0.013	0.016	0.016	0.013	0.038	0.038	0.099	0.096	0.093	0.080	0.086
Na	2.864	2.864	2.832	3.014	2.995	2.992	3.014	2.419	2.464	1.149	1.165	1.158	1.232	1.152
Ca	0.979	0.963	1.027	0.822	0.774	0.784	0.758	1.376	1.325	2.768	2.781	2.717	2.694	2.829
K	0.179	0.182	0.160	0.208	0.230	0.208	0.218	0.195	0.202	0.093	0.093	0.090	0.086	0.080
Total	19.987	19.984	19.990	20.013	19.978	19.962	19.968	19.994	19.994	19.994	20.013	19.968	20.006	20.026
An%	25	25	27	21	21	21	20	36	35	71	70	70	69	71
Or%	6	6	5	6	7	7	7	7	8	7	7	7	7	6

### Plagioclase analyses

Sample	I268	K232	K232	K232	K232	K232	K232	K226	K226	K226	K226	K226	A205	A205
Run	dja6	dja14	dja14	dja14	dja14	dja14	dja14	dja14	dja14	dja14	dja14	dja14	dja12	dja12
Analysis	9	52	54	60	63	64	65	43	44	45	41	42	41	51
Mineral	Plag	Plag	Plag	Plag	Plag	Plag	Plag	Plag	Plag	Plag	Plag	Plag	Plag	Plag
SiO <sub>2</sub>	66.1	59.54	59.68	59.45	59.25	59.97	59.22	49.59	49.81	50.43	50.87	50.55	56.78	59.86
TiO <sub>2</sub>	0.02	0	0.01	0.03	0.04	0.01	0.02	1.48	1.26	0.04	0	0.04	0.04	0.03
Al <sub>2</sub> O <sub>3</sub>	19.95	24.45	25.05	24.51	25.03	24.29	23.93	2.87	2.88	30.89	30.84	30.79	26.63	24.27
Cr <sub>2</sub> O <sub>3</sub>	0.01	0.02	0	0.02	0.04	0.01	0.04	0.2	0.18	0.04	0.04	0.04	0	0.03
FeO	0.21	0.15	0.2	0.29	0.25	0.24	0.23	10.23	9.85	0.57	0.52	0.56	0.32	0.3
MnO	0.03	0.02	0.04	0.03	0.02	0.02	0	0.32	0.29	0.03	0	0.02	0.03	0.01
MgO	0	0.02	0.01	0.01	0.01	0	0	15.86	15.79	0.13	0.15	0.17	0	0.02
CaO	2.93	6.78	7.04	6.53	7.2	6.32	6.32	18.43	18.53	14.17	14.14	13.97	8.27	6.11
Na <sub>2</sub> O	7.44	7.06	7.07	6.82	6.89	7.33	7.03	0.31	0.31	3.33	3.36	3.33	6	7.26
K <sub>2</sub> O	2.06	0.93	0.86	0.93	0.81	1	0.96	0.06	0.07	0.34	0.34	0.35	0.65	0.95
NiO	0.03	0.02	0.04	0.04	0.02	0.01	0	0.05	0.02	0.02	0.01	0	0.02	0.01
Total	98.78	98.99	100	98.66	99.53	99.2	97.75	99.4	98.99	99.99	100.3	99.82	98.74	98.85
Si	11.789	10.752	10.678	10.758	10.653	10.803	10.816	9.962	10.022	9.226	9.270	9.254	10.32	10.81
Al	4.195	5.203	5.283	5.229	5.306	5.158	5.152	0.678	0.682	6.659	6.624	6.643	5.702	5.165
Fe <sub>2</sub>	0.032	0.022	0.029	0.045	0.038	0.035	0.035	1.718	1.658	0.086	0.080	0.086	0.048	0.045
Na	2.573	2.470	2.451	2.394	2.403	2.560	2.490	0.122	0.122	1.181	1.187	1.181	2.115	2.541
Ca	0.560	1.312	1.350	1.267	1.386	1.219	1.235	3.968	3.994	2.778	2.762	2.739	1.61	1.181
K	0.467	0.214	0.195	0.214	0.186	0.230	0.224	0.016	0.019	0.080	0.080	0.083	0.15	0.218
Total	19.616	19.974	19.986	19.907	19.971	20.006	19.952	16.464	16.496	20.010	20.003	19.987	19.94	19.96
An%	18	35	36	35	37	32	33	97	97	70	70	70	43	32
Or%	15	8	7	8	7	8	8	12	14	6	6	7	7	8

Legend - Plag = plagioclase feldspar

## Appendix H (electron microprobe)

### Plagioclase analyses

Sample	A205	A210	A210	A210	A210	A210	A217	A217	A217	A217	A217	A217
Run	dja12	dja12	dja12	dja12	dja12	dja12	dja12	dja12	dja12	dja12	dja12	dja12
Analysis	52	53	54	55	59	61	3	4	14	16	17	18
Mineral	Plag	Plag	Plag	Plag	Plag	Plag	Plag	Plag	Plag	Plag	Plag	Plag
SiO <sub>2</sub>	59.37	59.23	60.77	60.93	58.92	57.34	60.55	60.59	60.19	57.99	57.76	58.14
TiO <sub>2</sub>	0.07	0.01	0.02	0	0	0.08	0	0.02	0.01	0.01	0.01	0.01
Al <sub>2</sub> O <sub>3</sub>	24.14	24.3	23.9	24.05	25.44	25.62	24.66	24.69	24.86	26.05	25.79	26.8
Cr <sub>2</sub> O <sub>3</sub>	0.02	0	0.04	0.02	0.02	0	0.04	0.01	0.01	0	0.04	0.04
FeO	0.22	0.21	0.22	0.21	0.24	0.18	0.2	0.29	0.25	0.24	0.28	0.2
MnO	0.03	0.03	0.01	0.05	0.01	0.03	0.03	0.03	0.02	0.01	0.03	0.03
MgO	0.02	0.01	0	0	0	0.01	0.02	0	0	0	0.02	0.01
CaO	6.04	6.35	5.72	5.82	6.97	7.78	6.42	6.35	6.5	7.86	7.86	8.24
Na <sub>2</sub> O	7.22	7.19	7.39	7.56	6.91	6.62	7.27	7.2	7.25	6.47	6.53	6.39
K <sub>2</sub> O	0.98	0.99	1.14	1.17	0.83	0.66	0.98	1.08	1.05	0.84	0.82	0.71
NiO	0.02	0.02	0.03	0.03	0.01	0.02	0.03	0.01	0.02	0.01	0.02	0.02
Total	98.13	98.34	99.24	99.84	99.35	98.34	100.2	100.3	100.2	99.48	99.16	100.6
Si	10.8	10.76	10.92	10.896	10.61	10.46	10.790	10.794	10.746	10.454	10.458	10.368
Al	5.178	5.206	5.062	5.0688	5.398	5.507	5.181	5.184	5.232	5.536	5.504	5.635
Fe <sub>2</sub>	0.032	0.032	0.032	0.032	0.035	0.029	0.029	0.045	0.038	0.035	0.042	0.029
Na	2.547	2.534	2.576	2.6208	2.413	2.339	2.512	2.486	2.509	2.262	2.291	2.211
Ca	1.178	1.235	1.101	1.1136	1.344	1.52	1.226	1.213	1.245	1.517	1.523	1.574
K	0.227	0.23	0.262	0.2656	0.192	0.154	0.224	0.246	0.240	0.192	0.189	0.160
Total	19.96	20	19.95	19.997	19.99	20.01	19.96	19.97	20.01	20	20.01	19.98
An%	32	33	30	30	36	39	33	33	33	40	40	42
Or%	8	8	9	9	7	6	8	9	9	8	8	7

### K-feldspar analyses

Sample	G8	G8	G8	G8	G8	E4	E4	E4	E4	E4	E4	E4	E2	E2
Run	dja1	dja1	dja1	dja2	dja2	dja15	dja15	dja15	dja15	dja15	dja15	dja15	dja15	dja15
Analysis	20	21	22	9	10	1	2	4	5	6	7	8	29	30
Mineral	Kf	Kf	Kf	Kf	Kf	Kf	Kf	Kf	Kf	Kf	Kf	Kf	Kf	Kf
SiO <sub>2</sub>	65.27	65.13	65.1	65.99	64.8	63.54	64.35	63.93	61.99	63.07	63.33	57.88	64.64	64.81
TiO <sub>2</sub>	0.01	0.03	0.01	0.01	0.02	0.38	0.39	0.34	0.46	0.39	0.3	0.26	0	0.08
Al <sub>2</sub> O <sub>3</sub>	18.39	18.22	18.4	18.33	18.19	17.83	18.65	19.26	18.5	19.39	19.48	23.48	19.08	19.16
Cr <sub>2</sub> O <sub>3</sub>	0.04	0.02	0.01	0	0.04	0.04	0.04	0.01	0.04	0.02	0.02	0.01	0.04	0.02
FeO	0.14	0.06	0.08	0.1	0.07	1.03	0.78	0.64	1.68	0.52	0.56	1.03	0.05	0.06
MnO	0.02	0.01	0	0.02	0.02	0.03	0.03	0	0.03	0.01	0.03	0.03	0	0.01
MgO	0	0	0	0	0	0.19	0.07	0.05	0.24	0.04	0.04	0.45	0	0
CaO	0.07	0.11	0.08	0.09	0.05	0.66	0.52	1.09	2.22	1.2	1.12	6.18	0.16	0.14
Na <sub>2</sub> O	2.1	1.45	2.31	2.66	2.08	2.99	3.28	3.66	3.43	3.23	3.29	4.65	2.92	2.98
K <sub>2</sub> O	13.84	14.59	13.52	13.11	14	11.06	11.46	10.61	9.88	10.63	10.68	4.66	12.46	12.46
NiO	0.02	0.02	0.01	0.03	0.02	0.02	0.02	0.02	0.01	0.01	0.02	0.02	0.02	0.01
Total	99.9	99.64	99.52	100.34	99.29	97.85	99.59	99.61	98.49	98.52	98.88	98.69	99.37	99.74
Si	11.990	12.016	11.987	12.029	11.990	11.872	11.824	11.722	11.584	11.683	11.690	10.678	11.882	11.869
Al	3.981	3.962	3.994	3.939	3.968	3.926	4.038	4.163	4.074	4.234	4.237	5.107	4.134	4.138
Fe <sub>2</sub>	0.022	0.010	0.013	0.016	0.010	0.160	0.118	0.099	0.262	0.080	0.086	0.160	0.006	0.010
Ti	0.000	0.003	0.000	0.000	0.003	0.054	0.054	0.048	0.064	0.054	0.042	0.035	0.000	0.010
Mg	0.000	0.000	0.000	0.000	0.000	0.054	0.019	0.013	0.067	0.010	0.010	0.125	0.000	0.000
Na	0.749	0.518	0.826	0.941	0.746	1.085	1.168	1.302	1.242	1.162	1.178	1.664	1.040	1.059
Ca	0.013	0.022	0.016	0.016	0.010	0.131	0.102	0.214	0.445	0.237	0.221	1.222	0.032	0.029
K	3.245	3.434	3.178	3.050	3.306	2.637	2.688	2.483	2.355	2.512	2.515	1.098	2.922	2.912
Total	20.000	19.965	20.013	19.990	20.032	19.920	20.013	20.045	20.093	19.971	19.978	20.090	20.016	20.026
An%	2	4	2	2	1	11	8	14	26	17	16	42	3	3
Or%	81	87	79	76	82	71	70	66	65	68	68	40	74	73

Legend - Plag = plagioclase feldspar, Kf = K-feldspar

## Appendix H (electron microprobe)

### K-feldspar analyses

Sample	E4	E4	E4	E4	E4	E4	E4	E2	E2	E2	E2	E2	VSE 1	VSE 1	VSE 1
Run	dja15	dja15	dja15	dja15	dja2	dja2	dja2	dja15	dja15	dja15	dja15	dja15	dja4	dja4	dja4
Analysis	9	10	11	12	25	28	29	24	25	26	27	28	4	9	11
Mineral	Kf	Kf	Kf	Kf	Kf	Kf	Kf	Kf	Kf	Kf	Kf	Kf	Kf	Kf	Kf
SiO2	61.61	61.76	61.7	63.25	63.76	63.89	64.39	64.78	64.19	63.75	64.92	64.65	76.07	64.86	63.5
TiO2	0.3	0.44	0.31	0.89	0.32	0.39	0.38	0.01	0.05	0.04	0.02	0.08	0	0.01	0
Al2O3	20.79	16.18	16.42	18.2	19.07	19.06	19.18	18.83	19.06	19.02	18.92	18.95	10.89	18.29	17.79
Cr2O3	0.03	0.01	0.04	0.04	0	0.04	0	0.04	0.04	0.04	0.04	0.03	0.04	0.02	0.02
FeO	0.9	4.65	4.2	1.3	0.54	0.35	0.36	0.03	0.03	0.03	0.02	0.02	0.06	0.04	0.08
MnO	0	0.03	0.03	0	0.01	0.03	0	0.03	0.04	0.02	0.02	0.03	0.03	0.01	0.05
MgO	0.01	0.98	1.23	0.08	0.01	0	0	0	0	0	0	0	0	0	0
CaO	2.82	1.46	1.76	1.25	1.2	1.22	1.24	0.14	0.15	0.14	0.16	0.12	0.01	0.01	0.2
Na2O	4.1	2.89	2.86	3.15	3.65	3.52	3.6	2.85	2.79	2.86	2.88	2.89	0.63	1.08	3.28
K2O	8.36	8.83	8.76	10.58	10.77	10.86	10.89	12.58	12.43	12.42	12.42	12.64	10.36	15.26	12.91
NiO	0.03	0.02	0.03	0.01	0.04	0.02	0.04	0	0.01	0.02	0.01	0.02	0.02	0.02	0.02
Total	98.97	97.34	97.39	98.77	99.37	99.38	100.1	99.29	98.82	98.35	99.46	99.46	98.11	99.6	97.85
Si	11.354	11.738	11.702	11.734	11.731	11.744	11.750	11.920	11.866	11.850	11.910	11.885	13.616	12.000	11.936
Al	4.515	3.626	3.670	3.981	4.134	4.128	4.125	4.083	4.154	4.166	4.093	4.106	2.298	3.990	3.942
Fe2	0.138	0.739	0.666	0.202	0.083	0.054	0.054	0.003	0.003	0.003	0.003	0.003	0.010	0.006	0.013
Na	0.042	0.064	0.045	0.125	0.045	0.054	0.051	0.000	0.006	0.006	0.003	0.010	0.000	0.000	0.000
Ca	0.003	0.278	0.349	0.022	0.003	0.000	0.000	0.000	0.000	0.000	0.000	0.000	0.000	0.000	0.000
K	1.466	1.066	1.053	1.133	1.302	1.254	1.274	1.018	0.998	1.030	1.024	1.030	0.218	0.387	1.197
Total	0.557	0.298	0.358	0.250	0.237	0.240	0.243	0.029	0.029	0.029	0.032	0.022	0.003	0.003	0.042
An%	1.965	2.141	2.118	2.506	2.528	2.547	2.534	2.954	2.931	2.944	2.909	2.963	2.365	3.603	3.098
Or%	20.038	19.949	19.962	19.952	20.064	20.022	20.032	20.006	19.987	20.029	19.974	20.019	18.509	19.990	20.227
	28	22	25	18	15	16	16	3	3	3	3	2	1	1	3
	57	67	67	69	66	67	67	74	75	74	74	74	92	90	72

### K-feldspar analyses

Sample	E20	VSE 1	VSE 1	VSE 1	VSE 1	VSE 1	VSE 8	VSE 8	VSE 8	VSE 8	VSE 8	VSE 8	VSE 22	VSE 8	VSE 8
Run	dja2	dja4	dja4	dja4	71	80	dja4	dja4	dja4	dja4	dja4	dja4	dja5	8	
Analysis	58	3	24	25	dja8	dja8	30	31	32	33	36	39	44	dja8	dja30
Mineral	Kf	Kf	Kf	Kf	Kf	Kf	Kf	Kf	Kf	Kf	Kf	Kf	Kf	Kf	Kf
SiO2	63.79	64.02	64.92	64.32	66.93	63.79	64.45	64.6	65.05	64.53	64.67	64.21	63.29	66.54	70.23
TiO2	0.01	0.01	0.02	0.01	0.01	0.08	0.02	0.02	0.02	0.03	0.01	0.03	0.03	0.04	0.02
Al2O3	18.42	17.86	18.13	17.96	18.42	24.36	17.98	18.69	18.32	18.08	18.13	17.89	17.82	19.66	20.36
Cr2O3	0.01	0.03	0.04	0.03	0.02	0.04	0	0	0.04	0.04	0.02	0.06	0	0.04	0.04
FeO	0.06	0.06	0.12	0.1	0.09	0.17	0.09	0.03	0.05	0.04	0.4	0.13	0.03	0.04	0.14
MnO	0.03	0.03	0.02	0.01	0.02	0.02	0.01	0.01	0.02	0.02	0	0.03	0.03	0	0.06
MgO	0	0	0	0	0	0	0	0	0	0	0.06	0	0	0.07	0.03
CaO	0.23	0.02	0.05	0.04	0.14	3.83	0.01	0.67	0.07	0.07	0.24	0	0.02	0.4	0.01
Na2O	2.88	1.13	1.95	1.31	1.05	6.04	1.26	2.66	3.51	1.11	4.65	1.57	0.75	2.75	0.25
K2O	12.32	15.35	14.23	15	10.11	0.76	15.02	12.72	11.92	15.31	9.91	14.79	15.72	11.04	15.72
NiO	0.02	0.02	0.01	0.02	0.02	0.04	0.01	0	0.02	0.04	0.02	0.02	0.02	0	0.02
Total	97.77	98.53	99.49	98.8	97.38	99.18	98.85	99.4	99.02	99.26	98.13	98.71	97.71	100.6	106.88
Si	11.926	12.003	12.000	12.006	12.294	11.251	12.016	11.901	11.981	11.997	11.962	12.000	11.987	11.949	12.016
Al	4.058	3.946	3.949	3.952	3.987	5.062	3.952	4.058	3.978	3.962	3.952	3.939	3.978	4.160	4.106
Fe2	0.010	0.010	0.019	0.016	0.013	0.026	0.013	0.003	0.006	0.006	0.061	0.019	0.003	0.006	0.019
Ti	0.000	0.000	0.003	0.000	0.000	0.010	0.003	0.003	0.003	0.003	0.003	0.000	0.003	0.006	0.003
Mg	0.000	0.000	0.000	0.000	0.000	0.000	0.000	0.000	0.000	0.000	0.016	0.000	0.000	0.019	0.006
Na	1.043	0.410	0.698	0.474	0.374	2.064	0.454	0.950	1.254	0.400	1.667	0.570	0.275	0.957	0.083
Ca	0.045	0.003	0.010	0.010	0.029	0.723	0.003	0.131	0.013	0.013	0.048	0.000	0.003	0.077	0.003
K	2.938	3.670	3.357	3.571	2.368	0.170	3.574	2.989	2.800	3.632	2.339	3.526	3.798	2.528	3.430
Total	20.019	20.042	20.035	20.029	19.066	19.306	20.016	20.035	20.035	20.013	20.048	20.054	20.048	19.702	19.667
An%	4	1	1	2	7	26	1	12	1	3	3	0	1	7	4
Or%	74	90	83	88	86	8	89	76	69	90	58	86	93	73	98

Legend - Kf = K-feldspar

## Appendix H (electron microprobe)

### K-feldspar analyses

Sample	VSE 1	VSE 1	VSE 1	VSE 1	VSE 1	VSE 1	VSE 1	VSE 8	VSE 8	VSE 8	I251	I251
Run	dja4	dja4	dja4	dja4	dja4	dja4	dja4	dja4	dja4	2	dja3	dja3
Analysis	12	17	18	19	20	22	23	46	47	dja8	8	9
Mineral	Kf	Kf	Kf	Kf	Kf	Kf	Kf	Kf	Kf	Kf	Kf	Kf
SiO2	64.46	51.18	64.93	64.37	63.43	84.13	82.6	63.15	64.38	76.78	65.68	65.56
TiO2	0.02	0.25	0.01	0.01	0.01	0.03	0.05	0.02	0.01	0.06	0.01	0.01
Al2O3	18.2	20.12	18.03	18.19	18.29	7.9	8.53	17.81	18.16	20.6	18.31	18.34
Cr2O3	0.02	0.01	0	0.04	0.01	0	0.01	0.01	0.02	0.02	0	0.04
FeO	0.04	7.24	0.09	0.07	0.13	0.1	0.13	0.05	0.15	0.02	0.04	0.01
MnO	0.02	0.07	0	0	0.02	0.03	0.03	0.03	0.03	0.01	0.02	0.03
MgO	0	4.16	0	0	0	0	0	0	0	0	0	0
CaO	0.06	0.11	0.54	0.07	0.03	0.05	0.05	0.02	0.09	0.12	0.14	0.12
Na2O	1.78	0.14	2.34	1.84	2.05	0.45	0.59	0.85	2.64	1.05	3.39	3.45
K2O	14.37	7.66	12.44	14.29	13.89	6.74	7.28	15.92	13.26	2.81	12.05	11.9
NiO	0.01	0.01	0.02	0.02	0.02	0.03	0.02	0.02	0.02	0.01	0.02	0.01
Total	98.98	90.95	98.4	98.9	97.88	99.46	99.29	97.88	98.76	101.55	99.66	99.47
Si	11.981	10.512	12.035	11.974	11.923	14.381	14.227	11.965	11.965	12.726	12.013	12.006
Al	3.987	4.870	3.939	3.987	4.051	1.590	1.731	3.978	3.978	4.026	3.949	3.958
Fe2	0.006	1.245	0.013	0.010	0.019	0.013	0.019	0.006	0.022	0.003	0.006	0.000
Ti	0.003	0.038	0.000	0.000	0.000	0.003	0.006	0.003	0.000	0.006	0.000	0.000
Mg	0.000	1.274	0.000	0.000	0.000	0.000	0.000	0.000	0.000	0.000	0.000	0.000
Na	0.640	0.054	0.842	0.662	0.746	0.150	0.198	0.314	0.950	0.336	1.203	1.226
Ca	0.013	0.026	0.109	0.013	0.006	0.010	0.010	0.003	0.019	0.022	0.029	0.022
K	3.408	2.006	2.941	3.392	3.331	1.469	1.600	3.846	3.142	0.595	2.813	2.781
Total	20.038	20.026	19.878	20.038	20.077	17.616	17.792	20.115	20.077	17.715	20.013	19.994
An%	2	32	11	2	1	6	5	1	2	6	2	2
Or%	84	97	78	84	82	91	89	92	77	64	70	69

### K-feldspar analyses

Sample	VSE 2	VSE 2	VSE 22	VSE 22	VSE 22	I251	I251	I251	I251	I251	I220	I220
Run	dja4	dja4	dja5	dja5	dja5	dja3	dja3	dja3	dja3	dja3	dja3	dja3
Analysis	57	58	35	36	43	5	6	7	17	18	41	42
Mineral	Kf	Kf	Kf	Kf	Kf	Kf	Kf	Kf	Kf	Kf	Kf	Kf
SiO2	63.62	63.73	63.53	64.35	57.67	65.28	65.77	66.03	65.64	66.14	65.26	65.38
TiO2	0.02	0.01	0.04	0.03	0.01	0.03	0.01	0.01	0.01	0.03	0.01	0.01
Al2O3	17.98	18.2	18.23	18.03	16.27	18.47	18.46	18.45	18.55	18.42	18.26	18.32
Cr2O3	0.01	0.04	0.02	0.01	0.02	0.02	0.02	0.01	0	0	0.02	0.04
FeO	0.02	0.01	0.08	0.06	0.1	0.04	0.03	0.08	0.03	0.05	0.06	0.08
MnO	0.03	0.03	0.02	0.03	0.02	0.03	0.01	0.03	0.03	0	0.02	0.03
MgO	0	0	0	0	0	0	0	0	0	0	0	0
CaO	0.13	0.07	0.19	0.14	0.16	0.19	0.16	0.13	0.16	0.15	0.13	0.16
Na2O	1.07	1.16	2.44	2.4	0.46	3.54	3.44	3.52	3.38	3.38	3.32	3.25
K2O	15.31	15.34	12.72	13.07	15.58	11.88	11.97	11.8	12.05	12.11	12.06	12.08
NiO	0.02	0.03	0.02	0.02	0	0.02	0	0.02	0.02	0.02	0.02	0.01
Total	98.21	98.62	97.29	98.14	90.29	99.5	99.87	100.08	99.87	100.3	99.16	99.36
Si	11.971	11.942	11.949	12.003	11.920	11.965	12.000	12.013	11.984	12.019	12.003	12.000
Al	3.987	4.019	4.042	3.965	3.965	3.990	3.971	3.955	3.990	3.946	3.958	3.965
Fe2	0.003	0.000	0.013	0.010	0.016	0.006	0.003	0.013	0.003	0.006	0.010	0.013
Ti	0.003	0.000	0.006	0.003	0.000	0.003	0.000	0.000	0.000	0.003	0.000	0.000
Mg	0.000	0.000	0.000	0.000	0.000	0.000	0.000	0.000	0.000	0.000	0.000	0.000
Na	0.390	0.422	0.890	0.867	0.186	1.258	1.216	1.242	1.197	1.190	1.184	1.155
Ca	0.026	0.013	0.038	0.029	0.035	0.038	0.032	0.026	0.032	0.029	0.026	0.032
K	3.674	3.667	3.053	3.110	4.109	2.778	2.787	2.739	2.806	2.806	2.829	2.829
Total	20.054	20.064	19.990	19.987	20.230	20.038	20.010	19.987	20.013	20.000	20.010	19.994
An%	6	3	4	3	16	3	3	2	3	2	2	3
Or%	90	90	77	78	96	69	70	69	70	70	70	71

Legend - Kf = K-feldspar

## Appendix H (electron microprobe)

### K-feldspar analyses

Sample	I251	I220	I268	I268	I268	I268	I268	K232	K232	I220	K232	A217
Run	dja3	dja3	dja6	dja6	dja6	dja6	dja6	dja14	dja14	dja3	dja14	dja12
Analysis	10	46	6	7	12	13	18	56	57	45	58	1
Mineral	Kf	Kf	Kf	Kf	Kf	Kf	Kf	Kf	Kf	Kf	Kf	Kf
SiO2	65.66	65.5	64.75	65.69	65.75	65.71	79.55	63.7	64.54	65.7	64.65	63.99
TiO2	0.01	0.01	0	0.01	0.01	0.02	0.01	0.03	0.05	0.02	0.01	0.08
Al2O3	18.4	18.27	18.44	18.64	18.63	18.7	10.86	18.4	18.7	18.36	18.72	18.9
Cr2O3	0.02	0.01	0.02	0.04	0.04	0.02	0.01	0.02	0.04	0.04	0.02	0.02
FeO	0.05	0.07	0.05	0.04	0.08	0.06	0.47	0.1	0.08	0.04	0.11	0.14
MnO	0.03	0.01	0.03	0.01	0.01	0.03	0.01	0.02	0.03	0.01	0.03	0.03
MgO	0	0	0.01	0	0	0	0	0	0	0	0	0
CaO	0.12	0.11	0.2	0.15	0.17	0.19	0.54	0.15	0.23	0.12	0.19	0.27
Na2O	3.29	3.39	3.56	3.63	3.51	3.6	3.05	2.81	2.83	3.36	2.94	2.88
K2O	12.21	11.95	11.31	11.47	11.46	11.64	4.53	12.22	12.22	12	12.24	11.87
NiO	0.03	0.01	0.01	0.01	0.01	0.01	0.02	0.01	0.02	0.02	0.02	0.02
Total	99.82	99.33	98.38	99.69	99.67	99.98	99.05	97.46	98.74	99.67	98.93	98.2
Si	12.000	12.016	11.971	11.981	11.990	11.965	13.747	11.936	11.926	12.010	11.93	11.882
Al	3.965	3.952	4.019	4.006	4.003	4.013	2.211	4.064	4.074	3.955	4.0704	4.1376
Fe2	0.006	0.010	0.006	0.006	0.013	0.010	0.067	0.016	0.013	0.006	0.016	0.0224
Ti	0.000	0.000	0.000	0.000	0.000	0.003	0.000	0.003	0.006	0.003	0	0.0096
Mg	0.000	0.000	0.003	0.000	0.000	0.000	0.000	0.000	0.000	0.000	0	0
Na	1.165	1.206	1.277	1.283	1.242	1.270	1.021	1.021	1.014	1.190	1.0528	1.0368
Ca	0.022	0.022	0.038	0.029	0.032	0.038	0.099	0.029	0.045	0.022	0.0384	0.0544
K	2.848	2.797	2.669	2.669	2.666	2.704	0.998	2.922	2.880	2.800	2.88	2.8128
Total	20.006	20.003	19.984	19.974	19.946	20.003	18.144	19.990	19.958	19.987	19.987	19.955
An%	2	2	3	2	3	3	9	3	4	2	4	5
Or%	71	70	68	68	68	68	49	74	74	70	73	73

### K-feldspar analyses

Sample	A217	A217	A217
Run	dja12	dja12	dja12
Analysis	11	12	13
Mineral	Kf	Kf	Kf
SiO2	65.45	64.75	64.63
TiO2	0.02	0.02	0.04
Al2O3	18.85	18.96	19
Cr2O3	0.02	0.01	0.01
FeO	0.26	0.08	0.12
MnO	0.01	0.03	0
MgO	0	0	0
CaO	0.35	0.16	0.2
Na2O	3.26	3.04	2.87
K2O	11.81	12.05	12.25
NiO	0.03	0.06	0.02
Total	100.06	99.16	99.14
Si	11.926	11.907	11.898
Al	4.048	4.1088	4.1216
Fe2	0.0384	0.0128	0.0192
Ti	0.0032	0.0032	0.0064
Mg	0	0	0
Na	1.152	1.0848	1.024
Ca	0.0672	0.032	0.0384
K	2.7456	2.8256	2.8768
Total	19.981	19.974	19.984
An%	6	3	4
Or%	70	72	74

Legend - Kf = K-feldspar



## Appendix H (electron microprobe)

### Biotite analyses

Sample Run Analysis	G8 dja1 6	G8 dja1 7	G8 dja1 17	G8 dja2 1	G8 dja2 2	G8 dja2 7	G8 dja2 8	E4 dja2 32	E4 dja2 34	E4 dja2 35	E4 dja10 1	E4 dja10 3	E4 dja10 7	E4 dja10 10	E4 dja10 11	E4 dja10 15
Mineral	biotite	biotite	biotite	biotite	biotite	biotite	biotite	biotite	biotite	biotite	biotite	biotite	biotite	biotite	biotite	biotite
SiO <sub>2</sub>	36.25	35.68	36.03	35.2	36.68	36.11	36.3	38.5	38.4	38.2	40.2	38.5	38.2	38.7	38.7	39.4
TiO <sub>2</sub>	4.12	3.99	4.24	4.67	4.14	4.32	4.31	5.39	5.09	5.03	4.65	5.09	5.17	4.98	5.1	4.88
Al <sub>2</sub> O <sub>3</sub>	13.15	13.56	13.17	13.96	13.12	13.63	13.59	13.4	13.8	13.9	13.1	14	14.1	14.1	14	14
Cr <sub>2</sub> O <sub>3</sub>	0.04	0.05	0.03	0	0.03	0.02	0.01	0.11	0.2	0.1	0.19	0.17	0.26	0.2	0.21	0.08
FeO	20.8	21.79	20.91	21.24	20.31	21.37	21.15	12.6	7.55	7.5	9.16	7.52	8.98	7.53	7.34	8.24
MnO	0.52	0.53	0.51	0.52	0.51	0.44	0.45	0.03	0.04	0.07	0.06	0.07	0.01	0.04	0.04	0.09
MgO	10.21	10.11	10.09	9.56	10.6	10.31	10.35	16.3	19.7	19.4	17.6	20.3	18.8	20.4	20	19.1
CaO	0.05	0	0.02	0.03	0.43	0.01	0.01	0.29	0.02	0.02	0.18	0.01	0.04	0.01	0.02	0.04
Na <sub>2</sub> O	0.24	0.14	0.18	0.32	0.3	0.16	0.14	0.52	0.45	0.46	0.46	0.39	0.48	0.49	0.48	0.49
K <sub>2</sub> O	9.53	9.5	9.32	9.13	9.15	9.47	9.58	8.43	9.87	9.79	8.53	9.81	9.51	9.71	9.67	9.31
NiO	0.01	0.01	0.02	0.02	0.02	0.04	0.03	0.06	0.06	0.03	0.1	0.03	0.07	0.03	0.06	0.05
Total	94.92	95.36	94.52	94.65	95.29	95.88	95.92	95.5	95.2	94.5	94.2	95.8	95.7	96.1	95.7	95.6
Si	5.639	5.553	5.628	5.502	5.656	5.568	5.588	5.647	5.573	5.577	5.856	5.542	5.546	5.551	5.568	5.667
Altet	2.361	2.447	2.372	2.498	2.344	2.432	2.412	2.314	2.363	2.389	2.144	2.372	2.418	2.378	2.383	2.333
Ttet	8.000	8.000	8.000	8.000	8.000	8.000	8.000	7.962	7.935	7.966	8.000	7.913	7.964	7.929	7.951	8.000
Aloct	0.050	0.041	0.052	0.074	0.041	0.045	0.054	0.000	0.000	0.000	0.116	0.000	0.000	0.000	0.000	0.034
Ti	0.482	0.466	0.497	0.550	0.480	0.502	0.499	0.594	0.554	0.552	0.510	0.552	0.563	0.537	0.552	0.528
Fe <sub>2</sub>	2.706	2.836	2.730	2.776	2.620	2.754	2.724	1.547	0.915	0.915	1.118	0.906	1.089	0.904	0.884	0.992
Mn	0.068	0.070	0.068	0.068	0.066	0.057	0.059	0.004	0.004	0.009	0.007	0.009	0.002	0.004	0.004	0.011
Mg	2.367	2.345	2.350	2.229	2.438	2.369	2.376	3.557	4.259	4.231	3.821	4.356	4.057	4.354	4.299	4.107
Toct	5.673	5.759	5.697	5.697	5.644	5.728	5.713	5.702	5.733	5.707	5.572	5.823	5.711	5.799	5.740	5.673
Ca	0.009	0.000	0.004	0.004	0.070	0.002	0.002	0.046	0.002	0.002	0.029	0.002	0.007	0.002	0.002	0.007
Na	0.073	0.042	0.055	0.097	0.090	0.048	0.042	0.147	0.128	0.130	0.130	0.108	0.134	0.136	0.134	0.136
K	1.892	1.885	1.857	1.822	1.800	1.863	1.881	1.580	1.828	1.824	1.588	1.802	1.760	1.778	1.775	1.709
Tint	1.973	1.927	1.916	1.923	1.960	1.914	1.925	1.773	1.958	1.956	1.747	1.912	1.901	1.916	1.912	1.852

### Biotite analyses

Sample Run Analysis	E68 dja10 16	E68 dja10 17	E68 dja10 18	E68 dja10 19	E20 dja2 39	E20 dja2 45	E20 dja2 46	E20 dja2 47	E20 dja2 48	E2 dja3 23	E2 dja3 24	E2 dja3 25	E2 dja3 26	E2 dja3 35	E5 dja14 1	E5 dja14 2
Mineral	biotite	biotite	biotite	biotite	biotite	biotite	biotite	biotite	biotite	biotite	biotite	biotite	biotite	biotite	biotite	biotite
SiO <sub>2</sub>	38.33	38.34	40.01	38.4	35.57	35.5	35.66	35.2	35.5	37.5	36.4	38	37.4	36.2	36.4	36
TiO <sub>2</sub>	5.11	5.17	5.76	5.19	4.59	4.68	4.77	4.51	4.49	4.18	4.3	4.09	4.16	4.34	4.83	4.86
Al <sub>2</sub> O <sub>3</sub>	13.84	14.04	13.97	13.96	14.88	14.75	14.83	15	15.2	13.8	13.5	13.8	13.5	13.7	14.1	13.9
Cr <sub>2</sub> O <sub>3</sub>	0.04	0.09	0.1	0.13	0	0.02	0.03	0.03	0.04	0.04	0.04	0.04	0.01	0.01	0.04	0.02
FeO	7.84	8.04	8.88	7.84	21.68	21.34	21.71	21.9	21.9	19.8	20.6	20.4	20.3	19.8	19.1	19.6
MnO	0.02	0.04	0.05	0.05	0.19	0.19	0.24	0.16	0.23		0.25	0.33	0.32	0.37	0.26	0.29
MgO	20.08	20	18.09	20	9.34	9.03	8.98	9.15	9.17	11.2	11.1	10.6	11	11.2	11.5	11.8
CaO	0.04	0.04	0.41	0.05	0.01	0	0.02	0	0.02	0.04	0.02	0.06	0.07	0.04	0	0.01
Na <sub>2</sub> O	0.58	0.57	0.55	0.62	0.46	0.52	0.56	0.48	0.49	0.55	0.6	0.57	0.55	0.56	0.48	0.48
K <sub>2</sub> O	9.59	9.61	7.55	9.78	9.16	8.89	9.12	9.04	9.09	9	8.95	8.84	9.12	9.13	8.95	9.04
NiO	0.07	0.1	0.04	0.06	0	0.02	0	0.02	0.02	0.05	0.02	0.01	0	0.05	0.02	0.05
Total	95.54	96.04	95.41	96.08	95.88	94.94	95.92	95.5	96.1	96.4	95.8	96.7	96.3	95.5	95.6	96.1
Si	5.542	5.522	5.724	5.529	5.478	5.507	5.491	5.452	5.454	5.665	5.575	5.722	5.676	5.559	5.540	5.487
Altet	2.358	2.383	2.276	2.369	2.522	2.493	2.509	2.548	2.546	2.335	2.425	2.278	2.324	2.441	2.460	2.501
Ttet	7.900	7.905	8.000	7.898	8.000	8.000	8.000	8.000	8.000	8.000	8.000	8.000	8.000	8.000	8.000	7.988
Aloct	0.000	0.000	0.081	0.000	0.180	0.204	0.182	0.195	0.204	0.125	0.019	0.171	0.092	0.043	0.065	0.000
Ti	0.557	0.561	0.620	0.561	0.532	0.546	0.552	0.526	0.519	0.475	0.495	0.464	0.475	0.502	0.554	0.557
Fe <sub>2</sub>	0.948	0.968	1.063	0.944	2.792	2.770	2.796	2.829	2.816	2.504	2.644	2.574	2.574	2.543	2.438	2.499
Mn	0.002	0.004	0.007	0.007	0.024	0.024	0.031	0.022	0.031	0.040	0.033	0.042	0.042	0.048	0.033	0.037
Mg	4.327	4.294	3.859	4.292	2.145	2.088	2.061	2.112	2.103	2.519	2.537	2.385	2.482	2.572	2.603	2.666
Toct	5.834	5.828	5.629	5.804	5.673	5.631	5.622	5.684	5.673	5.662	5.728	5.636	5.664	5.708	5.693	5.760
Ca	0.007	0.007	0.064	0.009	0.002	0.000	0.002	0.000	0.002	0.007	0.002	0.009	0.011	0.007	0.000	0.002
Na	0.163	0.158	0.152	0.174	0.136	0.156	0.167	0.143	0.145	0.161	0.178	0.167	0.163	0.167	0.141	0.141
K	1.769	1.767	1.377	1.797	1.800	1.760	1.791	1.786	1.784	1.736	1.751	1.701	1.767	1.789	1.740	1.756
Tint	1.938	1.932	1.593	1.980	1.938	1.916	1.960	1.929	1.932	1.903	1.932	1.877	1.940	1.962	1.881	1.899

## Appendix H (electron microprobe)

### Biotite analyses

Sample	E5	E5	E5	E5	E5	E5	E5	E5	E5	E5	E5	E5	E5	E5	UG29	UG29
Run	dja14	dja14	dja14	dja14	dja14	dja14	dja14	dja14	dja14	dja14	dja14	dja14	dja14	dja14	dja5	dja5
Analysis	3	4	5	6	8	9	10	11	16	20	21	22	23	24	2	3
Mineral	biotite	biotite	biotite	biotite	biotite	biotite	biotite	biotite	biotite	biotite	biotite	biotite	biotite	biotite	biotite	biotite
SiO2	35.9	36.1	36.4	35.7	36.3	36.1	35.7	36.2	35.7	35.8	36	36.5	36.3	36.7	37	37
TiO2	4.67	4.82	4.9	4.82	4.78	4.81	4.83	4.67	4.79	4.71	4.78	4.87	4.78	4.84	4.71	4.77
Al2O3	13.8	13.8	14	13.8	13.8	13.9	13.5	13.6	13.8	13.9	13.8	14	14.4	13.9	13.3	13.2
Cr2O3	0.01	0.03	0.04	0.02	0.03	0	0.04	0	0.01	0.02	0.03	0.04	0	0.02	0.03	0.01
FeO	19.7	19.5	19.8	19.5	19.6	19.5	19.3	19.9	19.6	19.9	20.1	19.9	20.1	20	16.3	16
MnO	0.26	0.31	0.3	0.34	0.29	0.32	0.34	0.3	0.29	0.32	0.3	0.34	0.27	0.31	0.38	0.35
MgO	11.4	11.5	11.5	11.3	11.6	11.7	11.5	11.5	11.4	11.3	11.4	11.5	11.3	11.6	13.9	13.7
CaO	0.01	0	0.02	0.73	0.01	0.05	0.07	0.02	0.04	0.01	0.05	0.01	0.01	0.01	0	0.01
Na2O	0.45	0.46	0.45	0.47	0.49	0.48	0.48	0.46	0.49	0.47	0.5	0.45	0.46	0.47	0.6	0.69
K2O	8.73	8.96	9.01	8.94	9.02	8.97	8.81	9.04	8.66	8.86	8.77	9.12	8.77	9.06	9.2	8.7
NiO	0.01	0.01	0.02	0.07	0.06	0.02	0.02	0.02	0.01	0.07	0.03	0.02	0.03	0.03	0.02	0.01
Total	94.8	95.5	96.5	95.7	96	95.8	94.7	95.7	94.8	95.3	95.8	96.8	96.4	97	95.4	94.4

Si	5.524	5.526	5.509	5.476	5.524	5.502	5.520	5.540	5.500	5.504	5.504	5.520	5.496	5.533	5.581	5.617
Altet	2.476	2.474	2.491	2.490	2.476	2.498	2.464	2.451	2.500	2.496	2.493	2.480	2.504	2.467	2.372	2.358
Ttet	8.000	8.000	8.000	7.966	8.000	8.000	7.984	7.990	8.000	8.000	7.997	8.000	8.000	8.000	7.953	7.975
Aloct	0.028	0.015	0.010	0.000	0.008	0.001	0.000	0.000	0.006	0.017	0.000	0.015	0.067	0.010	0.000	0.000
Ti	0.541	0.554	0.559	0.557	0.548	0.552	0.561	0.537	0.554	0.543	0.550	0.554	0.546	0.550	0.535	0.546
Fe2	2.534	2.501	2.515	2.495	2.493	2.493	2.497	2.543	2.532	2.554	2.572	2.521	2.552	2.521	2.053	2.033
Mn	0.033	0.040	0.040	0.044	0.037	0.042	0.044	0.040	0.037	0.042	0.040	0.044	0.035	0.040	0.048	0.044
Mg	2.616	2.614	2.607	2.585	2.638	2.651	2.642	2.633	2.625	2.585	2.594	2.587	2.552	2.609	3.128	3.111
Toct	5.752	5.724	5.730	5.680	5.724	5.739	5.744	5.753	5.754	5.741	5.755	5.721	5.752	5.730	5.764	5.733
Ca	0.002	0.000	0.002	0.121	0.002	0.009	0.011	0.002	0.007	0.002	0.009	0.002	0.002	0.002	0.000	0.002
Na	0.134	0.136	0.132	0.141	0.145	0.143	0.143	0.136	0.147	0.141	0.147	0.132	0.134	0.136	0.176	0.202
K	1.716	1.749	1.742	1.749	1.753	1.747	1.736	1.767	1.703	1.738	1.712	1.760	1.696	1.742	1.773	1.687
Tint	1.852	1.885	1.877	2.011	1.901	1.899	1.890	1.905	1.857	1.881	1.868	1.894	1.833	1.881	1.949	1.892

### Biotite analyses

Sample	UG29	UG29	UG29	UG29	VSE 1	VSE 2	VSE 2	VSE 2	VSE 2	VSE 2	VSE 2	VSE 2	VSE 2	VSE 2	VSE 2	VSE 8
Run	dja5	dja5	dja5	dja5	dja8	dja4	dja4	dja8	dja9	dja9	dja9	dja9	dja9	dja9	dja9	dja4
Analysis	5	6	15	16	78	53	54	38	17	21	24	26	27	28	29	28
Mineral	biotite	biotite	biotite	biotite	biotite	biotite	biotite	biotite	biotite	biotite	biotite	biotite	biotite	biotite	biotite	biotite
SiO <sub>2</sub>	37.1	37.1	37.3	37	42.6	36.7	36.7	37	36.5	36.9	36.6	36.5	36.3	36.7	36.6	36
TiO <sub>2</sub>	4.7	4.79	4.7	4.78	3.15	4.96	4.93	5.14	4.3	4.5	4.44	4.42	4.36	4.29	4.32	4.26
Al <sub>2</sub> O <sub>3</sub>	13.5	13.5	13.3	13.3	13.3	13.1	13.2	14	14	13.9	13.9	13.9	13.8	13.9	13.9	13.5
Cr <sub>2</sub> O <sub>3</sub>	0	0	0	0.04	0.03	0.04	0.04	0.03	0.02	0.04	0.02	0	0.01	0.04	0.01	0.02
FeO	16.1	16.2	16	15.8	19.5	15.4	15.5	16.3	16.4	16	15.8	17.4	17.6	17.7	17.5	22
MnO	0.35	0.36	0.39	0.39	0.37	0.4	0.33	0.31	0.29	0.28	0.23	0.29	0.31	0.35	0.27	0.57
MgO	13.9	13.8	14.2	14	9.71	14	14	13.9	13.8	14.1	13.9	13	13.1	13.3	13.3	9.56
CaO	0.01	0.02	0.03	0.01	0.18	0.04	0.07	0.01	0.01	0.04	0.07	0.03	0	0.03	0.04	0.01
Na <sub>2</sub> O	0.66	0.66	0.63	0.62	0.05	0.47	0.45	0.42	0.35	0.49	0.46	0.39	0.4	0.41	0.39	0.22
K <sub>2</sub> O	9.12	9.34	9.27	9.21	5.67	9.11	9.11	8.84	9.18	8.82	8.7	8.83	8.94	8.96	8.96	9.14
NiO	0.02	0.02	0.02	0.01	0	0.04	0	0.04	0.04	0.01	0.04	0.03	0.03	0.02	0.01	0.05
Total	95.4	95.8	95.8	95.2	94.9	94.3	94.4	96.3	94.8	95.1	94.1	94.7	94.9	95.7	95.4	95.3

Si	5.595	5.579	5.595	5.584	6.310	5.584	5.584	5.531	5.537	5.555	5.564	5.559	5.531	5.548	5.551	5.592
Altet	2.391	2.394	2.352	2.372	1.690	2.354	2.361	2.468	2.463	2.445	2.436	2.441	2.469	2.452	2.449	2.408
Tfet	7.986	7.973	7.946	7.955	8.000	7.938	7.944	7.999	8.000	8.000	8.000	8.000	8.000	8.000	8.000	8.000
Aloct	0.000	0.000	0.000	0.000	0.637	0.000	0.000	0.000	0.037	0.026	0.054	0.054	0.015	0.030	0.039	0.070
Ti	0.532	0.541	0.530	0.543	0.352	0.568	0.563	0.579	0.491	0.510	0.508	0.506	0.499	0.488	0.493	0.499
Fe2	2.024	2.033	2.006	2.000	2.420	1.965	1.976	2.035	2.077	2.022	2.015	2.215	2.251	2.235	2.218	2.858
Mn	0.044	0.046	0.051	0.051	0.046	0.051	0.042	0.040	0.037	0.035	0.029	0.037	0.040	0.044	0.035	0.075
Mg	3.115	3.089	3.179	3.153	2.145	3.183	3.177	3.089	3.128	3.172	3.144	2.946	2.988	2.985	2.999	2.218
Toct	5.716	5.709	5.766	5.746	5.600	5.766	5.757	5.742	5.770	5.765	5.750	5.759	5.792	5.783	5.783	5.719
Ca	0.002	0.002	0.004	0.002	0.029	0.007	0.011	0.002	0.002	0.007	0.011	0.004	0.000	0.004	0.007	0.002
Na	0.194	0.191	0.183	0.183	0.015	0.139	0.132	0.121	0.103	0.143	0.136	0.114	0.119	0.121	0.114	0.066
K	1.753	1.791	1.775	1.775	1.071	1.769	1.767	1.687	1.778	1.696	1.690	1.718	1.740	1.729	1.731	1.815
Tint	1.949	1.984	1.962	1.960	1.115	1.914	1.910	1.811	1.883	1.846	1.837	1.837	1.859	1.855	1.852	1.883

## Appendix H (electron microprobe)

### Biotite analyses

Sample	VSE 8	VSE 8	VSE 8	VSE 8	VSE 8	VSE 22	VSE 22	VSE 22	VSE 22	VSE 22	VSE 22
Run	dja4	dja9	dja9	dja9	dja9	dja10	dja10	dja10	dja10	dja10	dja10
Analysis	29.000	2.000	30.000	11.000	12.000	31.000	32.000	33.000	34.000	35.000	36.000
Mineral	biotite	biotite	biotite	biotite	biotite	biotite	biotite	biotite	biotite	biotite	biotite
SiO2	35.720	35.720	36.200	36.470	36.000	37.010	36.970	36.780	36.490	36.870	37.200
TiO2	4.210	4.600	4.250	4.280	4.330	4.990	5.020	5.010	4.910	5.000	4.850
Al2O3	13.230	13.470	13.370	13.250	13.140	13.480	13.440	13.340	13.250	13.500	13.340
Cr2O3	0.030	0.000	0.020	0.020	0.010	0.040	0.030	0.040	0.040	0.030	0.010
FeO	21.810	21.840	22.090	22.250	21.890	15.950	16.110	15.630	15.480	15.830	15.770
MnO	0.600	0.280	0.270	0.120	0.140	0.380	0.400	0.360	0.340	0.400	0.370
MgO	9.800	9.680	9.820	10.360	10.130	14.300	14.030	14.120	13.980	14.110	14.350
CaO	0.000	0.010	0.020	0.010	0.020	0.020	0.010	0.010	0.030	0.030	0.010
Na2O	0.190	0.200	0.170	0.140	0.150	0.450	0.470	0.440	0.480	0.480	0.470
K2O	9.210	9.120	9.420	9.520	9.490	8.920	8.970	8.910	8.980	8.990	9.190
NiO	0.010	0.020	0.010	0.030	0.030	0.020	0.040	0.020	0.050	0.020	0.020
Total	94.810	94.940	96.060	96.450	95.330	95.560	95.490	94.660	94.030	95.260	95.580
Si	5.588	5.568	5.608	5.601	5.597	5.555	5.562	5.568	5.568	5.555	5.586
Altet	2.412	2.432	2.392	2.398	2.403	2.385	2.383	2.380	2.383	2.398	2.361
Ttet	8.000	8.000	8.000	7.999	8.000	7.940	7.944	7.949	7.951	7.953	7.946
Alotct	0.028	0.043	0.050	0.000	0.004	0.000	0.000	0.000	0.000	0.000	0.000
Ti	0.495	0.539	0.495	0.495	0.506	0.563	0.568	0.570	0.563	0.568	0.548
Fe2	2.853	2.847	2.862	2.858	2.847	2.002	2.026	1.980	1.976	1.995	1.980
Mn	0.079	0.037	0.035	0.015	0.018	0.048	0.051	0.046	0.044	0.051	0.046
Mg	2.286	2.248	2.268	2.372	2.347	3.201	3.146	3.188	3.179	3.168	3.212
Toct	5.741	5.715	5.710	5.740	5.721	5.815	5.790	5.784	5.762	5.782	5.786
Ca	0.000	0.002	0.004	0.002	0.004	0.002	0.002	0.002	0.004	0.004	0.002
Na	0.057	0.059	0.051	0.042	0.046	0.132	0.136	0.130	0.143	0.141	0.136
K	1.839	1.813	1.861	1.866	1.881	1.709	1.723	1.720	1.749	1.727	1.760
Tint	1.896	1.874	1.916	1.910	1.932	1.844	1.861	1.852	1.896	1.872	1.899

### Magnetite analyses

Sample	G2	G2	G2	G2	G2	G2
Analysis	15.000	16.000	17.000	18.000	32.000	33.000
Run	dja7	dja7	dja7	dja7	dja7	dja7
Mineral	Magnetit	Magnetit	Magnetit	Magnetit	Magnetit	Magnetite
SiO2	0.020	0.030	0.040	0.500	3.700	1.030
TiO2	0.330	1.180	0.520	0.320	0.640	0.340
Al2O3	0.160	0.280	0.570	0.290	1.390	0.490
Cr2O3	0.040	0.050	0.060	0.000	0.020	0.040
FeO	82.170	80.820	77.820	80.380	72.260	78.830
MnO	0.150	0.370	0.230	0.170	0.060	0.060
MgO	0.010	0.030	0.010	0.020	0.900	0.230
CaO	0.060	0.070	0.010	0.180	0.480	0.280
Na2O	0.030	0.020	0.020	0.010	0.370	0.180
K2O	0.010	0.000	0.010	0.010	0.460	0.230
NiO	0.020	0.020	0.020	0.030	0.000	0.020
Total	83.000	82.870	79.310	81.910	80.280	81.730
O	32.000	32.000	32.000	32.000	32.000	32.000
Si	0.010	0.013	0.019	0.230	1.603	0.467
Al	0.086	0.150	0.320	0.157	0.710	0.262
Cr	0.016	0.019	0.022	0.000	0.006	0.013
Fe3+	15.764	15.249	15.451	15.378	12.990	15.120
Ti	0.115	0.403	0.186	0.112	0.208	0.115
Mg	0.006	0.019	0.006	0.013	0.582	0.157
Fe2+	7.966	8.137	8.029	8.095	7.885	7.753
Ca	0.029	0.035	0.006	0.090	0.224	0.138
Mn	0.058	0.141	0.093	0.067	0.022	0.022

Fe2+ and Fe3+ calculated using the method of Droop (1987)

## Appendix H (electron microprobe)

### Olivine analyses

Sample	226	226	226	226	226	226	226	226	226	226	226	226	226	226
Run	dja14	dja14	dja14	dja14	dja14	dja14	dja14	dja14	dja14	dja14	dja14	dja14	dja14	dja14
Analysis	25	26	27	28	29	30	31	32	46	47	48	49	50	51
Mineral	olivine	olivine	olivine	olivine	olivine	olivine	olivine	olivine	spar	olivine	olivine	olivine	olivine	olivine
SiO2	39.62	39.54	37.49	39.79	38.57	39.15	39.28	39.86	39.46	39.75	40.11	39.47	39.47	39.56
TiO2	0	0.04	0.01	0.01	0.01	0.01	0.04	0.01	0.04	0.01	0.01	0.01	0	0
Al2O3	0	0.02	0.04	0.02	0.03	0.05	0.02	0.01	3.07	0.02	0.01	0.01	0.11	0.01
Cr2O3	0	0.02	0.03	0.02	0.03	0.01	0.01	0.02	0.01	0.02	0.02	0.03	0.08	0
FeO	16.01	16.2	28.38	16.41	17.35	23.31	17.35	16.18	29.62	15.42	16.91	16.37	16.39	16.26
MnO	0.37	0.34	0.34	0.31	0.29	0.35	0.25	0.3	0.61	0.3	0.33	0.36	0.26	0.29
MgO	45.11	44.92	29.47	44.89	42.23	35.49	43.89	45.19	25.4	45.43	44.82	44.63	41.87	45.02
CaO	0.2	0.16	0.56	0.17	0.21	0.34	0.18	0.17	1.16	0.15	0.18	0.16	0.22	0.15
Na2O	0.02	0.02	0.07	0.02	0.02	0.05	0.02	0.01	0.64	0.01	0	0.01	0.03	0.01
K2O	0.01	0.02	0.13	0.02	0.05	0.14	0.01	0	0.14	0.01	0.01	0	0.21	0.01
NiO	0.18	0.14	0.12	0.19	0.18	0.11	0.09	0.22	0.03	0.27	0.16	0.1	0.24	0.18
Total	101.52	101.42	96.64	101.85	98.97	99.01	101.14	101.97	100.18	101.39	102.56	101.15	98.88	101.49
Si	0.987	0.986	1.042	0.989	0.993	1.032	0.988	0.988	1.056	0.988	0.991	0.988	1.011	0.986
Al	0.000	0.000	0.001	0.000	0.001	0.002	0.000	0.000	0.097	0.000	0.000	0.000	0.003	0.000
Ti	0.000	0.001	0.000	0.000	0.000	0.000	0.001	0.000	0.001	0.000	0.000	0.000	0.000	0.000
Fe2	0.334	0.338	0.660	0.341	0.374	0.514	0.365	0.336	0.662	0.321	0.350	0.343	0.351	0.339
Mg	1.675	1.671	1.221	1.663	1.621	1.395	1.645	1.670	1.013	1.684	1.651	1.665	1.599	1.674
Mn	0.008	0.007	0.008	0.006	0.006	0.008	0.005	0.006	0.014	0.006	0.007	0.008	0.006	0.006
Ca	0.005	0.004	0.017	0.004	0.006	0.010	0.005	0.004	0.033	0.004	0.005	0.004	0.006	0.004
Total	3.009	3.008	2.949	3.005	3.000	2.960	3.008	3.006	2.876	3.004	3.004	3.008	2.976	3.010

### Illite analyses

Sample	VSE 2	VSE 2	VSE 2	VSE 2	VSE 2	VSE 2	VSE 2	VSE 2	VSE 2	VSE 2	VSE 2	VSE 2	VSE 2	VSE 2
Run	dja4	dja4	dja4	dja4	dja8	dja8	dja8	dja8	dja35	dja35	dja35	dja35	dja35	dja35
Analysis	67	69	72	73	37	40	47	48	22	23	27	28	29	30
Mineral	Illite	Illite	Illite	Illite	Illite	Illite	Illite	Illite	Illite	Illite	Illite	Illite	Illite	Illite
Text Fig	4.2	4.2	4.2	4.2	4.2	4.2	4.2	4.2	4.2	4.2	4.2	4.2	4.2	4.2
SiO2	47.77	37.34	44.14	42.93	50.88	47.76	43.64	45.16	45.41	45.59	43.51	43.73	45.72	45.71
TiO2	1.39	0.05	0.16	0.14	0.09	0.09	0.09	0.05	0.56	0.42	0.29	0.1	0.27	0.21
Al2O3	23.47	19.29	30.6	27.52	34.86	37.16	15.81	15.45	28.06	25.81	28.96	34.24	32.23	32.82
Cr2O3	0.01	0.02	0.01	0.01	0.04	0.01	0	0.02	0.04	0.01	0.13	0.12	0.08	0.16
FeO	4.01	10.64	1.18	1.57	1.45	0.08	17.6	17.25	2.44	3.09	0.88	0.32	0.72	0.64
MnO	0.03	0.08	0.02	0.02	0.03	0.02	0.09	0.11	0.06	0.03	0.02	0.03	0.03	0.03
MgO	3.45	11.87	0.98	1.27	1.3	0.46	7.48	7.08	2.12	2.11	1.88	0.41	1.43	1.32
CaO	0.01	0.12	0.06	0.12	0.06	0.03	0.3	0.36	0.01	0.08	0.02	0.04	0	0.03
Na2O	0.12	0.07	0.6	0.84	0.31	0.37	0.11	0.11	0.24	0.27	0.6	0.35	0.51	0.62
K2O	11.1	4.91	5.75	8.34	4.46	2.19	3.94	3.53	9.95	9.73	7.71	3.07	6.97	6.26
NiO	0.04	0.01	0.02	0.02	0.02	0.04	0.06	0.11	0.01	0.02	0.02	0.02	0.05	0
Total	91.4	84.4	83.52	82.78	93.62	88.24	89.22	89.3	88.9	87.16	84.02	82.43	88.01	87.8
O	22	22	22	22	22	22	22	22	22	22	22	22	22	22
Si	6.785	5.916	6.499	6.547	6.585	6.409	6.653	6.822	6.523	6.697	6.472	6.347	6.420	6.400
Al	1.215	2.084	1.501	1.453	1.415	1.591	1.347	1.178	1.477	1.303	1.528	1.653	1.580	1.600
Ttet	8.000	8.000	8.000	8.000	8.000	8.000	8.000	8.000	8.000	8.000	8.000	8.000	8.000	8.000
Al	2.714	1.517	3.810	3.495	3.902	4.285	1.493	1.572	3.273	3.165	3.550	4.206	3.755	3.816
Ti	0.147	0.007	0.018	0.015	0.009	0.009	0.011	0.007	0.059	0.046	0.033	0.011	0.029	0.022
Fe2	0.477	1.410	0.145	0.200	0.156	0.009	2.244	2.180	0.293	0.381	0.110	0.040	0.084	0.075
Mg	0.730	2.803	0.216	0.288	0.251	0.092	1.701	1.595	0.453	0.462	0.416	0.088	0.299	0.275
Toct	4.069	5.737	4.188	3.999	4.318	4.395	5.449	5.354	4.078	4.054	4.109	4.344	4.166	4.188
Ca	0.002	0.020	0.009	0.020	0.009	0.004	0.048	0.057	0.002	0.013	0.002	0.007	0.000	0.004
Na	0.033	0.022	0.172	0.249	0.077	0.097	0.033	0.033	0.066	0.077	0.174	0.099	0.139	0.169
K	2.011	0.992	1.080	1.624	0.737	0.374	0.766	0.680	1.824	1.824	1.463	0.568	1.250	1.118
Tint	2.046	1.034	1.261	1.892	0.823	0.475	0.847	0.770	1.892	1.914	1.639	0.673	1.388	1.291

## Appendix H (electron microprobe)

### Illite analyses

Sample	VSE 1	VSE 2	VSE 2	VSE 2	VSE 2	VSE 2	VSE 2	VSE 2	VSE 2	VSE 2	VSE 2	VSE 2	VSE 2	VSE 8	VSE 8	VSE 8
Run	dja30	dja5	dja5	dja5	dja5	41	42	dja35	dja35	dja35	dja35	dja35	dja35	15	dja25	dja25
Analysis	26	45	46	47	48	dja10	dja10	8	9	12	13	14	15	dja9	34	35
Mineral	Illite	Illite	Illite	Illite	Illite	Illite	Illite	Illite	Illite	Illite	Illite	Illite	Illite	Illite	Illite	Illite
Text Fig	4.2	4.2	4.2	4.2	4.2	4.2	4.2	4.2	4.2	4.2	4.2	4.2	4.2	4.2	4.2	4.2
SiO2	47.5	47.1	47.3	47.3	47.3	46.8	47.3	46	43.8	47.31	44.8	46.3	47.6	45.2	49.7	50.6
TiO2	1.55	0.73	0.63	0.77	0.79	0.7	0.77	0.45	0.13	0.38	0.53	0.59	0.54	0.3	0.31	0.23
Al2O3	28.8	24.4	25.8	26.1	26.7	29	29.2	31.1	32.8	27.68	32.8	33	30.7	32.2	33.1	34.2
Cr2O3	0.03	0.01	0	0.05	0.04	0	0.01	0.05	0.02	0.04	0.02	0.02	0.03	0.02	0.01	0.02
FeO	3.83	3.3	3.31	4.52	4.22	2.61	2.9	2.5	0.56	3.27	1.29	1.44	1.9	2.04	2.64	2.55
MnO	0.03	0.02	0.02	0.03	0.05	0.04	0.01	0.02	0.03	0.04	0.03	0.03	0	0.02	0.02	0.03
MgO	1.92	2.65	2.42	2.75	2.62	2.04	2.13	1.74	0.51	2.36	1.07	1.36	2.16	0.95	1.36	1.33
CaO	0.01	0.15	0.06	0.02	0.03	0.04	0.03	0.2	0.36	0.05	0.09	0.02	0.01	0.01	0.01	0
Na2O	0.38	0.19	0.22	0.48	0.36	0.3	0.3	0.83	1.13	0.2	1.52	1.51	1.04	0.44	0.35	0.28
K2O	8.62	8.8	10.4	10.4	10.7	10.3	11	9.18	8.79	11.03	9.12	9.3	9.69	10.6	9.61	9.67
NiO	0.05	0.03	0.04	0.04	0.02	0.01	0.03	0.02	0.02	0.03	0.02	0.03	0.02	0	0.02	0.04
Total	92.7	87.4	90.2	92.5	92.8	91.8	93.7	92.1	88.1	92.39	91.3	93.6	93.6	91.8	97.1	99
O	22	22	22	22	22	22	22	22	22	22	22	22	22	22	22	22
Si	6.519	6.853	6.732	6.622	6.600	6.510	6.492	6.354	6.250	6.598	6.219	6.261	6.450	6.283	6.464	6.446
Al	1.481	1.147	1.268	1.378	1.400	1.490	1.508	1.646	1.750	1.402	1.781	1.739	1.550	1.717	1.536	1.554
Ttet	8.000	8.000	8.000	8.000	8.000	8.000	8.000	8.000	8.000	8.000	8.000	8.000	8.000	8.000	8.000	8.000
Al	3.180	3.042	3.068	2.936	2.985	3.268	3.209	3.414	3.768	3.147	3.583	3.530	3.352	3.568	3.539	3.585
Ti	0.161	0.079	0.068	0.081	0.084	0.073	0.079	0.046	0.013	0.040	0.055	0.059	0.055	0.031	0.031	0.022
Fe2	0.440	0.403	0.394	0.530	0.493	0.304	0.332	0.288	0.066	0.381	0.150	0.163	0.216	0.238	0.288	0.273
Mg	0.394	0.574	0.513	0.574	0.546	0.422	0.436	0.359	0.108	0.491	0.222	0.275	0.436	0.198	0.264	0.253
Toct	4.175	4.098	4.043	4.122	4.107	4.067	4.056	4.107	3.955	4.058	4.010	4.027	4.058	4.034	4.122	4.133
Ca	0.002	0.024	0.009	0.002	0.004	0.007	0.004	0.029	0.055	0.007	0.013	0.002	0.002	0.002	0.002	0.000
Na	0.101	0.053	0.062	0.130	0.097	0.081	0.079	0.222	0.312	0.055	0.409	0.396	0.273	0.119	0.088	0.068
K	1.509	1.635	1.881	1.866	1.910	1.830	1.929	1.617	1.602	1.962	1.615	1.606	1.676	1.888	1.595	1.573
Tint	1.613	1.712	1.951	1.998	2.011	1.918	2.013	1.868	1.969	2.024	2.037	2.004	1.951	2.009	1.685	1.641

### Smectite analyses from Red Formation siltstone (Emet Basin)

### Analyses of ignimbrite (see Text Figure 3.1a)

Sample	VSE 1	VSE 1	VSE 1	VSE 1	VSE 1	VSE 1	VSE 1	VSE 1	VSE 1	Sample	I251	I251	I251	I220	I220	I220
Analysis	dja8	dja8	dja8	dja8	dja8	dja8	dja8	dja30	dja30	Run	dja11	dja11	dja11	dja11	dja11	dja11
Run	84	85	86	87	88	89	90	18	20	Analysis	1	2	6	11	12	13
Mineral	Sm	Sm	Sm	Sm	Sm	Sm	Sm	Sm	Sm	Mineral	Matrix	Matrix	Matrix	Matrix	Matrix	Matrix
Text Fig	4.2	4.2	4.2	4.2	4.2	4.2	4.2	4.2	4.2	Text Fig	3.1 a	3.1 a	3.1 a	3.1 a	3.1 a	3.1 a
SiO2	49.9	46	47.4	47.1	48.9	47.4	48.8	42.9	48.2	SiO2	70.6	87	87.6	37.3	62	60.3
TiO2	0.61	1.8	1.79	0.35	0.37	0.42	0.86	0.97	1	TiO2	0.02	0.01	0.02	0	0.55	0.7
Al2O3	21.6	24.7	25.9	22.5	24.1	19.4	22.6	18	14.8	Al2O3	17.4	8.04	5.35	22.2	13.6	12.2
Cr2O3	0.04	0	0.04	0.04	0.02	0	0.04	0.02	0.01	Cr2O3	0.04	0.04	0.02	0.01	0.01	0.04
FeO	5.45	10.8	10.9	6.3	5.92	5.85	6.03	6.4	5.45	FeO	0.37	0.35	0.21	12.3	4.36	4.25
MnO	0.05	0.07	0.05	0.02	0.03	0.03	0.01	0.03	0	MnO	0.04	0.01	0.04	0.12	0.02	0.06
MgO	1.67	3.86	4.2	1.94	1.69	1.81	2.18	1.29	1.34	MgO	0.01	0	0.07	0.01	1.99	1.62
CaO	0.63	0.13	0.17	0.59	0.81	0.77	0.72	0.58	0.62	CaO	1.82	0.97	0.65	23.5	1.24	1.36
Na2O	0.31	0.17	0.11	0.21	0.25	0.07	0.27	0.41	0.16	Na2O	3.77	1.35	1.29	0.07	0.55	0.27
K2O	2.49	7.19	5.51	4.47	2.93	3.1	3.26	2.01	2.42	K2O	2.27	0.74	1.24	0.08	3.01	2.82
NiO	0.03	0.04	0.03	0.07	0.04	0.01	0.02	0.06	0.04	NiO	0.02	0	0.06	0.03	0.03	0.01
Total	82.9	95.1	96.3	83.9	85.2	78.9	84.9	72.6	74	Total	96.3	98.5	96.6	95.6	87.4	83.7
O	22	22	22	22	22	22	22	22	22	O	22	22	22	22	22	22
Si	7.383	6.400	6.413	7.071	7.108	7.436	7.143	7.333	7.971	Si	8.653	9.999	####	5.491	8.562	8.677
Al	0.617	1.600	1.587	0.929	0.892	0.564	0.857	0.667	0.029	Al	2.517	1.089	0.739	3.848	2.213	2.077
Ttet	8.000	8.000	8.000	8.000	8.000	8.000	8.000	8.000	8.000	Al	0.037	0.033	0.020	1.509	0.504	0.513
Al	3.156	2.448	2.545	3.059	3.224	3.024	3.040	2.952	2.855	Fe2	0.002	0.000	0.013	0.002	0.409	0.348
Ti	0.068	0.189	0.183	0.040	0.040	0.051	0.095	0.125	0.125	Mg	0.240	0.119	0.081	3.698	0.183	0.209
Fe2	0.673	1.256	1.232	0.792	0.719	0.768	0.739	0.915	0.755	Ca	0.895	0.301	0.293	0.020	0.147	0.075
Mg	0.367	0.801	0.847	0.433	0.365	0.422	0.475	0.330	0.330	Na	0.354	0.108	0.185	0.015	0.530	0.517
Toct	4.265	4.694	4.806	4.324	4.349	4.265	4.349	4.322	4.065	K						
Ca	0.099	0.020	0.024	0.095	0.125	0.130	0.112	0.106	0.110							
Na	0.088	0.046	0.029	0.062	0.070	0.022	0.077	0.136	0.051							
K	0.471	1.276	0.953	0.856	0.543	0.620	0.609	0.438	0.510							
Tint	0.658	1.342	1.005	1.012	0.739	0.772	0.799	0.680	0.671							

LEGEND: sm = smectite

## Appendix H (electron microprobe)

### Analyses of ignimbrite (see Text Figure 3.1a)

Sample Run	I220 dja11	I220 dja11	I220 dja11	I220 dja11	I220 dja11	I220 dja11	I220 dja11	I251 dja11	I220 dja11	I220 dja11	I220 dja11
Analysis	14	15	16	17	18	20	21	3	7	10	24
Mineral	Matrix	Matrix	Matrix	Matrix	Matrix	Matrix	Matrix	pumice	pumice	lass shar	lass shard
Text Fig	3.1 a	3.1 a	3.1 a	3.1 a	3.1 a	3.1 a	3.1 a	3.1 a	3.1 a	3.1 a	3.1 a
SiO <sub>2</sub>	61.5	60.78	61.7	63.65	51.23	62.71	67.35	79.51	77.92	77.75	79.17
TiO <sub>2</sub>	0.77	0.92	0.01	0.01	0.47	0.68	0.78	0	0	0.01	0.02
Al <sub>2</sub> O <sub>3</sub>	12.17	12.62	25.99	24.48	10.17	11.44	12.63	12.91	12.73	12.6	12.92
Cr <sub>2</sub> O <sub>3</sub>	0	0.02	0.02	0.02	0.02	0.03	0.05	0.03	0.03	0.01	0.04
FeO	4.12	4.55	0.37	0.34	6.08	4.9	5.43	0.74	0.22	0.2	0.24
MnO	0.05	0.07	0.01	0.02	0.13	0.15	0.14	0.09	0.04	0.07	0.07
MgO	1.43	1.77	0.02	0	1.87	1.69	2.41	0	0	0	0.01
CaO	1.21	1.28	7.22	5.89	0.96	1.08	1.23	0.53	0.59	0.5	0.57
Na <sub>2</sub> O	0.43	0.28	5.89	7.02	0.23	0.24	0.85	0.75	0.8	0.57	0.41
K <sub>2</sub> O	2.45	2.32	0.81	1.1	2.03	2.35	3.07	3.5	3.56	3.42	3.25
NiO	0.01	0.01	0.05	0.02	0.02	0.02	0	0.04	0.01	0.01	0
Total	84.14	84.62	102.09	102.55	73.21	85.29	93.94	98.1	95.9	95.14	96.7
O	22	22	22	22	22	22	22	22	22	22	22
Si	8.754	8.631	7.388	7.579	8.556	8.824	8.683	9.398	9.405	9.434	9.434
Al	2.042	2.112	3.667	3.436	2.002	1.896	1.921	1.800	1.811	1.802	1.815
Fe <sub>2</sub>	0.491	0.541	0.037	0.033	0.849	0.576	0.585	0.073	0.022	0.020	0.024
Mg	0.304	0.374	0.004	0.000	0.466	0.354	0.464	0.000	0.000	0.000	0.002
Ca	0.185	0.196	0.926	0.752	0.172	0.163	0.169	0.068	0.077	0.066	0.073
Na	0.119	0.077	1.368	1.621	0.075	0.066	0.213	0.172	0.187	0.134	0.095
K	0.444	0.420	0.123	0.167	0.433	0.422	0.506	0.528	0.548	0.530	0.495

### Analyses of altered feldspar in Emet Rhyolite

Sample Run	E18 dja16	E18 dja16	E18 dja16	E18 dja16	E18 dja16	E18 dja16	E18 dja16	E18 dja16	E18 dja16	Sample Run	E17 dja16	E17 dja16	E17 dja16
Analysis	1	2	3	4	9	10	13	14	15	Analysis	19	20	23
Mineral	Plag	Plag	Plag	Plag	Plag	Plag	Plag	Plag	Plag	Mineral	Kf	Kf	Kf
Text Fig	3.1 b	3.1 b	3.1 b	3.1 b	3.1 b	3.1 b	3.1 b	3.1 b	3.1 b	Text Fig	3.1 b	3.1 b	3.1 b
SiO <sub>2</sub>	64.14	64.23	64.28	63.22	60.67	62.21	62.9	63.47	64.49	SiO <sub>2</sub>	73	74.58	72.41
TiO <sub>2</sub>	0.01	0.03	0.07	0.01	0.02	0.01	0.01	0.03	0.01	TiO <sub>2</sub>	0.02	0.01	0
Al <sub>2</sub> O <sub>3</sub>	25.58	25.52	24.71	25.41	26.63	26.97	25.77	25.3	25.51	Al <sub>2</sub> O <sub>3</sub>	19.13	19.23	18.59
Cr <sub>2</sub> O <sub>3</sub>	0.04	0	0.04	0.03	0.04	0.03	0.04	0.04	0.04	Cr <sub>2</sub> O <sub>3</sub>	0.03	0.03	0.02
FeO	0.25	0.18	0.21	0.17	0.28	0.24	0.19	0.22	0.17	FeO	0.04	0.04	0.02
MnO	0.04	0.01	0.03	0	0	0.03	0.03	0.05	0.03	MnO	0.02	0.02	0
MgO	0	0.01	0	0.01	0.01	0	0	0	0	MgO	0	0	0
CaO	6.44	6.38	5.8	6.59	7.97	8.01	6.73	6.42	6.3	CaO	0.01	0.01	0.05
Na <sub>2</sub> O	7.72	7.56	7.87	7.54	6.78	2.75	7.5	7.63	3.17	Na <sub>2</sub> O	0.04	0.03	0.05
K <sub>2</sub> O	0.84	0.86	0.94	0.83	0.65	0.55	0.8	0.9	0.73	K <sub>2</sub> O	12.46	11.29	13.16
NiO	0.02	0.02	0.03	0	0.02	0.03	0.02	0.01	0.03	NiO	0.02	0.02	0.01
Total	105.13	104.81	104.01	103.84	103.08	100.83	104.03	104.1	100.49	Total	104.78	105.28	104.34
O	32	32	32	32	32	32	32	32	32	O	32	32	32
Si	10.867	10.899	10.992	10.845	10.534	10.819	10.781	10.867	11.178	Si	12.426	12.525	12.438
Al	5.107	5.104	4.979	5.139	5.450	5.530	5.206	5.104	5.210	Al	3.840	3.805	3.763
Fe <sub>2</sub>	0.035	0.026	0.029	0.026	0.042	0.035	0.029	0.032	0.026	Fe <sub>2</sub>	0.006	0.006	0.003
Na	2.538	2.486	2.608	2.509	2.282	0.928	2.493	2.534	1.066	Ti	0.003	0.000	0.000
Ca	1.168	1.162	1.062	1.213	1.482	1.491	1.235	1.178	1.171	Mg	0.000	0.000	0.000
K	0.182	0.186	0.205	0.182	0.144	0.122	0.176	0.195	0.160	Na	0.013	0.010	0.016
Total	19.898	19.862	19.875	19.914	19.933	18.925	19.920	19.910	18.810	Ca	0.003	0.003	0.010
										K	2.707	2.419	2.883
										Total	18.998	18.768	19.114

LEGEND: Plag = plagioclase, Kf = K-feldspar

## Appendix H (electron microprobe)

### Analyses of altered feldspar in Emet Rhyolite

Sample	E17	E5	E5	E17	E5	E5	E5	E5	E5	Sample	E18	E18
Run	dja16	dja16	dja16	dja16	dja16	dja16	dja16	dja16	dja16	Run	dja16	dja16
Analysis	24	40	45	26	33	34	35	36	39	Analysis	8	11
Mineral	Kf	Kf	Kf	Kf	Kf	Kf	Kf	Kf	Kf	Mineral	Kaol	Kaol
Text Fig	3.1 b	3.1 b	3.1 b	3.1 b	3.1 b	3.1 b	3.1 b	3.1 b	3.1 b	Text Fig	3.1 b	3.1 b
SiO <sub>2</sub>	72.88	68.61	74.15	63.06	73.49	75.56	72.59	75.19	71.56	SiO <sub>2</sub>	52.68	49.76
TiO <sub>2</sub>	0.01	0.01	0	0	0	0.02	0.01	0.01	0	TiO <sub>2</sub>	0.01	0.01
Al <sub>2</sub> O <sub>3</sub>	19.33	18.05	19.06	17.04	20.22	20.86	20.13	21.05	19.65	Al <sub>2</sub> O <sub>3</sub>	37.61	38.19
Cr <sub>2</sub> O <sub>3</sub>	0.04	0.01	0.02	0.04	0.04	0.05		0.04	0.02	Cr <sub>2</sub> O <sub>3</sub>	0.04	0.04
FeO	0.03	0.04	0.06	0.08	0.02	0.04	0.03	0.06	0.02	FeO	0.5	0.39
MnO	0.01	0.04	0	0.03	0.01	0.03	0.01	0.02	0.02	MnO	0.03	0.03
MgO	0	0	0	0	0	0	0	0.01	0	MgO	0.19	0.16
CaO	0.01	0	0.01	0.13	0.02	0.02	0.01	0.02	0	CaO	0.5	0.23
Na <sub>2</sub> O	0.08	0.05	0.01	0.12	0.04	0	0.04	0.01	0.04	Na <sub>2</sub> O	0	0.05
K <sub>2</sub> O	13.07	10.52	10.37	14.85	10.25	4.24	9.59	3.36	11.75	K <sub>2</sub> O	0.48	0.01
NiO	0.02	0.02	0.02	0.02	0.02	0.01	0.02	0.02	0.03	NiO	0.02	0.05
Total	105.49	97.38	103.73	95.42	104.12	100.86	102.48	99.8	103.12	Total	92.07	88.93
O	32	32	32	32	32	32	32	32	32	O	14	14
Si	12.371	12.470	12.570	12.138	12.413	12.662	12.416	12.666	12.342	Si	4.250	4.145
Al	3.869	3.866	3.808	3.866	4.026	4.122	4.058	4.179	3.994	Al	3.577	3.751
Fe <sub>2</sub>	0.003	0.006	0.010	0.013	0.003	0.006	0.003	0.010	0.003	Ti	0.000	0.000
Ti	0.000	0.000	0.000	0.000	0.000	0.003	0.000	0.000	0.000	Fe <sub>2</sub>	0.034	0.027
Mg	0.000	0.000	0.000	0.000	0.000	0.000	0.000	0.003	0.000	Mg	0.022	0.020
Na	0.026	0.019	0.003	0.045	0.013	0.000	0.013	0.003	0.013	Ca	0.043	0.021
Ca	0.003	0.000	0.003	0.026	0.003	0.003	0.003	0.003	0.000	Na	0.000	0.008
K	2.832	2.438	2.243	3.648	2.208	0.906	2.093	0.723	2.586	K	0.049	0.001
Total	19.104	18.800	18.637	19.734	18.666	17.702	18.586	17.587	18.938			

### Analyses of altered feldspar in Emet Rhyolite

Sample	E18	E17	E17	E17	E5	E5	E5	E5	E5	E5	E18	E18
Run	dja16	dja16	dja16	dja16	dja16	dja16	dja16	dja16	dja16	dja16	dja16	dja16
Analysis	12	16	17	18	30	31	32	37	38	43	5	6
Mineral	Kaol	Kaol	Kaol	Kaol	Kaol	Kaol	Kaol	Kaol	Kaol	Kaol	Kaol	Kaol
Text Fig	3.1 b	3.1 b	3.1 b	3.1 b	3.1 b	3.1 b	3.1 b	3.1 b	3.1 b	3.1 b	3.1 b	3.1 b
SiO <sub>2</sub>	49.99	48.69	50.03	43.98	49.06	48.99	50.62	49.69	47.76	48.33	48.17	48.04
TiO <sub>2</sub>	0.01	0.01	0.03	0.03	0.01	0.02	0.01	0.01	0.01	0	0.01	0.01
Al <sub>2</sub> O <sub>3</sub>	35.58	35.65	37.1	29.48	39.48	38.18	40.54	31.99	37.53	38.08	35.49	36.94
Cr <sub>2</sub> O <sub>3</sub>	0.04	0.04	0.04	0.05	0.01	0.01	0.02	0.02	0.01	0.03	0.04	0.03
FeO	1.11	0.59	0.34	0.5	0.47	0.42	0.4	1.36	0.6	0.3	0.86	0.79
MnO	0.02	0.01	0.03	0.03	0.01	0.01	0	0.02	0.01	0.03	0.03	0.01
MgO	0.55	0.46	0.36	0.49	0.16	0.04	0.07	1.07	0.24	0.03	0.34	0.31
CaO	0.77	0.51	0.35	0.45	0.1	0.05	0.08	0.51	0.17	0.04	0.61	0.73
Na <sub>2</sub> O	0.05	0.05	0.04	0.08	0.05	0.03	0.02	0.08	0.02	0.02	0.04	0.06
K <sub>2</sub> O	0.08	0.07	0.04	0.2	0.18	0.19	0.09	3.09	0.16	0.11	0.11	0.07
NiO	0.02	0.02	0	0.01	0.02	0	0.02	0.02	0.02	0.02	0	0.02
Total	88.28	86.13	88.4	75.34	89.63	87.95	91.89	87.89	86.57	87	85.79	87.07
O	14	14	14	14	14	14	14	14	14	14	14	14
Si	4.221	4.197	4.192	4.332	4.063	4.127	4.082	4.311	4.098	4.113	4.179	4.110
Al	3.542	3.623	3.664	3.423	3.854	3.791	3.853	3.270	3.795	3.819	3.629	3.725
Ti	0.000	0.000	0.001	0.003	0.000	0.001	0.000	0.000	0.000	0.000	0.000	0.000
Fe <sub>2</sub>	0.078	0.042	0.024	0.041	0.032	0.029	0.027	0.098	0.043	0.021	0.063	0.056
Mg	0.069	0.059	0.045	0.071	0.020	0.006	0.008	0.139	0.031	0.004	0.043	0.039
Ca	0.070	0.048	0.031	0.048	0.008	0.004	0.007	0.048	0.015	0.004	0.057	0.067
Na	0.008	0.008	0.007	0.015	0.008	0.006	0.003	0.014	0.003	0.003	0.007	0.010
K	0.008	0.007	0.004	0.025	0.020	0.021	0.010	0.342	0.018	0.013	0.013	0.007

LEGEND: Kf = K-feldspar, kaol = kaolinite

## Appendix H (electron microprobe)

### Analyses of altered feldspar in Emet Rhyolite

Sample Run	E18 dja16	E17 dja16	E17 dja16	E17 dja16	E18 dja16	E18 dja16	E5 dja16	E5 dja16	Sample Analysis Run	VSE 8 dja30	VSE 8 dja30
Mineral	Kaol	Kaol	Kaol	Kaol	Kaol	Kaol	Kaol	Kaol	Mineral	auth Kf	auth Kf
Text Fig	3.1 b	3.1 b	3.1 b	3.1 b	3.1 b	3.1 b	3.1 b	3.1 b	Text Fig	4.4	4.4
SiO <sub>2</sub>	51.24	49.29	50.47	44.1	51.92	47.71	45.35	51.11	SiO <sub>2</sub>	70.23	72.01
TiO <sub>2</sub>	0.01	0.01	0.04	0.01	0.01	0.03	0.01	0.01	TiO <sub>2</sub>	0.02	0.01
Al <sub>2</sub> O <sub>3</sub>	36.53	35.09	37.8	29.83	38.96	36.51	36.22	40.48	Al <sub>2</sub> O <sub>3</sub>	20.36	20.12
Cr <sub>2</sub> O <sub>3</sub>	0.03	0	0	0.04	0.04	0.04	0	0.04	Cr <sub>2</sub> O <sub>3</sub>	0.04	0.02
FeO	0.54	0.57	0.34	1.05	0.63	0.74	0.45	0.32	FeO	0.14	0.02
MnO	0.03	0	0.05	0.03	0.04	0.03	0.02	0.02	MnO	0.06	0.01
MgO	0.2	0.5	0.25	0.62	0.27	0.28	0.17	0.02	MgO	0.03	0
CaO	0.53	0.36	0.55	0.93	0.59	0.62	0.16	0.06	CaO	0.01	0.01
Na <sub>2</sub> O	0.01	0.01	0.07	0.07	0.01	0.03	0.02	0.01	Na <sub>2</sub> O	0.25	0.44
K <sub>2</sub> O	0.71	0.05	0.06	0.18	0.07	0.12	0.07	0.05	K <sub>2</sub> O	15.72	15.86
NiO	0.02	0.02	0.02	0.03	0.02	0.01	0.02	0.01	NiO	0.02	0
Total	89.88	85.92	89.68	76.96	92.6	86.16	82.52	92.14	Total	106.88	108.5
O	14	14	14	14	14	14	14	14	Si	12.016	12.115
Si	4.245	4.250	4.173	4.281	4.165	4.123	4.077	4.105	Al	4.106	3.990
Al	3.567	3.567	3.685	3.413	3.683	3.720	3.839	3.832	Fe <sub>2</sub>	0.019	0.003
Ti	0.000	0.000	0.003	0.001	0.000	0.001	0.000	0.000	Ti	0.003	0.000
Fe <sub>2</sub>	0.038	0.041	0.024	0.085	0.042	0.053	0.034	0.021	Mg	0.006	0.000
Mg	0.025	0.064	0.031	0.090	0.032	0.036	0.022	0.003	Na	0.083	0.144
Ca	0.048	0.034	0.049	0.097	0.050	0.057	0.015	0.006	Ca	0.003	0.003
Na	0.001	0.001	0.011	0.013	0.001	0.006	0.003	0.001	K	3.430	3.405
K	0.076	0.006	0.007	0.022	0.007	0.013	0.008	0.006	Total	19.667	19.661
									An%	4	2
									Or%	98	96

### Analyses of matrix in Borate Formation volcanoclastic siltstone (Emet Basin)

Sample Run	VSE 8 dja30	VSE 8 dja30	VSE 8 dja30	VSE 8 dja30	VSE 8 dja30	VSE 8 dja30	VSE 8 dja30	VSE 8 dja30	VSE 8 dja30	VSE 8 dja30	VSE 8 dja40	VSE 8 dja40	VSE 8 dja40
Analysis	11	16	21	23	17	18	19	20	22	24			
Phase	Matrix	Matrix	Matrix	Matrix	Matrix	Matrix	Matrix	Matrix	Matrix	Matrix	Matrix	Matrix	Matrix
Text Fig	4.4a	4.4a	4.4a	4.4a	4.4a	4.4a	4.4a	4.4a	4.4a	4.4a	4.4a	4.4a	4.4a
SiO <sub>2</sub>	45.8	70.41	65.68	47.2	46.82	44.5	52.28	49.64	47.31	60.74	47.903	46.752	48.57
TiO <sub>2</sub>	1.25	0.01	0.02	1.14	0.12	0.89	0.36	0.53	0.55	0.05	1.018	0.807	0.509
Al <sub>2</sub> O <sub>3</sub>	12.33	21.15	18.53	13.42	14.95	12.69	14.46	14.1	12.98	17.72	14.199	12.347	12.962
Cr <sub>2</sub> O <sub>3</sub>	0	0.01	0.01	0.01	0.04	0.01	0.04	0.03	0.04	0.01	0.036	0.036	0.005
FeO	7.96	0.05	0.33	7.21	3.1	5.74	4	6.01	4.54	0.73	8.476	6.431	4.816
MnO	0.07	0.01	0	0.02	0.01	0.05	0.01	0.04	0	0.03	0.057	0.007	0.011
MgO	4.07	0	0.26	4.04	2.83	2.73	2.58	3.99	2.9	0.46	4.873	3.12	2.87
CaO	0.93	1.33	0.09	0.85	0.72	0.82	0.67	0.6	2.38	1.22	0.872	0.447	0.85
Na <sub>2</sub> O	0.34	2.76	0.18	0.21	0.48	0.27	0.36	0.29	0.24	3.5	0.262	0.167	0.309
K <sub>2</sub> O	7.9	7.48	14.36	5.69	1.35	4.86	7.17	5.94	5.72	7.6	5.06	4.761	4.264
NiO	0.02	0.02	0.03	0.01	0	0.06	0.02	0.03	0.03	0.01	0.04	0.021	0.018
Total	80.67	103.23	99.49	79.8	70.42	72.62	81.95	81.2	76.69	92.07	82.797	74.897	75.185
O	22	22	22	22	22	22	22	22	22	22	22	22	22
Si	7.495	8.276	8.292	7.597	7.971	7.770	8.010	7.757	7.825	8.160	7.457	7.893	8.029
Al	2.378	2.930	2.757	2.545	3.001	2.611	2.611	2.596	2.530	2.805	2.605	2.457	2.526
Fe <sub>2</sub>	1.089	0.004	0.035	0.970	0.442	0.838	0.513	0.785	0.627	0.081	1.103	0.908	0.666
Mg	0.992	0.000	0.048	0.970	0.717	0.711	0.590	0.928	0.715	0.092	1.131	0.785	0.707
Ca	0.163	0.167	0.013	0.147	0.132	0.154	0.110	0.101	0.422	0.176	0.146	0.081	0.151
Na	0.108	0.629	0.044	0.066	0.158	0.092	0.108	0.088	0.077	0.911	0.079	0.055	0.099
K	1.650	1.122	2.312	1.168	0.293	1.082	1.401	1.184	1.208	1.302	1.005	1.025	0.899
Total	13.875	13.130	13.501	13.464	12.714	13.259	13.343	13.440	13.405	13.528	13.526	13.203	13.076

LEGEND: kaol = kaolinite



## Appendix H (electron microprobe)

### Analyses of altered plagioclase in Borate Formation siltstone (Borate Formation)

Sample	VSE 8	VSE 8	VSE 8	VSE 8	VSE 8	VSE 8	VSE 8	VSE 8	VSE 8	VSE 8	VSE 8	VSE 8
Analysis	dja8	dja8	dja8	dja8	dja8	dja8	dja8	dja8	dja8	dja8	dja8	dja8
Run	1	2	5	8	9	10	11	16	17	3	4	6
Mineral	plag/clay	plag/clay	plag/clay	plag/clay	plag/clay	plag/clay	plag/clay	plag/clay	plag/clay	plag/clay	plag/clay	plag/clay
Text Fig	4.4b	4.4b	4.4b	4.4b	4.4b	4.4b	4.4b	4.4b	4.4b	4.4b	4.4b	4.4b
SiO <sub>2</sub>	75.19	76.78	71.07	66.54	72.51	72.92	72.46	72.41	73.6	37.8	50.42	59.66
TiO <sub>2</sub>	0.08	0.06	0.05	0.04	0.03	0.01	0.05	0.07	0.06	0.11	0.01	0.07
Al <sub>2</sub> O <sub>3</sub>	20.31	20.6	22.96	19.66	20.41	22.37	22.06	21.75	19.83	25.18	33.53	28.04
Cr <sub>2</sub> O <sub>3</sub>	0.01	0.02	0.04	0.04	0.04	0	0.04	0.01	0.03	0.01	0.06	0.02
FeO	0.02	0.02	0.38	0.04	0.02	0.07	0.04	0.04	0.02	3.38	1.69	1.18
MnO	0.01	0.01	0.04	0	0	0.03	0.03	0.02	0.04	0.05	0.03	0.05
MgO	0	0	0.35	0.07	0	0	0	0	0	0.52	0.82	0.95
CaO	0.12	0.12	1.14	0.4	0.35	1.78	1.83	1.68	0.01	0.58	0.12	0.49
Na <sub>2</sub> O	2.4	1.05	6.16	2.75	5.43	6.2	5.06	5.44	0.04	0.81	0.3	2.93
K <sub>2</sub> O	5.54	2.81	1.78	11.04	0.15	0.25	0.22	0.3	10.13	9.89	8.23	5.35
NiO	0.02	0.01	0.05	0	0.02	0.02	0.01	0.02	0	0.02	0.01	0.02
Total	103.77	101.55	104.39	100.61	99.03	103.67	101.83	101.76	103.84	79	95.61	98.9
O	22	22	22	22	22	22	22	22	22	22	22	22
Si	8.595	8.749	8.140	8.215	8.532	8.287	8.340	8.353	8.569	6.316	6.580	7.363
Al	2.737	2.768	3.100	2.860	2.831	2.996	2.994	2.957	2.721	4.959	5.159	4.079
Fe <sub>2</sub>	0.002	0.002	0.037	0.004	0.002	0.007	0.004	0.004	0.002	0.473	0.185	0.121
Mg	0.000	0.000	0.059	0.013	0.000	0.000	0.000	0.000	0.000	0.130	0.161	0.174
Ca	0.015	0.015	0.141	0.053	0.044	0.218	0.227	0.207	0.002	0.103	0.018	0.064
Na	0.532	0.231	1.368	0.658	1.239	1.366	1.129	1.217	0.009	0.262	0.077	0.702
K	0.807	0.409	0.260	1.738	0.022	0.035	0.033	0.044	1.505	2.108	1.371	0.843

Sample	VSE 8	VSE 8	VSE 8	VSE 8
Analysis	dja8	dja8	dja8	dja8
Run	7	12	13	14
Mineral	plag/clay	plag/clay	plag/clay	plag/clay
Text Fig	4.4b	4.4b	4.4b	4.4b
SiO <sub>2</sub>	52.94	55.25	49.58	44.14
TiO <sub>2</sub>	0.02	0.09	0.12	0.23
Al <sub>2</sub> O <sub>3</sub>	29.65	34.76	27.48	15.36
Cr <sub>2</sub> O <sub>3</sub>	0.04	0.06	0.02	0.02
FeO	0.95	1.42	1.42	1.25
MnO	0.04	0.01	0.04	0.04
MgO	1	1.13	1.15	0.96
CaO	0.18	0.31	1.49	2.82
Na <sub>2</sub> O	0.52	0.36	0.76	2.46
K <sub>2</sub> O	7.36	7.3	4.31	2.89
NiO	0	0.02	0.02	0.05
Total	92.93	100.94	86.67	70.5
O	22	22	22	22
Si	7.011	6.739	6.994	7.731
Al	4.629	4.996	4.569	3.170
Fe <sub>2</sub>	0.106	0.145	0.167	0.183
Mg	0.198	0.205	0.242	0.251
Ca	0.026	0.040	0.224	0.530
Na	0.134	0.086	0.207	0.836
K	1.243	1.135	0.777	0.647

LEGEND: Plag = plagioclase

## Appendix I (XRF, PGAA, ICP-AES)

X-ray fluorescence (XRF) and inductively coupled plasma - atomic emission spectroscopy (ICP-AES) analyses were carried out at the University of Leicester, while prompt gamma activation analysis (PGAA) was completed at a commercial laboratory in Canada (Activation Laboratories). Major and trace elements were analysed by XRF, Li and the REES were analysed by ICP-AES and B was analysed by PGAA.

### **Sample preparation, analytical procedure and additional details**

Fine grained powders were used in all three analytical techniques. The powders were prepared at the University of Leicester using a fly press and an agate swing mill.

#### *XRF analysis*

Powder pellets and fusion beads were prepared for trace element and major element analysis respectively:

##### (i) Powder pellet preparation

Approximately 15g of fine powder was weighed into a beaker, to which a few drops of Mioviol 88 solution were added in order to bind the powder. When fully mixed the powder mixture was loaded into a hydraulic press, which compressed the material producing a circular powder pellet. This pellet was then ready to be loaded into the XRF spectrometer.

##### (ii) Fusion bead preparation

Ignited rock powders were used for the majority of fusion beads in this study. Before ignition, the powder was dried overnight in an oven at 110°C to remove low temperature absorbed volatiles. The dry powders were then weighed into Al<sub>2</sub>O<sub>3</sub> ceramic crucibles. The weight of the empty crucible (W1), and the weight of the crucible + sample prior to (W2), and, after ignition (W3), were recorded. The ignitions were carried out in a muffle furnace at 950°C for 1.5 hours. The percentage weight loss was calculated using the following formula:

$$LOI = 100 \cdot (W2 - W3) / (W2 - W1)$$

Before starting to make a batch of fusion beads, the weight loss on the flux (a mixture of lithium metaborate and lithium tetraborate) was determined. 5g of flux was weighed into a Pt / 5% Au crucible and placed over a Sparton gas burner until fully melted. Once cooled, the crucible and ignited flux was weighed and the weight loss on the flux determined. In order to make the fusion beads, 5g plus the previously determined weight loss of flux was accurately weighed into a Pt / Au crucible. 1 g of ignited sample was then weighed on top of the flux, and the two components were thoroughly mixed. The crucible and its contents were then placed on the Sparton gas burner. Once melted the mixture was

swirled around in the crucible to ensure complete mixing. The homogenised liquid was poured onto a heated casting plate, and allowed to cool. The resulting fusion bead was then ready for XRF analysis.

This method was used for most of the USEKA samples, but a slightly different procedure was employed for carbonate-rich samples. Igniting carbonates produces CaO or MgO, both of which are very effective at taking up H<sub>2</sub>O and CO<sub>2</sub> from the atmosphere. Hence, for the carbonate-rich samples, it proved more accurate to use 1g of dry, rather than ignited powder. Furthermore, SiO<sub>2</sub> and Al<sub>2</sub>O<sub>3</sub>-poor samples will not generally produce stable glasses with a mixture of lithium metaborate and lithium tetraborate. Therefore, lithium tetraborate was used as the flux, since it is capable of producing stable glasses by itself. Extra care was taken when melting these mixtures over the gas burner, since non-ignited powder releases volatiles at this stage.

Major and trace element analyses were carried out on Philips PW 1400 and ARL 8420+ XRF spectrometers. The analytical methods employed were those described by Tarney and Marsh (1991). The data from this study is presented in Tables I1, I2 and I3. The major element data has been recalculated incorporating the LOI values. Since analyses of carbonate-rich samples were conducted on non-ignited powders, the LOI values for these samples were simply added to their totals.

### *PGAA (B)*

The B concentrations of selected igneous rocks from the USEKA area were determined by PGAA at Activation Laboratories Ltd in Ontario, Canada. In order to activate samples, they are encapsulated and placed into or near the core of a neutron source (nuclear reactor). The neutrons interact with the target nucleus converting it into a radioactive nucleus (Hoffman 1992). The capture gamma rays emitted usually have very short half lives and can be measured during irradiation using a technique called PGAA. This technique is particularly well suited to the determination of B (Hoffman 1992).

One g of sample powder was weighed and encapsulated in a polyethylene vial. Samples were introduced into the thermalized neutron beam of the prompt gamma neutron beamport at the McMaster Nuclear Reactor. As the sample was being irradiated the prompt gamma rays emitted were measured using an n-type germanium detector for the 478 Kev Doppler broadened boron peak. The samples count rates were corrected for sodium interference and blank and boron were computed using CANMET SY-3 certified standard reference materials.

### *ICP-AES*

#### *(i) Li determination (sample preparation)*

Li was analysed in igneous and sediment samples from the USEKA area by ICP-AES, using a total digestion method. 100 mg of sample was weighed out into PTFE test tubes and 2 ml of 70 % nitric acid was added. The samples were placed in a hot block at 50°C overnight. 1 ml of 60 % perchloric acid and 5 ml of hydrofluoric acid were then added to the samples, which were subsequently returned to the hot block. The samples were left at 100°C for three hours, at 150°C for three hours and at 190°C for six hours. 1 ml of hydrochloric acid was added to each sample, before returning the samples to the hot

block at 50°C for half an hour. 9 ml of de-ionised water was then added to each tube, and the samples were left overnight. Finally, before analysis, the samples were centrifuged.

### (ii) REE determination (sample preparation)

The REE concentrations of selected igneous samples from the Emet and Kirka areas were determined by ICP-AES using methods described by Walsh et al. (1981) and Thompson and Walsh (1983). The samples were firstly ignited at 950°C for 1.5 hours. 0.5 g of this ignited sample was then weighed into a PTFE beaker and 15 ml hydrofluoric acid and 4 ml perchloric acid were added. The beakers were placed on a hot block at 180 - 200°C and evaporated to dryness. Another 4 ml of hydrofluoric acid was added and the beaker was evaporated to dryness again. 20 ml of 25 % hydrochloric acid was added to the beakers, which were warmed until the residue had dissolved. The solutions were then transferred into Pyrex beakers and the volume made up to 50 ml with de-ionised water.

Once the digestion had been completed, the samples were loaded into ion exchange columns. The following procedures are then carried out:

- (a) 450 ml of 1.7 N hydrochloric acid was run through the columns and collected in waste bottles.
- (b) 600 ml of 6 N hydrochloric acid was added to the columns and collected in sample bottles.
- (c) The samples were transferred from the sample bottles into 800 ml Pyrex beakers, which were placed on a sand bath and left to evaporate.
- (d) When the solutions had evaporated to about 50 ml, they were transferred to 50 ml Pyrex beakers and evaporation continued.
- (f) When the solutions had evaporated to about 10 ml, 2 ml of nitric acid was added and the solutions were evaporated to dryness.
- (g) Once re dissolved in 5 % nitric acid, the samples were ready for analysis.

### Accuracy and precision

#### *XRF*

TiO<sub>2</sub> was analysed in both fusion beads and powder pellets and it is clear from Figure I 1 that concentrations are similar in the pellet and bead of any given sample. This indicates that the samples have not been 'mixed up' during sample preparation and analysis. Data for standards run with samples from this study are presented in Tables I 4 and I 5. Averages of the measured international standards agree closely with accepted values from geostandards newsletters (Govindaraju 1994). The accuracy of the measured international standards for selected elements is also shown graphically in Figure I 2. The precision of the data is illustrated in Figure I 3, where international standard and USEKA sample concentrations measured in 1994 agree closely with analyses of the same samples carried out in 1995 and 1996.

#### *PGAA (B)*

## Appendix I (XRF, PGAA, ICP-AES)

---

In order to test the accuracy of the B data, international standards were sent for analysis by PGAA together with the USEKA samples. International standards sent to Canada for analysis are shown in Table I 6 and they clearly correlate closely with the accepted values in geostandards newsletters (Imai et al., 1996). The precision of the data can be seen by samples analysed in duplicate (Table I 6). There is close agreement between duplicate samples.

### *ICP-AES (Li & REE)*

The Li and REE concentrations in international standards measured in this study once again agree closely with the accepted values from geostandards newsletters (Table I 6) (Govindaraju 1994, Imai et al., 1996). Satisfactory precision was also obtained as illustrated by data from duplicate samples (Table I 6).

### *Comparison between XRF and ICP-AES*

As a further test of the accuracy of the data, comparisons have been made between XRF and ICP-AES. Since Nd, Ce and La were analysed by both techniques, they are plotted against each other in Figure I 4. Once again, there is reasonable agreement between the two data sources (Figure I 4).

## Appendix I (XRF, PGAA, ICP-AES)

**TABLE I1**  
**USEKA granitic and volcanic rocks**  
**XRF DATA**

Rock name	Erigöz Granite	Erigöz Granite	Erigöz Granite	Erigöz Granite	Erigöz Aplite	Erigöz Granite	Erigöz Granite
Locality	W Emet Basin	W Emet Basin	W Emet Basin	W Emet Basin	W Emet Basin	W Emet Basin	W Emet Basin
	Kusoyunagi Tepe	Kusoyunagi Tepe	E of Simav	E of Simav	E of Simav	E of Darci	E of Darci
Sample	G1	G2	G4	G5	G23	G7	G8
Fusion no.	LF3501	LF3498	LF3500	LF3505	LF3510	LF3499	LF3496
RUN	ARLF290	ARLF290	ARLF290	ARLF385	ARLF385	ARLF285	ARLF285
SiO <sub>2</sub>	70.09	70.27	74.67	75.61	78.92	72.89	71.68
TiO <sub>2</sub>	0.51	0.50	0.27	0.27	0.12	0.41	0.44
Al <sub>2</sub> O <sub>3</sub>	14.69	14.91	13.42	13.40	12.44	14.18	14.75
Fe <sub>2</sub> O <sub>3</sub>	3.32	3.27	1.85	1.79	0.99	2.75	2.93
MnO	0.06	0.06	0.04	0.03	0.02	0.05	0.05
MgO	1.09	1.08	0.44	0.42	0.12	0.93	1.03
CaO	2.56	2.62	1.55	1.45	0.68	2.25	2.51
Na <sub>2</sub> O	3.27	3.27	3.06	2.92	3.08	3.03	3.24
K <sub>2</sub> O	3.96	3.89	4.42	4.41	4.91	4.32	3.99
P <sub>2</sub> O <sub>5</sub>	0.17	0.17	0.07	0.07	0.03	0.13	0.14
LOI	0.35	0.35	0.39	0.41	0.29	0.43	0.47
Total	100.07	100.39	100.18	100.77	101.58	101.36	101.22
Pellet no.	L20509	L20499	L20510	L20505	L20494	L20511	L20501
RUN	T204,RT513	T205,RT514	T204,RT513	T204,RT513	T204,RT513	T204,RT513	T206,RT514
	RE155	RE156	RE155	RE155	RE155	RE155	RE156
Ba	1090	1058	751	79	180	885	843
Rb	159	157	157	154	235	165	161
Th	18	19	15	17	37	16	13
Nb	15.6	15.5	10.4	10.0	18.8	14.4	15.0
La	33	35	23	14	19	22	19
Ce	49	64	36	21	34	35	26
Nd	16	18	13	14	14	11	9
Sr	276	283	165	153	40	228	252
Zr	188	183	104	106	97	155	144
Y	35	31	18	17	38	24	24
Ga	17	16	15	14	14	16	17
Ni	1	BDL	BDL	BDL	BDL	BDL	BDL
Sc	10	13	7	3	5	10	10
V	60	58	35	10	15	50	54
Cr	6	10	6	4	4	6	13
Co	6	4	3	BDL	BDL	4	5
As	2	2	6	10	19	1	2

### PGAA

B	13	NA	NA	8	21	6	NA
---	----	----	----	---	----	---	----

### ICP-AES

Li	57	NA	NA	53	BDL	57	NA
La				31.2			
Ce				54.7			
Pr				5.08			
Nd				18.08			
Sm				3.19			
Eu				0.53			
Gd				3.1			
Dy				3.1			
Er				1.39			
Yb				1.28			
Lu				0.2			

NA = not analysed

BDL = below detection limit

Major elements in wt %, trace elements in ppm

## Appendix I (XRF, PGAA, ICP-AES)

**TABLE I1**  
XRF DATA

Rock name	Emet Rhyolite	Emet Rhyolite	Emet Latite	Emet Latite	Emet Rhyolite	Emet Rhyolite	Emet Rhyolite	Emet Rhyolite
Locality	Emet Basin Köprücek	Emet Basin Köprücek	Emet Basin Dereköy	Emet Basin Dereköy	Emet Basin Kurtlubeyler	Emet Basin Kurtlubeyler	Emet Basin NE of Yagcik	Emet Basin NE of Yagcik
Sample	E1	E2	E3	E4	E5	E6	E16	E17
Fusion no.	LF3484	LF3594	LF3509	LF3502	L3592	LF3479	LF3483	LF3512
RUN	ARLF284	ARLF286	ARLF285	ARLF294	ARLF286	ARLF284	ARLF284	ARLF285
SiO2	71.78	71.50	56.63	56.19	69.28	71.04	71.60	72.56
TiO2	0.36	0.37	1.88	1.91	0.58	0.59	0.40	0.39
Al2O3	14.90	14.70	14.05	14.05	15.34	15.13	14.69	14.71
Fe2O3	2.62	2.63	6.95	6.96	3.62	3.70	2.71	2.67
MnO	0.02	0.02	0.09	0.08	0.02	0.02	0.02	0.02
MgO	0.72	0.70	4.82	4.79	0.80	0.77	0.26	0.27
CaO	2.08	2.01	6.69	6.55	0.28	0.28	0.45	0.48
Na2O	3.19	3.16	2.21	2.20	0.69	0.64	1.44	1.46
K2O	3.78	3.87	5.84	5.79	6.43	5.97	7.53	7.31
P2O5	0.14	0.14	0.57	0.57	0.19	0.20	0.16	0.16
LOI	0.88	0.88	1.39	1.24	2.66	2.66	1.38	1.46
Total	100.48	99.99	101.11	100.33	99.90	101.01	100.63	101.49
Pellet no.	L20478	L20507	L20495	L20508	L20484	L20483	L20477	L20492
RUN	T205,RT514	T204,RT513	T205,RT514	T204,RT513	T205,RT514	T205,RT514	T205,RT514	T205,RT514
	RE156	RE155	RE156	RE155	RE156	RE156	RE156	RE156
Ba	939	962	459	478	1150	1139	857	952
Rb	103	106	258	243	265	254	335	321
Th	21	22	11	11	23	20	22	21
Nb	14.3	14.8	30.9	30.9	15.6	15.4	16.2	16.2
La	39	43	57	57	43	41	40	39
Ce	64	62	125	131	66	69	69	62
Nd	17	19	63	69	20	21	21	19
Sr	228	218	518	516	43	42	61	65
Zr	165	170	584	590	227	218	193	187
Y	21	22	24	24	25	24	25	24
Ga	18	17	20	22	17	17	17	17
Ni	0	0	115	115	1	1	0	0
Sc	11	8	17	18	6	10	7	7
V	39	37	170	177	70	75	33	36
Cr	9	3	281	288	4	5	2	1
Co	4	4	31	29	7	6	3	2
As	22	21	23	17	14	15	25	23

### PGAA

B	68	NA	13	NA	32	NA	61	NA
---	----	----	----	----	----	----	----	----

### ICP-AES

Li	24	NA	BDL	NA	37	NA	19	NA
La	21.2		49.9					
Ce	38.4		106.8					
Pr	5.1		13.89					
Nd	17.65		64.99					
Sm	2.93		8.96					
Eu	0.44		2.01					
Gd	2.8		6.8					
Dy	2.2		4.8					
Er	1.5		2.72					
Yb	0.77		1.78					
Lu	0.14		0.31					

## Appendix I (XRF, PGAA, ICP-AES)

**TABLE I1**  
XRF DATA

Rock name	Emet Rhyolite	Emet Rhyolite	Emet Rhyolite	Emet Rhyolite	Silicified Rhyolite	Emet shoshonite	Shoshonite
Locality	Emet Basin E of Yagcik	Emet Basin E of Yagcik	Emet Basin E of Yagcik	Emet Basin E of Yagcik	Emet Basin E of Yagcik	Emet Basin Dereköy	Usak-G Basin NW Eski Gediz
Sample	E18	E19	E20	E21	E22	E68	UG7
Fusion no.	LF3489	LF3488	LF3482	LF3480	LF9754	LF3535	LF3511
RUN	ARLF284	ARLF284	ARLF284	ARLF284	RHF415	ARLF286	ARLF285
SiO <sub>2</sub>	72.34	72.30	70.72	71.73	76.30	52.38	52.04
TiO <sub>2</sub>	0.42	0.38	0.33	0.34	0.01	1.66	1.17
Al <sub>2</sub> O <sub>3</sub>	14.34	14.45	13.86	14.05	0.27	13.19	16.00
Fe <sub>2</sub> O <sub>3</sub>	2.76	2.67	1.98	1.99	8.46	6.66	7.85
MnO	0.02	0.02	0.05	0.04	0.06	0.11	0.13
MgO	0.39	0.46	0.65	0.64	3.26	5.07	7.09
CaO	1.25	1.25	1.65	1.68	3.10	9.81	7.58
Na <sub>2</sub> O	2.49	2.37	2.22	2.15	0.00	2.30	2.85
K <sub>2</sub> O	5.38	5.18	5.31	5.27	0.00	5.27	3.16
P <sub>2</sub> O <sub>5</sub>	0.16	0.15	0.16	0.18	0.01	0.54	0.61
LOI	1.00	1.30	2.74	2.71	7.60	3.29	2.24
Total	100.52	100.55	99.68	100.79	99.04	100.28	100.70
Pellet no.	L20487	L20488	L20480	L20482	L30901	L20540	L20493
RUN	T205,RT514 RE156	T205,RT514 RE156	T205,RT514 RE156	T205,RT514 RE156		RT514,T206 RE156	T205,RT514 RE156
Ba	988	1007	756	745	BDL	503	1204
Rb	232	224	258	277	BDL	258	107
Th	22	22	17	18	1	10	19
Nb	16.1	15.4	15.9	15.8	BDL	29.5	19.3
La	39	38	32	35	BDL	59	60
Ce	62	60	54	54	BDL	116	111
Nd	19	19	19	20	BDL	58	44
Sr	145	142	183	178	50	579	982
Zr	181	178	169	163	6	538	272
Y	25	26	25	26	13	24	31
Ga	17	17	17	17	2	20	16
Ni	0	1	0	0	2266	132	114
Sc	5	8	6	7	11	14	17
V	35	38	27	31	13	162	172
Cr	5	5	5	3	2104	280	233
Co	6	3	2	2	98	30	29
As	42	41	14	14	71	40	2

### PGAA

B	57	NA	65	NA	NA	NA	16
---	----	----	----	----	----	----	----

### ICP-AES

Li	NA	NA	14	NA	NA	NA	38
La							58.8
Ce							112.1
Pr							12.7
Nd							41.48
Sm							9.18
Eu							2.29
Gd							7.4
Dy							6.2
Er							2.85
Yb							2.59
Lu							0.42



## Appendix I (XRF, PGAA, ICP-AES)

**TABLE I1**  
XRF DATA

Rock name	Shoshonite	Rhyolite	Rhyolite	Trachyte	Dacite	Trachyte	Latite
Locality	Usak-G Basin	Usak-G Basin	Usak-G Basin	Usak-G Basin	Usak-G Basin	Usak-G Basin	Usak-G Basin
	NW Eski Gediz	NW Eski Gediz	NW Eski Gediz	W of Yenikoy	E of Güre	E of Güre	S of Güre
Sample	UG8	UG28	UG29	UG58	UG63	UG64	UG65
Fusion no.	LF3508	LF3494	LF3495	LF3542	L3540	L3539	LF3538
RUN	ARLF285	ARLF285	ARLF294	ARLF286	ARLF286	ARLF286	ARLF286
SiO2	52.22	71.61	70.10	65.48	64.85	64.14	61.51
TiO2	1.19	0.43	0.41	0.99	0.72	2.41	0.73
Al2O3	16.08	15.58	15.45	14.04	16.95	13.81	16.31
Fe2O3	7.86	2.76	2.64	3.35	4.69	4.69	5.18
MnO	0.13	0.04	0.04	0.05	0.05	0.01	0.07
MgO	7.30	0.45	0.45	2.51	0.96	1.44	2.90
CaO	7.76	2.34	2.35	2.98	3.02	1.87	4.85
Na2O	2.58	3.63	3.67	2.12	2.65	1.57	2.63
K2O	3.14	4.17	4.17	6.23	3.71	7.10	3.84
P2O5	0.61	0.14	0.14	0.56	0.28	0.92	0.37
LOI	2.01	0.26	0.36	2.24	2.03	2.18	1.75
Total	100.87	101.41	99.76	100.57	99.91	100.13	100.13
Pellet no.	L20496	L20503	L20502	L20547	L20545	L20544	L20543
RUN	T205,RT514	T204,RT513	T204,RT516	T206,RT514	T206,RT514	T206,RT514	T206,RT514
	RE156	RE155	RE157	RE156	RE156	RE156	RE156
Ba	1210	1566	1643	1101	1132	852	1414
Rb	107	143	138	251	142	149	151
Th	17	33	32	36	24	29	32
Nb	19.8	17.1	16	32.5	16.9	69.9	17.2
La	62	49	52	60	57	109	68
Ce	117	78	73	115	104	237	115
Nd	45	19	18	44	39	98	43
Sr	913	392	403	655	644	638	911
Zr	277	192	179	502	250	1345	243
Y	31	18	17	22	24	25	29
Ga	17	17	17	19	21	25	20
Ni	115	0	0	20	8	277	20
Sc	19	9	11	14	12	17	16
V	169	51	48	105	69	163	128
Cr	232	6	0	121	53	737	65
Co	32	5	5	12	10	17	15
As	3	12	13	23	13	6	19

### PGAA

B	NA	53	NA	105	NA	NA	NA
---	----	----	----	-----	----	----	----

### ICP-AES

Li	NA	17	NA	27	NA	NA	NA
La							
Ce							
Pr							
Nd							
Sm							
Eu							
Gd							
Dy							
Er							
Yb							
Lu							

## Appendix I (XRF, PGAA, ICP-AES)

**TABLE I1**  
XRF DATA

Rock name	Trachyte	Trachyte	Latite	Trachyte	Trachyte	Trachyte	Latite
Locality	Usak-G Basin	Usak-G Basin	Usak-G Basin	Usak-G Basin	Usak-G Basin	Usak-G Basin	Usak-G Basin
	S of Güre	S of Güre	Zahman	S of Yenikoy	S of Yenikoy	N of Usak	S of Yenikoy
Sample	UG66	UG67	UG73	UG74	UG75	UG126	UG142
Fusion no.	LF3537	LF3536	L3531	LF3530	LF3529	LF3523	LF3521
RUN	ARLF286	ARLF286	ARLF286	ARLF286	ARLF285	ARLF285	ARLF285
SiO <sub>2</sub>	65.90	65.00	56.05	66.44	63.54	64.16	58.02
TiO <sub>2</sub>	0.89	0.89	1.59	1.31	1.16	0.93	1.94
Al <sub>2</sub> O <sub>3</sub>	16.34	16.42	14.97	15.14	13.86	17.15	13.92
Fe <sub>2</sub> O <sub>3</sub>	3.44	3.89	4.31	3.30	4.27	4.71	5.84
MnO	0.01	0.02	0.06	0.00	0.14	0.02	0.08
MgO	0.89	1.09	2.84	1.37	1.97	0.98	2.56
CaO	2.56	3.19	8.78	1.36	2.62	2.28	3.52
Na <sub>2</sub> O	2.46	2.69	2.35	1.71	2.52	2.34	1.89
K <sub>2</sub> O	4.93	4.89	5.13	7.06	6.56	4.68	8.37
P <sub>2</sub> O <sub>5</sub>	0.49	0.48	0.70	0.82	0.83	0.45	0.86
LOI	2.10	1.47	2.74	1.73	1.07	2.72	3.82
Total	100.02	100.05	99.52	100.24	98.52	100.41	100.83
Pellet no.	L20542	L20541	L20536	L20535	L20534	L20519	L20550
RUN	T206,RT514	T206,RT514	T206,RT514	T206,RT514	T206,RT514	T205,RT513	T206,RT514
	RE156	RE156	RE156	RE156	RE156	RE155	RE156
Ba	1601	1605	1166	1390	1504	1738	804
Rb	184	179	172	298	263	164	373
Th	30	27	15	18	18	34	22
Nb	24.4	24.2	31.2	27.1	24.4	25.1	51.6
La	69	75	70	49	58	81	91
Ce	124	145	146	86	113	136	185
Nd	48	62	61	35	51	50	77
Sr	932	998	647	649	712	786	751
Zr	389	382	603	694	618	362	1049
Y	32	51	30	31	24	28	22
Ga	19	21	20	22	21	22	23
Ni	27	28	94	55	39	14	343
Sc	18	17	25	12	12	18	20
V	147	139	166	115	125	146	178
Cr	173	166	344	232	268	54	779
Co	10	12	15	13	18	12	23
As	11	10	2	20	19	11	68

### PGAA

B	NA	NA	7	NA	54	22	NA
---	----	----	---	----	----	----	----

### ICP-AES

Li	NA	NA	27	NA	38	BDL	25
La					72	79.2	82.3
Ce					140.4	143.1	168.7
Pr					11.56	14.29	17.8
Nd					67.65	49.17	63.07
Sm					9.26	7.77	10.36
Eu					2.43	2.19	2.69
Gd					8.5	8.9	8
Dy					6.6	6.6	5.4
Er					2.77	2.03	2.17
Yb					2.95	2.17	0.79
Lu					0.44	0.35	0.09

## Appendix I (XRF, PGAA, ICP-AES)

**TABLE I1**  
XRF DATA

Rock name	Latite	Rhyolite	Rhyolite	Trachyte	Trachyte	Andesite	Andesite
Locality	Usak-G Basin	Selendi Basin	Selendi Basin	Selendi Basin	Selendi Basin	Selendi Basin	Selendi Basin
	SW of Zahman	E of Yumru dagi	E of Yumru dagi	E of Yumru Dagı	E of Yumru Dagı	SSW Saphane	SSW Saphane
Sample	UG145	SE1	SE2	SE3	SE4	SE12	SE13
Fusion no.	LF3520	LF5289	LF4904	LF5291	LF4907	LF6553	LF3487
RUN	ARLF290	ARLF412	ARLF411	ARLF412	ARLF411	ARLF459	ARLF284
SiO <sub>2</sub>	56.54	70.00	69.38	63.83	62.76	59.09	59.23
TiO <sub>2</sub>	2.03	0.54	0.52	0.66	0.65	0.81	0.81
Al <sub>2</sub> O <sub>3</sub>	12.73	14.65	15.21	16.66	16.41	16.78	16.44
Fe <sub>2</sub> O <sub>3</sub>	6.64	3.11	2.93	3.83	4.31	6.29	6.48
MnO	0.06	0.03	0.03	0.06	0.07	0.11	0.11
MgO	5.31	0.94	0.87	1.51	1.62	3.64	3.46
CaO	5.62	2.32	2.53	4.04	4.36	6.67	6.44
Na <sub>2</sub> O	2.31	3.36	3.61	3.55	3.78	3.07	2.87
K <sub>2</sub> O	6.14	4.45	4.43	3.82	3.92	2.61	2.61
P <sub>2</sub> O <sub>5</sub>	0.78	0.15	0.17	0.20	0.19	0.23	0.24
LOI	1.97	0.78	0.68	2.14	1.17	1.11	1.49
Total	100.12	100.33	100.35	100.30	99.25	100.43	100.17
Pellet no.	L20549	L22546	L21778	L22548	L21807	L20504	L20489
RUN	T206,RT514	LDA2	LDA3	LDA2	LDA3	T204,RT513	T205,RT514
	RE156					RE155	RE156
Ba	651	977	944	618	602	1206	1552
Rb	243	146	148	139	140	101	96
Th	22	20	18	11	18	21	19
Nb	55.2	16	14	12	11	10.9	11.5
La	92	31	30	28	31	206	46
Ce	201	61	67	69	64	446	67
Nd	87	28	25	31	33	193	25
Sr	634	250	301	380	409	674	669
Zr	1128	183	175	194	192	181	178
Y	26	19	20	17	20	29	29
Ga	23	17	16	22	19	20	18
Ni	236	BDL	7	BDL	11	9	10
Sc	21	8	8	14	9	18	14
V	153	61	57	71	67	201	156
Cr	529	10	24	17	24	240	17
Co	21	6	4	10	8	40	22
As	29	10	13	30	25	8	8

### PGAA

B	54	36	NA	112	NA	32	NA
---	----	----	----	-----	----	----	----

### ICP-AES

Li	30	23	NA	14	NA	42	NA
La							
Ce							
Pr							
Nd							
Sm							
Eu							
Gd							
Dy							
Er							
Yb							
Lu							

## Appendix I (XRF, PGAA, ICP-AES)

**TABLE 11**  
XRF DATA

Rock name	Rhyolitic tuff	Rhyolitic tuff	Latite	Latite	Alunite + Quartz	Rhyolite	Latite
Locality	Selendi Basin	Selendi Basin	Selendi Basin	Selendi Basin	Selendi Basin	Selendi Basin	Simav Basin
Sample	Taslik	Taslik	W of Abide	W of Abide	NW of Saphane	Saphane	Nasa
Fusion no.	SE24	SE25	SE26	SE27	SE71	SE72	SI14
RUN	LF3506	LF3507	LF3491	LF3483	LF3533	LF3532	LF3497
	ARLF285	ARLF285	ARLF284	ARLF284	ARLF294	ARLF286	ARLF285
SiO <sub>2</sub>	72.55	73.01	56.94	56.97	61.25	70.78	56.64
TiO <sub>2</sub>	0.45	0.46	1.62	1.62	0.23	0.33	1.23
Al <sub>2</sub> O <sub>3</sub>	12.56	12.76	10.49	10.58	13.40	13.79	15.98
Fe <sub>2</sub> O <sub>3</sub>	3.95	3.45	6.30	6.39	1.46	2.19	6.58
MnO	0.02	0.03	0.08	0.08	0.00	0.03	0.10
MgO	0.57	0.54	9.20	9.24	0.00	0.52	4.22
CaO	0.21	0.18	5.03	4.94	0.02	2.31	7.42
Na <sub>2</sub> O	0.58	0.58	1.31	1.33	0.00	2.74	2.89
K <sub>2</sub> O	9.48	9.47	7.05	7.00	3.82	4.17	4.14
P <sub>2</sub> O <sub>5</sub>	0.16	0.15	1.25	1.26	0.08	0.10	0.72
LOI	0.90	0.89	1.47	1.49	15.84	1.77	1.34
Total	101.43	101.52	100.73	100.90	96.05	98.72	101.26
Pellet no.	L20498	L20497	L20485	L20479	L20538	L20537	L20500
RUN	T205RT514	T205,RT514	T205,RT514	T205,RT514	RT514,T206	RT514T206	RT514,T206
	RE156	RE156	RE156	RE156	RE156	RH156	RE156
Ba	897	943	1888	1885	747	1181	1441
Rb	396	395	258	254	5	149	125
Th	18	17	15	14	30	25	15
Nb	12.2	12.3	48.1	48.2	13.6	13.4	31.1
La	32	35	53	54	41	44	78
Ce	52	52	103	100	61	57	141
Nd	11	13	47	44	6	16	58
Sr	58	72	967	978	255	201	791
Zr	151	156	831	827	200	156	544
Y	21	28	29	31	14	25	36
Ga	14	14	17	18	13	16	19
Ni	8	8	284	284	0	0	60
Sc	11	10	18	14	4	9	16
V	75	78	140	142	23	43	146
Cr	8	6	680	664	6	1	141
Co	9	10	34	32	2	1	20
As	145	167	6	6	204	4	3

### PGAA

B	34	NA	17	NA	3	NA	7
---	----	----	----	----	---	----	---

### ICP-AES

Li	BDL	NA	25	NA	BDL	NA	31
La					50.3		71.9
Ce					70.2		134.9
Pr					6.45		13.66
Nd					15.93		43.46
Sm					1.08		8.01
Eu					0.13		2.08
Gd					1.1		8.5
Dy					2		7
Er					1.63		1.87
Yb					1.64		0.64
Lu					0.26		0.09

## Appendix I (XRF, PGAA, ICP-AES)

**TABLE I1**  
XRF DATA

Rock name	Latite	Kirka Ignimbrite	Kirka Ignimbrite	Kirka Ignimbrite	Kirka Ignimbrite	Kirka Ignimbrite	Kirka Ignimbrite
Locality	Simav Basin	SE of Kirka Basin	SE of Kirka Basin	S of Kirka Basin	S of Kirka Basin	Kirka Basin	Kirka Basin
	Nasa	NW of Seyidler	NW Seyidler	Ayazini	Ayazini	Fetiye	Fetiye
Sample	SI15	I208	I209	I219	I220	I221	I222
Fusion no.	LF3490	LF4898	LF6881	LF6871	LF4895	LF6870	LF6874
RUN	ARLF284	ARLF411	RHF348	RHF348	ARLF411	RHF348	RHF340
SiO <sub>2</sub>	55.69	76.72	75.91	74.19	76.27	79.95	79.02
TiO <sub>2</sub>	1.20	0.09	0.11	0.07	0.06	0.08	0.05
Al <sub>2</sub> O <sub>3</sub>	15.71	12.39	12.18	12.96	12.92	10.94	10.43
Fe <sub>2</sub> O <sub>3</sub>	6.88	0.42	0.53	1.12	0.94	0.39	0.38
MnO	0.11	0.05	0.05	0.05	0.10	0.01	0.01
MgO	3.68	0.01	0.13	0.16	0.02	0.23	0.22
CaO	7.67	0.88	0.88	0.87	0.82	0.33	0.35
Na <sub>2</sub> O	2.83	2.52	2.40	2.49	2.71	1.09	1.12
K <sub>2</sub> O	4.05	4.99	4.68	4.94	5.31	5.16	5.25
P <sub>2</sub> O <sub>5</sub>	0.71	0.02	0.01	0.01	0.02	0.01	0.01
LOI	1.66	1.32	2.24	2.64	1.56	1.30	1.25
Total	100.20	99.41	99.1	99.49	100.72	99.49	98.08
Pellet no.	L20486	L21772	L22555	L22553	L21819	L22556	L22551
RUN	T205,RT514 RE156	LDA3	LDA2	LDA2	LDA3	LDA2	LDA2
Ba	1463	200	208	33	44	46	43
Rb	127	342	325	443	436	454	445
Th	15	40	42	35	31	28	33
Nb	31.5	42	38	42	47	42	33
La	79	26	24	18	16	19	17
Ce	143	53	58	39	41	38	38
Nd	60	24	20	20	17	12	25
Sr	799	77	67	NA	27	24	26
Zr	545	92	95	78	69	81	74
Y	36	34	35	52	55	59	52
Ga	19	14	15	19	17	16	16
Ni	92	4	3	11	4	12	11
Sc	17	5	2	6	5	5	4
V	146	8	12	11	7	8	8
Cr	134	21	4	BDL	BDL	5	4
Co	23	BDL	BDL	BDL	BDL	BDL	3
As	19	23	19	56	52	36	28

### PGAA

B	NA	71	NA	145	NA	NA	74
---	----	----	----	-----	----	----	----

### ICP-AES

Li	NA	11	NA	BDL	NA	NA	21
La							
Ce							
Pr							
Nd							
Sm							
Eu							
Gd							
Dy							
Er							
Yb							
Lu							

## Appendix I (XRF, PGAA, ICP-AES)

**TABLE I1**  
XRF DATA

Rock name	Kirka Ignimbrite	Kirka Ignimbrite	Kirka Ignimbrite	Kirka Ignimbrite	Kirka Ignimbrite	Kirka Ignimbrite	Kirka Ignimbrite
Locality	S of Kirka Basin Köroglukalesi	S of Kirka Basin Köroglukalesi	S of Kirka Basin Köroglukalesi	Kirka Basin Büyükyayla	Kirka Basin Büyükyayla	Kirka Basin Kümbet	Kirka Basin NE of Karaören
Sample	I250	I251	I252	I258	I259	I 260	I271
Fusion no.	LF7132	LF4882	LF4878	LF6872	LF6867	LF6883	LF6862
RUN	RHF341	ARLF389	ARLF389	RHF348	RHF340	RHF348	RHF340
SiO <sub>2</sub>	76.62	75.01	75.38	77.43	78.95	74.51	72.20
TiO <sub>2</sub>	0.06	0.05	0.05	0.06	0.05	0.08	0.08
Al <sub>2</sub> O <sub>3</sub>	12.32	12.63	12.67	12.00	10.10	12.30	12.78
Fe <sub>2</sub> O <sub>3</sub>	1.08	0.88	0.84	1.10	0.89	1.26	1.32
MnO	0.01	0.02	0.02	0.02	0.01	0.10	0.20
MgO	0.16	0.01	0.01	0.34	0.22	0.11	0.37
CaO	0.68	0.91	0.89	0.80	0.75	0.88	1.10
Na <sub>2</sub> O	2.19	3.16	3.14	1.95	2.32	2.69	2.61
K <sub>2</sub> O	4.66	4.09	4.12	4.69	3.95	5.51	5.21
P <sub>2</sub> O <sub>5</sub>	0.01	0.02	0.02	0.01	0.01	0.01	0.01
LOI	1.08	1.82	1.61	1.28	1.00	1.60	2.25
Total	98.86	98.61	98.74	99.68	98.26	99.04	98.12
Pellet no.	L22474	L22467	L22471	L22473	L28043	L22482	L28049
RUN	LDA2	LDA2	LDA2	LDA2	LDA8,9,10	LDA2	LDA8,9,10
Ba	40	44	39	38	43	126	82
Rb	334	385	386	382	367	320	418
Th	39	40	39	34	28	49	35
Nb	35	40	37	32	34	26	44
La	19	15	15	14	14	24	15
Ce	46	40	29	24	28	55	30
Nd	20	19	16	20	17	19	18
Sr	27	31	29	32	36	43	51
Zr	86	78	82	78	61	93	75
Y	26	43	43	34	49	40	63
Ga	18	19	18	17	NA	17	NA
Ni	4	9	9	5	NA	6	NA
Sc	2	4	3	4	NA	BDL	NA
V	7	10	7	10	9	10	2
Cr	5	7	6	BDL	8	6	7
Co	BDL	BDL	BDL	BDL	BDL	BDL	1
As	23	42	40	15	40	40	62

### PGAA

B	47	NA	120	NA	NA	NA	NA
---	----	----	-----	----	----	----	----

### ICP-AES

Li	49	NA	21	na	NA	NA	NA
La							
Ce							
Pr							
Nd							
Sm							
Eu							
Gd							
Dy							
Er							
Yb							
Lu							

## Appendix I (XRF, PGAA, ICP-AES)

**TABLE I1**  
XRF DATA

Rock name	Kirka shoshonite	Kirka shoshonite	Kirka shoshonite	Kirka Rhyolite	Kirka Rhyolite	Kirka Rhyolite	Kirka Rhyolite
Locality	Kirka Basin	Kirka Basin	Kirka Basin	Kirka Basin	Kirka Basin	Kirka Basin	Kirka Basin
	N of Sancar	Idrisyayla area	Idrisyayla area	Idrisyayla area	Idrisyayla area	Idrisyayla area	Idrisyayla area
Sample	K223	K225	K226	K227	K228	K229	K230
Fusion no.	LF5393	LF4902	LF4887	LF5392	LF4900	LF4896	LF4905
RUN	ARLF412	ARLF411	ARLF389	ARLF412	ARLF411	ARLF411	ARLF411
SiO <sub>2</sub>	51.05	55.32	55.89	76.00	76.76	73.68	74.00
TiO <sub>2</sub>	1.43	1.00	0.99	0.08	0.08	0.23	0.23
Al <sub>2</sub> O <sub>3</sub>	14.75	16.85	16.28	12.48	12.50	13.18	13.30
Fe <sub>2</sub> O <sub>3</sub>	7.10	7.16	6.96	0.38	0.35	2.14	2.09
MnO	0.11	0.12	0.11	0.01	0.01	0.05	0.05
MgO	7.49	5.07	5.03	0.11	0.16	0.24	0.22
CaO	7.75	7.16	6.93	0.19	0.22	1.09	1.12
Na <sub>2</sub> O	2.44	3.48	3.11	1.30	1.44	4.09	4.14
K <sub>2</sub> O	4.34	3.46	3.19	8.20	7.93	5.23	5.18
P <sub>2</sub> O <sub>5</sub>	0.58	0.49	0.48	0.04	0.05	0.07	0.07
LOI	2.02	0.70	0.48	1.06	1.00	0.23	0.26
Total	99.07	100.81	99.44	99.83	100.46	100.22	100.65
Pellet no.	L21777	L21776	L21827	L21773	L21774	L21818	L21779
RUN	LDA3	LDA3	LDA3	LDA3	LDA3	LDA2	LDA3
Ba	1217	1137	1192	111	98	426	424
Rb	137	127	126	446	430	187	193
Th	8	12	3	34	32	33	27
Nb	28	17	17	26	26	20	21
La	68	40	40	28	26	48	45
Ce	135	71	69	62	63	101	86
Nd	54	31	38	22	26	40	36
Sr	748	554	548	177	159	82	97
Zr	402	234	233	90	94	193	207
Y	24	24	26	11	18	23	22
Ga	16	15	16	16	16	17	15
Ni	155	120	113	3	2	BDL	BDL
Sc	16	20	17	4	2	6	4
V	153	128	131	3	10	25	19
Cr	272	211	197	BDL	BDL	BDL	4
Co	28	24	23	BDL	BDL	BDL	3
As	3	2	BDL	55	41	42	35

### PGAA

B	11	12	NA	53	NA	44	NA
---	----	----	----	----	----	----	----

### ICP-AES

Li	16	BDL	NA	35	NA	18	NA
La	61.8	39.7		22.3		48.3	
Ce	119.8	75.3		42.5		9.6	
Pr	13.17	9.31		4.7		8.85	
Nd	44.45	26.81		15.47		30.55	
Sm	8.45	6.91		3.89		5.81	
Eu	2.16	1.65		0.31		0.8	
Gd	6.7	6		3.7		5.1	
Dy	5.1	5.19		3.6		4.66	
Er	2.36	2.6		1.74		2.13	
Yb	1.95	2.39		2.28		2.11	
Lu	0.32	0.4		0.37		0.34	

## Appendix I (XRF, PGAA, ICP-AES)

**TABLE I1**  
XRF DATA

Rock name	Kirka Rhyolite	Kirka Trachyte	Kirka Trachyte	Kirka Dacite	Kirka Trachyte	Kirka Rhyolite	Kirka Rhyolite
Locality	Kirka Basin	Kirka Basin	Kirka Basin	Kirka Basin	Kirka Basin	Kirka Basin	Kirka Basin
	Idrisyayla area	Idrisyayla area	Idrisyayla area	Idrisyayla area	Idrisyayla area	Idrisyayla area	Idrisyayla area
Sample	K231	K232	K233	K234	K235	K236	K237
Fusion no.	LF4884	LF4891	LF4886	LF4881	LF7122	LF4880	LF4877
RUN	ARLF389	ARLF411	ARLF389	ARLF389	RHF348	ARLF389	ARLF411
SiO <sub>2</sub>	68.42	67.07	66.97	64.87	63.69	68.79	75.56
TiO <sub>2</sub>	0.58	0.61	0.59	0.67	0.77	0.53	0.08
Al <sub>2</sub> O <sub>3</sub>	15.88	16.46	15.42	15.30	15.47	14.88	12.44
Fe <sub>2</sub> O <sub>3</sub>	1.98	2.08	4.20	4.73	4.92	3.45	1.27
MnO	0.02	0.03	0.07	0.09	0.10	0.02	0.01
MgO	0.58	0.63	0.68	1.85	2.01	0.46	0.02
CaO	2.16	2.15	2.79	4.37	4.44	2.23	0.13
Na <sub>2</sub> O	3.34	4.03	3.63	3.61	3.97	3.37	1.22
K <sub>2</sub> O	4.08	4.54	3.99	3.55	3.77	4.34	7.30
P <sub>2</sub> O <sub>5</sub>	0.11	0.11	0.16	0.19	0.18	0.18	0.04
LOI	2.03	2.33	0.59	0.44	0.51	0.66	1.18
Total	99.19	100.03	99.08	99.66	99.84	98.9	99.24
Pellet no.	L22465	L21823	L21829	L22468	L21821	L22469	L22472
RUN	LDA2	LDA3	LDA3	LDA2	LDA3	LDA2	LDA2
Ba	983	999	969	1004	1011	990	95
Rb	156	155	158	138	137	190	418
Th	25	22	22	18	22	24	30
Nb	18	20	19	16	16	18	26
La	38	41	43	36	44	33	28
Ce	76	74	92	82	74	63	59
Nd	30	21	33	29	32	24	21
Sr	332	353	385	494	525	NA	90
Zr	190	185	176	178	174	176	96
Y	12	16	24	25	23	21	8
Ga	19	19	17	18	17	17	16
Ni	BDL	2	6	4	9	11	4
Sc	7	9	14	12	16	10	1
V	59	54	52	90	97	62	9
Cr	12	20	25	38	52	33	BDL
Co	3	6	13	12	14	8	3
As	29	39	26	31	29	19	58

### PGAA

B	NA	45	NA	24	NA	34	59
---	----	----	----	----	----	----	----

### ICP-AES

Li	NA	15	NA	19	NA	BDL	58
La		39.9		38.8			
Ce		70.8		69.3			
Pr		7.83		7.87			
Nd		22		23.3			
Sm		4.7		4.64			
Eu		0.96		0.44			
Gd		3.7		5.5			
Dy		3.4		5			
Er		1.82		2.6			
Yb		1.58		2.32			
Lu		0.27		0.4			



## Appendix I (XRF, PGAA, ICP-AES)

**TABLE I1**  
XRF DATA

Rock name	Kirka Rhyolite	Kirka Rhyolite	Kirka Rhyolite	Kirka Rhyolite	Kirka Rhyolite	Kirka Rhyolite	Kirka Rhyolite
Locality	Kirka Basin	Kirka Basin	Kirka Basin	Kirka Basin	Kirka Basin	Kirka Basin	Kirka Basin
	Idrisyayla area	Idrisyayla area	Idrisyayla area	Idrisyayla area	Idrisyayla area	Idrisyayla area	Idrisyayla area
Sample	K238	K239	K244	K245	K246	K247	K277
Fusion no.	LF4901	LF4879	LF7126	LF4885	LF4892	LF7116	LF6873
RUN	ARLF411	ARLF389	RHF341	ARLF389	ARLF411	RHF348	RHF348
SiO <sub>2</sub>	70.99	69.57	73.49	74.80	76.25	76.12	74.28
TiO <sub>2</sub>	0.51	0.53	0.21	0.19	0.08	0.09	0.23
Al <sub>2</sub> O <sub>3</sub>	14.11	14.46	13.03	12.60	11.41	11.85	13.31
Fe <sub>2</sub> O <sub>3</sub>	3.21	3.48	1.05	0.45	1.44	1.53	0.31
MnO	0.04	0.03	0.01	0.01	0.03	0.03	0.01
MgO	0.54	0.50	0.11	-0.05	0.00	0.06	0.13
CaO	2.17	2.27	0.24	0.14	0.17	0.17	0.25
Na <sub>2</sub> O	3.48	3.39	1.58	1.25	1.77	1.92	1.91
K <sub>2</sub> O	4.66	4.44	8.23	9.12	8.43	7.80	7.75
P <sub>2</sub> O <sub>5</sub>	0.17	0.18	0.04	0.05	0.06	0.01	0.03
LOI	0.45	0.41	0.93	0.26	0.41	0.41	1.11
Total	100.32	99.25	98.91	98.8	100.06	99.98	99.36
Pellet no.	L21775	L22470	L21820	L21828	L28054	L21811	L22480
RUN	LDA3	LDA2	LDA2	LDA3	LDA8,9,10	LDA3	LDA2
Ba	836	887	790	792	33	46	789
Rb	184	196	485	545	522	527	465
Th	21	19	32	20	44	27	22
Nb	17	18	20	19	30	31	21
La	38	40	49	40	23	27	34
Ce	71	73	82	82	66	55	62
Nd	27	29	24	27	30	28	24
Sr	289	280	124	106	18	9	96
Zr	181	164	113	121	139	146	115
Y	19	18	BDL	BDL	33	25	BDL
Ga	14	18	16	15	NA	16	15
Ni	5	5	8	5	NA	5	7
Sc	9	5	1	4	NA	4	BDL
V	48	53	22	14	1	5	20
Cr	29	19	5	5	13	BDL	BDL
Co	4	3	BDL	3	BDL	BDL	BDL
As	20	26	254	69	72	76	29

### PGAA

B	NA	NA	NA	67	42	NA	82
---	----	----	----	----	----	----	----

### ICP-AES

Li	NA	NA	NA	33	130	NA	55
La				37.9	25.4		
Ce				61.8	51.8		
Pr				5.58	6.23		
Nd				18.35	20.33		
Sm				2.51	4.85		
Eu				0.02	0.14		
Gd				3.1	4.6		
Dy				3	4.7		
Er				1.41	2.1		
Yb				0.81	2.56		
Lu				0.14	0.4		

## Appendix I (XRF, PGAA, ICP-AES)

**TABLE I1**  
XRF DATA

Rock name	Latite	Latite	Latite	Latite	Trachyte	Trachyte	Latite	Latite	Trachyte
Locality	Afyon area	Afyon area	Afyon area	Afyon area	Afyon area	Afyon area	Afyon area	Afyon area	Afyon area
Sample	Koprulu	Koprulu	Afyon	Afyon	Buyukkalecik	Buyukkalecik	NE Iscehisar	NE Iscehisar	Buyukkalecik
Fusion no.	A200	A201	A202	A203	A204	A205	A206	A207	A210
RUN	LF6644	LF6865	LF6860	LF6866	LF6858	LF6875	LF6652	LF6851	LF4909
	ARLF466	RHF340	RHF348	RHF340	RHF348	RHF248	ARLF466	RHF340	ARLF411
SiO <sub>2</sub>	55.70	55.68	61.88	61.74	62.76	61.99	54.46	54.76	62.40
TiO <sub>2</sub>	1.36	1.50	0.92	0.86	0.75	0.74	1.62	1.74	0.67
Al <sub>2</sub> O <sub>3</sub>	12.41	12.22	15.67	15.50	15.14	15.35	14.20	13.90	15.86
Fe <sub>2</sub> O <sub>3</sub>	6.70	7.04	4.77	5.51	4.89	5.20	7.43	7.94	4.92
MnO	0.08	0.08	0.06	0.06	0.11	0.10	0.40	0.26	0.10
MgO	5.86	5.48	1.84	1.46	2.46	2.88	3.65	3.37	2.19
CaO	6.65	6.46	4.18	3.47	3.93	4.92	6.35	6.45	4.56
Na <sub>2</sub> O	2.15	2.32	3.56	3.52	3.90	3.76	2.45	2.56	4.38
K <sub>2</sub> O	7.70	7.20	5.38	5.32	4.64	4.66	6.66	6.15	5.02
P <sub>2</sub> O <sub>5</sub>	0.99	1.02	0.59	0.58	0.44	0.43	1.15	1.16	0.45
LOI	0.47	0.58	0.45	0.87	0.31	0.27	0.89	0.94	0.26
Total	100.08	99.56	99.29	98.91	99.32	100.29	99.26	99.24	100.82
Pellet no.	L27158	L28046	L28039	L28045	L28041	L22554	L27159	L28044	L21809
RUN	LML1	LDA 8,9,10	LDA8,9,10	LDA8,9,10	LDA8,9,10	LDA2	LML1	LDA8,9,10	LDA3
Ba	1467	1724	1458	1475	1920	2231	2526	2617	1937
Rb	190	201	206	204	160	151	169	173	154
Th	32	38	40	42	45	51	19	17	39
Nb	41	43	34	32	24	22	29	31	23
La	113	108	77	73	92	92	78	69	95
Ce	251	239	154	150	169	186	161	148	166
Nd	100	103	71	68	72	77	59	69	67
Sr	1237	1309	1188	1192	1456	1701	985	1021	1609
Zr	598	707	450	443	268	316	607	729	284
Y	19	27	24	23	25	19	27	31	21
Ga	18	NA	NA	NA	NA	19	20	NA	18
Ni	148	NA	NA	NA	NA	17	154	NA	14
Sc	15	NA	NA	NA	NA	11	20	NA	16
V	128	105	127	114	91	103	184	160	90
Cr	548	591	53	47	19	32	467	431	57
Co	20	22	16	12	12	16	58	37	12
As	NA	11	21	14	17	15	NA	17	5

### PGAA

B	15	NA	38	NA	NA	NA	11	NA	35
---	----	----	----	----	----	----	----	----	----

### ICP-AES

Li	29	NA	15	NA	NA	NA	20	NA	24
La									
Ce									
Pr									
Nd									
Sm									
Eu									
Gd									
Dy									
Er									
Yb									
Lu									

## Appendix I (XRF, PGAA, ICP-AES)

**TABLE I1**  
XRF DATA

Rock name	Latite	Latite	Trachyte	Latite	Latite	Latite	Trachyte	Trachyte	Latite
Locality	Afyon area	Afyon area	Afyon area	Afyon area	Afyon area	Afyon area	Afyon area	Afyon area	Afyon area
Sample	Suhut	Suhut	Elvanpasa	Kayadibi	Kayadibi	Calkoy	Balmahmut	Balmahmut	Sandikli
Fusion no.	A213	A214	A216	A217	A218	A241	A242	A243	A248
RUN	LF4883	LF5419	LF6859	LF4917	LF4912	LF4890	LF4916	LF7117	LF4889
	ARLF389	ARLF412	RHF348	ARLF411	ARLF411	ARLF411	ARLF411	RHF348	ARLF411
SiO <sub>2</sub>	60.62	59.82	61.31	60.47	59.76	56.21	62.14	62.11	57.52
TiO <sub>2</sub>	0.92	0.95	0.70	0.71	0.70	0.61	0.59	0.70	1.01
Al <sub>2</sub> O <sub>3</sub>	14.32	14.78	17.02	16.68	16.52	13.36	16.54	16.10	14.67
Fe <sub>2</sub> O <sub>3</sub>	5.70	5.82	5.48	4.98	4.99	5.92	4.24	4.24	6.64
MnO	0.08	0.10	0.05	0.10	0.10	0.14	0.06	0.08	0.07
MgO	2.57	2.16	0.78	1.92	1.88	4.16	1.68	2.10	3.34
CaO	4.83	4.69	3.02	4.85	4.91	9.38	3.50	3.92	5.12
Na <sub>2</sub> O	3.20	3.44	3.99	4.05	3.97	3.30	3.46	3.75	3.16
K <sub>2</sub> O	5.61	6.07	5.70	4.71	4.67	2.73	5.27	5.64	6.09
P <sub>2</sub> O <sub>5</sub>	0.70	0.70	0.40	0.45	0.46	0.18	0.38	0.41	0.85
LOI	0.39	0.52	1.00	0.34	0.36	3.64	1.24	1.03	0.63
Total	98.94	99.02	99.46	99.27	98.31	99.6	99.08	100.08	99.09
Pellet no.	L22466	L21810	L28040	L21817	L21812	L21824	L21816	L21815	L21825
RUN	LDA2	LDA3	LDA8,9,10	LDA3	LDA3	LDA3	LDA3	LDA3	LDA3
Ba	1941	2044	2174	1696	1752	1248	1631	778	2739
Rb	266	256	182	170	166	86	192	163	243
Th	43	35	37	36	34	4	39	19	38
Nb	25	25	25	29	29	13	25	20	30
La	53	52	104	87	83	30	70	26	94
Ce	101	96	159	167	155	47	133	55	138
Nd	35	40	74	60	66	22	52	15	79
Sr	957	1013	1672	1320	1331	1074	1228	432	1251
Zr	325	322	359	322	317	132	265	113	383
Y	11	19	39	20	17	20	18	10	32
Ga	19	18	NA	18	18	15	16	13	17
Ni	27	37	NA	15	10	109	16	65	61
Sc	10	14	NA	14	9	21	7	6	13
V	119	116	83	84	86	84	82	23	121
Cr	60	91	9	42	47	262	50	87	174
Co	17	22	7	11	10	23	8	6	22
As	17	14	15	4	5	8	28	30	11

### PGAA

B	NA	NA	NA	31	NA	NA	90	NA	NA
---	----	----	----	----	----	----	----	----	----

### ICP-AES

Li	NA	NA	13	29	NA	NA	21	NA	NA
La									
Ce									
Pr									
Nd									
Sm									
Eu									
Gd									
Dy									
Er									
Yb									
Lu									

## Appendix I (XRF, PGAA, ICP-AES)

**TABLE I1**  
XRF DATA

Rock name	Latite	Shoshonite	Shoshonite
Locality	Afyon area	Afyon area	Afyon area
	Sandikli	Cepni	Cepni
Sample	A249	A253	A254
Fusion no.	LF7114	LF4906	LF4888
RUN	RHF348	ARLF411	ARLF389
SiO <sub>2</sub>	59.09	53.55	53.92
TiO <sub>2</sub>	0.96	1.34	1.27
Al <sub>2</sub> O <sub>3</sub>	15.60	17.00	16.50
Fe <sub>2</sub> O <sub>3</sub>	5.89	8.44	7.97
MnO	0.11	0.14	0.13
MgO	2.43	4.50	4.43
CaO	4.84	6.84	6.44
Na <sub>2</sub> O	3.54	3.77	3.27
K <sub>2</sub> O	6.08	4.39	4.01
P <sub>2</sub> O <sub>5</sub>	0.70	0.68	0.65
LOI	0.51	0.66	0.75
Total	99.74	101.31	99.36
Pellet no.	L21813	L21806	L21826
RUN	LDA3	LDA3	LDA3
Ba	2646	1729	1909
Rb	201	124	105
Th	27	10	18
Nb	23	21	19
La	63	41	48
Ce	122	94	85
Nd	53	44	38
Sr	1455	832	878
Zr	361	250	260
Y	25	24	27
Ga	18	17	19
Ni	25	37	36
Sc	16	17	15
V	115	150	119
Cr	71	82	69
Co	16	29	25
As	BDL	BDL	3

### PGAA

B	NA	NA	NA
---	----	----	----

### ICP-AES

Li	NA	NA	NA
La			
Ce			
Pr			
Nd			
Sm			
Eu			
Gd			
Dy			
Er			
Yb			
Lu			

## Appendix I (XRF, PGAA, ICP-AES)

**TABLE I2**                      **Volcaniclastic sediments from the USEKA area**  
XRF DATA

Rock name	Volcaniclastic	Volcaniclastic	Volcaniclastic	Volcaniclastic	Silt	Silt	Mudstone	Volcaniclastic
Basin	Emet Basin	Emet Basin	Emet Basin	Emet Basin	Emet Basin	Emet Basin	Emet Basin	Emet Basin
Unit	Red	Red	Red	Red	Borate	Borate	Borate	Borate
Locality	Section A	S of Hisarcik	NE of Yagcik	Section B	Section C	Section C	Section C	Section C
Sample	VSE1	VSE2	VSE3	VSE4	VSE5	VSE6	VSE 7	VSE8
Fusion no.	LF3516	LF3517	LF3518	LF3519	LF3595	LF3597	LF9293	LF3515
RUN	ARLF285	ARLF290	ARLF285	ARLF285	ARLF312	ARLF312	RHF390	ARLF285
SiO <sub>2</sub>	72.31	64.73	36.29	72.91	67.93	53.13	62.07	72.12
TiO <sub>2</sub>	0.57	0.31	0.23	0.11	0.50	0.45	0.42	0.42
Al <sub>2</sub> O <sub>3</sub>	14.84	12.13	9.27	11.47	13.96	11.93	12.83	14.33
Fe <sub>2</sub> O <sub>3</sub>	3.05	1.90	2.59	2.74	3.06	3.49	2.97	1.85
MnO	0.04	0.03	1.03	0.06	0.05	0.19	0.06	0.02
MgO	0.77	1.27	9.93	0.34	1.62	1.83	1.86	0.84
CaO	0.89	6.52	13.52	2.09	2.05	11.16	4.91	0.95
Na <sub>2</sub> O	2.60	0.19	0.06	1.67	1.63	1.20	1.52	1.93
K <sub>2</sub> O	3.47	4.91	3.84	4.97	5.25	4.43	4.81	7.46
P <sub>2</sub> O <sub>5</sub>	0.14	0.12	0.08	0.04	0.14	0.18	0.17	0.10
LOI	2.33	7.50	22.71	4.29	3.42	11.03	5.76	1.18
Total	100.99	99.61	99.56	100.68	99.61	99.02	97.37	101.22
Pellet no.	L20515	L20514	L20513	L20512	L20592	L20594	L20600	L20516
RUNS	T204	T204	T204	T204	LDA14	LDA14	RT524	T205
	RT513	RT513	RT513	RT513	RT524	RT524	RE159	RT513
	RE155	RE155	RE155	RE155	RE159	RE159	LDA16	RE155
Ba	570	436	815	257	860	610	694	660
Rb	177	409	315	309	435	420	363	426
Th	21	12	6	28	15	17	16	16
Nb	16.2	9.9	5.8	13.1	14	13	12.9	11.9
La	50	36	27	26	50	61	56	29
Ce	83	49	29	45	35	57	66	49
Nd	27	15	3	15	13	18	23	9
Sr	206	192	39	80	339	402	410	196
Zr	292	103	75	87	139	105	144	177
Y	29	17	13	22	19	32	22	15
Ga	17	14	11	13	NA	NA	15	16
Ni	8	76	14	14	NA	NA	11	6
Sc	13	8	13	9	NA	NA	20	9
V	63	55	49	22	67	64	69	61
Cr	25	111	21	32	24	20	23	14
Co	8	9	5	1	12	12	9	4
As	17	97	30	76	87	130	166	337
ICP-AES								
Li	35	76	48	16	118	119	125	59

### LEGEND

NA = not analysed

BDL = below detection limit

Major elements in wt %, trace elements in ppm

## Appendix I (XRF, PGAA, ICP-AES)

**TABLE I2**  
**XRF DATA**

Rock name	Silt & limestone	Limestone	Mudstone	Mudstone	Mudstone	Mudstone	Mudstone	Mudstone	Mudstone
Basin	Emet Basin	Emet Basin	Emet Basin	Emet Basin	Emet Basin	Emet Basin	Emet Basin	Emet Basin	Emet Basin
Unit	Borate	Borate	Borate	Borate	Borate	Borate	Borate	Borate	Borate
Locality	Section C	Section C	Section C	Section C	Section C	Section C	Section C	Section C	Section D
Sample	VSE9	VSE10	VSE11	VSE12	VSE13	VSE14	VSE15	VSE 16	VSE 17
Fusion no.	LF9294	LF9295	LF9296	LF9301	LF9300	LF9302	LF9299	LF9297	LF3627
RUN	RHF390	RHF390	RHF390	RHF390	RHF390	RHF390	RHF390	RHF390	ARLF313
SiO2	26.54	8.12	30.02	13.63	7.03	29.06	21.60	32.14	37.40
TiO2	0.11	0.02	0.31	0.16	0.10	0.24	0.17	0.28	0.24
Al2O3	3.86	0.54	7.46	3.65	2.25	5.77	4.24	7.96	9.43
Fe2O3	1.86	0.47	3.38	1.87	1.24	2.70	2.02	3.04	3.26
MnO	0.13	0.05	0.09	0.06	0.04	0.08	0.07	0.12	0.02
MgO	3.56	2.99	12.80	6.62	1.82	18.79	15.65	9.80	2.22
CaO	36.43	47.53	18.15	22.79	24.03	16.72	24.27	21.95	23.41
Na2O	0.23	0.37	0.19	0.31	0.24	0.16	0.17	0.37	0.08
K2O	1.80	0.25	2.69	1.54	0.88	1.78	1.53	3.46	1.48
P2O5	0.15	0.11	0.21	0.09	0.05	0.16	0.18	0.15	0.10
LOI	28.11	37.60	21.22	24.56	44.43	23.74	27.01	21.10	21.13
Total	102.78	98.05	96.51	75.28	82.10	99.20	96.92	100.36	98.78
Pellet no.	L20607	L21204	L20794	L20795	L20801	L20797	L20798	L20799	L21185
RUNS	LDA14	T217	LDA16	LDA16	LDA16	LDA16	LDA16	RT524	RT527
	RT524	RT527	RT524	RT524	RT524	RT524	RT524	RE159	RE160
	RE159	RE160	RE159	RE159	RE159	RE159	RE159	LDA16	T217
Ba	97	87	240	116	263	160	195	350	290
Rb	170	25	358	199	152	269	179	330	451
Th	7	BDL	12	6	2	8	7	13	11
Nb	6	1.3	8	4	2	6	4.4	8.1	9.5
La	30	13	59	32	21	49	34	47	68
Ce	166	23	329	238	28	641	2517	121	69
Nd	11	3	19	14	7	20	61	17	18
Sr	1656	2474	3889	5520	7578	5030	4111	2539	434
Zr	BDL	BDL	BDL	BDL	BDL	BDL	BDL	26	61
Y	10	BDL	13	5	BDL	7	6	16	13
Ga	NA	NA	NA	NA	NA	NA	NA	11	12
Ni	NA	NA	NA	NA	NA	NA	NA	23	124
Sc	NA	NA	NA	NA	NA	NA	NA	66	19
V	39	24	53	32	17	42	53	53	72
Cr	14	2	44	24	18	29	26	29	170
Co	6	BDL	12	6	5	7	8	8	10
As	1699	491	3048	2165	258	6047	20927	941	53
ICP-AES									
Li	203	92	718	368	196	986	715	494	135

## Appendix I (XRF, PGAA, ICP-AES)

**TABLE I2**  
XRF DATA

Rock name	Mudstone	Mudstone	Mudstone	Mudstone	Volcaniclastic	Mudstone	Mudstone	Mudstone
Basin	Emet Basin	Emet Basin	Emet Basin	Emet Basin	Emet Basin	Emet Basin	Selendi Basin	Selendi Basin
Unit	Borate	Borate	Borate	Borate	Borate	Borate	Inay	Inay
Locality	Section E	Section E	Section E	Section F	Section F	Section G	Section H	Section I
Sample	VSE18	VSE 19	VSE20	VSE 21	VSE 22	VSE 23	VSS 1	VSS 2
Fusion no.	LF9304	LF9303	LF9305	LF3639	LF3514	LF9307	LF7100	LF7111
RUN	RHF390	RHF390	RHF390	ARLF313	ARLF285	RHF390	RHF340	RHF340
SiO2	44.34	49.16	20.40	29.66	54.21	58.44	41.99	38.48
TiO2	0.43	0.43	0.20	0.22	0.38	0.52	0.58	0.45
Al2O3	12.36	12.97	5.68	6.90	6.17	11.64	12.41	10.44
Fe2O3	5.10	4.94	2.74	2.21	1.31	4.29	5.71	4.45
MnO	0.08	0.09	0.04	0.09	0.08	0.08	0.10	0.08
MgO	6.87	6.74	5.44	2.68	0.91	6.10	8.21	9.29
CaO	8.84	7.44	20.24	28.72	18.63	4.68	9.60	11.67
Na2O	0.28	0.32	0.16	0.35	1.61	0.27	0.73	0.88
K2O	4.18	4.42	1.66	1.51	1.16	4.01	2.90	3.78
P2O5	0.17	0.19	0.11	0.14	0.08	0.16	0.23	0.06
LOI	6.39	8.65	17.91	26.09	15.27	7.22	16.39	18.59
Total	89.04	95.34	74.58	98.58	99.82	97.39	98.84	98.16
Pellet no.	L21210	L21213	L21216	L21189	L20517	L21207	L23324	L26501
RUNS	RT527	RT527	RT527	T217	T205	T217	LDA17	LDA11
	RE160	RE160	RE160	RT527	RT513	RT527	LDA18	LDA12
	LDA14	LDA16	LDA14	RE160	RE155	RE160	LDA19	LDA13
Ba	440	563	272	461	296	419	365	402
Rb	420	347	174	410	73	395	157	161.4
Th	19	19	8	10	5	16	15	20.5
Nb	14	17	6	8	8.3	14.2	10.6	8.6
La	75	60	38	38	22	49	32	43
Ce	96	91	48	55	33	84	64	78.1
Nd	23	26	13	18	9	25	32	41.7
Sr	1941	696	3992	1339	352	1528	403	818.8
Zr	79	156	BDL	74	142	160	94	85
Y	15	24	12	15	16	21	29	41.7
Ga	NA	16	NA	8	5	15	17	NA
Ni	NA	195	NA	80	18	227	85	NA
Sc	NA	23	NA	28	11	14	19	NA
V	69	67	30	55	36	75	86	62.2
Cr	147	173	49	94	514	343	109	93
Co	20	18	10	6	2	18	19	9.7
As	328	185	206	204	112	321	19	29.7
ICP-AES								
Li	391	424	264	178	18	414	64	36

## Appendix I (XRF, PGAA, ICP-AES)

**TABLE I2**  
XRF DATA

Rock name	Mudstone	Mudstone	Volcaniclastic	Volcaniclastic	Volcaniclastic	Volcaniclastic	Volcaniclastic
Basin	Usak-Güre Basin	Usak-Güre Basin	Kirka Basin	Kirka Basin	Kirka Basin	Kirka Basin	Kirka Basin
Unit	Inay	Inay	Karaören	Karaören	Karaören	Karaören	Karaören
Locality	Section J	Section K	Teke Tepe	Teke Tepe	NW of Gemic	NW of Gemic	W of Gemic
Sample	VSUG 1	VSUG 2	VSK255	VSK256	VSK265	VSK266	VSK267
Fusion no.	LF7179	LF9306	LF7127	LF6889	LF6887	LF6885	LF6878
RUN	RHF342	RHF390	RHF341	RHF340	RHF340	RHF340	RHF348
SiO <sub>2</sub>	58.96	54.93	56.50	51.04	36.09	41.34	72.32
TiO <sub>2</sub>	0.35	0.52	0.04	0.04	0.14	0.17	0.08
Al <sub>2</sub> O <sub>3</sub>	7.19	12.24	9.37	8.53	7.42	8.19	12.01
Fe <sub>2</sub> O <sub>3</sub>	5.82	5.38	1.05	1.04	1.29	1.56	1.36
MnO	0.05	0.05	0.18	0.16	0.05	0.05	0.04
MgO	2.05	6.10	0.22	0.25	1.89	2.21	0.33
CaO	9.84	5.60	13.58	17.09	26.35	21.95	1.48
Na <sub>2</sub> O	0.30	0.29	1.96	1.90	0.93	0.86	2.10
K <sub>2</sub> O	1.71	2.84	3.95	3.49	1.12	1.34	5.87
P <sub>2</sub> O <sub>5</sub>	0.12	0.07	0.02	0.01	0.05	0.03	0.01
LOI	11.41	11.15	12.71	15.43	23.15	20.12	3.60
Total	97.80	99.20	99.59	99.00	98.47	97.81	99.20
Pellet no.	L26537	L26489	L28042	L22476	L22477	L22479	L22485
RUNS	LDA17	LDA11	LDA8,9,10	LDA2	LDA2	LDA2	LDA2
	LDA18	LDA12					
	LDA19	LDA13					
Ba	896	381.8	50	44	220	234	273
Rb	319	422.5	376	350	160	194	440
Th	10	18.1	28	22	13	18	360
Nb	4.5	17.8	25	23	11	15	29
La	91	81.5	20	21	36	51	49
Ce	170	117.1	34	35	37	40	72
Nd	14	28.1	20	16	14	20	26
Sr	650	408.5	53	53	282	284	NA
Zr	42	157.8	75	71	80	88	120
Y	bdl	14.4	44	33	21	28	26
Ga	9	NA	NA	15	10	13	18
Ni	442	NA	NA	9	35	92	8
Sc	9	NA	NA	10	14	19	6
V	119	92.7	0	9	39	68	14
Cr	200	366.1	11	5	29	32	3
Co	35	25.7	BDL	3	12	22	BDL
As	1416	665	38	25	14	12	34

### ICP-AES

Li	66	111	25	163	60
----	----	-----	----	-----	----



## Appendix I (XRF, PGAA, ICP-AES)

**TABLE I2**  
XRF DATA

Rock name	Volcaniclastic	Volcaniclastic	Volcaniclastic	Mudstone/doolomite	Mudstone	Dolomite	Mudstone
Basin	Kirka Basin	Kirka Basin	Kirka Basin	Kirka Basin	Kirka Basin	Kirka Basin	Kirka Basin
Unit	Karaören	Karaören	Karaören	Sarikaya	Sarikaya	Sarikaya	Sarikaya
Locality	NE of Karaören	N of Karaören	Damialikaagac	W of Sarikaya	W of Sarikaya	W of Sarikaya	Göçenoluk
Sample	VSK272	VSK273	VSK275	VSK1	VSK2	VSK3	VSK 4
Fusion no.	LF6877	LF6863	LF6861	LF9310	LF9308	LF7102	LF7103
RUN	RHF340	RHF340	RHF340	RHF390	RHF390	RHF340	RHF340
SiO <sub>2</sub>	74.49	72.63	54.63	14.48	34.94	2.27	57.27
TiO <sub>2</sub>	0.10	0.06	0.04	0.02	0.04	0.00	0.45
Al <sub>2</sub> O <sub>3</sub>	11.83	11.99	9.40	0.89	1.83	0.16	14.10
Fe <sub>2</sub> O <sub>3</sub>	1.33	1.01	0.71	0.23	0.51	0.06	4.45
MnO	0.06	0.49	0.05	0.02	0.02	0.02	0.09
MgO	0.13	0.32	0.43	22.61	23.82	21.80	8.40
CaO	0.90	1.15	15.20	20.91	12.13	26.87	0.82
Na <sub>2</sub> O	2.25	2.45	2.25	0.48	0.30	0.34	0.22
K <sub>2</sub> O	5.39	5.54	3.57	0.21	0.37	0.04	8.86
P <sub>2</sub> O <sub>5</sub>	0.01	0.01	0.01	0.03	0.02	0.04	0.05
LOI	1.95	2.53	13.16	35.35	23.83	45.40	3.77
Total	98.44	98.17	99.46	95.23	97.83	97.00	98.47
Pellet no.	L22484	L28048	L28050	L24456	L24454	L24457	L28059/24455
RUNS	LDA2	LDA8,9,10	LDA8,9,10	LDA17,18 LDA9(As) ARHT64	LDA17,18 LDA9(As) ARHT64	LDA17,18 LDA9(As) ARHT64	LDA17,18 LDA9(As) ARHT64
Ba	99	711	39	112	140	64	311
Rb	343	491	267	132.5	240.9	25.9	1052
Th	39	39	29	1.5	3	0.3	25.2
Nb	25	38	29	BDL	1	BDL	26.5
La	21	21	16	31	60	1	69
Ce	43	40	31	46	37	33	91
Nd	22	19	17	4	1	2	21
Sr	44	37	75	16598	9768	18171	566
Zr	99	77	56	12	21.1	4.7	117.9
Y	25	63	47	BDL	BDL	BDL	24.4
Ga	16	NA	NA	0.9	NA	BDL	NA
Ni	6	NA	NA	12	NA	4	NA
Sc	BDL	NA	NA	14	7	21	9
V	8	6	0	8	11	1	65
Cr	4	BDL	7	19	21	15	62
Co	BDL	1	BDL	BDL	BDL	BDL	9
As	34	85	47	16	30	5	344

### ICP-AES

Li	1895	3468	401	1697
----	------	------	-----	------

## Appendix I (XRF, PGAA, ICP-AES)

**TABLE I2**  
**XRF DATA**

Rock name	Volcaniclastic	Volcaniclastic	Volcaniclastic	Mudstone	Mudstone	Mudstone	Mudstone
Basin	Kirka Basin	Kirka Basin	Kirka Basin	Balmahmut area	Balmahmut area	Balmahmut area	Balmahmut area
Unit	Fetiye	Fetiye	Fetiye				
Locality	Salihye	Salihye	Kizilpınar	Section P	Section O	Balmahmut	Balmahmut
Sample	VSK261	VSK262	VSK274	VS B 1	VS B 3	VS B269	VS B270
Fusion no.	LF6879	LF6864	LF6850	LF7180	LF7108	LF6856	LF6888
RUN	RHF340	RHF340	RHF340	RHF342	RHF340	RHF340	RHF340
SiO <sub>2</sub>	41.28	39.81	62.26	56.39	69.93	62.47	63.27
TiO <sub>2</sub>	0.13	0.14	0.14	0.32	0.45	0.69	0.72
Al <sub>2</sub> O <sub>3</sub>	8.17	8.00	12.25	9.43	8.97	15.73	16.64
Fe <sub>2</sub> O <sub>3</sub>	1.57	1.55	1.94	1.72	3.23	5.34	2.18
MnO	0.09	0.08	0.05	0.03	0.03	0.03	0.03
MgO	1.14	1.12	1.39	0.92	3.44	1.17	1.21
CaO	22.91	23.87	8.06	15.21	2.65	2.97	2.92
Na <sub>2</sub> O	1.07	1.08	1.81	1.94	1.18	3.28	3.58
K <sub>2</sub> O	1.50	1.42	2.71	1.47	1.86	4.41	4.66
P <sub>2</sub> O <sub>5</sub>	0.04	0.05	0.06	0.31	0.43	0.37	0.44
LOI	20.45	21.04	8.46	12.46	4.93	2.10	1.75
Total	98.34	98.16	99.12	100.18	97.09	98.57	97.38
Pellet no.	L22486	L28047	L28052	L26512	L23348	L28051	L22475
RUNS	LDA2	LDA8,9,10	LDA8,9,10	LDA11	LDA11	LDA8,9,10	LDA2
				LDA12	LDA12		
				LDA13	LDA13		
Ba	223	213	108	1222.9	515.5	1475	1960
Rb	193	196	213	107.3	123.1	190	191
Th	18	20	31	14.5	13.9	40	41
Nb	21	19	27	10.8	10	24	27
La	21	23	24	41.7	25.1	66	78
Ce	29	35	42	74.5	53.3	127	161
Nd	13	16	23	30.3	23.3	57	66
Sr	152	139	76	1035.6	474.2	1367	1636
Zr	82	70	103	133.7	110	306	309
Y	28	29	48	10	12	24	13
Ga	11	NA	NA	NA	NA	NA	20
Ni	24	NA	NA	NA	NA	NA	3
Sc	13	NA	NA	NA	NA	NA	8
V	21	16	10	116.1	194.9	91	121
Cr	23	38	25	34.6	19.4	33	46
Co	4	2	3	7.3	10.8	14	5
As	10	20	25	18.6	21.1	39	29
ICP-AES							
Li		130		20	12		

## Appendix I (XRF, PGAA, ICP-AES)

**Table I3** As, Sr & Li concentrations of USEKA sediments

Rock type	Volcaniclastic	Volcaniclastic	Volcaniclastic	Volcaniclastic	Silt	Silt	Silt	Silt
Basin	Emet	Emet	Emet	Emet	Emet	Emet	Emet	Emet
Locality	Section A	S.Hisarcik	NE.Yagcik	Section B	Section C	Section C	Section C	Section C
m up section	5			1	103-104.8	104.8-106.6	106.6-108.4	108.4-110.2
Sample	VSE 1	VSE 2	VSE 3	VSE 4	VSE5		VSE6	
Pellet no.	L20515	L20514	L20513	L20512	L20592	L20593	L20594	L20595
XRF Run	RT513	RT513	RT513	RT513	RT524	RT524	RT524	RT524
XRF Run	RE155	RE155	RE155	RE155	RE159	RE159	RE159	RE159
As (XRF)	17	97	30	76	87	90	130	203
Sr (XRF)	206	192	39	80	339	384	402	501
Li (ICP)	35	76	48	16	119	102	119	209
Rock type	Silt	Silt	Silt	Silt	Mudstone	Volcaniclastic	Silt	Silt + Ist
Basin	Emet	Emet	Emet	Emet	Emet	Emet	Emet	Emet
Locality	Section C	Section C	Section C	Section C	Section C	Section C	Section C	Section C
m up section	110.2-112	112-113.8	113.8-115.6	115.6-117.4	117.4-119.2	119.2-121	121-122.8	122.8-124.6
Sample					VSE 7			
Pellet no.	L20596	L20597	L20598	L20599	L20600	L20601	L20602	L20603
XRF Run	RT524	RT524	RT524	RT524	RT524	RT524	RT524	RT524
XRF Run	RE159	RE159	RE159	RE159	RE159	RE159	RE159	RE159
As (XRF)	177	99	105	116	166	570	1207	1056
Sr (XRF)	404	302	306	320	410	1030	1213	1242
Li (ICP)	162	102	72	111	125	93	180	30
Rock type	Silt + Ist	Cong+silt	Volcaniclastic	Volcaniclastic	Lst	Volcaniclastic	Silt	Lst+mudstone
Basin	Emet	Emet	Emet	Emet	Emet	Emet	Emet	Emet
Locality	Section C	Section C	Section C		Section C	Section C	Section C	Section C
m up section	124.6-126.4	126.4-128.2	128.2-130	128	130-131.8	131.8-133.6	133.6-135.4	135.4-137.2
Sample				VSE 8	VSE 9			
Pellet no.	L20604	L20605	L20606	L20516	L20607	L20608	L20609	L21203
XRF Run	RT524	RT524	RT524	RT513	RT524	RT524	RT524	RT527
XRF Run	RE159	RE159	RE159	RE155	RE159	RE159	RE159	RE160
As (XRF)	1067	565	1931	337	1699	796	1158	475
Sr (XRF)	3066	407	3166	196	1656	2330	2475	2097
Li (ICP)	19	67	27	59	203	279	137	268
Rock type	Lst	Sst	Mudstone	Mudstone	Mudstone	Mudstone	Mudstone	Mudstone
Basin	Emet	Emet	Emet	Emet	Emet	Emet	Emet	Emet
Locality	Section C	Section C	Section C	Section C	Section C	Section C	Section C	Section C
m up section	137.2-139	139-140.8	145.8-147.8	147.8-149.4	149.4-151.2	151.2-153	151.2-153	153-154.8
Sample	VSE 10		VSE 11	VSE 12		VSE13	VSE14	VSE15
Pellet no.	L21204	L21205	L20794	L20795	L20796	L20801	L20797	L20798
XRF Run	RT527	RT527	RT524	RT524	RT524	RT524	RT524	RT524
XRF Run	RE160	RE160	RE159	RE159	RE159	RE159	RE159	RE159
As (XRF)	491	3268	3048	2165	1507	258	6047	20927
Sr (XRF)	2474	452	3889	5520	8296	7578	5030	4111
Li (ICP)	92	192	718	368	377	196	986	715
Rock type	Mudstone	Mudstone	Mudstone	Mudstone	Mudstone + ls	Lst	Chert	Mudstone
Basin	Emet	Emet	Emet	Emet	Emet	Emet	Emet	Emet
Locality	Section C	Section C	Section D	Section D	Section D	Section D	Section D	Section E
m up section	153-154.8	154.8-156.6	154-155.8	155.8-157.6	157.6-159.4	159.4-161.2	160	142-143.8
Sample		VSE16		VSE 17				VSE18
Pellet no.	L20802	L20799	L20803	L21185	L21186	L21187	L21188	L21210
XRF Run	RT524	RT524	RT524	RT527	RT527	RT527	RT527	RT527
XRF Run	RE159	RE159	RE159	RE160	RE160	RE160	RE160	RE160
As (XRF)	3957	941	34	53	75	83	130	328
Sr (XRF)	11940	2539	248	434	499	611	44	1941
Li (ICP)	124	494	180	135	122	BDL	BDL	391
Rock type	Mudstone	Mudstone	Mudstone	Mudstone	Mudstone	Mudstone	Mudstone	Mudstone
Basin	Emet	Emet	Emet	Emet	Emet	Emet	Emet	Emet
Locality	Section E	Section E	Section E	Section E	Section E	Section E	Section E	Section F
m up section	143.8-145.6	145.6-147.4	147.4-149.2	149.2-151	151-152.8	152.8-154.6	154.6-156.4	121-122.8
sample			VSE 19			VSE20		VSE 21
Pellet no.	L21211	L21212	L21213	L21214	L21215	L21216	L21217	L21189
XRF Run	RT527	RT527	RT527	RT527	RT527	RT527	RT527	RT527
XRF Run	RE160	RE160	RE160	RE160	RE160	RE160	RE160	RE160
As (XRF)	208	152	185	1011	180	206	202	204
Sr (XRF)	276	387	696	642	2876	3992	498	1339
Li (ICP)	374	347	424	355	166	264	440	178

LEGEND: Lst=limestone, Sst=sandstone, BDL=below detection limit, NA=not analysed

## Appendix I (XRF, PGAA, ICP-AES)

**Table I3** As, Sr & Li concentrations of USEKA sediments

Rock type	Mudstone	Siltstone	Sst	Volcaniclastic	Volcaniclastic	Mudstone	Mudstone	Mudstone
Basin	Emet	Emet	Emet	Emet	Emet	Emet	Emet	Emet
Locality	Section F	Section F	Section F	Section F	Section F	Section F	Section F	Section F
m up section	122.8-124.6	124.6-126.4	126.4-128.2	128.2-130	130	130-131.8	131.8-133.6	133.6-135.4
Sample					VSE 22			
Pellet no.	L21190	L21191	L21192	L21193	L20517	L21194	L21195	L21196
XRF Run	RT527	RT527	RT527	RT527	RT513	RT527	RT527	RT527
XRF Run	RE160	RE160	RE160	RE160	RE155	RE160	RE160	RE160
As (XRF)	268	488	878	322	112	228	113	215
Sr (XRF)	644	789	589	303	352	470	508	757
Li (ICP)	120	178	90	45	18	114	121	215
Rock type	Mudstone	Mudstone	Mudstone	Mudstone	Mudstone	Mudstone	Mudstone	Mudstone
Basin	Emet	Emet	Emet	Emet	Emet	Emet	Emet	Emet
Locality	Section F	Section F	Section F	Section F	Section F	Section F	Section G	Section G
m up section	135.4-137.2	137.2-139	139-140.8	140.8-142.6	142.6-144.4	144.4-146.2	151-152	151-152
Sample							VSE 23	
Pellet no.	L21197	L21198	L21199	L21200	L21201	L21202	L21207	L21209
XRF Run	RT527	RT527	RT527	RT527	RT527	RT527	RT527	RT527
XRF Run	RE160	RE160	RE160	RE160	RE160	RE160	RE160	RE160
As (XRF)	102	91	107	259	660	446	321	330
Sr (XRF)	1121	705	785	1007	990	848	1528	1645
Li (ICP)	192	169	316	368	259	216	414	340
Rock type	Mudstone	Mudstone	Mudstone	Mudstone	Mudstone	Mudstone	Mudstone	Mudstone
Basin	Emet	Selendi	Selendi	Selendi	Selendi	Selendi	Selendi	Selendi
Locality	Section G	Section H	Section H	Section H	Section H	Section H	Section H	Section H
m up section	152-153	0-1.8	1.8-3.6	3.6-5.4	5.4-7.2	7.2-9	9-10.8	10.8-12.6
Sample				VSS1				
Pellet no.	L21208	L23325	L23323	L23324	L23326	L23328	L23329	L23330
XRF Run	RT527	LDA6	LDA6	LDA19	LDA6	LDA6	LDA6	LDA6
XRF Run	RE160			LDA6				
As (XRF)	411	30	19	14	15	12	13	9
Sr (XRF)	2738	306	205	403	208	353	448	502
Li (ICP)	326	na	na	64	na	NA	NA	NA
Rock type	Mudstone	Mudstone	Mudstone	Mudstone	Mudstone	Mudstone	Mudstone	Cong
Basin	Selendi	Selendi	Selendi	Selendi	Selendi	Selendi	Selendi	Selendi
Locality	Section H	Section H	Section H	Section H	Section H	Section H	Section H	Section H
m up section	12.6-14.4	14.4-16.2	16.2-18	18-19.8	19.8-21.6	21.6-23.4	23.4-25.2	25.2-27
Sample								
Pellet no.	L23331	L23344	L23342	L23341	L23332	L23327	L23343	L26529
XRF Run	LDA6	LDA6	LDA6	LDA6	LDA6		LDA6	LDA6
As	5	14	19	15	18	16	17	6
Sr	212	519	611	208	244	346	169	411
Li	NA	NA	NA	NA	NA	NA	NA	NA
Rock type	Mudstone	Mudstone	Mudstone	Mudstone	Mudstone	Mudstone	Mudstone	Siltstone
Basin	Selendi	Selendi	Selendi	Selendi	Selendi	Selendi	Selendi	Selendi
Locality	Section H	Section H	Section H	Section H	Section H	Section H	Section H	Section I
m up section	27-28.8	28.8-30.6	30.6-32.4	32.4-34.2	34.2-36	36-37.8	37.8-39.6	0-1.8
Sample								
Pellet no.	L26520	L26497	L26530	L26516	L26519	L26528	L26518	L26491
XRF Run	LDA6	LDA6	LDA6	LDA6	LDA6	LDA6	LDA6	LDA6
As	25	24	24	45	41	83	93	15
Sr	409	664	295	1042	1068	1748	2071	157
Li	74	63	122	136	216	251	222	14
Rock type	Siltstone	Siltstone	Siltstone	Siltstone	Siltstone	Mudstone	Mudstone	Mudstone + ls
Basin	Selendi	Selendi	Selendi	Selendi	Selendi	Selendi	Selendi	Selendi
Locality	Section I	Section I	Section I	Section I	Section I	Section I	Section I	Section I
m up section	1.8-3.6	3.6-5.4	3.6-5.4	5.4-7.2	7.2-9	9-10.8	10.8-12.6	12.6-14.4
Sample								
Pellet no.	L26546	L26545	L26556	L26544	L26492	L26543	L26542	L26494
XRF Run	LDA6	LDA6	LDA6	LDA10	LDA6	LDA6	LDA6	LDA6
As	9	24	24	36	26	39	16	6
Sr	141	138	137	439	133	317	1080	549
Li	43	32	na	na	23	31	39	15

## Appendix I (XRF, PGAA, ICP-AES)

**Table I3** As, Sr & Li concentrations of USEKA sediments

Rock type	Mudstone	Mudstone	Mudstone	Mudstone	Mudstone	Mudstone	Mudstone + ls	Mudstone
Basin	Selendi	Selendi	Selendi	Selendi	Selendi	Selendi	Selendi	Selendi
Locality	Section I	Section I	Section I	Section I	Section I	Section I	Section I	Section I
m up section	14.4-16.2	16.2-18	18-19.8	19.8-21.6	21.6-23.4	23.4-25.2	25.2-27	27-28.8
Sample		VSS2						
Pellet no.	L26496	L26501	L26541	L26500	L26539	L26498	L26495	L26540
XRD Run	LDA6	LDA11	LDA6	LDA6	LDA6	LDA6	LDA6	LDA6
As	18	30	124	21	104	82	23	29
Sr	622	819	602	259	683	346	1268	625
Li	32	36	NA	37	NA	65	24	NA
Rock type	Mudstone	Mudstone + ls	Mudstone	Mudstone + ls	Mudstone	Mudstone + ls	Mudstone	Mudstone
Basin	Usak-Güre	Usak-Güre	Usak-Güre	Usak-Güre	Usak-Güre	Usak-Güre	Usak-Güre	Usak-Güre
Locality	Section J	Section J	Section J	Section J	Section J	Section J	Section J	Section J
m up section	0-1.8	1.8-3.6		3.6-5.4	5.4-5.6	5.4-7.2	7.2-9	9-10.8
Sample					VSUG1			
Pellet no.		L26531	L26532	L26538	L26537	L26535	L26534	L26499
XRD Run	L26536	LDA6	LDA6	LDA6		LDA6	LDA6	LDA6
As	97	338	203	412	1416	164	131	136
Sr	1855	910	2478	1508	650	845	1984	2119
Li	117	31	NA	72	66	38	81	52
Rock type	Mudstone	Mudstone	Mudstone	Mudstone	Mud + ls	Mudstone	Mudstone	Mudstone
Basin	Usak-Güre	Usak-Güre	Usak-Güre	Usak-Güre	Usak-Güre	Usak-Güre	Usak-Güre	Usak-Güre
Locality	Section J	Section K	Section K	Section K	Section K	Section K	Section K	Section K
m up section	10.8-12.6	0-1.8	1.8-3.6	3.6-5.4	5.4-7.2	7.2-9	9-10.8	10.8-12.6
Sample								VSUG2
Pellet no.	L26533	L26504	L26506	L26552	L26503	L26487	L26488	L26489
XRF Run	LDA6	LDA6	LDA6		LDA6	LDA6	LDA6	LDA13
As	135	40	152	67	177	252	240	665
Sr	2333	813	518	989	697	1418	580	409
Li	76	NA	38	65	NA	65	94	111
Rock type	Mudstone	Mudstone	Mudstone	Mudstone	Mudstone	Volcaniclastic	Volcaniclastic	Volcaniclastic
Basin	Usak-Güre	Usak-Güre	Usak-Güre	Usak-Güre	Usak-Güre	Kirka	Kirka	Kirka
Locality	Section K	Section K	Section K	Section K	Section K	Section M	Section M	Section L
m up section	12.6-14.4	14.4-16.2	16.2-18	18-19.8	19.8-21.6	6	6	110
Sample						VSK255	VSK256	VSK265
Pellet no.	L26490	L26486	L26505	L26514	L26493	L28042	L22476	L22477
XRF Run	LDA6	LDA6	LDA6	LDA6	LDA6	LDA8	LDA2	LDA2
As	179	243	196	138	238	38	25	14
Sr	1612	813	887	1719	1255	53	53	282
Li	67	112	88	83	97	NA	25	163
Rock type	Volcaniclastic	Volcaniclastic	Volcaniclastic	Volcaniclastic	Volcaniclastic	Mudstone	Mudstone	Carb
Basin	Kirka	Kirka	Kirka	Kirka	Kirka	Kirka	Kirka	Kirka
Locality	Section L	W Gemic	Section N	N Karaören	Damialikaagac	W of Sarikaya	W of Sarikaya	W of Sarikaya
m up section	110		3					
Sample	VSK266	VSK267	VSK272	VSK273	VSK275	VSK1	VSK2	VSK3
Pellet no.	L22479	L22485	L22484	L28048	L28050	L24456	L24454	L24457
XRF Run	LDA2	LDA2	LDA2	LDA8	LDA8	LDA9	LDA9	LDA9
XRF Run					LDA9	ARHT64	ARHT64	ARHT64
As	12	34	34	85	47	16	30	3
Sr	284	NA	44	37	75	16598	9768	18171
Li	NA	60	NA	NA	NA	1895	3468	401
Rock type	Mudstone	Volcaniclastic	Volcaniclastic	Volcaniclastic	Volcaniclastic	Volcaniclastic	Volcaniclastic	Silt
Basin	Kirka	Kirka	Kirka	Kirka	Kirka	Kirka	Kirka	Balmahmut
Locality	Göçenoluk	Salihye	Salihye	Curuttum	Curuttum	Kizilpınar	W Gemic	Section O
m up section								0-1.8
Sample	VSK 4	VSK261	94TV262	94TV263	94TV264	94TV274	94TV276	
Pellet no.	L28059/24455	L22486	L28047	L22478	L22481	L28052	L22483	L26515
XRF Run	LDA9	LDA2	LDA8	LDA2	LDA2	LDA8	LDA2	LDA6
XRF Run	ARHT64							
As	344	10	20	8	8	25	24	12
Sr	566	152	139	236	237	76	349	840
Li	1698	NA	130	NA	NA	NA	NA	25

## Appendix I (XRF, PGAA, ICP-AES)

**Table I3** As, Sr & Li concentrations of USEKA sediments

Rock type	Silt	Silt	Silt	Silt	Volcaniclastic	Volcaniclastic	Mudstone	Silt
Basin	Balmahmut	Balmahmut	Balmahmut	Balmahmut	Balmahmut	Balmahmut	Balmahmut	Balmahmut
Locality	Section O	Section O	Section O	Section O	Section O	Section O	Section O	Section O
m up section	1.3-3.6	3.6-5.4	5.4-7.2	7.2-9	9-10.8	10.8-12.6	10.8-12.6	12.6-14.4
Sample								
Pellet no.	L26508	L26522	L26509	L26523	L26521	L26511	L26512	L26513
XRF Run	LDA6	LDA6	LDA6	LDA6	LDA6	LDA11	LDA11	LDA6
As	14	9	7	9	31	26	19	16
Sr	1044	288	386	639	828	1641	1036	678
Li	22	8	29	8	BDL	6	20	9

Rock type	Silt	Volcaniclastic	Volcaniclastic	Mudstone	Mudstone	Mudstone	Mudstone	Lst
Basin								
Locality	Section O	Section P	Section P	Section P	Section P	Section P	Section P	Section P
m up section	14.4-16.2	0-1.8	1.8-3.6	3.6-5.4	5.4-7.2	9-10.8	10.8-12.6	13
Sample						VSB3)		
Pellet no.	L26502	L26526	L26548	L26524	L23347	L23348	L26527	L23345
XRF Run	LDA6	LDA6	LDA6	LDA6	LDA6	LDA11	LDA6	LDA6
As	13	29	47	140	38	21	38	31
Sr	245	1419	800	484	306	474	573	899
Li	12	24	BDL	34	BDL	12	13	BDL

Rock type	Mudstone
Basin	
Locality	Section P
m up section	14.4-16.2
Sample	
Pellet no.	L26525
XRF Run	LDA6
As	13
Sr	700
Li	26

## Appendix I (XRF, PGAA, ICP-AES)

**Table I4 - XRF Major Element International Standard Data**

Sample	Run	SiO2	TiO2	Al2O3	Fe2O3	MnO	MgO	CaO	Na2O	K2O	P2O5	Total
NIM-G	ARLF466	76.35	0.1	11.82	1.96	0.023	0.03	0.76	3.56	5.287	0.02	99.91
NIM-G	ARLF412	75.97	0.1	12.05	1.97	0.023	-0.01	0.77	3.56	5.117	0.01	99.56
NIM-G	ARLF411	75.49	0.1	12.17	1.99	0.023	-0.01	0.78	3.75	5.191	0.01	99.49
NIM-G	RHF340	76.45	0.11	11.77	2.13	0.022	0.12	0.79	3.8	5.11	0.01	100.3
NIM-G	ARLF466	76.35	0.1	11.82	1.96	0.023	0.03	0.76	3.56	5.287	0.02	99.91
NIM-G	RHF348	76.44	0.12	12.17	2.02	0.024	0.08	0.79	3.47	5.071	0.01	100.2
NIM-G	ARLF459	77.08	0.1	12.05	1.95	0.023	0.03	0.76	3.62	5.031	0.01	100.7
NIM-G	ARLF412	75.97	0.1	12.05	1.97	0.023	0	0.77	3.56	5.117	0.01	99.56
NIM-G	ARLF411	75.49	0.1	12.17	1.99	0.023	0	0.78	3.75	5.191	0.01	99.49
NIM-G	RHF390	76.23	0.09	12.34	2.02	0.027	-0.05	0.78	3.4	4.998	0.01	99.85
NIM-G	Stdev	0.48	0.01	0.19	0.05	0.00	0.05	0.01	0.13	0.10	0.00	0.40
NIM-G	Average	76.18	0.10	12.04	2.00	0.02	0.02	0.77	3.60	5.14	0.01	99.89
NIM-G	Accepted	75.70	0.09	12.08	1.88	0.02	0.06	0.78	3.36	4.99	0.01	
JR-1	ARLF466	76.24	0.11	12.54	0.89	0.107	0.11	0.68	4.2	4.729	0.02	99.63
JR-1	ARLF284	74.9	0.11	12.29	0.9	0.1	0.04	0.66	3.78	4.445	0.02	97.26
JR-1	ARLF290	74.31	0.11	12.19	0.9	0.1	0.05	0.67	3.78	4.467	0.02	96.61
JR-1	ARLF285	75.07	0.11	12.32	0.9	0.1	0.05	0.6	3.78	4.452	0.02	97.47
JR-1	ARLF286	74.31	0.11	12.27	0.9	0.1	0.05	0.67	3.79	4.462	0.02	96.68
JR-1	ARLF466	76.21	0.11	12.54	0.89	0.107	0.11	0.68	4.2	4.729	0.02	99.63
JR-1	RHF390	75.67	0.11	12.9	0.93	0.108	0.07	0.71	3.83	4.461	0.02	98.8
JR-1	Stdev	0.82	0.00	0.24	0.01	0.00	0.03	0.03	0.20	0.13	0.00	1.32
JR-1	Average	75.24	0.11	12.44	0.90	0.10	0.07	0.67	3.91	4.54	0.02	98.01
JR-1	Accepted	75.41	0.10	12.89	0.90	0.10	0.09	0.63	4.10	4.41	0.02	
MRG-1	ARLF466	39.66	3.79	8.47	18.26	0.177	13.81	14.91	0.82	0.202	0.07	100.2
MRG-1	ARLF412	39.3	3.87	8.44	18.59	0.179	13.76	15.07	0.77	0.196	0.07	100.2
MRG-1	ARLF411	39.76	3.93	8.44	18.68	0.181	14.33	15.78	0.85	0.201	0.07	102.2
MRG-1	ARLF411	39.32	3.87	8.6	18.56	0.174	13.78	15.1	0.82	0.183	0.07	100.5
MRG-1	ARLF312	40.05	3.79	8.38	17.81	0.166	14.08	14.52	0.55	0.177	0.07	99.6
MRG-1	ARLF313	40.01	3.78	8.37	17.8	0.165	14.08	14.53	0.55	0.174	0.07	99.52
MRG-1	ARLF290	40	3.8	8.33	17.85	0.17	14.06	14.57	0.55	0.176	0.07	99.57
MRG-1	RHF341	39.23	3.86	8.34	18.09	0.179	13.86	14.96	0.67	0.183	0.06	99.44
MRG-1	ARLF466	39.66	3.79	8.47	18.26	0.177	13.81	14.91	0.82	0.202	0.07	100.2
MRG-1	ARLF412	39.3	3.87	8.44	18.59	0.179	13.76	15.07	0.77	0.196	0.07	100.2
MRG-1	RHF390	39.62	3.51	8.77	17.75	0.179	13.91	15.15	1.01	0.196	0.07	100.2
MRG-1	Stdev	0.31	0.11	0.13	0.36	0.01	0.18	0.36	0.15	0.01	0.00	0.77
MRG-1	Average	39.63	3.81	8.46	18.20	0.18	13.93	14.96	0.74	0.19	0.07	100.16
MRG-1	Accepted	39.12	3.77	8.47	17.02	0.17	13.55	14.70	0.74	0.18	0.08	
JA-2	ARLF466	57.37	0.69	15.58	6.35	0.114	7.88	6.59	3.12	1.762	0.16	99.62
JA-2	ARLF312	58.39	0.71	15.85	6.3	0.102	7.48	6.12	2.78	1.808	0.17	99.71
JA-2	ARLF313	59.24	0.71	16.1	6.32	0.104	7.37	6.11	2.74	1.819	0.17	100.7
JA-2	RHF340	57.55	0.79	15.37	6.79	0.115	8.29	6.46	3.15	1.731	0.16	100.4
JA-2	Stdev	0.86	0.04	0.32	0.23	0.01	0.42	0.24	0.22	0.04	0.01	0.59
JA-2	Average	58.14	0.73	15.73	6.44	0.11	7.76	6.32	2.95	1.78	0.16	100.01
JA-2	Accepted	56.18	0.67	15.3	5.73	0.11	7.68	6.48	3.08	1.8	0.15	
W-1	ARLF466	52.47	1.08	15.2	11.08	0.175	6.64	10.98	2.34	0.635	0.14	100.8
W-1	ARLF411	51.6	1.1	15.42	11.29	0.167	6.86	11	2.35	0.581	0.14	100.5
W-1	RHF340	51.81	1.19	14.8	11.51	0.174	6.79	10.91	2.34	0.624	0.14	100.3
W-1	RHF341	51.71	1.18	14.78	11.48	0.174	6.75	10.89	2.32	0.622	0.14	100.1
W-1	ARLF459	52.31	1.07	14.82	10.89	0.17	6.77	10.67	2.17	0.592	0.13	99.59
W-1	Stdev	0.39	0.06	0.29	0.26	0.00	0.08	0.13	0.08	0.02	0.00	0.45
W-1	Average	51.98	1.12	15.00	11.25	0.17	6.76	10.89	2.30	0.61	0.14	100.24
W-1	Accepted	52.51	1.07	15	10.19	0.17	6.62	10.99	2.16	0.64	0.13	
NIM-N	ARLF466	52.35	0.19	16.56	8.86	0.178	7.51	11.24	2.58	0.235	0.02	99.71
NIM-N	ARLF411	51.15	0.19	16.75	9.12	0.175	7.63	12.39	2.54	0.216	0.02	100.2
NIM-N	ARLF312	52.7	0.19	16.18	8.88	0.17	7.57	11.05	2.16	0.228	0.02	99.15
NIM-N	ARLF313	52.59	0.19	16.14	8.89	0.17	7.54	11.08	2.17	0.228	0.02	99.03
NIM-N	ARLF276	53.34	0.19	16.27	8.84	0.17	7.56	11.01	2.15	0.23	0.02	99.78
NIM-N	ARLF284	53.29	0.19	16.26	8.36	0.17	7.55	11.02	2.14	0.227	0.02	99.72
NIM-N	ARLF294	52.66	0.19	16.21	8.87	0.17	7.59	11.04	2.15	0.228	0.02	99.13
NIM-N	ARLF290	52.76	0.19	16.11	8.89	0.17	7.54	11.13	2.15	0.228	0.02	99.2
NIM-N	ARLF285	53.43	0.19	16.3	8.87	0.17	7.59	11.03	2.15	0.229	0.02	99.97
NIM-N	ARLF286	52.87	0.19	16.18	8.89	0.17	7.58	11.09	2.13	0.231	0.02	99.35
NIM-N	RHF341	52.03	0.21	15.98	9.19	0.176	7.57	11.25	2.46	0.234	0.02	99.12
NIM-N	RHF348	52.56	0.21	16.6	8.86	0.182	7.67	11.44	2.49	0.236	0.02	100.3
NIM-N	ARLF411	51.15	0.19	16.75	9.12	0.175	7.63	12.39	2.54	0.216	0.02	100.2

## Appendix I (XRF, PGAA, ICP-AES)

**Table I4 - XRF Major Element International Standard Data**

Sample	Run	SiO2	TiO2	Al2O3	Fe2O3	MnO	MgO	CaO	Na2O	K2O	P2O5	Total
NIM-N	Stdev	0.73	0.01	0.25	0.20	0.00	0.04	0.49	0.19	0.01	0.00	0.46
NIM-N	Average	52.53	0.19	16.33	8.90	0.17	7.58	11.32	2.29	0.23	0.02	99.60
NIM-N	Accepted	52.64	0.2	16.5	8.1	0.18	7.5	11.5	2.46	0.25	0.03	
JA-3	ARLF412	61.99	0.72	15.86	6.61	0.11	3.49	6.35	3.4	1.451	0.12	100.1
JA-3	ARLF411	61.85	0.71	16.07	6.66	0.111	3.68	6.46	3.58	1.483	0.12	100.7
JA-3	ARLF312	62.14	0.7	15.26	6.52	0.098	3.7	6.09	2.9	1.361	0.12	98.89
JA-3	ARLF313	62.86	0.7	15.4	6.5	0.099	3.68	6.07	2.89	1.36	0.12	99.67
JA-3	ARLF284	62.91	0.7	15.33	6.49	0.1	3.69	6.05	2.9	1.354	0.12	99.64
JA-3	ARLF294	62.3	0.7	15.28	6.52	0.1	3.71	6.07	2.9	1.364	0.12	99.06
JA-3	ARLF290	62.2	0.7	15.2	6.52	0.1	3.7	6.1	2.92	1.362	0.12	98.92
JA-3	ARLF285	63.03	0.7	15.38	6.5	0.1	3.69	6.06	2.91	1.358	0.12	99.85
JA-3	ARLF286	62.25	0.7	15.32	6.52	0.1	3.71	6.12	2.92	1.367	0.12	99.13
JA-3	Stdev	0.43	0.01	0.30	0.06	0.00	0.07	0.15	0.26	0.05	0.00	0.62
JA-3	Average	62.39	0.70	15.46	6.54	0.10	3.67	6.15	3.04	1.38	0.12	99.55
JA-3	Accepted	62.26	0.68	15.6	6.05	0.11	3.65	6.28	3.17	1.41	0.11	
BHVO-1	ARLF411	48.74	2.78	13.85	12.61	0.171	7.4	12.4	2.48	0.512	0.29	101.2
PCC-1	ARLF312	44.69	0.01	0.59	8.69	0.12	45.84	0.51	-0.15	0	0.01	100.3
PCC-1	ARLF313	45.09	0.01	0.6	8.69	0.12	45.36	0.5	-0.15	-0.001	0.01	100.2
PCC-1	ARLF290	44.82	0.01	0.57	8.72	0.12	45.94	0.51	-0.15	-0.001	0.01	100.6
PCC-1	Stdev	0.20	0.00	0.02	0.02	0.00	0.31	0.01	0.00	0.00	0.00	0.16
PCC-1	Average	44.87	0.01	0.59	8.70	0.12	45.71	0.51	-0.15	0.00	0.01	100.37
PCC-1	Accepted	41.71	0.01	0.68	7.78	0.12	43.4	0.52	0.03	0.01	0	
AC-E	ARLF284	71.85	0.11	14.63	2.55	0.05	-0.06	0.33	6.13	4.621	0.02	100.2
AC-E	ARLF294	71.04	0.11	14.61	2.56	0.05	-0.06	0.34	6.16	4.651	0.02	99.49
AC-E	ARLF290	71.07	0.11	14.53	2.57	0.05	-0.07	0.34	6.17	4.665	0.01	99.45
AC-E	ARLF290	71.1	0.11	14.5	2.57	0.06	-0.06	0.34	6.15	4.659	0.02	99.45
AC-E	ARLF285	72.04	0.11	14.65	2.56	0.05	-0.06	0.34	6.15	4.655	0.02	100.5
AC-E	ARLF286	71.35	0.11	14.6	2.56	0.05	-0.06	0.34	6.15	4.644	0.02	99.77
AC-E	Stdev	0.43	0.00	0.06	0.01	0.00	0.00	0.00	0.01	0.02	0.00	0.45
AC-E	Average	71.41	0.11	14.59	2.56	0.05	-0.06	0.34	6.15	4.65	0.02	99.82
AC-E	Accepted	70.35	0.11	14.7	2.41	0.06	0.03	0.34	6.54	4.49	0.01	
SO-2	ARLF284	61.5	1.67	16.91	8.97	0.1	0.99	2.97	2.57	3.374	0.85	99.9
SO-2	ARLF294	60.8	1.67	16.9	9	0.1	0.99	2.97	2.58	3.404	0.84	99.24
SO-2	ARLF290	60.99	1.68	16.83	9.02	0.1	0.99	3	2.6	3.408	0.85	99.46
SO-2	ARLF285	61.8	1.67	17	8.99	0.1	0.99	2.97	2.58	3.397	0.84	100.3
SO-2	ARLF286	60.92	1.67	16.92	9	0.1	0.99	2.99	2.61	3.393	0.84	99.44
SO-2	Stdev	0.43	0.00	0.06	0.02	0.00	0.00	0.01	0.02	0.01	0.00	0.44
SO-2	Average	61.20	1.67	16.91	9.00	0.10	0.99	2.98	2.59	3.40	0.84	99.68
SO-2	Accepted	53.42	1.43	15.1		0.09	0.89	2.77	2.48	2.94	0.69	



## Appendix I (XRF, PGAA, ICP-AES)

**TABLE I5 - XRF Trace Element International Standard data**

	Runs	As	Nb	Zr	Y	Sr	Rb	Th	Ga	Ni	Sc	V	Cr	Co	Ba	La	Ce	Nd
:JR-1	RE155,RT513	13	16	104	46	28	253	28	16	BDL	NA	NA	NA	NA	NA	NA	NA	NA
:JR-1	RE160,RT527	14	16	105	44	28	255	27	17	BDL	NA	NA	NA	NA	NA	NA	NA	NA
:JR-1	RE159,RT524	15	15	104	45	27	254	28	16	BDL	NA	NA	NA	NA	NA	NA	NA	NA
:JR-1	LDA3	19	16	104	44	29	259	24	16	3	7	8	BDL	BDL	51	17	54	26
:JR-1	LDA2,ARHT32	18	15	101	44	25	249	26	17	6	4	13	BDL	BDL	47	15	41	26
:JR-1	LDA8,LDA9,LDA10	17	16	100	48	29	258	29	NA	NA	NA	4	8	2	41	19	46	25
:JR-1	LML1	NA	13	106	37	34	250	31	17	5	5	17	BDL	BDL	36	18	44	24
:JR-1	LDA6	13	NA	102	45	27	NA	NA	NA	NA	NA	NA	NA	NA	NA	NA	NA	NA
:JR-1	LDA9b	15	NA	NA	NA	NA	NA	NA	NA	NA	NA	NA	NA	NA	NA	NA	NA	NA
stdev		2	1	2	3	3	4	2	0	2	2	6			7	2	6	1
average		15	15	103	44	28	254	27	17	5	5	11	8	2	44	17	46	25
Accepted		16	16	101	45	30	257	27	18	1	5	NA	2	1	40	20	47	24
:NIM-G	RE156,RT514,T20	13	55	301	142	11	329	53	28	8	3	9	26	1	106	110	199	75
:NIM-G	RE155,RT513,T20	12	55	302	144	11	326	53	30	7	1	11	28	2	109	109	201	76
:NIM-G	RE160,RT527	12	55	302	142	11	326	53	28	10	-1	13	27	1	104	107	203	74
:NIM-G	RE157,RT516	13	55	301	140	11	326	52	28	8	1	11	28	2	109	109	201	76
:NIM-G	LML1		54	267	133	17	327	49	28	16	BDL	13	BDL	3	83	101	190	67
:NIM-G	LDA2,ARHT32	15	55	275	151	9	323	47	27	23	BDL	8	22	BDL	108	97	198	73
:NIM-G	LDA3	10	56	280	144	11	319	52	29	16	1	6	15	BDL	110	103	198	72
:NIM-G	LDA8,LDA9,LDA10	18	55	293	142	11	324	52	NA	NA	NA	BDL	25	2	104	105	197	75
:NIM-G	LDA11,12,13	19	55	294	144	12	331	54	NA	NA	NA	BDL	18	0	109	103	201	75
:NIM-G	LDA14,16	NA	NA	NA	NA	NA	NA	NA	NA	NA	1	2	11	5	112	109	195	72
:NIM-G	RE159,RT524	13	55	301	142	11	325	53	29	9	NA	NA	NA	NA	NA	NA	NA	NA
:NIM-G	LDA17	NA	NA	NA	NA	NA	NA	NA	NA	NA	NA	2	23	BDL	106	NA	NA	NA
:NIM-G	LDA18,LDA19	14	54	290	137	11	326	52	29	23	NA	NA	NA	NA	NA	99	200	75
stdev		3	1	12	4	2	3	2	1	6	1	4	6	2	8	4	4	3
average		14	55	291	142	12	326	52	28	13	1	8	22	2	105	105	198	74
Accepted		15	53	300	143	10	320	51	27	8	1	2	12	4	120	109	195	72
:BE-N	RE156,RT514	2	109	268	31	1377	50	12	17	274	NA	NA	NA	NA	NA	NA	NA	NA
:BE-N	LML1		113	262	29	1364	54	12	18	277	25	267	411	61	1080	101	196	77
stdev			3	4	1	9	3	0	0	2								
average		2	111	265	30	1371	52	12	18	275	25	267	411	61	1080	101	196	77
Accepted		2	105	260	30	1370	47	10	17	267	22	235	360	60	1025	82	152	67
:STM-1	RE156,RT514	4	267	1444	49	714	122	33	37	0	NA	NA	NA	NA	NA	NA	NA	NA
:STM-1	RE159,RT524	5	267	1442	48	714	122	33	39	1	NA	NA	NA	NA	NA	NA	NA	NA
:STM-1	RE160,RT527	5	266	1446	47	711	123	34	38	0	NA	NA	NA	NA	NA	NA	NA	NA
:STM-1	LML1		287	1220	47	718	118	35	35	2	BDL	12	BDL	BDL	561	132	248	77
:STM-1	LDA2	5	267	1341	53	8	123	38	36	BDL	BDL	3	5	BDL	556	126	247	85
:STM-1	LDA3	7	267	1337	45	761	117	32	37	4	2	9	10	3	575	124	254	86
:STM-1	LDA6	5	NA	1271	49	700	NA	NA	NA	NA	NA	NA	NA	NA	NA	NA	NA	NA
:STM-1	ARHT64	NA	262	1371	49	722	123	32	38	4	NA	NA	NA	NA	NA	NA	NA	NA
stdev		1	8	84	2	252	3	2	1	2		5	4		10	4	4	5
average		5	269	1359	48	631	121	34	37	2	2	8	8	3	564	127	250	83
Accepted		5	268	1210	46	700	118	31	36	3	1	9	4	1	560	150	259	79
		As	Nb	Zr	Y	Sr	Rb	Th	Ga	Ni	Sc	V	Cr	Co	Ba	La	Ce	Nd
:JA-1	RE156,RT514	3	2	84	30	251	12	1	18	2	NA	NA	NA	NA	NA	NA	NA	NA
:JA-1	RE155,RT513	3	1	85	30	251	12	1	18	1	NA	NA	NA	NA	NA	NA	NA	NA
:JA-1	RE157,RT516	3	1	84	30	254	12	0	17	1	NA	NA	NA	NA	NA	NA	NA	NA
:JA-1	LML1		BDL	94	36	256	8	BDL	16	BDL	30	94	BDL	BDL	313	BDL	21	15
:JA-1	ARHT32					250												
:JA-1	LDA2	3	2	87	35	NA	10	bdl	19	bdl	29	95	7	11	285	5	7	10
:JA-1	LDA3	BDL	BDL	79	33	265	13	5	15	bdl	32	106	4	14	297	2	28	11
:JA-1	LDA8,LDA9,LDA10	2	1	83	31	256	12	1	NA	NA	NA	89	6	11	298	4	16	12
:JA-1	LDA11,12,13	3	1	82	31	255	11	BDL	NA	NA	NA	92	1	14	295	5	10	13
:JA-1	LDA6	6	NA	84	37	245	NA	NA	NA	NA	NA	NA	NA	NA	NA	NA	NA	NA
:JA-1	LDA17	NA	NA	NA	NA	NA	NA	NA	NA	NA	NA	103	13	12	295	NA	NA	NA
:JA-1	LDA18,LDA19	3	1	84	10	258	11	1	16	6	NA	NA	NA	NA	NA	5	8	12
stdev		1	0	4	8	5	1	2	1	2	2	7	4	2	9	1	8	2
average		3	1	85	30	254	11	1	17	2	30	97	6	12	297	4	15	12
Accepted		3	2	88	31	266	12	1	17	2	28	105	7	12	307	5	14	11
:AC-E	T205	NA	NA	NA	NA	NA	NA	NA	NA	NA	6	6	0	29	51	60	167	95
:AC-E	T206	NA	NA	NA	NA	NA	NA	NA	NA	NA	4	7	BDL	31	53	60	159	94
:AC-E	T204	NA	NA	NA	NA	NA	NA	NA	NA	NA	4	12	BDL	30	49	62	166	96
stdev											1	3		1	2	1	5	1
average											5	9	BDL	30	51	61	164	95
Accepted											0	3	3	0	55	59	154	92

## Appendix I (XRF, PGAA, ICP-AES)

**TABLE I5 - XRF Trace Element International Standard Data**

		As	Nb	Zr	Y	Sr	Rb	Th	Ga	Ni	Sc	V	Cr	Co	Ba	La	Ce	Nd
:BR	T205	NA	NA	NA	NA	NA	NA	NA	NA	NA	22	239	370	57	1190	80	151	61
:BR	T206	NA	NA	NA	NA	NA	NA	NA	NA	NA	21	247	372	62	1192	82	149	62
stdev											1	6	2	3	2	1	2	1
average											22	243	371	60	1191	81	150	61
Accepted											25	235	380	52	1050	82	151	65
:W-2	T205	NA	NA	NA	NA	NA	NA	NA	NA	NA	30	248	89	47	181	12	19	10
:W-2	T206	NA	NA	NA	NA	NA	NA	NA	NA	NA	29	239	94	45	180	14	23	12
stdev											1	6	3	1	0	1	3	2
average											30	243	92	46	181	13	21	11
Accepted											35	262	93	44	182	11	24	14
MRG-1	RT155,RT513,T20	0	20	110	14	271	9	1	20	192	NA	NA	NA	NA	NA	NA	NA	NA
MRG-1	RE156,RT514,T20	1	19	110	15	270	8	2	20	195	NA	NA	NA	NA	NA	NA	NA	NA
MRG-1	LDA8,LDA9,LDA10	BDL	20	104	15	268	5	1	NA	NA	NA	563	555	88	62	12	27	21
MRG-1	LDA11,12,13	BDL	19	104	15	268	6	1	NA	NA	NA	568	566	92	63	12	28	22
MRG-1	T217	NA	NA	NA	NA	NA	NA	NA	NA	NA	56	587	503	87	62	8	22	20
MRG-1	LDA6	BDL		109	13	267	NA	NA	NA	NA	NA	NA	NA	NA	NA	NA	NA	NA
MRG-1	ARHT64	NA	20	108	15	289	9	2	19	202	NA	NA	NA	NA	NA	NA	NA	NA
MRG-1	LDA17	NA	NA	NA	NA	NA	NA	NA	NA	NA	NA	606	492	94	58	NA	NA	NA
stdev			0	3	1	8	2	1	1	5		20	37	3	2	2	3	1
average		0	20	109	15	280	9	2	20	197	56	584	524	91	60	12	27	21
Accepted		1	20	108	14	266	9	1	17	193	55	526	430	87	61	10	26	19
:AN-G	RE157,RT516	1	1	10	8	75	2	0	19	32	NA	NA	NA	NA	NA	NA	NA	NA
:AN-G	LDA2	NA	BDL	21	11	NA	1	BDL	19	28	13	65	46	23	28	BDL	8	8
:AN-G	ARHT64	NA	NA	13	9	77	2	2	18	34	NA	NA	NA	NA	NA	NA	NA	NA
stdev				2	1	1	0	2	1	2								
average		1	1	11	9	76	2	1	18	33	13	65	46	23	28		8	8
Accepted		0	1	11	8	76	1	0	18	35	10	70	50	25	34	2	5	2
W-1	RE157,RT516	1	6	97	23	185	23	1	19	70	NA	NA	NA	NA	NA	NA	NA	NA
W-1	LDA14,16	NA	NA	NA	NA	NA	NA	NA	NA	NA	42	216	119	47	161	10	22	11
average		1	6	97	23	185	23	1	19	70	42	216	119	47	161	10	22	11
Accepted		2	10	99	26	186	21	2	17	75	35	257	119	47	162	11	23	15
SO-1	RE160,RT527	2	12	88	26	316	125	13	24	83	NA	NA	NA	NA	NA	NA	NA	NA
Accepted		2	12	84	25	331	141	12	24	92								
SO-4	RE160,RT527	8	10	289	24	156	64	8	11	18	NA	NA	NA	NA	NA	NA	NA	NA
Accepted		7	10	156	22	168	69	9	11	24								
GXR3	LDA9b	3970	NA	NA	NA	NA	NA	NA	NA	NA	NA	NA	NA	NA	NA	NA	NA	NA
Accepted		3970																
GXR4	LDA9b	108	NA	NA	NA	NA	NA	NA	NA	NA	NA	NA	NA	NA	NA	NA	NA	NA
Accepted		98																
<b>Standard data for As from runs in 1994 (ie. same calibration as for RE155, 156 &amp; 157 which included samples from this study)</b>																		
GXR3	RE152	4023																
GXR3	RE153	4006																
GXR3	RE154	3997																
Accepted		3970																
GXR6	RE152	315																
GXR6	RE153	311																
GXR6	RE154	311																
Accepted		330																
BXN	RE152	121																
BXN	RE153	119																
BXN	RE154	118																
Accepted		115																

FIGURE I1 - Powder pellet  $\text{TiO}_2$  vs fusion bead  $\text{TiO}_2$

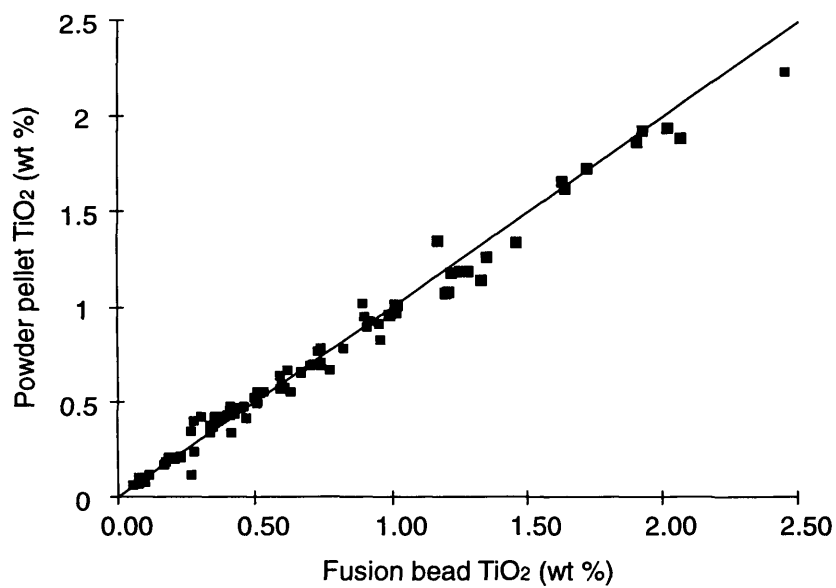
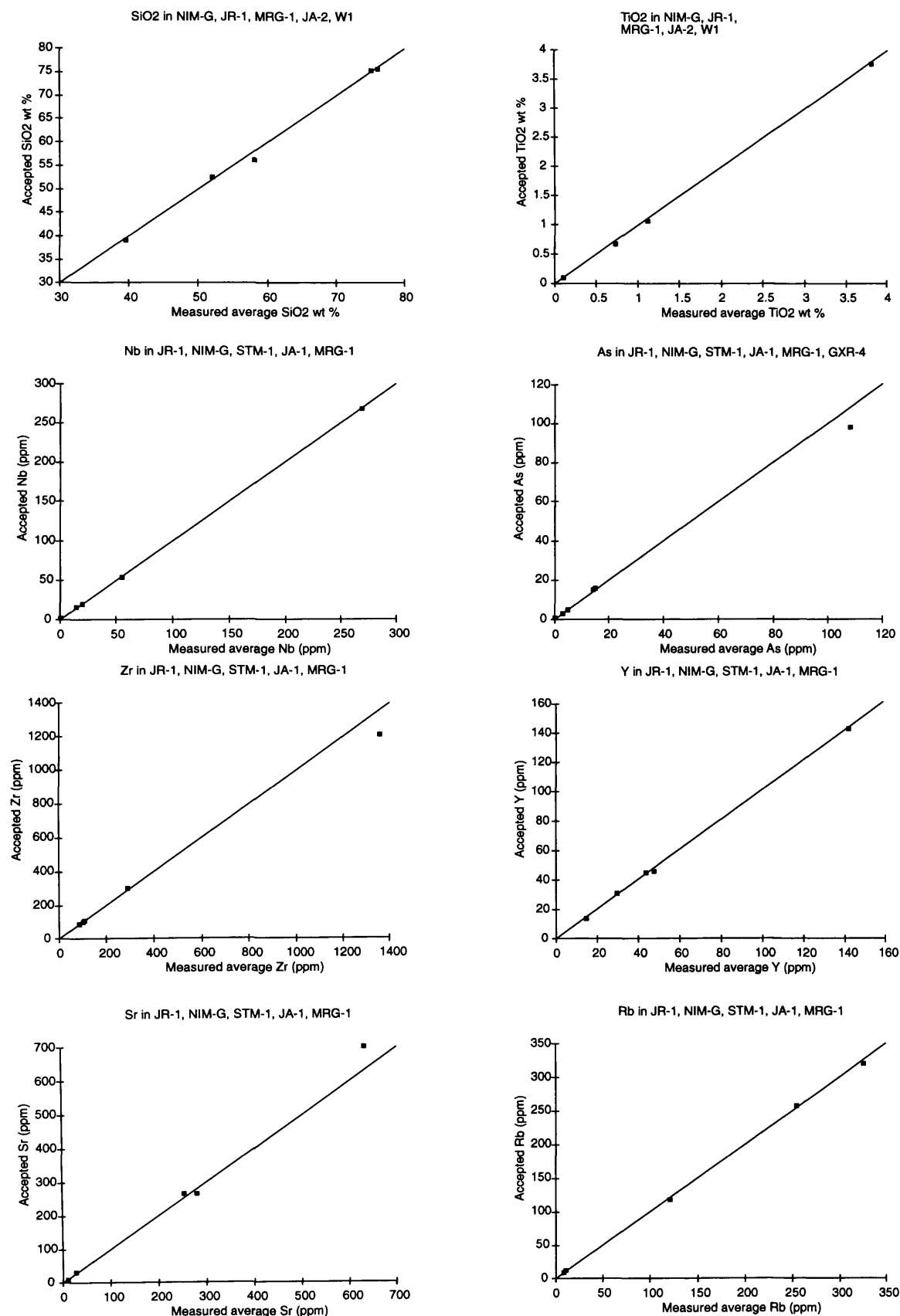
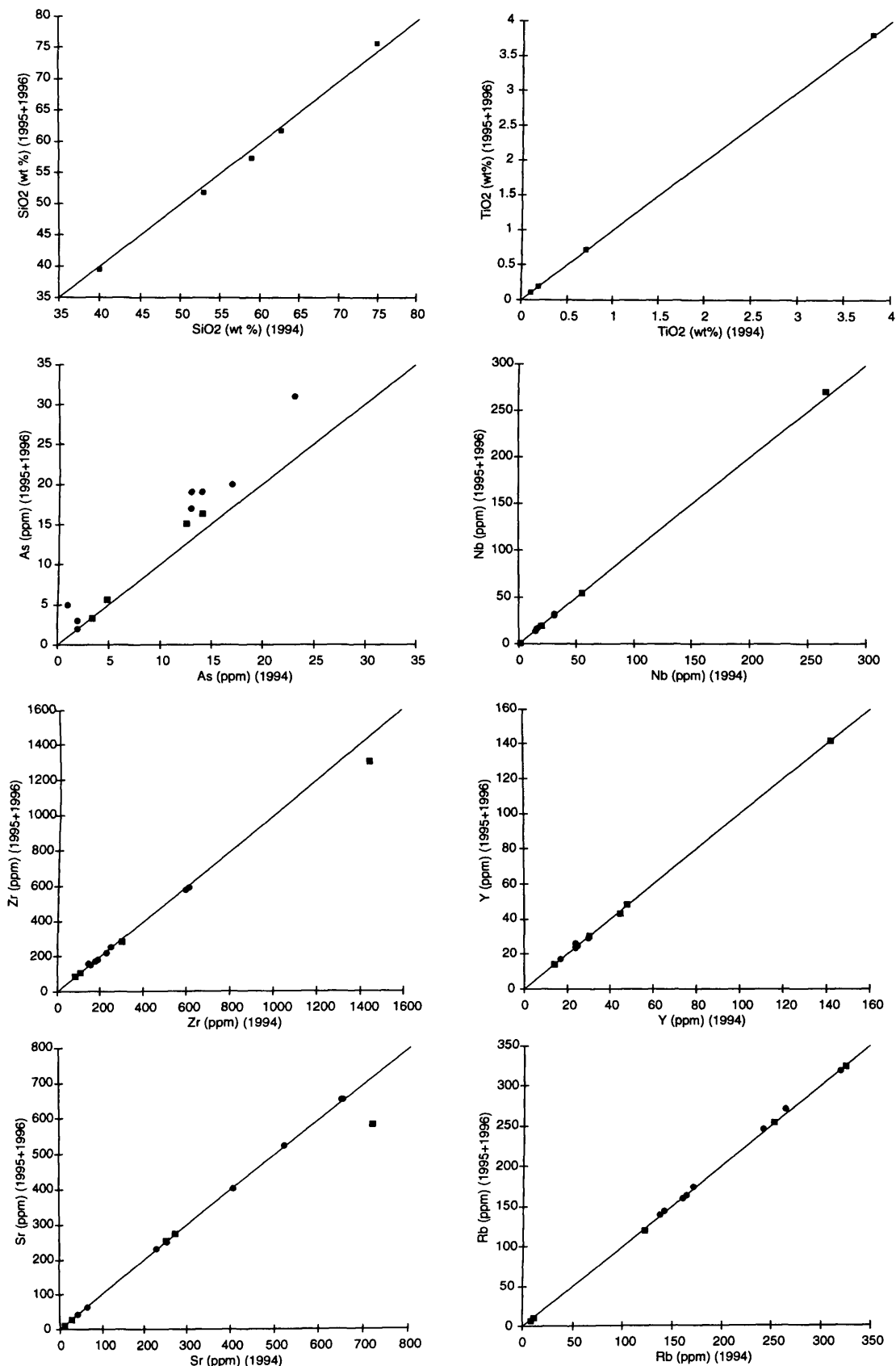


**FIGURE I2 - accuracy of XRF analyses - concentrations of selected major and trace elements in international standards (accepted values from the literature vs average measured values from this study)**



(Accepted values from Geostandards Newsletter, Govindaraju 1994)

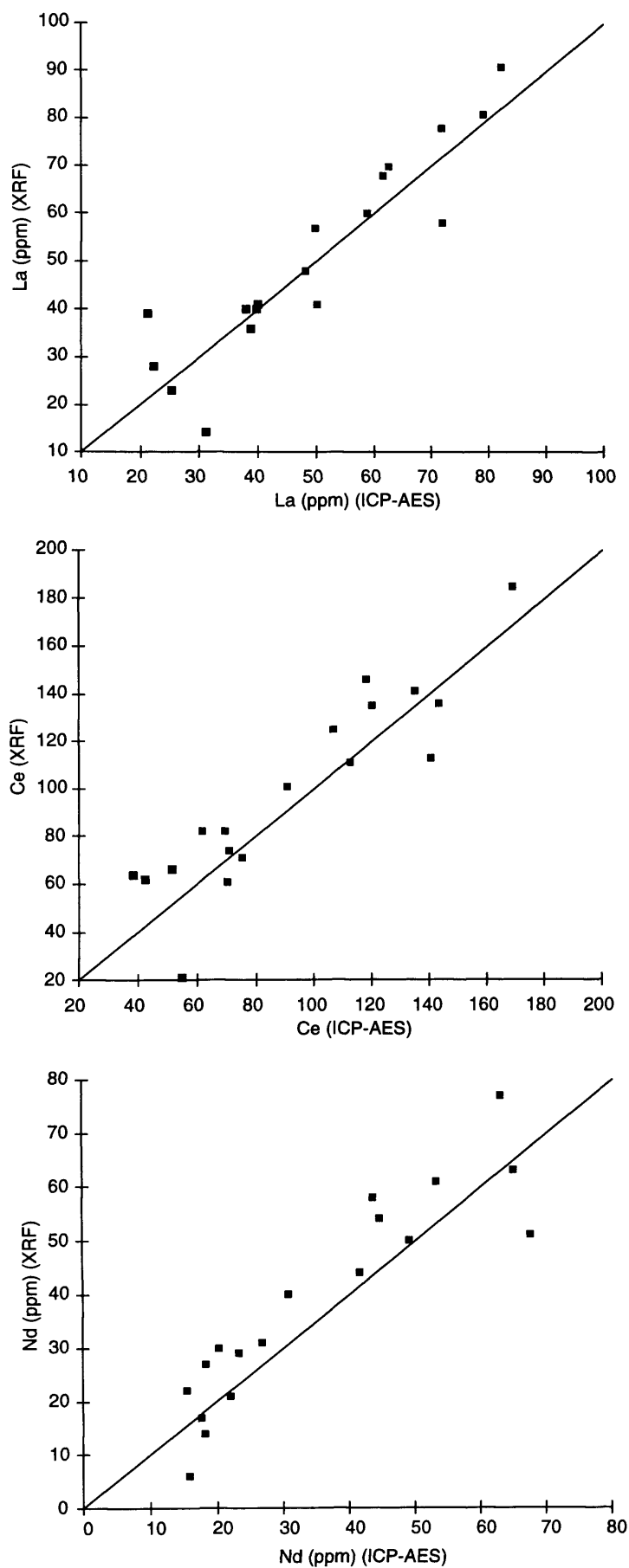
**FIGURE I3 - precision of XRF analyses (concentrations of selected major and trace elements in international standards and USEKA samples analysed by XRF in 1994 and 1995/1996)**



**Legend**

- USEKA samples analysed in 1994 and 1995/1996 (the same powder pellets analysed twice)
- Average 1994 and 1995/1996 international standard analyses (Major elements - JR-1, MRG-1, JA-2, MIN-N, JA-3, Trace elements - JR-1, NIM-G, STM-1, JA-1, MRG-1)

FIGURE I 4 - comparison between XRF and ICP-AES La, Ce & Nd data



## Appendix I (XRF, PGAA, ICP-AES)

**TABLE I6 - B, Li, REE standard data (accuracy & precision)**

### PGAA (B)

(standards run with USEKA igneous suite)

<i>Accuracy</i>	B	<i>Precision</i>	B
Measured JR-1	126	E20	65
Measured JR-1	105	E20	73
St Dev	15	St Dev	6
Average	116		
Accepted	117	UG73	7
		UG73	9
Measured JA-1	25	St Dev	1
Measured JA-1	21		
St Dev	3	K277	82
Average	23	K277	86
Accepted	21	St Dev	3
Measured JB-2	33		
Accepted	30		

### ICP-AES (Li)

(i) standards run with USEKA sediments

<i>Accuracy</i>	Li	<i>Precision</i>	Li
Measured SO-1	69	VSE 16	494
Measured SO-1	53	VSE 16	503
Measured SO-1	50	St Dev	6
St Dev	10		
Average	57	VSE 2	76
Accepted	48	VSE 2	76
		St Dev	0
Measured SO-2	16		
Measured SO-2	9	VSE 23	414
St Dev	5	VSE 23	423
Average	13	St Dev	6
Accepted	9		
Measured JLK-1	53	Sect I-10.8-12.1	39
Measured JLK-1	52	Sect I-10.8-12.1	37
Measured JLK-1	53	St Dev	1
St Dev	1		
Average	53		
Accepted	52		

(ii) standards run with USEKA igneous suite

<i>Accuracy</i>	Li	<i>Precision</i>	Li
Measured JR-1	62	K227	35
Measured JR-1	67	K227	35
Measured JR-1	63	St Dev	0
St Dev	3		
Average	64	K234	19
Accepted	61	K234	19
		St Dev	0
Measured JR-2	81		
Accepted	79	K237	58
		K237	61
Measured JB-2	BDL	St Dev	2
Measured JB-2	BDL		
Measured JB-2	BDL	SE3	14
Measured JB-2	BDL	SE3	15
Accepted	8	St Dev	1
Measured JA-2	29		
Accepted	27		

### ICP-AES (REE)

<i>Accuracy</i>	La	Ce	Pr	Nd	Sm	Eu	Gd	Dy	Er	Yb	Lu
Measured JA-2	16.4	32.8	4.05	17.40	3.29	0.82	3.4	3.2	2.12	1.66	0.3
Accepted	16.3	32.7	4.38	13.80	3.12	0.94	3.1	3.0	1.37	1.67	0.3
Measured JR-2	17.8	40.6	5.56	24.57	5.20	0.24	5.2	5.8	4.07	4.05	0.7
Accepted	16.9	38.8	4.93	21.10	5.71	0.15	6.3	6.9	4.50	5.46	0.9
Measured JR-1	20.0	48.1	6.41	25.89	5.88	0.25	4.8	7.4	4.02	4.20	0.6
Accepted	19.7	47.1	5.62	23.50	6.07	0.30	5.2	5.8	3.78	4.49	0.7
Measured JA-3	9.5	21.5	3.38	12.46	3.40	0.77	3.6	3.6	1.65	1.90	0.3
Accepted	9.0	23.3	2.25	12.30	3.14	0.85	2.9	3.0	1.46	2.18	0.3
<i>Precision</i>											
V3	49.9	106.8	13.89	64.99	8.96	2.01	6.8	4.8	2.72	1.79	0.3
V3	42.8	90.5	10.97	55.93	7.51	1.74	5.7	4.4	2.13	1.51	0.3
Stdev	5	12	2	6	1	0	1	0	0	0	0
93TG5	31.2	54.7	5.08	18.08	3.19	0.53	3.1	3.1	1.40	1.28	0.2
93TG5	34.8	61.0	6.71	21.08	4.12	0.78	3.2	3.0	1.59	1.32	0.2
Stdev	3	4	1	2	1	0	0	0	0	0	0
94TV246	25.4	51.8	6.23	20.33	4.86	0.14	4.6	4.7	2.11	2.56	0.4
94TV246	25.5	51.5	5.32	19.64	4.47	0.14	4.4	4.8	2.01	2.59	0.4
Stdev	0	0	1	0	0	0	0	0	0	0	0

B and Li Japanese standard data is from Imai et al., 1996, all other standard data is from Govindaraju 1994

## Appendix J - Nd and Sr isotope data

### Analytical procedure

Radiogenic isotope ratios, and Nd and Sm concentrations, were analysed at the NERC Isotope Geosciences Laboratory. Sr and Nd were separated from common dissolutions of 150 - 400 mg powdered samples using ultra clean reagents and conventional cation exchange columns. Procedural blanks for Sr, Nd and Sm averaged 450 pg, 120 pg, and 110 pg respectively. All Sr isotopic compositions were measured in static mode on a Finnigan MAT 262 multicollector mass spectrometer; the Nd isotopic compositions were measured in dynamic mode on a VG 354 multicollector mass spectrometer.  $^{87}\text{Sr}/^{86}\text{Sr}$  was normalised to  $^{86}\text{Sr}/^{88}\text{Sr} = 0.1194$ ,  $^{143}\text{Nd}/^{144}\text{Nd}$  was normalised to  $^{146}\text{Nd}/^{144}\text{Nd} = 0.7219$ . Within-run precision for Sr and Nd isotope ratios, expressed as one standard error of the mean, was always better than 10 ppm of the measured ratio, i.e. 0.000007 and 0.000005 for  $^{87}\text{Sr}/^{86}\text{Sr}$  and  $^{143}\text{Nd}/^{144}\text{Nd}$  respectively. Results for isotope standards during the periods of these measurements were: NBS 987  $^{87}\text{Sr}/^{86}\text{Sr} = 0.710187 \pm 0.000028$  (n=13), Johnson-Matthey Nd  $^{143}\text{Nd}/^{144}\text{Nd} = 0.511123 \pm 0.000012$  (n=65), La Jolla Nd  $^{143}\text{Nd}/^{144}\text{Nd} = 0.511864 \pm 0.000008$  (n=2), all errors: two standard deviations). Internal errors on individual measurements were always much smaller than the standard reproducibility reported here and therefore the ability to reproduce the standards should be taken as the limiting factor in interpreting the uncertainty of any given analysis.

### Results

Experimental data for the determination of  $^{87}\text{Sr}/^{86}\text{Sr}_i$

Sample	Rb (ppm)	Sr (ppm)	Rb/Sr	$^{87}\text{Rb}/^{86}\text{Sr}$	$^{87}\text{Sr}/^{86}\text{Sr}_m$	Age (Ma)	$^{87}\text{Sr}/^{86}\text{Sr}_i$
E1	103	228	0.452	1.309	0.709131	20.2	0.708755
E5	265	43	6.144	17.792	0.713474	20.3	0.708344
E20	258	183	1.408	4.076	0.710465	20	0.709307
E16	335	61	5.498	15.919	0.712734	20	0.708212
UG28	143	392	0.364	1.053	0.708008	17.6	0.707745
E3	258	518	0.498	1.440	0.707929	14.9	0.707624
SE13	96	669	0.143	0.414	0.708276	16.8	0.708177
SI14	125	791	0.158	0.457	0.707478	15	0.707381
V26	258	967	0.266	0.771	0.707608	15	0.707444
G5	154	153	1.007	2.914	0.709987	17.7	0.709255
G8	161	252	0.637	1.845	0.709489	20.5	0.708952
UG75	263	712	0.370	1.071	0.707856	15.9	0.707614
UG63	142	644	0.220	0.638	0.707556	14.6	0.707424
UG145	243	634	0.384	1.112	0.708799	15.5	0.708554
SE1	146	251	0.583	1.687	0.709323	18.9	0.708870
V226	126	548	0.230	0.665	0.70755	9	0.707465
V228	430	159	2.704	7.830	0.710788	17	0.708898
V231	156	332	0.470	1.359	0.709021	17	0.708693
V210	154	1609	0.096	0.277	0.705622	12.2	0.705574
V217	170	1320	0.129	0.373	0.706162	13.6	0.706090
V241	86	1074	0.080	0.232	0.706095	12.2	0.706055
V242	192	1228	0.156	0.452	0.706176	12.2	0.706098
V249	201	1455	0.138	0.400	0.706496	12.2	0.706427
888/2	120	689	0.174	0.504	0.711718	18	0.711589



## Appendix J (Nd and Sr isotope data)

Experimental data for the determination of  $\epsilon_{Nd}$

Sample	Nd (ppm)	Sm (ppm)	Sm/Nd	$^{147}\text{Sm}/^{144}\text{Nd}$	$^{143}\text{Nd}/^{144}\text{Nd}$ d m	Age (Ma)	$^{143}\text{Nd}/^{144}\text{Nd}$ d l	I t CHUR	$\epsilon_{Nd}$
E1	27.72	5.15	0.1857	0.1123	0.512386	20.2	0.512371	0.512612	-4.7
E5	34.22	6.16	0.1799	0.1088	0.512362	20.3	0.512348	0.512612	-5.2
E20	26.32	5.14	0.1955	0.1182	0.512346	20	0.512331	0.512612	-5.5
E16	28.33	5.29	0.1866	0.1128	0.51239	20	0.512375	0.512612	-4.6
UG28	28.51	4.72	0.1655	0.1001	0.512422	17.6	0.512410	0.512615	-4.0
E3	61.38	10.37	0.1689	0.1022	0.512429	14.9	0.512419	0.512619	-3.9
SE13	32.96	6.31	0.1914	0.1158	0.512391	16.8	0.512378	0.512616	-4.6
SI14	62.74	10.61	0.1692	0.1023	0.51243	15	0.512420	0.512619	-3.9
V26	56.33	10.67	0.1893	0.1145	0.512472	15	0.512461	0.512619	-3.1
G5	21.04	3.73	0.1773	0.1072	0.512353	17.7	0.512341	0.512615	-5.4
G8	23.62	4.66	0.1974	0.1194	0.512355	20.5	0.512339	0.512612	-5.3
UG75	44.12	7.96	0.1804	0.1091	0.512434	15.9	0.512423	0.512618	-3.8
UG63	46.01	7.87	0.1711	0.1035	0.512391	14.6	0.512381	0.512619	-4.6
UG145	86.06	12.90	0.1499	0.0907	0.512305	15.5	0.512296	0.512618	-6.3
SE1	27.84	4.94	0.1775	0.1073	0.512356	18.9	0.512343	0.512614	-5.3
V226	32.77	6.18	0.1885	0.1140	0.512459	9	0.512452	0.512626	-3.4
V228	18.40	4.25	0.2307	0.1395	0.512364	17	0.512348	0.512616	-5.2
V231	26.85	4.81	0.1790	0.1083	0.512371	17	0.512359	0.512616	-5.0
V210	74.27	11.39	0.1534	0.0927	0.512513	12.2	0.512506	0.512622	-2.3
V217	66.25	10.03	0.1514	0.0916	0.51248	13.6	0.512472	0.512621	-2.9
V241	25.90	4.98	0.1923	0.1163	0.512393	12.2	0.512384	0.512622	-4.7
V242	58.21	8.75	0.1503	0.0909	0.512494	12.2	0.512487	0.512622	-2.6
V249	55.73	9.84	0.1765	0.1068	0.512497	12.2	0.512488	0.512622	-2.6
888/2	123.30	24.69	0.2002	0.1211	0.512102	18	0.512088	0.512615	-10.3